Transactions

of the

ASME

Furnace Heat Absorption in Paddy's Run Pulverized-Coal-Fired Steam Generator, Using Turbulent Burners, Louisville, Ky.:

Part I Variation in Heat Absorption as Shown by Measurement of Surface Temperature of Exposed Side of Furnace Tubes. . *R. I. Wheater and M. H. Howard* 893

Part II Furnace Heat-Absorption Efficiency as Shown by Temperature and Composition of Gases Leaving the Furnace . . . . *R. C. Corey and Paul Cohen* 925

Part III Comparison and Correlation of the Results of Furnace Heat-Absorption Investigation . . . . . *H. H. Hemenway and R. I. Wheater* 937

Discussion of Preceding Papers 945

The Evaluation of Steam-Power-Plant Losses by Means of the Entropy-Balance Diagram . . . . . *Allen Keller* 949

The Gas-to-Gas Heat Exchanger as Applied to an Oxygen Plant . . . . . *Clyde Simpelaar and David Aronson* 955

Design of Regenerators for Gas-Turbine Service . . . . . *David Aronson* 967

Correlation of Plastic Deformation During Metal Cutting With Tensile Properties of the Work Material. . . . . *J. T. Lapsley, Jr., R. C. Grassi, and E. G. Thomsen* 979

Improved Nails . . . . . *E. George Stern* 987

Head and Flow Observations on a High-Efficiency Free Centrifugal-Pump Impeller. . . . . *W. C. Osborne and D. A. Morelli* 999

The Flow Through Centrifugal Compressors and Pumps . . . . . *H. E. Sheets* 1009

Possibilities of the Regenerative Steam Cycle at Temperatures Up to 1600 F . . . . . *P. H. Knowlton and R. W. Hartwell* 1017

Oil Holes and Grooves in Plain Journal Bearings . . *S. A. McKee and H. S. White* 1025

Film Thickness Between Gear Teeth. . . . *M. D. Hersey and D. B. Lowdenslager* 1035

Thermal-Shock and Other Comparison Tests of Austenitic and Ferritic Steels for Main Steam Piping . . . . . *W. C. Stewart and W. G. Schreitz* 1043

OCTOBER, 1950

VOL. 72, NO. 7

Transactions

of The American Society of Mechanical Engineers

Published on the tenth of every month, except March, June, September, and December

---

Published monthly by The American Society of Mechanical Engineers. Publication office at 20th and Northampton Streets, Easton, Pa. The editorial department is located at the headquarters of the Society, 29 West Thirty-Ninth Street, New York 18, N. Y. Cable address, "Dynamic," New York. Price $1.50 a copy, $12.00 a year for Transactions and the *Journal of Applied Mechanics;* to members and affiliates, $1.00 a copy, $6.00 a year. Changes of address must be received at Society headquarters three weeks before they are to be effective on the mailing list. Please send old as well as new address.... By-Law: The Society shall not be responsible for statements or opinions advanced in papers or ... printed in its publications (B13, Par. 4).... Entered as second-class matter March 2, 1928, at the Post Office at Easton, Pa., under the Act of August 24, 1912.....

Furnace Heat Absorption in Paddy's Run Pulverized-Coal-Fired Steam Generator, Using Turbulent Burners, Louisville, Ky.

Part I Variation in Heat Absorption as Shown by Measurement of Surface Temperature of Exposed Side of Furnace Tubes

By R. I. WHEATER[1] and M. H. HOWARD,[2] NEW YORK, N. Y.

This report is one of three current formal reports (1)[3] covering the activities of the ASME Special Research Committee on Furnace Performance Factors in connection with the furnace performance tests which were conducted at the Paddy's Run Station of the Louisville Gas and Electric Company in Louisville, Kentucky. The furnace heat absorption and its distribution in the furnace, as reported in this paper, were determined by the "ΔT method," which consists of using the difference in temperature between the surface of the exposed face of the tube and the mixture within the tube to measure the heat absorption at representative locations. The companion paper, Part II, covers the furnace performance as measured by a heat balance of the furnace. Part III presents a correlation of the results.

Introduction

IT IS desirable at this point to review briefly the history of the extensive test program which has been undertaken by the ASME Special Research Committee on Furnace Performance factors. This program was actually initiated in 1943 for the purpose of gaining more factual and fundamental knowledge of the various factors which affect the performance of large central-station furnaces. In order to accomplish this, it was also necessary to establish methods of measuring the amount and distribution of heat absorbed in such furnaces.

The first furnace to be tested was a completely water-cooled, dry-bottom furnace, fired tangentially by eight pulverized-coal burners which could be tilted up or down 30 deg from the horizontal. These tests were made in 1945 at the Ohio Power Company's Tidd Station, using the No. 11 boiler, which is a conventional, 3-drum, bent-tube boiler. Four papers (2) were presented in June, 1947, covering the furnace performance obtained with this design under several operating variables, as well as the results of several different means of measuring the furnace heat absorption and its distribution in the furnace.

The subject tests were conducted at the Paddy's Run Station of the Louisville Gas and Electric Company in 1948, in order to establish the furnace performance of another completely water-cooled furnace which is fired horizontally by eight turbulent pulverized-coal burners.

The object of this paper is to establish the distribution and amount of heat absorption in this furnace, as measured by the "ΔT method" for the various operating conditions investigated, and to study the effect of these operating variables on furnace performance. The operating variables studied were (*a*) burner adjustments, (*b*) furnace rating, (*c*) excess air for combustion, and (*d*) various combinations of burners in service at 50 per cent full load.

Test Equipment

The No. 3 unit at Paddy's Run Station is designed for a maximum continuous output of 640,000 lb of steam per hr at a pressure of 950 psig and a temperature of 900 F. It was first placed in operation on September 25, 1947, and normally has carried an output of 600,000 to 640,000 lb of steam per hr at design conditions. This unit, shown in Fig. 1, is of the single-drum bent-tube type, containing a conventional water-cooled furnace, a bare-tube pendant-type convection superheater, both a bare-tube and an extended-surface boiler section, an extended-surface economizer, a regenerative-type air preheater, and two ball-mill firing systems.

The dry-bottom furnace is approximately 31 ft in width and 24 ft in depth. The height of the furnace from the roof to the center line of the hopper throat at the bottom of the furnace is about 90 ft. The furnace walls are composed of 3-in-OD, 0.220-in. minimum wall, carbon-steel tubes spaced on $3^1/_4$-in. centers. This tube spacing exists throughout the furnace. Near the top, the rear-wall tubes bend into the furnace and then extend up vertically to form the slag screen. These rear-wall tubes are bent to form four rows of slag-screen tubes on 13-in. centers. The front-wall tubes bend at the top of the furnace to form the furnace roof. Both the front and rear-wall tubes bend into the furnace to form the hopper throat at the bottom of the furnace. This throat is therefore parallel to the front or firing wall. The furnace contains 8884 sq ft total projected wall surface, which includes the outlet aperture.

This steam-generating unit is fired by eight horizontal intervane burners which are located in the lower front wall and arranged in two horizontal rows of four burners each. These burners are

---

[1] Assistant to the Manager, Service Department, Foster Wheeler Corporation, New York, N. Y. Mem. ASME.

[2] Manager, Service Department, Foster Wheeler Corporation, New York, N. Y. Mem. ASME.

[3] Numbers in parentheses refer to Bibliography at end of paper.

Contributed by the Special Research Committee on Furnace Performance Factors, and the Fuels, Power, and Heat Transfer Divisions, and presented at the Annual Meeting, New York, N. Y., November 27–December 2, 1949, of The American Society of Mechanical Engineers.

Note: Statements and opinions advanced in papers are to be understood as individual expressions of their authors and not those of the Society. Paper No. 49—A-118.

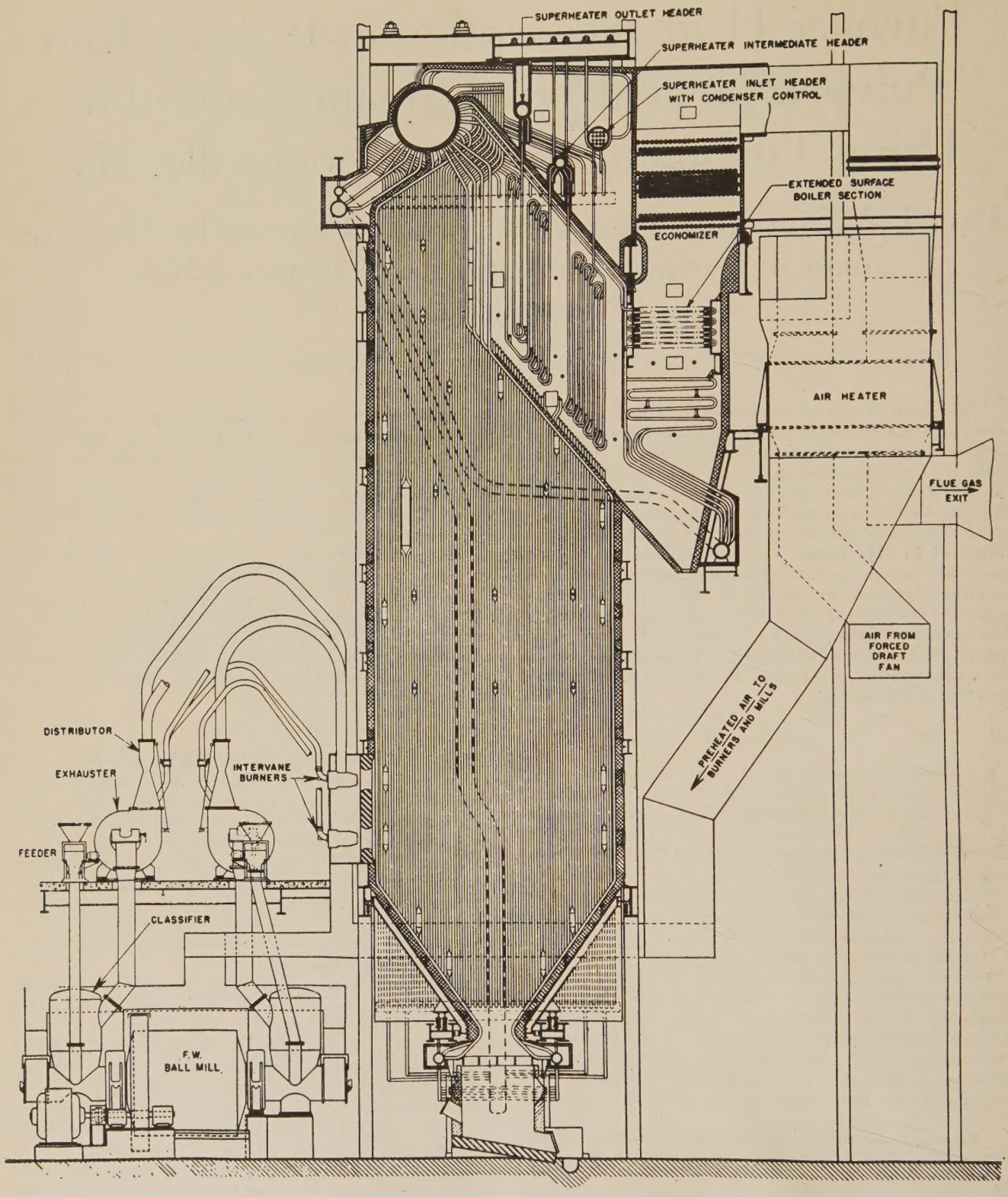

FIG. 1 GENERAL ARRANGEMENT OF BOILER NO. 3

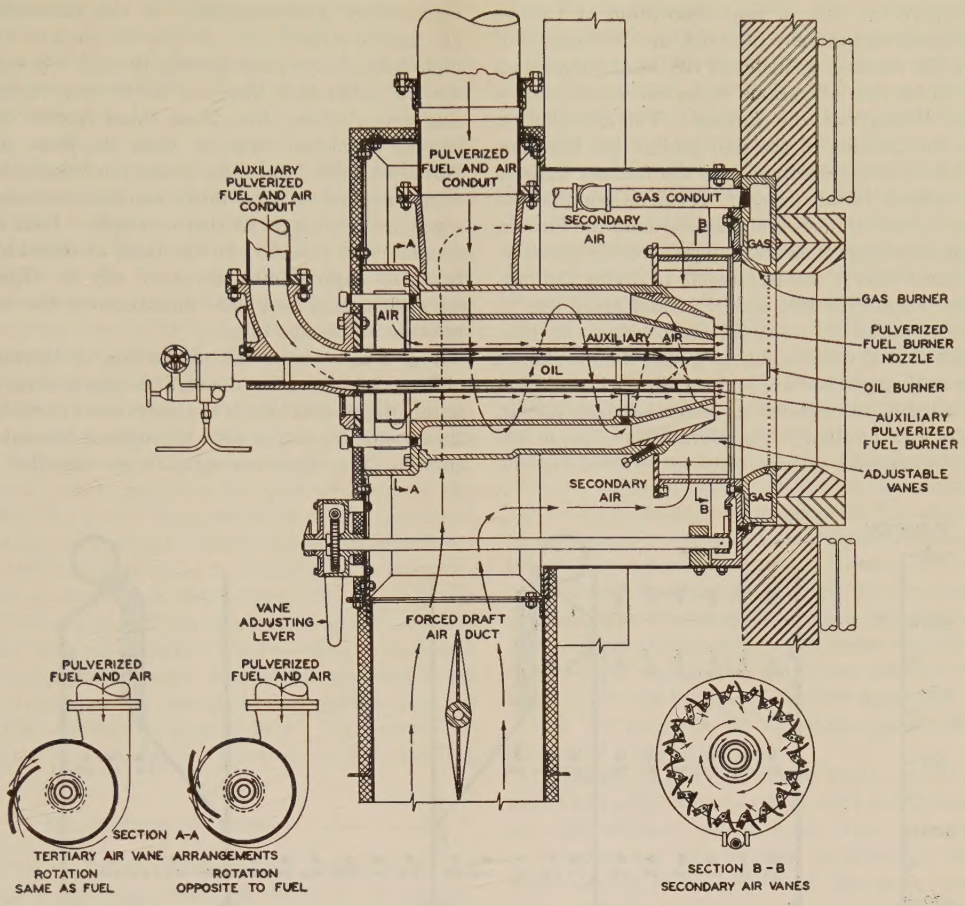

FIG. 2 GENERAL ARRANGEMENT OF HORIZONTAL INTERVANE BURNERS

of the turbulent type and may fire either pulverized coal or natural gas. However, at the time of these tests, natural gas was not yet available at the plant and only pulverized-coal-firing was investigated. The burners are supplied with pulverized coal by two ball-mill systems each containing two exhausters. The two lower inside burners and the two upper outside burners are part of one mill system, and the remaining burners are part of the other mill system. Each burner conduit is equipped with a shutoff valve which permits individual burners to be removed from service.

Fig. 2 shows the horizontal intervane burners which are used. Each burner contains two coal nozzles, a main nozzle, and a smaller auxiliary nozzle. This arrangement is designed for the purpose of extending the load range per burner. The primary air and coal leaving the main nozzle has an angular velocity which is created by the tangential inlet to the burner body. A similar rotation is given to the coal leaving the auxiliary nozzle by means of vanes located near the outlet. The velocity of the primary mixture leaving these nozzles may be varied by use of the auxiliary air dampers which are located in the exhauster inlets.

Secondary air for combustion is admitted to the burner throat through adjustable vanes which control the angular velocity of the secondary air. These vanes are adjustable from 0 to 100 per cent open, which corresponds to an actual range up to about 70 deg open. The rotation of the secondary air is in the same direction as that of the primary mixture. Tertiary air also can be admitted to the burner throat through the annular space between the coal nozzles and controlled by an adjustable vane to create a rotation either with or against the rotation of the burner.

The burner adjustments mentioned provide means of changing the flame shape and furnace conditions. The effects of the various adjustments are as follows:

1 When the secondary-air vane opening is increased at a constant air flow, the following takes place:

(*a*) The ignition zone moves away from the burner tip.
(*b*) The flame is lengthened and the flame angle reduced.
(*c*) The burner-box pressure is reduced.
(*d*) The angular velocity of the fuel-air mixture leaving the burner throat is decreased.
(*e*) The mixing of the fuel and air is changed.

When the secondary-air vane opening is decreased at a constant air flow, the following occurs:

(*a*) The ignition zone moves closer to the burner tip.
(*b*) The flame is shortened and the flame angle increased.
(*c*) The burner-box pressure is increased.
(*d*) The angular velocity of the fuel-air mixture leaving the burner throat is increased.
(*e*) The mixing of the fuel and air is changed.

2 When the tertiary air is used with rotation of the burner the flame is lengthened, and conversely, when used against rotation the flame is shortened.

3 When the auxiliary air damper is opened, the burner velocities are increased and the ignition zone moves away from the burner tip.

From the foregoing it will be seen that changes in air flow can change flame shape, depending upon whether the air flow is varied at constant secondary-air vane opening, constant burner-box pressures, or by changes to both vane opening and burner-box pressure.

In order to measure the rate of heat absorption at various representative locations and thereby establish the distribution of heat absorption in the furnace, we installed 128 thermocouples on the furnace-face center line of various waterwall tubes and at various elevations throughout the furnace. This installation was made during the erection of the unit and at the locations shown in Fig. 3, which is a development of the furnace walls as viewed from the "outside" of the furnace. It can be seen that the thermocouples were installed in several bands around the furnace and arranged to give coverage of as nearly equal areas as possible. It will also be realized that it was impossible to divide the projected areas of the waterwalls into exactly equal areas due to existing interference caused by tiebacks, beams, and the like. Since it was not felt that it was possible to install thermocouples on the upper rear-wall sloped section and obtain an installation which would be reliable throughout an extended test period, these thermocouples were omitted. Therefore this section of the rear wall is not represented satisfactorily or covered by the furnace-face thermocouples. In this particular area the tubes are backed with $2^1/_2$ in. of tile, the back of which is exposed to high-temperature gases passing through the superheater. It will also be noted that there are no thermocouples installed on the slag-screen tubes, since these tubes receive convection transfer as well as radiant transfer from the flame and furnace gases. However, aside from these areas, the furnace-face thermocouples were installed to give fairly complete coverage and relatively equal area coverage per thermocouple. Four additional thermocouples were installed on the back of individual rear waterwall tubes at approximate elevation 463 ft. These thermocouples were then used as a base indication of the temperature of the mixture within the tube.

Fig. 3 also shows the numbering of thermocouples, location of furnace observation doors, and details of the installation. The numbering shown here is the instrument numbering of the various thermocouples and is used throughout the subsequent data and curves. The thermocouples were installed substantially as

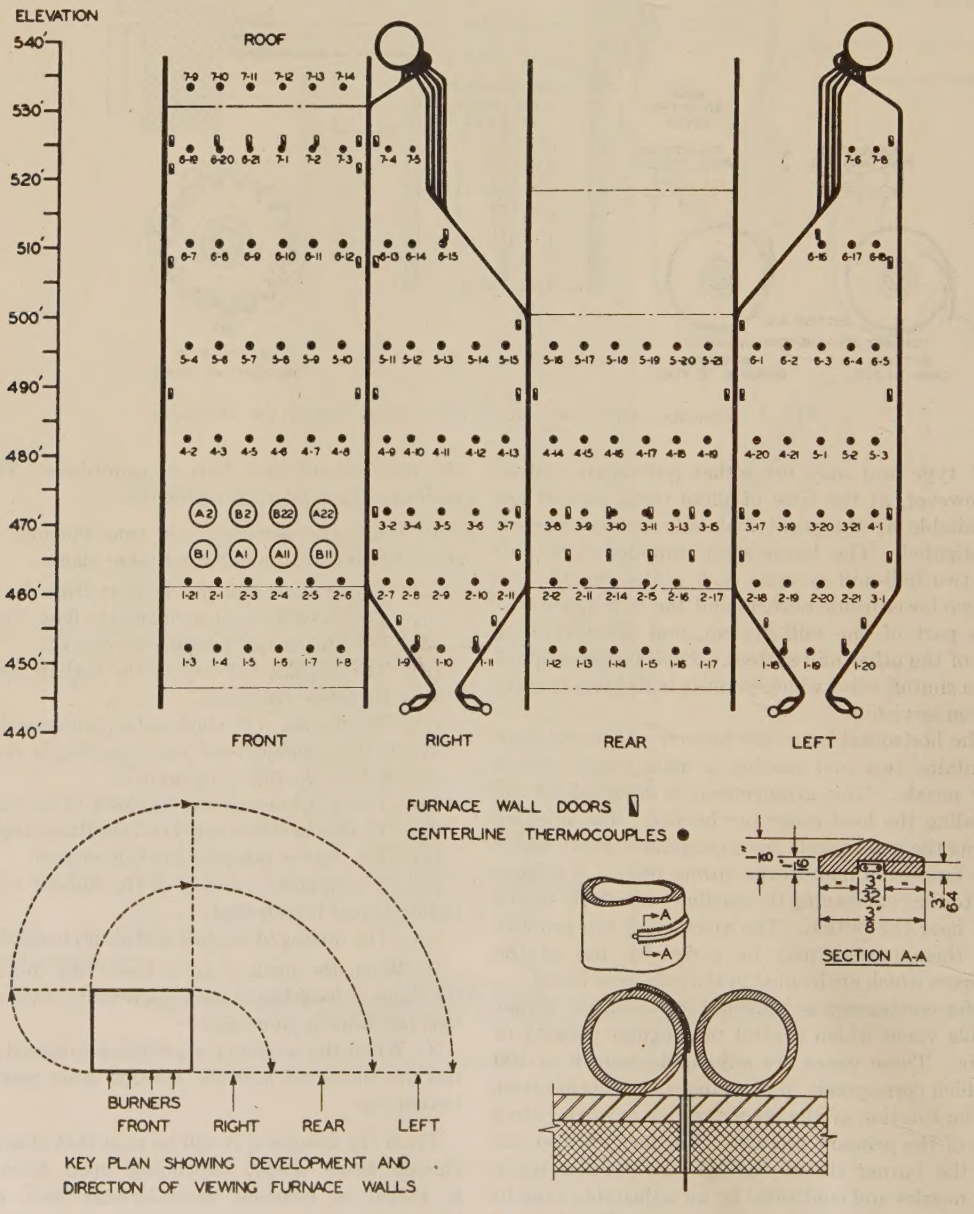

FIG. 3 KEY PLAN AND THERMOCOUPLE LOCATION IDENTIFICATION DIAGRAM

described by Humphreys (3), a method which was used satisfactorily on the previously described Tidd Station tests. The thermocouples were installed at the center line of the furnace face of the tubes and consisted of No. 22 gage, glass-fiber, insulated, chromel-alumel wire.

The instrument originally used to record the thermocouple data was the same 21-point Leeds & Northrup Micromax high-speed potentiometer-recorder which had been used during the Tidd tests. However, owing to the difficulties which were experienced with this original instrument on the first series of tests, the committee replaced the Micromax with a Speedomax recorder. The latter instrument is much more suited to our particular purpose since it has the ability to handle exceptionally high lead wire resistances at a high speed of recording. The instrument was supplemented by a switching unit which contained seven groups of 21 contacts each, or a total of 147 points.

Thermocouples were identified by numbering all of the seven groups from 1 to 21, inclusive. The group identification number, which is one of the 21 points, prints at the upper extremity of the chart and identifies the group being recorded at the particular time. The switching mechanism is entirely automatic and allows the 147 points (140 thermocouples) to be recorded in approximately 30 minutes or about 12 seconds per thermocouple. While it was possible to increase greatly the speed of recording and thus decrease the time interval required for recording a complete cycle with the latter arrangement, it was felt unnecessary to do so since the variations existing during the test period were too small to warrant the additional volume of data. Fig. 4 shows the instrument mounted in a convenient location on the operating floor.

Description of Tests

The test program at Paddy's Run Station consisted of two series of tests, each requiring about 10 days for completion. The first series of tests, containing test Nos. 1 to 14, inclusive, were run in February, 1948. The second series of tests, containing test Nos. 15 to 30, inclusive, were run in October, 1948.

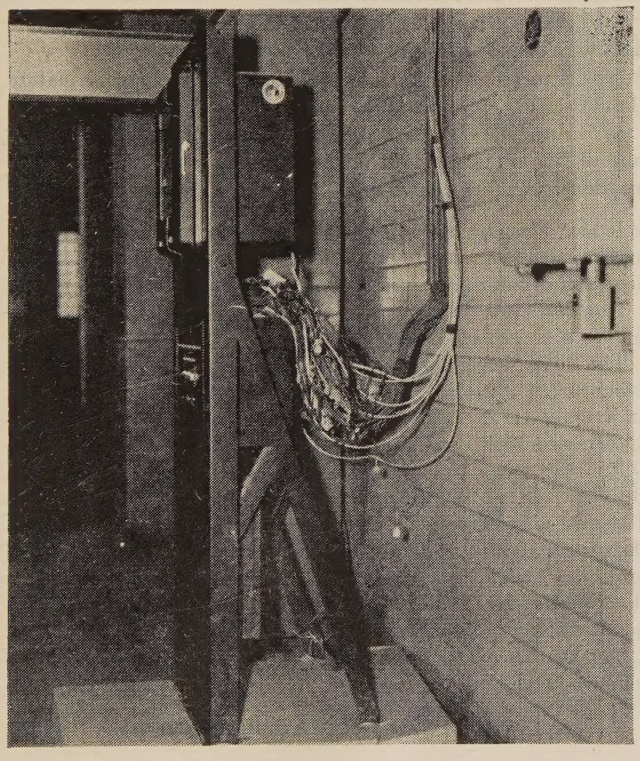

Fig. 4 View of L&N 140 Point Speedomax Recording Unit

We are sorry to report that due to difficulties experienced with the original Micromax recorder, we did not obtain any thermocouple data of value during the first series of tests.

However, the heat-balance data taken on test Nos. 1 to 14, inclusive, did establish that flame shape has a definite effect upon furnace performance and warranted further investigation. It was also found that the effect of varying the amount of excess air for combustion on furnace performance was a very difficult factor to isolate. On this series of tests, the committee attempted to investigate the effect of changing excess air under as near to normal operating conditions as possible, which includes the adjustment of secondary-air vanes to obtain the most desirable furnace conditions. It was found that these adjustments to the secondary-air vanes affected the furnace performance obtained for various amounts of excess air. Hence it became apparent that our test program should include an investigation of the effect of flame shape on furnace performance, and also that the effect of variations in excess air, which were important, would have to be determined at constant secondary-air vane opening even though this is not normal operation. It is readily realized that it is impossible to measure flame shape, but it is possible to establish definitely the secondary-air vane opening and burner-box pressure. Since the secondary-air vanes control the flame shape over a wide range, the committee decided to investigate the effect of varying secondary-air vane opening.

The test program for the second series of tests as actually completed is shown in Table 1.

Originally, it had been hoped that it would be possible to run individual series of tests (those tests at the same load and excess air with different secondary-air vane openings) consecutively, on the same test day, in order to determine the effect of varying vane opening with a minimum change in operating conditions, such as accumulation of ash on furnace walls. However, in actually running the tests it was found that the time necessary to establish equilibrium at the desired operating conditions made it impossible to complete three tests in a reasonable test day, and it was also found that the accumulation of ash on the furnace walls did not vary greatly during the entire test period.

It was also necessary to eliminate test Nos. 20 and 23, owing to insufficient time available in the test schedule.

Prior to each test period the retractable soot blowers, located between the slag screen and the first row of superheater elements, were blown, as well as the air-heater soot blowers. No other efforts were made to clean the unit prior to tests since the furnace remained relatively clean.

TABLE 1 TEST PROGRAM FOR SECOND TEST SERIES

Test no.	Date	Heat input to furnace, per cent full load	Excess air at furnace outlet, per cent	Secondary-air vane position, per cent open	No. of burners in service	Duration of test, hr
15	10/22/48	93.2	23.0	40	8	4.0
15A[a]	10/27/48	91.6	24.8	40	8	4.5
16	10/22/48	92.2	25.0	60	8	4.0
17	10/28/48	92.3	26.2	50	8	4.0
18	10/28/48	90.6	16.9	40	8	5.0
19	10/20/48	89.5	17.0	60	8	4.0
21	10/25/48	92.8	29.7	45	8	4.0
22	10/25/48	92.3	30.2	60	8	4.0
24	10/24/48	68.7	21.4	35	8	4.0
25	10/24/48	68.9	23.4	50	8	4.0
26	10/24/48	69.0	24.5	65	8	5.0
27	10/27/48	50.2	23.6	30	8	3.75
28	10/30/48	49.3	21.7	50	4 upper	4.0
29	10/29/48	49.2	23.0	50	4 lower	4.0
30	10/30/48	49.5	21.5	50	2 upper and 2 lower	4.0

[a] Test 15A was run under same conditions as test No. 15 and 5 days later as a check test.

When equilibrium was established at the desired test conditions, the instrument was placed in operation and all of the thermocouple data recorded, obtaining 8 to 11 complete cycles of temperature measurement for each test period. All board data and other pertinent data were recorded throughout the test period at regular intervals. One or two complete inspections of the furnace-wall surfaces were made during each test period to establish furnace cleanliness conditions. We also took a pulverized-coal fineness sample from each burner conduit during the test period in accordance with the ASTM Code for Pulverized Coal Sampling.

Methods of Analyzing Test Data

Distribution of pulverized-coal flow to the various burners was determined by using the pulverized-coal fineness samples as a measure. In taking these samples, we traversed all burner conduits from two directions without changing the cyclone-vent position, once it had been set to provide the correct average recovery rate. Therefore the weight of sample collected in each conduit, divided by the total weight of sample collected from all burner conduits, was considered representative of the distribution of pulverized coal between burners. It is of interest to note how well the distribution of coal flow between mill systems, as measured by this method, checks that determined by use of the coal scales. Table 2 shows the comparison of total flow to the A-mill system by both methods.

TABLE 2 COMPARISON OF COAL FLOW TO A-MILL SYSTEM BY DIFFERENT METHODS

Test no.	Per cent of total coal flow to A mill (coal scales)	Per cent of total flow to A mill (fineness samples)
15	48.2	50.5
15A	49.4	48.6
16	49.9	49.7
17	49.6	50.1
18	47.5	47.6
19	46.2	45.8
21	47.9	47.8
22	48.5	49.1
24	50.3	51.2
25	51.0	52.5
26	50.0	50.3
27	50.0	50.3
28	50.5	47.6
29	43.3	43.6
30	..	..

The ΔT-value referred to on these tests is the difference between the temperature of the exposed surface of the furnace-wall tube, measured on the tube center line at various locations, and the average temperature of the mixture within the tube, as indicated by the base thermocouples.

The distribution of heat absorption over the furnace walls has been represented by Figs. 5 to 19, inclusive, by use of isothermal ΔT-diagrams. Each diagram is actually a development of the furnace walls as viewed from "outside of the furnace." The ΔT-values shown on these particular diagrams use the saturation temperature at drum pressure, correcting for difference in elevation, as the average temperature of the mixture within the tube. While the base used does not affect the distribution of heat absorption, these ΔT-values may be changed to the thermocouple base by applying the correction noted under each isothermal ΔT-diagram. It has been found that the base thermocouples provide a better indication of the temperature of the mixture within the tube than is obtained by using the saturation temperature. The small arrows indicated on the circles representing burner openings in the front wall denote the rotation of the fuel mixture leaving the particular burner throat. Important test conditions are also noted on each diagram.

Ash-coverage diagrams are also included in Figs. 5 to 19, inclusive, to represent the ash conditions observed on the furnace walls during each test period. Fig. 20 must be used in conjunction with these ash-coverage diagrams, since it describes various types of ash found and referred to on the ash-coverage diagrams. Each area, on the diagram, contains the authors' estimate of the per cent coverage, average depth of ash, and type of ash. The locations of observation doors used for these furnace observations are also shown. The small arrows represent a general indication of the direction of gas flow noted at various points throughout the furnace. We have also attempted to indicate an approximate flame angle leaving the burner throats for all tests.

The distribution of heat absorption over the height of the furnace is represented for various series of tests in Figs. 22 to 28, inclusive. This distribution is shown by plotting the average ΔT of all thermocouples located at a particular elevation against the height of the furnace in feet above the center line of the hopper throat. Average rate of heat absorption at the various elevations may be approximated by multiplying the average ΔT-value by a factor of 1060 Btu/(sq ft) (hr) (deg F).

The ΔT-values obtained for these tests do, of course, present a means of estimating the total amount of furnace heat absorption if certain assumptions are to be made. However, any such calculations are subject to many possible errors, some of which are constant and others variable. Some of the inherent errors, which must be remembered whenever considering results obtained from such calculations, are as follows:

(*a*) Possible variation of true temperature measurement with the age of the thermocouple.

(*b*) Errors due to the effect of ash accumulating at the thermocouple location and not on the surrounding surface, caused by the protective shield, and thus not giving an accurate temperature measurement of the exposed surface represented by the thermocouple.

(*c*) Variations of the internal cleanliness of the tube.

(*d*) Variations of inside-film conductance under various conditions of load and internal cleanliness.

(*e*) Errors caused by improper weighting of thermocouple data with respect to the surface represented.

(*f*) Errors due to the impossibility of covering adequately the entire projected area of the furnace waterwalls.

(*g*) Errors due to the difficulty in obtaining the true temperature of the mixture within the tube at the many thermocouple locations.

It also must be recognized that a 1-deg error in temperature measurement can result in an 8 per cent error in the furnace heat-absorption results at 50 per cent full load.

However, we have made calculations using assumptions similar to those used by Schueler (2).

The thermal conductivity of the tube metal was assumed to be 348 Btu/(sq ft-hr)/in., and by using the tube OD of 3 in. with an average ID of 2.524 in., we obtained a value for metal conductance of 1342 Btu/(sq ft) (hr) (deg F) when referred to the OD of the tube. A film conductance was assumed to be 5000 Btu/(sq ft) (hr) (deg F) when referred to the OD of the tube. The over-all conductance through the tube metal and film was then calculated to be 1060 Btu/(sq ft) (hr) (deg F). The total projected area of the furnace is 8884 sq ft, which includes the projected area of all waterwall surface in the furnace above the hopper throat and the projected area of the outlet aperture.

Total furnace heat absorption was then determined by the following equation:

$$\text{Absorption} = U_o S \Delta T, \text{ Btu per hr}$$

where

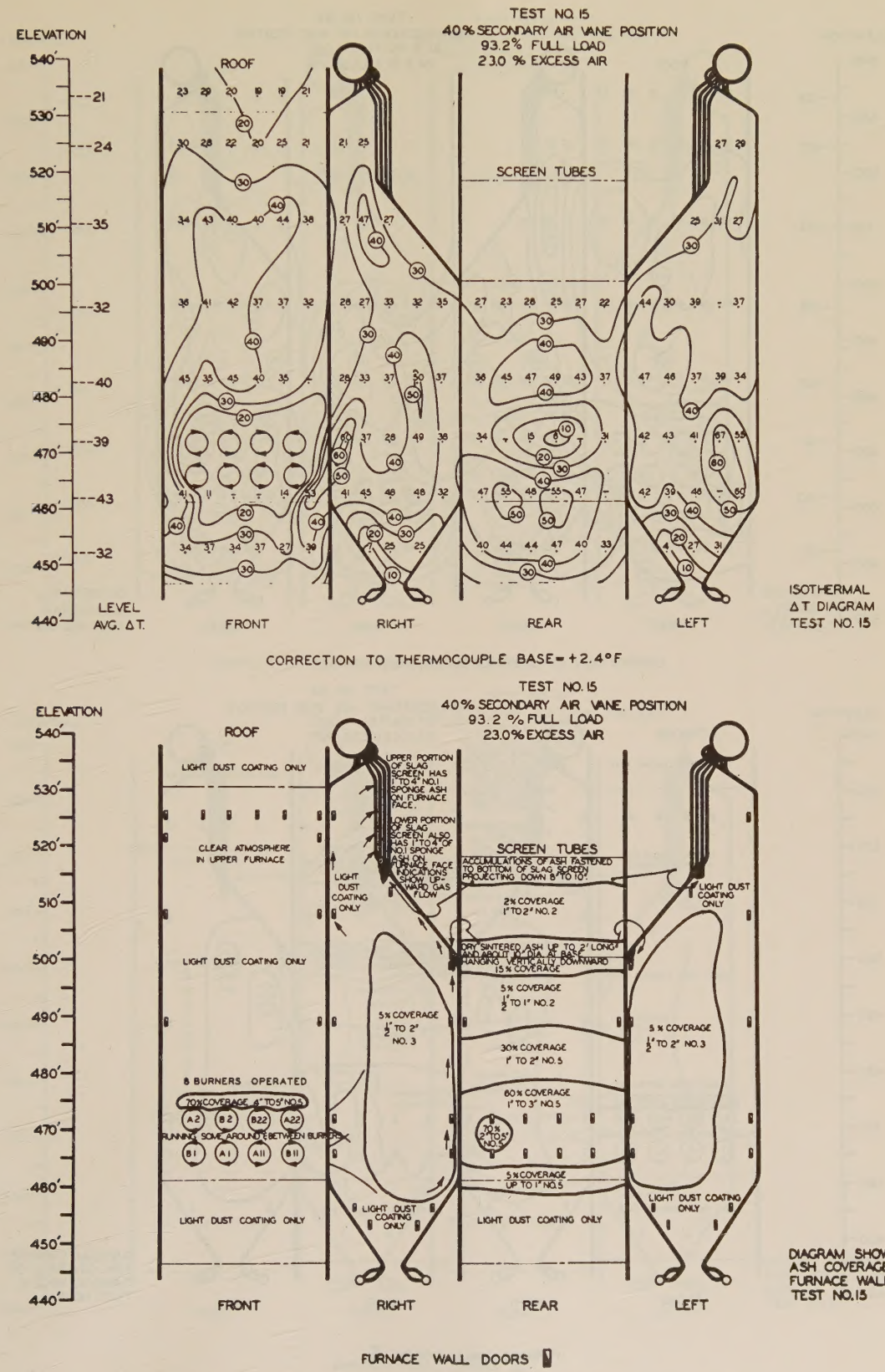

FIG. 5 ISOTHERMAL ΔT AND ASH-COVERAGE DIAGRAM TEST NO. 15

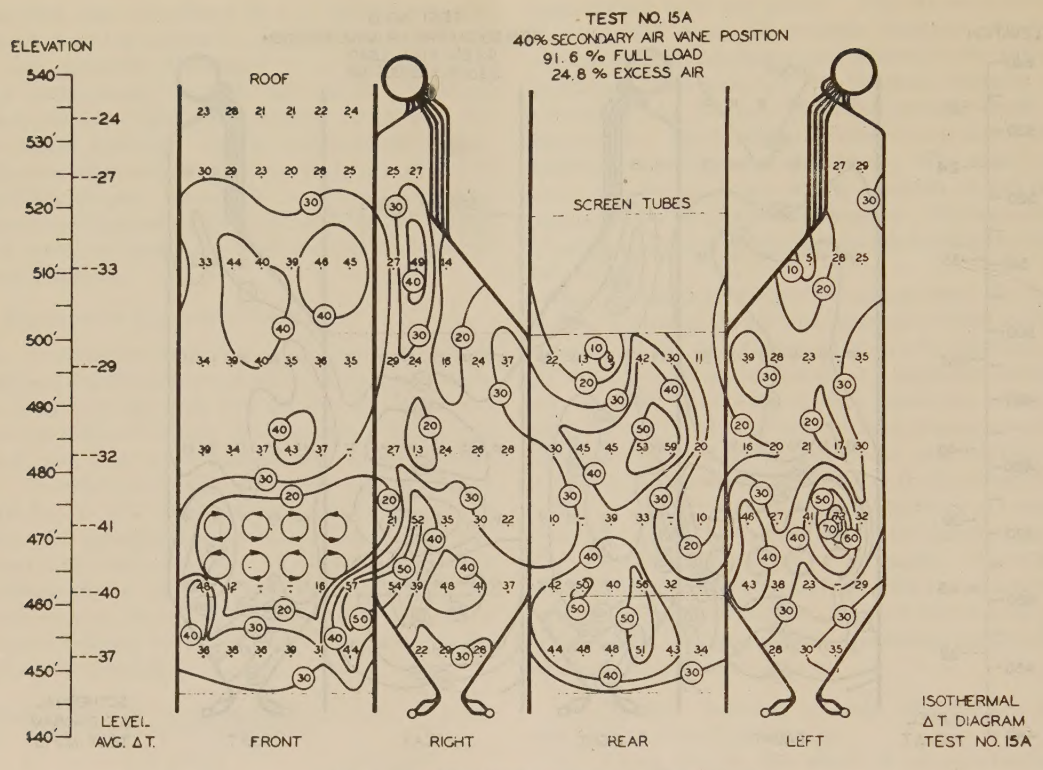

CORRECTION TO THERMOCOUPLE BASE = + 0.0°F

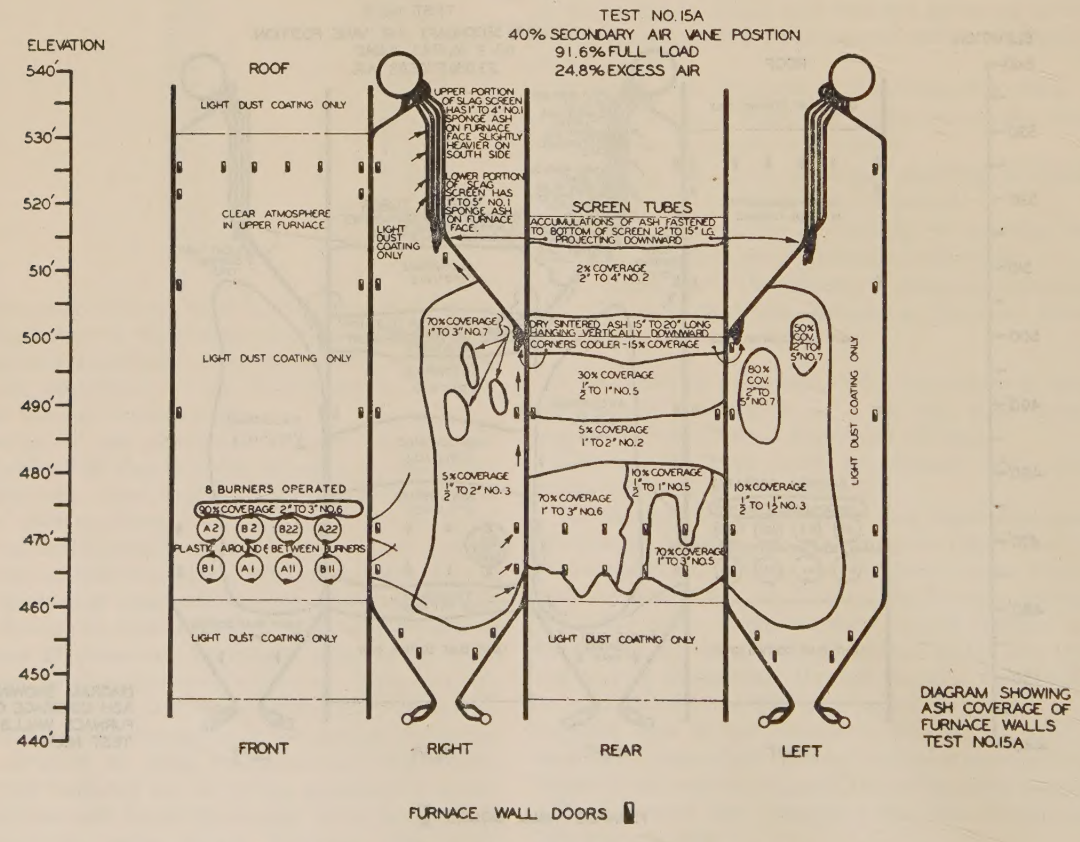

FIG. 6 ISOTHERMAL ΔT AND ASH-COVERAGE DIAGRAM TEST NO. 15A

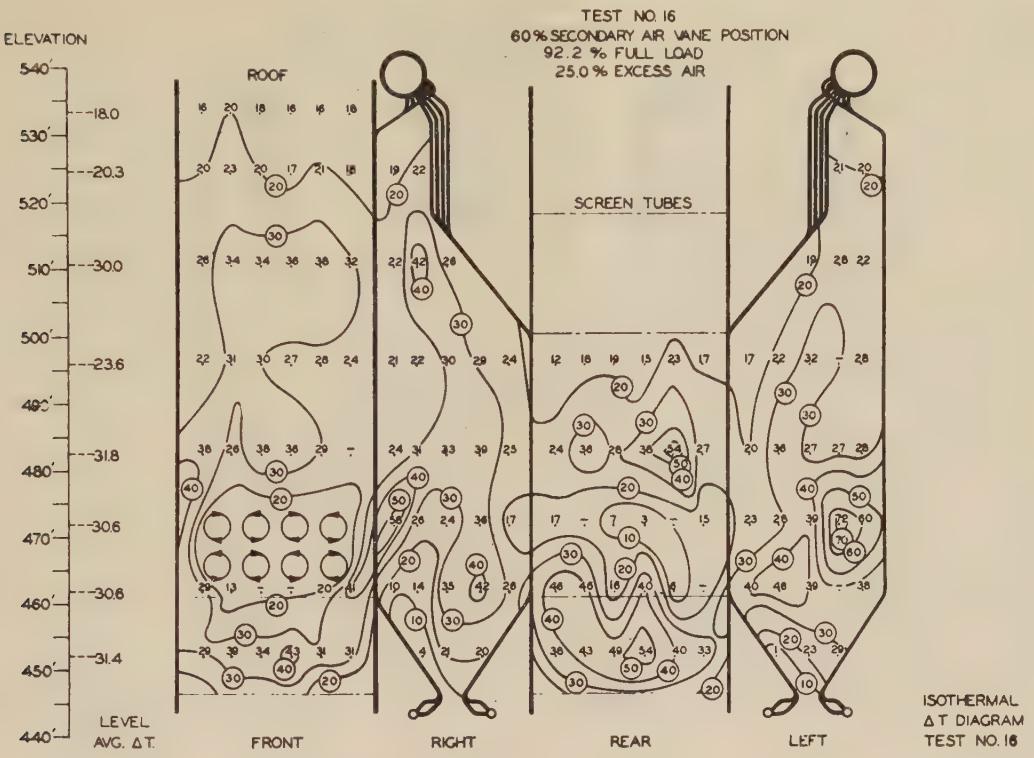

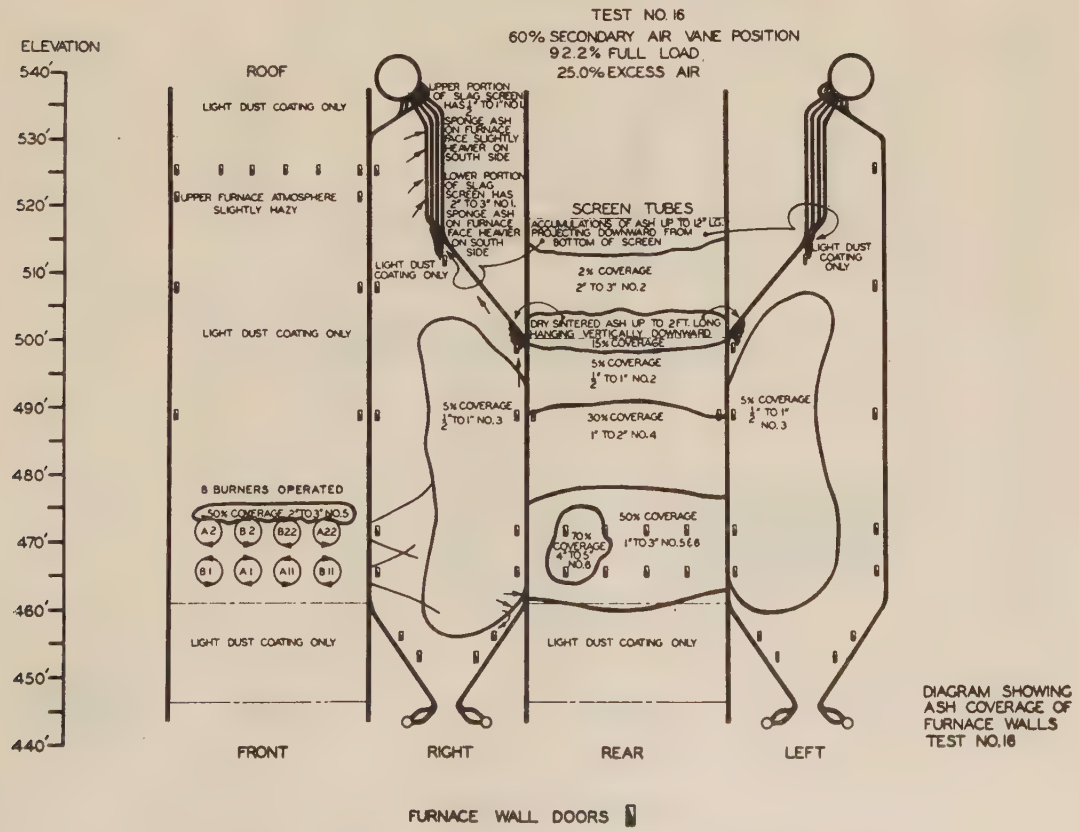

FIG. 7 ISOTHERMAL ΔT AND ASH-COVERAGE DIAGRAM TEST NO. 16

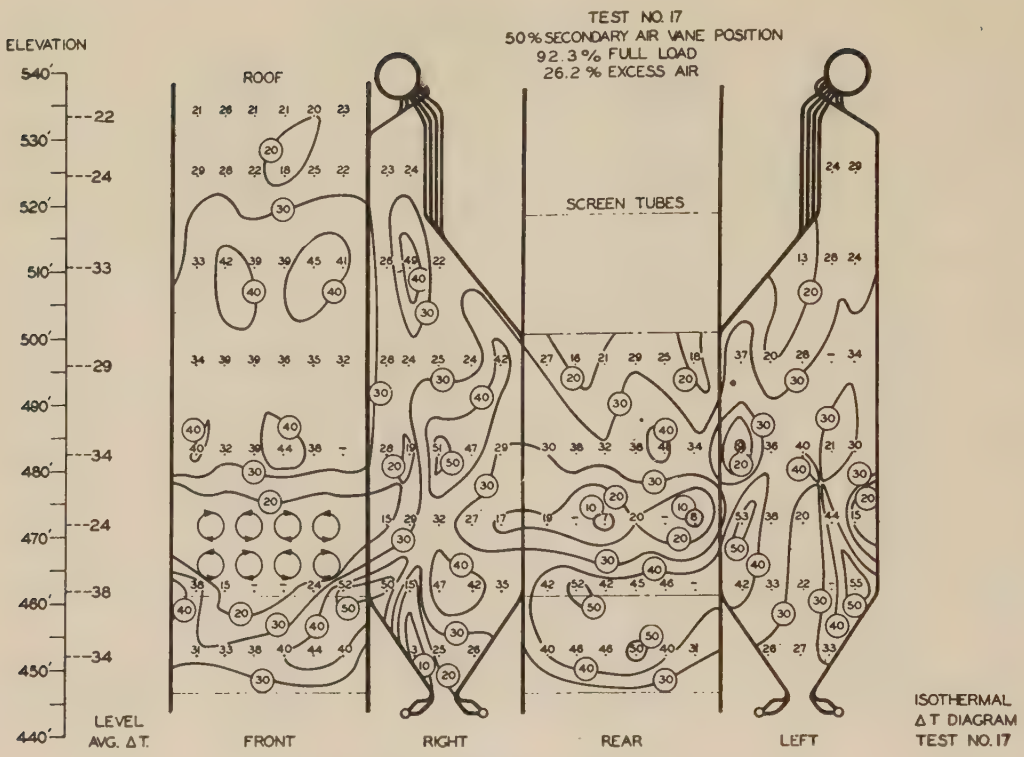

CORRECTION TO THERMOCOUPLE BASE = + 1.4°F

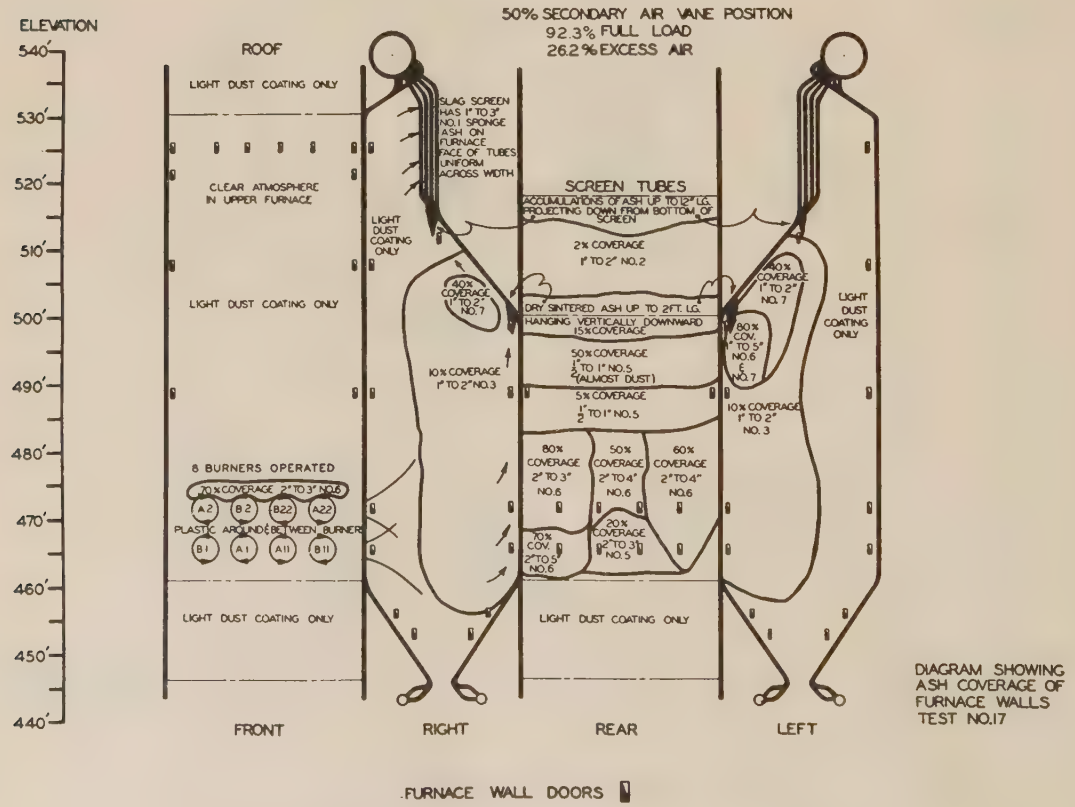

FIG. 8 ISOTHERMAL ΔT AND ASH-COVERAGE DIAGRAM TEST NO. 17

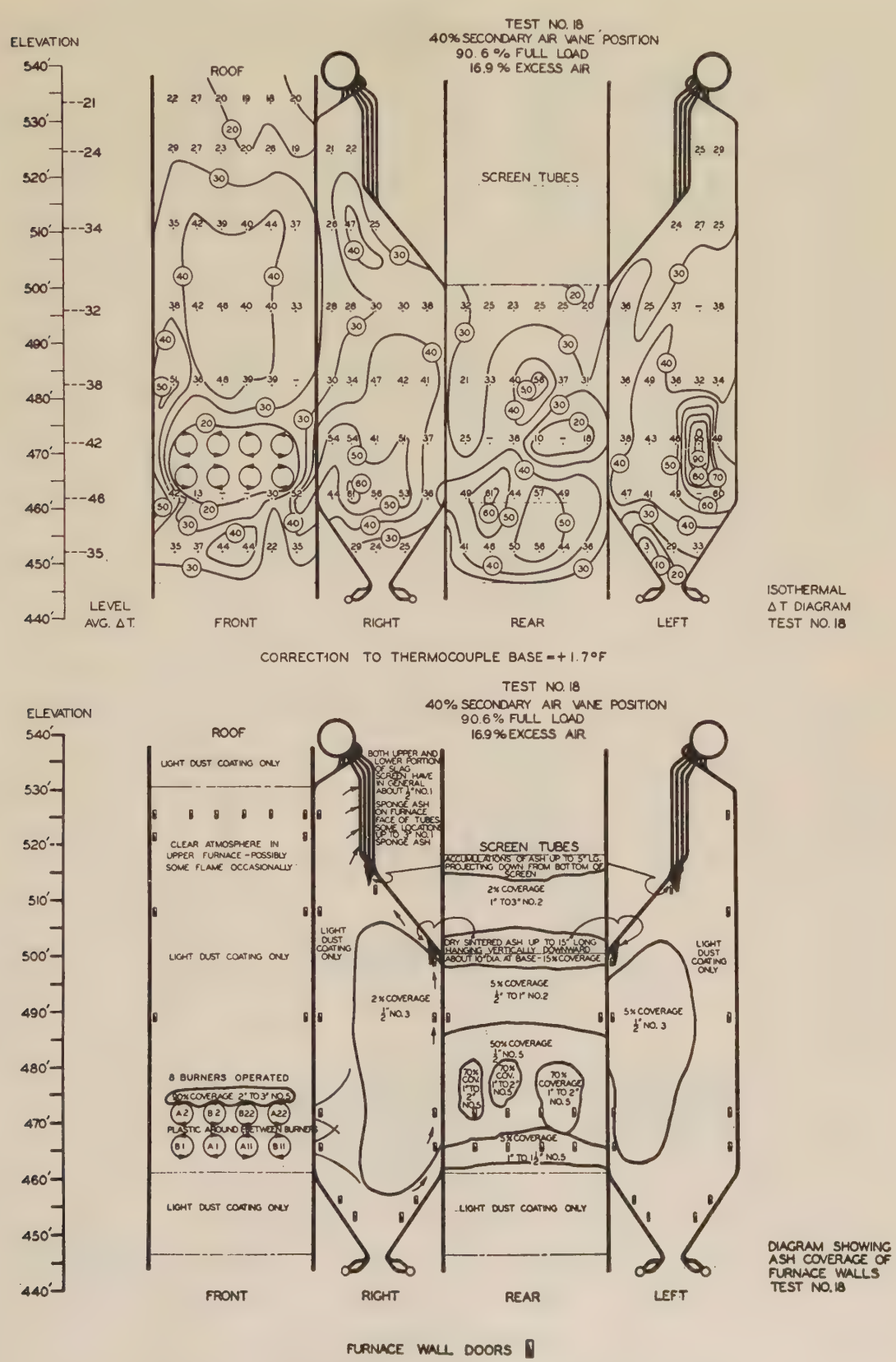

FIG. 9 ISOTHERMAL ΔT AND ASH-COVERAGE DIAGRAM TEST NO. 18

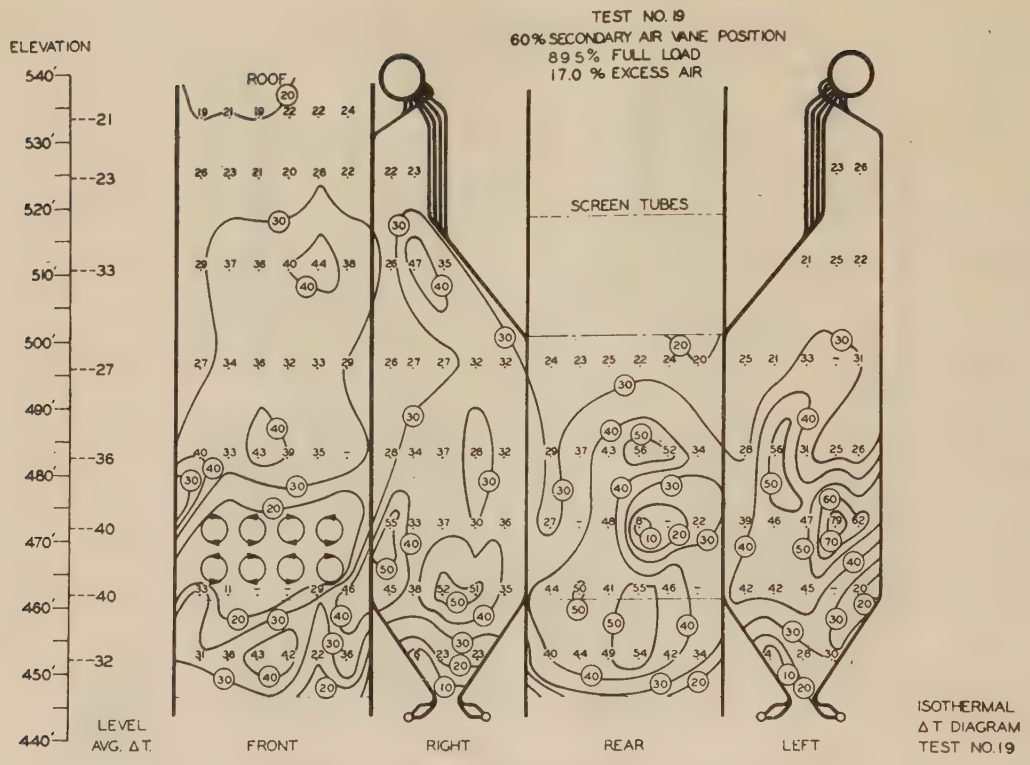

CORRECTION TO THERMOCOUPLE BASE = +2.0°F

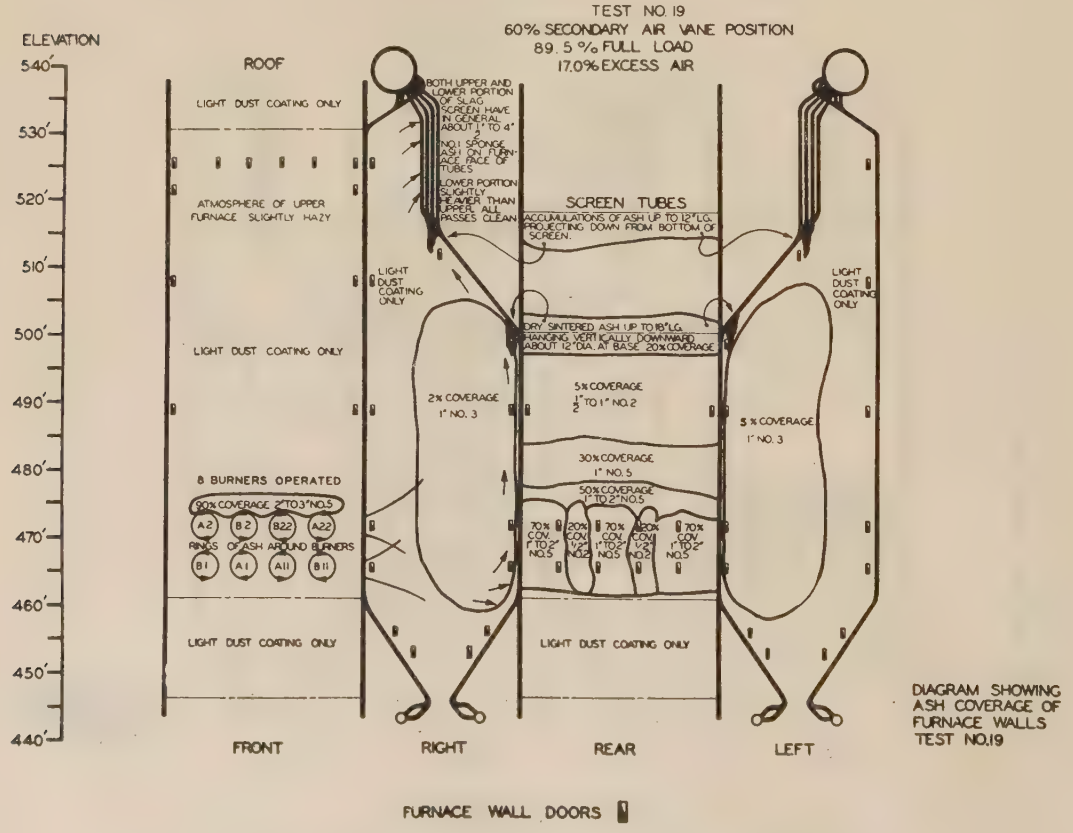

FIG. 10 ISOTHERMAL ΔT AND ASH-COVERAGE DIAGRAM TEST NO. 19

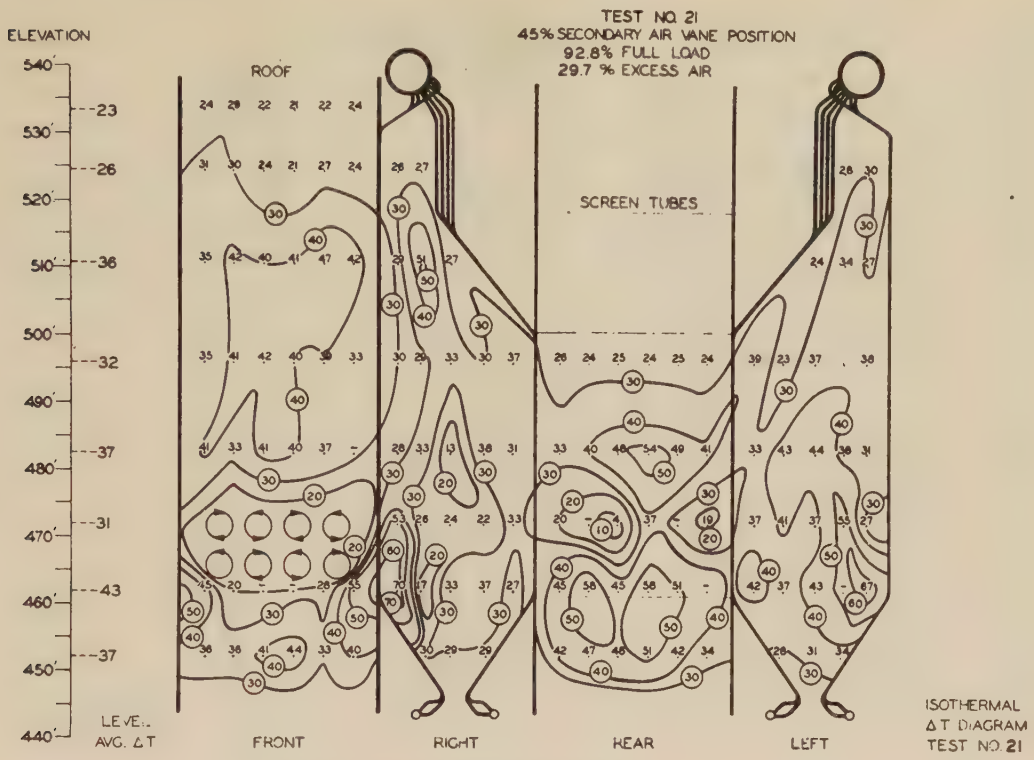

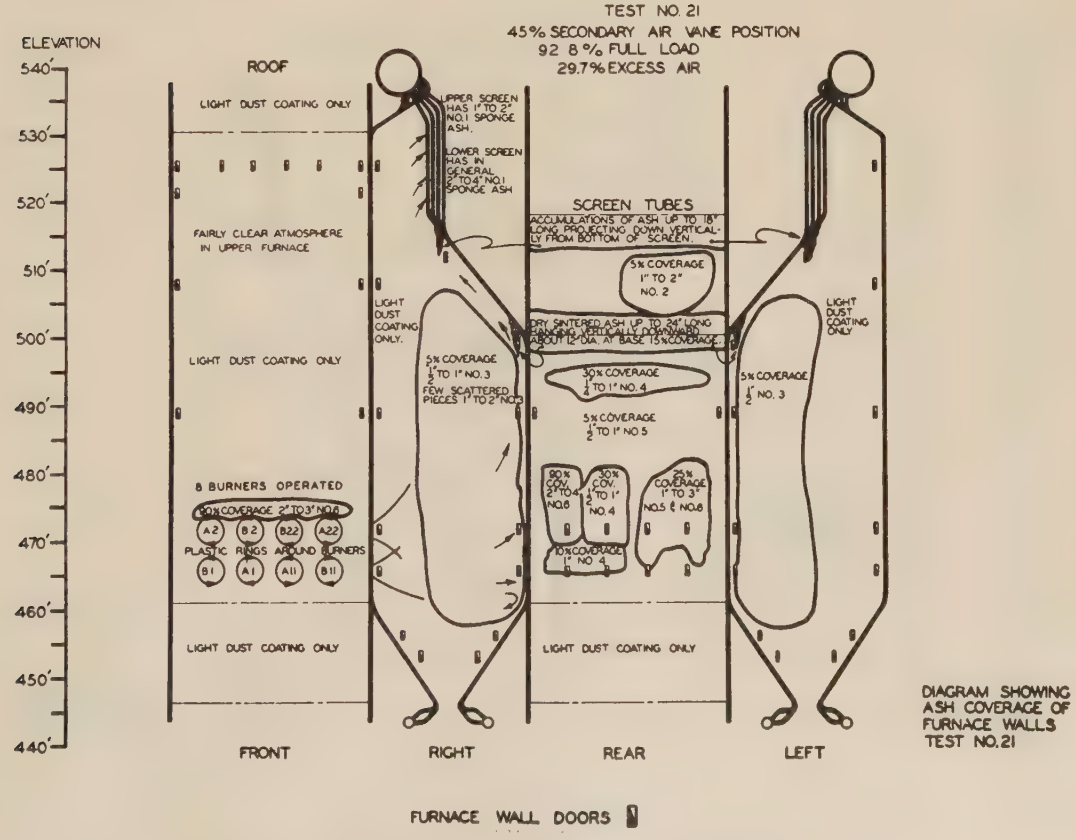

FIG. 11 ISOTHERMAL ΔT AND ASH-COVERAGE DIAGRAM TEST NO. 21

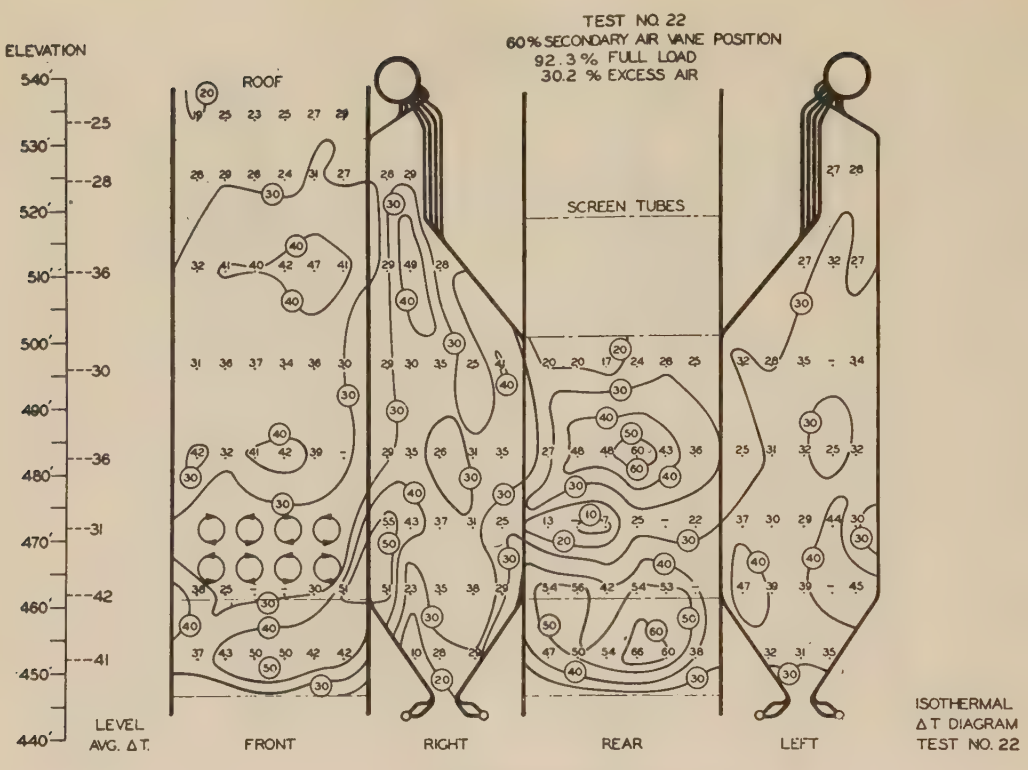

CORRECTION TO THERMOCOUPLE BASE = −0.5°F

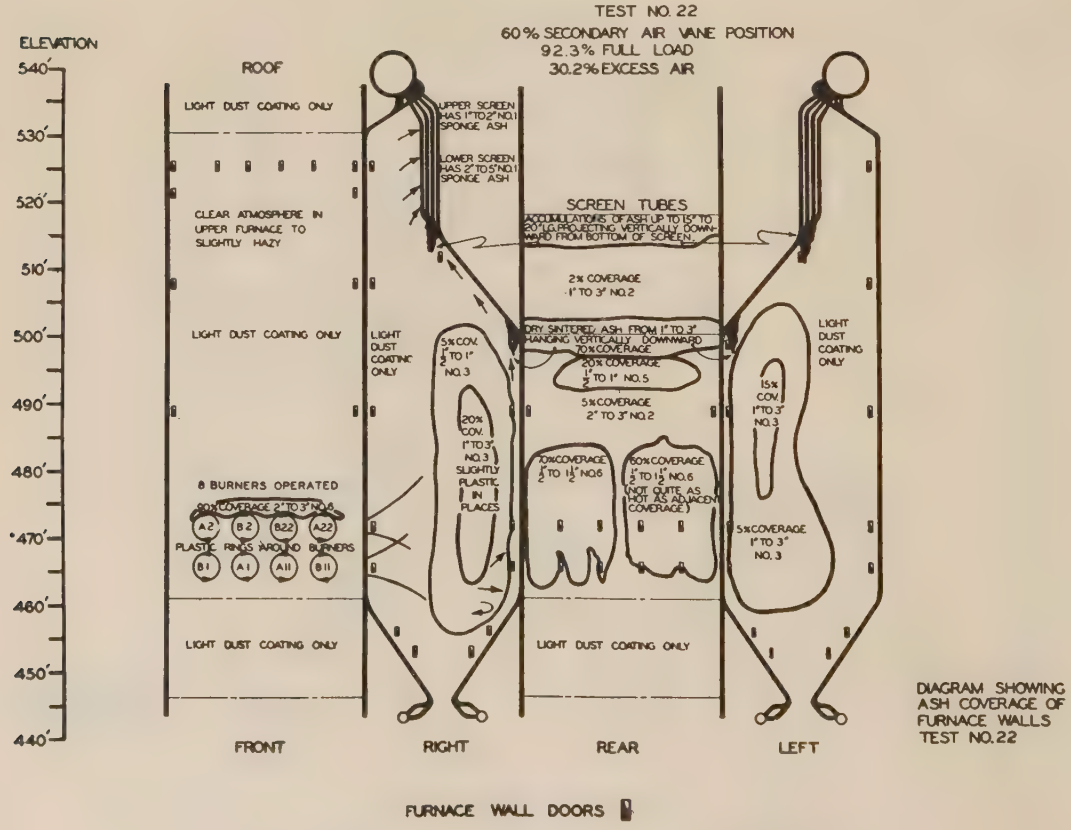

FIG. 12 ISOTHERMAL ΔT AND ASH-COVERAGE DIAGRAM TEST NO. 22

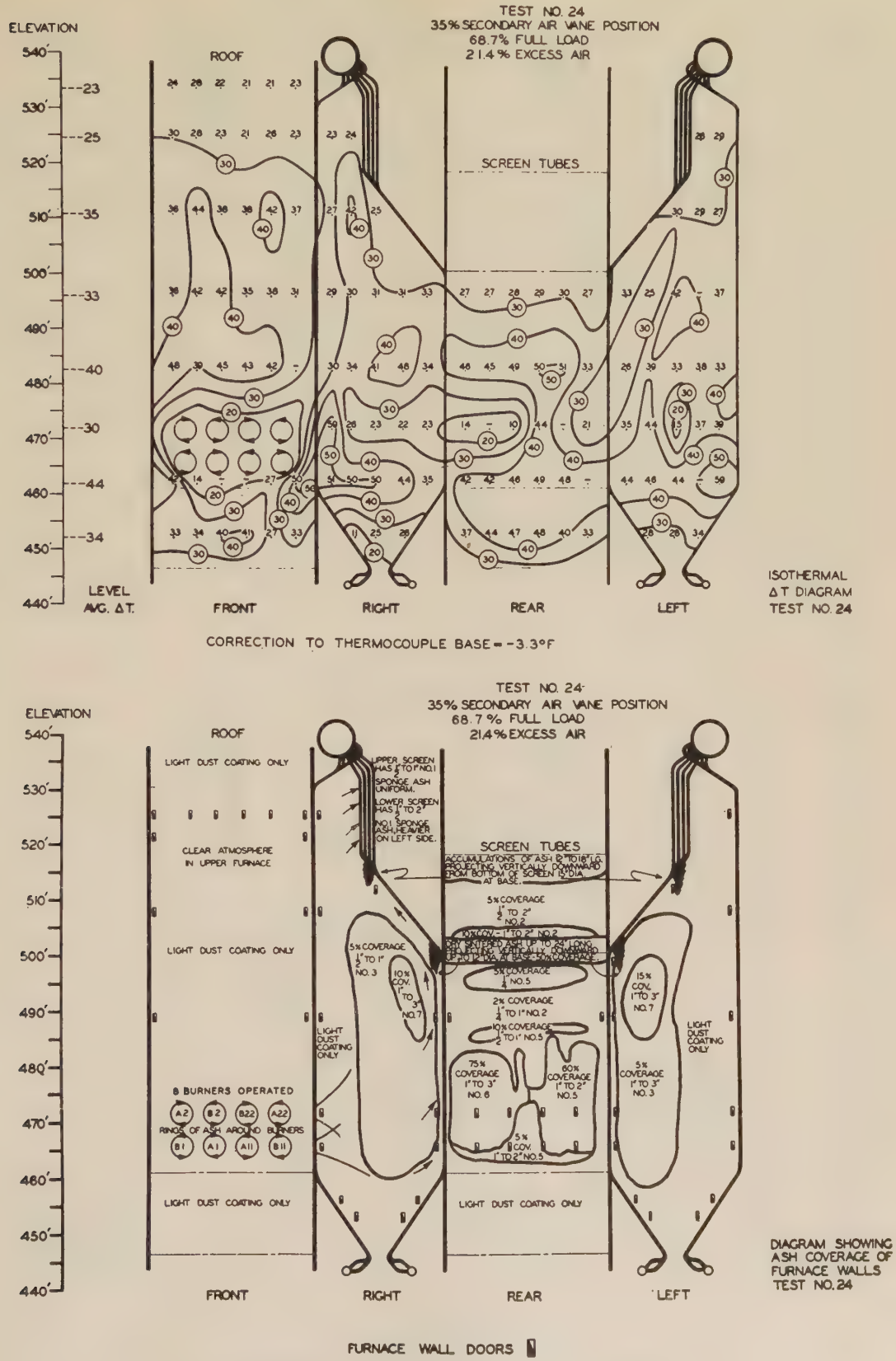

FIG. 13 ISOTHERMAL ΔT AND ASH-COVERAGE DIAGRAM TEST NO. 24

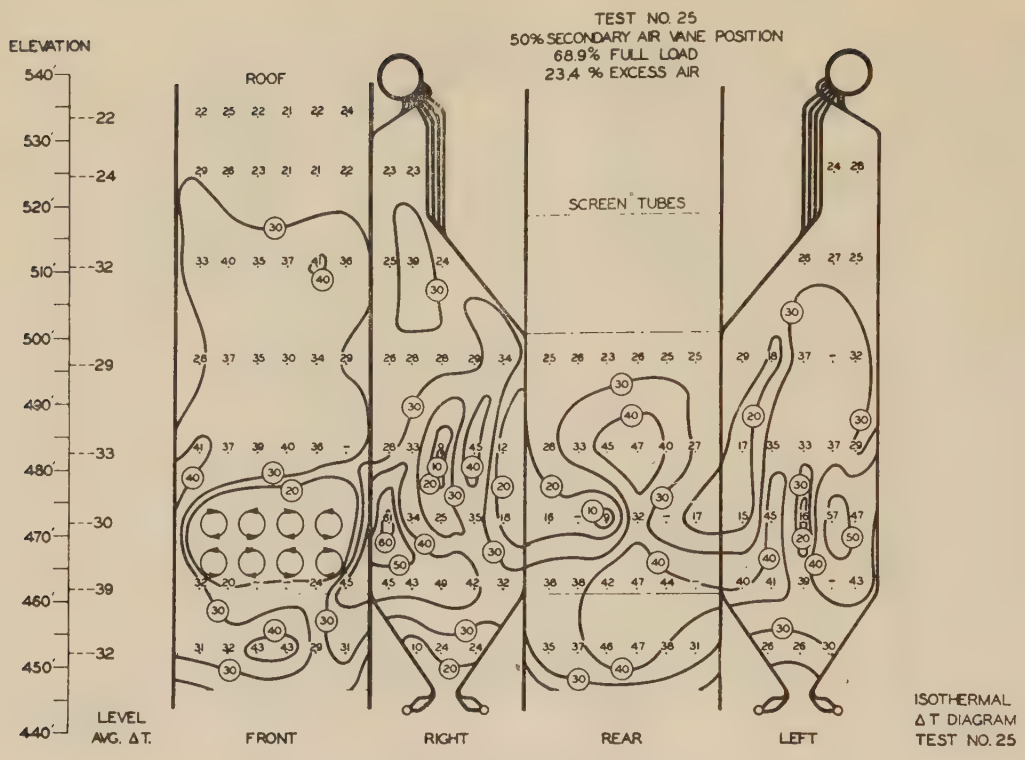

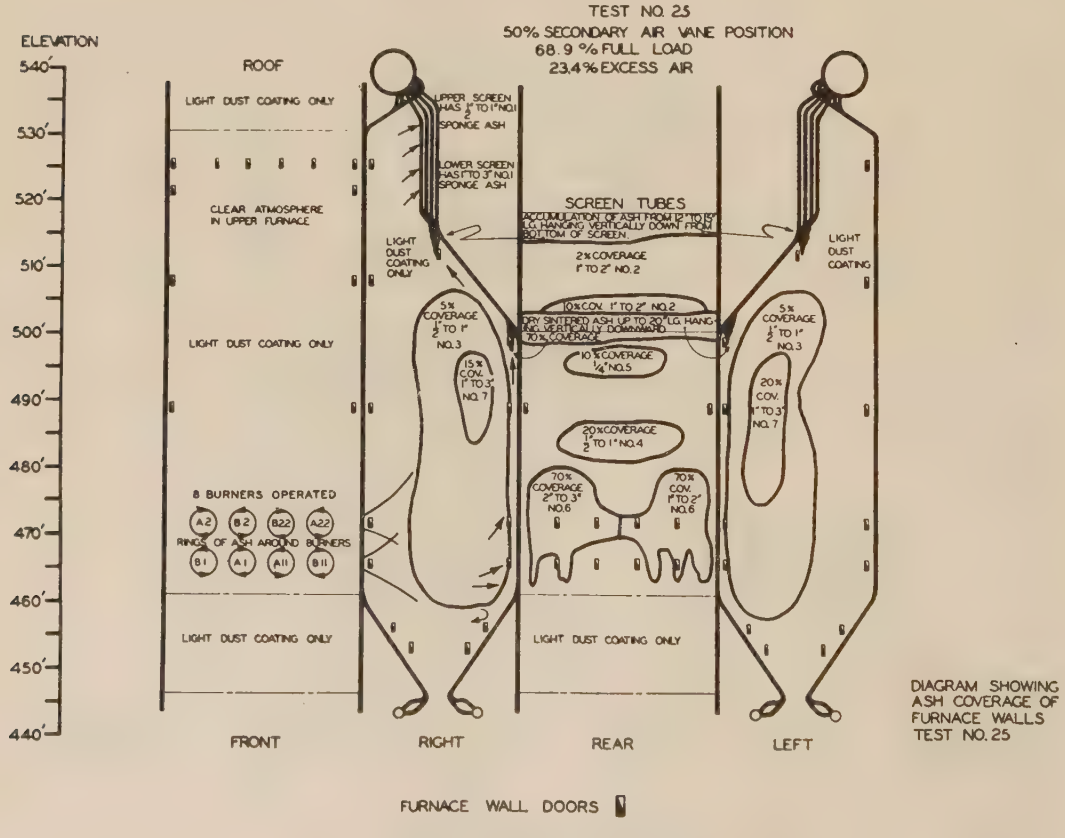

FIG. 14 ISOTHERMAL ΔT AND ASH-COVERAGE DIAGRAM TEST NO. 25

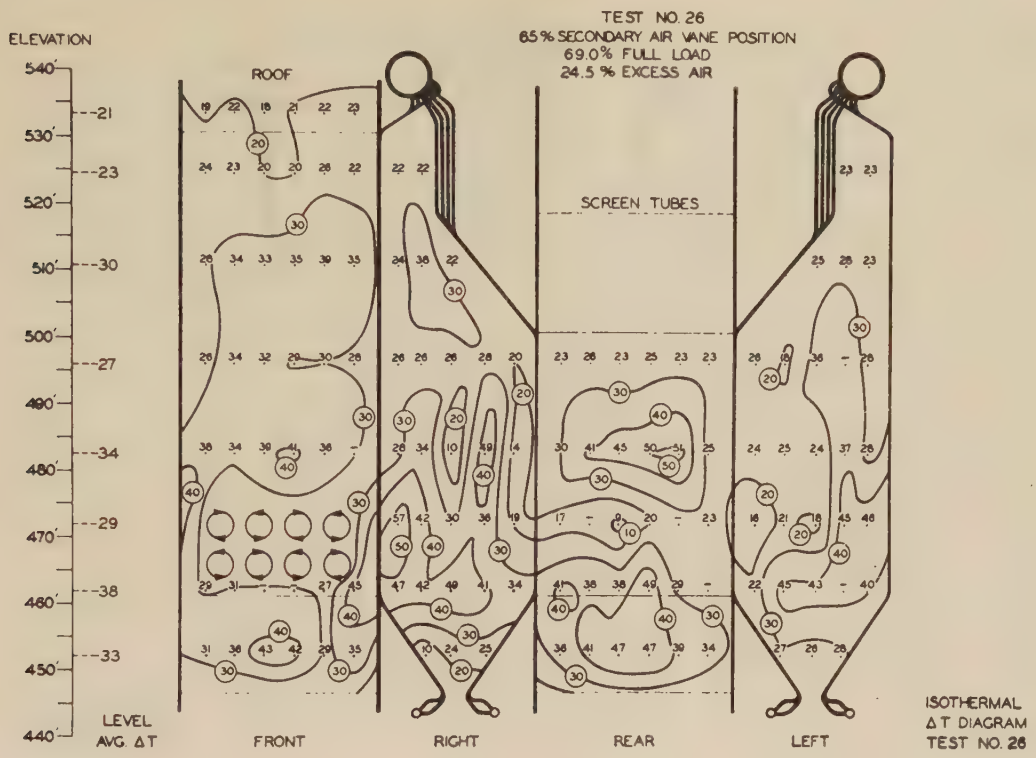

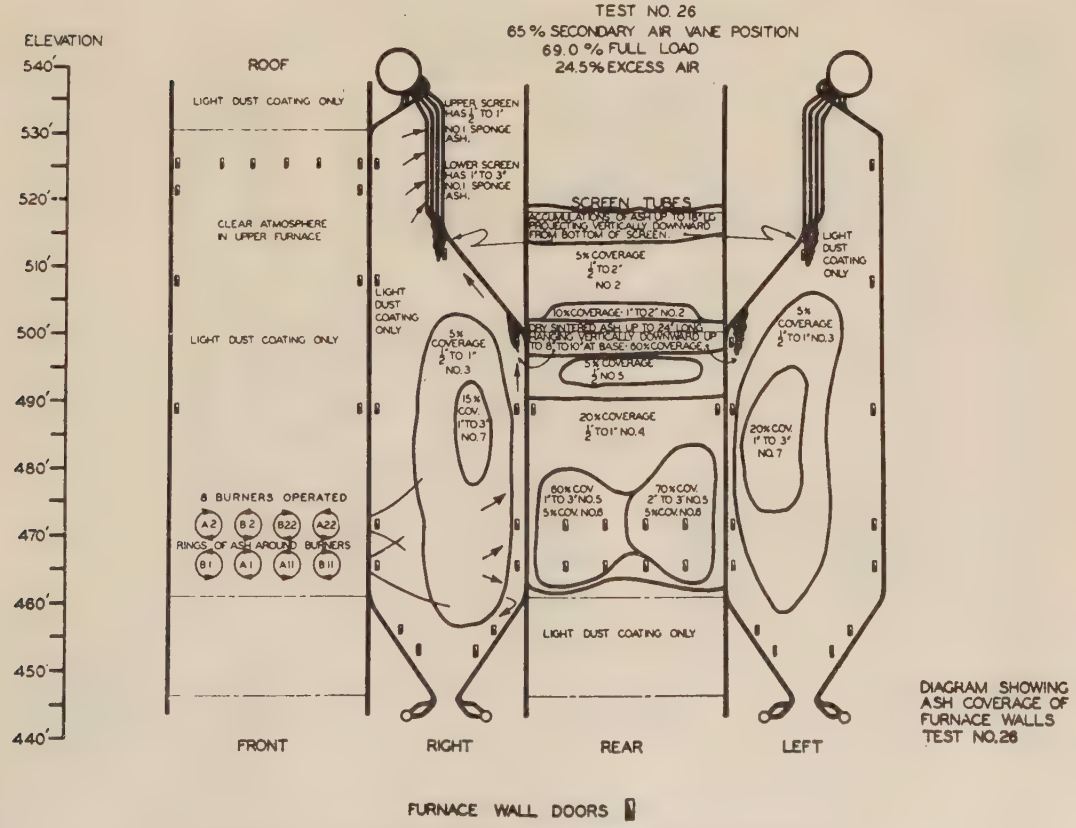

FIG. 15 ISOTHERMAL ΔT AND ASH-COVERAGE DIAGRAM TEST NO. 26

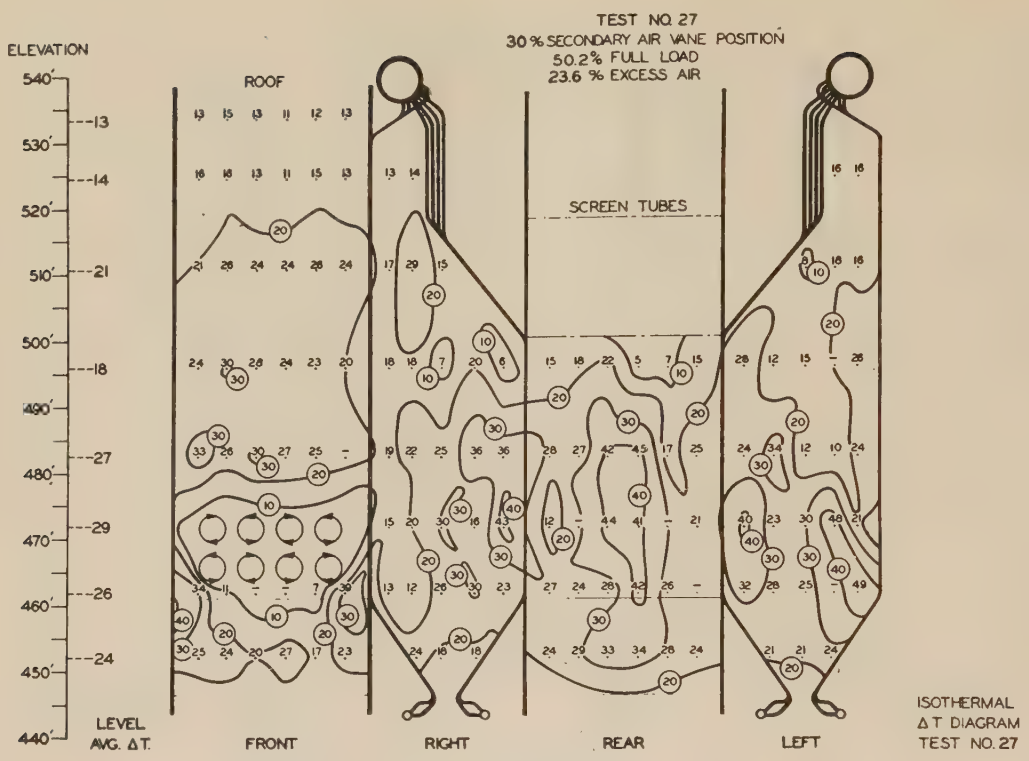

CORRECTION TO THERMOCOUPLE BASE=+0.3°F

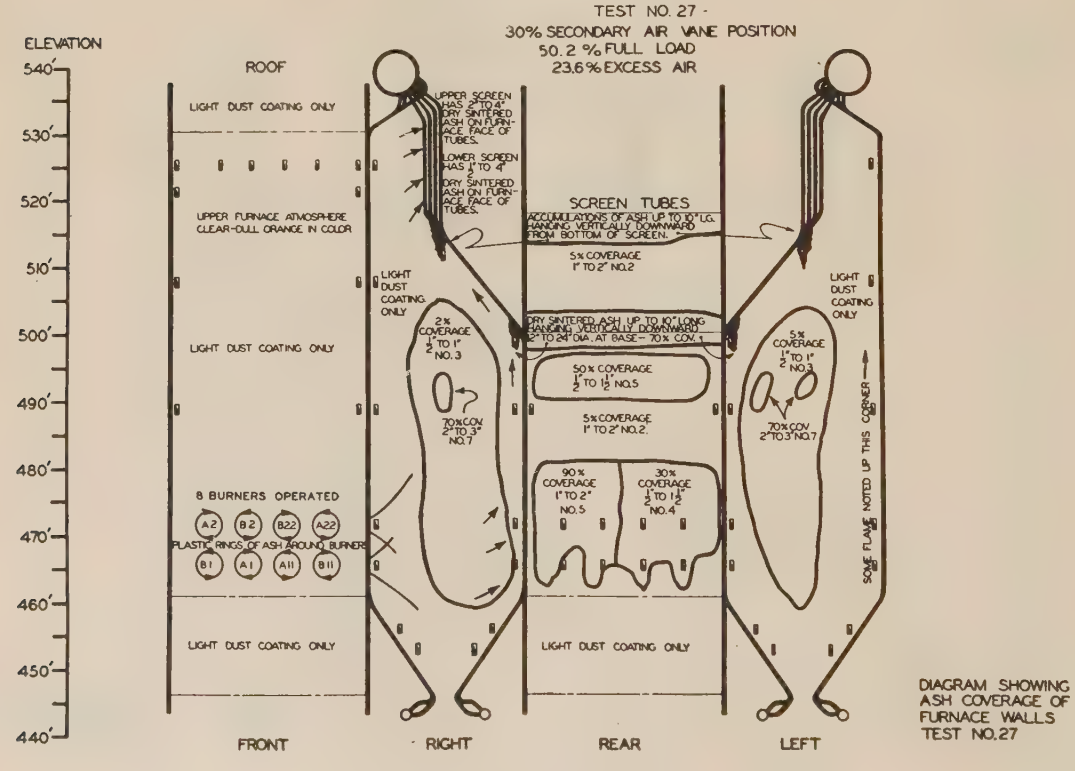

FIG. 16 ISOTHERMAL ΔT AND ASH-COVERAGE DIAGRAM TEST NO. 27

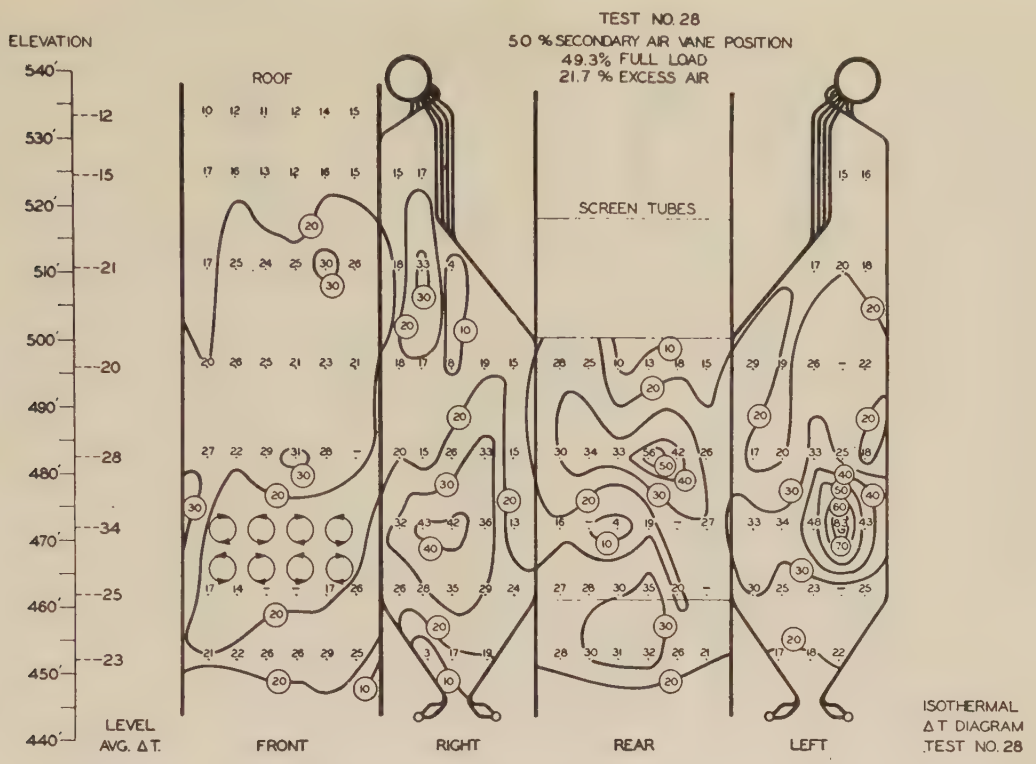

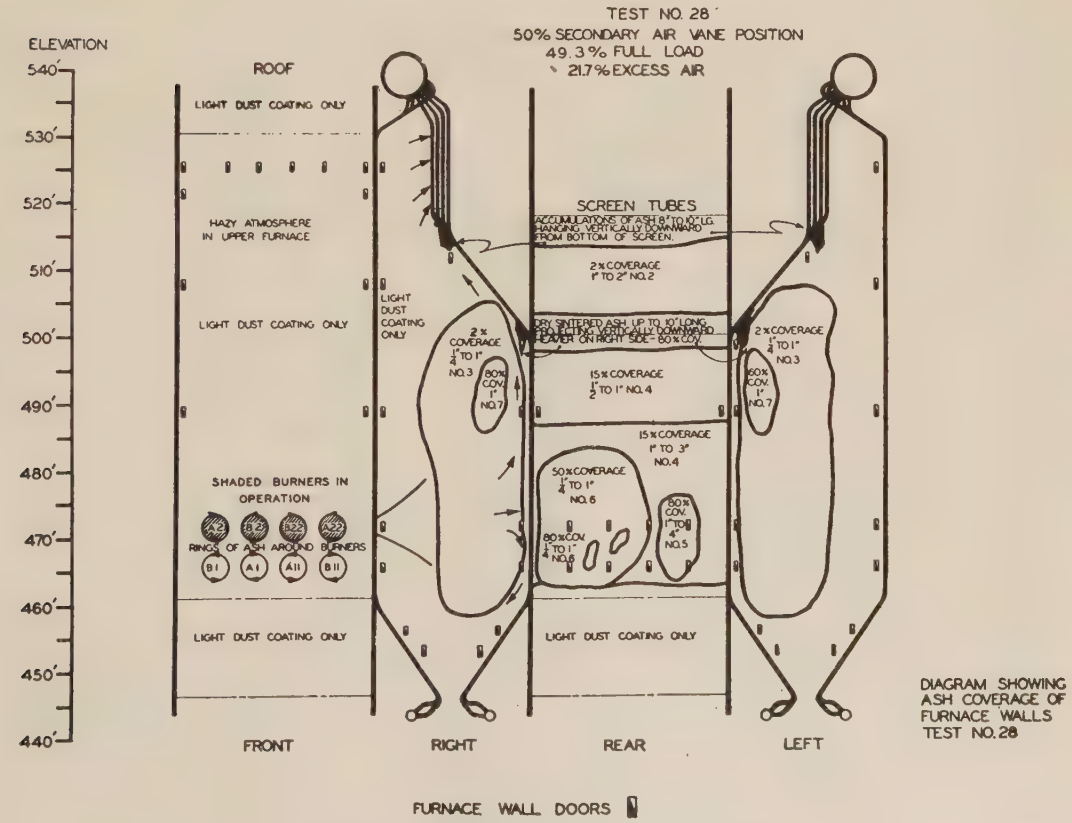

FIG. 17 ISOTHERMAL ΔT AND ASH-COVERAGE DIAGRAM TEST NO. 28

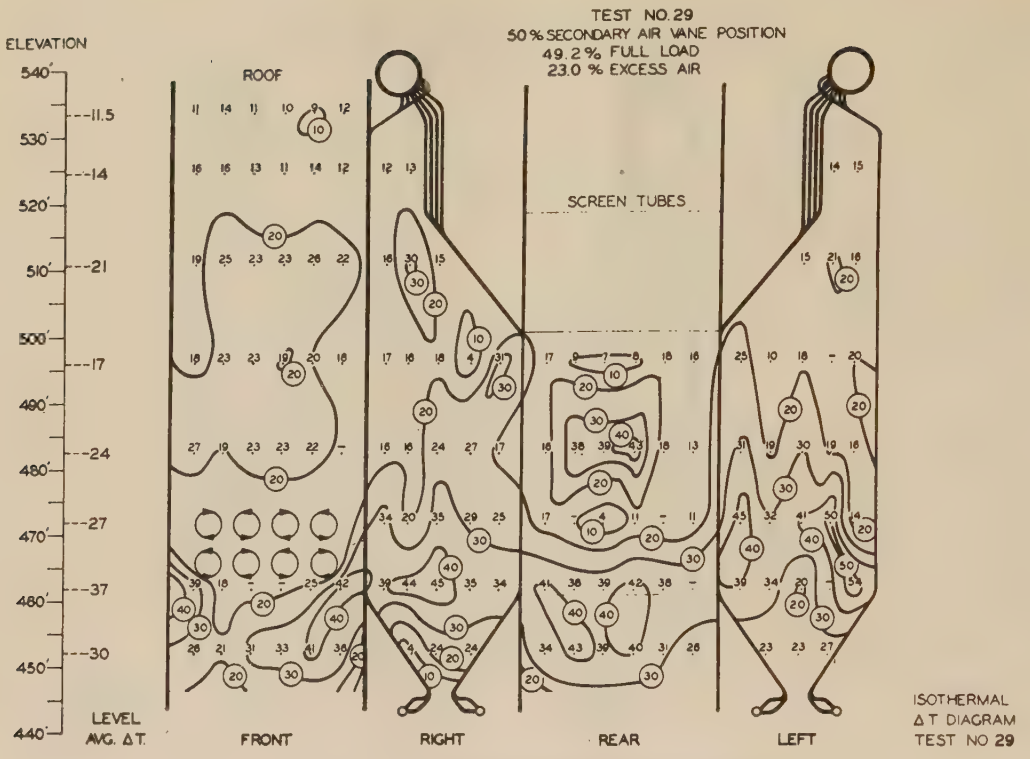

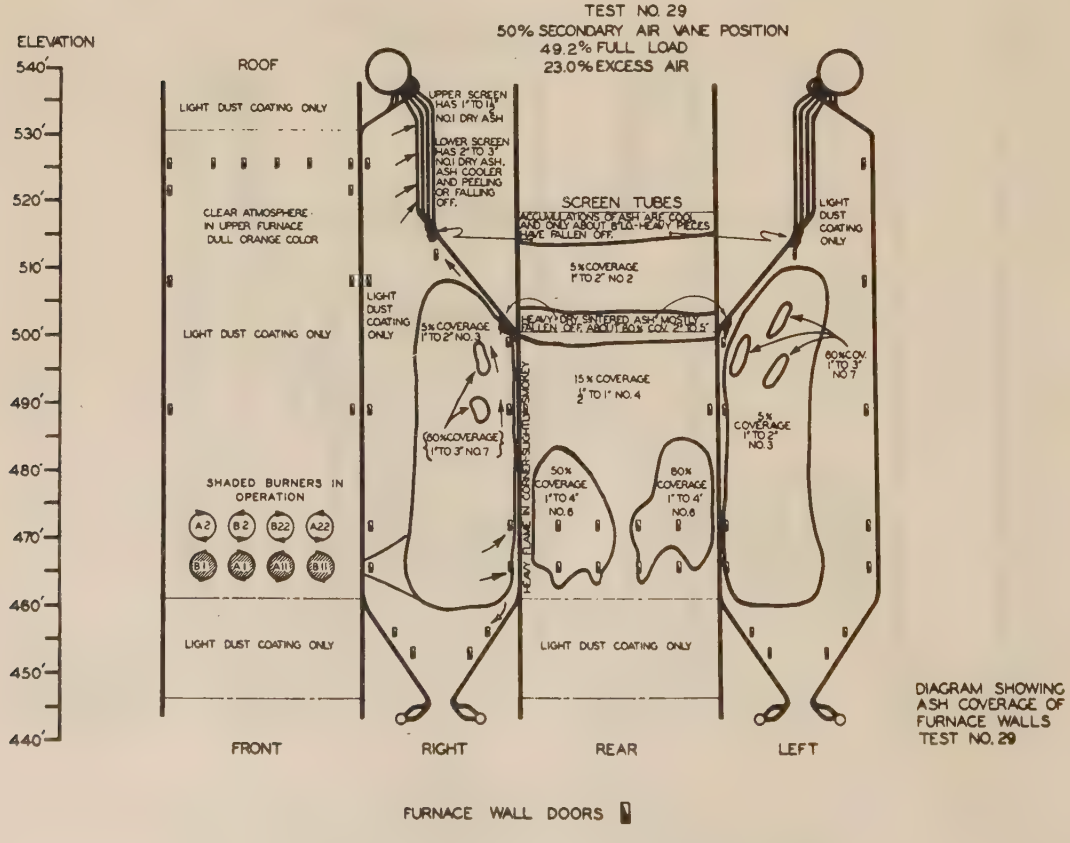

FIG. 18 ISOTHERMAL ΔT AND ASH-COVERAGE DIAGRAM TEST NO. 29

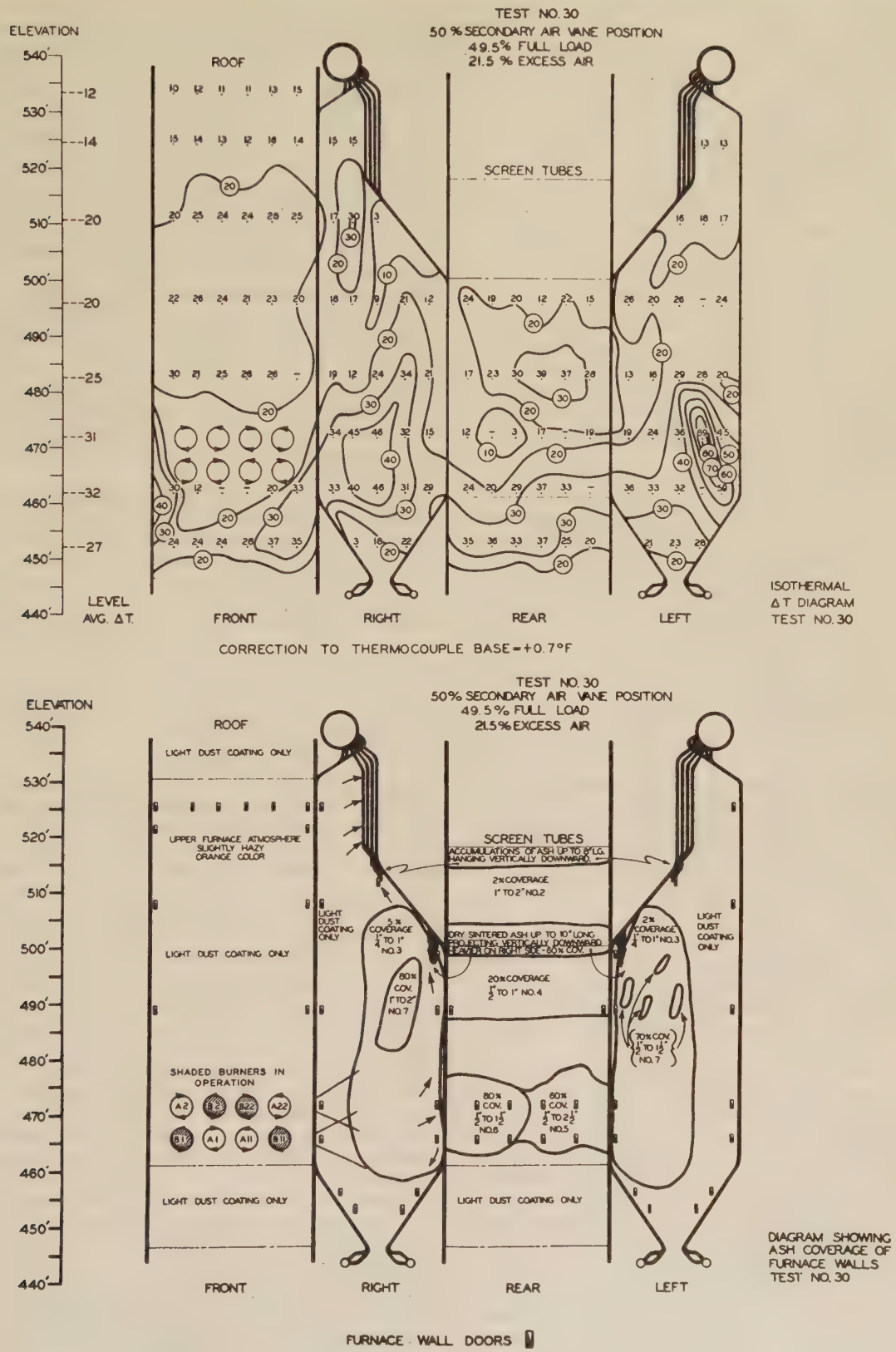

FIG. 19 ISOTHERMAL ΔT AND ASH-COVERAGE DIAGRAM TEST NO. 30

U_o = over-all conductance of metal and film = 1060 Btu/(sq ft) (hr) (deg F)
S = total projected area of furnace surface = 8884 sq ft
ΔT = average difference in temperature between surface at furnace-face center line and temperature of mixture within tube as indicated by base thermocouples

$$U_o S \Delta T = 1060 \times 8884 \times \Delta T$$
$$= 9{,}417{,}000 \times \Delta T, \text{ Btu per hr}$$
$$= 9.417 \times \Delta T \text{ MKB per hr}$$

Furnace heat-absorption efficiency then becomes

$$\text{Efficiency} = \frac{9.417 \times \Delta T}{\text{Net heat available to furnace}} \times 100$$

The value of heat absorption for the ΔT method has been determined for each complete test as well as furnace heat-absorption efficiency. Fig. 21 shows a comparison of the furnace heat absorption as obtained from the ΔT-results with the furnace heat absorption as determined by heat-balancing the furnace. This curve shows that, in general, a fairly good correlation is obtained between the two methods.

Analysis of Results

Table 3 shows the average of all board data and all other pertinent operating data, such as burner-box pressures, burner settings, pulverized-coal fineness, etc., taken during the tests.

Table 4 shows the distribution of pulverized coal between burners on each test in per cent of total coal flow to the furnace.

Table 5 shows the average value of ΔT obtained at each furnace-face thermocouple location.

Table 6 presents a summary of the important test conditions and results for all complete tests.

Figs. 5 to 19, inclusive, show the distribution of heat absorption in the furnace and furnace-wall cleanliness for all of the operating conditions studied.

Figs. 22 to 28, inclusive, show the distribution of heat absorption over the height of the furnace for all of the operating conditions, and these curves are arranged in groups to facilitate the study of the effect of the various operating variables.

Figs. 29 to 32, inclusive, show the furnace heat-absorption efficiency, as determined by the ΔT-results for all of the operating conditions studied.

Owing to the inherent errors involved in any calculations, based upon the ΔT-values, the analysis of these data necessarily must be qualitative. The curves have been drawn to indicate trends in the distribution of heat absorption and furnace efficiency for this particular furnace under the operating conditions studied.

Referring to the ash-coverage diagrams, it is found that, in general, the furnace walls remain relatively clean under all of the operating conditions investigated. The only furnace-wall surface which accumulated any appreciable amount of ash is that surface of the rear wall located directly opposite the burners. In this location the ash coverage varies with operating conditions and the surface periodically cleans itself. The ash coverage on the side walls is negligible and is confined to small fingers which project out from between the tubes toward the direction of gas flow. The front-wall surface has no ash coverage other than a light dust coating about $^1/_{16}$ in. thick. Heavy formations of ash somewhat similar to stalactites were found hanging vertically down from the bottom of the slag-screen opening on all tests. These formations varied in size for the different tests since their accumulated weight occasionally would cause them to break away and fall to the ash pit. The average diameter of these formations at their base was 8 to 10 in. and their length approximately 12 to 18 in. They were held in place by their base, forming at the location where the rear-wall tubes were bent out of line to form the slag screen. Similar ash formations were found at the bottom of the rear-wall sloped section. Here the ash appeared to be dry and sintered and again built up until the accumulated weight caused it to break away. These pieces were of the same general size as described previously and could be broken off easily. It is possible that a small eddy was located in this corner of the furnace and aided the growth of these formations.

Referring to the isothermal ΔT-diagrams, it may be seen that zones of relatively high absorption rates existed in that area of the side walls adjacent to the burners under all operating conditions. These zones, in general, indicated absorption rates in the vicinity of 50,000 to 75,000 Btu/(sq ft-hr), whereas the average absorption rate for the entire furnace is approximately 40,000 to 45,000 Btu/(sq ft-hr) at full load. The absorption rates found in these zones for some operating conditions are probably higher than those experienced in the normal operation of this furnace, since normally the secondary-air vanes are adjusted as required to obtain the optimum furnace conditions with no flame impingement. On these tests we used the vane adjustments to provide changes in flame shape so that we might study its effect upon furnace performance.

The sloping section of the rear wall which forms part of the ash hopper also showed relatively high heat-absorption rates in all cases, apparently due to the cleanliness of the surface in this area and the fact that this surface has an excellent "view" of the flames. The heat absorbed by the rear wall, where the surface is not affected by ash coverage, is generally higher than found on the other walls. The highest average absorption rates for any elevation are found in the lower part of the furnace and usually reach their maximum at the elevation just below the burners. The maximum might occur at the burner elevation if the furnace-wall surface in this area were not affected by ash accumulations.

A wide variation in absorption rate is found at the burner elevation for the various operating conditions studied, again indicating that this area is affected by ash accumulation which varies with operating conditions, or cleans itself periodically. On the curves representing the distribution of heat-absorption rates over the height of the furnace, it is found that the heat-absorption rates decrease in going to the higher furnace elevations, but that a second peak of increased absorption rates occurs in that part of the furnace where the cross-sectional area is reduced by the sloping section of the rear wall. Since this same characteristic is noted for all operating conditions, it seems that, at least partially, it is caused by an increase in convection transfer in this region due to the "scrubbing" action of the furnace gases against the wall surface as the cross-sectional area of the furnace is reduced. This is also shown by the isothermal ΔT-diagrams where zones of slightly higher absorption rates are found at this elevation on the side walls and the front wall.

The furnace heat-absorption efficiency was indicated to be approximately 41 per cent at full load, under normal operating conditions.

The effects of the various operating variables on distribution of heat absorption in the furnace and furnace efficiency are analyzed under separate headings which follow:

Effects of Varying Secondary-Air Vane Opening. Based upon our experience with these burners, we investigated this variable in the range of 40 to 60 per cent vane opening at full load and 35 to 65 per cent vane opening at 75 per cent full load. These ranges of vane opening provide sufficient variations in flame shape and still maintain satisfactory furnace conditions.

(*a*) 100 per cent full load—25 per cent excess air (test Nos. 15 to 17, inclusive): Under these conditions, it was found that the amount of ash accumulated on the rear wall opposite the

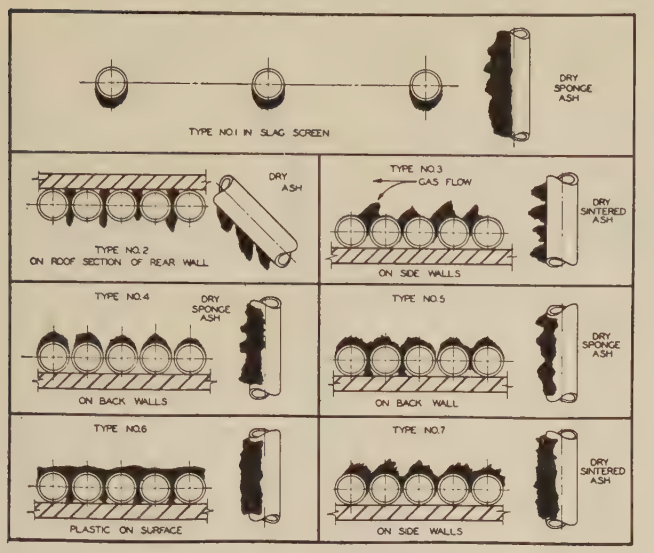

FIG. 20 KEY SHOWING VARIOUS TYPES OF ASH
(To be used with diagrams showing ash conditions on furnace-wall tubes.)

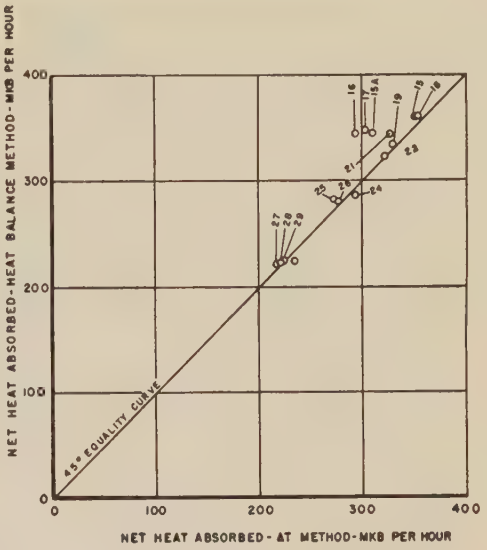

FIG. 21 COMPARISON OF FURNACE HEAT ABSORPTION COMPUTED FROM WALL TUBE ΔT-DATA WITH FURNACE HEAT ABSORPTION COMPUTED FROM FURNACE EXIT-GAS TRAVERSE

TEST NO.	HEAT AVAILABLE MKB/HR.	% FULL LOAD	EXCESS AIR %	SEC. AIR VANE POS % OPEN	BURNERS
× 15	793.7	93.2	23.0	40	8
○ 15A	780.5	91.6	24.8	40	8
○ 16	785.2	92.2	25.0	60	8
△ 17	787.2	92.3	26.2	50	8

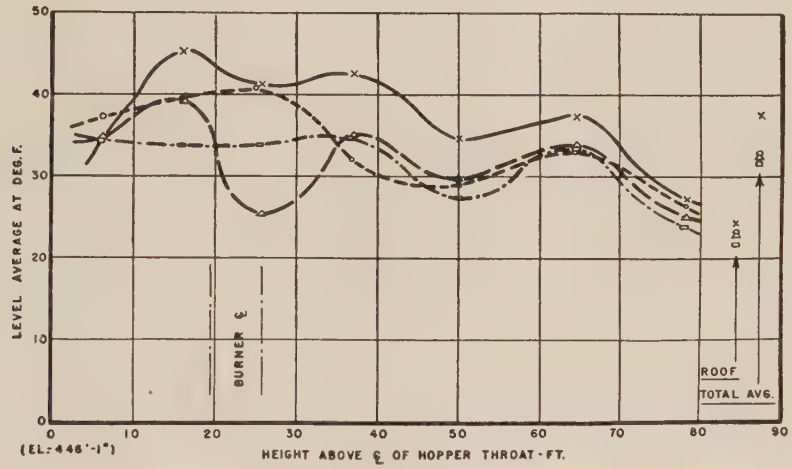

FIG. 22 FURNACE TUBE AVERAGE ΔT-VARIATION WITH LEVEL FOR THREE SECONDARY-AIR VANE POSITIONS AT FULL LOAD AND ABOUT 25 PER CENT EXCESS AIR AT FURNACE OUTLET

burners increased slightly as the vanes were opened. This, of course, was accompanied by a decrease in absorption rate in this area. While the front-wall surface remains clean during these changes in vane opening, the heat absorbed by this surface decreased as the vanes were opened. The distribution of heat absorption in the side walls did not vary greatly, although there are some indications that the zones of relatively high absorption rates near the burners contain lower absorption rates at 50 per cent vane opening. Considering the distribution of heat absorption over the height of the furnace, it was found that at the 6-ft elevation there was little change in the average heat-absorption rates. However, between the 6-ft and 35-ft elevation, the heat absorption varied considerably for the different vane openings, apparently caused by the variations in ash coverage of the rear wall in this area. From elevation 35 ft to the top of the furnace, the trends in absorption rates are the same for various vane openings, but the tests with the higher vane openings show lower absorption rates. The furnace heat-absorption efficiency decreased about 4 per cent as the vane openings were increased from 40 to 60 per cent.

(*b*) 100 per cent full load—17 per cent excess air (test Nos. 18 and 19): Again, it was found that the heat absorption in the front wall decreased as the vanes were opened, while the cleanliness in this area remained constant. The ash coverage of the rear wall did not vary appreciably between tests. The zones of relatively high heat absorption on the side walls near the burners did not change greatly as the vane openings were varied, but it did appear that the absorption rates found in these zones were reduced as the vane openings were increased. In studying the distribution of heat absorption over the height of the furnace, it

TEST NO	HEAT AVAILABLE MKB/HR.	HEAT AVAILABLE % FULL LOAD	EXCESS AIR %	SEC. AIR VANE POS. % OPEN	BURNERS
○18	772.4	90.6	16.9	40	8
×19	761.5	89.5	17.0	60	8

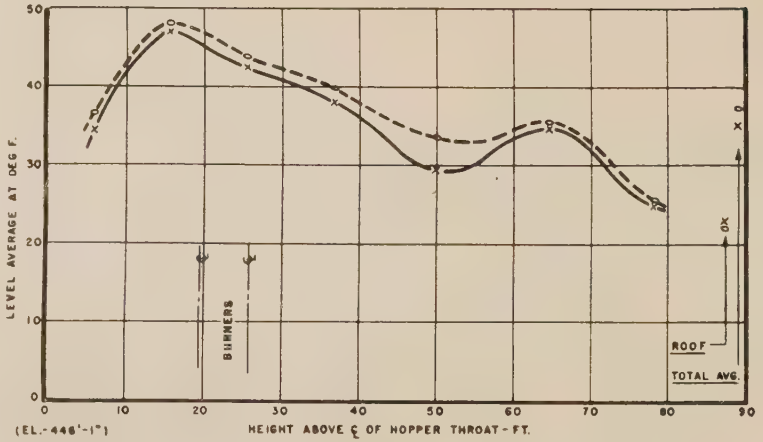

FIG. 23 FURNACE TUBE LEVEL AVERAGE ΔT-VARIATION FOR TWO SECONDARY-VANE POSITIONS AT FULL LOAD AND ABOUT 17 PER CENT EXCESS AIR AT FURNACE OUTLET

TEST NO.	HEAT AVAILABLE MKB/HR	HEAT AVAILABLE % FULL LOAD	EXCESS AIR %	SEC. AIR VANE POS. % OPEN	BURNERS
○21	792.3	92.8	29.7	45	8
×22	788.0	92.3	30.2	60	8

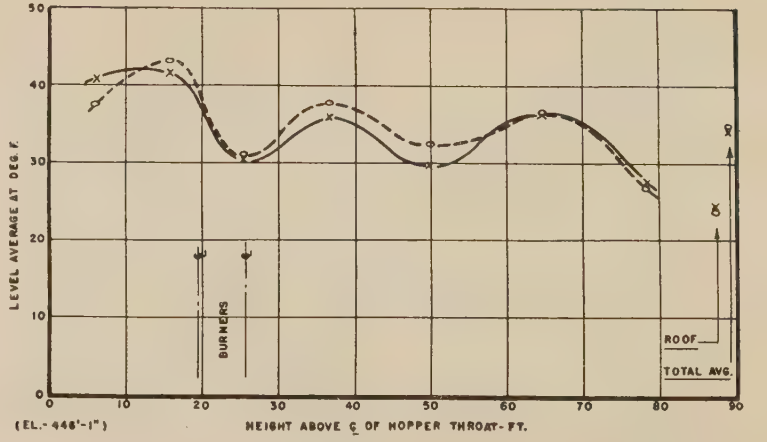

FIG. 24 FURNACE TUBE LEVEL AVERAGE ΔT-VARIATION FOR TWO SECONDARY-AIR VANE POSITIONS AT FULL LOAD AND ABOUT 30 PER CENT EXCESS AIR AT FURNACE OUTLET

TEST NO.	HEAT AVAILABLE MKB/HR	HEAT AVAILABLE % FULL LOAD	EXCESS AIR %	SEC. AIR VANE POS. % OPEN	BURNERS
○24	584.9	68.7	21.4	35	8
×25	586.9	68.9	23.4	50	8
△26	587.4	69.0	24.5	65	8

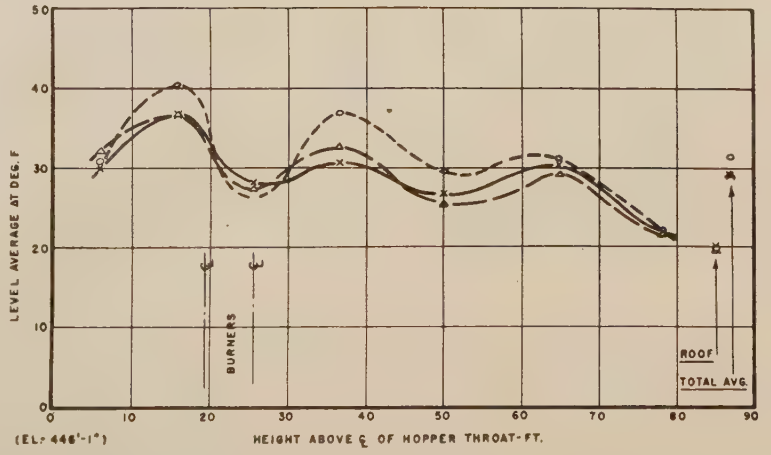

FIG. 25 FURNACE TUBE LEVEL AVERAGE ΔT-VARIATION FOR THREE SECONDARY-AIR VANE POSITIONS AT 75 PER CENT LOAD AND ABOUT 25 PER CENT EXCESS AIR AT FURNACE OUTLET

TEST NO.	HEAT AVAILABLE MKB/HR.	HEAT AVAILABLE % FULL LOAD	EXCESS AIR %	SEC. AIR VANE POS. % OPEN	BURNERS
○27	427.1	50.2	23.6	30	8
×28	418.2	49.3	21.7	50	4 UPPER
△29	418.3	49.2	23.0	50	4 LOWER
●30	419.6	49.5	21.5	50	4 NORMAL

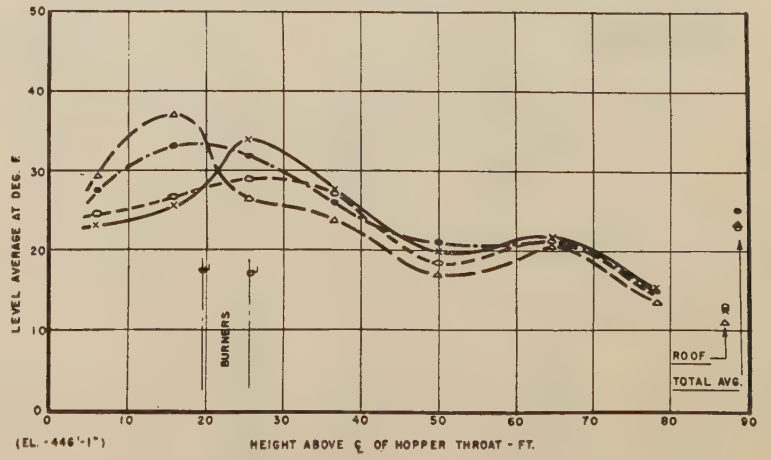

FIG. 26 FURNACE TUBE LEVEL AVERAGE ΔT-VARIATION WITH DIFFERENT BURNER FIRING ARRANGEMENTS AT 50 PER CENT LOAD AND ABOUT 25 PER CENT EXCESS AIR AT FURNACE OUTLET

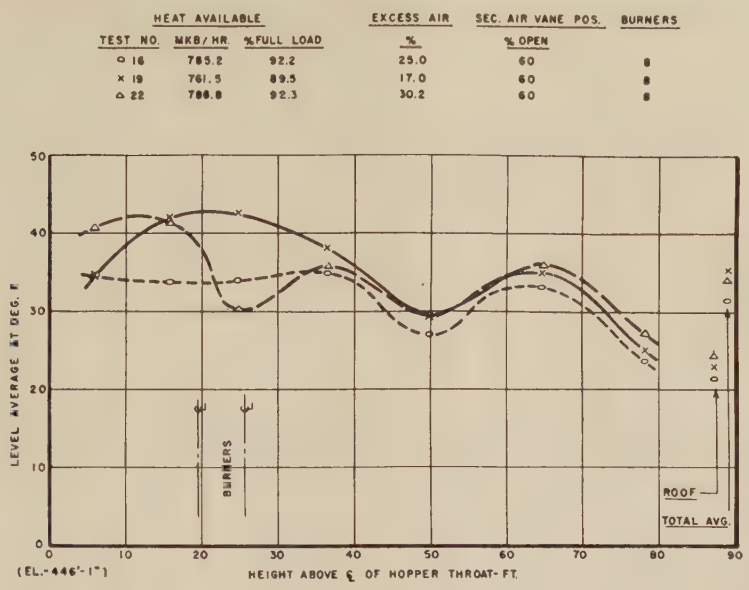

FIG. 27 FURNACE TUBE LEVEL AVERAGE ΔT-VARIATION WITH EXCESS AIR AT FULL LOAD AND 60 PER CENT SECONDARY-AIR VANE POSITION

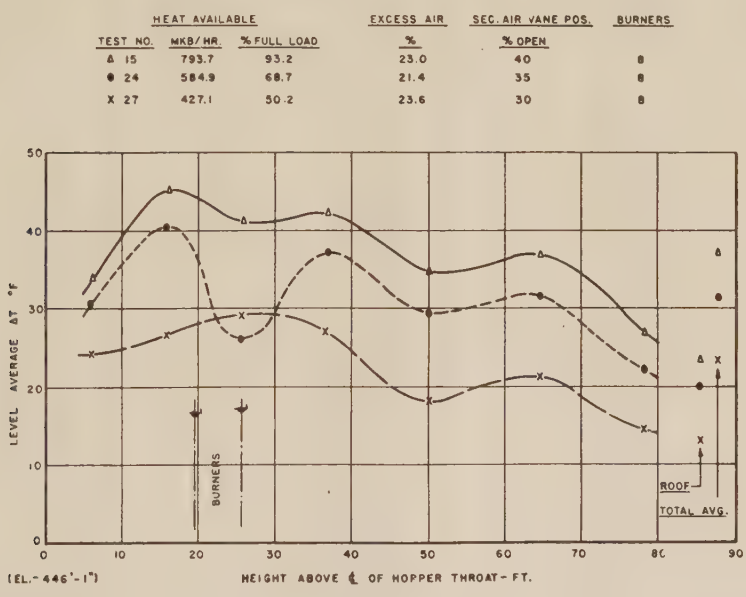

FIG. 28 FURNACE TUBE LEVEL AVERAGE ΔT WITH VARIATIONS IN NET HEAT AVAILABLE TO FURNACE FOR NORMAL SECONDARY-AIR VANE POSITIONS AND ABOUT 25 PER CENT EXCESS AIR

was found that the trends obtained for both of these vane openings were the same but that slightly lower absorption rates were found over the height of the furnace with the higher vane opening. It was noted that there was little variation in absorption at the burner elevation, which indicates that the ash accumulation in this region and its variations were small on both of these tests. The furnace efficiency decreased about 2 to 3 per cent as the vanes were opened from 40 to 60 per cent.

(*c*) 100 per cent full load—30 per cent excess air (test Nos. 21 and 22): The heat absorbed by the front wall decreased as the vanes were opened. The absorption rates in the zones of relatively high absorption on the side walls decreased as the vanes were opened. The ash coverage of the rear wall opposite the burners apparently increased as the vanes were opened, causing a decrease in absorption rates in this area. The distribution of the heat absorption over the height of the furnace was not changed greatly as the vane openings were varied; On both tests it is indicated that ash coverage at the burner elevations caused a reduction in heat-absorption rates in this area. The furnace efficiency remained nearly constant as the vane openings were varied, since a decrease of only 1 per cent was shown as the vane openings were increased from 45 to 60 per cent.

(*d*) 75 per cent full load—25 per cent excess air (test Nos. 24 to 26, inclusive): The heat absorbed by the front wall decreased when the vane openings were increased. The high absorption zones on the side walls did not appear to change significantly as the vane openings were varied. The distribution of heat absorption over the height of the furnace did not change greatly as the vane openings were varied although higher rates

TABLE 3 SUMMARY OF OPERATING AND TEST DATA FOR TEST NO. 15 THROUGH 30

TEST NUMBER		15	15-A	16	17	18	19	21	22	24	25	26	27	28	29	30
DATE - 1948		10-22	10-27	10-22	10-28	10-28	10-20	10-25	10-25	10-24	10-24	10-24	10-27	10-30	10-29	10-30
TIME - START		1000	2000	1600	0154	1200	1915	1600	1000	1030	0545	2400	0150	0100	0115	0600
DURATION - HOURS		4	4.5	4	4	5	4	4	4	4	4	5	3.75	4	4	4
INTEGRATORS:																
CORRECTED STEAM FLOW	M LBS PER HR	625.4	625.9	625.3	628.1	624.2	623.7	626.1	623.4	459.1	459.9	464.3	331.7	329.8	331.0	329.1
CORRECTED FEEDWATER FLOW	M LBS PER HR	626.4	627.5	625.4	627.8	625.3	624.6	628.6	623.1	473.6	471.2	470.4	347.4	345.8	347.6	343.0
SUPERHEATER CONDENSER FLOW	% VALVE OPENING	23	33	43	35	8	10	32	49	9	24	21		0		
COAL FLOW - 3A MILL	M LBS PER HR	34.03	32.50	35.27	32.06	32.26	32.12	32.31	32.40	26.40	26.32	26.18	18.97	18.61	16.31	
COAL FLOW - 3B MILL	M LBS PER HR	36.53	33.35	35.35	32.52	35.69	37.37	35.19	34.40	26.09	25.27	26.18	18.98	18.21	20.47	36.17
TOTAL COAL FLOW	M LBS PER HR	70.66	65.85	70.62	64.58	67.95	69.49	67.50	66.80	52.49	51.59	52.36	37.95	36.82	36.78	36.17
TEMPERATURE RECORDERS:																
FINAL STEAM TEMPERATURE	°F	899	893	902	900	897	895	900	901	892	898	901	861	852	837	856
FEEDWATER ENTERING ECONOMIZER	°F	400	401	400	401	400	400	398	401	375	375	378	358	349	348	347
FEEDWATER LEAVING ECONOMIZER - NORTH	°F	491	498	501	498	480	488	499	512	459	466	465	430	425	425	427
FEEDWATER LEAVING ECONOMIZER - SOUTH	°F	479	488	491	487	469	478	487	504	445	455	455	420	418	414	417
FEEDWATER LEAVING SUPERHEATER CONDENSER - NORTH	°F	539	534	528	535	541	538	530	529	533	534	530				
FEEDWATER LEAVING SUPERHEATER CONDENSER - SOUTH	°F	539	532	528	533	541	538	530	529	531	530	530				
GAS TEMPERATURE ENTERING ECONOMIZER	°F															
GAS TEMPERATURE LEAVING ECONOMIZER - NORTH	°F	653	667	657	665	640	650	669	673	590	595	591	533	519	520	525
GAS TEMPERATURE LEAVING ECONOMIZER - SOUTH	°F	648	659	655	656	629	648	666	670	583	589	589	520	515	508	515
GAS TEMPERATURE LEAVING AIR HEATER - NORTH	°F	317	315	321	316	310	307	312	325	300	302	303	314	311	310	316
GAS TEMPERATURE LEAVING AIR HEATER - SOUTH	°F	315	320	320	314	314	319	314	312	311	308	306	302	301	301	296
AIR ENTERING AIR HEATER - NORTH	°F	91	93	96	89	90	93	88	82	84	82	85	81	85	81	81
AIR ENTERING AIR HEATER - SOUTH	°F	90	91	95	86	89	80	85	80	82	80	81	77	83	80	79
AIR LEAVING AIR HEATER - NORTH	°F	580	589	585	586	568	565	582	592	540	543	540	510	498	499	500
AIR LEAVING AIR HEATER - SOUTH	°F	572	584	585	579	563	565	582	586	534	538	537	496	491	486	490
AIR ENTERING 3A MILL	°F		279	453	373		439	346	410	322	332	393	376	320	320	319
AIR ENTERING 3B MILL	°F		288	463	365		419	400	418	360	366	367	374	328	329	317
PRESSURES:																
SUPERHEATER OUTLET HEADER	PSIG	882	876	878	875	885	884	882	890	875	878	883	888	888	878	885
DRUM	PSIG	959	953	954	952	960	960	959	965	900	903	908	916	917	906	914
PULVERIZED FUEL SYSTEM:																
NUMBER OF PULVERIZERS IN SERVICE		2	2	2	2	2	2	2	2	2	2	2	2	2	2	1
NUMBER OF MAIN BURNERS IN SERVICE		8	8	8	8	8	8	8	8	8	8	8	8	4	4	4
NUMBER OF AUXILIARY BURNERS IN SERVICE		8	8	8	8	8	8	8	8	8	8	8	0	4	4	4
SECONDARY AIR VANE POSITION - 3A2	% OPEN	40	40	60	50	40	60	45	60	35	50	65	30	50	0	0
SECONDARY AIR VANE POSITION - 3B2	% OPEN	40	40	60	50	40	60	45	60	35	50	65	30	50	0	50
SECONDARY AIR VANE POSITION - 3B22	% OPEN	40	40	60	50	40	60	45	60	35	50	65	30	50	0	50
SECONDARY AIR VANE POSITION - 3A22	% OPEN	40	40	60	50	40	60	45	60	35	50	65	30	50	0	0
SECONDARY AIR VANE POSITION - 3B1	% OPEN	40	40	60	50	40	60	45	60	35	50	65	30	0	50	50
SECONDARY AIR VANE POSITION - 3A1	% OPEN	40	40	60	50	40	60	45	60	35	50	65	30	0	50	0
SECONDARY AIR VANE POSITION - 3A11	% OPEN	40	40	60	50	40	60	45	60	35	50	65	30	0	50	0
SECONDARY AIR VANE POSITION - 3B11	% OPEN	40	40	60	50	40	60	45	60	35	50	65	30	0	50	50
AUXILIARY AIR DAMPER POSITION - 3A1	INS OPEN	2.0	2.8	2.0	2.7	2.0	4.0	2.8	2.8	2.2	2.1	2.2	1.8	0	2.7	0
AUXILIARY AIR DAMPER POSITION - 3A2	INS OPEN	2.0	2.9	2.0	2.8	2.0	1.5	2.8	2.8	2.3	2.3	2.2	1.9	3.1	0	0
AUXILIARY AIR DAMPER POSITION - 3B1	INS OPEN	2.0	2.3	2.0	2.2	2.0	2.0	2.3	2.4	1.9	1.8	1.7	1.6	0	2.7	2.7
AUXILIARY AIR DAMPER POSITION - 3B2	INS OPEN	2.0	2.7	2.0	2.8	2.0	2.0	2.8	2.8	2.1	2.1	2.0	1.8	2.9	0	2.8
CAPACITY DAMPER POSITION - 3A1	% OPEN	28	28	29	27	25	25	28	28	22	21	21	18	0	27	0
CAPACITY DAMPER POSITION - 3A2	% OPEN	28	29	30	28	26	27	28	28	23	23	22	19	31	0	0
CAPACITY DAMPER POSITION - 3B1	% OPEN	24	23	26	22	24	24	23	24	19	18	19	16	0	27	27
CAPACITY DAMPER POSITION - 3B2	% OPEN	26	27	28	28	26	27	28	28	21	21	20	18	29	0	28
MISCELLANEOUS DRAFTS:																
INDUCED DRAFT AT FAN B	INS WG	9.9	10.2	10.1	10.1	8.3	8.0	10.7	10.8	6.0	6.2	6.0	6.1	4.0	4.0	4.0
INDUCED DRAFT AT FAN A	INS WG	8.9	9.1	9.1	9.1	8.1	9.0	9.5	9.4	5.4	5.5	5.8	6.3	3.7	3.4	3.7
AIR HEATER DIFFERENTIAL B	INS WG	3.5	3.4	3.5	3.4	3.0	3.0	3.5	3.6	2.1	2.1	2.2	1.3	1.3	1.4	1.3
AIR HEATER DIFFERENTIAL A	INS WG	3.4	3.4	3.5	3.4	2.9	3.1	3.5	3.5	2.2	2.2	2.1	1.3	1.4	1.3	1.4
ECONOMIZER DIFFERENTIAL B	INS WG	1.9	2.2	2.0	2.2	1.8	1.9	2.4	2.4	0.9	1.0	1.0	0.6	0.6	0.6	0.6
ECONOMIZER DIFFERENTIAL A	INS WG	2.1	2.4	2.2	2.4	1.8	1.7	2.5	2.5	1.0	1.0	1.0	0.7	0.7	0.7	0.7
EXTENDED SURFACE DIFFERENTIAL	INS WG	0	0	.01	0	0	0	0	0	0	0	0	0	0	0	0
SUPERHEATER DIFFERENTIAL	INS WG	2.4	2.6	2.4	2.5	2.2	2.2	2.5	2.6	1.5	1.6	1.6	1.0	1.0	1.0	1.0
SLAG SCREEN DIFFERENTIAL	INS WG	0	0	0	0	0	0	0	0	0	0	0	0	0	0	0
UPPER FURNACE	INS WG	.36	.32	.43	.33	.41	.34	.37	.36	.40	.40	.44	.40	.42	.40	.40
LOWER FURNACE	INS WG	.90	.89	1.00	.89	1.00	.62	.90	.84	.90	1.00	1.00	.85	.96	.90	.90
FORCED DRAFT AT FAN A	INS WG	12.4	13.0	9.9	11.1	9.9	8.4	13.0	10.0	6.0	5.0	4.6	2.8	4.9	4.1	4.8
FORCED DRAFT AT FAN B	INS WG	11.9	12.4	9.2	10.9	9.3	7.7	12.5	10.3	5.8	4.6	4.2	2.8	4.7	4.0	4.5
FORCED DRAFT DUCT PRESSURE A	INS WG	6.7	7.0	3.7	5.3	4.9	3.2	6.8	4.2	2.9	1.6	1.3	0.9	3.1	2.4	2.8
FORCED DRAFT DUCT PRESSURE B	INS WG	6.6	7.1	3.9	5.4	5.0	3.3	6.8	4.4	3.0	2.0	1.6	1.4	3.4	2.7	3.1
SECONDARY AIR PRESSURE	INS WG															
BURNER NUMBER A 1	INS WG	5.9	6.2	3.1	4.5	4.6	2.6	5.9	2.9	2.9	1.5	1.0	1.1	0	2.1	0
BURNER NUMBER A 11	INS WG	6.2	6.5	3.5	4.9	4.8	3.0	6.1	3.8	3.4	2.0	1.6	1.6	0	2.8	0
BURNER NUMBER A 2	INS WG	6.1	6.8	3.3	4.9	4.8	3.0	6.5	3.9	3.0	1.8	1.3	1.3	3.1	0	0
BURNER NUMBER A 22	INS WG	6.9	7.4	4.1	5.6	5.3	3.8	7.1	4.5	4.0	2.6	2.1	2.3	4.0	0	0
BURNER NUMBER B 1	INS WG	6.6	6.9	3.6	5.0	5.0	3.2	6.4	3.9	3.2	2.0	1.3	1.6	0	2.9	3.2
BURNER NUMBER B 11	INS WG	6.1	6.7	3.4	4.9	5.0	3.0	6.1	3.8	3.2	2.0	1.6	1.7	0	2.6	3.1
BURNER NUMBER B 2	INS WG	4.8	5.1	2.2	3.5	3.6	2.0	4.6	2.5	2.3	1.0	0.6	1.0	2.1	0	2.0
BURNER NUMBER B 22	INS WG	4.6	4.8	2.0	3.2	3.3	1.9	4.4	2.4	2.1	1.0	0.4	0.8	2.0	0	2.0
MILL DIFFERENTIAL A 1	INS WG	3.0	2.8	3.1	2.9	2.9	2.8	2.9	3.0	2.1	1.9	2.0	1.4	0	3.0	0
MILL DIFFERENTIAL A 2	INS WG	3.0	3.0	3.1	3.0	2.9	2.8	3.0	2.9	2.2	2.3	2.0	1.4	3.7	0	0
MILL DIFFERENTIAL B 1	INS WG	2.6	2.7	2.8	2.6	2.8	2.9	2.5	2.8	2.0	1.9	2.0	1.4	0	3.1	3.0
MILL DIFFERENTIAL B 2	INS WG	2.6	2.8	2.8	3.0	2.8	2.9	2.7	2.9	2.0	2.0	2.0	1.5	3.5	0	2.9
HIGH LEVEL DIFFERENTIAL - A MILL	INS WG	1.2	1.4	1.3	1.2	1.3	1.2	1.3	1.2	1.0	1.0	1.0	1.0	0.9	1.0	0
HIGH LEVEL DIFFERENTIAL - B MILL	INS WG	0.9	1.0	1.0	0.9	1.1	1.1	0.9	1.0	0.8	0.8	0.8	0.7	0.8	0.9	1.1
LOW LEVEL DIFFERENTIAL - A MILL	INS WG	1.5	1.5	1.5	1.5	1.5	1.4	1.5	1.5	1.5	1.5	1.5	1.6	1.5	1.6	0
LOW LEVEL DIFFERENTIAL - B MILL	INS WG	1.4	1.4	1.3	1.4	1.5	1.5	1.3	1.4	1.5	1.5	1.4	1.5	1.5	1.4	1.4
MILL SUCTION - A MILL	INS WG	2.1	2.0	2.1	1.9	2.1	2.0	2.3	2.3	2.4	2.3	2.3	2.0	2.0	2.0	0
MILL SUCTION - B MILL	INS WG	2.0	2.0	2.0	2.0	2.0	2.0	2.0	2.1	2.0	2.0	2.0	2.0	2.0	2.0	2.0
COAL AIR TEMPERATURE LEAVING MILL:																
COAL AIR TEMPERATURE A 1	°F	147	150	151	151	150	138	150	146	143	141	147	150		139	
COAL AIR TEMPERATURE A 2	°F	134	137	140	139	138	150	138	134	130	128	132	133	136		
COAL AIR TEMPERATURE B 1	°F	138	139	140	140	138	139	138	137	138	140	140	139		137	136
COAL AIR TEMPERATURE B 2	°F	140	141	141	143	140	140	140	142	138	140	140	142	139		140
PULVERIZED COAL FINENESS:																
THRU 50 MESH	%	99.9	99.9	99.9	99.9	99.9	99.9	99.9	99.9	99.9	99.9	99.9	100.0	100.0	99.9	99.8
THRU 100 MESH	%	97.8	98.1	97.9	98.2	98.2	98.0	97.9	98.1	98.8	98.7	98.6	99.2	98.9	98.5	97.4
THRU 200 MESH	%	86.3	88.9	87.2	89.1	88.4	87.9	88.3	88.4	91.0	90.9	90.4	92.4	92.2	91.0	85.9
ASH TEMPERATURES:																
INITIAL DEFORMATION	°F	2000	1970	2050	1920	1940	1900	1970	1940	1930	1940	1940	1940	1970	1970	1950
SOFTENING	°F	2050	2030	2130	1940	2100	2100	2080	2030	1990	2050	2050	2000	2010	2010	2040
FLUID	°F	2260	2210	2280	2260	2340	2310	2260	2210	2310	2260	2280	2310	2260	2130	2290
RAW COAL ANALYSIS:																
GRINDABILITY	HARDGROVE NUMBER	65	62	64	62	62	64	64	61	67	61	59	60	66	64	63
HEAT CONTENT (AS RECEIVED)	BTU PER LB	10,960	11,260	10,430	11,610	10,960	10,640	11,120	11,190	10,770	10,990	10,870	11,200	11,320	11,250	11,470
HEAT CONTENT (M & A FREE)	BTU PER LB															
MOISTURE (AS RECEIVED)	%	20.7	8.4	11.0	7.8	9.8	11.6	8.4	8.9	9.5	9.3	9.1	9.2	8.4	8.7	8.1
ASH (AS RECEIVED)	%	12.2	12.6	15.5	11.4	13.5	13.8	13.9	12.7	14.4	13.9	14.1	12.2	12.1	12.5	11.3
VOLATILE (AS RECEIVED)	%	33.8	34.2	32.5	36.6	35.2	33.2	35.0	36.0	34.4	35.0	33.5	35.1	35.3	34.3	34.9
H (M & A FREE)	%	5.4	5.2	5.2	5.3	5.3	5.4	5.1	5.3	5.2	5.2	5.2	5.2	5.2	5.2	5.3
C (M & A FREE)	%	61.0	62.5	58.1	64.1	61.0	59.2	61.8	62.0	59.3	61.0	60.4	62.3	62.5	62.3	63.5
N (M & A FREE)	%	1.3	1.2	1.2	1.3	1.3	1.2	1.2	1.3	1.3	1.2	1.2	1.2	1.2	1.2	1.3
O (M & A FREE)	%	16.7	14.1	16.5	13.7	15.1	16.6	14.2	15.1	14.6	14.6	14.2	15.2	15.0	14.5	14.6
S (M & A FREE)	%	3.4	4.4	3.5	4.2	3.8	3.8	3.9	3.6	5.2	4.2	4.3	3.9	4.0	4.3	4.0
MINE		---------- 90% FROM MUHLENBURG COUNTY - WESTERN KENTUCKY ----------														
HEAT INPUT IN FUEL AND AIR	MKB PER HR	795.3	781.9	787.0	788.7	774.4	764.4	792.3	788.0	586.4	588.5	588.9	428.8	420.8	420.1	521.9
HEAT AVAILABLE TO FURNACE	MKB PER HR	793.7	780.5	785.2	787.2	772.4	761.5	791.0	786.8	584.9	586.9	587.4	427.1	418.2	418.3	419.6
AVERAGE FURNACE EXIT GAS TEMPERATURE	(MHVT) °F	2000	2050	2020	2035	2075	2095	1995	2070	1875	1885	1875	1750	1740	1690	1725
AVERAGE FURNACE WALL THERMOCOUPLE Δ T	°F	34.8	32.9	28.2	30.9	35.7	33.0	34.6	34.6	34.6	31.2	30.4	22.8	23.4	24.1	24.3
EXCESS AIR AT FURNACE OUTLET	%	23.0	24.8	25.0	26.2	16.9	17.0	29.7	30.2	21.4	23.4	24.5	23.6	21.7	23.0	21.5

SYMBOLS:

- D - DOWN
- U - UP
- CW - CRACKED WITH ROTATION
- C - CLOSED
- MKB - MILLION BTU
- M - MOISTURE
- A - ASH
- MHVT - MULTIPLE HIGH VELOCITY THERMOCOUPLE

TABLE 4 PULVERIZED-COAL DISTRIBUTION BETWEEN BURNER CONDUITS IN PER CENT OF TOTAL FLOW TO UNIT

Burner conduit test no.	3A1	3A11	3A2	3A22	3B1	3B11	3B2	3B22
15	12.5	13.4	12.2	12.4	13.4	11.6	12.5	12.0
15A	11.6	13.4	12.0	11.6	13.8	13.8	11.5	12.3
16	12.6	13.8	12.1	11.2	12.5	12.6	12.6	12.6
17	13.7	13.6	11.2	11.6	12.3	13.2	11.7	12.7
18	12.6	13.4	11.0	10.6	13.1	13.9	12.9	12.5
19	11.3	12.3	11.2	11.0	13.6	13.5	13.3	13.8
21	12.0	12.9	11.9	11.0	13.5	12.5	13.5	12.7
22	13.0	13.4	11.6	11.1	14.0	13.3	11.5	12.1
24	13.6	14.0	12.3	11.3	12.8	12.3	12.3	11.4
25	13.2	14.2	14.1	11.0	13.7	12.5	11.5	9.8
26	13.5	13.0	11.7	12.1	12.7	12.8	12.8	11.4
27	12.0	12.8	12.2	13.3	14.4	12.4	11.6	11.3
28			23.0	24.6			27.0	25.4
29	23.1	20.5			28.3	28.1		
30					25.6	27.0	22.9	24.5

TABLE 5 CENTER-LINE THERMOCOUPLE AVERAGE TEMPERATURE DIFFERENTIALS FOR ALL COMPLETE TESTS

TEST #	15	15-A	16	17	18	19	21	22	24	25	26	27	28	29	30
TC #															
1-2															
1-3	36	36	32	32	36	33	36	36	30	29	30	25	21	26	25
1-4	39	38	42	34	38	38	36	42	31	30	35	24	22	21	25
1-5	36	36	37	39	45	45	41	49	37	41	42	20	26	31	25
1-6	39	39	46	41	45	44	44	49	38	41	41	27	26	33	29
1-7	29	31	34	45	23	24	33	41	24	27	28	17	29	41	38
1-8	41	44	34	41	36	38	40	41	30	29	34	23	25	36	36
1-9	9	22	7	4	30	8	30	9	8	8	9	24	3	4	4
1-10	27	29	24	26	25	25	29	27	22	22	23	18	17	24	19
1-11	27	28	23	27	26	25	29	28	23	22	24	18	19	24	23
1-12	42	44	41	41	42	42	42	46	34	33	35	24	28	34	36
1-13	46	48	46	47	47	46	47	49	41	35	40	29	30	43	37
1-14	46	48	52	47	51	51	48	53	44	44	46	33	31	39	34
1-15	49	51	57	51	57	56	51	65	45	45	46	34	32	40	38
1-16	42	43	43	41	45	44	42	55	37	36	38	28	26	31	26
1-17	35	34	36	32	35	36	34	37	30	29	33	24	21	26	21
1-18	6	28	4	27	4	6	28	31	25	24	26	21	17	23	22
1-19	29	30	26	28	30	30	31	30	25	24	25	21	18	23	24
1-20	33	35	32	34	34	32	34	34	31	28	27	24	22	27	29
1-21	43	48	32	39	43	35	45	37	39	30	28	34	17	39	34
2-1	13	12	16	16	14	13	20	24	11	18	20	11	14	18	13
2-3															
2-4															
2-5	16	16	23	25	31	31	28	29	24	22	26	7	17	25	21
2-6	55	57	44	53	53	48	55	50	47	43	44	39	26	42	34
2-7	43	54	13	51	45	47	70	50	48	43	46	13	26	39	34
2-8	47	39	17	16	62	40	17	22	47	41	41	12	28	44	41
2-9	50	48	38	48	57	54	33	34	47	47	48	26	35	45	47
2-10	50	41	45	43	54	53	37	37	41	40	40	30	29	35	32
2-11	34	37	29	36	37	37	27	28	32	30	33	23	24	34	30
2-12	49	42	49	43	50	46	45	53	39	36	40	27	27	41	25
2-13	57	50	49	53	62	52	58	55	39	36	37	24	28	38	21
2-14	50	40	19	43	45	43	45	41	43	40	37	28	30	39	30
2-15	57	56	43	46	58	57	58	53	46	45	48	42	35	42	38
2-16	49	32	9	47	50	47	51	52	45	42	28	26	20	38	34
2-17															
2-18	44	43	43	43	48	44	42	46	41	38	21	32	29	39	37
2-19	41	38	49	34	42	44	37	43	43	39	44	28	25	34	34
2-20	48	23	42	23	50	47	43	38	41	37	42	25	23	20	33
2-21															
3-1	62	29	41	56	61	22	67	44	56	41	39	49	25	54	58
3-2	62	21	61	16	55	57	53	54	56	59	56	15	32	34	35
3-3															
3-4	39	52	29	30	55	35	26	42	23	32	41	20	43	20	46
3-5	30	35	27	33	42	39	24	36	20	23	29	30	42	35	47
3-6	51	30	39	28	52	32	22	30	19	33	25	16	36	29	33
3-7	40	22	20	18	38	38	33	24	20	16	18	43	13	25	16
3-8	36	10	20	20	26	29	20	12	11	14	16	12	16	17	13
3-9															
3-10	17	39	10	8	39	50	4	6	7	7	8	44	4	4	4
3-11	8	33	6	21	11	10	37	24	41	30	19	41	19	11	18
3-12	*														
3-13															
3-14	*														
3-15	33	10	18	9	19	24	19	21	18	15	22	21	27	11	20
3-16	*														
3-17	44	46	26	54	39	41	37	36	32	13	15	40	33	45	20
3-18	*														
3-19	45	27	31	39	44	48	41	29	41	43	20	23	34	32	25
3-20	43	41	42	21	47	49	37	28	12	14	17	30	48	41	37
3-21	69	71	75	45	96	81	55	43	34	55	44	48	83	50	90
4-1	57	32	63	16	50	64	27	29	36	45	45	21	43	14	46
4-2	47	39	41	41	52	42	41	41	35	39	37	33	27	27	31
4-3	37	34	29	33	37	35	33	31	36	35	33	26	22	19	22
4-5	47	37	41	40	49	45	41	40	42	37	38	30	29	23	26
4-6	43	43	39	45	40	41	40	41	40	38	40	27	31	23	27
4-7	37	37	32	39	40	37	37	38	39	34	35	25	28	22	27
4-8															
4-9	30	27	27	29	31	30	28	28	27	26	27	19	20	16	20

TEST #	15	15-A	16	17	18	19	21	22	24	25	26	27	28	29	30
TC #															
4-10	35	13	34	20	35	36	33	34	31	31	33	22	15	16	13
4-11	39	24	36	52	48	39	13	25	38	7	9	25	26	24	25
4-12	52	26	42	48	43	30	38	30	45	43	48	36	33	27	35
4-13	39	28	28	30	42	34	31	34	31	10	13	36	15	17	22
4-14	38	30	27	31	22	31	33	26	43	26	29	28	30	16	18
4-15	47	45	39	39	34	39	40	47	42	31	40	27	34	38	24
4-16	49	45	31	33	41	45	48	47	46	43	44	42	33	39	31
4-17	51	53	41	39	57	58	54	59	47	45	49	45	56	43	40
4-18	45	59	57	42	38	54	49	42	48	38	50	17	42	18	38
4-19	39	20	30	35	32	36	41	35	30	25	24	25	26	13	29
4-20	49	16	23	10	37	30	33	24	23	15	23	24	17	31	14
4-21	48	20	39	37	50	58	43	30	36	33	24	34	20	19	17
5-1	39	21	30	41	37	33	44	31	30	31	23	12	33	30	30
5-2	41	17	30	22	33	27	38	24	35	35	36	10	25	19	29
5-3	36	30	31	31	35	28	31	31	30	27	27	24	18	16	21
5-4	38	34	25	35	39	29	35	30	33	26	25	24	20	18	23
5-6	43	39	34	40	43	36	41	35	39	35	33	30	26	23	27
5-7	44	40	33	40	47	38	42	36	39	33	31	28	25	23	25
5-8	39	35	30	37	41	34	40	33	32	28	28	24	21	19	22
5-9	39	36	31	36	41	35	39	35	35	32	29	23	23	20	24
5-10	34	35	27	33	34	31	33	29	28	27	27	20	21	18	21
5-11	30	29	24	29	29	28	30	28	26	24	25	18	18	17	19
5-12	29	24	25	25	29	29	29	27	27	26	25	18	17	16	18
5-13	35	16	33	26	31	29	33	34	28	26	25	7	8	18	10
5-14	34	24	32	25	31	34	30	24	28	27	27	20	19	4	22
5-15	37	37	27	43	39	34	37	40	30	32	19	6	15	31	13
5-16	29	22	15	28	33	26	26	19	24	23	22	15	28	17	25
5-17	25	13	21	17	26	25	24	19	24	24	25	18	25	9	20
5-18	30	9	22	22	24	24	25	16	25	21	22	22	10	7	21
5-19	27	42	18	30	26	24	24	23	26	24	24	5	13	8	13
5-20	29	30	26	26	26	26	25	27	27	23	22	7	18	18	23
5-21	24	11	20	19	21	22	24	24	24	23	22	15	15	16	16
6-1	46	39	20	38	37	27	39	31	30	27	25	28	29	25	27
6-2	32	28	25	21	26	23	23	27	22	16	17	12	19	10	21
6-3	41	23	35	29	38	35	37	34	39	35	35	15	26	18	27
6-4															
6-5	39	35	31	35	39	33	38	33	34	30	27	26	22	20	25
6-7	36	33	29	34	36	31	35	31	33	31	27	21	17	19	21
6-8	45	44	37	43	43	39	42	40	41	38	33	26	25	25	26
6-9	42	40	37	40	40	38	40	39	35	33	32	24	24	23	25
6-10	42	39	39	40	41	42	41	41	35	35	34	24	25	23	25
6-11	46	46	41	46	45	46	47	46	39	39	38	26	30	26	29
6-12	40	45	35	42	38	40	42	40	34	34	34	24	26	22	26
6-13	29	27	25	27	27	28	29	28	24	23	23	17	18	16	18
6-14	49	49	45	50	48	49	51	48	39	37	37	29	33	30	31
6-15	29	14	29	23	26	37	27	27	22	22	21	15	4	15	4
6-16	27	5	22	14	25	23	24	26	27	24	24	8	17	15	17
6-17	33	28	31	29	28	27	34	31	26	26	27	18	20	21	19
6-18	29	25	24	25	26	24	27	26	24	23	22	16	18	16	18
6-19	32	30	23	30	30	28	31	27	27	27	23	16	17	16	16
6-20	30	29	26	29	28	25	30	28	25	24	22	16	16	16	15
6-21	24	23	23	23	24	22	24	25	20	21	19	13	13	13	14
7-1	22	20	20	19	21	22	21	23	18	19	19	11	12	11	13
7-2	27	28	24	26	27	30	27	30	23	19	25	15	16	14	17
7-3	23	25	21	23	20	24	24	26	20	20	21	13	15	12	15
7-4	23	25	22	23	22	24	26	27	20	21	21	13	15	12	16
7-5	27	27	25	25	23	25	27	28	21	21	21	14	17	13	16
7-6	29	27	24	25	26	25	28	26	23	24	22	16	15	14	14
7-8	31	29	23	30	30	28	30	27	26	26	22	16	16	15	14
7-9	25	23	19	22	23	21	24	18	21	20	18	13	10	11	11
7-10	31	28	23	27	28	23	29	24	25	23	21	15	12	14	13
7-11	22	21	21	22	21	21	22	22	19	20	17	13	11	11	12
7-12	21	21	19	22	20	24	21	24	18	19	20	11	12	10	12
7-13	21	22	19	21	19	24	22	26	18	20	21	12	14	9	14
7-14	23	24	21	24	21	26	24	28	20	22	22	13	15	12	16

* Saturation base thermocouple

TABLE 6 SUMMARY OF CONDITIONS AND RESULTS OF TESTS NOS. 15 THROUGH 30

Test Number	Date	Net Heat Available to Furnace MKB/Hr.	Net Heat Input to Furnace % Full Load	Excess Air at Furnace Outlet %	Secondary Air Vane Position % Open	Number of Burners in Service	Average ΔT Deg. F	Average Burner Box Pressure Ins. W.G.	Net Heat Absorbed in Furnace (ΔT Method) MKB/Hr	Furnace Efficiency %
15	10-22-48	793.7	93.2	23.0	40	8	37.2	5.9	350.3	44.2
15A	10-27-48	780.5	91.6	24.8	40	8	32.9	6.3	309.8	39.7
16	10-22-48	785.2	92.2	25.0	60	8	31.2	3.1	293.8	37.4
17	10-28-48	787.2	92.3	26.2	50	8	32.3	4.6	304.2	38.6
18	10-28-48	772.4	90.6	16.9	40	8	37.4	4.6	352.2	45.4
19	10-20-48	761.5	89.5	17.0	60	8	35.0	2.8	329.6	43.3
21	10-25-48	791.0	92.8	29.7	45	8	34.7	5.9	326.8	41.3
22	10-25-48	786.8	92.3	30.2	60	8	34.1	3.5	321.1	40.8
24	10-24-48	584.9	68.7	21.4	35	8	31.3	3.0	294.8	50.4
25	10-24-48	586.9	68.9	23.4	50	8	29.1	1.7	274.0	46.6
26	10-24-48	587.4	69.0	24.5	65	8	29.4	1.2	276.9	47.2
27	10-27-48	427.1	50.2	23.6	30	8	23.1	1.4	217.5	50.9
28	10-30-48	418.2	49.3	21.7	50	4*	23.5	2.8	221.3	52.9
29	10-29-48	418.3	49.2	23.0	50	4**	24.0	2.9	226.0	54.0
30	10-30-48	419.6	49.5	21.5	50	4***	25.0	2.6	235.4	56.1

* - upper
** - lower
*** - normal

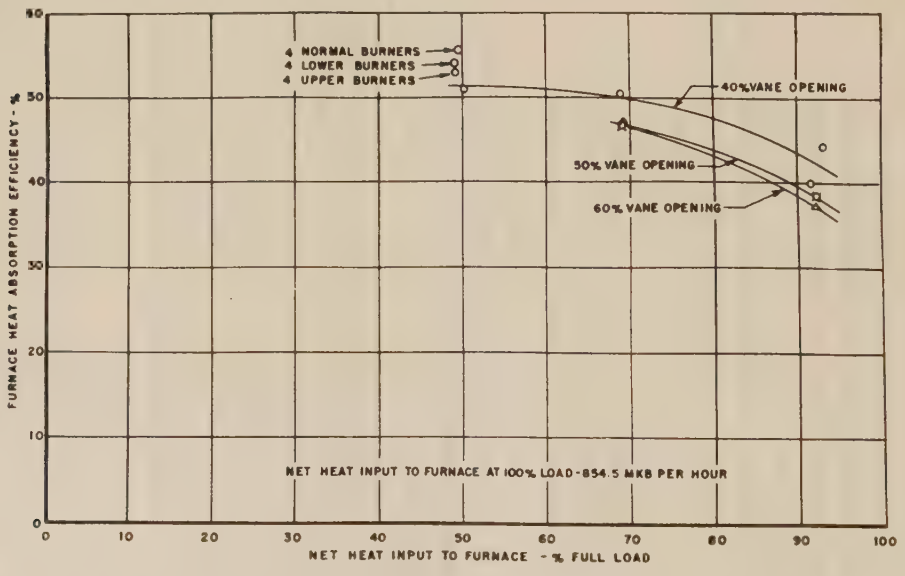

FIG. 29 VARIATIONS OF FURNACE HEAT-ABSORPTION EFFICIENCY WITH NET HEAT INPUT TO FURNACE FOR THREE DIFFERENT SECONDARY-AIR VANE POSITIONS WITH EIGHT BURNERS IN SERVICE AND APPROXIMATELY 25 PER CENT EXCESS AIR AT FURNACE OUTLET

of absorption were found on the tests at the lower vane openings. The heat-absorption rates at the burner elevations were low on all of these tests, apparently owing to the ash coverage in this area. It is also possible that this ash was deposited on some of full-load tests and that the change in furnace rating was not sufficient to allow it to clean itself. Increasing the vane opening under these conditions caused a decrease in furnace heat-absorption efficiency of about 3 to 4 per cent.

(*e*) General: Summarizing the foregoing results, it is found that increasing the vane opening results in decreasing the heat absorbed in the front wall and usually causes a reduction in absorption in the rear wall owing to an increase in ash coverage. The rate of heat absorption in those zones of relatively high absorption rates on the side walls near the burners usually decreases as the vanes are opened. The distribution of heat absorption over the height of the furnace does not vary greatly in any range of elevation other than in the vicinity of the burners, but lower absorption rates are found throughout the furnace as the vane openings are increased. The effect of varying vane opening on furnace heat-absorption efficiency at full load seems

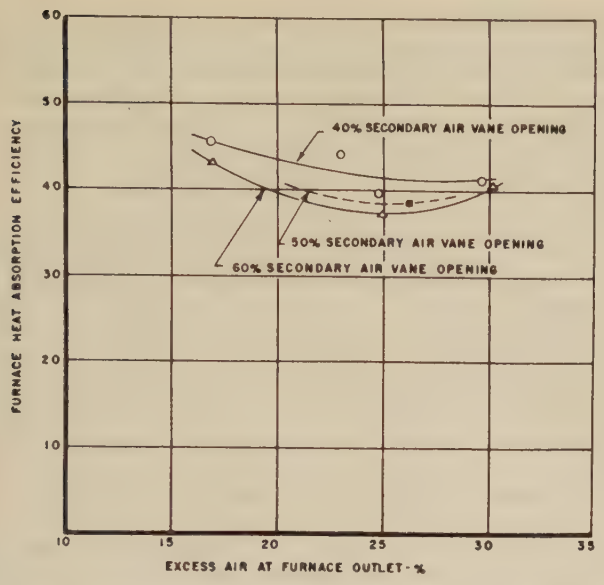

Fig. 30 Variation of Furnace Heat-Absorption Efficiency With Secondary-Air Vane Opening at Approximately 100 Per Cent Full Load for Three Different Excess-Air Values at Furnace Outlet

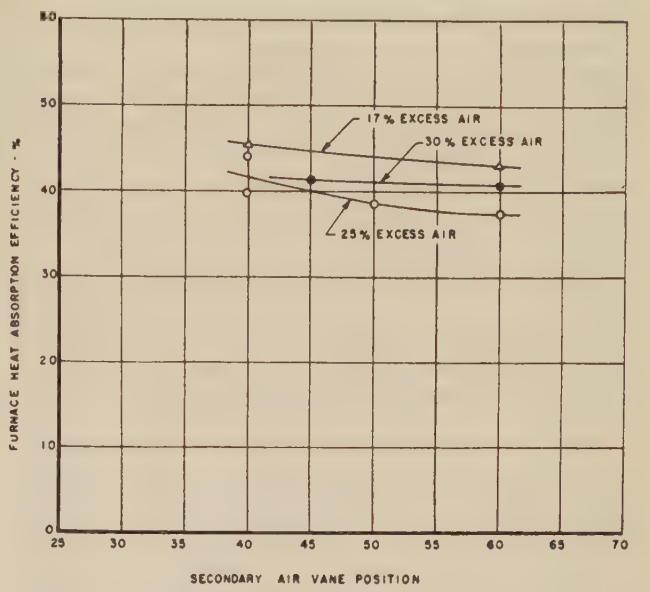

Fig. 31 Variation of Furnace Heat-Absorption Efficiency With Excess Air at Furnace Outlet for Three Different Secondary-Air Vane Settings at Approximately 100 Per Cent Full Load

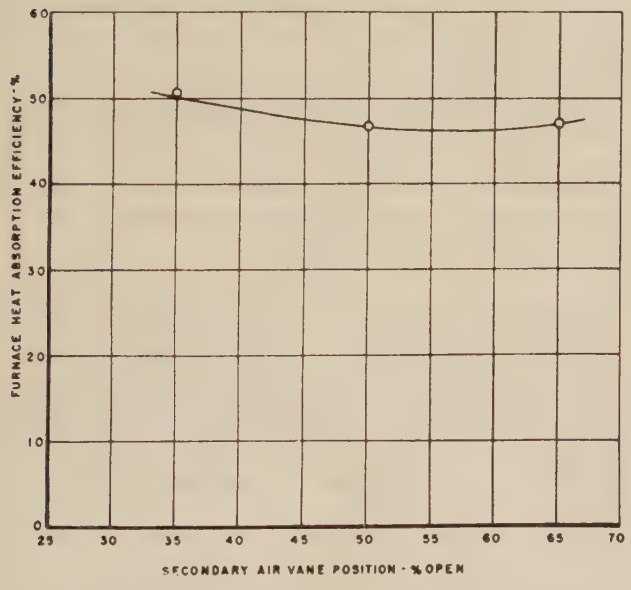

Fig. 32 Variation of Furnace Heat-Absorption Efficiency With Secondary-Air Vane Position for Approximately 75 Per Cent Full Load With 25 Per Cent Excess Air at Furnace Outlet

to change depending upon the excess air used. At 17 and 25 per cent excess air, we found a decrease of approximately 2 to 4 per cent as the vanes were opend, but found only a slight decrease in efficiency as the vane opening was increased at 30 per cent excess air. The effect of vane openings on furnace efficiency seems to be slightly reduced as the furnace rating is reduced.

Effect of Varying Heat Input to Furnace. The effect of varying heat input was studied between the approximate range of 50 to 93 per cent full load at 25 per cent excess air at the furnace outlet with eight burners in service. The effect of this variable alone is probably best shown by comparing test Nos. 15, 25, and 27, where the secondary-air vane openings were 40, 35, and 30 per cent open, respectively. Other comparisons in the range of about 70 per cent to 93 per cent full load may also be made. Test Nos. 17 and 25 were run at 50 per cent vane opening, and test Nos. 16 and 26 were made at 60 to 65 per cent vane opening.

Comparing test Nos. 15, 24, and 27, it is found that the distribution of heat absorbed in the front wall does not vary greatly, regardless of the heat input, although, of course, it increases in amount as the heat input is increased. The location of the zones of higher absorption found on the side walls near the burners does not change greatly as the heat input is increased, but the rate of heat absorption in these zones increases. The rear wall is less affected by ash accumulation at the lower heat inputs with the result that it has a more uniform and nearly as great absorption at the lower loads as are obtained at the high load. In general, the isothermal diagrams become a little more spotted at 50 per cent full load.

Comparing the distribution over the height of the furnace, it is found that the general trends remain the same, except at the burner elevations. At full load, it is noted that there is a small reduction in the absorption in this particular area when comparing it to elevations both above and below this region. At about 70 per cent full load, there is a considerable reduction in absorption at the burner elevation, but it is felt that this is caused by ash coverage on the rear wall which was accumulated during some of the various operating conditions at full load and did not clean itself, thus distorting the true distribution at this load.

At 50 per cent load, it is found that the distribution of heat absorption over the height of the furnace is much more uniform than found under the preceding conditions and reaches a maximum at the burner elevation. This indicates that at 50 per cent load the distribution of heat absorption is not affected by ash coverage and that the ash coverage is negligible. The other tests show about the same results for the range in which they were investigated.

The furnace heat-absorption efficiency for test Nos. 15, 24, and 27 indicates that, as the heat input is increased in the range from 50 to 70 per cent full load, there is only a slight decrease in furnace efficiency, but that increasing the heat input in the range from 70 to 93 per cent causes an appreciable reduction in furnace efficiency (about 7 per cent). Comparing the other

tests at 50 and 60 per cent vane opening in the range from 70 to 93 per cent, the same results are noted.

Effect of Varying Excess Air at Furnace Outlet. The effect of varying excess air at the furnace outlet was studied at approximately full load in the range between 17 to 30 per cent. Test Nos. 15, 18, and 21 were all run with approximately 40 per cent secondary-air vane opening. Test Nos. 16, 19, and 22 were all run with 60 per cent vane opening. It is found that the distribution of heat absorption on the various furnace walls varies only a small amount as the excess air is increased, although there are some indications that the absorption rates in the rear wall are decreased as the excess air is increased, apparently due to an increase in ash coverage. The zones of high absorption on the side walls near the burners do not seem to vary significantly as the excess air is changed, although the rates of heat absorption found were a little higher at the low excess air.

In studying the distribution of heat absorption over the height of the furnace at 60 per cent vane opening, it is noted that from elevation 35 ft to the top of the furnace there is little change in distribution regardless of the amount of excess air used, but that considerable variations are found from the hopper throat up to the 35-ft elevation.

At 17 per cent excess air the heat-absorption rate reaches a maximum at the burner elevations. At 25 per cent excess air, the absorption rate is rather constant over this range of elevation. At 30 per cent excess air there is a considerable reduction in the heat absorption at the burner elevations, but the heat absorption is higher just under the burner elevations than is noted under the other conditions. These same general characteristics are noted in comparing the tests at 40 per cent secondary-air vane opening.

It was indicated that the furnace heat-absorption efficiency at 40 per cent vane opening decreased rather rapidly as the excess air was changed from 17 to 25 per cent, and then remained approximately constant as the excess air was increased from 25 to 30 per cent. It was also indicated that at 60 per cent vane opening the furnace efficiency decreased rapidly between 17 and 25 per cent excess air, and then increased slightly as the excess air was increased from 25 to 30 per cent. This indicates that, as the excess air is increased at constant vane opening from 17 to 25 per cent excess air, there is a reduction in furnace efficiency which can be recovered partially by increasing the excess air further. This might be caused by the increase in the angular velocity of the mixture leaving the burner throat. Both the study of variations of the amount of excess air and the study of variations in secondary-air vane opening seem to indicate that an increase in the angular velocity of the fuel mixture leaving the burner throats results in improving the mixing of the fuel and air and possibly increases the rate of combustion of the fuel particles. Thus it seems possible that the temperature of the flame envelope might be changed as well as its shape as the angular velocity of the fuel mixture is changed.

Effect of Various Combinations of Burners in Service at 50 Per Cent Full Load. Test Nos. 27 to 30, inclusive, were run at about 50 per cent full load with approximately 25 per cent excess air at the furnace outlet. Test No. 27 was run with all eight burners in service, Test No. 28 with only the four upper burners, Test No. 29 with only the four lower burners, and Test No. 30 with the two upper inside burners and the two lower outside burners in service. It was found that the distribution and amount of heat absorbed by the front wall did not vary greatly on any of these tests. The heat absorption by the rear wall did change considerably depending upon which burners were used. The absorption by this wall was much more uniform when all eight burners were used and also much less affected by ash coverage. It was found that the location of higher absorption rates on the rear wall changed with the combinations of burners in service. They were located highest on the rear wall with the four upper burners in operation and lowest when the four lower burners were used. The zones of high absorption rates on the side walls near the burners did not vary greatly but yet tended to shift up and down, depending upon which burners were used. These zones contained the lowest absorption rates when all eight burners were used.

When studying the distribution of heat absorption over the height of the furnace for these tests, it was found that from the 35-ft elevation to the top of the furnace there was little change in distribution. However, from the ash-hopper throat up to the 35-ft elevation, the distribution was changed considerably for the various burner combinations. With the four lower burners in operation, the maximum absorption rates were found just below the lower burner elevations. With the four upper burners in operation, the maximum absorption rate was found at the elevation of these upper burners. When the two upper and two lower burners were used, the maximum heat-absorption rate was found to be less than those obtained with the other four burner combinations and spread over a wider range of elevation, reaching its maximum near the elevation of the lower burners. When eight burners were used, the absorption rate in this region was much lower and much more constant, reaching its maximum value at the elevation of the upper burners.

It was indicated that the lowest furnace efficiency was obtained with eight burners in operation and increased in the following order; four upper burners, four lower burners, and two upper and two lower burners. However, using the convection superheater as an indication of furnace efficiency, it was found that the four lower burner operation resulted in a higher furnace efficiency than was obtained with the two upper and two lower burner operation. It also seems that the difference in efficiency between four lower burner operation and two upper and two lower burner operation is too small to establish definitely by the ΔT-method, which is the more efficient.

Conclusions

Based upon the foregoing data and analysis of results, we have formed the following conclusions concerning the performance of this furnace under the operating conditions investigated:

1 Ash does not collect in sufficient quantities to affect the heat absorption by the furnace-wall surface at any location other than the area of the rear wall at the burner elevations, where there is a tendency to accumulate and shed ash under some of the operating conditions studied.

2 Considering the distribution of heat absorption over the height of the furnace, it is found that the average absorption rates are usually highest at the elevation just below the burners, although indications show that the maximum might be found at the burner elevations if it were not for the effect of ash coverage in this area. A second peak of higher absorption rates occurs at the elevation where the cross-sectional area of the furnace is reduced, near the top, by the rear-wall sloping section.

3 Variations in absorption rates for clean furnace surface throughout the furnace do not exceed a magnitude of 3 or 4 to 1. Zones of 60,000 to 75,000 Btu/(sq ft-hr) absorption rates exist in that area of the side walls near the burners, and relatively high rates of absorption occur in that area of the rear wall which forms part of the hopper throat at the bottom of the furnace under all of the operating conditions studied.

4 Opening the secondary air vanes, in the ranges studied, causes (*a*) a reduction in heat absorbed by the front walls; (*b*) an increase in ash accumulation on the rear wall opposite the burners, accompanied by a decrease in absorption in this area; (*c*) a reduction in absorption rates in the zones of higher absorption

on the side walls near the burners; (*d*) a decrease in absorption at the burner elevations and lower absorption rates throughout the furnace; and (*e*) a decrease in furnace efficiency, which varies with excess-air and heat-input conditions.

5 Increasing the excess air for combustion, in the range from 17 to 30 per cent, causes (*a*) a reduction in heat absorption at the burner elevations; (*b*) an increase in ash coverage in that area of the rear wall directly opposite the burners; and (*c*) a decrease in furnace heat-absorption efficiency with varying characteristics, depending upon which secondary-air vane opening is used.

6 Variations in the combination of burners in service, at 50 per cent full load, causes (*a*) changes in the ash coverage on the rear-wall area opposite the burners; (*b*) variations in the average absorption rates at the burner elevations, and the locations of higher absorption zones shift up and down, depending upon the burners used; and (*c*) variations in furnace heat-absorption efficiency in the range of approximately 5 per cent.

7 The ΔT-method provides a good means of determining the distribution of heat absorption in the furnace and many of its inherent errors apparently cancel themselves in the determination of the furnace heat-absorption efficiency. However, it is recommended that wherever furnace efficiency is concerned, the reader should also refer to the heat-balance data contained in Part II of the investigation at Paddy's Run Station.

The data, diagrams, and curves which have been included in this paper should be of considerable assistance to the furnace designer and operator in predicting performance characteristics of similar furnaces, although it must be recognized that other operating variables, such as different characteristics of the fuel fired, may revise or modify some of the results which have been found.

Acknowledgments

The authors wish to express their appreciation for the assistance rendered by the following in making this extensive investigation possible:

The ASME Special Research Committee on Furnace Performance Factors for the opportunity of participating in this investigation.

The officials of the Louisville Gas and Electric Company, Mr. A. G. Rosenbaum, General Superintendent, and Mr. F. B. Tetzel, Superintendent of Power Production, who made the No. 3 unit at Paddy's Run Station available to the committee for testing, and co-operated with the committee in every possible way throughout the extended test program.

Mr. John Blizard, Mr. Martin Frisch, Mr. A. R. Mumford, and Mr. Fred Ely for their very helpful criticisms and suggestions.

The personnel of Paddy's Run Station of the Louisville Gas and Electric Company: Mr. J. D. Brecker, Plant Engineer; Mr. S. P. Connor, Assistant Plant Engineer; Mr. H. C. Scherffieus, Economy Engineer; and their assistants who gave capable and willing assistance in accomplishing the test program.

The Combustion Research Section of the U. S. Bureau of Mines whose contributions on this test project have been outstanding.

The members of the Service Department, Steam Division and Research Department of the Foster Wheeler Corporation, who gave generously of their time and experience in the running of tests and analysis of results.

BIBLIOGRAPHY

1 "Furnace Heat Absorption in Pulverized-Coal-Fired Steam Generator Using Turbulent Burners at Paddy's Run Station, Louisville, Ky."

Part I "Variation in Heat Absorption as Shown by Measurement of Surface Temperature of Exposed Side of Furnace Tubes," by R. I. Wheater and M. H. Howard, subject paper.

Part II "Furnace Heat-Absorption Efficiency as Shown by the Temperature and Composition of Gases Leaving the Furnace," by R. C. Corey and Paul Cohen, published in this issue of the Transactions, pp. 925–935.

Part III "Comparison and Correlation of the Results of Furnace Heat-Absorption Investigation," by H. H. Hemenway and R. I. Wheater, published in this issue of the Transactions, pp. 937–944.

2 "An Investigation of the Variation in Heat Absorption in a Pulverized-Coal-Fired Water-Cooled Steam-Boiler Furnace."

Part I "Variations in Heat Absorption as Shown by Measurement of the Surface Temperature of the Exposed Side of Furnace Tubes," by L. B. Schueler, Trans. ASME, vol. 70, 1948, pp. 553–567.

Part II "Furnace Heat-Absorption Efficiency as Shown by Temperature, Composition, and Flow of the Gases Leaving the Furnace," by W. T. Reid, Paul Cohen, and R. C. Corey, Trans. ASME, vol. 70, 1948, pp. 569–585.

Part III "Variation in Heat Absorption as Shown by Density and Velocity Measurements of the Fluid Within a Tube," by A. R. Mumford and C. G. R. Humphreys, Trans. ASME vol. 70, 1948, pp. 587–600.

Part IV "Comparison and Correlation of the Results of Furnace Heat-Absorption Investigations," by A. R. Mumford and G. W. Bice, Trans. ASME, vol. 70, 1948, pp. 601–614.

3 "Thermocouples for Furnace-Tube Surface Temperature Measurement," by C. G. R. Humphreys, *Combustion*, October, 1944, pp. 43–45.

Furnace Heat Absorption in Paddy's Run Pulverized-Coal-Fired Steam Generator, Using Turbulent Burners, Louisville, Ky.

Part II Furnace Heat-Absorption Efficiency as Shown by Temperature and Composition of Gases Leaving the Furnace

By R. C. COREY[1] and PAUL COHEN,[2] PITTSBURGH, PA.

This paper is part of the second of a series of formal reports on investigations of heat absorption and distribution of heat transfer in representative pulverized-coal-fired boiler furnaces, sponsored by the ASME Special Research Committee on Furnace Performance Factors. The results are presented of fifteen determinations of heat absorption in the furnace of a 640,000 lb per hr boiler with horizontal firing, operating at 950 psig and 900 F at the superheater outlet. The effect on furnace heat-absorption efficiency is shown for variation of (*a*) the heat available in the furnace, (*b*) the excess air, (*c*) the setting of the secondary-air vanes of the turbulent burners, and (*d*) at low loads, the number and location of the burners used. Detailed data are given for the distribution of excess air and gas temperature at the furnace outlet. The heat-absorption data are analyzed in terms of radiation heat transfer, and the significance of flame location, volume, and shape is discussed.

Introduction

THIS paper presents the results of determinations of the heat-absorption efficiency of a central-station, pulverized-coal-fired, steam-boiler furnace, for a variety of operating conditions. It is a part of the report of the second[3] of a series of comprehensive investigations of heat transfer in boiler furnaces by the Special Research Committee on Furnace Performance Factors of the Society. The unit studied in this second investigation is boiler No. 3, Paddy's Run Station, Louisville Gas & Electric Company, Louisville, Ky., a single-drum boiler, with a dry-bottom furnace, fired from the front wall with eight horizontal turbulent burners arranged in two rows and rated at 640,000 lb of steam per hr at 950 psig and 900 F at the superheater outlet.

The investigation of this unit by the committee consisted of two parts, namely, determination of the total heat absorption in the furnace, which is the subject of this paper, and determination of the distribution of heat absorption in the furnace, the subject of another paper of this symposium. The furnace heat-absorption tests were made by the Combustion Research Section of the Bureau of Mines, concurrently with the other studies, as part of the Bureau of Mines co-operative research program with the committee to study the effect of ash and slag on furnace performance.

Fifteen tests were made to determine the effect on furnace heat absorption of variations of load, excess air, adjustment of the turbulent burners, and, at low loads, the number and location of the burners used. The heat absorption is defined as the heat transferred by convection to the furnace walls, not including the screen, and the heat transferred by radiation to the furnace walls, including the screen. With slight modification, the test procedure is that of Method *b* of the ASME Test Code for Stationary Steam-Generating Units. The heat absorption in the furnace is obtained as the difference between the net heat available in the furnace (the low heat value of the fuel fired, corrected for unburned combustible, plus the sensible heat in the air used for combustion) and the sensible heat in the furnace-outlet gases and the refuse, and the heat transferred from the furnace casing.

The sensible heat in the furnace-outlet gas was calculated from the temperature and composition determined by techniques appropriate for furnace testing.[4] Measurements were made at a number of positions approximating the furnace outlet within the limitations of the available means of access to the furnace. Because of the significance of the distribution of the temperature and composition of the gases at the furnace outlet, the complete test data are tabulated in the paper.

Methods of Test and Calculation

Description of Furnace. Fig. 1 is a sectional side elevation of the boiler, showing the general arrangement of the components. The furnace is 78 ft high from the top of the hopper to the center line of the drum, 31 ft 0 1/2 in. wide between side-wall tubes, 24 ft 3 in. deep, and the volume is 47,100 cu ft. All furnace walls consist of 3-in-OD tubes on 3 1/4-in. centers, backed by tile. The front portion of the furnace roof is formed by the direct continuation of the front-wall tubes, and the rear portion of the roof is formed by the back-wall tubes bent forward and covered on the outside with a tile baffle. The slag screen is formed from the back-wall tubes expanded into four rows of tubes with a 9-in. center-to-center spacing between rows and a 13-in. center-to-

---

[1] Supervising Engineer, Combustion Research Section, Bureau of Mines. Mem. ASME.

[2] Fuel Engineer, Combustion Research Section, Bureau of Mines. Mem. ASME.

[3] The report on the first unit studied, Boiler No. 11, Tidd Station, has already been published: "An Investigation of the Variation in Heat Absorption in a Pulverized-Coal-Fired Water-Cooled Steam-Boiler Furnace," by L. B. Schueler, et al, Trans. ASME, vol. 70, 1948, pp. 553–619.

Contributed by the Special Research Committee on Furnace Performance Factors, and the Fuels, Power, and Heat Transfer Divisions and presented at the Annual Meeting, New York, N. Y., November 27–December 2, 1949, of The American Society of Mechanical Engineers.

Note: Statements and opinions advanced in papers are to be understood as individual expressions of their authors and not those of the Society. Paper No. 49—A-42.

[4] "Methods and Instrumentation for Furnace Heat-Absorption Studies: Temperature and Composition of Gases at Furnace Outlet," by P. Cohen, R. C. Corey, and J. W. Myers, Trans. ASME, vol. 70, November, 1949, pp. 965–978.

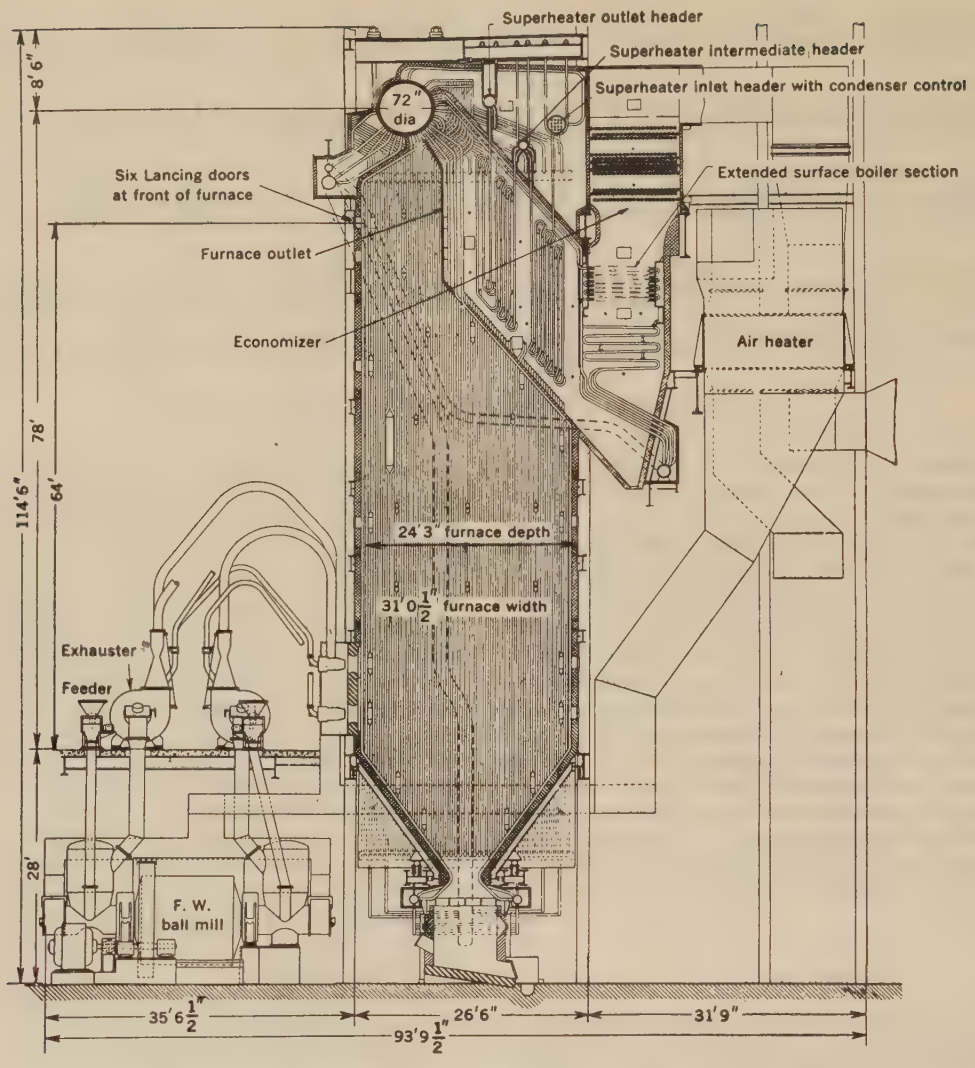

FIG. 1 SECTIONAL SIDE ELEVATION OF BOILER NO. 3, PADDY'S RUN STATION

center spacing between lanes. The front row of screen tubes is 8 ft 11½ in. from the front-wall tubes, center-to-center distance. The furnace outlet is 18 ft 4 in. high and 30 ft 9½ in. wide. The area of projected radiant-heating surface in the furnace is 8884 sq ft, including the developed area of the furnace outlet, 564 sq ft.

The furnace is fired with eight intervane burners in the front wall, arranged in two rows of four each with center lines 4 ft 4 in. and 10 ft 4 in. above the top of the hopper, respectively. Fuel is supplied by two ball-mill pulverizers equipped with two exhausters each. The north mill fires the two inner upper burners and the two outer lower burners, and the south mill, the other four burners. Forced-draft fans, induced-draft fans, and regenerative air heaters are all in duplicate and arranged at the back of the unit. Interconnecting dampers permit operation at low loads with but one set of fans and air heater, but, in the tests, both sets of auxiliaries were always used to assure the best balance in the furnace and beyond.

Location of Test Points. After consideration of the available access doors, it was decided to make all measurements from six lancing doors at the front of the furnace, 64 ft above the top of the hopper. A large proportion of the furnace outlet could be reached by inserting a 14-ft water-cooled high-velocity thermocouple probe through these doors and swinging the probe at various angles from the horizontal. Thirty sampling positions were used in the tests, arranged in six columns (A, B, C, D, E, and F), corresponding to the location of the lancing doors in the front wall, each column having five sampling points, designated +6, +3, 0, —3, and —6, which are approximate vertical distances in feet from the midplane of the furnace outlet. The actual sampling points were 6 in. in front of the screen at the elevations shown. The resulting distribution of sampling points is shown in Fig. 2, a map of the developed furnace-outlet area, drawn to scale. The furnace outlet is also shown by the heavy line in Fig. 1.

To facilitate manipulation of the long and heavy water-cooled thermocouple holder and to provide reproducibility of the location of the sampling positions, a special insert was built for the lancing doors, which provided means for convenient and accurate manipulation of the probe and also permitted rather complete sealing of the door during sampling, with asbestos-board plates. Fig. 3 gives the general details of this special insert.

Instrumentation and Analyses. The temperature and composition of the gas at the furnace outlet were determined with instrumentation and technique previously described.[4] The following brief review will be helpful:

(*a*) The temperature of the gas at the furnace outlet was determined with high-velocity thermocouples (platinum, 10 per cent rhodium-platinum elements), using two new designs of multiple shields shown as types E and G in Fig. 4. Direct compari-

son between the shields, and the B&W MHVT (multiple high-velocity thermocouple), also shown in Fig. 4, were made in the subject furnace. The corrections of the observed temperatures, to the B&W MHVT basis were small, 30 F and 40 F for types E and G, respectively, at 2000 deg F. Because of the short length of the Pt Rh-Pt couple and the high gas-flow rates used in the probes, the temperature of the junction between the lead wire and couple in the probe exceeded the value at which the two were matched, and an additional minor correction was required because of the difference in thermoelectrical properties of the couple and lead wire. The emf of the thermocouples was recorded with a high-speed electronic potentiometer recorder equipped with a 1-hr clock, and representative average values of the temperature of the gas at a sampling point could be obtained from records of $^1/_2$ to 1 min duration.

(*b*) Gas analyses and temperature measurements were made simultaneously by connecting a Bailey oxygen recorder, with a 1-hr clock, in series with the aspirating system of the high-velocity thermocouple. Routine complete analysis of the gases being sampled by the Bailey oxygen recorder served both to check the calibration of the Bailey oxygen recorder and to correlate the oxygen content of the furnace-outlet gas with that of the other gas constituents. As with the temperature measurements, significant average values for the oxygen content of the gas at a sampling point could be obtained from records of $^1/_2$ to 1 min duration.

(*c*) Except for analysis of the flue gas entering the air heaters, for which the technique just described was employed, all other required observations were made with plant instrumentation. The temperatures of the flue gas and air entering and leaving the air heaters were recorded at the control board by two resistance thermometers properly situated in each duct at which measurements were made. Coal feed rates were ascertained by recording at regular intervals the time and the number of the trip at each of the four coal scales (two for each mill). Increments of the coal were taken at the scales, following ASTM specifications, and were stored during the test in 10-gal milk pails. The samples were reduced to approximately 35 lb and shipped to Pittsburgh in sealed cans for analysis by the Coal Analysis Section of the Bureau of Mines.

The quantity of fly ash in the gas entering the Cottrell precipitators was determined by the staff of the Louisville Gas & Electric Company, using the methods of the Research Corporation and with equipment supplied by the latter company. The fly ash was analyzed by the Coal Analysis Section of the Bureau of Mines.

The humidity of the air was determined by sling psychrometer at the F.D. fan inlet.

General Test Procedure. The superheaters and air heaters were blown routinely before each test, and, as required, excess slag deposits on the furnace screen were removed by hand lancing. The necessary burner adjustments were made, the load was adjusted to the desired value, and the fans were balanced as closely as possible. A preliminary analysis of the furnace gas was made through door C, and the air flow was then adjusted accordingly to give the desired excess air at the furnace outlet. Because of occasional nonuniformity of the gas at the furnace outlet, this procedure involved some guesswork and did not always yield the desired excess air. Coal-scale readings were started as soon as the unit was stabilized, and the test continued for a period of about 4 hr, the time necessary to make a complete set of all the

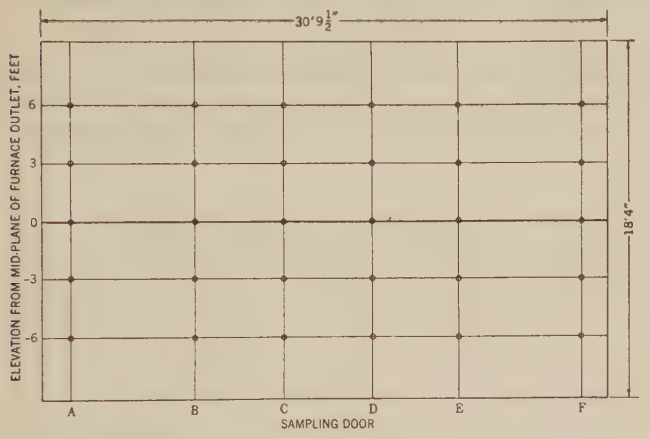

Fig. 2 Distribution of Sampling Points at Furnace Outlet

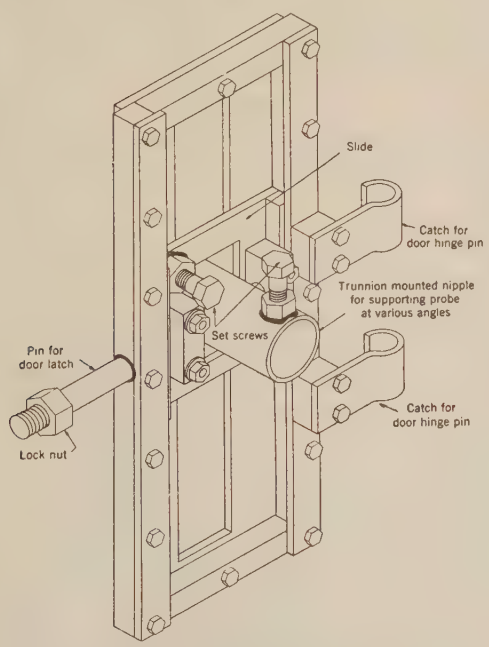

Fig. 3 Lancing-Door Insert for Supporting Water-Cooled High-Velocity Thermocouple Probe

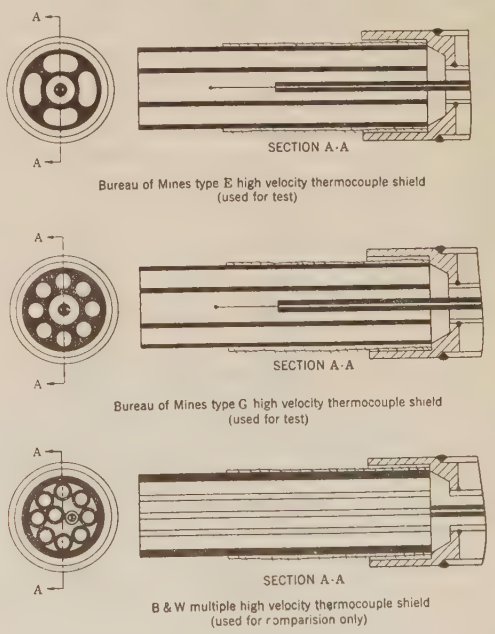

Fig. 4 Radiation Shields for High-Velocity Thermocouple

measurements required for the committee's investigation. The survey at the furnace outlet usually required less than 3 hr.

Methods of Calculation. (*a*) *Temperature and Gas-Composition Data.* Because the sampling points are quite uniformly distributed over the furnace-outlet area, simple numerical averages were calculated of the observed temperature and oxygen-concentration data. These averages, with appropriate corrections, were then used in all subsequent calculations, as previous considerations[4] had shown that more rigorous treatment can rarely be justified.

(*b*) *Furnace Heat Balance.* The heat absorption in the furnace is calculated as the difference between the net heat available in the furnace and the heat lost from the furnace in the products of combustion, and by radiation and convection from the furnace casing. The net heat available in the furnace is the sum of the low-heat value of the fuel fired (corrected for unburned combustible) and the sensible heat in the preheated air. Combustible losses were calculated from the analysis of the fly ash, the fly ash concentration, and the calculated quantities of the gases at the entrance to the Cottrell precipitator. The sensible heat in the preheated air was calculated from a heat balance on the air heaters, employing the known temperatures of the gas and air streams entering and leaving the air heaters, the average composition of the gas entering the air heater, and an assumed value for the air leakage in the preheater equal to 5 per cent by weight of the gas entering the heater.[5]

The enthalpy of the furnace-outlet gas was calculated from the quantities of the respective gases at the furnace outlet (computed from the gas composition and corrected fuel analysis), and the heat contents of the individual gases at the average temperature of the furnace-outlet gas, obtained from the tables of Heck.[6]

For the purpose of these calculations it was assumed that all the ash left the furnace at the temperature of the gases; the heat content was calculated using a mean specific heat of 0.27 Btu per lb deg F. The heat loss from the furnace casing was taken as one half that of the entire unit as given by the ABMA Standard Radiation Loss Chart.

Results of Tests

Description of Tests. The operating data and the results obtained in the fifteen tests are summarized in Table 1. The tests are divided into three groups; group 1, consisting of eight tests at full load, numbers 15, 15A, 16, 17, 18, 19, 21, and 22, was made to determine the effect on furnace heat absorption of variations of excess air and secondary-air vane settings at the test load. Group 2, consisting of three tests at three-quarters load, numbers 24, 25, and 26, was made to determine the effect of secondary-air vane settings at the test load; and group 3, consisting of four tests at half-load, numbers 27, 28, 29, and 30, was made to determine the effect of the number and location of the burners, at the test load. The fuel burned in these tests consisted of a quite uniform mixture of high-volatile C West Kentucky coals. There was little variation in coal composition from test to test, as shown in Table 1.

Temperature and Gas Composition at the Furnace Outlet. Of considerable interest, in addition to the calculated furnace heat absorption, is the distribution of the temperature and composition of the gases at the furnace outlet. These data are given in Tables 2 and 3, respectively. The temperature data in Table 2 are the values observed with the shields used in the particular test; for the heat-absorption calculations, the averages of these values were corrected to the B&W MHVT basis and for lead-junction errors as shown in Table 4. The gas compositions in Table 3 are expressed as per cent excess air, as possibly affording more familiar and representative values than the oxygen percentages actually observed. A recent discussion[4] showed that these values are quite representative of the average conditions for which the tests were made, and, when plotted on a map of the furnace outlet, yield consistent and significant distribution patterns. This is illustrated in Figs. 5 and 6, which are distribution plots of the temperature and composition of the gas at the furnace outlet, respectively, for test 22.

These plots demonstrate some of the outstanding characteristics of the type of firing used in the subject boiler. One of these is the considerable spread of temperature of the gases at the furnace outlet, compared to the spread in gas composition. Thus the gas at sampling point D+6, excess air 33.7 per cent, leaves the furnace at 1920 F, whereas the gas at sampling point D—6, excess air 32.9 per cent, or practically the same as that of the gas at D+6, leaves the furnace at 2320 F. It is evident that the coal-air mixtures from which these streams of gases originated were quite similar, but had considerably different experiences in traversing the furnace volume from the burner to the furnace outlet. The gas leaving the furnace at D+6 has lost considerably more heat to the walls than the gas leaving the furnace at D—6; this is probably due to a longer residence time in the furnace, and probably a lower average velocity in the furnace. This is in accord with visual observations of the velocity of the gases leaving

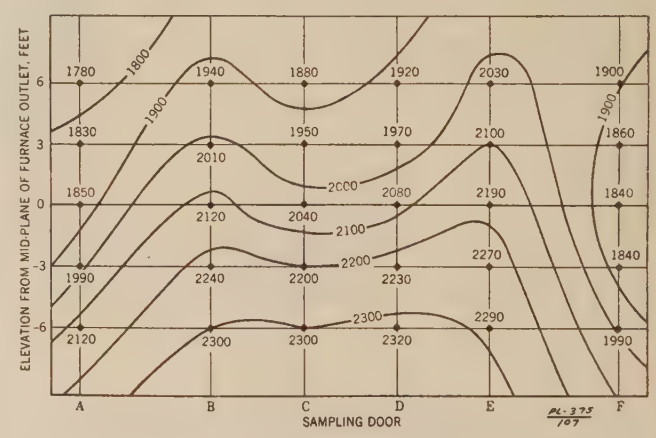

Fig. 5 Distribution of Temperature, Deg F, at Furnace Outlet, Test No. 22

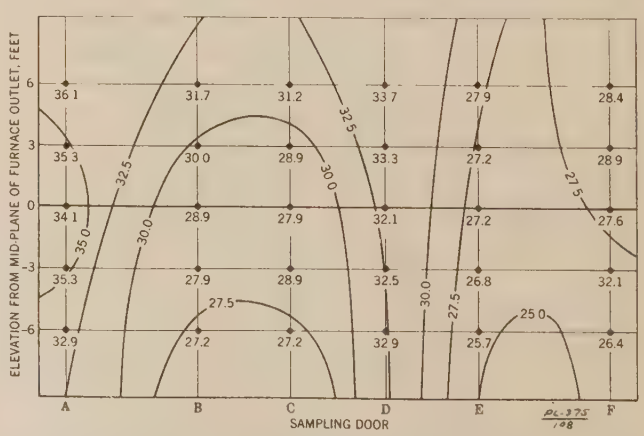

Fig. 6 Distribution of Excess Air, Per Cent, at Furnace Outlet, Test No. 22

[5] "Heat Transfer and Fluid Resistances in Ljungström Regenerative-Type Air Preheaters," by Hilmer Karlsson and Sven Holm, Trans. ASME, vol. 65, 1943, pp. 61–72.

[6] "The New Specific Heats," by R. C. H. Heck, *Mechanical Engineering*, vol. 62, 1940, pp. 9–12.

TABLE 1 SUMMARY OF DATA AND RESULTS. ASME FURNACE HEAT-ABSORPTION TESTS. BOILER NO. 3, PADDY'S RUN STATION, LOUISVILLE GAS & ELECTRIC COMPANY, OCTOBER 20-30, 1948

		October 20 - 30, 1948.															
1	Test number	15	15A	16	17	18	19	21	22	24	25	26	27	28	29	30
2	Date	10-22-48	10-27-48	10-22-48	10-28-48	10-20-48	10-20-48	10-25-48	10-25-48	10-24-48	10-24-48	10-24-48	10-27-48	10-30-48	10-29-48	10-30-48
3	Start of Test[a]	9:59 A.M.	8:11 P.M.	4:09 P.M.	1:57 A.M.	11:56A.M.	6:20 P.M.	4:10 P.M.	10:02A.M.	11:00A.M.	5:57 A.M.	1:11 A.M.	1:49 A.M.	12:44A.M.	1:19 A.M.	6:08 A.M.
4	End of Test[b]	1:15 P.M.	11:44P.M.	7:20 P.M.	5:15 A.M.	3:46 P.M.	10:12P.M.	7:19 P.M.	1:28 P.M.	1:25 P.M.	9:06 A.M.	4:03 A.M.	4:44 A.M.	4:07 A.M.	4:48 A.M.	9:22 A.M.
5	Corrected steam flow, M lb per hr	625.4	625.9	625.3	628.1	624.2	623.7	626.1	623.4	469.1	459.9	464.3	331.7	329.8	331.0	329.1
6	Corrected feed water flow, M lb per hr	626.4	627.5	625.4	627.8	625.3	624.6	628.6	623.1	473.6	471.2	470.4	347.4	345.8	347.6	343.0
7	Superheater outlet header pressure, psig	882	876	878	875	885	884	882	890	876	878	883	888	888	878	885
8	Final Steam Temperature, F	899	893	902	900	897	895	900	901	892	898	901	861	852	837	856
9	Number of burners used and arrangement	8[c]	8[c]	8[c]	8[c]	8[c]	8[c]	8[c]	8[c]	8[c]	8[c]	8[c]	8[c]	4-Upper[e]	4-Lower[f]	4-Normal[g]
10	Secondary air vane position, percent open	40	40	60	50	40	60	45	60	35	50	65	30	50	50	50
11	Coal feed rate, as fired weight, lb per hr	69,130	65,780	71,870	64,360	67,890	68,830	67,170	66,640	52,270	51,790	52,370	37,710	36,680	36,870	36,280
	Coal, proximate analysis, per cent as fired															
12	Moisture	10.7	8.4	11.0	7.8	9.8	11.6	8.4	8.9	9.5	9.1	9.1	9.2	8.4	8.7	8.1
13	Volatile matter	33.8	34.2	32.5	36.6	35.2	33.2	35.0	36.0	34.4	35.0	33.5	35.1	35.3	34.3	34.9
14	Fixed carbon	43.3	44.8	41.0	44.2	41.5	41.4	42.8	42.4	41.7	42.1	42.7	43.5	44.2	44.5	45.7
15	Ash	12.2	12.6	15.5	11.4	13.5	13.8	13.8	12.7	14.4	13.8	14.7	12.2	12.1	12.5	11.3
	Coal, ultimate analysis, per cent as fired															
16	Hydrogen	5.4	5.2	5.2	5.3	5.3	5.4	5.1	5.3	5.2	5.2	5.2	5.2	5.2	5.2	5.3
17	Carbon	61.0	62.5	58.1	64.1	61.0	59.2	61.8	62.0	59.3	61.0	60.4	62.3	62.5	62.3	63.5
18	Nitrogen	1.3	1.2	1.2	1.3	1.3	1.2	1.2	1.3	1.3	1.2	1.2	1.2	1.2	1.2	1.3
19	Oxygen	16.7	14.1	16.5	13.7	15.1	16.6	14.2	15.1	14.6	14.6	14.2	15.2	15.0	14.5	14.6
20	Sulfur	3.4	4.4	3.5	4.2	3.8	3.8	3.9	3.6	5.2	4.2	4.3	3.9	4.0	4.3	4.0
21	High heating value, as fired, Btu per lb	10,960	11,260	10,430	11,610	10,960	10,640	11,120	11,190	10,770	10,990	10,870	11,200	11,320	11,250	11,470
22	Grindability, Hardgrove index	63	62	64	62	62	64	64	61	67	62	59	60	66	64	63
	Ash cone fusion temp., F (ASTM)															
23	I.D.T.	2000	1970	2050	1920	1940	1900	1970	1940	1930	1940	1940	1940	1970	1970	1950
24	S.T.	2050	2030	2130	1940	2100	2100	2080	2030	1990	2050	2050	2000	2010	2010	2040
25	F.T.	2260	2210	2280	2260	2340	2310	2260	2210	2310	2260	2280	2310	2260	2130	2290
	Pulverized[h] coal fineness															
26	Per cent thru 50 mesh	99.9	99.9	99.9	99.9	99.9	99.9	99.9	99.9	99.9	99.9	99.9	100.0	100.0	99.9	99.8
27	Per cent thru 100 mesh	97.8	97.9	98.0	98.3	98.2	98.0	97.9	98.1	98.8	98.7	98.6	99.2	98.9	98.5	97.4
28	Per cent thru 200 mesh	86.3	88.9	87.2	89.1	88.4	87.9	88.3	88.4	91.0	90.9	90.4	92.4	92.2	91.0	85.9
29	Average temperature of gases at furnace outlet, F (MHVT)[i]	2020	2070	2045	2065	2045	2120	2015	2095	1885	1900	1890	1755	1740	1690	1730
	Average composition of gases at furnace outlet, percent dry gas[j]															
30	$CO_2 + SO_2$	14.67	14.60	14.55	14.31	15.52	15.40	13.87	13.88	14.81	14.64	14.48	14.67	14.84	14.69	14.69
31	O_2	4.04	4.28	4.31	4.48	3.12	3.16	4.94	5.00	3.81	4.10	4.24	4.12	3.86	4.03	3.82
32	N_2	81.29	81.12	81.14	81.21	81.36	81.45	81.19	81.12	81.38	81.26	81.28	81.21	81.30	81.28	81.29
33	Excess air at furnace outlet, per cent	23.0	24.8	25.0	26.2	16.9	17.0	29.7	30.2	21.4	23.4	24.5	23.6	21.7	23.0	21.5
34	Dry air at furnace outlet, lb per lb coal as fired	10.53	10.87	10.09	11.37	9.97	9.75	11.30	11.29	10.27	10.58	10.62	10.75	10.65	10.77	10.79
35	Wet gas at furnace outlet, lb per lb coal as fired	11.42	11.77	10.96	12.27	10.83	10.61	12.17	12.19	11.12	11.46	11.49	11.63	11.52	11.66	11.68
	Average composition of gases at air preheater inlet, per cent dry gas[k]															
36	$CO_2 + SO_2$	13.75	13.72	13.76	13.55	14.74	14.44	13.20	13.27	14.05	13.96	13.80	13.89	13.92	13.89	13.86
37	O_2	5.11	5.28	5.22	5.37	4.03	4.25	5.70	5.70	4.68	4.89	5.01	5.02	4.94	4.94	5.01
38	N_2	81.14	81.00	81.02	81.08	81.23	81.31	81.10	81.03	81.27	81.15	81.19	81.09	81.14	81.17	81.13
39	Excess air at air preheater inlet, per cent	31.1	32.6	32.0	33.2	22.9	24.6	36.1	36.1	27.7	29.3	30.3	30.4	29.6	29.7	30.2
40	Dry air at air preheater inlet, lb per lb coal as fired	11.21	11.56	10.65	11.99	10.48	10.38	11.86	11.80	10.81	11.08	11.13	11.34	11.33	11.38	11.57
41	Wet gas at air preheater inlet, lb per lb coal, as fired	12.11	12.45	11.53	12.90	11.35	11.24	12.73	12.70	11.67	11.96	12.00	12.23	12.21	12.27	12.47
42	Average temperature of gas entering air preheater, F.	651	663	656	661	635	649	667	671	587	592	590	527	517	514	520
43	Average temperature of gas leaving air preheater, F.	316	317	321	315	312	313	313	319	305	305	305	308	306	306	306
44	Average temperature of air entering air preheater, F.	91	92	96	87	89	87	87	81	83	81	83	79	84	81	80
45	Average temperature of air leaving air preheater, F.	576	587	585	583	565	565	582	589	537	541	539	503	495	493	495
46	High heating value of coal fired, kB per hr[l]	757,700	740,700	749,600	747,200	744,100	732,400	746,900	745,700	568,300	569,200	569,300	422,400	415,200	414,800	416,100
47	Low heating value of coal fired, kB per hr	723,300	709,200	715,200	715,800	710,900	698,100	715,400	713,200	543,100	544,400	544,200	404,300	397,600	397,100	398,400
48	Sensible heat above 80 F in air kB per hr[m]	72,000	72,700	71,900	72,900	63,500	66,300	76,900	74,800	43,300	44,200	44,700	24,500	23,200	23,000	23,500
49	Total net heat supplied in air and fuel, kB per hr	795,300	781,900	787,000	788,700	774,400	764,400	792,300	788,000	586,400	588,500	588,900	428,800	420,800	420,100	421,900
50	Heat loss in furnace due to unburned carbon, kB per hr	300	100	600	300	800	1,700	100	000	300	400	200	400	1,400	600	1,100
51	Heat loss by radiation from furnace, kB per hr[n]	1,300	1,300	1,300	1,300	1,300	1,300	1,300	1,300	1,300	1,300	1,300	1,300	1,300	1,300	1,300
52	Total heat loss from unburned carbon and radiation, kB per hr	1,500	1,400	1,800	1,600	2,100	2,900	1,400	1,300	1,600	1,500	1,500	1,600	2,600	1,900	2,300
53	Net heat available in furnace, kB per hr	793,700	780,600	786,200	787,200	772,400	761,500	791,000	786,800	584,900	586,900	587,400	427,100	418,200	418,300	419,600
54	Sensible heat above 80 F in wet gas at furnace outlet, kB per hr	429,300	430,900	434,500	436,000	405,700	420,600	440,700	458,500	294,200	300,000	302,400	202,200	193,000	189,800	192,400
55	Sensible heat above 80 F in ash and fly ash leaving furnace, kB per hr	4,400	4,600	5,900	3,900	4,900	5,200	4,800	4,600	3,700	3,500	3,800	2,100	2,000	2,000	1,800
56	Total sensible heat above 80 F in products of combustion, kB per hr	433,700	435,400	440,400	439,900	410,600	425,800	445,600	463,100	297,900	303,500	306,200	204,300	195,000	191,900	194,200
57	Heat absorbed in furnace, kB per hr	360,000	345,100	344,800	347,200	361,800	335,700	345,400	323,700	287,000	283,400	281,300	222,800	223,200	226,400	225,400
58	Furnace heat absorption efficiency, per cent	45.4	44.2	43.9	44.1	46.8	44.1	43.7	41.1	49.1	48.3	47.9	52.2	53.4	54.1	53.7
59	Total net heat available in furnace, kB per hr and ft² [o]	89.3	87.8	88.4	88.6	86.9	85.7	89.1	88.6	65.8	66.0	66.1	48.0	47.1	47.1	47.2
60	Heat absorption in furnace, kB per hr and ft² [o]	40.6	38.9	38.9	39.1	40.7	37.8	38.9	36.4	32.3	31.9	31.7	25.1	25.1	25.5	25.4

a/ Central standard time; time of last coal scale reading preceding period of test surveys
b/ Central standard time; time of first coal scale reading following period of test surveys
c/ Main and auxiliary burners
d/ Main burners only
e/ Main and auxiliary burners; two mills
f/ Main and auxiliary burners; two mills
g/ Two inner upper, two outer lower main and auxiliary burners, north mill only
h/ Determined by Foster-Wheeler Corp.
i/ Average of thirty determinations, corrected to B&W MHVT basis, see table 4.
j/ Average of thirty determinations
k/ Average of twelve determinations
l/ This and subsequent figures were rounded after calculation
m/ Calculated from heat balance on air heater
n/ One half full load loss for entire unit as given by ABMA Standard Radiation Chart.
o/ Based on total projected heat receiving surface of 8,884 ft²

Additional data are available on fly ash analysis and distribution, and humidity of combustion air. For tests 16, 19, 24, 30, the forms of sulfur and carbonate in coal were determined, as well as the ash cone softening temperatures in an oxidizing atmosphere.

TABLE 2 OBSERVED[a] GAS TEMPERATURES DEG F, AT FURNACE OUTLET, ASME FURNACE HEAT-ABSORPTION TESTS, BOILER NO. 3, PADDY'S RUN STATION

Test No.[b]		15	15A	16	17	18	19	21	22	24	25	26	27	28	29	30
Door[c]	Position[c]															
A	+6	1740	1710	1820	1730	1780	1760	1740	1780	1600	1590	1660	1510	1440	1450	1450
	+3	1880	1750	1770	1880	1950	1870	1880	1830	1690	1700	1670	1500	1610	1480	1460
	0	2060	1910	1750	2020	2210	2010	2060	1850	1930	1850	1710	1640	1710	1580	1550
	-3	2130	1960	1880	2130	2270	2040	2090	1990	1990	1980	1800	1750	1740	1660	1600
	-6	2110	1970	2050	2200	2300[d]	2160	2140	2120	2020	1940	1970	1870	1750	1750	1800
B	+6	1990	2030	1980	1990	2040	1890	1950	1940	1850	1860	1800	1710	1570	1650	1630
	+3	2010	2070	2070	2030	2090	2000	1960	2010	1870	1880	1870	1770	1610	1680	1700
	0	2030	2150	2160	2100	2150	2100	2010	2120	1930	1940	1960	1840	1670	1750	1770
	-3	2080	2150	2260	2180	2190	2210	2070	2240	1990	2030	2010	1900	1750	1810	1840
	-6	2160	2230	2360[d]	2170	2250	2340	2160	2300	2090	2180	2160	1980	1860	1870	1840
C	+6	1890	1970	1940	1950	1910	1900	1890	1880	1800	1760	1710	1650	1550	1590	1580
	+3	1880	1970	1980	1940	1930	1980	1880	1950	1820	1790	1760	1650	1590	1640	1630
	0	1940	2060	2050	2000	2020	2050	1970	2040	1860	1810	1810	1720	1660	1710	1680
	-3	2070	2170	2180	2070	2130	2220	2030	2200	1920	1920	1920	1790	1770	1780	1760
	-6	2190[d]	2270	2350[d]	2190	2240	2350[d]	2150	2300	2000	2130	2090	1970	1900	1860	1860
D	+6	1850	1890	1770	1900	1860	1970	1830	1920	1730	1770	1690	1620	1610	1570	1620
	+3	1900	1950	1830	1940	1930	2060	1870	1970	1750	1870	1710	1650	1620	1650	1650
	0	1960	2070	1930	2010	1980	2150	1970	2080	1840	1960	1790	1700	1670	1720	1690
	-3	2090	2160	2050	2080	2060	2310	2040	2230	1910	2050	1830	1780	1800	1800	1780
	-6	2230	2230	2250	2210	2150	2330	2180	2320	2010	2180	1940	1920	1950	1860	1870
E	+6	1840	1950	1850	1870	1790	2020	1840	2030	1740	1660	1820	1630	1660	1570	1660
	+3	1880	2030	1940	1930	1850	2070	1900	2100	1810	1700	1910	1690	1720	1630	1700
	0	2010	2120	2060	2010	1920	2180	2030	2190	1910	1750	2030	1750	1790	1690	1790
	-3	2080	2220	2150	2110	2060	2270	2120	2270	1960	1820	2100	1800	1870	1730	1850
	-6	2200	2190	2260	2300	2200	2350	2190	2290	2040	1870	2120	1820	1970	1800	1870
F	+6	1740	1810	1720	1810	1710	1830	1740	1900	1630	1700	1740	1580	1520	1420	1590
	+3	1760	1790	1740	1800	1730	1810	1780	1860	1630	1710	1700	1560	1610	1480	1620
	0	1800	1810	1780	1830	1680	1800	1790	1840	1630	1690	1650	1530	1690	1490	1580
	-3	1840	1990	1880	1900	1750	1900	1830	1840	1680	1810	1750	1540	1730	1460	1610
	-6	1910	2130	2070	2050	1900	2130	1970	1990	1800	1930	1900	1620	1760	1480	1700
Average[a]		1975	2024	1997	2011	1999	2069	1969	2046	1848	1861	1852	1715	1705	1654	1691

a/ Uncorrected; for corrections see Table 4.

b/ For test conditions, see Table 1.

c/ For location at furnace outlet, see Figure 2.

d/ Data not taken; extrapolated value

the furnace, being greatest at the bottom of the outlet and lowest at the top. The effect of this behavior on the radiation heat transfer in the furnace will be considered in a later part of this paper.

Detailed distribution data of the type shown in Figs. 5 and 6 assist in understanding ash deposition and slagging of the screen and superheater. The wide spread in temperatures at the furnace outlet demonstrates the readiness with which excessive temperatures can exist, even though the mean value is less than some assumed safe limit.

The distribution plots for the other tests are not given, but may readily be constructed from the data in Tables 2 and 3.

Furnace Heat Absorption. For readier reference, a condensed summary of the test conditions and results is presented in Table 5 in which each test is given a reference letter. In Fig. 7 the observed furnace heat-absorption efficiency has been plotted against excess air for the various combinations of the other test variables. The furnace heat-absorption efficiency is used in Fig. 7 because it is less sensitive than furnace heat absorption to the unavoidable variations in the net heat available in the tests at each particular boiler load. Lines have been drawn in Fig. 7 indicating the effect of excess air on furnace heat-absorption efficiency, for the various settings of the secondary-air vanes at full and three-quarters load; and for the various locations and number of burners used, at half-load. At full load there are enough experimental points to establish these lines, and, except for points B and C, tests 15A and 16, respectively, the relationships are quite definite. At three-quarters and half-load, the variations of furnace heat-absorption efficiency with excess air can only be inferred; these lines (dashed) have been given successively lower slopes as the load decreases, in accord with the behavior found in another furnace.[3]

TABLE 4 CORRECTIONS OF OBSERVED AVERAGE TEMPERATURE TO B&W MHVT BASIS. ASME FURNACE HEAT-ABSORPTION TESTS. BOILER NO. 3, PADDY'S RUN STATION, LOUISVILLE GAS & ELECTRIC COMPANY. OCTOBER 20–30, 1948.

Observed average temp., deg F	Total correction (to MHVT basis and for lead-junction error), deg F: Type E shield	Type G shield
1600	25	31
1700	30	37
1800	35	43
1900	41	50
2000	46	56
2100	51	62

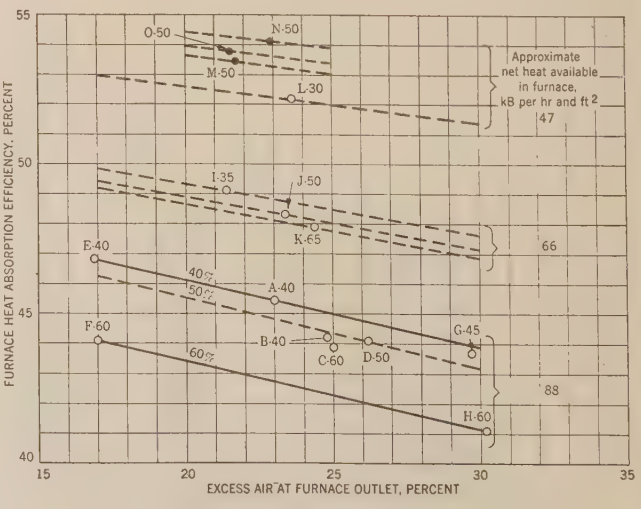

FIG. 7 FURNACE HEAT-ABSORPTION EFFICIENCY AS AFFECTED BY EXCESS AIR, NET HEAT AVAILABLE IN FURNACE, SECONDARY-AIR VANE SETTINGS, AND NUMBER AND LOCATION OF BURNERS USED

(O, Eight burners, ●, four burners; letter designates test, see Table 5; number after letter is secondary-air vane opening, per cent.)

TABLE 3 OBSERVED GAS COMPOSITION AT FURNACE OUTLET, EXPRESSED AS PER CENT EXCESS AIR, ASME FURNACE HEAT ABSORPTION TESTS. BOILER NO. 3, PADDY'S RUN STATION

Test No.[a]		15	15A	16	17	18	19	21	22	24	25	26	27	28	29	30
Door[b]	Position[b]															
A	+6	31.9	30.6	28.2	36.7	23.0	25.7	39.0	36.1	29.2	34.6	36.4	31.1	31.1	33.9	25.6
	+3	28.3	27.7	28.2	32.5	20.5	25.3	35.4	35.3	27.4	30.0	35.7	31.3	25.3	35.2	24.9
	0	26.4	27.7	29.2	30.2	18.5	23.7	32.6	34.1	22.2	28.0	32.8	28.6	24.9	32.3	26.1
	-3	27.7	28.5	29.2	28.8	23.4	24.1	30.9	35.3	22.6	27.0	31.6	28.6	24.2	28.8	27.2
	-6	26.8	27.2	27.3	32.1	24.4	23.7	34.2	32.9	21.6	27.4	25.5	26.9	24.6	30.7	24.2
B	+6	25.4	27.2	26.4	30.2	16.7	19.2	32.6	31.7	20.5	25.5	27.4	23.8	25.3	28.4	21.7
	+3	24.6	25.9	25.0	27.6	16.7	17.8	29.6	30.0	21.2	24.7	26.1	23.8	26.7	26.6	22.4
	0	26.8	25.5	24.1	28.3	16.4	17.4	30.0	28.9	21.2	24.4	25.0	23.0	23.1	24.8	22.8
	-3	25.4	26.4	23.2	26.7	16.9	17.8	29.2	27.9	20.5	22.7	24.7	23.8	23.1	26.2	20.4
	-6	26.4	26.4	23.7	27.6	17.4	17.1	27.6	27.2	19.8	20.8	23.7	23.0	23.6	25.5	21.7
C	+6	26.8	27.2	27.3	28.6	20.0	18.1	30.9	31.2	22.6	27.4	25.5	25.4	25.6	25.5	21.0
	+3	26.8	25.9	24.6	27.6	17.4	16.7	30.4	28.9	23.3	25.0	27.0	26.9	24.9	24.1	21.0
	0	25.4	25.9	25.0	27.2	16.0	17.4	27.6	27.9	22.2	25.5	25.0	24.6	24.2	22.7	21.7
	-3	22.8	24.3	25.0	26.4	15.7	14.4	27.6	28.9	20.5	23.6	25.0	25.0	23.1	24.1	23.6
	-6	23.2	25.5	25.0	26.4	16.4	16.0	27.6	27.2	19.5	19.8	21.2	23.0	20.6	24.1	22.0
D	+6	20.2	26.7	25.8	26.7	17.6	16.4	30.9	33.7	21.9	21.2	23.3	23.0	22.0	24.4	20.4
	+3	21.5	23.9	23.7	24.7	15.7	14.6	28.8	33.3	22.6	20.8	24.0	22.2	19.9	22.0	21.0
	0	19.4	22.7	22.8	23.6	15.7	13.8	28.4	32.1	20.5	18.8	22.9	21.9	21.0	22.0	22.4
	-3	19.8	23.9	21.5	25.1	15.3	11.6	28.4	32.5	19.8	18.2	22.6	23.0	18.2	20.9	21.0
	-6	19.8	23.1	21.5	24.3	15.0	14.6	28.8	32.9	18.8	16.8	18.8	22.7	17.1	20.6	23.6
E	+6	20.6	23.5	25.4	23.1	15.3	15.7	28.0	27.9	19.5	22.6	19.6	22.7	22.0	19.2	19.0
	+3	20.6	22.7	22.8	23.1	14.6	16.0	27.6	27.2	20.5	21.2	21.2	21.9	19.0	18.2	20.6
	0	18.1	22.7	22.3	20.8	13.8	13.0	27.6	27.2	20.5	19.6	20.5	20.4	17.9	17.6	19.9
	-3	20.6	21.6	24.1	21.1	14.0	14.0	26.4	26.8	18.6	18.8	19.2	20.4	17.4	14.8	19.3
	-6	18.1	21.9	21.9	23.5	14.6	14.6	26.0	25.7	16.6	19.2	18.5	16.7	15.1	15.7	17.4
F	+6	20.6	23.9	26.8	25.5	15.7	16.0	30.0	28.4	21.9	24.0	23.3	20.7	24.2	19.9	19.3
	+3	20.6	22.4	25.4	23.9	14.0	16.0	29.2	28.9	21.6	24.4	22.6	21.5	20.6	17.3	18.6
	0	20.6	23.1	25.8	23.1	16.7	14.6	29.2	27.6	23.6	25.5	23.6	21.5	17.9	16.6	21.0
	-3	20.6	21.6	25.0	22.7	14.6	16.0	30.9	32.1	22.2	24.4	22.6	21.1	17.9	19.2	19.8
	-6	20.6	18.9	24.6	19.3	15.0	14.4	26.8	26.4	21.9	23.6	18.5	21.9	17.9	15.7	18.6

a/ For test conditions, see Table 1.

b/ For location at furnace outlet, see Figure 2.

From Fig. 7 it will be noted that the effect of secondary-air vane setting is quite pronounced at full load; a change in the setting from 60 to 40 per cent open at 17 per cent excess air increases the furnace heat-absorption efficiency from 44.1 to 46.8 per cent. Also, the effect of secondary-air vane setting is considerably reduced at three-quarters load; a change in the setting from 65 to 35 per cent open, at 23 per cent excess air, increases the furnace heat-absorption efficiency by only 0.6 per cent. The effect at half-load may be presumed to be negligible. Further, the effect of secondary-air vane setting at full load appears to be quite independent of excess air, the change in furnace heat-absorption efficiency due to change in secondary-air vane setting from 60 to 40 per cent open being 2.7, 2.7, and 2.7 per cent at 17, 23, and 29 per cent excess air, respectively. Similarly, the effect of change of excess air, at constant secondary-air vane opening, appears to be independent of the opening of the secondary-air vanes. Figs. 8 and 9 are similar plots of the experimental results showing the furnace heat absorption and the average temperature of the furnace-outlet gases, respectively.

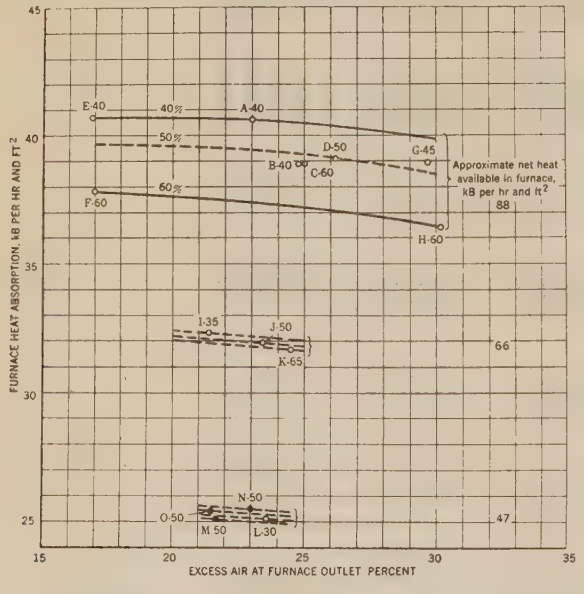

FIG. 8 FURNACE HEAT ABSORPTION AS AFFECTED BY EXCESS AIR, NET HEAT AVAILABLE IN FURNACE, SECONDARY-AIR VANE SETTINGS, AND NUMBER AND LOCATION OF BURNERS USED

(O, Eight burners, ●, four burners; letter designates test, see Table 5; number after letter is secondary-air vane opening, per cent.)

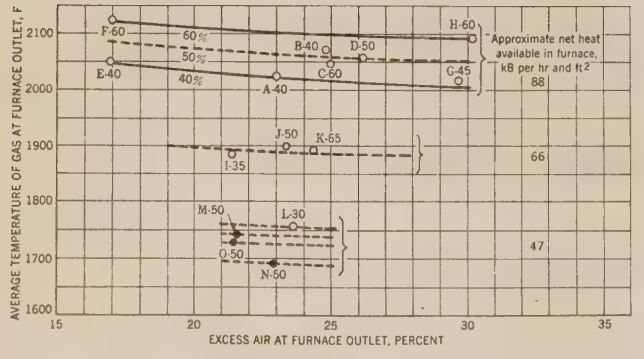

FIG. 9 AVERAGE TEMPERATURE OF FURNACE-OUTLET GAS AS AFFECTED BY EXCESS AIR, NET HEAT AVAILABLE IN FURNACE, SECONDARY-AIR VANE SETTINGS, AND NUMBER AND LOCATION OF BURNERS USED

(O, Eight burners, ●, four burners; letter designates test, see Table 5; number after letter is secondary-air vane opening, per cent.)

The rather complicated relationships between the variables cannot be represented simply, and a number of curves are required. Fig. 10 shows the effect of net heat available in the furnace on furnace heat absorption for three different values for the excess air at the furnace outlet, all at one setting of the secondary-air vanes, 40 per cent open. The curve for 23 per cent excess air is drawn with a full line, because all the necessary data are available. The effect of excess air is known only at full loads; therefore the curves for 17 and 29 per cent excess air are drawn with dashed lines.

The upper part of Fig. 10 shows the effect of secondary-air vane opening. The corrections to the furnace heat absorption for secondary-air vane settings other than 40 per cent open are plotted as a function of net heat available in the furnace for secondary-air vane openings of 50 and 60 per cent. Since the effect of secondary-air vane openings is independent of excess air, at least at high loads, Fig. 8, only one set of correction curves is required.

The relationships shown in Fig. 10 apply only to operation

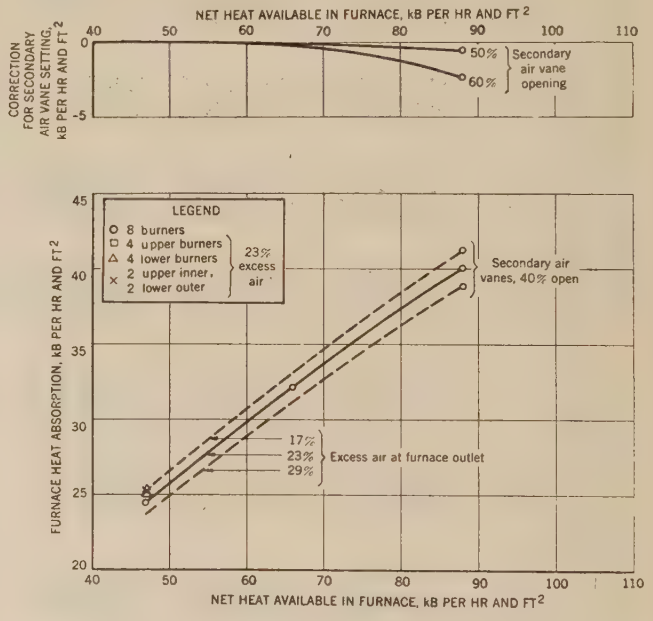

FIG. 10 FURNACE-PERFORMANCE CHARACTERISTICS

with eight burners. The effect of operation with four burners is shown on the lower part of the plot by the additional points representing the results for various combinations of the burners.

The qualitative relationship of all the variables is best conveyed by the isometric three-variable plot in Fig. 11, which readily shows the decrease in furnace heat absorption with increased excess air at all loads, the almost linear increase in furnace heat absorption with increase in net heat available in the furnace, between 47 and 88 kB per hr and ft², and the decrease of furnace heat absorption with increase in the opening of the secondary-air vanes, this effect being independent of excess air, but increasing rapidly with net heat available in the furnace, between 66 and 88 kB per hr and ft².

CORRELATION OF TEST RESULTS

The correlation of the test conditions and results so far given is purely empirical, without reference to the mechanism for heat transfer in the furnace. The information presented, though as comprehensive as the data on which it is based, nevertheless lacks generality because no account has been taken of the fundamental processes involved. Because of the complexity of the problem,

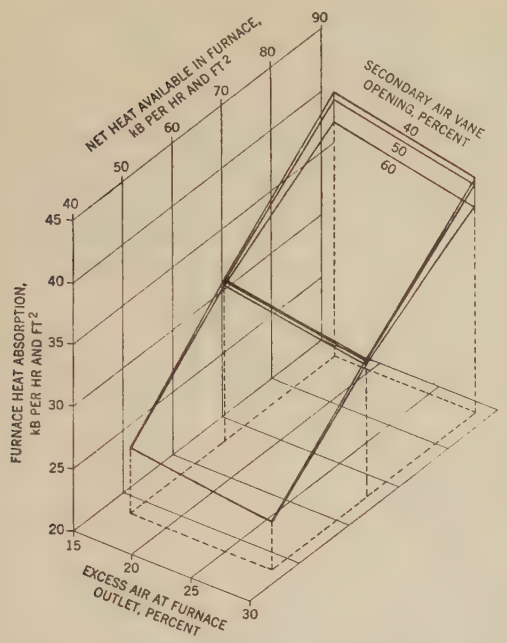

FIG. 11 THREE-VARIABLE REPRESENTATION OF FURNACE-PERFORMANCE CHARACTERISTICS FOR EIGHT-BURNER OPERATION

progress in fundamental analysis has been slow, and confined largely to semiempirical correlations based either on the average temperature of the gases at the furnace outlet,[7,8] or on a radiant mean temperature between the adiabatic temperature and the temperature of the gases leaving the furnace.[9] Of these procedures the first is more convenient, and is applied to the data of this investigation in Fig. 12 in which the furnace heat absorption, kB per hr and ft², has been plotted against the fourth power of the average temperature of the gases leaving the furnace, deg R; the letter and point symbols correspond to Table 5. For comparison, line *Z-Z* shows the calculated black-body radiation from a source at the average temperature of the furnace-outlet gas, to the furnace walls at a constant temperature. In view of the cleanliness of the furnace walls, the latter temperature has been taken as 1050 R.

It will be seen that the unit heat transfer, based on the heat-receiving surface, is considerably less than that of a black body at the temperature of the furnace outlet gas, line *Z-Z*. Expressed in terms of an equivalent gray body at the temperature of the furnace-outlet gases, the heat transfer corresponds to that from a source with an emissivity of about 0.7, for the low-load tests and decreasing at high loads. It is further evident that if the correlation had been based on a radiation mean temperature, according to Blizard,[9] the apparent emissivity of the source would be still lower. For one test at high load an approximate value of 0.28 was calculated for the apparent emissivity of the source on this basis. This is in sharp contrast to the high emissivities predicted from the work of Sherman[10] for flames having the dimensions of the subject furnace. As an example, Sherman predicted that even after combustion was essentially complete, the gas and suspended ash from Illinois coal would have total emissivities of 0.83 and 0.97 for 12 and 20-ft thicknesses, respectively.

The source of this discrepancy is found readily. The high-temperature gases do not fill the entire furnace volume, and not only is the exposed area of the radiation source less than that of the heat-receiving surface on which the unit heat transfer is calculated, but the mean beam lengths for radiation probably are considerably lower than would be calculated from the furnace dimensions. The ratio of area of flame to area of wall may be estimated as follows: As a first approximation, assuming wall emissivity of unity and flame emissivity equal to flame absorptivity, the net radiation heat transfer from flame to furnace walls, Btu per hr, may be written as

$$Q = \sigma \epsilon_F A_F (T_F^4 - T_W^4)$$

The subscripts F and W denote the flame and furnace wall, respectively, and

σ = radiation constant
A = area (of envelope for flame; of projected area for wall surface)
T = radiant mean temperature, abs
ϵ = emissivity

This equation may be rewritten as

$$Q = \sigma A_W \epsilon_F \frac{A_F}{A_W} (T_F^4 - T_W^4)$$

in which the product $\epsilon_F(A_F/A_W)$ may be considered an apparent emissivity of the flame, ϵ_F', calculated from heat transfer per unit wall area, A_W. From an assumed value of true mean emissivity of the flame, $\epsilon_F = 0.9$, and a value of 0.28 for ϵ_F' previously calculated for one of the high-load tests, A_F/A_W may be obtained as the ratio of $\epsilon_F'/\epsilon_F = 0.28/0.9 = 0.31$. So low an indicated area of the flame, and therefore its volume, must include a significant effect of decreased true mean flame emissivity arising from smaller mean beam lengths, and the true value of A_F/A_W is undoubtedly somewhat higher than the value of 0.31 calculated. For the purposes of the present argument, no further refinement of the calculation is warranted.

Somewhat similar considerations were applied by Mumford and Bice[11] to the analysis of the effect of tilting the burner in a tangentially fired furnace previously studied by the committee. They concluded that multiplication of the observed rates of heat transfer for different inclination of the burners by the ratios of area of heat-receiving surface to area of flame envelope would have brought all the data into line. No estimate was made by them of the apparent emissivity of the flame, but the unit heat transfer based on the average temperature of the furnace-outlet gas was higher in the tangentially fired furnace than in the subject furnace, indicating that the apparent emissivities were higher.

This discussion has of necessity been only semiquantitative, and has undoubtedly exaggerated the true picture; for instance, the flame never achieves the adiabatic temperature. Also, only the general level of heat transfer has been considered; interpretation of the effect of burner adjustments on heat transfer at constant load is still required. So far it can only be concluded that the heat transfer in the furnace is considerably less than theoretically achievable levels.

[7] "An Investigation of Powdered Coal as Fuel for Power-Plant Boilers," by Henry Kreisinger, John Blizard, C. E. Augustine, and B. J. Cross, U. S. Bureau of Mines, Government Printing Office, Washington, D. C., Bulletin 223, 1923.

[8] "Evaluation of Effective Radiant Heating Surface and Application of the Stefan-Boltzmann Law to Heat Absorption in Boiler Furnaces," by H. F. Mullikin, Trans. ASME, vol. 57, 1935, pp. 517–529.

[9] "Absorption of Heat by Walls of a Furnace," by John Blizard, ASME Furnace Performance Factors Pamphlet, May, 1944, pp. 79–82. Bound with Trans. ASME, vol. 66, 1944.

[10] "Burning Characteristics of Pulverized Coals and the Radiation From Their Flames," by R. A. Sherman, *Combustion*, vol. 5, December, 1933, pp. 30–38.

[11] "An Investigation of the Variation of Heat Absorption in a Pulverized-Coal-Fired Water-Cooled Steam Boiler Furnace IV—Comparison and Correlation of the Results of Furnace Heat-Absorption Investigations," by A. R. Mumford and G. W. Bice, Trans. ASME, vol. 70. 1948. pp. 601–614.

TABLE 5 CONDENSED SUMMARY OF OPERATING CONDITIONS AND RESULTS, ASME FURNACE HEAT-ABSORPTION TESTS. BOILER NO. 3, PADDY'S RUN STATION

1	Test number	15	15A	16	17	18	19	21	22	24	25	26	27	28	29		30		
2	Designation	A○	B○	C○	D○	E○	F○	G○	H○	I○	J○	K○	L○	M●	N●		O●		
3	Number and arrangement of burners	8	8	8	8	8	8	8	8	8	8	8	8	4 upper	4 lower	2 inner-upper & 2 outer-lower	8		
4	Burner secondary air vane opening, per cent	40	40	60	50	40	60	45	60	35	50	45	30	50	50		60		
5	Steam generation, M lb per hr	626.4	626.9	625.3	628.1	624.2	623.7	626.1	623.4	459.1	459.9	464.3	331.7	329.8	331.0		329.1		
6	Excess air at furnace outlet, per cent	23.0	24.8	25.0	26.2	16.9	17.0	29.7	30.2	21.4	23.4	24.5	23.6	21.7	23.0		21.5		
7	Net heat available in furnace, kB per hr and ft^2	89.3	87.8	88.4	88.6	86.9	85.7	89.1	88.6	65.8	66.0	66.1	48.0	47.1	47.1		47.2		
8	Heat absorption in furnace, kB per hr and ft^2	40.6	38.9	38.9	39.1	40.7	37.8	38.9	36.4	32.3	31.9	31.7	25.1	25.1	25.5		25.4		
9	Heat absorption efficiency, per cent	46.4	44.2	43.9	44.1	46.8	44.1	43.7	41.1	49.1	48.3	47.9	52.2	53.4	54.1		53.7		
10	Average temperature of gas at furnace outlet, t_o, deg F.	2020	2070	2045	2065	2045	2120	2015	2096	1885	1900	1890	1765	1740	1690		1730		
11	, T_o, deg R.	2480	2530	2505	2515	2506	2580	2475	2555	2345	2360	2350	2215	2200	2150		2190		
12	$\left(\frac{T_o}{1000}\right)^4$	37.8	41.0	39.4	40.0	39.4	44.3	37.5	42.6	30.2	31.0	30.5	24.1	23.4	21.4		23.0		

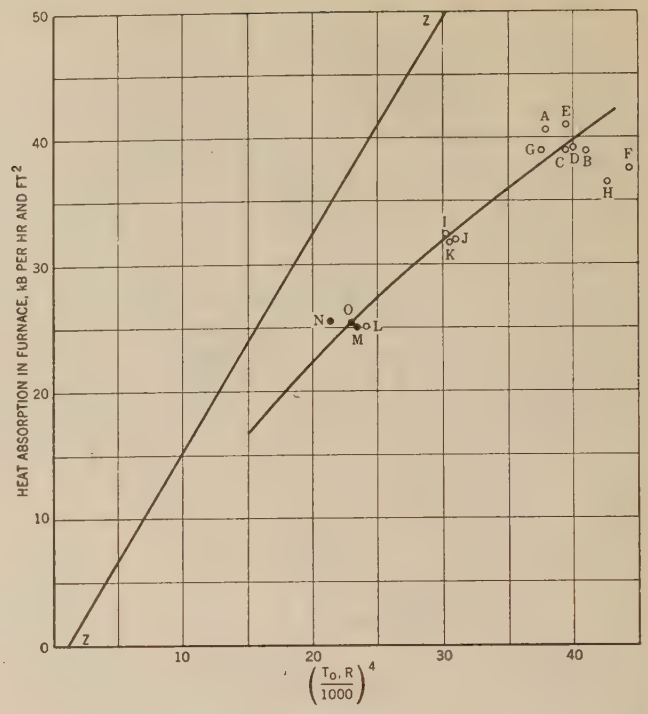

FIG. 12 CORRELATION OF HEAT TRANSFER IN FURNACE WITH FOURTH POWER OF ABSOLUTE TEMPERATURE OF GASES AT FURNACE OUTLET

(○, Eight burners, ●, four burners; letter designates test, see Table 5.

As previously noted, the gases at the furnace outlet display a characteristic temperature distribution which has been attributed to varying velocities of the respective portions of the gas stream in traversing the furnace volume. One of the possible means by which the setting of the secondary-air vanes may affect heat transfer in the furnace is by changing the velocity-distribution patterns in the furnace. That this probably does not occur, however, is seen from examination of the temperature-distribution data. For example, in both tests 18, and 19, 17 per cent excess air, and 40 and 60 per cent secondary-air vane openings, respectively, the average deviation of the temperature of the gases at the furnace outlet from their mean is 150 F. Thus if the distribution of temperature at the furnace outlet is taken as a criterion, the change in burner vane settings does not affect appreciably the velocity distribution of the gases in the furnace. The effect of secondary-air vane settings must be sought in the delayed combustion which occurs at high secondary-air vane openings. Under these conditions heat release is delayed, and thus radiation is decreased, compared to the turbulent bushy flame conditions obtained with lower secondary-air vane openings.

At the lower burning rates, the temperature and the velocity of the gas leaving the furnace are more uniform, as would be expected, because the total residence time of the gases in the furnace is greater. Similarly, because the percentage heat absorption is greater at low loads, the effect of burner adjustments on heat absorption is less pronounced.

Another factor, which should be considered as affecting the temperature distribution at the furnace outlet, is the tendency for ash deposits to be heavier on the rear than on the front wall of the unit, due to the flame-path characteristics. Thus the insulating effect of the ash would produce higher gas temperatures along the rear than along the front wall, and any temperature gradient at the furnace outlet caused by higher gas velocity along the rear wall, which was discussed previously, would be increased further.

The unique characteristics of each of the different methods of firing pulverized coal have long been recognized and need no emphasis here. Indeed, they form an essential basis for the design of the test program of the Furnace Performance Factors Committee. The important fact brought out by the results of this investigation is that detailed consideration must be given to burner location, flame shape, and volume, and all other factors which affect flame radiation, if a rational basis is to be found for predicting the heat absorption in boiler furnaces. The problem is tremendously complicated, and special attention must be given to these details to obtain basic generalizations.

Summary and Conclusions

The absorption of heat in the furnace of the Paddy's Run boiler was measured to provide basic performance data and to determine the relationship between the rate of heat transfer and the observed temperature drop across the furnace-wall tubes. The furnace heat absorption was determined as the difference between the heat input to the furnace, corrected for losses, and the sensible heat in the furnace-outlet gas obtained from measurements of the temperature and composition employing techniques appropriate for furnace testing. The effect on furnace heat absorption of load, excess air, burner setting, and, at low loads, the number and location of the burners, was studied in a series of fifteen tests.

In all tests, the temperature of the gas at the furnace outlet varied considerably with position, being highest at the bottom and lowest at the top. At full load, the spread in temperature exceeded 500 F; at lower loads the spread was somewhat less. In contrast, the composition of the gas at the furnace outlet was considerably more uniform than the temperature. There was little variation of gas composition in any of the tests from the top to the bottom of the outlet, but occasionally nonuniform distribution from side to side. In such cases the excess air was always highest on the left or south side of the furnace. From these observations it is concluded that the variations of the temperature of the gas with position at the outlet originated from variations in the velocity of the gas streams in the furnace. Visual observations of the gas streams did indicate that the velocity of the gas was highest at the bottom of the outlet and decreased toward the top of the outlet. Because of lack of suitable access, no velocity measurements were made to check these observations.

At full load, the furnace heat-absorption efficiency decreased with both increase of excess air, and opening of the secondary-air vane settings. The effect of excess air was independent of the secondary-air vane setting, and the effect of secondary-air vane setting was independent of excess air, over the range of the variables studied. Thus the furnace heat-absorption efficiency decreased about 2.7 per cent for an increase in secondary-air vane opening from 40 to 60 per cent, and decreased about 2.8 per cent for an increase in excess air from 17 to 29 per cent. The corresponding changes in the average temperature of the gases leaving the furnace were about 75 and 30 F, respectively.

At three-quarter load, the furnace heat-absorption efficiency decreased about 0.6 per cent for an increase in secondary-air vane opening from 35 to 65 per cent. The effect of excess air was not determined at this load.

At half-load, only the effect of the number and location of the burners was studied. With eight burners, the secondary-air vanes had to be set at 30 per cent open for good operation; with four burners, the secondary-air vane settings were 50 per cent open. The furnace heat-absorption efficiency was highest when the four lower burners were used; was 0.6 per cent lower when the four upper burners were used; 1.9 per cent lower when all eight burners were used; and about 0.4 per cent lower when the 2 upper inner and 2 lower outer burners were used. The over-all variation in the average temperature of the gases leaving the furnace for the four combinations of burners was about 75 F.

For otherwise constant conditions, furnace heat absorption increases and furnace heat-absorption efficiency decreases as the heat available in the furnace increases. With eight burners, 40 per cent secondary-air vane opening and 23 per cent excess air, the heat absorption increases almost linearly from about 24 kB per hr and sq ft, at 47 kB per hr and sq ft heat available, to about 40 kB per hr and sq ft at 88 kB per hr and sq ft heat available in the furnace. The corresponding furnace heat-absorption efficiencies are approximately 52 and 45 per cent, respectively. The corresponding average temperatures of the gases leaving the furnace were 1755 and 2020 F, respectively.

At low load, the heat transfer in the furnace corresponded to that by radiation from a body having the area of the heat-receiving surface, the average temperature of the furnace-outlet gas, and an emissivity of 0.67. At higher loads, the apparent emissivity decreased. Analysis of the test results indicates that the area of the envelope of hot gases in the furnace must be considerably less than that of the heat-receiving surfaces. A ratio of 0.31, which is probably somewhat low, was calculated for full-load conditions, on the assumption that the coal is burned instantaneously. This, however, is evidently not the case. Indeed, the effect of burner secondary-air vane settings on furnace heat absorption can best be interpreted in terms of the effect on the rate of combustion of the coal.

This investigation has provided detailed knowledge of the properties of the gas leaving the furnace, and of furnace performance for a wide range of significant operating variables. Although the heat-transfer process in the furnace has not been evaluated quantitatively, a beginning has been made toward better understanding of this basic aspect of the problem of furnace performance.

Acknowledgments

The authors gratefully acknowledge, with appreciation and thanks, the contributions to this investigation made by the following:

The Special Research Committee on Furnace Performance Factors of The American Society of Mechanical Engineers, for the opportunity to participate in this work, and the individual committee members for advice and help whenever required.

Dr. A. C. Fieldner, Chief, Fuels and Explosives Division, and Dr. R. L. Brown, Chief, Coal Branch, Bureau of Mines, who authorized the work and made many helpful suggestions.

The engineers and assistants of the Combustion Research Section: Messrs. J. W. Myers, J. Jonakin, C. H. Schwartz, J. J. Pfeiffer, G. Kollar, and H. Perry, who capably made the difficult tests that form the basis for this paper.

The officials of the Louisville Gas & Electric Company: A. G. Rosenbaum, Superintendent of Steam Power, Fred Tetzel, Assistant Superintendent of Steam Power, and J. D. Brecher, Plant Engineer, Paddy's Run Station, and their staffs, for willing and able assistance in the arrangement of the tests.

The Bailey Meter Company, for the loan of a recording oxygen meter.

Mr. Fred Ely of the Research and Development Division, Babcock & Wilcox Company, for the loan of a high-speed recording potentiometer.

Furnace Heat Absorption in Paddy's Run Pulverized-Coal-Fired Steam Generator, Using Turbulent Burners, Louisville, Ky.

Part III Comparison and Correlation of the Results of Furnace Heat-Absorption Investigation

By H. H. HEMENWAY[1] and R. I. WHEATER,[2] NEW YORK, N. Y.

In this paper, the results of the two companion papers (Parts I[3] and II[4]) are compared. Some of the possible sources of error are noted. Slightly revised calculated results are obtained by taking weighted averages of the data. The revised results are examined to determine which tests are the most dependable. An equation showing the relationship between furnace exit-gas temperature and furnace heat-absorption rate for a fixed burner adjustment is developed. From the revised results the effect of various factors on furnace performance is shown.

Introduction

THIS is the third of three papers presenting the results of investigations of furnace performance in the pulverized-coal-fired boiler No. 3 at Paddy's Run. These investigations were conducted under the sponsorship of the ASME Special Research Committee on Furnace Performance Factors. The first paper, Part I,[3] of this series presents results and analyses of the data obtained by measuring the furnace face temperatures of waterwall tubes. The second paper, Part II,[4] of this series presents the results and analyses of the data obtained by measuring the temperature and composition of the gas leaving the furnace and entering the slag screen. This paper deals with the comparison and correlation of the data presented in the first two papers.

Part I and Part II adequately describe the arrangement and dimensions of the furnace tested, the methods of testing, the methods of calculation, and the results obtained by each method of testing. By means of the two methods of testing, which will be referred to herein as the ΔT-method and the heat-balance method, the average heat-absorption rate expressed as MKB/(hr) for each test was determined. In Fig. 1, which is a copy of Fig. 21 of Part I, the results obtained by both methods of testing are compared, and an examination of this figure shows that except for a few of the full-load tests, the 45-deg equality line falls fairly well within the pattern of test points.

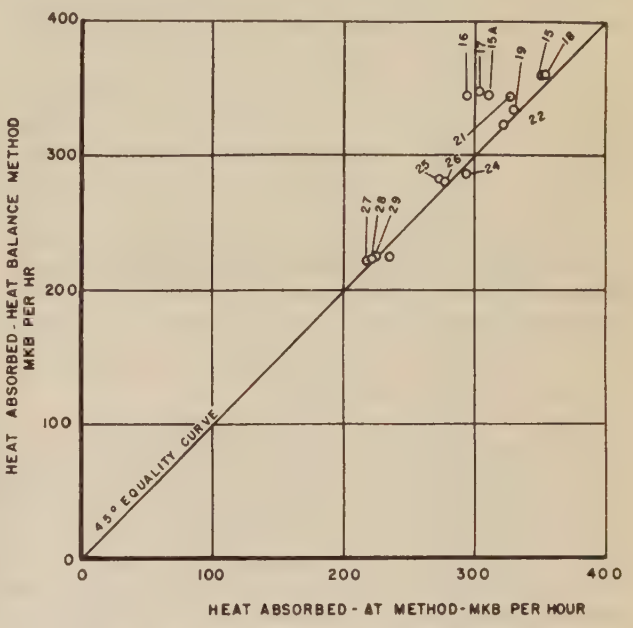

FIG. 1 COMPARISON OF FURNACE HEAT ABSORPTION, COMPUTED FROM WALL-TUBE ΔT-DATA WITH FURNACE HEAT ABSORPTION COMPUTED FROM FURNACE EXIT-GAS TRAVERSE
(Number designates test.)

The heat-absorption rate per unit of furnace radiant projected area determined from the heat balance, divided by the average temperature difference between the furnace-tube face and saturated water temperature, ΔT, yields the average over-all heat-transfer coefficient U_o. In Fig. 2 U_o is plotted against ΔT. This figure shows that the average over-all heat-transfer coefficient of 1060 Btu/(hr) (F) (sq ft of projected area), which was assumed in Part I in the calculation of furnace heat absorption by the ΔT-method, does not differ greatly from the values obtained from the heat balance.

The ΔT-Method

Some Sources of Error. The principal sources of error in the ΔT-method which are considered here are as follows:

(*a*) Errors in measurement.
(*b*) Errors in averaging.
(*c*) Errors in the assumptions.

Errors in measurement include the errors in the instruments

[1] Executive Assistant, Foster Wheeler Corporation. Jun. ASME.
[2] Assistant to the Manager, Service Department, Foster Wheeler Corporation. Mem. ASME.
[3] "Part I—Variation in Heat Absorption Shown by Measurement of Surface Temperature of Exposed Side of Furnace Tubes," by R. I. Wheater and M. H. Howard, published in this issue of the Transactions, pp. 893–923.
[4] "Part II—Furnace Heat-Absorption Efficiency as Shown by the Temperatures and Composition of the Gases Leaving the Furnace," by R. C. Corey and Paul Cohen, published in this issue of the Transactions, pp. 925–935.

Contributed by the Research Committee on Furnace Performance Factors, and the Fuels, Power, and Heat Transfer Divisions and presented at the Annual Meeting, New York, N. Y., November 27–December 2, 1949, of THE AMERICAN SOCIETY OF MECHANICAL ENGINEERS.

NOTE: Statements and opinions advanced in papers are to be understood as individual expressions of their authors and not those of the Society. Paper No. 49—A-117.

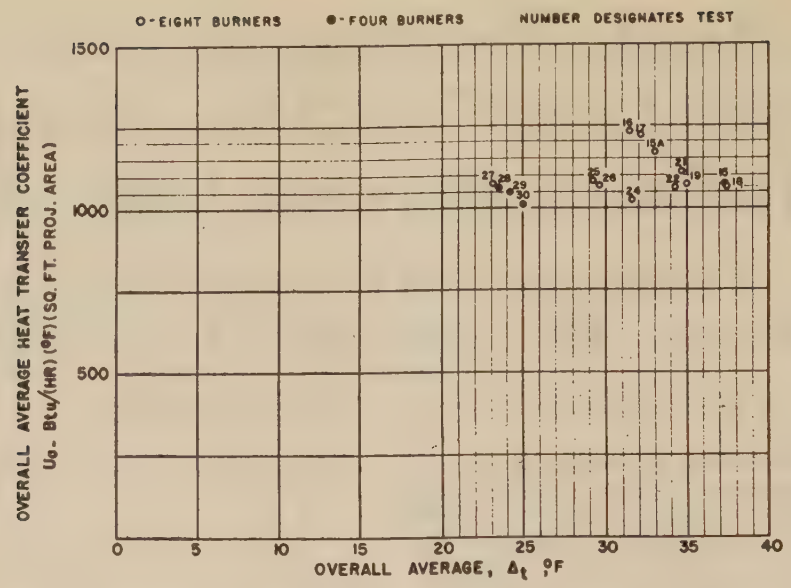

FIG. 2 CORRELATION OF FURNACE WALL-TUBE OVER-ALL AVERAGE HEAT-TRANSFER COEFFICIENT WITH ΔT

which were used in the tests. In addition, they include errors which may have been introduced in the temperature measurements of the front face of the wall tubes by the fact that the thermocouple shield probably served as a shelf for ash deposit and the resulting insulating or shading effect caused the temperature of the couple to be lower than the temperature of the wall of the tube remote from the shield.

In Part I the average over-all ΔT was assumed to be the arithmetic average of the ΔT-values for each live furnace-face thermocouple. Eight of the 128 thermocouples were dead and hence were not included in the averaging. The thermocouples could not be installed at uniform intervals, and none was installed on the rear wall roof or the slag screen. Thus there are reasons to suppose that the use of simple arithmetic averaging introduced some error in the results. In addition, since only one set of readings was taken during each 30-min period, the average value over this period may have differed slightly from the single value recorded owing to the small variations caused by operation with automatic controls.

In making the calculations it was assumed that the average tube-wall thickness at the thermocouple was 0.238 in., that the tube-wall conductivity was 348 (Btu) (in.)/(sq ft) (hr) (F), and that the heat-transfer coefficient from the tube to the water and steam mixture in the tube had a constant value of 5900 Btu/(hr) (F) (sq ft of inner surface of tube). The first two assumptions are probably tolerably accurate, but the third is subject to considerable error. It was assumed also that the heat transferred to the walls of the furnace as a whole was equal to the calculated unit rate of heat absorption multiplied by the projected area of the furnace walls. Since the walls do not have plane surfaces, this assumption, while approximate, is not exact.

In spite of all the possible errors which may have crept into the estimates of the heat absorption calculated by the ΔT-method, nevertheless the average error could not have been great because of the close agreement of the results obtained by this method and the heat-balance method.

Measurement of Saturation Temperature. It was originally assumed that the average temperature of the mixture of boiling water and steam in the tubes of all walls and at all elevations might be represented by the saturation temperature corresponding to the drum pressure. It was noted in analyzing the results that the temperature measured by the thermocouples peened to the backs of four rear waterwall tubes just above the hopper at elevation 463 ft did not check the temperature obtained from drum pressure readings. A review of the data indicates that the average pressure drop from the drum to the superheater outlet based on gage readings is as follows:

Evaporation (a) 1000 lb of steam per hr	Pressure drop (b), psi	$\frac{(b) \times 10{,}000}{(a)^2}$
625	77	1.97
460	25	1.18
330	29	2.66

From this table it is obvious that one or both pressure gages are in error. A change of 25 psi represents a change of 3.23 deg F in saturation temperature at a pressure of 950 psig. Hence a 25-psi error in pressure-gage measurement introduces in the ΔT-method an error of about 10 per cent in the calculated rate of heat absorption at full load, and of about 14 per cent at half load. With regard to the back-face thermocouple temperature measurements, differences as great as 7 F were measured between adjacent tubes in one round of measurements. Thus, while the averaging of all readings may have eliminated most of the error, some error probably still exists. After some consideration it was decided by the authors of Part I to use the thermocouple measurements to determine saturation temperature.

The assumption that saturation temperature is constant for all elevations is inexact, however, since the pressure and hence the saturation temperature is higher at the lower levels and lower at the upper levels of the furnace. Since the fluid along the length of the furnace tubes consists of saturated water and steam in varying proportions, it is necessary to know something about the circulation characteristics of the unit in order to determine the change in pressure with change in elevation. Circulation tests run in September, 1948, indicated that there was no material change in the total weight flow rate of water in the furnace tubes between half load and full load. From circulation calculations it was estimated that for all tests the saturation temperature was approximately 0.4 F higher in the hopper tubes at the lowest thermocouple elevation, and about 1.7 F lower in the roof tubes at the highest thermocouple location than in the tubes at the 463-ft elevation. The over-all correction was calculated to be plus 0.7 F.

Weighted-Average Values of ΔT. A sketch of the development of the furnace walls showing the location of thermocouples is found in Fig. 3. The dead thermocouples are underlined. The furnace is divided into several areas from A to Q, inclusive. The average ΔT for each area is the average of the ΔT-averages of the rows in the area. The sum of the products of each area by the average ΔT of the area, divided by the total area in which the thermocouples were installed, yields a weighted average ΔT. The weighted average ΔT-values thus calculated, including the +0.7 F correction mentioned, are tabulated in column 10 of Table 1.

As previously stated, thermocouples were not installed on the inclined rear-wall roof (K), or on the slag screen (I and J). After examination of the data it was thought reasonable to assume that, (1) the average ΔT due to radiation only in the upper screen (I) was equal to the average ΔT of roof (A); (2) the average ΔT in lower slag screen (J) due to radiation only was equal to the average ΔT of the front wall at elevation 525 ft; and (3) the average ΔT of the rear-wall roof (K) was equal to the average ΔT for the other three walls at elevation 511 ft. Applying these values of ΔT to areas (I), (J), and (K), the weighted average ΔT for each test for all furnace areas was calculated. The results, including the +0.7 F correction, are tabulated in column 11 of Table 1.

In column 12 of Table 1 is tabulated the difference between the final weighted average ΔT and the average ΔT taken from Part I for each test. While the differences are within the probable error of the tests and might be neglected, the weighted-average values of ΔT should be more accurate and will be used hereafter in this paper.

Heat-Balance Method

Some Sources of Error. Part II describes the methods of test and calculation of the heat-balance data. That paper notes that measurements of gas flow and direction were not taken and that the average gas temperature and gas composition for each test were calculated from simple numerical averages of the measurements with appropriate corrections. A possible small source of error lies in the air-heater heat balance, in which it was assumed that for all tests the air leakage into the gas was equal to 5 per cent by weight of the gas entering the air heater. Probably the greatest source of error outside of the possible error in the corrections to the thermocouple measurements lies in the fact that only one traverse of the gases leaving the furnace could be made on each test. In this connection it should be noted that at full load the spread of temperature of the gas leaving the furnace was over 500 F. However, the gas composition was quite uniform, the deviation in per cent excess air rarely exceeding 10 per cent.

Weighted-Average Values of Furnace Exit-Gas Temperature. The sampling doors used for gas-temperature and gas-analysis measurements are not uniformly spaced across the boiler. For this reason simple numerical averages of the measurements where the spread is large may lead to error in the results. A method of obtaining a weighted-average furnace exit-gas temperature is shown in Fig. 4 in which isothermal lines of gas temperature for test No. 15A are drawn. Note that sampling

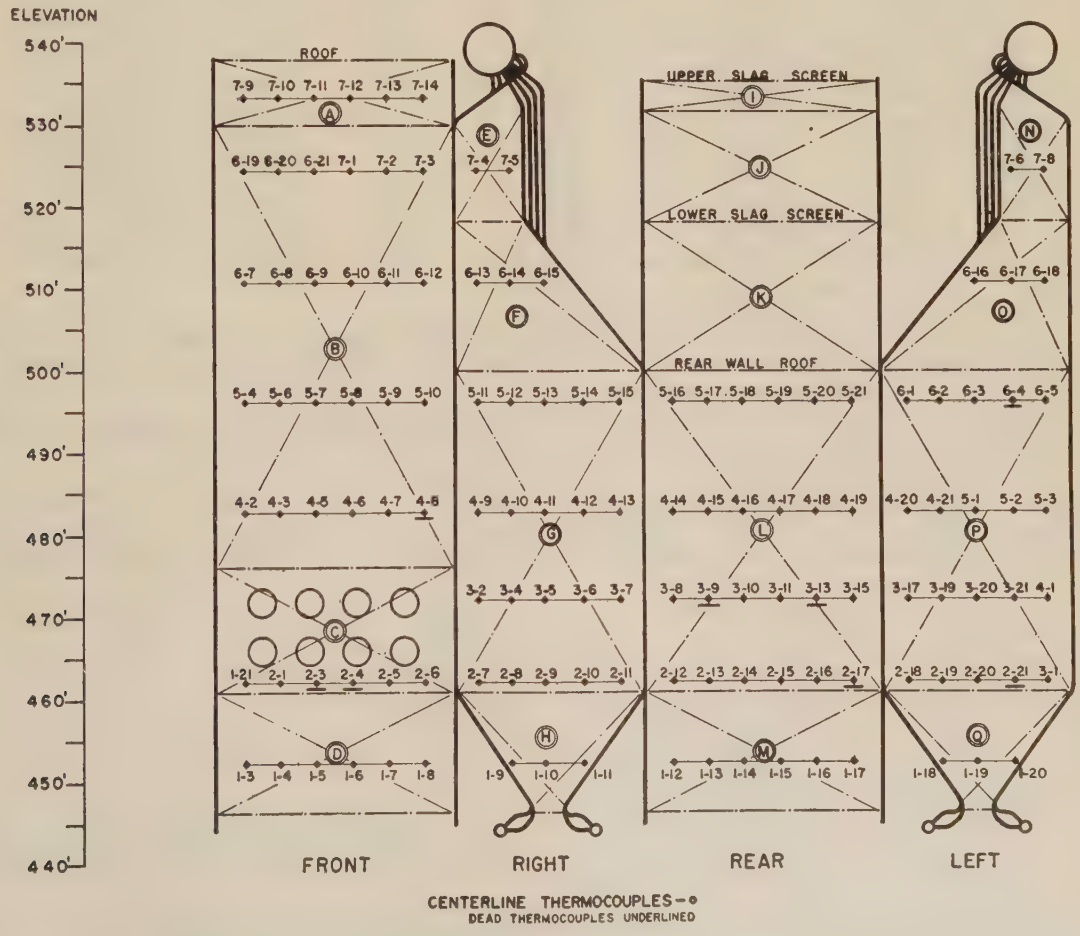

Fig. 3 Division of Furnace Walls Into Areas for Computing Weighted Average Values of ΔT

TABLE 1 SUMMARY OF CONDITIONS AND RESULTS BY ΔT-METHOD

1	2	3	4	5	6	7	8
Test	Net Heat Available Above 80F In Furn. MKB/Hr.	Net Heat Available Above 80F In Furn. KB/(hr) (sq.ft.)	Excess Air At Furn. Outlet %	Secondary Air Vane Position % Open	Number Burners In Service	Heat Abs. In Furn. from Part I KB/(hr)(F) (sq.ft.)	Furn. Heat Absorpt. Effy. from Part I Percent
15	793.7	89.3	23.0	40	8	39.4	44.2
15A	780.5	87.9	24.8	40	8	34.9	39.7
16	785.2	88.4	25.0	60	8	33.1	37.4
17	787.2	88.6	26.2	50	8	34.2	38.6
18	772.4	86.9	16.9	40	8	39.6	45.4
19	761.5	85.7	17.0	60	8	37.1	43.3
21	791.0	89.0	29.7	45	8	36.8	41.3
22	786.8	88.6	30.2	60	8	36.2	40.8
24	584.9	65.8	21.4	35	8	33.2	50.4
25	586.9	66.1	23.4	50	8	30.9	46.6
26	587.4	66.1	24.5	65	8	31.2	47.2
27	427.1	48.1	23.6	30	8	24.5	50.9
28	418.2	47.1	21.7	50	4 upper	24.9	52.9
29	418.3	47.1	23.0	50	4 lower	25.4	54.0
30	419.6	47.2	21.5	50	4 normal	26.5	56.1

1	9	10	11	12	13	14
Test	Avg. Δ T From Part I °F	Weighted Average Δ T for Furn. areas not incl. I,J&K In Fig. 3 °F	Weighted Avg. Δ T for all Furn. Areas A to Q incl. in Fig.3 °F	Corr. to Δ T (Col. 11 - Col. 9) °F	Corr. Heat Absorp. In Furn. from Δ T col. 11 KB/(hr)(F) (sq.ft.)	Corrected Furnace Heat Abs. Effy. from col. 13 Percent
15	37.2	38.1	37.8	+0.6	40.1	44.8
15A	32.9	33.6	33.8	+0.9	35.8	40.8
16	31.2	32.1	32.0	+0.8	33.9	38.4
17	32.3	34.0	34.2	+1.9	36.3	40.9
18	37.4	38.5	38.0	+0.6	40.3	46.3
19	35.0	36.0	35.7	+0.7	37.8	44.1
21	34.7	36.1	36.0	+1.3	38.2	42.9
22	34.1	35.8	35.6	+1.5	37.7	42.6
24	31.3	32.0	31.8	+0.5	33.7	51.2
25	29.1	30.3	30.2	+1.1	32.0	48.5
26	29.4	30.6	30.3	+0.9	32.1	48.6
27	23.1	24.0	23.5	+0.4	24.9	51.8
28	23.5	24.1	23.7	+0.2	25.1	53.4
29	24.0	24.8	24.0	0.0	25.4	54.0
30	25.0	25.1	24.6	-0.4	26.1	55.2

doors A and F are relatively close to the side walls where the gas temperatures are lower on the average than the temperatures closer to the center of the furnace.

The furnace outlet is divided into 3 vertical strips (R), (S), and (T). Center strip (S) contains temperature measurements taken through sampling doors (B), (C), (D), and (E) which are uniformly spaced. The width of strip (S) equals 4 times the uniform door spacing. Side strips (R) and (T) are equal in width. The center-line temperatures of strips (R) and (T) were determined by making an isothermal map for each test and by interpolating between the isothermals.

The sum of the average strip temperatures, each of which was multiplied by the ratio of the respective strip area to the total, yielded a weighted-average furnace exit-gas temperature. However, the calculated weighted-average temperatures vary only 5 F to 15 F from the temperatures obtained by simple arithmetic averaging in Part II. Values of furnace exit-gas temperature obtained by both methods of averaging, as well as the differences, are given in Table 2. While there are many other methods of averaging, the method just described was used, since it corrects for the lower gas temperatures measured near the walls but places a minimum of reliance on values which do not represent actual measurements.

Comparison of Furnace Exit-Gas-Temperature Data With Other Data. Inspection of furnace exit-gas-temperature data, as compared to other test data, indicates that there may be relatively large errors in the values of average gas temperatures of a few

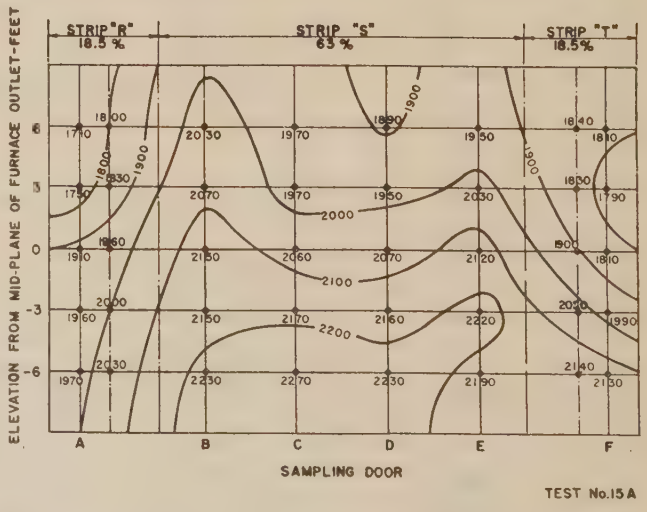

FIG. 4 DISTRIBUTION OF TEMPERATURE, DEG F, AND DIVISION OF FURANCE GAS OUTLET INTO AREAS FOR COMPUTING WEIGHTED-AVERAGE FURNACE EXIT-GAS TEMPERATURE, TEST NO. 15A

TABLE 2 SUMMARY OF HEAT-BALANCE DATA WITH CORRECTIONS

1	2	3	4	5	6	7	8
Test	Heat Absorption in Furnace from Part II KB/(hr)(F) (sq. ft.)	Furnace Heat Absorption Efficiency from Part II Percent	Average Furnace Exit Temperature from Part II °F	Weighted Average Furnace Exit Gas Temperature °F	Correction to Furnace Exit Gas Temperature °F	Corrected Heat Absorption in Furnace from Gas Temperature in Column 5 KB/(hr)(F) (sq. ft.)	Corrected Furnace Heat Absorption Efficiency from Column 7 Percent
15	40.5	45.4	2020	2030	+10	40.3	45.1
15A	38.8	44.2	2070	2085	+15	38.4	43.8
16	38.8	43.9	2045	2050	+ 5	38.7	43.8
17	39.1	44.1	2055	2065	+10	38.8	43.8
18	40.7	46.8	2045	2055	+10	40.5	46.5
19	37.8	44.1	2120	2130	+10	37.5	43.8
21	38.9	43.7	2015	2020	+ 5	38.7	43.5
22	36.4	41.1	2095	2110	+15	36.0	40.7
24	32.3	49.1	1885	1890	+ 5	32.2	48.9
25	31.9	48.3	1900	1905	+ 5	31.8	48.1
26	31.7	47.9	1890	1905	+15	31.4	47.4
27	25.1	52.2	1755	1765	+10	24.9	51.9
28	25.1	53.4	1740	1750	+10	25.0	53.1
29	25.5	54.1	1690	1695	+ 5	25.4	54.0
30	25.4	53.7	1730	1740	+10	25.2	53.4

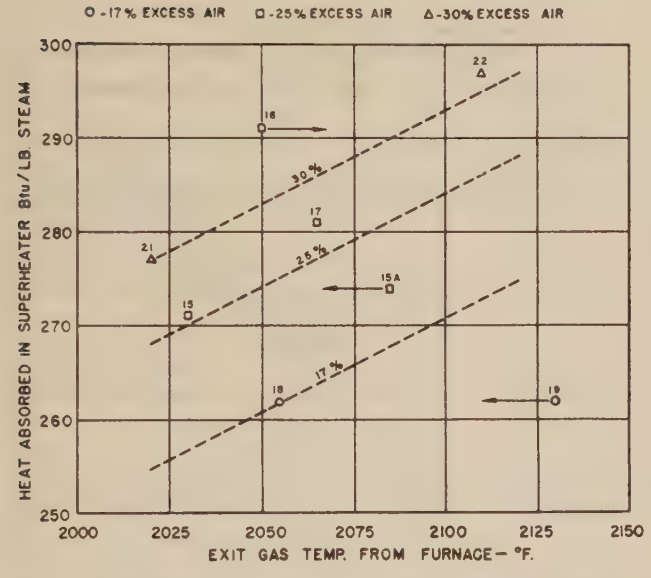

FIG. 5 COMPARISON OF SUPERHEATER HEAT DUTY AND FURNACE EXIT-GAS TEMPERATURE, DEG F, AT FULL LOAD
(Number designates test.)

of the full-load tests. Several means are available to determine for which tests the temperature data appear to be the least reliable. One method of analysis is to compare gas temperature with convection-superheater duty at constant load and constant excess air. In Part I the necessary data for determining superheater duty is given except for the heat given up by the condensation of saturated steam in the inlet-superheater header to the condenser coils provided to maintain a constant final steam temperature. The rate of flow of water through the condenser coils was determined from a calibration curve of the condenser control valve. From the flow rate and the observed water-temperature rise, the heat transferred in the inlet-superheater header was estimated. Calculated superheater duty for the full-load tests is plotted against weighted-average furnace exit-gas temperature in Fig. 5.

Full-load-performance calculations were made of the rate of change of superheater duty with change in furnace exit-gas temperature at constant excess air, and of superheater duty at constant gas temperature for three rates of excess air, namely, 17, 25, and 30 per cent. From these calculations the slope of and spacing between the lines drawn in Fig. 5 were determined. It was assumed that the 30 per cent excess-air line passes through the point for test No. 21. We may draw the tentative conclusion that values of gas temperature appear high for tests Nos. 15A and 19, and low for test No. 16.

Another method of analysis is to make plots of furnace exit-gas temperature against per cent excess air at constant secondary-air vane position, and also against secondary-air vane position at constant excess air. These plots are shown in Figs. 6 and 7 and corroborate the tentative conclusion drawn from Fig. 5 except for test No. 19. A check of ΔT and heat-balance data indicates that at 17 per cent excess air, an increase in the secondary-air vane position from 40 per cent (test No. 18) to 60 per cent (test No. 19) results in reduced heat absorption in the furnace and in a higher exit-gas temperature. It appears that the observed position of the condenser control valve for test No. 19 may have been an error.

Relationship of Furnace Exit-Gas Temperature to Furnace Heat-Absorption Rate. In predicting furnace performance, designers depend upon empirical data to calculate the rate of furnace heat absorption and the corresponding furnace exit-gas temperature. In Fig. 8 are plotted values of furnace heat-absorption rate per square foot of furnace projected area against average absolute furnace exit-gas temperature to the 4th power.

The straight line drawn in Fig. 8 represents the equation

$$Q = C\left[\left(\frac{T_o}{1000}\right)^4 - \left(\frac{T_w}{1000}\right)^4\right]$$

where

Q = furnace heat-absorption rate, Btu/(hr) (sq ft of projected area)
C = const = 1060
T_o = average furnace exit-gas temperature, deg R
T_w = average furnace tube-wall temperature, assumed to be 1040 deg R

Note that this line passes through those points for which the secondary-air vane position was approximately 40 per cent (neglecting test No. 15A), that those points representing tests having a secondary-air vane position of 50 per cent fall below

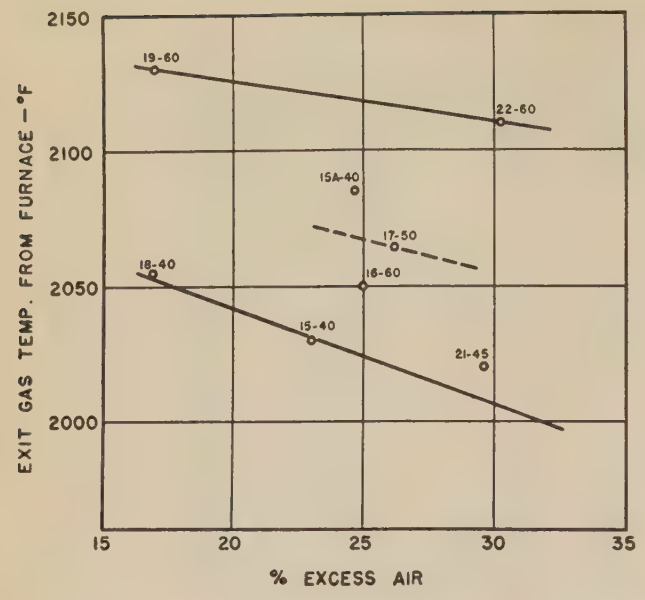

Fig. 6 Relation Between Furnace Exit-Gas Temperature, Deg F, and Excess Air for Three Secondary-Air Vane Positions at Full Load

(First number designates test; second number designates per cent opening of secondary-air vanes.)

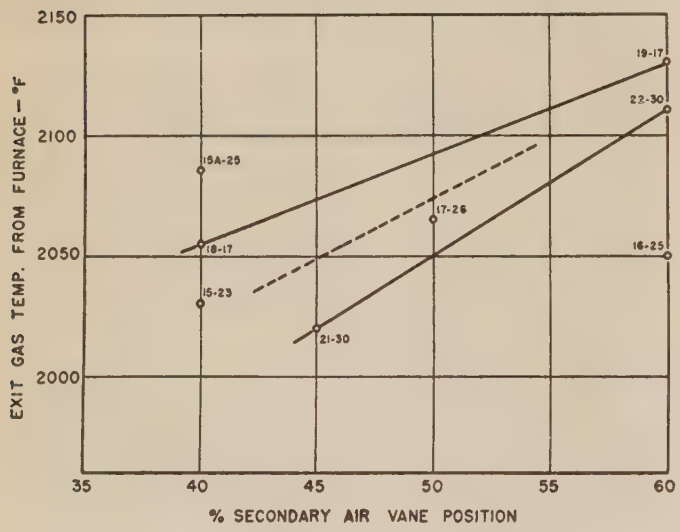

Fig. 7 Relation Between Furnace Exit-Gas Temperature, Deg F, and Secondary-Air Vane Positions for Three Values of Excess Air at Full Load

(First number designates test; second number designates per cent excess air.)

the line, and those that represent tests having a secondary-air vane position of 60 per cent fall off even farther below the line. Fig. 8 shows that for eight-burner operation with the burner secondary-air vanes set for maximum heat-absorption efficiency (40 per cent open), the furnace heat-absorption rate is related to furnace exit-gas temperature by the foregoing equation. It follows that for the operating conditions given, if the furnace heat input and excess air at the furnace outlet are known, the heat-absorption rate and exit-gas temperature from the furnace may be calculated. For four-burner operation, particularly when the lower row of burners is fired (test No. 29) the value of C in the equation is greater, and may be as high as 1240. Where the vane position is 50 or 60 per cent open, the equation holds tolerably well at three-quarters load but at full load the value of C drops off to approximately 980 and 850, respectively.

Correlation of ΔT and Heat-Balance Data

In Fig. 9 furnace heat-absorption efficiency, calculated by the ΔT and heat-balance methods is plotted against excess air for the full-load tests. Note that the points for tests Nos. 15A and 16 are not in agreement with the other data, and also that the furnace heat-absorption efficiency, calculated by the ΔT-method for test No. 17 appears to be out of line. In Fig. 10 furnace heat-absorption efficiency, calculated by both methods, is plotted against secondary-air vane position for the full-load tests. Again, notice that the points for the tests previously mentioned are not in agreement.

It had previously been found that furnace exit-gas-temperature measurements for test Nos. 15A and 16 seemed less reliable than for the other full-load tests. It now appears that the ΔT-data for these tests are also less reliable and by a greater margin. The maximum deviation from the lines drawn in Figs. 9 and 10 is about 10 per cent for the ΔT-data (test No. 16) and

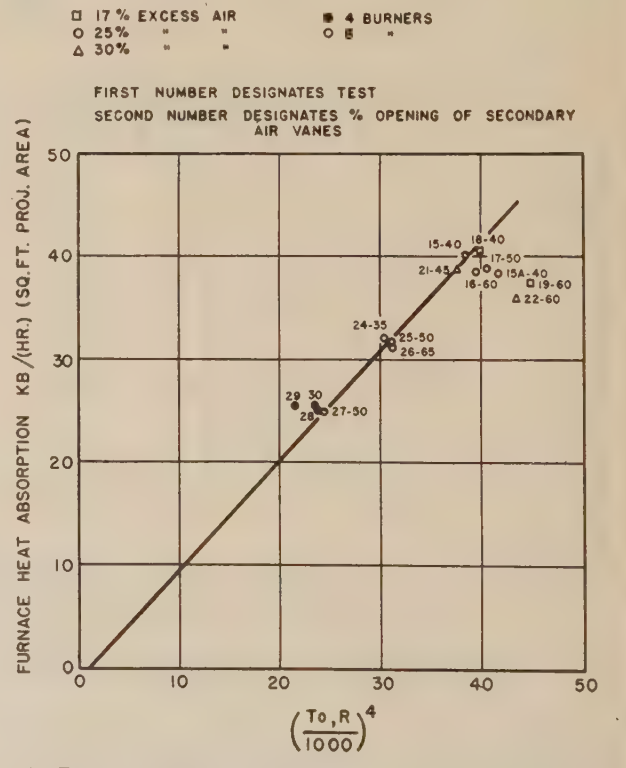

Fig. 8 Relation Between Furnace Heat-Absorption Rate and Furnace Exit-Gas Temperature T_o, Deg R

about 3 per cent for the heat-balance data (test No. 16). These values are by no means excessive and indicate that reasonably accurate results of furnace performance may be obtained by either method of testing.

From Figs. 9 and 10 it appears:

1 That the furnace heat-absorption efficiency decreases as excess air is increased at constant secondary-air vane position.

2 That the furnace heat-absorption efficiency decreases as the secondary-air vanes are opened at constant excess air.

Statement (1) confirms past observations of the performance of radiant superheaters which give a lower steam temperature as the excess air is increased. Statement (2) applies to the adjustment of the burners used on the Paddy's Run boiler and shows

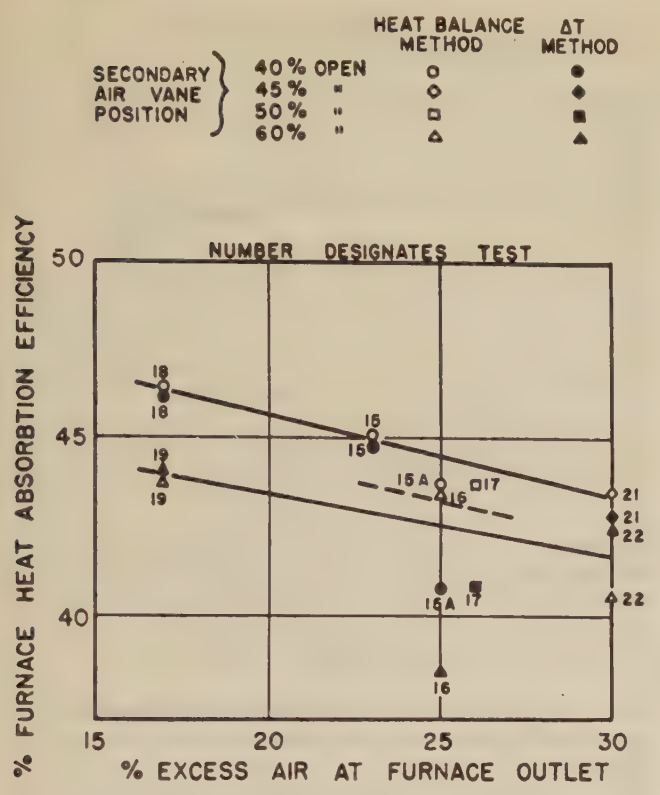

FIG. 9 RELATION BETWEEN FURNACE HEAT-ABSORPTION EFFICIENCY AND EXCESS AIR FOR THREE SECONDARY-AIR VANE POSITIONS AT FULL LOAD

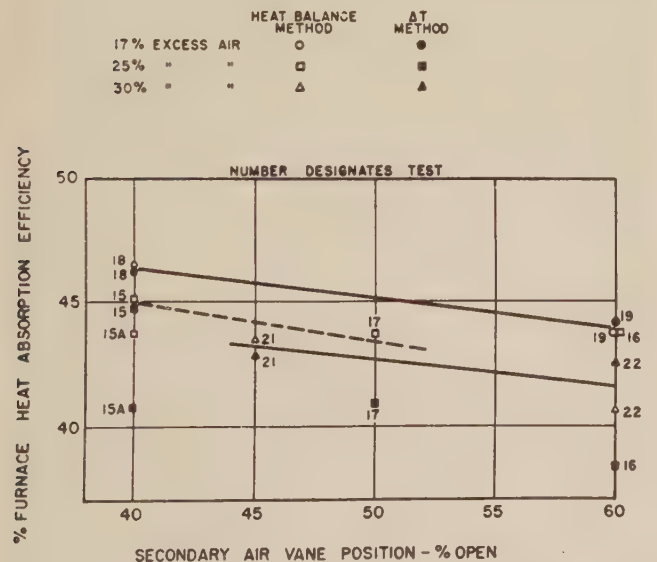

FIG. 10 RELATION BETWEEN FURNACE HEAT-ABSORPTION EFFICIENCY AND SECONDARY-AIR VANE POSITION FOR THREE VALUES OF EXCESS AIR AT FULL LOAD

that by means of burner adjustment, the heat absorption in the furnace may be varied.

In Fig. 11 the values of heat absorption obtained by both methods are compared. On the whole, the data appear to be in excellent agreement as do the data in Fig. 12 in which U_o, the over-all average heat-transfer coefficient, is plotted against ΔT. If runs Nos. 15A, 16, and 17 are neglected, Fig. 12 shows that

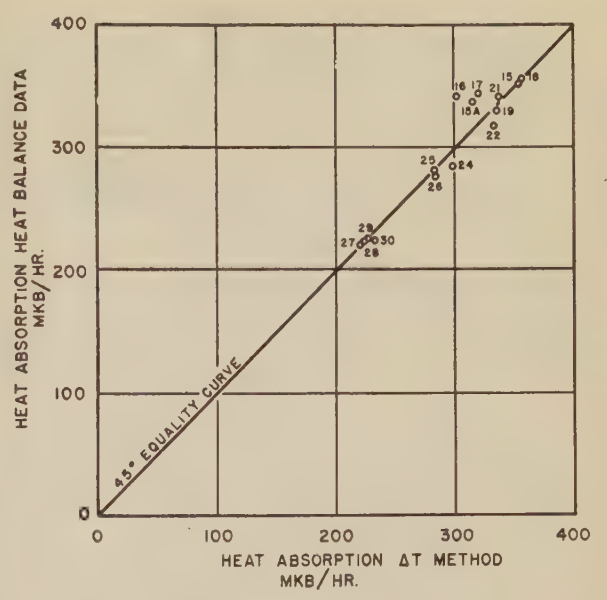

FIG. 11 COMPARISON OF CORRECTED FURNACE HEAT ABSORPTION COMPUTED BY HEAT-BALANCE AND ΔT-METHODS (Number designates test.)

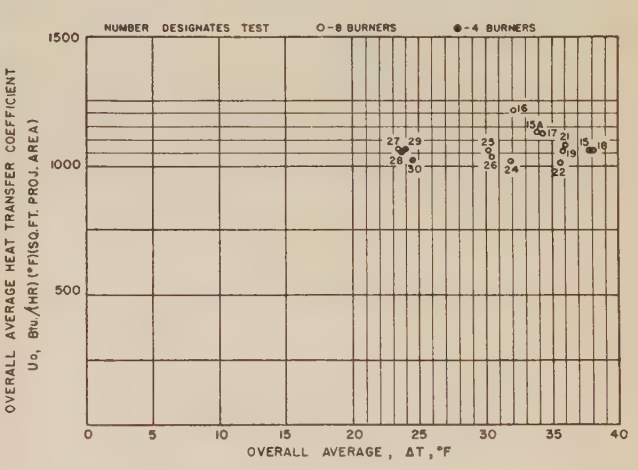

FIG. 12 CORRELATION OF CORRECTED FURNACE-WALL TUBE OVER-ALL AVERAGE HEAT-TRANSFER COEFFICIENT WITH CORRECTED VALUES OF ΔT

a fair average value of U_o for all runs would lie between 1030 and 1050 Btu/(hr) (F) (sq ft of projected area).

In Fig. 13 the furnace heat-absorption rate is plotted against the net heat available in the furnace above 80 F for the tests in which the secondary-air vanes were 40 per cent open. In Fig. 14 furnace heat-absorption efficiency is plotted against the heat available for the same tests. Only one curve is drawn in each figure showing the heat absorption at 25 per cent excess air, since only single points are available for 17 and 30 per cent excess air. It has been shown that at full load, the heat-absorption efficiencies decreased on opening the secondary-air vanes. At three-quarters load, maximum heat-absorption efficiency was obtained at a setting of 35 per cent open. At one-half load only one test was run with 8 burners and that with a vane position of 30 per cent open.

CONCLUSIONS

The following conclusions have been reached in this study.

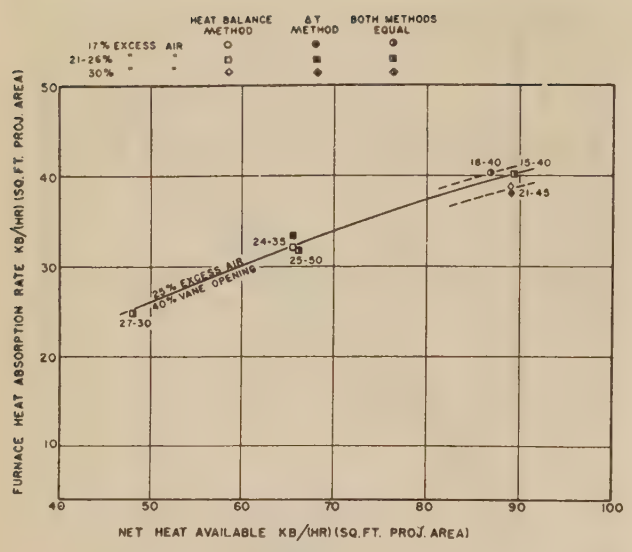

FIG. 13 RELATION BETWEEN FURNACE HEAT ABSORPTION AND NET HEAT AVAILABLE TO FURNACE

(First number designates test; second number designates per cent opening of secondary-air vanes.)

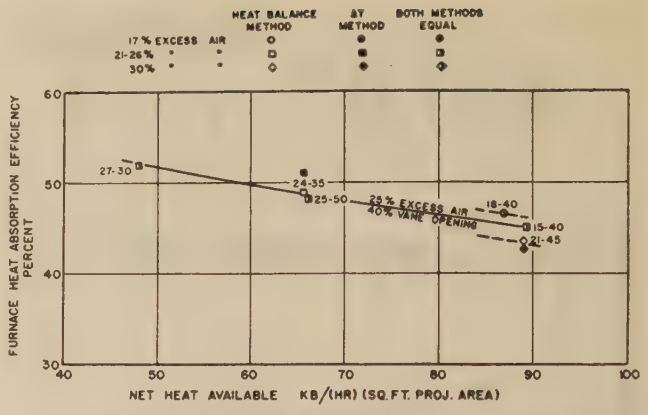

FIG. 14 RELATION BETWEEN FURNACE HEAT-ABSORPTION EFFICIENCY AND NET HEAT AVAILABLE TO FURNACE

(First number designates test; second number designates per cent opening of secondary-air vanes.)

1 With care in testing, furnace performance may be determined by either the heat-balance method or by the ΔT-method with a fair degree of accuracy.

2 The over-all average heat-transfer coefficient U_o, through the tube wall and inside tube film was 1030 to 1050 Btu/(hr) (F) (sq ft projected area). From this, the calculated film coefficient is 5500 Btu/(hr) (F) (sq ft of inside tube-wall surface).

3 For eight-burner operation with secondary-air vanes 40 per cent open, the average furnace heat-absorption rate Q, the average furnace exit-gas temperature T_o, and the average furnace tube-face temperature T_w, are related as follows

$$Q = 1060 \left[\left(\frac{T_o}{1000} \right)^4 - \left(\frac{T_w}{1000} \right)^4 \right]$$

4 In general, the conclusions of Part I and Part II, with some slight modifications to the calculated results found in Tables 1 and 2 of this paper are valid.

ACKNOWLEDGMENT

The authors wish to express their appreciation to Mr. John Blizard for his very helpful criticisms and suggestions.

Furnace Heat Absorption in Paddy's Run Pulverized-Coal-Fired Steam Generator, Using Turbulent Burners—Discussion

THE following discussion applies to the three papers published in this issue of the Transactions as Parts I,[1] II,[2] and III,[3] under the subject title.

OLLISON CRAIG.[4] The tests made on the boiler at Paddy's Run Station determine heat absorption by radiation in the furnace walls by measurement of gases leaving the furnace and not by measuring the temperatures of the boiler tubes in the furnace, as was done on a test at Tidd Station. The method used at Paddy's Run no doubt gives determination of heat absorption by radiation in the furnace more accurately. With two exceptions the average of measured temperatures leaving the furnace checks reasonably close with temperatures calculated from Orrok's modified formula. One of these exceptions is test No. 29 and is accounted for by the fact that the lower burners were used at the light load. The other exception is test No. 22, and there is no apparent explanation.

The distribution of temperature as indicated in Fig. 5 explains, as pointed out in the paper,[2] why, in practice, slag troubles are encountered even though the average temperature of the gases is below the slagging temperature of the ash. Due to the way in which the gases approach and flow to and through the furnace exit, the temperature of the gases at the lower part of the exit are some 300 deg higher than the average gas temperatures. An explanation is given in the paper to the effect that this is because of the difference in velocity of exit at the top and bottom of the exit openings. Actually, it would seem that those gases which leave at the top of the exit opening may have been in the entire furnace for a longer period of time and on the average may have radiated heat to furnace water tubes from a shorter distance than was the case with most of the gases which entered at the bottom of the furnace exit. In addition, there has been a greater distance and a greater time interval between the point at which combustion was completed in the furnace and the top point of exit of the gases than would be the case with the bottom point of furnace exit.

Slag formation at a furnace exit can be materially different with the same amount of coal burned with the same excess air in the same furnace, depending upon the point at which combustion is completed. This is a fact well known in stoker operation and is one of the reasons for using overfire jets in stoker operation.

A knowledge of heat absorption in a furnace envelope is necessary because, (1) it is necessary to have the gases leave under such temperature conditions that slag will not be formed in the gas passes of the boiler and in the superheater region; (2) the temperature of the gases entering the superheater region must be known, in order to determine the design of the superheater. The results of the tests at Paddy's Run are excellent from both of these viewpoints. Similar information is desirable with other methods of burning fuels and also with other fuels than coal. The results which are obtained with other methods of firing and with other fuels are surprisingly different.

F. G. ELY.[5] The authors[1,2,3] have made an excellent presentation of test data dealing with a subject which involves many complexities. It is encouraging to find that their correlations are comparatively good, which may in part be attributed to improved techniques of traversing and to the circumstance that ash deposits on the furnace-wall surfaces remained generally consistent on comparative tests.

For critical appraisal of the data, the authors have made use of the superheater as a calorimeter, and from its indications find justification for considering tests Nos. 15-A and 16 less reliable than the other tests.

This procedure of cross-checking results by study of the performance of component equipment seems very proper and desirable and extends the facilities of testing beyond the limitations of the ΔT-method and the heat-balance method.

In this design of unit, the furnace boundary itself comprises the major portion of the steam-generating surface, and it is possible to draw a further comparison by calculating the steam-generating duty from enthalpy of saturation, feedwater leaving economizer, and metered steam output. In Fig. 1, herewith, the test points of

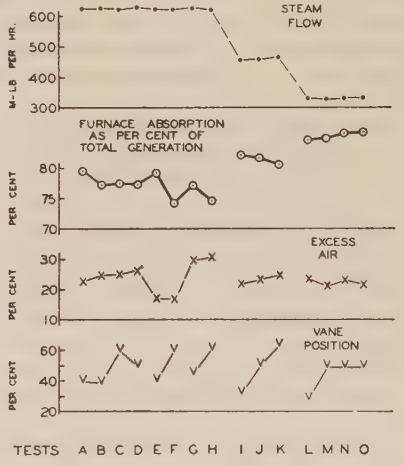

FIG. 1 FURNACE ABSORPTION AS PER CENT OF TOTAL GENERATION

furnace heat absorption by the heat-balance method are plotted as percentages of total generation and are shown to range from 74 to 86 per cent, depending upon load and operating conditions.

If it be assumed that the proportioning between furnace and convection bank is a function of excess air alone, the results for tests Nos. 19 and 21 are cast in doubt, and the influence of burner vane position is minimized. If, however, the influence of the

[1] Part I—"Variation in Heat Absorption as Shown by Measurement of Surface Temperature of Exposed Side of Furnace Tubes," by R. I. Wheater and M. H. Howard, pp. 893–923.

[2] Part II—"Furnace Heat-Absorption Efficiency as Shown by the Temperature and Composition of Gases Leaving the Furnace," by R. C. Corey and Paul Cohen, pp. 925–935.

[3] Part III—"Comparison and Correlation of the Results of Furnace Heat-Absorption Investigation," by H. H. Hemenway and R. I. Wheater, pp. 937–944.

[4] Vice-President, Riley Stoker Corporation, Worcester, Mass. Fellow ASME.

[5] Research Engineer, Research and Development Department, Babcock & Wilcox Company, Alliance, Ohio. Mem. ASME.

burner vanes is considered primary, some question would exist for the relationship of tests Nos. 15, 16, and 17.

Discrepancies of this order may lie in the inherent errors of temperature measurement by traverse, or in the variations caused by ash deposit on the furnace walls. On the latter point it is recommended that the S-A factors as developed by Mumford and Bice[6] be applied to observed furnace conditions to note their effect in correlation of the test points.

It is further recommended that for future programs of furnace testing, more emphasis be placed on obtaining check or repeated tests, to give statistical weight to the averaged results, and to disclose the range of performance that may occur in day-to-day operation of the equipment.

H. F. Mullikin.[7] MHVT furnace outlet-gas temperatures as obtained by Messrs. Corey and Cohen[2] appear low to the writer. The temperatures of 2060 F at a furnace heat-available rate of 95,000 Btu/(sq ft)(hr) and 1730 F at a furnace heat-available rate of 50,000 Btu/(sq ft)(hr), as given in Fig. 9 of the paper, are about 190 deg F and 130 deg F below values that would be expected, according to the writer's experience.[8] Is it possible that the special design HVT thermocouples read low during the test? Platinum thermocouples tend to lose calibration rapidly. Were they checked before and after every test? Was difficulty experienced with ash plugging toward the end of a run?

The authors are to be complimented on the completeness of the test procedure.

A. A. Orning.[9] The statement by the authors of Part I,[1] that it is impossible to measure flame shape, merits further consideration. The inference probably intended was that flame shape is not a readily measurable quantity, while secondary-air vane opening and burner-box pressure, factors which determine flame configuration in the furnace considered, are quantities subject to measure and control. It should not be inferred that flame shape is incapable of estimation. The objective of the furnace-performance tests, to relate furnace heat absorption and its distribution in the furnace to furnace geometry and operating variables, scarcely can be accomplished without some estimate of flame configuration as the intermediate between operating conditions and heat transfer.

Since the flame originated at the burners and followed some systematic path toward the furnace outlet, the ΔT-contours at any level should have relation to those at other levels. The prevalence of ash deposits on the back wall opposite the burners accounts for low heat transfer to that surface, although it probably was blanketed by the most intense flame within the furnace. The flame became less intense or occupied a smaller cross-sectional area at higher levels in the furnace. The gas temperatures and compositions reported in Part II[2] indicate two flame cores entered the furnace outlet. The ΔT-contours suggest only one radiant core except near the front wall just below the furnace outlet.

The rotation imparted at each of the eight burners was of such a sense as to create a pattern of eight eddies across the furnace. However, they probably degenerated into two eddies which best filled the rectangular cross section, and each contained a maximum of radiant intensity. Placed near the center of the furnace, the two centers of maximum intensity would not be reflected in the ΔT-contours. However, the sloping back forced the flame against the front wall so that the two maxima appeared on the front wall just below the furnace outlet. Flame sweeping near the front wall would account for the third maximum generally appearing in Figs. 22–28, inclusive, of Part I.[1] It would be interesting to know whether visual observation suggested two flame cores sweeping near the front wall at that level.

The ΔT data are missing for some points indicated on the thermocouple-location identification diagram. Had the corresponding couples completely failed? Other couples appear to be faulty. The ΔT's reported for positions 6–14 and 7-10 are generally high under all operating conditions. What criteria were used to determine that a given couple was faulty?

L. B. Schueler.[10] The three papers[1,2,3] presenting the test data and analytical report on the Paddy's Run boiler offer another set of complete information of interest and use to the boiler-furnace designer and user. The data appear to be well taken and have benefited from some improvement in instrumentation and technique since the Tidd boiler tests of several years ago. Favorable furnace-outlet location and profile, together with improved instrumentation, indicate that the gas-temperature and composition data should be most reliable.

A study of the furnace tube ΔT isotherms in Part I[1] indicates that the rather compact bunching of all burners in one wall is not conducive to uniform and effective heat transfer to the furnace walls. The front, or burner wall, shows only moderate absorption rates probably because the flame is traveling away from the wall, and the wall is partially screened by the cold layer of coal and air leaving the burners. The side walls show fairly good absorption rates, due to greater exposure to active flame, and a beneficial sweeping action of the flame without much slag deposition. However, these walls have less area than the front and rear so that their effect is thereby minimized. The rear wall, which should benefit most by virtue of its position opposite the burners, suffers somewhat from slag deposition by flame impact in the middle zone, although the hopper slope performs remarkably well. The upper portion of the entire furnace appears to suffer from lack of proximity and direct exposure to active flame.

All in all, it would appear that burner position, furnace shape, or both could well be changed to achieve more effective heat absorption throughout much of the furnace. The physical and operating convenience of grouping all burners in one wall at the main operating level must be weighed against the evident unfavorable flame pattern produced in a conventional furnace.

The uniformity of gas composition at the furnace outlet, as brought out in Part II,[2] is testimony of good coal and air distribution and combustion. The indicated effects of changing burner vane positions are interesting but not as pronounced as might be hoped for. It is possible that the extremely high pulverized-coal fineness for all tests acts to minimize the effects of vane position, and it would be interesting to determine whether the effects are greater with coal of normal fineness, say, 70 per cent through 200 mesh. Correspondingly, the present tests show virtually no carbon loss whereas vane manipulation with lower fineness and lower volatile fuels might encounter high carbon losses as a consequence.

Closure by R. I. Wheater and M. H. Howard

We agree with Mr. Ely that it would be advisable to verify the furnace-performance characteristics by incorporating additional check tests in future programs of this nature. Considera-

[6] Part IV—"An Investigation of the Variation in Heat Absorption in a Pulverized-Coal-Fired Water-Cooled Steam-Boiler Furnace," by A. R. Mumford and G. W. Bice, Trans. ASME, vol. 70, 1948, p. 601.

[7] Head, Department of Mechanical Engineering, Montana State College, Bozeman, Mont. Mem. ASME.

[8] "Determining Furnace Heat Transfer by Gas Temperature Measurement," by H. F. Mullikin, *Power Generation*, vol. 52, August, 1948, pp. 68–71, 116–122, Figs. 5 and 9.

[9] Coal Research Laboratory, Carnegie Institute of Technology, Pittsburgh, Pa. Mem. ASME.

[10] Engineer, Mechanical Engineering Division, American Gas & Electric Service Corporation, New York, N. Y. Mem. ASME.

tion should be given to reducing the duration of each test, which would permit running more check tests and reduce the volume of data to be analyzed. This would also hold operating variables to a minimum.

Dr. Orning is correct in emphasizing that it is not impossible to measure flame shape. However, due to the difficulties involved in accurately measuring flame shape and duplicating it under various test conditions, burner settings, which could be duplicated and do control flame shape, were used as a reference.

The relation of the ΔT contours at various levels is not only affected by the ash accumulations on the rear wall but it is also affected by eddies in the flow path and by shielding of the emitting body. While some of the ΔT contours indicate two radiant cores existing in the upper part of the furnace, they were not visible through the available doors and no flames existed at this elevation.

On several occasions prior to the tests, the thermocouples were checked as the unit was taken off the line to assure that they indicated saturation temperature, as the pressure was reduced without fire in the furnace. The thermocouple at the location omitted from the ΔT data had either failed or consistently recorded a temperature considerably below saturation temperature.

Mr. Schueler has presented an excellent analysis of the distribution of heat absorption by the walls and its relation to the burner locations. The location of the burners and the furnace shape both affect the distribution of heat absorption by the walls but additional data is required to determine the optimum firing arrangement. Available data has however indicated that maximum furnace efficiency is obtained when the fires are located as near as possible to the bottom of the furnace.

Comparison of these results with additional heat absorption distribution data as it becomes available should enable the designer to locate the burners and shape the furnace to obtain the optimum heat-absorption distribution throughout much of the furnace.

Closure by R. C. Corey and Paul Cohen

Mr. Craig's explanation for the vertical temperature gradient at the furnace outlet agrees with that proposed by the authors. The gas-residence time of the stream lines leaving the top of the furnace outlet is believed to be longer, and therefore the linear velocity lower, than those leaving the lower portion of the outlet. Also considered as a possible factor was the heavier ash deposits on the rear than on the front wall, causing less net heat transfer from the gases along the rear wall. He calls attention to the need for similar investigations of furnaces fired by other methods. The Committee recognizes that all types of firing must be investigated if fundamental furnace heat-transfer relations are to be discovered. To the present time, however, it has been expedient to concentrate upon pulverized-coal-fired units, but during 1950 it is expected that a series of tests with a spreader-fired unit will be completed.

Mr. Ely makes an interesting comparison between the operating variables, excess air and vane opening, and the furnace heat absorption as per cent of total steam generation.

The question raised is whether tests 19 and 21, or tests 15A, 16, and 17 are in error, depending upon whether the relative heat-absorption efficiency of the furnace is affected by the excess air alone, or is influenced primarily by the vane opening. However, it will be noted from the three-variable plot, Fig. 11 of Part II, that each of the variables influences furnace heat absorption, the effect being greatest at full load. If it is assumed as a rough approximation that excess air and vane opening have the same relative effect in the ranges that were studied, then Mr. Ely's plot indicates test No. 15A to be somewhat low and No. 16 to be somewhat high. But it is not known definitely whether the deviations were due to instrumental errors or to unusual ash patterns on the furnace walls for these two tests.

The authors agree with Mr. Ely that check runs should be made as often as possible in these furnace investigations. However, because of the number of independent variables that must be considered in the limited time available for such tests, it has not been possible to make as many duplicate tests as desired.

Mr. Mulliken suggests that the furnace-outlet temperatures seem low for heat-release rates of 95,000 and 50,000 Btu/(sq ft) (hr). Rigorous tests, in which direct comparisons were made in the furnace between B&W MHVT and the modified shields, showed the latter to be approximately 50 F lower. The test results were corrected accordingly and used for the enthalpy calculations. In addition, to detect possible contamination of the junctions, the test couples were calibrated frequently against a standard couple in a special electric furnace, and defective junctions were renewed.

Plugging of the shields always is a problem, particularly at full load and low excess air. However, the aspirating system was arranged so that the pressure drop across the shield was known at all times, and when it became too high the shield was replaced. Generally, the temperature at a given location in the furnace outlet was found to be the same with the new shield as with the one that was replaced, suggesting that inaccuracies due to reduction of cross section of the shield by ash were negligible. It was interesting to find that the emf of couples fitted with type E or G shields did not change noticeably, at constant mass flow of gas, even when as much as 90 per cent of the free area of the shield became plugged with ash.

Mr. Schueler's suggestion that the effect of vane setting might be more pronounced with coarser coal is probably correct. That is, for a given coal and excess air, the rate of change of flame surface with respect to vane opening may increase as the coal fineness decreases. Of course a relation of this kind would apply only within the limits of stable ignition.

Closure by H. H. Hemenway and R. I. Wheater

Mr. Craig observes that the averages of the measured temperatures leaving the furnace check reasonably with temperatures calculated from Orrok's modified formula except for test Nos. 29 and 22. General equations such as Orrok's for calculating furnace performance deal only with those few factors having the greatest influence on furnace heat absorption and are usually fairly accurate. One factor not normally considered is flame shape on which subject Mr. Orning has some very interesting comments. On the Paddy's Run unit, flame shape was varied by changing the

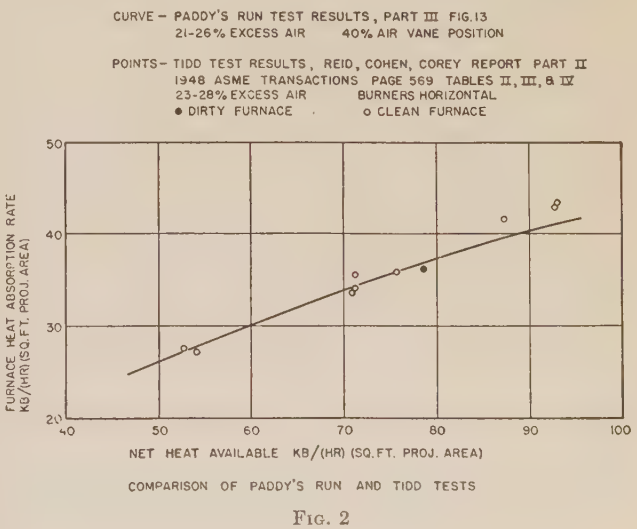

Fig. 2

position of the burner secondary-air vanes to alter the whirl imparted to the air before it entered the furnace. By opening these vanes this whirl was reduced which increased the length and reduced the spread of the flame causing a lowering of furnace heat absorption. This reduction of heat absorption on test No. 22, run with 60 per cent vane opening, probably caused the results to deviate from the results calculated by the Orrok equation.

Mr. Ely's plot of furnace absorption as per cent of total generation provides an excellent means of cross checking results. If the point for test No. 15A (B) is raised and the point for test No. 16 (C) lowered as suggested in Part III, the resulting plot will show rather well the effects of excess air and per cent vane opening on furnace heat absorption.

The authors may have been remiss in omitting the use of the S-A factors developed by Mumford & Bice[6] and recommended by Mr. Ely but the ash deposits on the furnace-wall surfaces were so minor in nature and varied so little between tests that early examination of the data indicated little change in the correlation of the test points.

Mr. Schueler expresses the opinion that the furnace-wall surfaces might be more effectively used by making changes in burner grouping, furnace shape, or both. The relatively poor results obtained on tests with the secondary air vanes open greater than 40 per cent may have led to this observation. At Paddy's Run the vane settings were varied to study the effect of this particular factor on furnace performance. Normally the air vanes are set at the position giving optimum performance. In this case the setting is 40 per cent open. As a matter of interest a comparison was made of the results of the tests on the Tidd tangentially fired furnace when the burners are horizontal, and the Paddy's Run furnace with burner air vanes 40 per cent open, both at approximately 25 per cent excess air. This comparison is shown in Fig. 2. Note the closeness of the results obtained by the two different methods of firing.

The Evaluation of Steam-Power-Plant Losses by Means of the Entropy-Balance Diagram

By ALLEN KELLER,[1] LYNN, MASS.

This paper deals with a method of isolating and evaluating the various cycle losses of a condensing steam power plant. Each loss in the steam cycle causes an increase of entropy. By considering each of these entropy increases on a "per hour" basis instead of a "per pound" basis, the heat rejection to the condenser caused by each individual loss can be evaluated quickly.

Nomenclature

The following nomenclature is used in the paper:

G = mass flow, lb per hr
H = enthalpy flow, 1000 Btu per hr
p = pressure, psia
q = sensible-heat flow, Btu per hr
Q = sensible heat, Btu
s = specific entropy, Btu/deg F/lb
S = entropy flow, Btu/deg F/hr
S' = entropy, Btu/deg F
t = ordinary temperature, deg F
T = absolute temperature, deg F
v = specific volume, cu ft per lb

Introduction

The concept of a flow of entropy can, at times, be used advantageously to evaluate the different losses in a condensing steam power plant and to get quick answers as to the over-all effect of design changes. An entropy-balance diagram can do this, because entropy is a measure of the unavailability of energy from the standpoint of a complete power plant consisting of boiler, turbine, condenser, feedwater heaters, pumps, and so forth.

Definition of an Entropy-Balance Diagram

When sensible heat is added to a quantity of matter, the change of entropy is given by the equation

$$dS' = \frac{dQ}{T} \quad [1]$$

Conventional steam tables assume that the entropy of saturated water at 32 F is zero. For water at temperatures above 32 F and for steam, the entropy is greater than zero because the sensible-heat content is greater than that for saturated water at 32 F. For steam, water, or ice at any condition, the entropy may be obtained by making a proper integration of Equation [1] from saturated water at 32 F to steam, water, or ice at the condition specified.

Equation [1] makes no mention of the quantity of matter to which heat is added because, as a differential equation, it may be integrated to determine the entropy of any quantity of matter. Conventional steam tables give the result of this integration for 1 lb (mass) of water. Thus the steam table lists values of "specific entropy" or entropy per pound of fluid.

If entropy per pound of fluid be multiplied by the fluid-mass flow, in pounds per hour, the product is the entropy flow per hour. An entropy-balance diagram is, then, a chart similar to a heat-balance diagram on which is represented the rate of flow of entropy throughout the entire steam cycle of a power plant. There is, however, one important difference between a heat-balance diagram and an entropy-balance diagram. On the heat-balance diagram, the boiler, turbine, feedwater pumps, and condenser are the only places where heat (or more properly enthalpy) is added to or subtracted from the thermodynamic medium itself. At all other points in the cycle, enthalpy is only transferred, as from steam to water in a feedwater heater. On the other hand, on an entropy-balance diagram the total entropy of the thermodynamic fluid is increased whenever a cycle loss takes place. For example, consider an extraction steam pipe leading from the turbine to a feedwater heater. The pressure drop in this pipe will cause an increase in the entropy of the steam flowing in the pipe, and the hourly entropy increase taking place within the pipe will be a direct measure of the cycle output loss caused by the pipe fluid friction.

Construction of an Entropy-Balance Diagram

Fig. 1 is a conventional heat-balance diagram for a typical steam-turbine power plant having an 11,500-kw AIEE-ASME preferred standard turbine-generator set operating at rated load. On this diagram, the heat-radiation loss is assumed to be zero, and the power required to drive the hot-well pump and boiler feed pump is neglected. (If desired, feedwater-pumping power can be taken into account without affecting the validity of the entropy balance as a means of evaluating losses.)

The derivation of Fig. 1 is not described in this paper.

Fig. 2 is the entropy-balance diagram corresponding to Fig. 1. It is based upon the flows given on the heat-balance diagram. At each point on the diagram, the mass flow is multiplied by the specific entropy to get the entropy flow. Whenever the total entropy leaving a given piece of apparatus is greater than the total entropy entering the same apparatus, the difference between the two entropy flows is the entropy increase caused by the cycle loss taking place in the apparatus. For example, consider the steam-extraction pipe from the turbine to the No. 2 feedwater heater. The entropy flow at the pipe discharge is 9319.1 Btu/deg F/hr. This value was calculated by multiplying 5338 lb per hr flow by 1.7458 Btu/deg F/lb specific entropy.[2] At the pipe inlet the entropy flow is 5338 lb per hr × 1.7344 Btu/deg F/lb or 9258.2 Btu/deg F/hr. Therefore the 10 per cent pressure drop in this pipe causes an entropy increase of 60.9 Btu/deg F/hr.

Fig. 2 shows that 143,479.2 Btu/deg F/hr is the entropy

---

[1] Assistant Division Engineer, Turbine Engineering Division, General Electric Company. Mem. ASME.

Contributed by the Power Division and presented at the Annual Meeting, New York, N. Y., November 27–December 2, 1949, of The American Society of Mechanical Engineers.

Note: Statements and opinions advanced in papers are to be understood as individual expressions of their authors and not those of the Society. Paper No. 49—A-65.

[2] All properties of steam used in this paper were read from "Thermodynamic Properties of Steam," by J. H. Keenan and F. G. Keyes, John Wiley and Sons, New York, N. Y., 1936 edition.

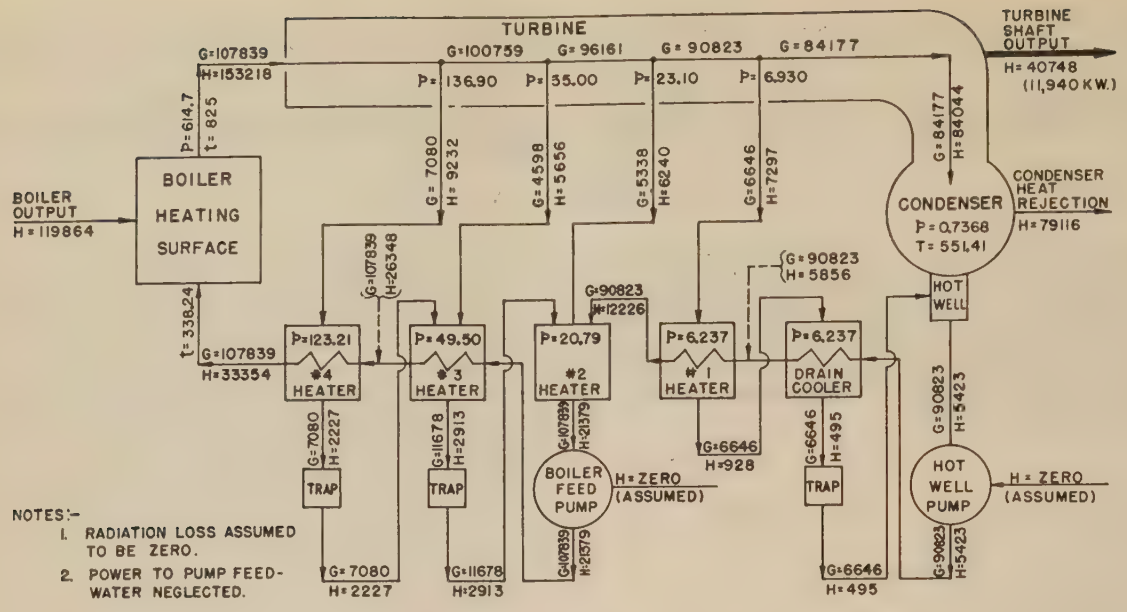

FIG. 1 TYPICAL HEAT-BALANCE DIAGRAM

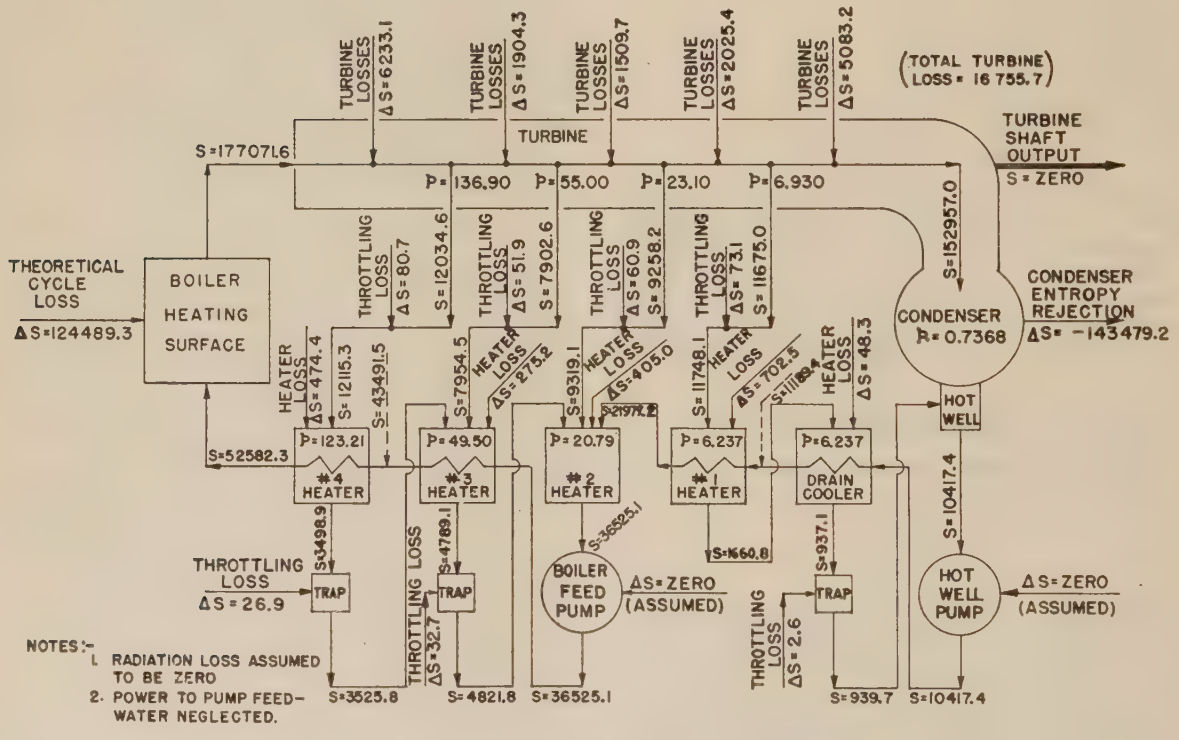

FIG. 2 TYPICAL ENTROPY-BALANCE DIAGRAM

rejection[3] to the condenser circulating water. This value represents the sum of all entropy increases (ΔS) in Fig. 2. The largest single entropy increase is the 124,489.3 Btu/deg F/hr added by the boiler. This quantity represents the theoretical cycle losses for the particular flow, boiler-inlet feedwater condition, and superheated steam-outlet condition shown in Fig. 1.

[3] In this paper, all values have been computed on an electrical computing machine merely to reduce the round-out errors and insure essentially perfect totals for all summations. For ordinary work such refinements usually will not be necessary.

EVALUATION OF LOSSES

Substantially all condensing power plants operate with wet steam exhausts. For such plants, the turbine-exhaust-steam temperature is a function of the exhaust pressure only. Thus when Equation [1] is applied to the heat-transfer phenomenon in the condenser, the temperature T is a constant.

Figs. 1 and 2 are based upon $1^1/_2$ in. Hg abs exhaust pressure. At this pressure the saturation temperature of steam is 91.72 F or 551.41 F abs ($T = t + 459.69$).

With constant temperature, Equation [1] may be written in the form

$$\Delta q = T\Delta S \quad [1a]$$

Thus the condenser heat rejection corresponding to the 143,479.2 Btu/deg F/hr condenser entropy rejection in Fig. 2 must be

$$\Delta q = 551.41 \times 143{,}479.2 = 79{,}115{,}866 \text{ Btu per hr}$$

This value agrees with the condenser heat rejection calculated by heat-balance methods as shown in Fig. 1.

To illustrate the method of evaluating individual losses, consider again the steam-extraction pipe to the No. 2 heater. A previous calculation has shown the entropy increase in this pipe to be 60.9 Btu/deg F/hr. This entropy increase must be rejected at the condenser at 551.41 F abs temperature. The corresponding heat rejection at the condenser is

$$\Delta q = 551.41 \times 60.9 = 33{,}581 \text{ Btu per hr}$$

This is the heat equivalent of 9.85 kw. Thus the 10 per cent pressure drop from the turbine shell to the No. 2 feedwater heater is causing a power output loss of 9.85 kw or 0.0825 per cent of the 11,940-kw turbine shaft output.

Tabulation of All Losses for Figs. 1 and 2 Power Plant

Table 1 isolates and evaluates each loss in the Fig. 1 heat-balance diagram, and Fig. 2 entropy-balance diagram. This table is an illustration of the type of over-all picture of power-plant losses which may be prepared relatively quickly by means of the entropy-balance diagram.

Table 1 shows the losses associated with feedwater heating while many readers are accustomed to think of gains from feedwater heating. This difference is only a matter of viewpoint. Feedwater heating results in an efficiency gain relative to the Rankine cycle without feedwater heating. On the other hand, an actual feedwater-heating installation always results in a loss relative to the perfect regenerative feedwater-heating cycle. This latter is the viewpoint in this paper.

The derivation of Table 1 needs some explanation.

For each individual loss, column B of Table 2 lists the entropy increase as shown in Fig. 2. The total of all entropy increases is the entropy rejection to the condenser, which agrees with the value shown in Fig. 2.

The two asterisked entries require special explanation. The turbine-shaft power output of 11,940 kw has a heat equivalent of 40,748,235 Btu per hr. At 551.41 F abs temperature, this amount of heat flow would have an entropy flow equivalent of 73,898.3 Btu/deg F/hr. This number has been included in Table 1 as the first asterisked quantity.

The 217,377.5 Btu/deg F/hr entropy increase shown as the boiler output in Table 1 was calculated as follows: Fig. 1 shows a boiler output of 119,864,000 Btu per hr. At 551.41 F abs temperature, this amount of heat flow is equivalent to 217,377.5 Btu/deg F/hr. This quantity represents the entropy equivalent at condenser temperature of the boiler heat output.

Column C shows the power output loss corresponding to each entropy increase. These were calculated by the formula

$$\text{Kw loss} = \frac{\left\{\begin{array}{c}\text{Hourly}\\ \text{entropy}\\ \text{increase}\\ \text{Btu/deg F/hr}\end{array}\right\} \times \left\{\begin{array}{c}\\ \text{temperature at}\\ \text{condenser, deg F abs}\end{array}\right\}}{3412.75} \quad [2]$$

Column D shows the percentage ratio of each individual loss to the turbine output and column E shows the percentage ratio of each loss to the boiler output.

The values in column C may be used to "capitalize" each of the individual losses. Again, using the No. 2 heater steam-extraction pipe as an example, if 1 kw of extra power output at constant input is worth, say, $100, then a capital expenditure of $980 would be justified to eliminate completely the pressure drop in this pipe, or a capital expenditure of about $500 to decrease the pressure drop from 10 to 5 per cent.

TABLE 1 EVALUATION OF INDIVIDUAL LOSSES OF FIG. 1 HEAT BALANCE

(A)	(B)	(C)	(D)	(E)
	Entropy increase	Power loss		
Item	Btu/deg F/hr	Kw	Per cent of turbine power output	Per cent of boiler output
Drain cooler	48.3	7.8	0.065	0.022
Drain-cooler trap	2.6	0.4	0.003	0.001
No. 1 heater	702.5	113.5	0.951	0.323
No. 1 heater steam-extraction pipe	73.1	11.8	0.099	0.034
No. 2 heater	405.0	65.4	0.548	0.186
No. 2 heater steam-extraction pipe	60.9	9.8	0.082	0.028
No. 3 heater	275.2	44.5	0.373	0.127
No. 3 heater steam-extraction pipe	51.9	8.4	0.070	0.024
No. 3 heater trap	32.7	5.3	0.044	0.015
No. 4 heater	474.4	76.7	0.642	0.218
No. 4 heater steam-extraction pipe	80.7	13.0	0.109	0.037
No. 4 heater trap	26.9	4.4	0.037	0.012
Theoretical cycle losses	124489.3	20114.2	168.461	57.270
Turbine losses	16755.7	2707.3	22.674	7.708
Total losses	143479.2	23182.5	194.158	66.005
Turbine power output	*73898.3	11940.0	100.000	33.995
Boiler output	*217377.5	35122.5	294.158	100.000

* See text for an explanation of asterisked entries.

TABLE 2 INCREASE OF SPECIFIC ENTROPY CAUSED BY 10 PER CENT THROTTLING PRESSURE DROP

Extraction point	Specific entropy of steam in turbine stage, Btu/deg F/lb	Specific entropy of steam at heater entrance, Btu/deg F/lb	Change of specific entropy Btu/deg F/lb
No. 4 heater	1.6998	1.7112	+0.0114
No. 3 heater	1.7187	1.7300	+0.0113
No. 2 heater	1.7344	1.7458	+0.0112
No. 1 heater	1.7567	1.7677	+0.0110
Equation [3a]			+0.0114

Feedwater-Heating-Cycle Losses

Fig. 3 shows the cumulative loss in the feedwater-heating cycle as a function of the feedwater temperature. This shows that a perfect feedwater-heating system would improve the over-all plant efficiency (at constant boiler efficiency) by about 6 per cent.

It is difficult, if not impossible, to extract superheated steam

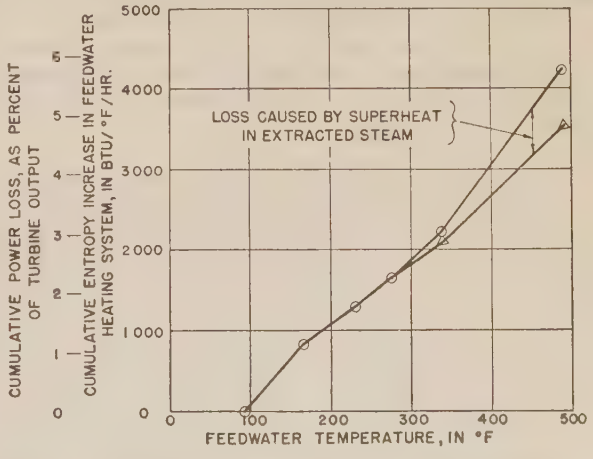

Fig. 3 Cumulative Loss in Feedwater-Heating System

for feedwater-heating purposes without taking a loss relative to the extraction of wet steam. This results from the fact that the feedwater temperature leaving a heater usually is determined by the pressure of the extracted steam without regard to its superheat. Even when a feedwater heater is designed to use the superheat in extracted steam to decrease the heater terminal-temperature difference, the temperature of the feedwater leaving the heater is many degrees below the temperature of the extracted steam.

Fig. 3 indicates the portion of the loss in the feedwater-heating cycle that is caused by superheat in the extracted steam. This loss was evaluated by calculating the extra "entropy of superheat" that would have been extracted if the heat of superheat were available at saturation temperature. Fig. 3 shows that the loss from this source amounts to about 0.2 per cent at the 338 F feedwater temperature leaving the No 4 heater.

To get an over-all idea of the feedwater-heating loss, the Fig. 3 curves cover the entire feedwater-temperature range from hot well to boiler saturation. To calculate the point at the 489 F boiler saturation temperature, a fictitious fifth stage of feedwater heating was assumed which delivers saturated water to the boiler at 614.7 psia pressure, heated by steam extracted from the turbine throttle. For this imaginary condition, the boiler heat output was kept unchanged from the actual 119,864,127 Btu per hr value by assuming a boiler mass flow of 126,685 lb per hr which is converted by the boiler from saturated water at 614.7 psia pressure to superheated steam at 614.7 psia pressure 825 F temperature. Of this 126,685 lb per hr boiler flow, 18,846 lb per hr is then extracted from the turbine throttle to the imaginary heater, leaving 107,839 lb per hr to flow to the turbine first stage, the same as before. With this imaginary feedwater heater in the picture, the entire feedwater-heating system from hot well to boiler saturation temperature extracts 4244.5 Btu/deg F/hr less entropy from the turbine than it adds to the feedwater. This 4244.5 Btu/deg F/hr value represents the saving which could be made if a perfect feedwater-heating system were available which delivered saturated water to the boiler.

Reheat Effects

The entropy-balance diagram is strictly correct for showing where cycle losses actually take place; however, it gives slightly conservative values when used to evaluate the gains which would be made if losses were eliminated or reduced.

Again, as an example, consider the No. 2 heater extraction pipe. Suppose that the pressure drop in this pipe were reduced and at the same time the extraction point in the turbine moved downstage slightly so as to maintain the same heater pressure. The state line enthalpy of the extracted steam would then be reduced slightly so that more extraction steam flow would be required to get the necessary heat for the feedwater heater. This increased extraction flow necessarily would cause less mass flow through the turbine low-pressure stages and hence less entropy flow to the condenser.

In evaluating the increased output that would result if the No. 2 heater extraction-pipe pressure drop were eliminated, it has been assumed that the decrease of entropy flow to the turbine exhaust would exactly equal the entropy increase in the extraction pipe. This is true except for one thing, namely, turbine stages are not 100 per cent efficient, and any reduction in the flow through a stage will also reduce the stage loss. Thus the entropy flow to condenser will always be decreased slightly more than any increase in the amount of entropy extracted.

At the turbine flange extracting to the No. 2 heater, the specific entropy is 1.7344 Btu/deg F/lb. At the turbine exhaust it is 1.8171 Btu/deg F/lb. Thus the "reheat factor" that must be applied to entropy extraction at the No. 2 heater opening is approximately 1.8171/1.7344 or 1.048. The word "approximately" is used in the foregoing expression because an entropy of liquid must be subtracted from both numbers, which will make the true reheat factor more complicated than the simple quotient shown.

If a turbine were 100 per cent efficient relative to the Rankine cycle and had an isentropic expansion line, all reheat factors would be 1.00. Since all large turbines have Rankine-cycle efficiencies between 80 and 90 per cent, the reheat factors can never get appreciably above 1.00. About 1.10 to 1.15 is the highest reheat factor that will be encountered in any normal installation; thus considering it as unity will cause no great error in perspective for a given study.

Simplified Calculation Methods

It can be shown that for a throttling process

$$ds = -0.1850 \frac{pv}{T} d \log_e p \quad [3]$$

Since the value of pv/T generally changes very little along a turbine-expansion line, it may be considered as approximately a constant.

Using 0.585 as an approximate value of pv/T, Equation [3] becomes

$$\Delta s = +0.108 \log_e \frac{p_1}{p_2} \quad [3a]$$

in which p_1/p_2 is the pressure ratio of a throttling process, and p_1 is the higher pressure.

Table 2 shows the actual increase of specific entropy associated with the 10 per cent pressure drop in each of the four extraction pipes of Figs. 1 and 2, together with the values calculated by Equation [3a]. Table 2 shows that Equation [3a] is quite accurate as a means of estimating entropy increases caused by throttling.

Simple procedures also can be worked up for estimating quickly the entropy increases associated with heater terminal-temperature differences, and the like, without reference to a steam table.

Conclusions

The entropy-balance method is a fundamentally sound and easily applied method of isolating and evaluating the different losses in the steam cycle of a condensing power plant. Although a sizable amount of calculation work is required to make a complete analysis of a given installation, any one question may be answered quite quickly after a heat balance is available. Preliminary estimates of many losses also may be made prior to a heat-balance calculation by making judicious assumptions as to the mass flows involved.

The entropy-balance diagram is not a substitute for other methods of analysis. It is another way of looking at a problem which should be used when it is helpful and not used when other methods seem more straightforward to apply.

Discussion

R. E. Hansen.[4] The evaluation of cycle losses by calculation of entropy generation is convenient, particularly when losses under study are too small to show up in a heat-balance computation.

The author states on the second page of the paper that the entropy rejection (a better word than "loss") of the theoretical

[4] Engineer, Elliott Company, Jeannette, Pa. Mem. ASME.

cycle is equal to the entropy received in the boiler. He does not define his theoretical cycle, but if the intention is to use as a reference the cycle defined by Selvey and Knowlton,[5] the theoretical heat rejection would be increased by an amount given in the writer's paper[6] of 1945.

It is not clear to the writer why, in Table 1, a fictitious entropy quantity representing turbine output is added to total entropy rejection in the cycle. This total does not appear to provide any additional information. Thermal efficiency of the turbine cycle may be found by dividing kw output by boiler output in kw, i.e., 11940/35122, or 34.0 per cent. Plant efficiency would be found by deducting auxiliary power before making this division, then multiplying the quotient by boiler efficiency.

The question of radiation loss is side-stepped by the assumption of zero. However, radiation can be handled quite readily in this type of computation. It may be of value to consider two types of entropy change, one by transfer, the other by generation. Entropy is increased by transfer in the boiler, and decreased by the same means wherever radiation or conduction losses occur. Entropy generation, as by pressure drop or internal heat transfer with a temperature difference, always results in an increase. Heat rate of the cycle becomes

$$\frac{3412.75\ \Delta H_B}{\Delta H_B - (\Sigma T\,\Delta S)_r - (T\,\Delta S)_c} \quad \ldots\ldots\ldots\ldots [4]$$

where ΔH_B is the heat received in the boiler, $(\Sigma T\,\Delta S)_r$ is the summation of all entropy losses through radiation or conduction, multiplied by the temperature at which the loss occurs, and $(T\,\Delta S)_c$ is the entropy rejection in condenser multiplied by condensing temperature. Where radiation and pressure drop occur simultaneously, the entropy rejection due to radiation must be computed separately from the entropy generation due to pressure drop, in order to evaluate $(\Sigma T\,\Delta S)_r$; the net change affects $(T\,\Delta S)_c$.

The author's evaluation of the effect of an individual loss is substantially correct in so far as capacity value is concerned, unless capacity limitation lies in the generator. There is an additional value, however, due to fuel savings. For example, with a load factor such that 6000 kwhr can be generated annually from each kw of capacity, and where energy cost due to fuel averages 1 mill per kwhr the fuel saving amounts to $60 annually. Assuming 12 per cent fixed charges, capitalized value of the saving becomes $500 per kw, or $4900 in the example cited by the author. This value is obtained regardless of capacity limitation, as fuel input may be reduced at the burner. Both values must of course be corrected to a plant value, by considering the effect of boiler efficiency and auxiliary loss, which increases the value of the savings.

[5] "Theoretical Regenerative-Steam-Cycle Heat Rates," by A. M. Selvey and P. H. Knowlton, Trans. ASME, vol. 66, 1944, pp. 489–512.

[6] "Irreversibility in the Theoretical Regenerative Steam Cycle," by R. E. Hansen, Trans. ASME, vol. 67, 1945, pp. 557–560.

Whenever entropy is discussed, the question arises as to what it is and why it is useful. Most forms of energy represent the product of a potential, such as force or voltage, by a quantity, such as distance or current. In the case of heat, temperature is the potential, but there is no readily perceived quantity by which to multiply it. This difficulty is solved by inferring the existence of entropy, and computing its value mathematically. There is no need to know any more than this about its nature, and no probability that we ever will.

Author's Closure

The comments of R. E. Hansen are all quite pertinent.

The theoretical cycle the author used as a reference on page 950 is the completely reversible regenerative cycle in which the feedwater is heated by extracting heat from the turbine at the same temperature as the feedwater. This could be accomplished, theoretically, by flowing the feedwater, in a counterflow direction, through a water jacket around the turbine shell and heating the feedwater by transferring heat at constant temperature through the turbine shell. The losses relative to the foregoing cycle caused by extracting superheated steam, as discussed on page 951 of the author's paper, are the same as those discussed in the R. E. Hansen paper,[6] except that they are evaluated for an actual cycle with a finite number of feedwater heaters and a less than 100 per cent efficient turbine.

In Table 1 the fictitious entropy quantity representing turbine output was inserted for checking purposes only. The text on page 950 explains how the 217,377.5-Btu/F/hr entropy increase assigned to the boiler was calculated. By calculating a similar entropy flow value which, at condenser temperature, would be equivalent to the turbine power output, a check was established that turbine-power output plus turbine, condenser, and feedwater-heating-system losses equaled the boiler output, as expressed in entropy units.

Radiation as well as many other considerations were sidestepped to keep the paper short. For example, the entropy balance concept can be used to evaluate boiler feed-pump losses, which was also sidestepped by stating that boiler feed-pump power had been neglected. The purpose of the paper is to present a concept for isolating and evaluating different kinds of losses to which each engineer can fill in the necessary detail to adapt the concept to his own needs.

Much has already been written on the subject of steam-power-plant efficiencies and heat balances. Mr. J. K. Salisbury has given much thought to this subject, and his 1949 ASME paper[7] presents another approach to the problem of evaluating power-plant losses. The entropy balance concept is just another tool which a power-plant designer may use in his work.

[7] "Power-Plant Cycle Evaluation," by J. K. Salisbury, Trans. ASME, vol. 71, 1949, pp. 593–604.

The Gas-to-Gas Heat Exchanger as Applied to an Oxygen Plant

Plate and Interrupted Strip-Fin Design

By CLYDE SIMPELAAR[1] and DAVID ARONSON[2]

The construction and performance of high-efficiency (95 per cent) counterflow heat exchangers is reported. These exchangers are of the finned-plate type employing interrupted strip fins. Comparison is made between test-core results and performance of large-size units installed in a tonnage gaseous-oxygen plant. Heat-transfer results were in good agreement but measured pressure drops on the large-size units were considerably higher than predicted from test-core results, possibly due to losses at end connections. Successful development of the true counterflow gas-to-gas exchanger adds flexibility to the design of low-pressure gas cycles as in oxygen plants, permitting the substitution of heat exchangers for regenerators.

Nomenclature

The following nomenclature is used in the paper:

a/s = ratio of total heat-transfer surface to minimum cross-sectional area per unit of length

A = total heat-transfer and/or friction area, sq ft ($A = A_f + A_w$). This definition of area differs from Norris and Spofford (1)[3] A, which is the sum of half the direct surface plus the full indirect surface)

A_c = minimum cross-sectional area for flow, sq ft

A_f = surface area of fins, sq ft

A_w = surface area of direct surface, sq ft

b = width of strip fin (distance from leading edge to trailing edge in direction of air flow), ft

c_p = gas unit heat capacity, Btu/(lb)(deg F)

D_e = equivalent passage diameter, $D_e = 4r_H = 4A_c/(A/L)$, ft

f = Fanning friction factor (see dimensionless groupings)

G = core air-mass velocity, (lb)/(hr)(ft² of A_c)

g = conversion factor, $g = \dfrac{32.2\ (\text{ft})\ (\text{lb-matter})}{(\text{sec})\ (\text{sec})\ (\text{lb-force})}$

(for time in hours, $g = 4.17 \times 10^8$)

h = surface heat-transfer coefficient referred to fin average surface temperature, not to temperature at base of fin, Btu/(hr)(ft²)(deg F). Note that for conditions of test, distinction between surface temperature and base of fin is unimportant

j = heat-transfer factor (see dimensionless groupings)

k = thermal conductivity of gas, Btu/(hr)(ft²)(deg F/ft)

k_e = thermal conductivity of fin material, Btu/(hr)(ft²) (deg F/ft)

L = length of flow passage, ft

m = $(2h/k\delta)^{0.5}$, 1/ft

P = gas pressure, psia

ΔP = pressure drop, lb/in.² or lb/ft²

t = temperature, deg F

T = temperature, deg R

δt = temperature change of gas from inlet to outlet, deg F

Δt_m = temperature difference between gas and metal surface, deg F

U = over-all heat-transfer coefficient, gas_h to gas_c based on total area, A

W = mass-flow rate, lb per sec or lb per hr

x_f = effective fin length, ft

δ, Δ = prefixes denoting difference

δ = thickness of fin, ft

η = fin efficiency, dimensionless

η = $(\tanh x_f m)/x_f m$, approximate[4]

μ = viscosity, lb/(hr ft)

ρ = gas density, lb per cu ft

ψ = fin perimeter, ft, $\psi = 2(b + \delta)$

Dimensionless Groupings

St = (h/Gc_p), Stanton's number, a heat-transfer modulus

Pr = $(c_p\ \mu/k)$, Prandtl's number, a fluid-property modulus evaluated for arithmetic-mean bulk fluid temperature

j = $(St)\ (Pr)^{2/3}$ = generalized heat-transfer grouping (this factor, j versus Re, defines heat-transfer characteristic of surface)

Re = $(D_e G/\mu)$, Reynolds number, a flow-property modulus characterizing "turbulence"

R_ψ = $(\psi G/\mu)$ modified Reynolds number based on fin perimeter

$f = \dfrac{\Delta P\ 2g\ \rho}{G^2\ (A/A_c)}$ = Fanning friction factor (the f—Replot defines friction characteristic of surface)

NTU = $\delta t/\Delta t$ = number of core "heat-transfer units," a dimensionless expression of "heat-transfer size" of core; $NTU = (\eta)(Ah/Wc_p) = (\eta)(h/Gc_p)\ (A/A_c)$

Subscripts

c refers to cooler fluid, i.e., one being heated

h refers to warmer fluid, i.e., one being cooled

---

[1] Chief Research Engineer, Modine Manufacturing Company, Racine, Wis. Mem. ASME.

[2] Process Engineer, Elliott Company, Jeannette, Pa.

[3] Numbers in parentheses refer to the Bibliography at the end of the paper.

Contributed by the Heat Transfer and Gas Turbine Power Divisions and presented at the Annual Meeting, New York, N. Y., November 27–December 2, 1949, of The American Society of Mechanical Engineers.

 Paper No. 49—A-153.

[4] Within the accuracy of the data it is considered justifiable to apply the fin efficiency to the entire surface. The indirect surface constitutes 85 per cent of the total surface so the uncertainty of the relative effectiveness of direct and indirect surface can have only a small effect on over-all performance.

Introduction

This new type of heat-exchanger surface for gas-to-gas service is a development of the company of one of the authors.[1] The application to commercial-size heat exchangers was carried through in co-operation with the company of the second author,[2] for use in its oxygen pilot plant. The importance of proper heat-exchange design in the satisfactory functioning of the oxygen plant is indicated in a separate report (2) on the performance of this pilot plant.

A broad review of oxygen technology, including a consideration of heat-exchanger requirements, was featured in an AIChE symposium in December, 1946, and was later reported (3). The newer designs of oxygen plants involve heat transfer to gases at comparatively low density and require exchangers of very high efficiency. For such service as well as other applications involving gases at low density some form of extended surface is indicated from the standpoint of economy in cost, size, and weight. Tests of several types of extended surface are reported by Norris and Spofford (1), by London and Ferguson (4, 5) and by Trumpler and Dodge (3). These were all built in comparatively small size.

The present paper describes commercial-size units built around a fin pattern corresponding to sample No. 10 of the Norris and Spofford paper (1) and core J of the London and Ferguson paper (4). The core structure which is illustrative of the flat plate and strip construction is shown in Figs. 1, 2, and 3. Fin elements are built up from thin channel sections of copper which interlock into one another to give rigidity to the structure prior to soldering. The fins are formed by slitting the web of the channel at intervals corresponding to the fin width b, and then offsetting each alternate strip. This gives an arrangement of fins staggered by two's.

Somewhat different methods of construction were employed in the cores tested by the other authors. Norris and Spofford had each fin element consisting of a separate strip of copper. London and Ferguson's cores were made by folding a strip of aluminum back and forth to form a serpentine pattern of fin elements resembling the filler elements of corrugated fiberboard. These variants of fin construction result in only second-order effects in performance.

A radically different arrangement is described by Trumpler and Dodge. The cores, which were developed by Prof. S. C. Collins, consisted of a multiple-annulus tube in which each annulus was packed with closely coiled copper ribbon, soldered to the tube walls, so that a rather complex fin pattern resulted.

The methods which can be employed for assembling small core elements into large-size commercial units vary with the type of core and the intended service. For use in low-temperature plants (oxygen, liquid air, etc.), the following requirements were set for the commercial heat exchangers employing the fin pattern shown in Fig. 1:

1 An arrangement having a very close approach to true counterflow.

2 A single metallically bonded unit of reasonably large size to reduce the number of units per plant, thus eliminating excessive manifolding.

3 A unit capable of withstanding relatively high pressures.

After the initial units for the pilot plant under consideration were built, these parameters of design were increased by the addition of the following elements:

4 A structure of sufficient strength to resist operating pressures without the use of external tie rods, braces, etc.

5 A design to permit close stacking of individual units to minimize exposed surfaces.

6 A structure susceptible of being bonded into a complete unit, including end connections, in one operation.

7 A unit of relatively standardized design giving uniform performance.

8 A design eliminating all possibility of pass-to-pass leakage.

The improved design is shown in Figs. 4 and 5.

Description of Equipment

Core Structure—Fin Pattern. Both test cores and full-scale exchangers were built with fin elements arranged as shown in Fig. 1. Channels are nested twelve to the inch, with alternate strips offset $^1/_{24}$ in. so that a symmetrical pattern is obtained.

This fin pattern was tested with three modifications as given in Table 1.

TABLE 1 FIN PATTERNS TESTED

Core no.	Fin width, b, in.	Nominal fin length, i.e., passage height, $2x_f$, in.	Section tested
1	$^1/_8$	$^1/_2$	3″ × 3″ × 3″ core
2	$^3/_{32}$	$^1/_2$	1−$^1/_2$″ × 3″ and full scale
3	$^3/_{32}$	$^1/_4$	Full scale

Test Cores and Test Equipment. Heat-transfer and pressure-drop results were obtained on test cores 1 and 2. Test core 1 was tested water to air. Description of this core is as follows:

Air side:

5 passages $^1/_2$ in. high and 3 in. wide × 3 in. long
Total heat-transfer surface, A = 4.37 sq ft
Net open cross section, A_c = 0.0492 sq ft
Ratio: surface/cross section, A/A_c = 89

Water side: Cross-flow to air

6 passages 0.08 in. high × 3 in. wide × 3 in. long
Total heat-transfer surface 0.657 sq ft

This core was made up with the 3 in. × 3 in. fin slabs soldered into individual units. These slabs were then separated with U-shaped brass strips soldered in place along the front edges so that the water passage was, in effect, a flat tube 3 in. × 0.080 in. There was thus one water tube between each $^1/_2$-in. air passage.

Test core 2 of the following description was tested steam to air:

Air side:

1 passage $^1/_2$ in. high × 6 in. wide × 3 in. long
Total heat-transfer surface, A = 1.70 sq ft
Net open cross section, A_c = 0.0191 sq ft
Ratio: Surface/cross section, A/A_c = 89

Steam side:

2 passages same as air side, except 3 in. wide × 6 in. long

For heat-transfer tests, core lengths in the direction of air flow were kept small in order to maintain sufficiently high temperature differences between steam and discharge air; for example, an 18-in. length would have resulted in about 0.1 deg F temperature difference, too low for accurate interpretation.

The arrangement of the test stand is shown in Fig. 6. Air flow was measured by a special orifice chamber which had been calibrated by volumetric displacement. Inlet and discharge-air temperatures were measured with unshielded copper-constantan thermocouples inserted in the middle of wooden ducts, the walls of which were close to the air temperature. An excess of steam was passed through the core in order to insure uniformly high rates of heat transfer by condensation with absence of subcooling.

No mixing baffles or straightening vanes were used in the inlet or discharge connections, since the large number of fins in series

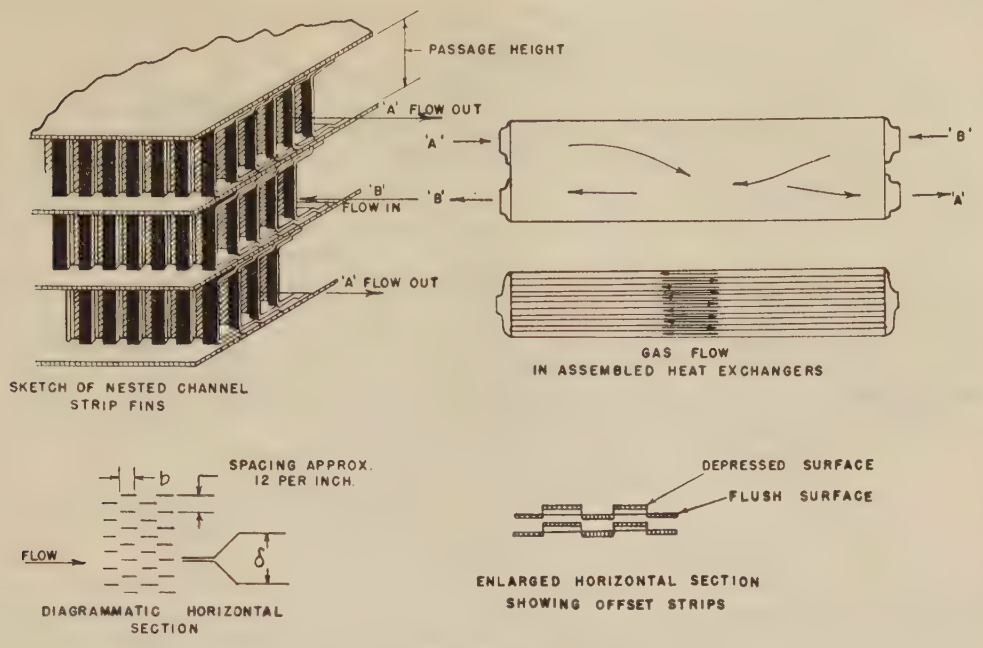

FIG. 1 CORE-STRUCTURE DETAILS

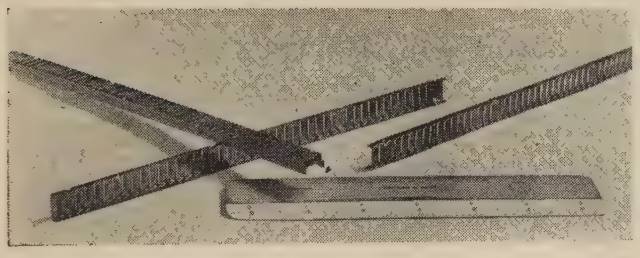

FIG. 2 FIN ELEMENTS

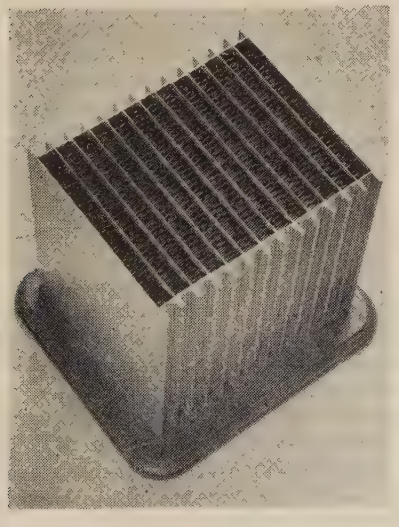

FIG. 3 CORE ASSEMBLY

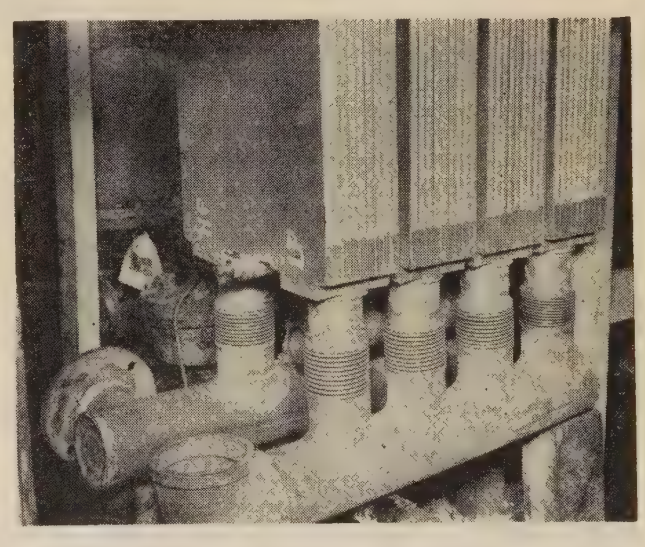

FIG. 4 ASSEMBLY OF IMPROVED DESIGN OF SLAB HEAT EXCHANGERS

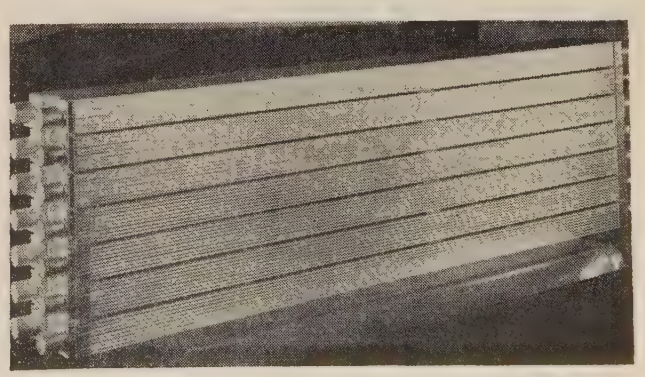

FIG. 5 IMPROVED DESIGN OF SLAB HEAT EXCHANGERS

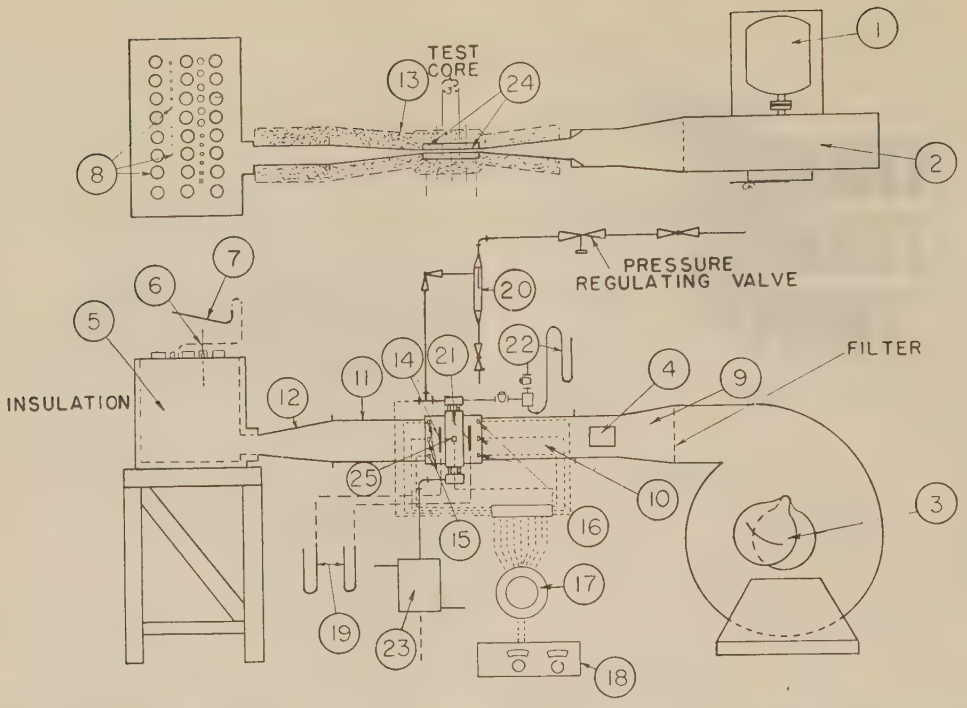

FIG. 6 EQUIPMENT FOR TESTING SMALL CORE SECTIONS

(1) Induction motor, 7.5 hp, 3470 rpm
(2) Blower, centrifugal 1296 cfm 20 in. sp
(3) Air-flow regulator
(4) Air-flow by-pass
(5) Orifice box
(6) Orifice box thermometer
(7) Orifice box draft gage
(8) Orifice plugs
(9) Transition from round to rectangular duct
(10) Transition 6 × 3 in. to 6 × 1/2 in. duct
(11) Transition 6 × 1/2 in. to 6 × 3 in. duct
(12) Transition 6 × 3 in. to 3 × 3 in. duct
(13) Hair-felt insulation
(14) Piezometer rings
(15) Downstream thermocouple grid
(16) Upstream thermocouple grid
(17) Selector switch
(18) Leeds & Northrop portable precision potentiometer No. 8662
(19) Draft gages
(20) Moisture trap
(21) Test core
(22) Mercury manometer
(23) Condenser
(24) Insulated duct
(25) Wall-temperature thermocouple

effected adequate mixing. Flow was fully turbulent in all tests. Reynolds number in the ducts ranged from 4000 to 40,000. A thermocouple, attached to the separating wall of test core no. 2, was used to measure wall temperatures. These values ranged from 0.5 to 1.3 deg F lower than condensing-steam temperatures. The wall temperature in the test of core 1 was calculated on the basis of waterside coefficient being given by

$$hD/k = 0.023\ (DG/\mu)^{0.8}(c_p\mu/k)^{1/3}$$

Large Units and Test Equipment. For convenience in manufacturing and subsequent handling, the finned length of the large units was made 7 1/2 ft. Two types of exchangers were built, each suited to its special application in the oxygen pilot plant. The low-pressure type has equal areas for flow of the two streams since they are both at approximately atmospheric pressure, and the flow quantities are about equal. The high-pressure type has twice as much flow area for the gas at atmospheric pressure as for the one at 6 atm. This pattern results in economy of exchanger volume.

The heat exchangers were built in sections of seven passages, and then the required number of sections were bonded together to make up the final unit. Each section consists of an outer brass plate, a layer of copper fins, a brass separating plate, another layer of fins, another separating plate, and so on, for seven layers of fins, with a final outer plate. The entire assembly was soldered together in a special oven.

For the low-pressure exchangers, the inner passages consist of of 1/2-in. fins, and the two outer passages of 1/4-in. fins, as illustrated in Fig. 7(*a*). This results in a material balance across

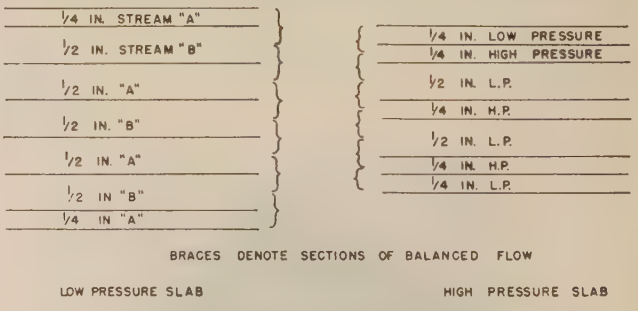

FIG. 7 ARRANGEMENT OF HEAT-EXCHANGER PASSAGES

each separating plate so that heat need be transferred only from the middle of any one passage to the separating plate. Were an even number of passages of equal height used, then, in the outer passages, the heat flow would have to take place across the full passage height which would mean a lower fin effectiveness, the length of the fin then being taken as 1/2 in. for calculating fin effectiveness instead of 1/4 in.

For the high-pressure exchangers having a smaller flow area for the high-pressure stream, there are in each slab section three passages for the high-pressure stream, each passage being 1/4 in. high; and for the low-pressure stream, two 1/2-in. plus two 1/4-in. passages as shown in Fig. 7(*b*).

In the later improved design, the size of the individual slab sections is larger and each slab is provided with standard sweat-solder-type end connections so that each slab becomes a complete heat exchanger. Any number of these individual exchang-

TABLE 4 TEST-CORE RESULTS

Run No.	Air Flow LB/HR	Air Flow Rate, LB/(HR)(FT²)	Air Pressure In, PSIA	Air Pressure Out, PSIA	Pressure Drop PSI	Air Temp. In °F	Air Temp. Out °F	Air Temp. Change δT	Avge. Water or Steam Temp. °F	h Air	h Water	j	f*	R_e**	R_ψ
						Core 1									
1	868	17,650	14.72	14.59	.13	94.2	150.7	56.5	198.5	55.5	2,000	.0104	.040	4,430	8,100
2	647	13,130	14.68	14.60	.081	100.7	160	59.3	198.7	47.5	2,000	.0119	.044	3,250	5,950
3	432	8,770	14.64	14.60	.041	102.6	168.9	66.3	198.0	37.9	2,000	.0143	.050	2,160	3,940
4	216	4,390	14.60	14.59	.014	102.1	180.1	78.0	199.5	24.1	2,000	.0180	.070	1,080	1,970
						Core 2									
1	574	29,900	15.2	14.75	.47	109.3	161.0	51.7	216.4	62.3		.0062	.046	6,620	9,350
2	515	26,820	15.1	14.7	.37	113.6	166.2	52.6	216.5	59.9		.0072	.044	5,910	8,340
3	466	24,250	15.0	14.7	.32	116.0	169.2	53.2	216.6	56.9		.0076	.046	5,330	7,520
4	386	20,100	14.9	14.65	.24	112.1	172.1	60.0	216.5	52.4		.0085	.050	4,420	6,240
5	346	18,030	14.83	14.62	.20	111.4	174.2	62.8	216.7	49.8		.0089	.052	3,970	5,610
6	285	14,850	14.75	14.61	.141	109.9	177.1	67.2	216.8	44.1		.0096	.053	3,260	4,600
7	245	12,750	14.7	14.58	.109	108.8	181.1	72.3	217.5	41.5		.0105	.056	2,800	3,950
8	202	10,520	14.65	14.58	.087	107.4	184.1	76.7	217.3	37.1		.0114	.065	2,315	3,270
9	148	7,720	14.62	14.6	.050	106.6	190.1	83.5	217.5	31.3		.0131	.071	1,690	2,380
10	97.5	5,080	14.6	14.58	.031	107.2	195.7	88.5	218.7	22.6		.0144	.099	1,120	1,580
11	54.4	2,840	14.6	14.56	.013	109.0	201.9	92.9	215.6	16.1		.0184	.131	621	880

* f. values were obtained from pressure drops measured during heating runs. Density was calculated at arithmetic average of inlet and outlet temperature.

** Based on average film temperature.

ers can be connected in parallel simply by connecting them to suitable manifolds. Such an assembly is shown in Fig. 5.

A list of the physical characteristics of the low-pressure exchangers which are called the "clean-up" exchangers is given in Table 2. The term clean-up is used because in operation, water, carbon dioxide, and hydrocarbons from the air are deposited on the metal surfaces as a rime and then removed or "cleaned up" with a stream of warmer nitrogen every 4 hr.

TABLE 2 PHYSICAL CHARACTERISTICS OF LOW-PRESSURE EXCHANGERS

Nitrogen passages (for a single exchanger):
18 passages 1/2 in. high × 12 in. wide × 90 in. long
Total heat-transfer surface, A = 1858 sq ft
Net open cross section, A_c = 0.70 sq ft
Ratio: surface/cross section, A/A_c = 2655
a/s = 354 per ft of length
Fin perimeter ψ = 0.0166 ft
$D_e = 4rH$ = 0.0117 ft
Air passages (for a single exchanger):
12 passages 1/2 in. high × 12 in. wide × 90 in. long
Plus 12 passages of 1/4 in. high × 12 in. wide × 90 in. long; for purpose of heat-transfer and pressure-drop calculations, set is considered as 18 passages, 1/2 in. high, i.e., identical with nitrogen passages

There are four units of this type, identified as C-1, C-2, D-1, and D-2. Two of these units, C-1 and C-2, in one set and D-1 and D-2 in the other set, are operated in series.

There are two sets of high-pressure heat exchangers termed A and B. The B exchanger consists of two 7.5-ft units, each having the dimensions given in Table 3.

TABLE 3 PHYSICAL CHARACTERISTICS OF HIGH-PRESSURE EXCHANGERS

Low-pressure side:
The same as the air passages of the clean-up exchangers
High-pressure side:
18 passages 1/4 in. high × 12 in. wide × 90 in. long
Total heat-transfer surface, A = 1.019 sq ft
Net open cross section, A_c = 0.388 sq ft
Ratio: surface/cross section, A/A_c = 3020
a/s = 403 per ft of length

The A exchanger consists of a single 7.5 ft unit identical in every respect to the B units, except that the A unit has only one third the number of passages as the individual B units and therefore one third the surface area and net open area. The value of the ratio A/A_c is the same in both A and B exchangers.

Temperatures were measured with copper-constantan thermocouples which had been calibrated in an ice bath against mercury-in-glass thermometers and by immersion in boiling oxygen of 99.5 per cent purity. The thermocouples were soldered to the ends of thin-wall stainless-steel tubes which were inserted into the inlet and outlet ducts.

The thermocouple leads were carried without intermediate junctions to a Brown electronic indicating potentiometer, having a response time of about 4 sec. Therefore a complete record of temperature conditions in an exchanger could be taken in less than 1 min.

Test Results

Core Tests. Core-test results are given in Table 4. Values of f and j obtained with the first sample having 1/8-in-wide strip fins were slightly higher than reported by Norris and Spofford (1), as shown in Fig. 8. Tests of the second sample with 3/32-in-wide fins gave, over most of the range, lower values of j and higher values of f than predicted by the tests of Norris and Spofford (1). The results with 3/32-in. fins were confirmed by the tests of Kays and London (6) made on core sample 9 3/4 in. × 8 3/8 in. × 3.844 in. air-flow length, as shown in Fig. 9. The values of friction factor obtained by Kays and London at the low flows (hence low pressure drops) are believed to be more reliable and are the values used in the construction of Fig. 8.

The plotted values of the Norris and Spofford tests are shown lower than given in their paper. They used a surface area of the full fin surface plus one half the direct surface. In the present paper and in the work of London and Ferguson (4), the area is considered the full fin surface plus the full direct surface. Either method of representation is, of course, purely arbitrary.

The effective diameter to be employed for calculating Reynolds number is different in the two plots. Norris and Spofford proposed the fin perimeter, $\psi = 2(b + \delta)$ as a suitable correlating term. London and Ferguson pointed out that this is inadequate to cover all types of surface, and suggested that representation be made on the basis of the mean hydraulic diameter, $D_e = 4A_c/(A/L)$. There is probably no simple method of representation which will show the effect on performance of fin size, shape, passage spacing, etc.

Failure to realize improvement in j-values for the fins of reduced perimeter (as predicted by the Norris and Spofford correlation) is apparently due to the corresponding reduction in distance between in-line surfaces.

The values of friction factor f, obtained with all test cores, were higher than predicted by Norris and Spofford, as shown in Fig. 8. This may be attributed to difference in thickness of fins and condition of leading edges. Fin dies were of a preliminary nature and did not produce fin edges completely free of burr.

Performance of Assembled Heat Exchangers. The assembled heat exchangers were tested as part of the operation of the oxygen

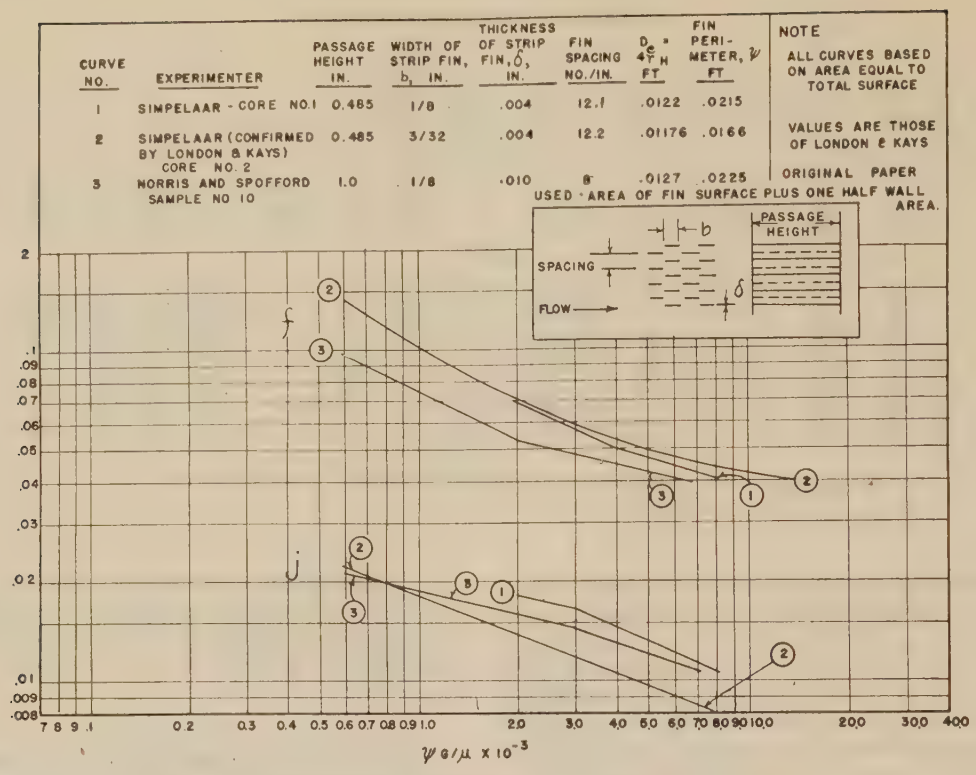

FIG. 8 COMPARISON OF PERFORMANCE OF DIFFERENT STRIP FINS
(Tests of Simpelaar and Aronson and of Norris and Spofford.)

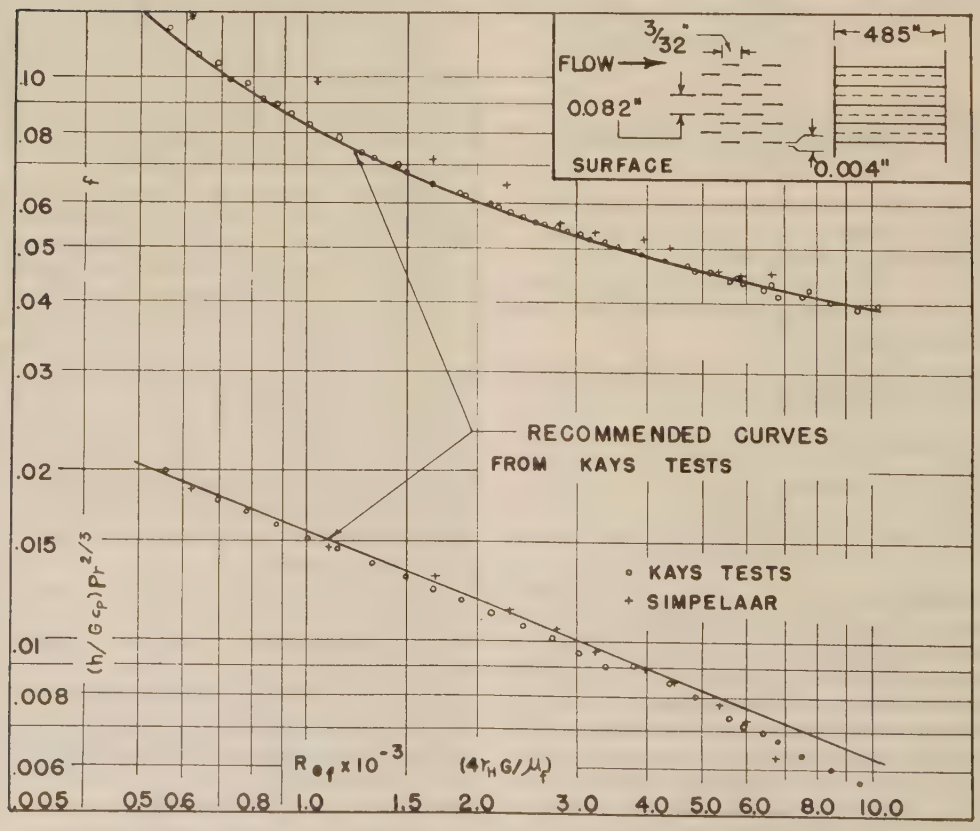

FIG. 9 PERFORMANCE OF STRIP-FIN TEST CORE
(Comparison of test results of Simpelaar and Aronson and Kays and London.)

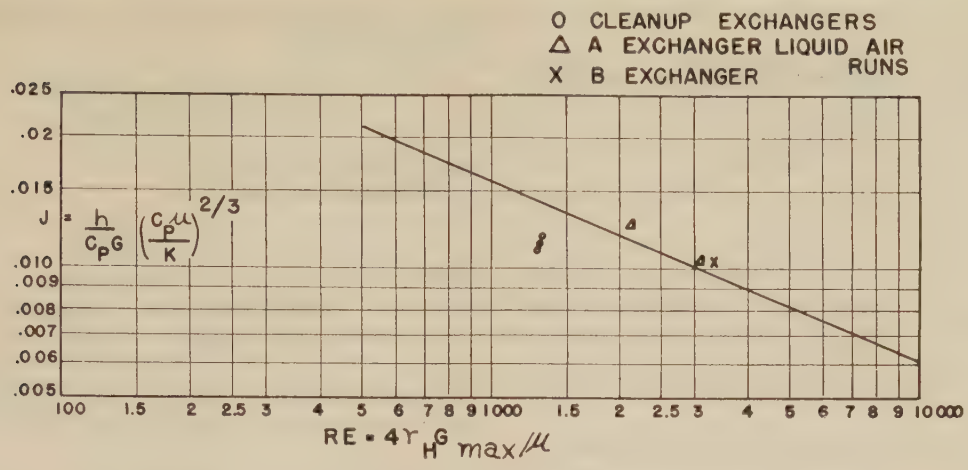

Fig. 10 Heat-Transfer Factors for Heat Exchangers

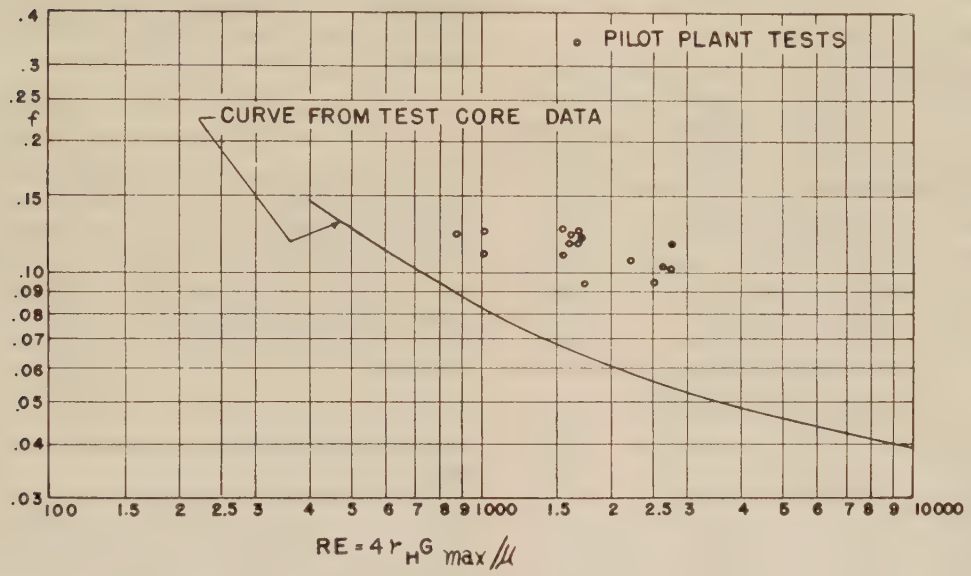

Fig. 11 Friction Factors for Heat Exchangers

pilot plant. Comparison of performance between assembled units and test cores is presented in Figs. 10 and 11. The reasonably good agreement of heat-transfer performance indicates that inefficiencies introduced when building up from test core to large-scale assembly are of small magnitude. The apparently poorer results indicated on the low-pressure clean-up exchangers may be attributed partly to errors in thermocouple readings and partly to a real decrease in efficiency due to nonuniform flow distribution. These exchangers have different-type end connections than the high-pressure exchangers, so that there may be a difference in the pattern of flows down the passages. An unbalance in flow of 2 per cent from one side of an exchanger passage to the other side results in an increase in end-temperature difference of 5.2 per cent, which represents just that much poorer performance. This lack of good flow balance is likely to be the only reason for poorer heat-transfer results in large-scale units.

Heat balances of the exchangers were made as part of the check of the over-all plant performance. In view of the extremely small end-temperature differences, such heat balances can only check the order of magnitude of the calculated performance.

Table 6 is a sample sheet showing the step-wise method of calculating the performance of exchanger B. A discussion of the factors involved is given in the Appendix. The variation of temperature with length of the heat exchanger is shown graphically in Fig. 12.

The over-all pressure drops measured on the assembled heat exchangers are greater than those predicted from results on test cores as may be seen from Fig. 11, showing friction factor plotted against Reynolds number. This higher pressure drop is attributed to losses in the end connections, the magnitude of which can only be estimated from the observed over-all performance. The end connections which provide for distribution of the flow from the relatively narrow inlet nozzle to the full width of the exchanger slab are built up of a number of hollow rectangular tubes placed in the form of a grid. These tubes support the separating plates, at the same time permitting flow to take place in two directions. The arrangement of these spacer tubes is shown in Fig. 13. For the clean-up exchangers, the "low-pressure-pass" arrangement is used on both air and nitrogen passes. For the high-pressure exchangers A and B, the arrangements are as indicated, respectively, for the two sets of passes.

Table 7 gives typical pressure-drop results for the pilot-plant

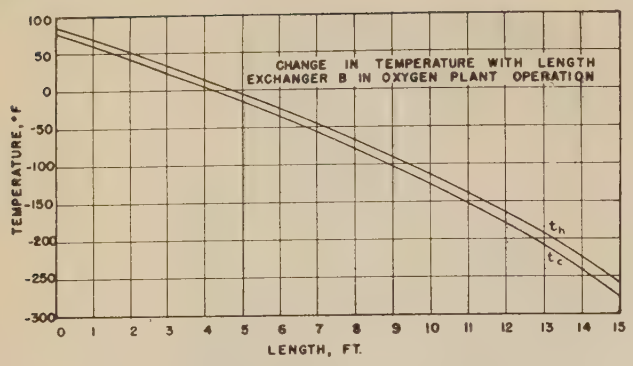

FIG. 12 CHANGES IN TEMPERATURE WITH LENGTH FOR EXCHANGER B IN OXYGEN-PLANT OPERATION

TABLE 5 CLEAN-UP EXCHANGERS—RECYCLE RUNS

Exchanger And Date	Section	Temperature In °F	Temperature Out °F	Temperature Difference Observed	Calc.	Discrepancy
(D-1 (D-2 2/19/48 Full Flow	Warm	50	40.5	9.5		
	Middle	-140	-150.5	10.5		
3,550 lb/hr	Temp.Change	190.	191.			
	Average			10.0	8.9	-12%
	Middle	-140	-150.5	10.5		
	Cold	-287.3	-301.5	14.2		
	Temp.Change	147.3	151.			
	Average			12.3	8.5	-45%
(C-1 (C-2 2/21/48 Full Flow	Warm	45	34.8	10.2		
	Middle	-139.2	-148.5	9.3		
3,550 lb/hr	Temp.Change	184.2	183.3			
	Average			9.8	8.6	-14%
	Middle	-139.2	-148.5	9.3		
	Cold	-290.8	-303.0	12.2		
	Temp.Change	151.6	154.5			
	Average			10.7	8.7	-23%
(D-1 (D-2 2/20/48 Full Flow	Warm	46.5	37.8	8.7		
	Middle	-144.5	-153.8	9.3		
3,550 lb/hr of air	Temp. Change	191.0	191.6			
	Average			9.0	8.9	-1%
	Middle	-144.5	-153.8	9.3		
	Cold	-288.0	-303.5	15.5		
	Temp. Change	143.5	149.7			
	Average			12.4	8.5	-46%
(C-1 (C-2 2/20/49 Full Flow	Warm	43.5	33.0	10.5		
	Middle	-139.9	-149.0	9.1		
3,550 lb/hr	Temp.Change	183.4	182.0			
	Average			9.8	8.5	-15%
	Middle	-139.9	-149.0	9.1		
	Cold	-289.9	-303.8	13.9		
	Temp.Change	150.0	154.8			
	Average			11.5	8.7	-32%

runs. The friction factors have been calculated using the following relationships

$$\Delta P = \frac{f \times G^2 \times 4L}{2g\rho D_e}$$

where Δp is in lb per sq ft.

For 90-inch core length

$$4L/D_e = 2655$$

Then

$$f = \frac{2(4.17)\ (10^8)\ (\Delta P)\rho}{G^2\ (2655)} = \frac{(31.4)\ (10^4)\ (\Delta P)\rho}{G^2}$$

The gas densities and viscosities were calculated at the arithmetic average of the inlet and discharge temperature.

Conclusions

Thermal efficiency of large-size heat exchangers agreed reasonably well with values predicted from test-core results. The heat-transfer performance for this particular strip fin can be represented by

$$j = \frac{h}{cG}\left(\frac{c_p\mu}{k}\right)^{2/3} = 0.245\ (D_eG/\mu)^{-0.4}$$

Large-size heat exchangers had larger pressure losses than predicted from test-core results. Improved design of end connections and distributing sections would reduce pressure losses. This would make it possible to increase the velocity through the core for the same pressure loss and thus increase the heat-transfer capacity of a given core. Over the range of Reynolds number from 2000 to 10,000, the friction factor for the test cores can be represented by

$$f = 0.393\ (D_eG/\mu)^{-0.25}$$

In the actual full-size cores the apparent f was almost double this value.

True counterflow heat exchangers, having an efficiency of 95 per cent in a 7.5-ft length, have proved satisfactory in the operation of a tonnage gaseous oxygen plant. The use of an interrupted strip fin having a high surface area per unit volume (300 sq ft total transfer area per cu ft of volume) makes possible close end-temperature differences with a compact heat exchanger. The design is suitable for gas-to-gas applications for pressures up to about 150 psig and temperatures from about 250 deg F (limited by strength of solder) down to as low as required.

TABLE 6 CALCULATION OF EXCHANGER B PERFORMANCE

High Pressure Temp. t_h	Net Joule-Thomson Δt	Adjustment for Unbalanced Flow	(a) Net Temp. Diff. $t_h - t_c$	Low Pressure Temp. t_c	Low Pressure Temp. Change δt_c	(b) δt_c x.896	(c) High Pressure Temp.Change δt_h	(e) $\left(\frac{\mu_t}{\mu_{100}}\right)^{0.4}$	(d)= (b)+(c)	Relative $\Delta l = \frac{(d)}{(a)(e)}$	Δl feet
85	0.0	0.0	6.5	78.5							
84			6.5	77.5	2.0	1.80	2.0	0.993	3.80	0.589	.1192
83	0.0	0.0	6.5	76.5							
66.5			6.8	59.7	33.6	30.1	33.0	0.980	63.1	9.48	1.916
50	0.2	0.4	7.1	42.9							
25			7.6	17.4	51.1	45.8	50	0.950	95.8	13.25	2.680
0	0.6	1.1	8.2	-8.2							
-25			8.7	-33.7	51.1	45.8	50	0.921	95.8	11.95	2.418
-50	1.1	1.7	9.3	-59.3							
-75			10.0	-85.0	51.4	46.1	50	0.880	96.1	10.93	2.220
-100	1.9	2.3	10.7	-110.7							
-125			11.6	-136.6	51.7	46.3	50	0.837	96.3	9.92	2.007
-150	3.0	2.9	12.4	-162.4							
-175			13.6	-188.6	52.4	47.0	50	0.787	97.0	9.06	1.832
-200	4.8	3.5	14.8	-214.8							
-215			15.9	-230.9	32.3	29.0	30	0.741	59.0	5.00	1.012
-230	6.7	3.9	17.1	-247.1							
-243.2			18.7	-261.9	29.6	26.5	26.5	0.720	53.0	3.94	.797
-256.5	9.5	4.2	20.2	-276.7							
										74.12	15.001

TABLE 7 PRESSURE DROP; PILOT-PLANT EXCHANGERS

Run	Exchanger	Flow lb/hr	Mass Flow Rate lb/(hr)(ft)^2	Avge.* Temp. °F	Avge.* Pressure psia	Pressure Drop $\frac{\Delta p}{2}$ in.Hg.	Pressure Drop $\frac{\Delta p}{2}$ ft^2	Reynolds Number $D_e G/\mu$	Friction Factor f
1/22/48 2:30 A.M.	D-1	2,080	2,970	-54	17.1	0.45	31.7	1,010	.124
	D-2	2,080	2,970	-231	17.3	0.25	17.6	1,710	.123
1/22/48 6:30 A.M.	C-1	2,080	2,970	-57	17.1	0.40	28.2	1,020	.111
	C-2	2,080	2,970	-232	17.3	0.20	14.1	1,720	.095
1/22/48 9:30 P.M.	C-1	1,730	2,470	-70	16.8	0.30	21.1	870	.122
	C-2	1,730	2,470	-248	17.0	0.15	10.6	1,530	.114
1/22/48 2:30 A.M.	B-1	3,420	4,880	+ 3	15.8	1.55	109.	1,510	.128
	B-2	3,420	4,880	-168	16.4	0.80	56.3	2,210	.108
2/7/48 3:30 A.M.	D-1	3,460	4,760	-40	17.2	1.15	80.8	1,570	.119
	D-2	3,460	4,760	-211	17.6	0.55	39.3	2,490	.095
2/7/48 6:30 A.M.	C-1	3,460	4,760	-56	17.2	1.15	80.8	1,640	.124
	C-2	3,460	4,760	-234	17.6	0.60	42.2	2,760	.119
2/7/48 10:30 A.M.	B-1	3,460	4,760	-60	18.3	1.0	70.4	1,650	.117
	D-2	3,460	4,760	-232	18.6	0.5	35.2	2,730	.104
2/7/48 3:30 A.M.	B-1	3,880	5,540	-15	16.2	1.75	123.2	1,750	.122
	B-2	3,880	5,540	-181	16.8	0.9	63.4	2,600	.104

* Arithmetic average of inlet and discharge conditions.

Note: Nitrogen gas used in all of the above tests.

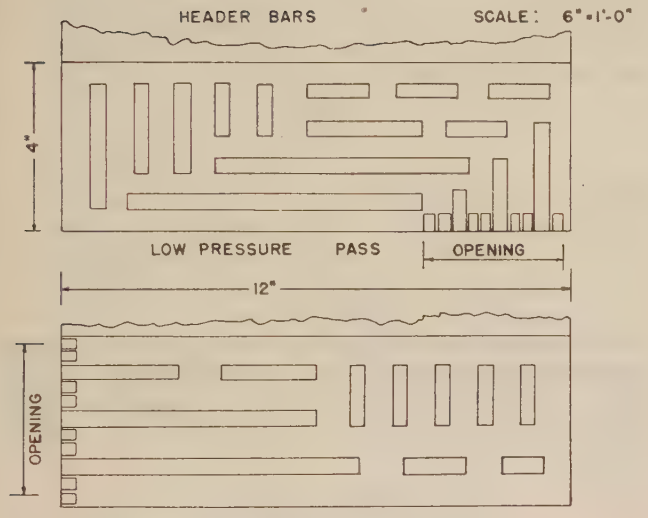

FIG. 13 PATTERNS OF SPACER TUBES IN END MANIFOLDS OF HEAT EXCHANGERS

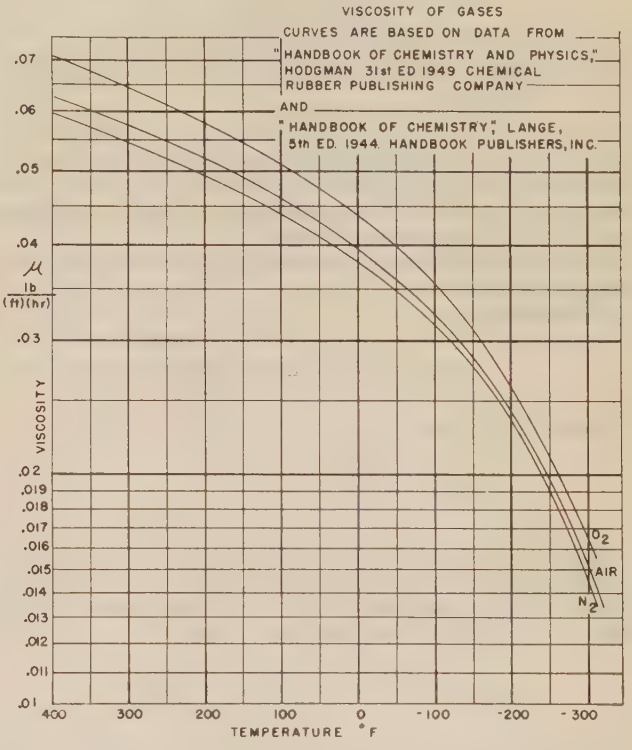

FIG. 14 CHART OF VISCOSITIES FOR AIR, NITROGEN, AND OXYGEN

ACKNOWLEDGMENTS

The successful construction of these heat exchangers is due largely to the untiring efforts of Mr. Don Huggins, Mechanical Engineer at Modine Manufacturing Company, who supervised exchanger assembly. Core tests were the work of Mr. Huggins and Modine laboratory technicians. Performance values on the large heat exchangers were obtained by the plant engineers responsible for the design and operation of the Elliott Company oxygen pilot plant, Messrs. Duffer Crawford, Joseph Cost, Carroll Claitor, and Mack Atcheson.

The authors also wish to express their appreciation of the contribution of Modine Manufacturing Company and the Elliott Company who underwrote this project and agreed to publication of the results.

BIBLIOGRAPHY

1 "High-Performance Fins for Heat Transfer," by R. H. Norris and W. A. Spofford, Trans. ASME, vol. 64, 1942, pp. 489–496.

2 "The Elliott Oxygen Pilot Plant," by I. Roberts, D. Aronson, M. Atcheson, L. C. Claitor, J. L. Cost, and D. B. Crawford, *Industrial and Engineering Chemistry*, vol. 41, 1949, pp. 2661–2669.

3 "The Design of Ribbon Packed Exchangers for Low Temperature Air Separation Plants," by P. R. Trumpler and B. F. Dodge, Trans. AIChE, vol. 43, Feb., 1947, pp. 75–84.

4 "Gas Turbine Plant Regenerator Surfaces—Basic Heat Transfer and Flow Friction Data," by A. L. London and C. K. Ferguson, Bureau of Ships Research Memorandum no. 2–46 Navships (250-338-3), July, 1946.

5 "Test Results of High-Performance Heat-Exchanger Surfaces Used in Aircraft Intercoolers and Their Significance for Gas-Turbine Regenerator Design," by A. L. London and C. K. Ferguson, Trans. ASME, vol. 71, 1949, pp. 17–26.

6 "Tests of a Strip-Fin Heat Exchanger Surface," by W. M. Kays, Technical Report no. 4, Navy Contract N6-ONR-251 Task Order VI (NR-035-104), Department of Mechanical Engineering, Stanford University, A. L. London, Project Supervisor.

7 "Thermodynamics," by G. N. Lewis and M. Randall, second edition, McGraw-Hill Book Company, Inc., New York, N. Y., 1923, pp. 65–68.

8 "Thermodynamic Properties of Oxygen, Nitrogen, and Air," by L. C. Claitor and D. B. Crawford, Trans. ASME, vol. 71, 1949, pp. 885–895.

Appendix

Calculation of Exchanger Performance

The method of stepwise calculation of exchanger performance has been developed as follows:

For each set of passages of incremental length, Δl, the incremental NTU is

$$\Delta NTU_c = \frac{\delta t_c}{\Delta t_c} = \frac{j_c (a/s)_c (\Delta l)}{0.818}$$

$$\Delta NTU_h = \frac{\delta t_h}{\Delta t_h} = \frac{j_h (a/s)_h (\Delta l)}{0.818}$$

where

δt_h = temperature change of hot fluid over length of exchanger
$\Delta t_h = t_h - t_m$ = temperature difference between hot fluid and metal wall
$\Delta t_c = t_m - t_c$ = temperature difference between metal wall and cold fluid
$t_h - t_c$ = temperature difference between two gases
a/s = ratio of total surface to net open area per unit of length

The equations for NTU are applicable over a short length for which the conditions of physical properties and temperature differences between the two gases are essentially constant. The performance for the full exchanger length is obtained by adding up the NTU for each elemental length.

The over-all NTU can be determined as a ratio of the NTU for either of the two streams:

For the hot stream

$$NTU_h = \frac{\delta t_h}{t_h - t_c} = \frac{\delta t_h}{\Delta t_h + \Delta t_c}$$

For the cold stream

$$NTU_c = \frac{\delta t_c}{t_h - t_c} = \frac{\delta t_c}{\Delta t_h + \Delta t_c}$$

Arbitrarily, the over-all NTU, based on the hot stream, will be used for calculating the exchanger performance. The final answer would be identical were the NTU based upon the cold stream. For the NTU based on the hot stream

$$NTU_h = \frac{\delta t_h}{t_h - t_c} = \frac{j_h \eta_h (a/s)_h (\Delta l) (\Delta t_h)}{(\Delta t_h + \Delta t_c)(0.818)}$$

To find the value of the ratio $\Delta t_h/(\Delta t_h + \Delta t_c)$ in terms of the known physical characteristics and temperature changes

$$\Delta t_h = \frac{\delta t_h (0.818)}{j_h \eta_h (a/s)_h (\Delta l)}$$

$$\Delta t_c = \frac{\delta t_c (0.818)}{j_c \eta_c (a/s)_c (\Delta l)}$$

$$\frac{\Delta t_h}{\Delta t_h + \Delta t_c} = \frac{\delta t_h (0.818)}{[j_h \eta_h (a/s)_h (\Delta l)] \left[\frac{\delta t_h (0.818)}{j_h \eta_h (a/s)_h (\Delta l)} + \frac{\delta_c t_c (0.818)}{j_c \eta_c (a/s)_c (\Delta l)}\right]}$$

which simplifies to

$$\frac{\Delta t_h}{\Delta t_h + \Delta t_c} = \frac{\delta t_h}{\delta t_h + \delta t_c \left(\frac{j_h}{j_c}\right)\left(\frac{\eta_h}{\eta_c}\right)\left[\frac{(a/s)_h}{(a/s)_c}\right]}$$

Substituting the value of this ratio in the equation for NTU

$$NTU_h = \frac{\delta t_h}{t_h - t_c} = \frac{j_h \eta_h (a/s)_h (\Delta l) (\delta t_h)}{0.818 \left[\delta t_h + \delta t_c \left(\frac{j_h}{j_c}\right)\left(\frac{\eta_h}{\eta_c}\right)\frac{(a/s)_h}{(a/s)_c}\right]}$$

Rearranging this equation

$$\Delta l = \frac{(0.818)\left[\delta t_h + \delta t_c \left(\frac{j_h}{j_c}\right)\left(\frac{\eta_h}{\eta_c}\right)\frac{(a/s)_h}{(a/s)_c}\right]}{j_h \eta_h (a/s)_h (t_h - t_c)}$$

The ratio of the two heat-transfer factors is a function of the modified Reynolds number to the 0.4 power (as indicated by test-core results)

$$\frac{j_h}{j_c} = \frac{0.245/(D_e G/\mu)_h^{0.4}}{0.245/(D_e G/\mu)_c^{0.4}}$$

The value of the effective diameter D_e for the two streams is taken as being equal.

The viscosities of the two gases, hot gas and the cold gas, within the same small increment of length, under conditions of operation, may be considered equal; hence

$$\frac{j_h}{j_c} = \left(\frac{G_c}{G_h}\right)^{0.4}$$

Then

$$\Delta l = \frac{(0.818)\left[\delta t_h + \delta t_c \left(\frac{G_c}{G_h}\right)^{0.4}\left(\frac{\eta_h}{\eta_c}\right)\frac{(a/s)_h}{(a/s)_c}\right]}{j_h \eta_h (a/s)_h (t_h - t_c)}$$

The calculation of exchanger performance can be handled by relating the performance at any section (and any temperature) to the performance at an arbitrary temperature. This arbitrary standard temperature is taken as 100 F. The ratio of performance is given by

$$\frac{j_{100}}{j_t} = \frac{0.245/(D_e G_{100}/\mu_{100})^{0.4}}{0.245/(D_e G_t/\mu_t)^{0.4}}$$

Since D_e and G are constant along the length of the exchanger

$$j_{100}/j_t = (\mu_{100}/\mu_t)^{0.4}$$

Substituting the value of $(j_h)_{100}$ in the equation for performance

$$\Delta l = \frac{0.818\left[\delta t_h + \delta_{tc}\left(\frac{G_c}{G_h}\right)^{0.4}\left(\frac{\eta_h}{\eta_c}\right)\frac{(a/s)_h}{(a/s)_c}\right]}{(j_h)_{100}\left(\frac{\mu_t}{\mu_{100}}\right)^{0.4} \eta_h (a/s)_h (t_h - t_c)}$$

From this equation the incremental length for each temperature range can be calculated and then the value of $(j_h)_{100}$ determined from the conditions in any particular interval of length. The method of calculating performance is illustrated by the following example:

Exchanger B is handling a flow of 4220 lb per hr of nitrogen in the high-pressure passages and 4270 lb per hr in the low-pressure passages. The respective average pressures are 85 psia and 18 psia. The observed end temperature conditions are as follows:

	Temperature, deg F		
	High pressure	Low pressure	Difference
Warm end	85	78.5	6.5
Cold end	—256.5	—276.7	20.2
Temperature change	341.5	355.2	

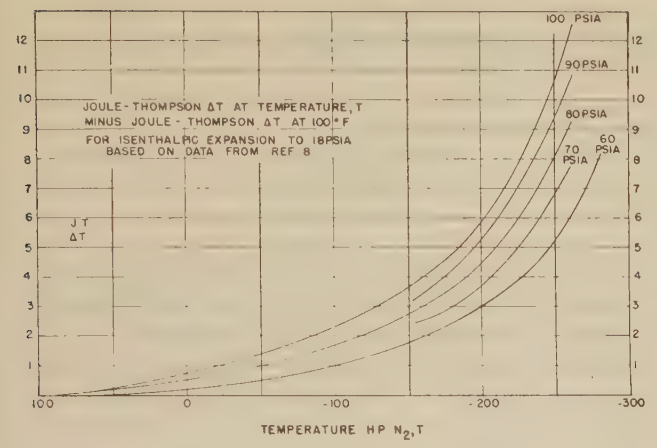

FIG. 15 NET JOULE-THOMSON ΔT

The detailed calculations are handled in tabular form as shown in Table 6. The multiplier for the temperature change δt_c of the cold fluid is

$$\left(\frac{G_c}{G_h}\right)^{0.4} \frac{\eta_h}{\eta_c} \frac{(a/s)_h}{(a/s)_c} = \left(\frac{6100}{12{,}500}\right)^{0.4} \left(\frac{0.967}{0.922}\right) \left(\frac{403}{354}\right) = 0.896$$

The ratio of fin effectiveness for the hot fluid to that of the cold fluid at 100 F is 0.967/0.922 and is taken as being constant over the entire length of the exchanger. Variation of this ratio with temperature is negligible.

The first five columns of the table are used to calculate a heat balance over each incremental length. The balance could be made by taking enthalpy values from a temperature-enthalpy chart or table but as a practical method the scheme shown is easier to handle. The high-pressure temperature is split into convenient intervals with the first increment taken as small as 2 deg in order to reduce the effect of averaging in using this interval for calculating the value of j_{100}. The net Joule-Thomson effect (7) is the difference between the Joule-Thomson effect at an arbitrary temperature (taken at 100 F) and the Joule-Thomson effect at the particular temperature interval. Values are plotted in Fig. 15. The adjustment for unbalance flow is calculated by allowing a higher or lower temperature change for the low-pressure stream than for the high-pressure stream, inversely proportional to the difference of the two molal flows. The column next to the last is calculated as an incremental length which is converted to actual incremental lengths in the last column.

The value of the heat-transfer factor at 100 F is then calculated by using the performance values over any increment of length

$$j_{100} = \frac{0.818 \left[\delta t_h + (\delta t_c) \left(\frac{G_c}{G_h}\right)^{0.4} \frac{\eta_h}{\eta_c} \frac{(a/s)_h}{(a/s)_c} \right]}{\Delta l \left(\frac{\mu_t}{\mu_{100}}\right)^{0.4} \eta_h (a/s)_h (t_h - t_c)}$$

Substituting the values from the table for the interval 85 deg to 83 deg

$$j_{100} = \frac{0.818 \, [2 + 2 \, (0.896)]}{(0.1192) \, (0.993) \, (0.967) \, (403) \, (6.5)} = 0.0104$$

Reynolds number at 100 deg F for the given conditions of flow is

$$D_e G/\mu = (0.0117) \, (12{,}500)/(0.044) = 3320$$

From the temperature and incremental length values in Table 6, the change of temperature along the length of the exchanger can be plotted, as has been done in Fig. 12.

Design of Regenerators for Gas-Turbine Service

By DAVID ARONSON[1]

This paper presents a method for designing gas-turbine regenerators with particular reference to the condition of space being the principal limitation on design. For the plate-fin structure a procedure is given for arriving at maximum performance attainable in a given volume of regenerator core, and for calculating the fin patterns and plate spacings required to obtain such maximum performance. For the tubular-type regenerator a method of arriving at optimum tube spacings is presented.

Nomenclature

A = heat-transfer area, sq ft

a = factor in determining fin effectiveness, $a = (2h/kt)^{0.5}$

B = constant $\dfrac{j/(f/2)_g \eta_g R L_c^2}{(NTU)(W_g v_g)^2 (\mathrm{Pr})^{2/3}}$

b = wetted perimeter, ft

c = fraction of total length, L_c, given to cold stream:
$L_c(c)$ = total height in no-flow direction of all cold-stream passages, ft
$L_c(1 - c)$ = total height in no-flow direction of all hot-stream passages, ft

c_p = specific heat at constant pressure, Btu/(lb F)

C = air or gas capacity rate, $C = Wc_p$, Btu/(hr F)

C_2, C_3, C_4, C_5 = constants related to f, j, and $j/(f/2)$

C_7, C_8, C_9 = constants relating performance inside to outside of tubes

D_e = equivalent diameter of passage, for rectangular passages, ft

$$D_e = 4r_h = \frac{4S}{b} = \frac{4(D_1 D_2)}{2(D_1 + D_2)} = \frac{2D_1 D_2}{D_1 + D_2}$$

D_1 = width of rectangular passage, ft or in.

D_2 = height of rectangular passage, ft or in.

D_i = inside diameter of round tubes, ft or in.

D_o = outside diameter of round tubes, ft or in.

F = ratio of design factors, dimensionless (see text)

f, f_o = see dimensionless groupings

G = mass velocity, lb/(hr ft²) or lb/(sec ft²) $G = V\rho$ or $= V/v$

G_o = mass velocity at minimum opening between tubes, lb/(hr ft²) or lb/(sec ft²)

g = proportionality factor, $g = 32.2$ lb ft/# sec² $= 4.17 \times 10^4$ lb ft/# hr²

h = unit conductance for thermal convection heat transfer, Btu/(hr ft² F)

j = see dimensionless groupings

k = thermal conductivity, Btu/(hr ft² F/ft)

L = flow length, ft

L_a = length of passage for flow of gas, ft

L_b = length of passage for flow of air, ft

L_c = length of assembly of passages in no-flow direction for crossflow plate-fin type exchanger, or length in no-flow direction for tubular exchanger, ft

L_n = dimension in direction of stream flowing across outside of tubes, ft

L_T = length of tubes, ft

N = number of tubes in direction of flow across tubes, dimensionless $N = L_n/S_L$

NTU = see dimensionless groupings

P = pressure, #/in.² or #/ft²

$(\Delta P/P)$ = pressure-drop ratio, dimensionless

R = gas constant; for air $R = 53.3$ ft #/(lb F)

r = ratio of volume flow of two streams, dimensionless

$$r = \frac{(W/\rho)_a}{(W/\rho)_g} = \frac{W_a v_a}{W_g v_g}$$

r_h = hydraulic radius, ft

S = free flow area, sq ft

S_T/D_o = tube-spacing ratio, center to center in direction normal to gas flow, dimensionless

S_L/D_o = tube-spacing ratio, center to center in direction of gas flow, dimensionless

T = temperature, R

t = temperature, F

$\Delta t_{\ln}$ = long mean temperature difference, F

$$t_{\ln} = \frac{[(t_1)_g - (t_2)_a] - [(t_2)_g - (t_1)_a]}{\ln\left[\dfrac{(t_1)_g - (t_2)_a}{(t_2)_g - (t_1)_a}\right]}$$

Δt_m = mean-effective-temperature difference to be used in determining efficiency for crossflow heat exchangers, F

$$\Delta t_m = Y(\Delta t_{\ln})$$
$$\Delta t_m = (\Delta t_m)_g + (\Delta t_m)_a$$

$(\Delta t_m)_a$ = mean-effective-temperature difference between air and metal wall

$(\Delta t_m)_g$ = mean-effective-temperature difference between gas and metal wall

Δt_o = difference between bulk fluid temperature and temperature of metal wall at base of fin

δt = change in temperature of fluid going through regenerator, F, $\delta t = t_1 - t_2$

U = unit over-all thermal conductance, Btu/(hr ft² F of A)

V = velocity of fluid, at average air or gas temperature, fps

v = specific volume, at average air or gas temperature, ft³/lb

---

[1] Section Engineer, Heat Process, Elliott Company, Jeannette, Pa. Mem. ASME.

Contributed by the Heat Transfer and Gas Turbine Power Divisions and presented at the Annual Meeting, New York, N. Y., Nov. 27–Dec. 2, 1949, of The American Society of Mechanical Engineers.

 Paper No. 49—A-144.

W = flow rate, lb/sec or lb/hr

x_f = effective length of fin

Y = correction factor to apply to log-mean-temperature difference to obtain effective temperature difference, dimensionless

$$Y = \Delta t_m / \Delta t_{\ln}$$

from which $NTU = \delta t/(Y \Delta t_{\ln})$

Values of Y are summarized on page 147 of (15)[2] from report of Bowman, Mueller, and Nagle (16).

δ, Δ = prefixes denoting difference

ϵ = heat-exchanger effectiveness, a function of NTU, C_a/C_g, and flow arrangement, dimensionless (see Fig. 2)

$$\epsilon = \frac{(t_2)_a - (t_1)_a}{(t_1)_g - (t_1)_a} = X \text{ of McAdams (15)}$$

η = combined fin and metal-wall effectiveness, dimensionless

$$\eta = \eta_e \frac{D_2}{D_1 + D_2} + 1.00 \frac{D_1}{D_1 + D_2}$$

η_e = fin effectiveness, dimensionless

$$\eta_e = \frac{\tanh ax_f}{ax_f}$$

μ = absolute viscosity, lb/(hr ft)

ρ = fluid density, lb/ft^3

σ = ratio of free flow to frontal area, dimensionless

Dimensionless Grouping

A/S = ratio of surface area to net open area. $A/S = 4L/D_e$

$f = \dfrac{(\Delta P)(v)}{(V^2/2g)\,(A/S)}$ = Fanning friction factor. The f versus Re plot defines the friction characteristic of the surface

$= \dfrac{(\Delta P)(v)}{(V^2/2g).N}$ = friction factor for flow across tubes. The f_o versus Re plot defines the friction characteristic of the tube pattern. The velocity, V, is that at the minimum opening between tubes and N is the number of such openings in the direction of flow

f_o is related to f by:

$$f_o \frac{(S_T/D_o - 1)}{\pi/4} = \phi \Rightarrow f$$

j = (St) (Pr)$^{2/3}$ = generalized heat-transfer grouping. This factor, j versus Re, defines the heat-transfer characteristic of the surface

NTU = number of core "heat-transfer units," a dimensionless expression of the "heat-transfer size" of the core. NTU is customarily based on the minimum weight flow.

$$NTU = UA/C_{\min} = \frac{\delta t_a}{\Delta t_m} = \frac{\text{Temperature change of air}}{\text{Over-all mean-temperature difference}}$$

[2] Numbers in parentheses refer to the References at end of the paper.

NTU_a = NTU for the air side of the core. $NTU_a = \eta_a h_a A_a / C_a$

$$= j_a (\mathrm{Pr})^{-2/3} \eta_a (A/S)_a = \frac{\delta t_a}{(\Delta t_m)_a}$$

NTU_g = NTU for the gas side of the core

$$NTU_g = \eta_g h_g A_g / C_g = j_g (\mathrm{Pr})^{-2/3} \eta_g (A/S)_g = \frac{\delta t_g}{(\Delta t_m)_g}$$

Pr = $(C_p \mu / k)$, Prandtl number, a fluid property modulus

Re = (DG/μ), Reynolds number, a flow property modulus characterizing the "turbulence"

St = (h/Gc_p), Stanton's number, a heat-transfer modulus

$\phi = \dfrac{(\Delta P)(v)}{(V^2/2g)\,(A/S)}$ friction factor for flow across tubes based on ratio of surface area to minimum open area

Subscripts

a = air-side condition

g = gas-side condition

i = condition on inside of tube

o = condition on outside of tube

1 = fluid entrance condition to heat exchanger

2 = fluid condition at exit of heat exchanger

Miscellaneous

lb = pounds mass in distinction to

= pounds force

Introduction

This paper develops a design procedure for the gas-turbine regenerator. It is particularly applicable to those installations where space available for the regenerator is limited. Both the extended surface, plate-fin type, and the tubular type are considered.

In regenerator design there is an optimum ratio between the heat-transfer coefficients and surface areas on the cold side to those on the hot side which will result in the lowest over-all pressure drop $\Delta P/P$ for a given regenerator effectiveness ϵ. In the past this ratio was arrived at by tedious trial-and-error calculations. By using the relationships developed in this paper the designer may reduce the number of such trials or eliminate them completely. Further aid in design is to be found in the work of Soderberg and Smith (1) which shows the effect of regenerator thermal effectiveness on cycle efficiency, and in the paper of London and Kays (2) which is a comparison of several types of heat-transfer surfaces for regenerator application.

General Design Procedure

The design of a gas-turbine regenerator is simplified if one works mainly with dimensionless ratios. The two important ratios are:

$$\frac{\delta t}{\Delta t_m} = \frac{\text{Temperature change of one fluid}}{\text{Over-all mean temperature difference between one fluid and the other}}$$

$$\frac{\Delta P}{P} = \frac{\text{Pressure drop of fluid going through regenerator}}{\text{Absolute pressure of fluid}}$$

By simple algebraic rearrangement of the well-known expressions for heat transfer and pressure drop, it is possible to develop the relationship between these two ratios. At the same time one obtains equations relating these ratios to the physical design of the regenerator.

A balance between the quantity of heat to be transferred and the force producing the transfer is given by

$$Wc_p\delta t = UA\Delta t_m \quad \ldots\ldots [1]$$

which can be rearranged to

$$UA/Wc_p = \delta t/\Delta t_m \quad \ldots\ldots [2]$$

This ratio of temperature change to temperature difference is expressed as NTU, number of transfer units. The performance on each side of the regenerator may be expressed similarly. For the gas side

$$W_g(c_p)_g\,(\delta t)_g = h_g\eta_g A_g\,(\Delta t_m)_g \quad \ldots\ldots [3]$$

which rearranges to

$$NTU_g = \frac{(\delta t)_g}{(\Delta t_m)_g} = \frac{h_g\eta_g A_g}{W_g(c_p)_g} = \frac{h_g\eta_g A_g}{C_g} \quad \ldots\ldots [4]$$

This ratio can be calculated directly from the heat-transfer factor j and the ratio of surface to net open area A/S

$$j = \frac{h}{Gc_p}\left(\frac{c_p\mu}{k}\right)^{2/3} = \frac{h}{(W/S)c_p}\left(\frac{c_p\mu}{k}\right)^{2/3} \quad \ldots\ldots [5]$$

Substitution of the value of j from Equation [5] in Equation [4] gives

$$NTU_g = \frac{j_g(A/S)_g\eta_g}{(c_p\mu/k)^{2/3}} \quad \ldots\ldots [6]$$

A similar development applies to the air side.

The pressure drop for flow in tubes or continuous passages is given by

$$\Delta P = \frac{fV^2\,(A/S)}{2gv} \quad \ldots\ldots [7]$$

and by dividing through both sides by the absolute pressure P, the dimensionless form is obtained

$$\Delta P/P = \frac{fV^2\,(A/S)}{2gPv} \quad \ldots\ldots [8]$$

and since

$$Pv = RT$$

$$\Delta P/P = \frac{f\,V^2\,(A/S)}{2gRT} \quad \ldots\ldots [9]$$

For conditions in a regenerator the values of P, v, and T may be taken as the arithmetic average of inlet and outlet conditions without introducing significant error.

Equations [6] and [9] may be combined to give the relationship between NTU and $\Delta P/P$

$$NTU_g = \frac{[j/(f/2)]_g\,(\Delta P/P)_g\,gRT_g\eta_g}{V_g^2\,(C_p\mu/k)^{2/3}} \quad \ldots\ldots [10]$$

The value of $j/(f/2)$ is a function of both Reynolds number and passage geometry. For flow through round tubes at Re from 5000 to 200,000 the values of f and j, respectively, may be approximated by

$$f = 0.046/\mathrm{Re}^{0.2}$$
$$j = 0.023/\mathrm{Re}^{0.2}$$

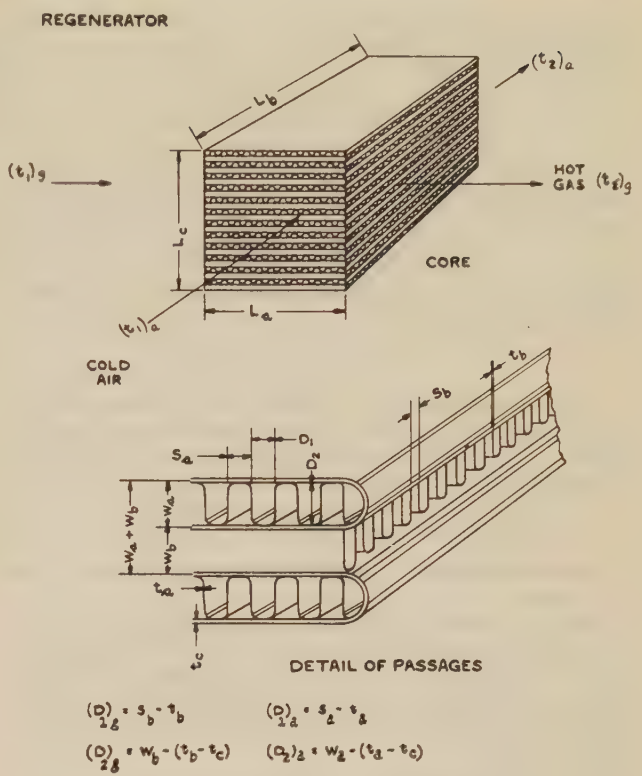

FIG. 1 ARRANGEMENT OF SURFACES IN PLATE-FIN-TYPE REGENERATOR

so that

$$j/(f/2) = 1.0$$

At values of Re less than 5000 this ratio becomes less than unity and is dependent on the length-to-diameter ratio of the passage. Test values of different types of fins are reported in (3), (4), (5), (6), and (7). For the type of construction here considered, the values of $j/(f/2)$ vary from about 0.5 to 1.0. (See Fig. 1.)

A Relationship Between Individual and Over-All Performance Values.

The reciprocals of the NTU_g and NTU_a may be added to give the reciprocal of the over-all NTU, shown as follows

$$\frac{1}{UA} = \frac{1}{h_gA_g\eta_g} + \frac{1}{h_aA_a\eta_a} \quad \ldots\ldots [11]$$

In a gas turbine the weight flows and the heat capacities of the two streams are approximately equal so that

$$C_g = C_a \quad \ldots\ldots [12]$$

Dividing Equation [11] by [12]

$$\frac{\dfrac{1}{UA}}{C_a} = \frac{1}{\dfrac{h_gA_g\eta_g}{C_g}} + \frac{1}{\dfrac{h_aA_a\eta_a}{C_a}} \quad \ldots\ldots [13]$$

which from Equations [2] and [4] is identical with

$$\frac{1}{NTU} = \frac{1}{NTU_g} + \frac{1}{NTU_a} \quad \ldots\ldots [14]$$

Where no subscript is used, NTU will be read as the over-all number of transfer units. The over-all NTU can be related to the individual pressure-drop ratios by substituting Equation [10] in [14]

$$\frac{1}{NTU} = \frac{(V_g)^2\,(\mathrm{Pr})^{2/3}}{[j/(f/2)]_g \eta_g (\Delta P/P)_g\, gRT_g} + \frac{(V_a)^2\,(\mathrm{Pr})^{2/3}}{[j/(f/2)]_a \eta_a (\Delta P/P)_a\, gRT_a} \quad [15]$$

The individual pressure-drop ratios can be shown by thermodynamic analysis to have an effect on the cycle proportional to their sum

$$\Delta P/P = (\Delta P/P)_g + (\Delta P/P)_a \quad [16]$$

This develops from the expression for the entropy gain due to pressure loss which is given by

$$-R \ln (P_2/P_1)$$

where P_1 is the pressure at the inlet to the regenerator and P_2 is the pressure at the outlet. For the small pressure ratios involved in regenerator design the logarithm of the ratio may be approximated by

$$\ln P_2/P_1 = \ln (1 - \Delta P/P_{avg}) = -\Delta P/P_{avg}$$

B Optimum Relations Between Performance in Air and in Gas Passages.

There are optimum ratios between the individual NTU and the individual $\Delta P/P$ which give the highest over-all NTU for a given $\Delta P/P$, or for a given NTU, the lowest total $\Delta P/P$. Partial differentiation with respect to the possible variables and setting the resulting partial differentials equal to zero gives the optimum conditions.

The following relationships are developed in order to arrive at equations suitable for differentiation

$$V_g = (W_g v_g)/S_g \quad [17a]$$

$$V_a = (W_a v_a)/S_a \quad [17b]$$

Let

$$r = (W_a v_a)/(W_g v_g) \quad [18]$$

and

$L_c(c)$ = length in ft in no-flow direction given to cold-stream passages [19a]

$L_c(1 - c)$ = length in ft in no-flow direction given to hot-stream passages [19b]

The space occupied by metallic separating walls is neglected. The areas for flow are, respectively

$$S_g = (L_b)\,(L_c)\,(1 - c) \quad [20]$$

$$S_a = (L_a)\,(L_c)\,(c) \quad [21]$$

Substituting Equations [18], [19a], and [19b], in Equations [17a] and [17b] gives

$$V_g = \frac{(W_g v_g)}{(L_a)(L_c)(1 - c)} \quad [22]$$

$$V_a = \frac{(W_a v_a)}{(L_a)(L_c)(c)} = \frac{r(W_g v_g)}{(L_a)(L_c)(c)} \quad [23]$$

Inserting these values of V in Equation [15]

$$\frac{1}{NTU} = \frac{(W_g v_g)^2\,(\mathrm{Pr})^{2/3}}{j/(f/2)_g \eta_g (\Delta P/P)_g gRT_g\,(L_b)^2(L_c)^2(1 - c)^2} + \frac{r^2\,(W_g v_g)^2\,(\mathrm{Pr})^{2/3}}{j/(f/2)_a \eta_a\,(\Delta P/P)_a gRT_a\,(L_a)^2(L_c)^2(c)^2} \quad [24]$$

To simplify the analysis one can assume that the following terms are equalities (which is approximately true)

$$j/(f/2)_g = j/(f/2)_a$$

$$\eta_g = \eta_a$$

$$(\mathrm{Pr})_g^{2/3} = (\mathrm{Pr})_a^{2/3}$$

and that the change in value of $j/(f/2)$ in the range of possible design variations may be considered a second-order effect. Let

$$\frac{j/(f/2)_g \eta_g R L_c^2}{(NTU)\,(W_g v_g)^2\,(\mathrm{Pr})^{2/3}} = B$$

then Equation [24] becomes

$$B = \frac{1}{(\Delta P/P)_g T_g\, L_b^2 (1 - c)^2} + \frac{r^2}{(\Delta P/P)_a T_a L_a^2 c^2} \quad [25]$$

Let

$$F = NTU_g/NTU_a \quad [26]$$

$$F = \frac{1/NTU_a}{1/NTU_g} = \frac{r^2}{\dfrac{(\Delta P/P)_a T_a L_a^2 c^2}{(\Delta P/P)_g T_g L_b^2 (1 - c)^2}} \quad [27]$$

Substituting Equation [27] in [25] and solving for the individual values of $\Delta P/P$ gives

$$(\Delta P/P)_g = \frac{(F + 1)}{B\,(L_b)^2\,(1 - c)^2\,T_g} \quad [28]$$

$$(\Delta P/P)_a = \frac{(F + 1)}{(F)\,(B)\,(L_a)^2\,(c)^2\,T_a} \quad [29]$$

Substituting Equations [28] and [29] in Equation [16] gives the general equation

$$\Delta P/P = \frac{(F + 1)}{B\,(L_b)^2\,(1 - c)^2\,T_g} + \frac{(F + 1)\,r^2}{(F)\,B\,(L_a)^2\,(c)^2\,T_a} \quad [30]$$

The value of F and c for minimum $\Delta P/P$ are found by partial differentiation as mentioned above

$$\left(\frac{\partial(\Delta P/P)}{\partial c}\right)_F = 0 = +\frac{(F + 1)\,2}{B(L_b)^2\,(1 - c)^3\,T_g} - \frac{(F + 1)}{(F)}\,\frac{2\,r^2}{B(L_a)^2 c^3 T_a} \quad [31]$$

$$\left(\frac{c}{1 - c}\right)^3 = \frac{(rL_b/L_a)^2\,(T_g/T_a)}{F} \quad [32]$$

$$\left(\frac{\partial(\Delta P/P)}{\partial F}\right)_a = 0 = \frac{1}{BL_b^2(1 - c)^2 T_g} - \frac{r^2}{F^2\,(B)\,(L_a)^2(c)^2\,T_a} \quad [33]$$

$$F^2 = (rL_b/L_a)^2 \left(\frac{1 - c}{c}\right)^2 (T_g/T_a) \quad [34]$$

Substituting the value of F obtained from Equation [34] in Equation [32] gives

$$\frac{c}{1 - c} = (rL_b/L_a)^{0.5}\,(T_g/T_a)^{0.25} \quad [35]$$

Substituting Equation [35] in Equation [34] gives

$$F = (r\,L_b/L_a)^{0.5}\,(T_g/T_a)^{0.25} \quad [36]$$

Comparing Equation [36] with Equation [35] one notes that

$$F = \frac{c}{1 - c} \quad [37]$$

Equation [27] can be rewritten as

$$F = \frac{r^2 (\Delta P/P)_g T_g L_b^2 (1 - c)^2}{(\Delta P/P)_a T_a L_a^2 (c)^2} \quad \ldots\ldots [38]$$

which combined with Equation [34] gives

$$F = \frac{(\Delta P/P)_a}{(\Delta P/P)_g} \quad \ldots\ldots [39]$$

These relationships can be more readily visualized by equating them all to F.

$$F = \frac{(\Delta P/P)_a}{(\Delta P/P)_g} = \frac{c}{1 - c} = \frac{(D_2)_a}{(D_2)_g} = \frac{(NTU)_g}{(NTU)_a} = \left(\frac{rL_b}{L_a}\right)^{0.5} \left(\frac{T_g}{T_a}\right)^{0.25} \quad \ldots\ldots [40]$$

$(D_2)_a$ and $(D_2)_g$ are the heights, respectively, of the cold and hot stream passages, on the basis that there is the same number of passages for both streams.

The over-all NTU can be related to the over-all pressure-drop ratio and the velocity of either stream by rearrangement of the relationships given in Equation [40]

$$NTU = \frac{(\Delta P/P)\eta [j/(f/2)]\, gRT_g}{(1 + F)^2 (V_g)^2 (\mathrm{Pr})^{2/3}} = \frac{F^2 (\Delta P/P)\eta [j/(f/2)]\, gRT_a}{(1 + F)^2 (V_a)^2 (\mathrm{Pr})^{2/3}} \quad \ldots\ldots [41]$$

In the foregoing analysis no allowance has been made for losses other than frictional pressure drops. These other losses are small enough as not to affect significantly the design relationships, but they should of course be included in the calculation of over-all performance.

For the general case in which

$$C_a/C_g = Z \neq 1$$
$$W_g/W_a = M \neq 1$$
$$(c_p)/(c_p)_g = ZM \neq 1$$

the analysis is similar to that already presented, except that the ratios of the two flows must be included. The final equations so derived are

$$F = \frac{(\Delta P/P)_a}{M(\Delta P/P)_g} = \frac{NTU_g}{Z(NTU)_a} = \left[\frac{(c_p)_g}{(c_p)_a}\right]^{0.25} \left[\frac{(r)(L_b)}{(L_a)}\right]^{0.5} \left[\frac{T_g}{T_a}\right]^{0.25} \quad \ldots\ldots [42]$$

C Design of Exchanger Passages.

The spacings of exchanger passages can be calculated by means of Equations [6] and [40], and from plots of the j values for the particular fin design chosen. The *ratio* of passage heights is given by Equation [40], but the absolute value to be used is a matter of judgment on the part of the designer. He must balance high fin effectiveness against increased cost and weight as the height of individual passages is reduced. Conversely, as fin height is increased fin thickness must be maintained adequate to provide reasonable values of fin effectiveness. The fin effectiveness is given by

$$\eta_e = (\Delta t)_m/(\Delta t)_o = (\tanh ax_f)/(ax_f) \quad \ldots\ldots [43]$$

where

$a = (hb/kS)^{0.5} = (2h/kt)^{0.5}$ for uniform rectangular section fin
x_f = effective length of fin

This length will vary from one half the passage height to the full passage height depending on the method of assembling the individual passages. If the regenerator is built up by assembling individual flat "tubes" consisting of one gas passage and one air passage as shown in sketch B of Fig. 3, then the fin height is the full passage height. If made with one center passage for air and two half-passages for gas as shown in sketch A of Fig. 3, the fin height is taken as one half the center passage height for the air side and the height of the half-passage for the gas side. If there are an even number of passages bonded together as shown in Fig. 1, then the fin height is some value between one half and the full passage height.

The direct surface effectiveness may be taken as unity, so that the over-all effectiveness is

$$\eta = \eta_e \left(\frac{D_2}{D_1 + D_2}\right) + \left(\frac{D_1}{D_1 + D_2}\right) \quad \ldots\ldots [44]$$

The effective diameter, D_e, for smooth continuous fins may be obtained approximately by substitution in Equation [6] of the relationship between j and Reynolds number

$$NTU = j(4L/D_e)(\mathrm{Pr})^{-2/3} = 0.023\,(\mathrm{Re})^{-0.2}(4L/D_e)(\mathrm{Pr})^{-2/3} \quad \ldots\ldots [45]$$

D Example—Over-All Performance.

The design of a regenerator for a locomotive gas turbine will illustrate the handling of the foregoing relationships:

The following are the approximate properties of the two streams (exact values not being known until the regenerator has been designed):

	Gas side	Air side
Weight flow, W, lb/sec	60	60
Average density, lb/ft^3	0.0333	0.166
Average specific volume, v, ft^3/lb	30.0	6.0
Average viscosity, μ, lb/(ft) (hr)	0.076	0.068
Heat capacity, c_p, Btu/(lb) (F)	0.25	0.25
Prandtl number, $c_p\mu/k$	0.67	0.67
Average temperature, T, deg R	1210	980
Average pressure, P, psia	14.9	60.0

The regenerator is to have a core of the following dimensions:

Length of flow path for hot gas, L_a, 3 ft
Length of flow path for cold gas, L_b, 7 ft
No flow direction, L_c, 6 ft

As a first step in the design one can determine the relationship between pressure-drop ratio and NTU. With this information the turbine designer can decide upon the optimum NTU for the turbine cycle.

The design parameter F is given by Equation [36]

$$F = [(0.2)(7/3)]^{0.5}(1210/980)^{0.25} = 0.72$$

(The first figure of 0.2 is obtained from $r = v_a/v_g = 6/30 = 0.2$)

Assuming that the ratio of net free area to gross cross-sectional area for the sum of the two streams ($\sigma_g + \sigma_a$) is 0.85 and that it is about proportional to the relative net free area of each, then the velocities of the gases are

$$V_a = \frac{W_a v_a}{(L_a)(L_c)\left(\frac{(F)}{1 + F}\right)(\sigma)} = \frac{(60)(6)}{(3)(6)[(0.72)/1.72](0.85)} = 56.2 \text{ ft/sec}$$

$$V_g = \frac{W_g/v_g}{(L_b)(L_c)[1/(1 + F)](\sigma)} = \frac{(60)(30)}{(7)(6)(1/1.72)(0.85)} = 88.7 \text{ ft/sec}$$

Either of these values can be substituted in the appropriate part of Equation [41] to give the relationship between pressure-drop ratio and NTU. The following values are assumed for this preliminary study:

$$\text{Fin effectiveness, } \eta, = 0.85$$

$$j/(f/2) = 0.75$$

The ratio of j to the half friction factor is higher than 0.75 but is reduced to allow for pressure losses at inlet and discharge and for losses or gains due to acceleration or deceleration of the fluid streams.

Based on gas stream

$$NTU \text{ over-all} = \frac{(\Delta P/P)\,(0.85)\,(0.75)\,(32.2)\,(53.3)\,(1210)}{(1.72)^2\,(86.7)^2\,(0.77)} = 77.2\,(\Delta P/P)$$

Based on air stream

$$NTU \text{ over-all} = \frac{(\Delta P/P)\,(0.85)\,(0.75)\,(32.2)\,(53.3)\,(980)\,(0.72)^2}{(1.72)^2\,(56.2)^2\,(0.77)} = 77.2\,(\Delta P/P)$$

If the $\Delta P/P$ for the cycle is limited to 3 per cent, then the maximum NTU obtainable in the given volume is

$$NTU \text{ over-all} = (77.2)\,(0.03) = 2.31$$

which for a single pass crossflow unit gives an efficiency ϵ of 64 per cent, Fig. 2.

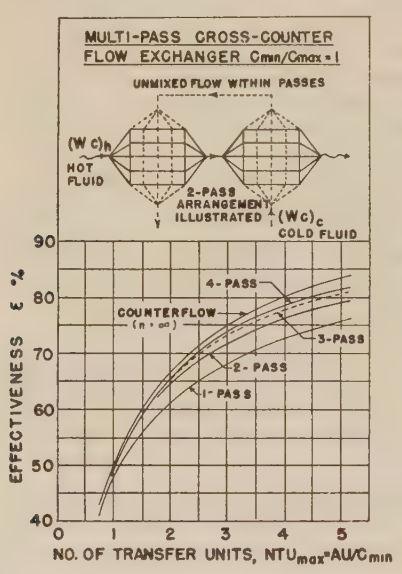

Fig. 2 Plot of NTU Versus Exchanger Effectiveness

E Example Design of Passages.

The calculations to arrive at passage and fin spacings for an over-all NTU of 2.31 are as follows

From Equation [40]

$$NTU_g = (1 + F)\,(NTU) = (1.72)\,(2.31) = 3.98$$

$$NTU_a = \left(\frac{1 + F}{F}\right)(NTU) = \left(\frac{1.72}{0.72}\right)(2.31) = 5.52$$

$$F = \frac{(D_2)_a}{(D_2)_g} = 0.72$$

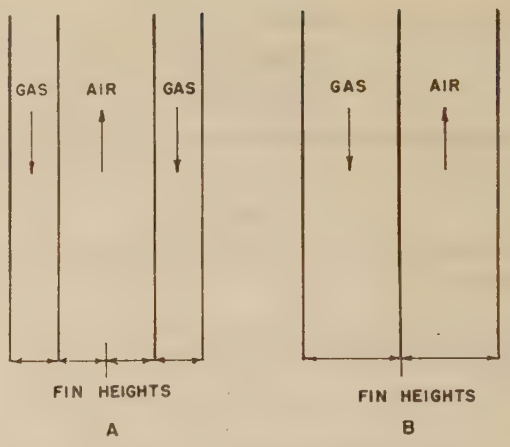

Fig. 3 Heat-Flow Pattern in Finned Sections

From Equation [45] the equivalent diameter of the two passages are found. Using the values of Pr and η assumed

$$NTU = 0.023(0.85)\,(\mathrm{Re})^{-0.2}\,(4L/D_e)\,(0.67)^{-2/3}$$

and assuming that $\mathrm{Re}_g = 3000$ and $\mathrm{Re}_a = 10{,}000$

$$(L/D_e)_g = (3.98)\,(3.000)^{0.2}\,(0.76)/[(0.023)\,(0.85)\,(4)] = 193$$

$$(D_e)_g = 3.0/193 = 0.0155 \text{ ft} = 0.186 \text{ in.}$$

$$(L/D_e)_a = (5.52)\,(10{,}000)^{0.2}\,(0.76)/[(0.023)\,(0.85)\,(4)] = 343$$

$$(D_e)_a = 7.0/343 = 0.0204 \text{ ft} = 0.245 \text{ in.}$$

With these calculated values of equivalent diameter, the assumed Reynolds numbers can be checked and corrections made if there are significant differences. Calculation of passage heights and fin spacings follow customary procedure. After allowances are made for such factors as actual fin efficiencies, area occupied by metal walls, entrance and exit effects, according to the method suggested by London and Kays (2), the final predicted performance values given in Table 1 are obtained.

Design of Tubular Regenerators

From the standpoint of maximum performance for a given volume of heat-exchanger core, the use of bare tubes results in lower thermal efficiency than possible with extended-surface plate-fin construction. The foregoing analysis of extended-surface design showed that if there were no limit on the amount of surface and if the fins and separating plates could be made comparatively thin, the over-all NTU obtainable in a given volume is directly proportional to pressure-drop ratio. A similar proportion exists for tubular design but the NTU compared to extended surface is lower for the same allowable pressure-drop ratio.

The use of tubular design is often indicated on the basis of lower cost, better mechanical design, and suitability for high-pressure as well as high-temperature service. A full discussion of this subject is not within the scope of this paper.

In connection with the design of radiators and intercoolers for aircraft service, a type of heat exchanger comparable to a regenerator, a number of design charts, and methods of preparation of such charts for selecting the proper size of core have been developed (8), (9), (10), (11), (12), and (13). The procedures given usually refer to the selection of a core which has already been designed having a fixed pattern of tube spacing and diameters, or plate and fin arrangements. Tubular regenerators, on the other hand, will usually be designed for a particular model of gas turbine, so that there is a choice of both tube diameters and tube spacings. The tube length and the other dimensions will in many cases be fixed by the over-all turbine design.

TABLE 1 COMPARISON OF REGENERATOR DESIGNS FOR LOCOMOTIVE SERVICE

	Extended surface inconel	Tubular: High effectiveness	Tubular: Low effectiveness
ϵ, per cent	64	64	52
$\Delta P/P$, per cent	2.92	7.78	3.01
NTU	2.35	2.35	1.22
Weight, lb (core only)	7,000	3,600	4,400
Total surface, ft²	24,800	9,300[a]	6,550[a]
Direct surface, ft²	7,100		
Indirect surface, ft²	17,700		
Unit heat-transfer coefficient, U, based on direct surface	35.8[b]	25.5[c]	18.8[c]
Number of tubes		9,709	3,825
Outer diameter of tubes, in.		0.280	0.500
Inner diameter of tubes, in.		0.242	0.435
Spacing of tubes:			
in direction of gas flow, S_L/D_o		1.75	1.40
in no-flow direction, S_T/D_o		1.94	1.92
Thickness of separating plate, in.	0.020		
Gas side			
$\Delta P/P_g$, per cent	1.75	3.05	1.38
NTU_g	4.01	4.05	2.09
h, Btu/(hr ft² F)	16.9	43.8	32.3
η, fin effectiveness	0.80		
Total surface, ft²	16,000	4,990	3,500
Direct surface, ft²	3,550		
Indirect surface, ft²	12,450		
Number of fins per inch	7.7		
Fin thickness, in.	0.010		
Passage height, in.	0.45		
G, lb/(hr ft²)	10,420	10,600	10,670
V, ft/sec	86.7	86.5	89
Re	2,120	3,240	5,850
Air side			
$\Delta P/P_a$, per cent	1.17	4.73	1.63
NTU_a	5.70	5.58	2.94
h, Btu/(hr ft² F)	36.5	69.6	52.1
η, fin effectiveness	0.85		
Total surface, ft²	8,800	4,340	3,050
Direct surface, ft²	3,550		
Indirect surface, ft²	5,250		
Number of fins per inch	4.8		
Fin thickness, in.	0.010		
Passage height, in.	0.337		
G, lb/(hr ft²)	33,600	74,400	55,000
V, ft/sec	56.2	121.6	92
Re	10,100	22,000	29,200

[a] The total surface for the tubular design is given as the sum of the outside surface and the inside surface in order to give a true comparison with the total surface of the extended surface units

[b] The over-all heat-transfer coefficient U for the extended-surface design is based on one half the total direct surface to put it on a basis comparable with the tubular design.

[c] For the tubular design the coefficient U is based on the outside tube-surface area.

A General Design Relationships.

The design of tubular regenerators to some extent can follow the procedure given for the extended-surface type. The ratios of NTU's for optimum performance can be expressed by a design parameter F, but it should be noted that this parameter, given in Equation [46], is independent of the over-all dimensions of the regenerator. The relationships for a tubular design are

$$F = \frac{NTU_o}{NTU_i} = \frac{h_o A_o / C_o}{h_i A_i / C_i} \quad \ldots\ldots [46]$$

For gas-turbine regenerator one may consider that

$$C_o = C_i$$

For a bare-tube design

$$A_o/A_i = D_o/D_i$$

so that Equation [46] becomes

$$F = \frac{NTU_o}{NTU_i} = \frac{h_o}{h_i}\frac{D_o}{D_i} \quad \ldots\ldots [47]$$

The ratio of the two heat-transfer coefficients (h_o/h_i) is obtained from the ratio of the mass velocities on the two sides which will give the highest over-all conductance U for the minimum total friction power. This ratio of mass velocities when applied to the expressions for heat transfer and incorporated in Equation [47] gives

$$F = \frac{C_8}{(D_o G_o \mu_o)^{0.17}} \left[\left(\frac{D_o}{D_i}\right)\left(\frac{v_i}{v_o}\right)\right]^{0.444} \left(\frac{T_o}{T_i}\right)^{0.222} \left(\frac{\mu_o}{\mu_i}\right)^{0.111} \quad \ldots [48]$$

The constant C_8, which is a function of tube configurations, is shown in Figs. 13 and 14. Employing this ratio of the two NTU's, one can calculate the absolute values of the individual NTU's for

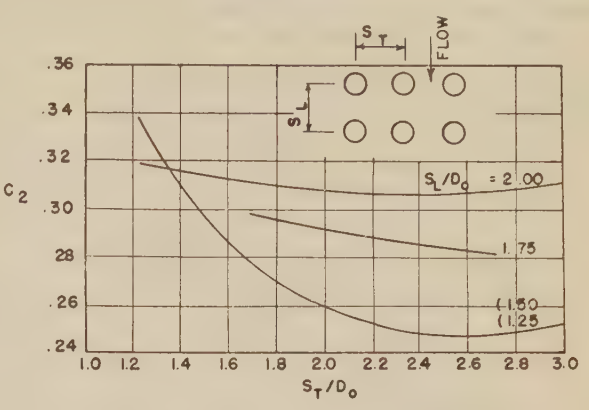

FIG. 4 CONSTANT C_2 AS A FUNCTION OF TUBE SPACING; FLOW OF AIR ACROSS IN-LINE TUBES. CHART FROM (8)

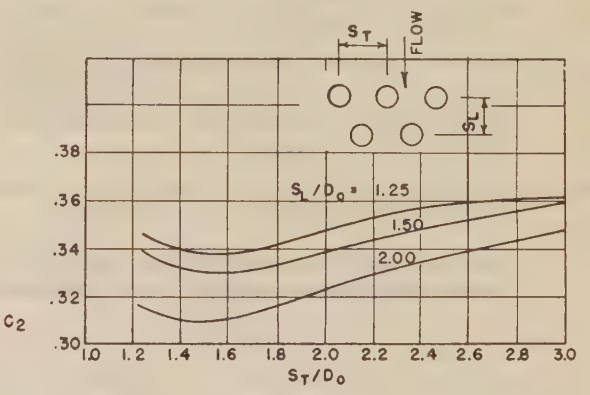

FIG. 5 CONSTANT C_2 AS A FUNCTION OF TUBE SPACING; FLOW OF AIR ACROSS STAGGERED TUBES. CHART FROM (8)

a given value of over-all NTU. From the NTU_i the L/D_i of the tube is obtained by using Equation [45a]

$$NTU_i = \frac{0.023\,(4L_T/D_i)}{(\mathrm{Re}_i)^{0.2}(\mathrm{Pr})^{2/3}} \quad \ldots\ldots [45a]$$

The pressure drop for flow inside the tube is given by Equation [9a]

$$(\Delta P/P)_i = f\frac{V^2}{2g}\frac{4L_T/D_i}{RT_i} \quad \ldots\ldots [9a]$$

Equation [45a] may often give a tube diameter smaller than considered practical. One can redesign the unit for multipass on the tube side so that the effective tube length is increased, or accept a design which will not give the maximum $NTU/(\Delta P/P)$ ratio for the given volume. In the latter case more surface is required for the same NTU.

The tube spacings required for the optimum ratios of heat-transfer coefficients are given by

$$(S_L/D_o)\,(S_T/D_o - 1) = \frac{100\,(C_2/F)^{1.25}\,(D_i/D_o)\,(L_n/L_T)\,(\mu_o/\mu_i)^{0.25}}{(D_o G_o/\mu_o)^{0.25}} \quad \ldots [49]$$

for the case of in-line tube arrangements and staggered tube arrangements having the minimum opening in the transverse spacings. While Equation [49] does not give the absolute values of

the spacings, one can be guided by the general principle that S_T/D_o should be made as small as mechanical design limitations permit because this results in the highest heat transfer for a given friction power as indicated roughly by the plots of Figs. 6, 7, and 8 where C_5 is related to the factor $j/(f/2)$ by

$$j/(f/2) = C_5/(D_oG/\mu)^{0.27} \quad [50]$$

and C_5 is

$$C_5 = \frac{1.10\ C_2}{2C_4\ (S_T/D_o - 1)} \quad [51]$$

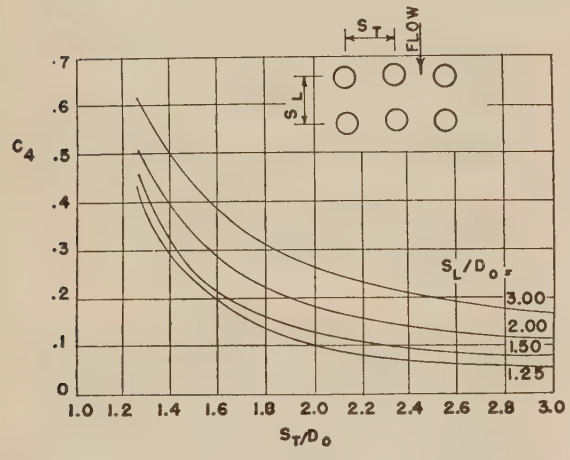

Fig. 6 Constant C_4 as a Function of Tube Spacing; Flow of Air Across In-Line Tubes. Chart From (8)

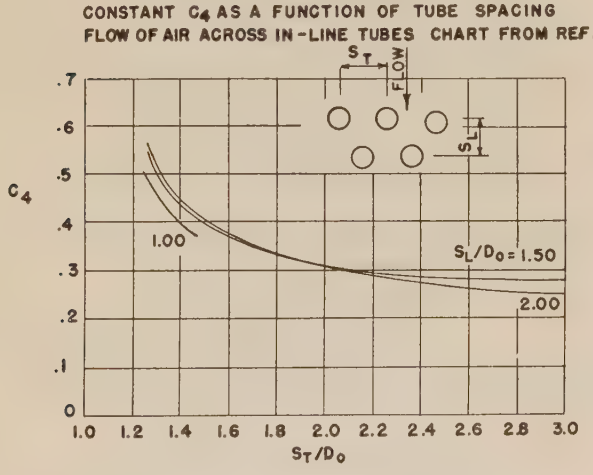

Fig. 7 Constant C_4 as a Function of Tube Spacing. Flow of Air Across Staggered Tubes. Chart From (8)

Often tube spacings will be limited by minimum ligament requirements in the tube sheet. (In the design of the regenerator for locomotive service shown in Fig. 17, close tube spacings were obtained by bending the tubes into an arc.)

The values of C_2 and C_4 are functions of Reynolds number and tube arrangement. Wood and Brevoort (8) have prepared simplified correlations, Figs. 4, 5, 6, and 7 of the data of Pierson and Huge as correlated by Grimison (14), for heat transfer and friction factors for flow across tubes. The values of the several authors are related as follows:

$C_2 = 0.31\ F_a$ where F_a is the arrangement factor of Grimison and C_2, the constant given by Wood and Brevoort in

$$hD/k = C_2\ \mathrm{Re}^{0.6} \quad [52]$$

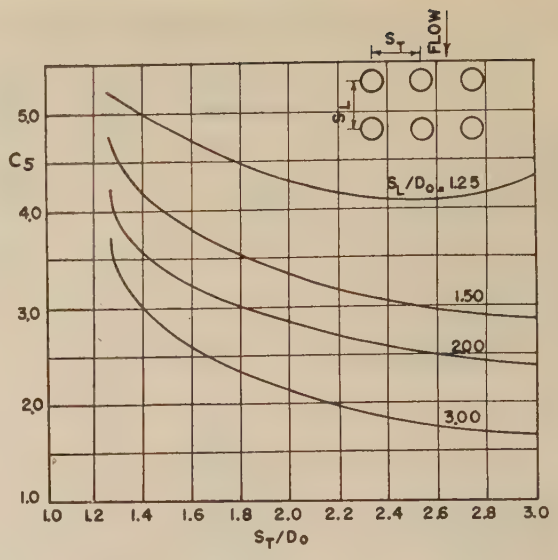

Fig. 8 Constant C_5 as a Function of Tube Spacing; Flow of Air Across In-Line Tubes

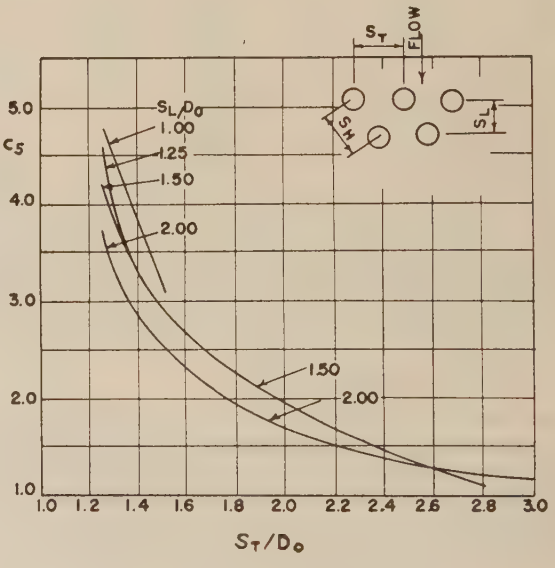

Fig. 9 Constant C_5 as a Function of Tube Spacing; Flow of Air Across Staggered Tubes

In the preparation of their plots Wood and Brevoort incorporated the value of Prandtl number in the constant C_2. In order to cover a wider range of gas properties the Prandtl number is reintroduced, and in line with the treatment followed earlier in the paper, the heat-transfer expression is transformed into the Stanton number thus

$$h/c_pG = 1.10\ C_2\ \mathrm{Pr}^{-2/3}\ \mathrm{Re}^{-0.4} \quad [52a]$$

The pressure drop on the outside of tubes is given by

$$(\Delta P/P)_o = \frac{4f_oNG^2v}{2gP} = \frac{4f_oNV^2}{2gPv} = \frac{4f_oN}{RT}\ \frac{V^2}{2g} \quad [53]$$

where

$$f_o = C_4/(\mathrm{Re})^{0.13} = f_{\text{Grimison}} \quad [54]$$

The value of NTU_o can be obtained from Equation [52a] by incorporating the ratio of surface to net free area

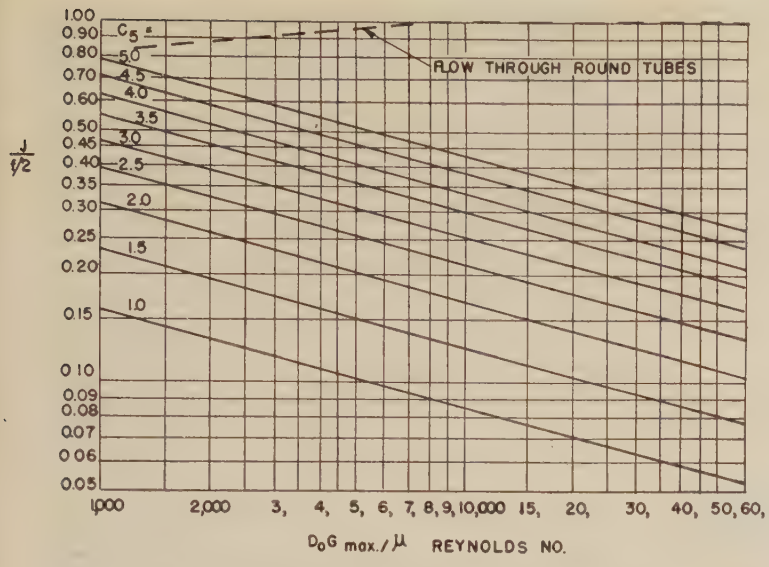

FIG. 10 VALUES OF $j/(f/2)$ FOR FLOW ACROSS TUBES FOR VARIOUS VALUES OF C_5 AND OF REYNOLDS NUMBER

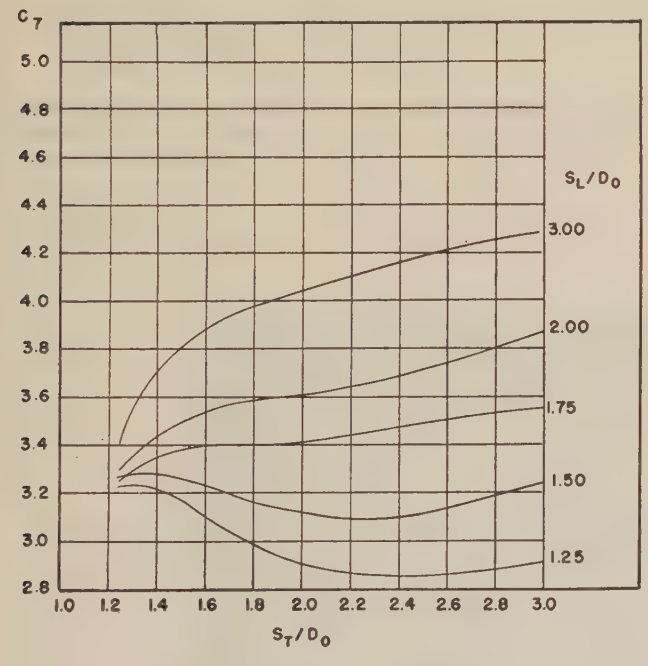

FIG. 11 CONSTANT C_7 AS A FUNCTION OF TUBE SPACING; FLOW OF AIR ACROSS IN-LINE TUBES

$$NTU_o = \frac{1.10\ C_2 N}{(\mathrm{Pr})^{2/3}\,(S_T/D_o - 1)\,(\mathrm{Re})^{0.4}} \quad \cdots\cdots [55]$$

The equations here presented are sufficient for the design of a tubular regenerator which will make the most effective use of the surface employed.

B Derivation of Relationship for Optimum Performance.

The analysis of tubular design for optimum performance is predicated on the thesis that the ratio of the mass velocities on the two sides is the primary variable. The effect of tube configuration on the optimum ratio of mass velocities is treated as a second-order effect.

The several design equations must be arranged to express the variation of total friction power loss and of total resistance to heat flow with the ratio of G_o to G_i. The following are taken as equalities

$$W_o = W_i$$

$$(c_p)_o = (c_p)_i$$

The analysis will be based on the performance of a single tube in a tube bank and the length of tube to be considered will be taken as equal to the outside diameter. This does not affect the validity of the analysis since the regenerator is merely a multiple of such an elemental area with all factors in proportion.

The performance on the inside of the tube will be considered only for the case of turbulent flow for which

$$f = 0.046/\mathrm{Re}^{0.2}$$

and

$$j = 0.023/\mathrm{Re}^{0.2}$$

The pressure-drop ratio is then expressed as

$$(\Delta P/P)_i = \frac{0.046}{(D_i G_i/\mu_i)^{0.2}} \frac{G_i^2 v_i^2\, 4(D_o/D_i)}{2gRT_i} \quad \cdots\cdots [56]$$

The amount of fluid flowing is $W = GS = G\,(\pi/4)\,D_i^2$ which, substituted in Equation [56], gives

$$(\Delta P/P)_i W_i = \left[\frac{0.046\ (\mu_i)^{0.2}\,\pi\,(D_o)^{1.8}\,v_i^{2.0}}{2g(D_o/D_i)^{0.8}\,RT_i}\right] G_i^{2.8} \quad \cdots\cdots [57]$$

To simplify the handling of the equations the terms inside the brackets can be called K_i

$$K_i = \frac{0.046\ (\mu_i)^{0.2}\,(D_o)^{1.8}\,v_i^{2.0}}{2g(D_o/D_i)^{0.8}\,RT_i} \quad \cdots\cdots [58]$$

$$(\Delta P/P_i)\,W_i = K_i G_i^{2.8} \quad \cdots\cdots [59]$$

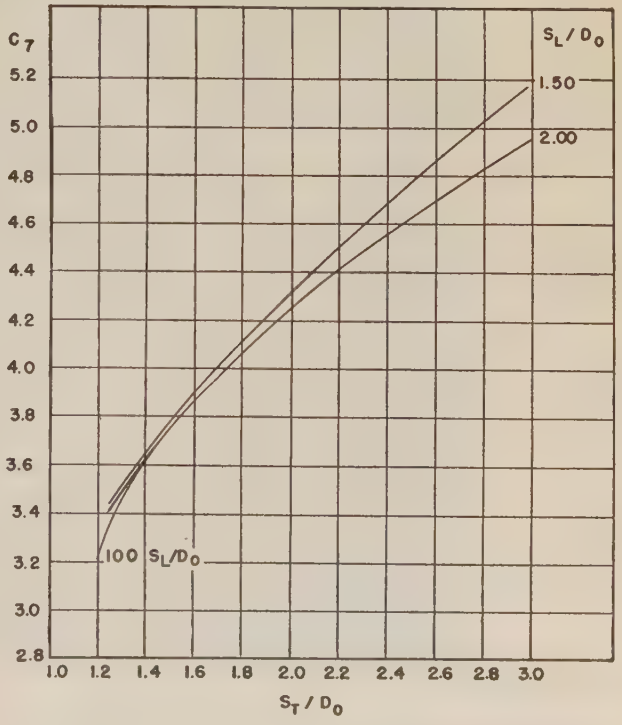

FIG. 12 CONSTANT C_7 AS A FUNCTION OF TUBE SPACING; FLOW OF AIR ACROSS STAGGERED TUBES

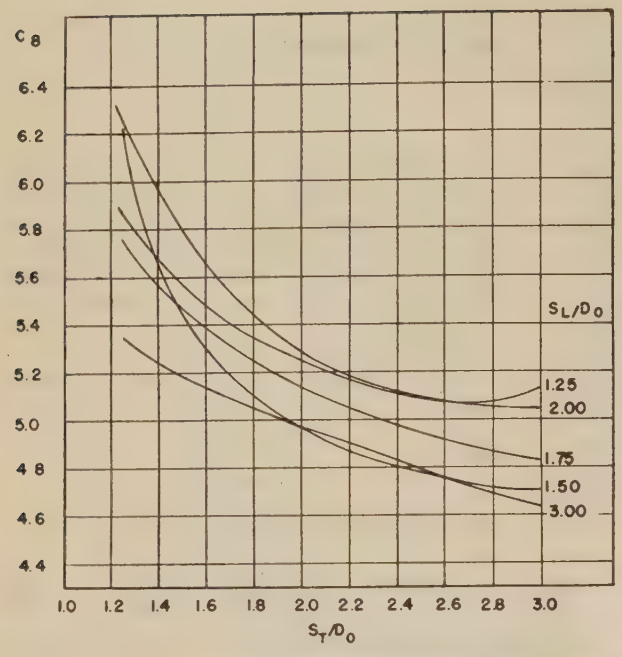

FIG. 13 CONSTANT C_8 AS A FUNCTION OF TUBE SPACING; FLOW OF AIR ACROSS IN-LINE TUBES

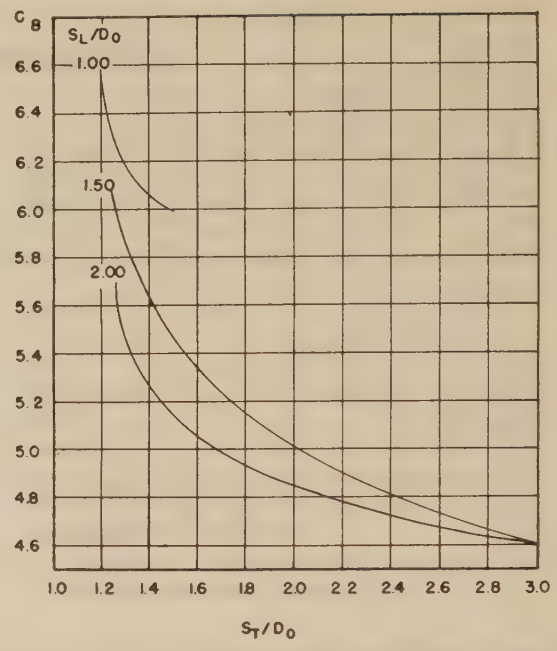

FIG. 14 CONSTANT C_8 AS A FUNCTION OF TUBE SPACING; FLOW OF AIR ACROSS STAGGERED TUBES

The heat transfer on the inside of the tube is given by Equation [45] which becomes

$$h_i A_i = \left[\frac{0.023\,(\mu_i)^{0.2}\,D_o^{1.8}\pi(c_p)_i}{\mathrm{Pr}^{2/3}\,(D_o/D_i)^{0.8}}\right] G_i^{0.8} \quad \ldots\ldots [60]$$

Let

$$H_i = \left[\frac{0.023\,(\mu_i)^{0.2} D_o^{1.8}\pi(c_p)_i}{\mathrm{Pr}^{2/3}\,(D_o/D_i)^{0.8}}\right] \quad \ldots\ldots [61]$$

$$h_i A_i = H_i G_i^{0.8} \quad \ldots\ldots [62]$$

For the fluid on the outside of the tube a similar rearrangement is carried through. From Equation [53]

$$(\Delta P/P)_o = 4f_o \frac{G_o^2}{2g}\frac{v_o^2}{RT_o} = \frac{4C_4}{(D_o G_o/\mu_o)^{0.13}}\frac{G_o^2}{2g}\frac{v_o^2}{RT_o} \quad [63]$$

Instead of a friction factor f_o based on the number of tubes, N, in the direction of gas flow, one can express pressure loss by a drag factor ϕ based on the ratio of surface area to net open area

$$A/S = [\pi D_o/(S_T - D_o)] = \pi/(S_T/D_o - 1)$$

$$(\Delta P/P)_o = \phi \frac{G^2}{2g}\frac{v_o^2}{RT_o}(A/S)$$

$$= \frac{C_9}{(D_o G_o/\mu_o)^{0.13}}\frac{G_o^2}{2g}\frac{v_o^2}{RT_o}\frac{\pi}{(S_T/D_o - 1)} \quad \ldots\ldots [64]$$

so that

$$C_9 = \frac{C_4(S_T/D_o - 1)}{\pi/4} \quad \text{(values for } C_9 \text{ are given in Figs. 15 and 16)}$$

$$\ldots\ldots [65]$$

Multiplying both sides of Equation [64] by $W = GS$

$$(\Delta P/P_o)W_o = \left[\frac{C_9}{(D_o G_o/\mu_o)^{0.13}}\right]\left(\frac{G_o^3}{2g}\right)\left(\frac{v_o^2}{RT_o}\right)(A_o) \quad [66]$$

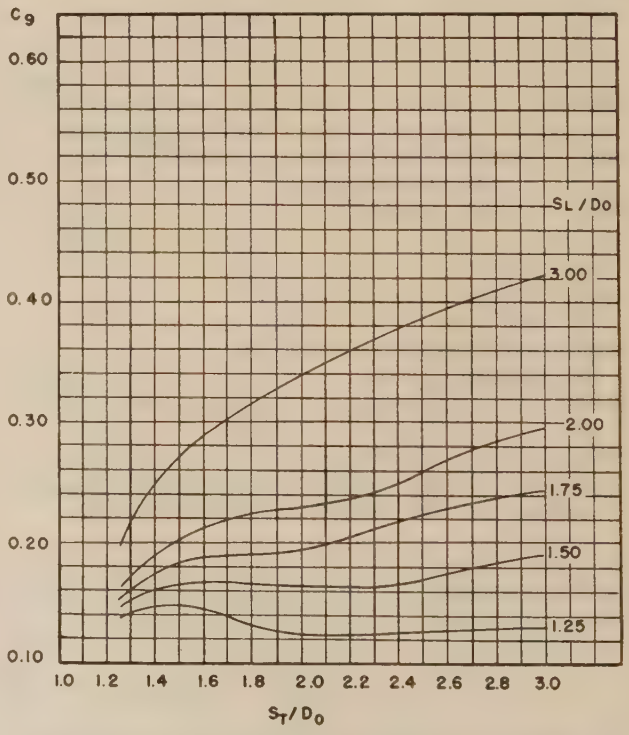

FIG. 15 CONSTANT C_9 AS A FUNCTION OF TUBE SPACING; FLOW OF AIR ACROSS IN-LINE TUBES

which simplifies to

$$(\Delta P/P_o)W_o = \frac{C_9\pi\,(\mu_o)^{0.13}\,D_o^{1.87}\,v_o^2}{2gRT_o} G_o^{2.87} \quad \ldots\ldots [66a]$$

Let

$$K_o = \left[\frac{C_9\pi(\mu_o)^{0.13}D_o^{1.87}\,v_o^2}{2gRT_o}\right] \quad \ldots\ldots [67]$$

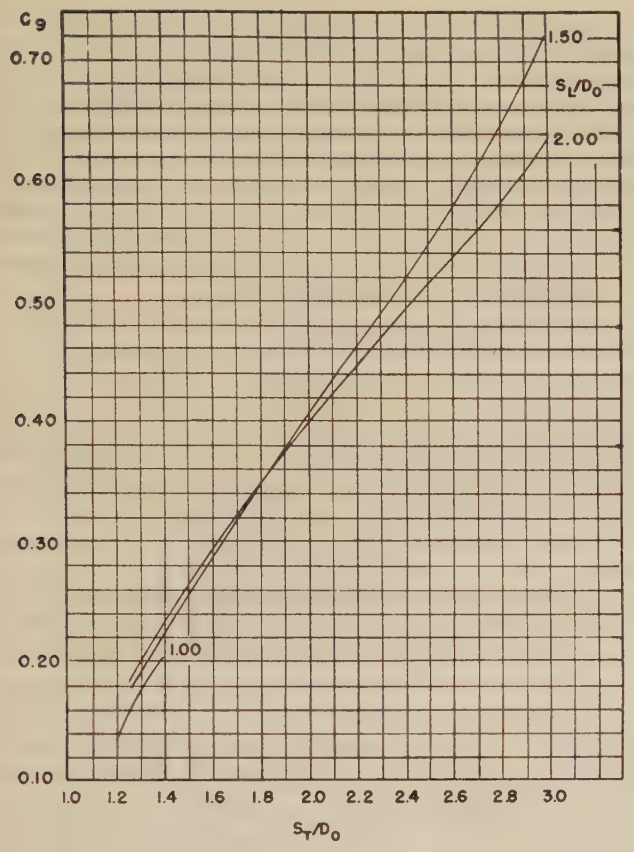

FIG. 16 CONSTANT C_9 AS A FUNCTION OF TUBE SPACING; FLOW OF AIR ACROSS STAGGERED TUBES

then

$$(\Delta P/P_o)W_o = K_o G_o^{2.87} \quad [68]$$

The heat-transfer equation is obtained from Equation [52]

$$h_o A_o = \frac{1.10\, C_2 (c_p)_o G_o}{\mathrm{Pr}^{2/3}\, \mathrm{Re}^{0.4}} A_o \quad [69]$$

$$= \left[\frac{1.10\, C_2 (c_p)_o D_o^{1.6} (\mu_o)^{0.4}}{\mathrm{Pr}^{2/3}}\right] G_o^{0.6}$$

Let

$$H_o = \frac{1.10\, C_2 (c_p)_o D_o^{1.6} (\mu_o)^{0.4}}{\mathrm{Pr}^{2/3}} \quad [70]$$

then

$$h_o A_o = H_o G_o^{0.6} \quad [71]$$

This completes the establishment of equations to represent performance on each side of the heat exchanger. The over-all performance is given by

$$\frac{1}{UA} = \frac{1}{h_i A_i} + \frac{1}{h_o A_o} = R \text{ (resistance)} \quad [72]$$

Substituting Equations [62] and [71] in Equation [72] and rearranging

$$R = \frac{1}{H_i G_i^{0.8}} + \frac{1}{H_h G_o^{0.6}} \quad [73]$$

or

$$\frac{1}{H_o G_o^{0.6}} = R - \frac{1}{H_i G_i^{0.8}} \quad [74]$$

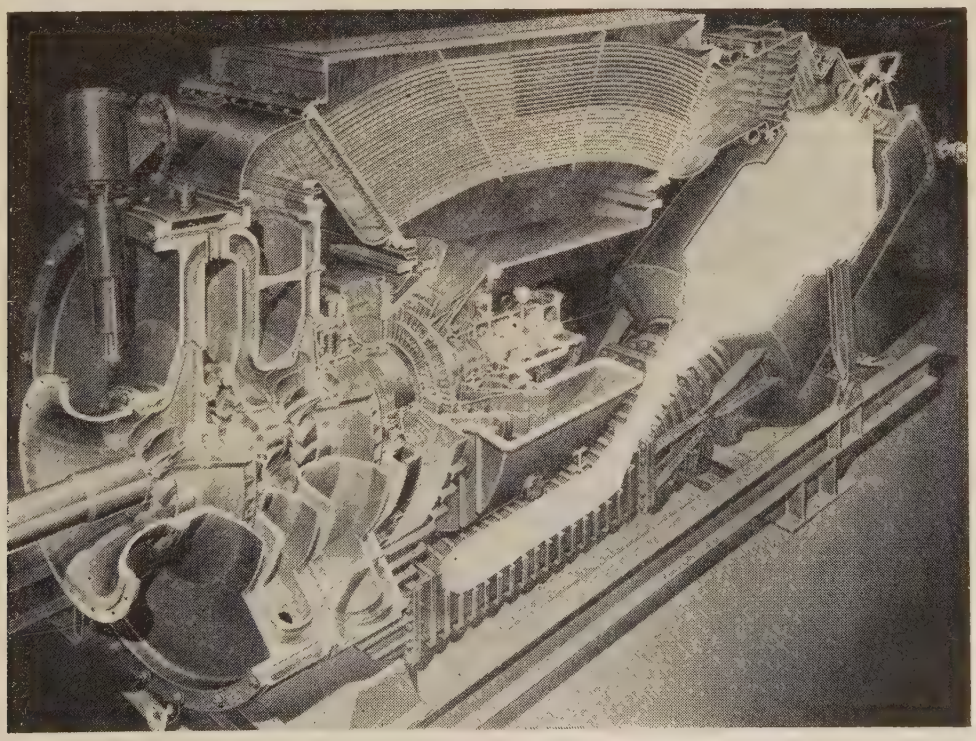

FIG. 17 TUBULAR REGENERATOR ON LOCOMOTIVE GAS TURBINE

solving for G_0 gives

$$G_o = \left[\frac{1}{(H_o)\,(R-1)/H_i G_i^{0.8})}\right]^{1/0.6} \quad \ldots\ldots\ldots [75]$$

The total friction power loss is given by

$$(\Delta P/P)W = (\Delta P/P)_i W_i + (\Delta P/P)_o W_o \ldots\ldots [76]$$

Substituting the values of the individual friction power losses from Equations [59] and [68] in Equation [76] gives

$$(\Delta P/P)W = K_i G_i^{2.8} + K_o G_o^{2.87} \ldots\ldots\ldots [77]$$

Substituting the value of G_o from Equation [75] in Equation [77] gives

$$(\Delta P/P)W = K_i G_i^{2.8} + \frac{K_o}{[(H_o)(R-1/H_i G_i^{0.3})]^{2.87/0.6}} \ldots [78]$$

The optimum arrangement to obtain a given over-all heat transfer coefficient UA occurs when $(\Delta P/P)W$ is a minimum

$$\left[\frac{\partial(\Delta P/P)W}{\partial G}\right]_{UA} = 2.8\,K_i G_i^{1.8} + \frac{K_o\,(-2.87/0.6)\,(0.8/H_i)}{H_o^{2.87/0.6}\,(R-1/H_i G_i^{0.8})^{3.47/0.6}\,(G_i)^{1.8}}$$

Setting this derivative equal to zero will give the minimum for $(\Delta P/P)W$

$$0 = 2.8\,K_i G_i^{3.6} - \left(\frac{2.87}{0.6}\right)\frac{(K_o)\,(0.8)}{H_i\,[H_o^{2.47/0.6}\,(1/H_o G_o^{0.6})^{3.47/0.6}]}$$

$$0 = 2.8\,K_i G_i^{3.6} - \frac{(2.87)\,(0.8)}{(0.6)}\left(\frac{K_o H_o}{H_i}\right) G_o^{3.47}$$

$$\frac{G_i^{3.6}}{G_o^{3.47}} = \frac{(2.87)\,(0.8)}{(2.8)\,(0.6)}\,\frac{K_o H_o}{K_i H_i} = 1.37\,\frac{K_o H_o}{K_i H_i} \ldots\ldots [79]$$

Substituting the values of $K_o H_o / K_i H_i$ in Equation [79] and simplifying, results in the ratio of G values for optimum performance

$$\frac{G_i}{G_o} = \frac{1}{(D_o G_o/\mu_o)^{0.037}}\left\{\left[\frac{(1.10)\,(C_2)\,(C_9)\,(1.37)}{(0.046)\,(0.023)}\right]\left(\frac{\mu_o}{\mu_i}\right)^{0.4}\left(\frac{D_o}{D_i}\right)^{1.6}\left(\frac{v_o}{v_i}\right)^{2}\left(\frac{T_i}{T_o}\right)\right\}^{0.278} \ldots\ldots [80]$$

Let $C_7 = \left[\frac{1.37\,(1.10)\,(C_2)\,(C_9)}{(0.046)\,(0.023)}\right]^{0.278}$ (the values of C_7 are given in Figs. 11 and 12)

$$\frac{G_i}{G_o} = \frac{C_7}{(D_o G_o/\mu_o)^{0.037}}\left(\frac{\mu_o}{\mu_i}\right)^{0.11}\left(\frac{D_o}{D_i}\right)^{0.444}\left(\frac{v_o}{v_i}\right)^{0.555}\left(\frac{T_i}{T_o}\right)^{0.278} \ldots [81]$$

This ratio of mass velocities is seen to be largely a function of the ratio of specific volumes. The value of the constant C_7 changes only slightly with tube configuration. Reynolds number on the outside of the tubes comes in only to a low power. The viscosity, temperature, and diameter ratios have only a small effect. This optimum ratio can be used to arrive at the design parameter F given in Equation [48] or it can be used in any other design procedure to arrive at final performance values.

These equations have been used for designing a tubular regenerator for the same conditions as given previously for the extended-surface type. Predicted performance values are given in Table 1 for two alternate tubular designs. In one design the effectiveness is kept the same as for the extended surface. The much higher pressure drop for tubular design is strikingly apparent. In the other design the pressure drop is kept approximately the same as for the extended-surface type and as a result the effectiveness is considerably reduced. Offsetting this poorer thermal performance is the much smaller amount of actual metal-surface area employed in the tubular design.

Comparisons under other conditions can readily be made by means of the equations presented here.

Acknowledgments

The author wishes to express his indebtedness to Mr. L. C. Claitor who developed the relationships for optimum performance of tubular regenerators, and to the Elliott Company who supported this study and agreed to publication of the analysis.

REFERENCES

1 "The Gas Turbine as a Possible Marine Prime Mover," by C. R. Soderberg and A. B. Smith, Trans. of the American Society of Naval Architects and Marine Engineers, vol. 51, 1943, pp. 115–155.

2 "The Gas-Turbine Regenerator—The Use of Compact Heat-Transfer Surfaces," by A. L. London and W. M. Kays, Trans. ASME, vol. 72, 1950, pp. 611–621.

3 "Gas Turbine Plant Regenerator Surfaces," by A. L. London and C. K. Ferguson, Bureau of Ships Research Memorandum No. 2–46, NavShips (250–338–3) July, 1946.

4 "Test Results of High-Performance Heat-Exchanger Surfaces Used in Aircraft Intercoolers and Their Significance for Gas-Turbine Regenerator Design," by A. L. London and C. K. Ferguson, Trans. ASME, vol. 71, 1949, pp. 17–26.

5 "The Basic Heat-Transfer and Flow-Friction Characteristics of Plain Plate-Fin Heat-Exchanger Surfaces," by W. M. Kays, Technical Report No. 5, Navy Contract N6-ONR-251 Task Order VI (NR-035-104), Department of Mechanical Engineering, Stanford University, Stanford, Calif.

6 "High-Performance Fins for Heat Transfer," by R. H. Norris and W. A. Spofford, Trans. ASME, vol. 64, 1942, pp. 489–496.

7 "Laminar-Flow Heat-Transfer Coefficients for Ducts," by R. H. Norris and D. D. Streid, Trans. ASME, vol. 62, 1940, pp. 525–533.

8 "Design, Selection, and Installation of Aircraft Heat Exchangers," by G. P. Wood and M. J. Brevoort, NACA Report No. ARR-3G-31, July, 1943.

9 "Generalized Equations for Selection Charts for Heat Exchangers in Aircraft," by Arthur N. Tifford and George P. Wood, NACA Report, ACR-April, 1942.

10 "Generalized Selection Charts for Harrison and Tubular Intercoolers," by George P. Wood and Arthur N. Tifford, NACA Report, ARR-December, 1942.

11 "Intercooler Design for Aircraft," by M. J. Brevoort, U. T. Joyner, and M. Leifer, NACA Report, ACR-September, 1939.

12 "Design Charts for Cross-Flow Tubular Intercoolers," by J. George Reuter and Michael F. Valerino, NACA Report, ACR-January, 1941.

13 "The Cross-Flow Plate-Type Intercooler," by Benjamin Pinkel, J. George Reuter, and Michael F. Valerino, NACA Report, ACR-April, 1942.

14 "Correlation and Utilization of New Data on Flow Resistance and Heat Transfer for Cross Flow of Gases Over Tube Banks," by E. D. Grimison, Trans. ASME, vol. 59, 1937, pp. 583–594.

15 "Heat Transmission," by W. H. McAdams, second edition, McGraw-Hill Book Company, Inc., New York, N. Y., 1942.

16 "Mean Temperature Difference in Design," by R. A. Bowman, A. C. Mueller, and W. M. Nagle, Trans. ASME, vol. 62, 1940, pp. 283–294.

Correlation of Plastic Deformation During Metal Cutting With Tensile Properties of the Work Material

By J. T. LAPSLEY, JR.,[1] R. C. GRASSI,[2] and E. G. THOMSEN,[3] BERKELEY, CALIF.

An experimental correlation of plastic deformation occurring during metal cutting with the plastic deformation in tension of the work material; an analysis permitting comparison of these two states of strain is presented. Orthogonal cutting of seamless steel tubing was employed for feeds of 0.0025–0.0085 in. per revolution (ipr), and positive rake angles of 25–45 deg. Deformation and forces of cutting were obtained from chip measurement and from a tool dynamometer employing resistance strain gages. The agreement obtained indicates that the tensile properties of the work material may offer a useful index to metal-cutting performance.

Nomenclature

The following nomenclature is used in the paper:

F_T = thrust force, lb; measured in direction of motion of tool by tool dynamometer in orthogonal cutting

F_C = cutting force, lb; measured perpendicular to direction of motion of tool by tool dynamometer in orthogonal cutting

l, l_o = final and original length, respectively, in.; refers to chip length in metal cutting and gage length in tension testing

D_o, D = original and instantaneous diameter, respectively, of neck in a tension bar, in.

α = rake angle, deg; measured in plane perpendicular to cutting edge

ϕ = shear angle, deg; angle between shear plane and surface being generated, measured in plane perpendicular to cutting edge

A_s = area of shear plane, sq in.

τ_{xz} = mean shear stress on shear plane (in metal cutting) psi

γ_{xz} = shearing strain of chip during removal in metal cutting

$\bar{\sigma}_x$, $\bar{\sigma}_y$, $\bar{\sigma}_z$ = normal true stresses at a point in a deformed metal, measured parallel to three co-ordinate directions x, y, z, respectively, psi

τ_{xy}, τ_{yz}, τ_{zx} = shearing stresses on planes perpendicular to co-ordinate axes of first subscript, and in direction of second subscripts, psi

$\bar{\epsilon}_x$, $\bar{\epsilon}_y$, $\bar{\epsilon}_z$ = finite plastic true strains associated with the normal stresses $\bar{\sigma}_x$, $\bar{\sigma}_y$, $\bar{\sigma}_z$, respectively

γ_{yx}, γ_{yz}, γ_{zx} = shearing strains associated with shearing stresses τ_{xy}, τ_{yz}, τ_{zx}, respectively

Effective true stress =

$$\sqrt{\frac{(\bar{\sigma}_x - \bar{\sigma}_y)^2 + (\bar{\sigma}_y - \bar{\sigma}_z)^2 + (\bar{\sigma}_z - \bar{\sigma}_x)^2}{2} + 3(\tau_{xy}^2 + \tau_{yz}^2 + \tau_{zx}^2)}$$

(complex stress function, psi)

Effective finite plastic strain =

$$\frac{2}{3}\sqrt{\frac{(\bar{\epsilon}_x - \bar{\epsilon}_y)^2 + (\bar{\epsilon}_y - \bar{\epsilon}_z)^2 + (\bar{\epsilon}_z - \bar{\epsilon}_x)^2}{2} + \frac{3}{4}(\gamma_{xy}^2 + \gamma_{yz}^2 + \gamma_{zx}^2)}$$

W_c = work done in cutting per unit volume of metal removed, in-lb/in.^{3}

W_s = work done in shearing per unit volume of metal removed, in-lb/in.^{3}

$\log_e$ = natural logarithm

t_o = initial thickness of chip, in.

w_o = initial chip width, in.

Introduction

Tool life, the time a tool remains serviceable under a given set of conditions, is probably the most important practical index of machinability. An appreciable amount of data is now available which can be expressed by the formula $VT^n = C$, where V is cutting velocity in feet per minute, T is tool life in minutes, n and C are constants depending on the cutting conditions, nature of work material, and other factors. While this relationship between velocity and tool life is quite general, the constants n and C hold only for specific conditions. For each new condition of metal cutting for which no information is available, time-consuming and costly experiments must be performed to find the numerical values of these constants. Consequently, a correlation of tool life with physical constants pertaining to the cutting condition, similar to the correlation of friction factor with Reynolds modulus in hydrodynamics, would be an important contribution.

In order to establish a general functional relationship of tool life with physical constants of tool work, conditions in the cutting zone, such as temperature, abrasiveness of the work at this temperature, the mechanics of metal cutting, and the state of plastic deformation of the chip must be established. It is the purpose of this paper to discuss the mechanism of metal cutting and to correlate the state of plastic deformation of metal cutting with that of the tension test.

In this investigation, orthogonal cutting of seamless steel tubing was used with values of feed from 0.0025 to 0.0085 in. per revolution (ipr) and positive back-rake angles on the cutting tool of 25 deg, 35 deg, 40 deg, and 45 deg. Cutting was done dry with a high-speed-steel tool at approximately 90 fpm.

[1] Assistant Professor of Mechanical Engineering, University of California.

[2] Assistant Professor of Mechanical Engineering, University of California. Mem. ASME.

[3] Associate Professor of Mechanical Engineering, University of California.

Contributed by the Production Engineering Division and presented at the Annual Meeting, New York, N. Y., November 27–December 2, 1949, of The American Society of Mechanical Engineers.

Note: Statements and opinions advanced in papers are to be understood as individual expressions of their authors and not those of the Society. Paper No. 49—A-121.

Experimental Technique

Orthogonal cutting, in which a straight-edged cutting tool moved relative to the workpiece in a direction perpendicular to its cutting edge, was employed. The cutting conditions were such as to yield continuous chip formation without a built-up edge on the tool. This type of chip formation has been designated as a type-2 chip (1).[4]

The force system for orthogonal cutting, developed by Merchant (2) is shown in Fig. 1. The resultant force R may be resolved into components, the cutting force F_C, and the thrust force

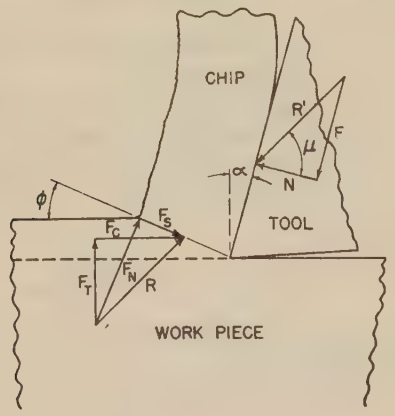

Fig. 1 Force System Acting on Chip During Orthogonal Cutting

F_T, which were measured by the tool dynamometer employed. Resolution of the force R along the shear plane, designated by the shear angle ϕ, results in F_S, the shearing force, and F_N, the force perpendicular to the shear plane. The force of friction is represented by F, and the force component perpendicular to the tool face by N. The friction angle and back-rake angle are represented by μ and α, respectively. The lack of collinearity of R and R' is not significant and has been so shown by others (2).

On the basis of Merchant's analysis, it has been shown that the work of cutting is

$$W_c = F_C/t_o w_o \quad \ldots\ldots\ldots\ldots\ldots\ldots [1]$$

where t_o and w_o are original chip thickness and width, respectively.

The work of shear is obtained from the relationship

$$W_s = \tau_{zz}\gamma_{zz} \quad \text{or} \quad (W_s = S_s\epsilon, \text{ according to Merchant}) \ldots [2]$$

where $\gamma_{zz} = \cot\phi + \tan(\phi - \alpha)$, and τ_{zz} is the shear stress on the plane designated by the angle ϕ.

The shear angle ϕ, is determined from the chip geometry by the following expression providing the chip width remains constant

$$\tan\phi = \frac{l}{l_o}\cos\alpha \Big/ \left(1 - \frac{l}{l_o}\sin\alpha\right) \quad \ldots\ldots\ldots [3]$$

where l_o and l are the initial and final chip lengths, respectively.

Metal cutting was done by machining the end of a short section of 6-in-OD, 0.475-in wall thickness, seamless steel tubing. The tubing was in the "as-received" or unannealed condition. The cutting tool, of high-speed steel, was clamped in a special holder mounted on the compound rest of an engine lathe. The tool was set on center and fed perpendicularly to the end of the tube which was clamped in a four-jaw chuck. Cutting was done dry, at 57 rpm, or approximately 90 fpm. This cutting speed was selected to obtain a moderate strain rate in the chip.

[4] Numbers in parentheses refer to the Bibliography at the end of the paper.

The tool dynamometer had as its measuring elements SR4 type A-5 electrical strain gages. The gages were mounted as shown in Fig. 2, with two active gages in adjacent legs of a conventional bridge circuit for each force determination. This arrangement increased sensitivity and also provided a means of eliminating temperature effects. Coolant was circulated through

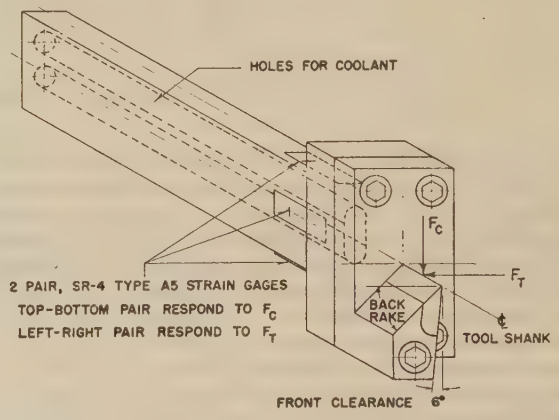

Fig. 2 Schematic Drawing of Tool Dynamometer Used in Measuring Orthogonal Cutting-Force Components, F_C and F_T

the tool shank so that heat generated during cutting did not produce a temperature differential between the strain gages. The stability of the gages was maintained by protection with wax, Ozite, and a metal shield.

The calibration of the dynamometer utilized a 5000-lb proving ring. The calibration for the thrust force F_T, was accomplished with the tool clamped in the holder used for cutting and mounted on the compound rest. Force was uniformly applied to the cutting edge through the proving ring by means of special adapters and manual carriage motion. The dynamometer calibration for the cutting force F_C, was performed with the tool mounted in its holder and clamped to the table of an upright drill press. The force was applied uniformly to the cutting edge (similar to F_T), by using manual spindle travel.

The dynamometer was designed so that the measurement of one force was independent of the other. The calibrations proved that this design criterion had been achieved. Simultaneous recording of F_T and F_C was obtained by using strain recorders. The time of cutting varied with conditions and was dependent upon attaining equilibrium values of forces and a representative number of chips. Since the chip width remained constant, the relationships previously presented are applicable. The initial conditions of chip thickness, and length, t_o and l_o, were determined from the feed and outside diameter of the tube, respectively. A reference point for measuring the final chip length, l, was established by cutting a shallow longitudinal slot in the outside surface of the tube. This measurement was facilitated by the fact that the chips did not curl during removal.

Specimens for the tension test were cut from the tube wall so that their axes coincided with that of the tube. The gage section was $1\frac{1}{4}$ in. long and 0.250 in. diam.

Experimental Results

The experimental data of the metal-cutting tests are presented in Table 1 and are shown graphically in Figs. 3 to 6, inclusive. Although these data are not the primary objective of this investigation, they show some interesting trends which also establish their consistency.

Figs. 3 and 4 indicate the effect of back rake and feed, respectively, on the tool forces. It may be noted that the change in

TABLE 1 TABULATED TEST DATA AND CALCULATED RESULTS; ORTHOGONAL END CUTTING OF SEAMLESS STEEL TUBING

(Conditions: Dry cutting, 90 fpm, and constant chip width, i.e., 0.475 in.)

Back-rake angle, deg	Feed, ipr	Cutting ratio, l/l_c	Cutting force, F_C, lb	Thrust force, F_T lb	Shear angle, ϕ, deg	Shear strain γ_{zs}	Work of shear, W_s, 1000 in-lb/in.^{3}	Work of cutting, W_c 1000 in-lb/in.^{3}	Effective strain, $\frac{\sqrt{3}}{3}\gamma_{zs}$	Effective stress, 1000 psi, $\sqrt{3}\,\tau_{zs}$
25	0.0025	0.358	380	224	20.9	2.55	209	319	1.47	143
	0.0035	0.366	475	281	21.5	2.48	180	286	1.43	126
	0.005	0.407	643	357	24.0	2.23	169	270	1.29	131
	0.006	0.345	728	398	20.1	2.65	175	255	1.53	114
	0.0085	0.383	992	551	22.4	2.38	159	246	1.37	116
35	0.0025	0.527	254	102	31.6	1.56	112	214	0.90	125
	0.0035	0.528	306	122	31.9	1.55	96.4	184	0.89	108
	0.005	0.529	433	166	32.0	1.55	96.5	182	0.89	108
	0.006	0.533	507	184	32.2	1.54	95.5	178	0.90	108
	0.0085	0.532	675	234	32.0	1.55	91.3	167	0.89	102
40	0.0025	0.585	232	71	35.7	1.32	94.0	195	0.76	124
	0.0035	0.580	296	87	35.4	1.33	87.8	178	0.77	116
	0.005	0.611	412	112	37.5	1.26	83.1	173	0.73	114
	0.006	0.606	475	127	37.2	1.27	81.1	167	0.73	111
	0.0085	0.606	634	153	37.2	1.27	78.1	157	0.73	107
45	0.0025	0.670	232	68	41.9	1.06	74.8	195	0.61	123
	0.0035	0.670	285	77	41.9	1.06	68.5	172	0.61	112
	0.005	0.649	386	94	40.2	1.10	69.6	162	0.64	110
	0.006	0.642	443	102	39.6	1.01	62.7	156	0.58	107
	0.0085	0.646	581	117	39.9	1.11	65.0	144	0.64	102

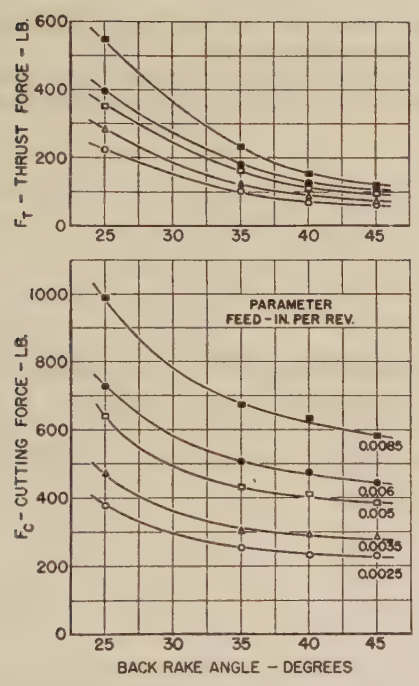

FIG. 3 EFFECT OF BACK-RAKE ANGLE ON CUTTING FORCES FOR CONSTANT FEED VALUES

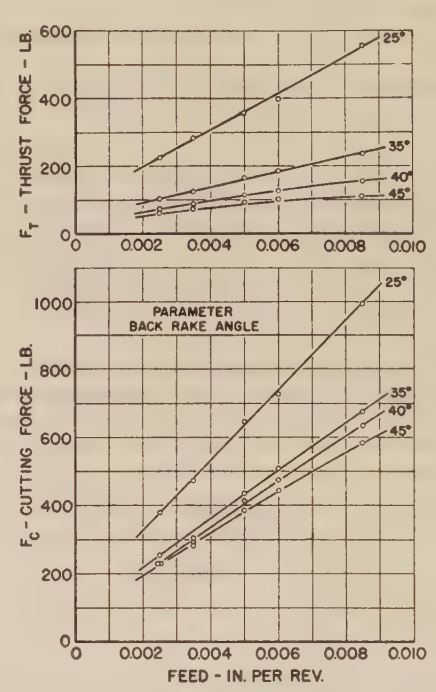

FIG. 4 EFFECT OF FEED ON CUTTING FORCES FOR CONSTANT BACK-RAKE ANGLES

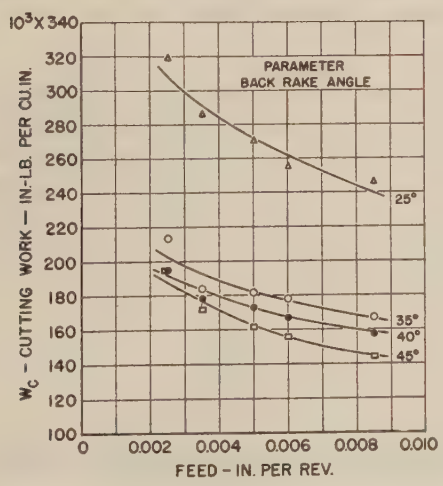

FIG. 5 EFFECT OF FEED ON WORK OF CUTTING FOR CONSTANT BACK-RAKE ANGLES

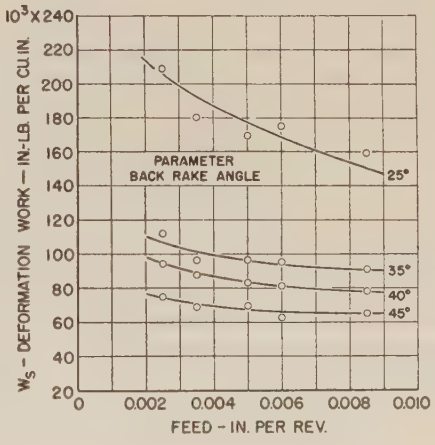

FIG. 6 EFFECT OF FEED ON WORK OF SHEAR DEFORMATION FOR CONSTANT BACK-RAKE ANGLES

feed results in a greater change in the cutting force than in the thrust force. Figs. 5 and 6 show the amount of work expended per unit volume of metal removed in cutting and in shear deformation, respectively. Examination of these figures indicates that the work expended for rake angles 45 deg, 40 deg, and 35 deg is appreciably lower than that expended for the 25-deg back-rake angle. This behavior might be attributable to the presence of a nonobserved built-up edge.

Discussion

The metal of the chip during metal cutting is severely deformed and, therefore, is in a highly work-hardened state. It is possible to compare this state of work-hardening with that obtained by any other deformation process by application of a theory of plasticity (3, 4), providing the states are calculable and the metal under consideration satisfies the assumptions made in the ideal theory. The assumptions are as follows:

(*a*) The metal is isotropic.
(*b*) The metal is homogeneous.
(*c*) The stresses are linear functions of the infinitesimal plastic strains.
(*d*) Temperature, deformation rate, and hydrostatic pressure do not affect the state of plastic deformation.

While real metals do not behave ideally, it has been shown (5) that low-strength aluminum alloys, magnesium alloys, and mild steel satisfy the foregoing assumptions to a good degree of approximation when equivalent states of work-hardening in tension, compression, and torsion are compared. The following section will be devoted to the development necessary for correlation between the plastic state in a chip and in a tension bar by application of this theory of plasticity.

If the previously stated assumptions are satisfied, it can be shown that equivalent states of work-hardening can be represented on an effective stress-effective plastic strain curve. Two complex stress and strain functions utilized in the correlation are

Effective stress =

$$\sqrt{\frac{(\bar{\sigma}_x - \bar{\sigma}_y)^2 + (\bar{\sigma}_y - \bar{\sigma}_z)^2 + (\bar{\sigma}_z - \bar{\sigma}_x)^2}{2} + 3(\tau_{xy}^2 + \tau_{yz}^2 + \tau_{zx}^2)} \quad [4]$$

Effective plastic strain =

$$\frac{2}{3}\sqrt{\frac{(\bar{\epsilon}_x - \bar{\epsilon}_y)^2 + (\bar{\epsilon}_y - \bar{\epsilon}_z)^2 + (\bar{\epsilon}_z - \bar{\epsilon}_x)^2}{2} + \frac{3}{4}(\gamma_{xy}^2 + \gamma_{yz}^2 + \gamma_{zx}^2)} \quad [5]$$

The work of plastic deformation for any particular state of deformation is given by the area under the curve from zero strain to the value under consideration.

While the stress or strain path employed does not affect the validity of the universality of the effective stress-effective plastic strain curve, it is only possible to determine the plastic state in a few simple cases. The infinitesimal plastic strains, from which the finite strains under the radical of the effective strain are constructed, are not perfect differentials. The finite strains are, therefore, path dependent and can be obtained by integration only if the stress or strain path is known. In the present investigation it is assumed that the stress ratios remain constant during the entire deformation, thus permitting the evaluation of the finite strains in terms of quantities measurable before and after the deformation. With this additional assumption, it is possible to calculate the plastic states for tension and metal cutting.

The Tension Test. Let the x-co-ordinate axis be coincident with the axis of the test bar. Therefore, $\bar{\sigma}_x$, is the true stress resulting from the applied axial load

$$\bar{\sigma}_x = \frac{\text{Axial load}}{\text{Instantaneous area}} \quad [6]$$

Since $\bar{\sigma}_x$ is the only stress, the effective stress reduces to

$$\text{Effective stress (in tension)} = \bar{\sigma}_x \quad [7]$$

The finite plastic strain $\bar{\epsilon}_x$ in the axial direction can be determined from measurements of the original gage length and the length at any stage of the deformation up to the maximum load

$$\bar{\epsilon}_x = \log_e \frac{l}{l_o} \quad [8]$$

where l_o and l are initial and final gage length, respectively.

After the maximum load has been exceeded, the specimen necks and the deformation ceases to be uniform over the gage length. The axial strain, however, can be obtained from measurements of the minimum diameter in the neck for constant volume deformation

$$\bar{\epsilon}_x = 2 \log_e \frac{D_o}{D} \quad [9]$$

where D_o and D are initial and instantaneous diameter, respectively, at any stage of deformation.

By use of the constant-volume relationship, the effective plastic strain can be evaluated in terms of the normal strains

$$\bar{\epsilon}_x + \bar{\epsilon}_y + \bar{\epsilon}_z = 0 \quad [10]$$

but

$$\bar{\epsilon}_y = \bar{\epsilon}_z$$

therefore

$$-\bar{\epsilon}_y = -\bar{\epsilon}_z = \frac{1}{2}\bar{\epsilon}_x \quad [11]$$

Substituting these values of strain into Equation [5] results in

$$\text{Effective plastic strain (tension)} = \bar{\epsilon}_x \quad [12]$$

Consequently, the effective stress-effective plastic strain curve is identical with the true stress-true plastic strain curve in tension.

When necking occurs, the stress ceases to be uniform as has been shown by Bridgman (6). In general, however, the error introduced by assuming a constant stress across the section is not significant.

Metal Cutting. Merchant (7) has shown that it is possible to obtain an analysis of the metal-cutting process by assuming that the deformation is simple shear. The shearing process is visualized to take place on a plane making an angle ϕ with the original work surface, as shown in Fig. 1. The slight curvature of the shear plane observed from photomicrographs has been neglected in the analysis. The deformation stress τ_{xz} on this plane is obtainable from the measured tool forces, while the shearing strain γ_{xz} is calculable from chip-deformation measurements

$$\tau_{xz} = \frac{F_C \sin\phi \cos\phi - F_T \sin^2\phi}{t_o w_o} \quad [13]$$

$$\gamma_{xz} = \cot\phi + \tan(\phi - \alpha) \quad [14]$$

where t_o and w_o are the initial thickness and width of chip, respectively.

In addition to the shearing stress, a normal stress $\bar{\sigma}_z$ acts on the shear plane

$$\bar{\sigma}_z = \frac{F_C \sin^2 \phi + F_T \sin \phi \cos \phi}{t_o w_o} \quad \ldots\ldots\ldots [15]$$

Since the analysis is based only on the shear strain, the effective strain reduces to

$$\text{Effective strain (metal cutting)} = \frac{\sqrt{3}}{3} \gamma_{xz}; \quad \gamma_{xz} = \gamma_{zx} \quad [16]$$

However, a further assumption must be made in order to calculate the effective stress. Since τ_{xz} is the only shear stress acting, $\tau_{yz} = \tau_{xy} = 0$. Of the normal stresses, only $\bar{\sigma}_x$ is known; it is therefore necessary to assign values to $\bar{\sigma}_y$ and $\bar{\sigma}_z$. While values cannot be fixed, a priori, it is reasonable to assume that the state of stress is that of hydrostatic pressure on the shear plane. Under this condition, the three normal stresses are equal and are eliminated from the effective-stress expression, Equation [4]. The effective stress, therefore, reduces to

$$\text{Effective stress (metal cutting)} = \sqrt{3}\, \tau_{xz}; \quad \tau_{zx} = \tau_{xz} \ldots [17]$$

Correlation Between Tension and Metal Cutting. Fig. 7 shows the calculated metal-cutting data and the stress-strain curve obtained from tension tests for the same material. The solid line represents the experimental data from tension tests which were extrapolated to higher values of strains than those achievable in tension, as shown by the dashed portion of the curve. Such extrapolation is not unreasonable; for example, higher strains may be obtained in torsion. It is evident that there is good agreement between the tension data and the metal-cutting data.

The fact that the effective stress values for a given rake-angle group about a particular strain value indicates that factors not taken into account are active. Merchant (7) proposes that the normal stress on the shear plane (a condition of hydrostatic pressure in the present analysis) influences the shear stress. While this may be an important factor, it is not clearly proved to be the only factor, as the experimental data, reported by Merchant, show scatter when the normal stress is considered. Further investigation is necessary to establish which assumptions are not valid and what other variables must be considered.

Fig. 8 shows a comparison of the work of deformation per unit volume of metal removed as calculated from the shear work of metal cutting and from the tension test. The deformation work based upon tension was obtained by evaluating areas under the

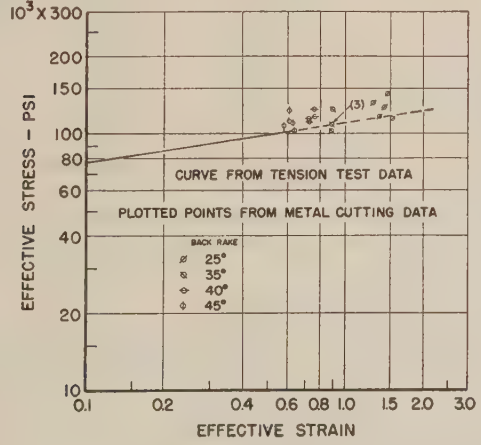

Fig. 7 Correlation Between Effective Stress-Effective Plastic Strain Values as Calculated From (1) Plasticity Analysis of Metal-Cutting Deformation; (2) Tension Test of Work Material

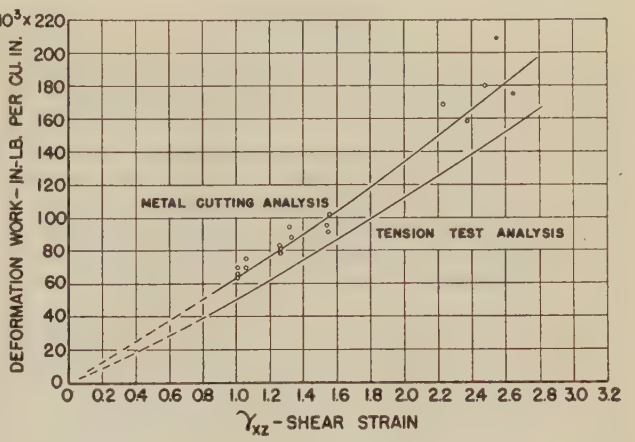

Fig. 8 Work of Deformation as Function of Shear Strain, γ_{xz}, for (1) Shear Stress-Shear Strain Analysis of Metal Cutting as Developed by Merchant; (2) Effective Stress-Effective Plastic Strain Analysis Based on Tension-Test Data

effective stress-effective plastic strain curve, presented in Fig. 7. An empirical equation was determined for this curve

$$\text{Effective stress} = 110 \times 10^3 (\text{effective plastic strain})^{0.152} \ldots [18]$$

Work of deformation for given shear-strain values was determined by integration of the equation between limits of zero strain and the corresponding effective plastic-strain value.

From the comparison it is seen that the work of deformation, as determined from the metal-cutting analysis, exceeds the deformation work based upon the tension test for all cutting conditions employed in this investigation. It is felt that the present information is insufficient for an adequate explanation of this anomaly and that further investigation should be made.

Conclusions

1 The results of the investigation have shown that metal-cutting data can be correlated with tension data for orthogonal cutting and the test conditions employed.

2 The tension properties of a material may offer a useful index of cutting performance.

3 The work done by shear deformation, calculated from metal-cutting data, results in larger values than that determined from the tension test for equivalent states of deformation.

4 Further application of the plasticity theory should yield information which could give a more basic understanding of metal cutting.

BIBLIOGRAPHY

1 "Physics of Metal Cutting," by H. Ernst, *Machining of Metals*, American Society for Metals, 1938, p. 24.

2 "Mechanics of the Metal Cutting Process. I Orthogonal Cutting and a Type 2 Chip," by M. E. Merchant, *Journal of Applied Physics*, vol. 16, no. 5, 1945,p p. 267–275.

3 "Plastic Flow of Metals," by J. J. Jelinek, A. J. Latter, E. G. Thomsen, and J. E. Dorn, OPRD Report No. W-200, May, 1945.

4 "The Ductility of Metals Under General Conditions of Stress and Strain," by J. E. Dorn and E. G. Thomsen, Trans. ASM, vol. 39, 1947, pp. 741–772.

5 "Investigation of the Validity of an Ideal Theory of Elasto-Plasticity for Wrought Aluminum Alloys," by E. G. Thomsen, I. Cornet, I. Lotze, and J. E. Dorn, NACA Technical Note No. 1552, July, 1948.

6 "The Stress Distribution at the Neck of a Tensile Specimen," by P. W. Bridgman, Trans. ASM, vol. 32, 1944, pp. 553–574.

7 "Mechanics of the Metal Cutting Process. II Plasticity Conditions in Orthogonal Cutting," by M. E. Merchant, *Journal of Applied Physics*, vol. 16, no. 6, 1945, pp. 318–324.

Discussion

M. Eugene Merchant.[5] The authors have contributed some much-needed information by carrying out cutting tests and tensile tests on the same material, and then comparing the mechanical properties of the material as calculated from the data obtained on the two types of tests. They are to be congratulated on the manner in which they have carried through the test work and analysis; such information serves to clarify further the fundamentals of the cutting process and their relation to the mechanical properties of the metal being machined.

The mathematical analysis which the authors have used to compare the metal-cutting results with those from the tensile tests provides good correlation between the two sets of data. However, this mathematical analysis is based on certain assumptions which are questionable when applied to the metal-cutting process. Therefore it appears somewhat fortuitous that such good agreement was obtained. In particular, the main basis for the mathematical theory used to compare the two sets of data is that states of work-hardening occur in the plastic deformation taking place on the shear plane in metal-cutting which are equivalent to those obtained in a normal tensile test. The fallacy here is brought out by Drucker,[6] who points out that in the process of metal cutting virtually no work-hardening of the metal occurs on the shear plane because of the extremely high strain rates involved in the cutting process. (The "work-hardening" actually observed in hardness measurements on chips virtually all occurs after deformation on the shear plane is complete, since work-hardening is a "rate-process," like a chemical reaction!)

In the tensile test, of course, work-hardening does occur, since the rate of strain is quite low. Further, the very fact that an extremely high strain rate is involved in the cutting process, compared to the very low strain rates involved in tensile tests, will have a marked effect on the actual shear strength of the metal in the two cases; shear strength is known to increase with increasing strain rate. Therefore, in the two types of deformation in actuality there can be no comparable states of work-hardening, and so the basic premise of the authors' theory is not met.

Nevertheless, it appears from the test results reported by the authors (as well as from data obtained in the writer's laboratory, as will be shown shortly) that reasonable agreement can be obtained between mechanical properties observed from cutting tests and those observed from low-strain-rate tests. The reason for this fortunate result is not immediately evident; it appears, however, that the complicating factors involved tend to balance each other. Presumably, the "weakening" effects of the absence of work-hardening and the local heating on the shear plane in cutting offset the "strengthening" effect of the very high strain rate reasonably well. The net result apparently makes the stress values obtained from the two types of tests very nearly equal, for the range of strains and strain rates usually found in machining.

Another factor which the authors have (admittedly) neglected in making the comparison between the tensile-test data and those from metal-cutting is the effect of compressive stress (or hydrostatic pressure) on the actual values of shear strength calculated from metal-cutting data.

As pointed out previously by the writer,[7] the shear strength of the metal on the shear plane in metal cutting is raised by the presence of a high value of compressive stress acting on that plane. No such compressive stress acts on the slip processes occurring in the tensile tests. (In fact, the reverse is true.) Therefore the values of shear strength calculated from the authors' metal-cutting data ought, in all fairness, to be corrected to a value of zero compressive stress (at least), if they are to be compared with strength values from the tensile tests. This can be done, approximately, for the data presented by the authors, by extrapolating the shear-strength versus compressive-stress data back to zero compressive stress, making use of metal-cutting theory. When this is done, it is found that the calculated shear strength (τ_{xz}) for the steel used by the authors is approximately 60,000 psi (this value is independent of strain since no work-hardening occurs in the metal-cutting process, as previously mentioned). Thus the effective stress value ($\sqrt{3}\tau_{xz}$) is approximately 100,000 psi. This value is still in reasonable agreement with the authors' tensile-test data.

Actually, to be wholly fair, the tensile-test data ought also to be corrected to a value of zero hydrostatic pressure, which would increase the effective stress values somewhat. No effort has been made to do this, however, since the effect probably would be slight, and no provision for such correction has been made in the theory of plastic deformation used by the authors in analyzing the tensile tests.

Comparisons between metal-cutting data and data obtained from low strain-rate tests of mechanical properties, somewhat similar to the comparison reported by the authors, have been carried out in the writer's laboratory[8,9] recently. However, these low-strain-rate tests were made by quite a different method from the tensile tests employed by the authors; a method developed by Bridgman[10] was used wherein notched tubular specimens are tested in torsion while subjected to an axial compressive force. Here again, surprisingly good correlation between the metal-cutting data and those obtained from this torsion-compression type of test was obtained, even though the strain rates and corresponding work-hardening states were very different. A comparison of the values of shear strength calculated from the two types of tests at comparable values of compressive stress and shearing strain are given in Table 2 of this discussion. It may be seen that the shear-strength values calculated from the two types of tests agree surprisingly well, considering the great differences that exist between the conditions of deformation in the two cases.

TABLE 2 COMPARISON OF SHEAR-STRENGTH VALUES OBSERVED FROM TORSION-COMPRESSION-TYPE TESTS WITH THOSE OBSERVED FROM METAL-CUTTING TESTS, AT EQUIVALENT VALUES OF COMPRESSIVE STRESS

(Shearing strain = 2.4 — 3.0)

Steel	Value of compressive stress at which compared, 1000 psi	Observed values of shear strength, 1000 psi: Torsion-compression test	Observed values of shear strength, 1000 psi: Metal-cutting test
SAE 1117	60	63	67
SAE 3150 (spheroidized)	110	81	89
SAE 3150 (pearlitic)	110	88	86
SAE 3450	110	93	88

In metal cutting three mechanical properties of the material being machined control the forces acting on the cutting tool.[7] These are as follows:

1 Shear strength of the material.

2 Machining constant of the material (a property of the material, the value of which, in theory, depends upon the rate of increase of shear strength with applied compressive stress).

[5] Senior Research Physicist, The Cincinnati Milling Machine Company, Cincinnati, Ohio. Mem. ASME.

[6] "An Analysis of the Mechanics of Metal Cutting," by D. C. Drucker, *Journal of Applied Physics*, vol. 20, 1949, pp. 1013–1021.

[7] Refer to authors' bibliography (7).

[8] "Torsion-Compression Testing," by J. Kemeny, University of Cincinnati Thesis, 1947.

[9] "Torsion-Compression Testing," by E. J. Krabacher and K. W. Whisler, University of Cincinnati Thesis, 1949.

[10] "On Torsion Combined With Compression," by P. W. Bridgman, *Journal of Applied Physics*, vol. 14, 1943, pp. 273–283.

3 The coefficient of friction between the cutting tool and the flowing chip.

Of these three quantities needed to predict cutting forces in machining, only the first can be obtained from a tensile test by the methods used by the authors. The torsion-compression type of test mentioned has the advantage not only of giving values of shear strength, but also of providing theoretical values of machining constant; the increase in (torsional) shear strength as increasing axial compressive force is applied to the tubular test specimen can be observed in this type of test. Again, reasonably good correlation with metal-cutting data is obtained, as shown by the values of machining constant given in Table 3 herewith. Here the agreement is not as good as for the shear strength values (Table 2), but still serve well enough for a first approximation.

TABLE 3 COMPARISON OF VALUES OF MACHINING CONSTANT OBSERVED FROM TORSION-COMPRESSION TYPE TESTS WITH THOSE OBSERVED FROM METAL-CUTTING-TESTS, AT EQUIVALENT VALUES OF SHEARING STRAIN

Steel	Value of shearing strain at which compared	Observed values of machining constant, degrees: Torsion-compression test	Observed values of machining constant, degrees: Metal-cutting test
SAE 1117	2.15	85.0	77.0
SAE 3150 (spheroidized)	3.11	84.5	76.0
SAE 3150 (pearlitic)	3.15	74.0	70.8
SAE 3450	2.96	83.0	77.9

In conclusion, we again wish to congratulate the authors for their fine beginning on the exploration of fundamentals in metal cutting. It is pleasing to note from the concluding paragraph of the paper that the present work does, in truth, mark only a beginning and that we may look forward to further interesting reports in this field from the authors.

Milton C. Shaw.[11] The authors have presented a most interesting discussion of the application of the distortion-energy theorem of plasticity to the cutting of metals. This idea of considering the states of stress in two bodies as equivalent when the same energy of distortion is associated with each is another of the many contributions of James Clerk Maxwell (1856).[12] The distortion-energy theorem represents the plasticity condition that has been most successful to date in relating the flow characteristics of two homogeneous bodies of different geometry and stress distribution. This method is one way of introducing the effect of strain-hardening into the theory of cutting.

The authors have listed carefully the assumptions upon which the distortion-energy theorem is based. These might be considered briefly in light of the experimental results. Despite the fact that all metals are far from homogeneous, the size or mean period of the inhomogeneity is generally very small compared with the size of the body undergoing plastic flow, and good results are obtained by treating the material as a homogeneous continuum. However, when the specimen is small, the fact that the material is actually inhomogeneous becomes more important. For example, the distortion-energy theorem indicates that all tensile-test specimens made from a given material should have the same ultimate stress regardless of diameter of the specimen. This is not the case however, for it is found that as the diameter is decreased below a particular diameter, the ultimate stress increases. This size effect is to be expected whenever strain hardening occurs in an inhomogeneous material.

In the cutting process, the depth of cut corresponds to the diameter of the tensile-test specimen, and it is apparent that in cutting we are generally dealing with small specimens. It is not surprising, therefore, that the authors' test points fall above the tensile-test data for the $^1/_4$-in-diam specimen in Fig. 7 of the paper, and further that the cutting-data points lie an increasing distance above the tensile curve as the chip size decreases.

The writer recently has completed work on a theory of cutting which takes strain-hardening and the inhomogeneity of the metal cut into consideration. This analysis, which will be published elsewhere, is in good agreement with the authors' data and shows quantitatively that the shear work to remove a cubic inch of material increases as the depth of cut decreases, as may be seen in Table 1, Fig. 8, of the paper. It might be remarked at this point that the reason for the increase in specific shear work with rake angle (for a given depth of cut), as shown in Fig. 8, is due to the increase in the shear strain arising in the cutting process as the depth of cut is decreased.

The assumption regarding the unimportance of temperature and the rate of strain in application of the distortion-energy theorem might also be considered. The true stress-strain curve is usually obtained under essentially static conditions, while the cutting process, on the other hand, involves a very high rate of strain. From photomicrographs it is evident that nearly all of the large strain that occurs in cutting takes place as the metal crosses the "shear plane." If this were truly a mathematical plane, we would have, in the cutting process, strain at an infinite rate. Actually, we may say the rate of strain in cutting is very high.

Since nearly all of the energy associated with the plastic-straining of metals appears in the form of heat, it is evident that a significant temperature rise is to be expected in the essentially adiabatic straining process of cutting, while a relatively small temperature rise is to be expected on the shear plane in the nearly isothermal-straining process of the ordinary true stress-strain test. The temperature on the shear plane is apt to be far more significant in the cutting process than in other processes to which the distortion-energy theorem is applied. Thus it is evident that the extreme conditions of size and rate of strain that are met in the cutting process provide a serious test of the assumed independence of strain mechanism and the temperature effect in Maxwell's distortion-energy theorem.

The authors have assumed the normal stress on the shear plane to be a manifestation of the presence of a hydrostatic pressure. This leads naturally to the result that the state of stress in cutting is independent of the normal stress on the shear plane, which, however, is in disagreement with Merchant's theory of cutting. The fact that the authors' analysis is in such good agreement with experiment (except for the afore-mentioned size effect) indicates strain-hardening and not the influence of normal stress on the shear plane to be the important item. It is therefore enlightening to examine the authors' data according to Merchant's analysis.[7]

In Fig. 9, herewith, the authors' data are shown plotted with normal stress against shear stress. According to Merchant, all of these points should be along a single straight line. Therefore we might choose either of the lines shown. According to Merchant's plasticity condition, when the observed shear angle ϕ is plotted against the quantity $(\tau - \alpha)$, where τ is the friction angle, and α the rake angle, a straight line should be obtained whose equation is

$$\phi = {}^1/_2 (\tau - \alpha) + \cot^{-1} K \quad [19]$$

where K is the slope of the line in Fig. 9.

The authors' data points are shown as circles in Fig. 10 of this

[11] Associate Professor of Mechanical Engineering, Massachusetts Institute of Technology, Cambridge, Mass. Mem. ASME.

[12] Letter by Maxwell to William Thomson dated Dec. 18, 1856, published in Proceedings of Cambridge Philosophical Society, Part V, vol. 32.

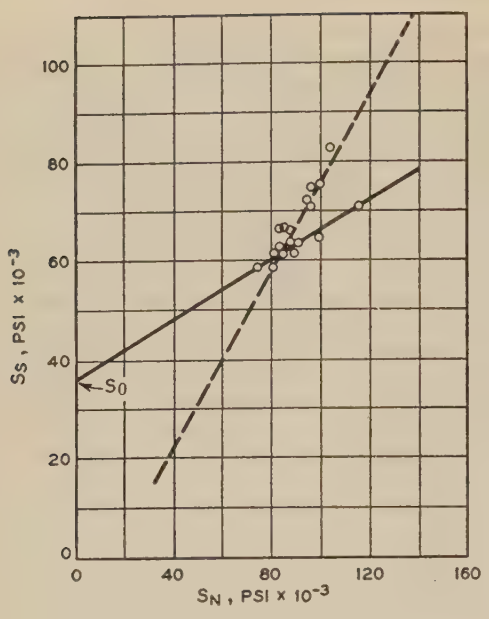

FIG. 9

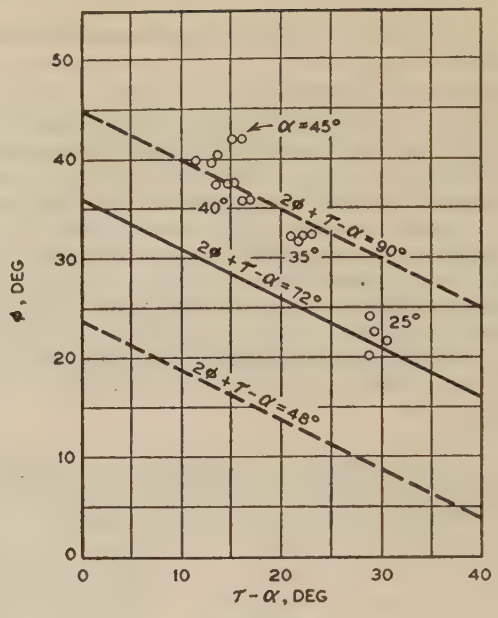

FIG. 10

discussion, while the two lines corresponding to those of Fig. 9 are shown solid and dotted. The dash line corresponds to a value of K of zero (i.e., the case corresponding to the authors' finding that shear strength is independent of normal stress on the shear plane). Most of the authors' data are seen to be in better agreement with the dash line corresponding to $K = 0$. Only those points corresponding to a rake angle of 25 deg are in agreement with the solid curve, and there is apparently no justification for the dotted curves in Figs. 9 and 10.

Actually, it would appear that the test points lie along or somewhat below the dash line in Fig. 10, the distance below the line increasing as the rake angle decreases. The increase in temperature on the shear plane which accompanies strain has not been included in the analysis leading to the upper line in Fig. 10, but if included would move the line vertically downward an increasing amount as the shear energy increased. This could account for the fact that points fall progressively farther below the upper line in Fig. 10, as the rake angle is increased, for as previously mentioned, the amount of strain, and hence the shear work required to remove a cubic inch of metal, also increases as the rake angle is decreased. It would thus appear that the authors' data are in full support of the view that strain-hardening is an important consideration in the metal-cutting process, and further that the influence of normal stress on the shear plane is relatively insignificant.

AUTHORS' CLOSURE

The authors are appreciative of the discussions submitted by Dr. Merchant and Professor Shaw. It is gratifying to note their interest in the paper as evidenced by the comments. However, there exist some areas of disagreement which we believe will be resolved only by further experimental investigations.

Merchant's comments hinge essentially upon two considerations, (1) absence of work-hardening effect during metal cutting as postulated by Drucker and (2) the effect of compression upon shear strength as reported by Bridgman. The large variation in strain rates is the basis for Merchant's comment that the two states of work-hardening (metal cutting and tension test) are not comparable. The authors' simplifying assumption (*d*) regarding strain rate should be modified if and when experimental data establish the order of importance of strain rate. However, in the absence of such experimental data, the authors cannot agree with the comment of Merchant based upon Drucker's theoretical analysis that work-hardening does not occur during metal cutting because of the relatively high strain rates involved.

The effect of normal stress on the shear strength or flow stress, referred to by Merchant, has been neglected by the authors because this effect has not been clearly demonstrated. The results of Bridgman cited in Merchant's paper (Bibliography 7) did not demonstrate clearly that the effect holds for all metals. In fact, Bridgman concludes that the shear stress at a definite strain value of unity increases with normal stress only for drill rod, but for SAE 1045 carbon steel the variation was within the order of experimental accuracy. If subsequent experimental work shows the normal stress factor to be appreciable, it can be incorporated in the plasticity analysis.

The authors agree in general with comments made by Shaw. The assumptions stated in the paper, such as homogeneity and isotropy of the work material, are simplifying assumptions only and should not be considered as hard and fast rules. Refinements can be applied to the plasticity theory, based on Maxwell's original hypothesis and restated by others in several ways, as certain effects not incorporated in this theory are isolated.

The authors have also applied Merchant's criteria for metal cutting as shown in the graphs of Figs. 9 and 10. In view of the hypothesis, however, that the effect of work-hardening in metal cutting is important, they have felt that insufficient data were available to isolate this effect, inasmuch as comparisons ought only to be made at equivalent states of work-hardening.

In conclusion, the authors wish to thank the discussers for their interest and to state that the approach presented in their paper should be regarded as a basis for further investigation. Additional experimental work, now in progress, indicates that the analysis correlates also for materials other than that reported.

Improved Nails

Their Driving Resistance, Withdrawal Resistance, and Lateral Load-Carrying Capacity

By E. GEORGE STERN,[1] BLACKSBURG, VA.

Approximately 3600 tests were performed on the driving resistance, withdrawal resistance, lateral load-carrying capacity, withdrawal, and deformation of 2, 2 1/2, 3, 3 1/2, and 4-in-long plain-shank, spirally grooved, and annularly grooved nails in southern yellow pine, white oak, and beech, in order to make available comparative test and design information on these nails. Data on nail properties, as influenced by nail type, size, point, shank pilot, steel composition, heat-treatment, cement coating, wood species, wood density, and annual rings of the wood are presented to help in determining the type of nail most suitable for specific applications. At a later date a report will be issued on the effects of change in moisture content and elapsed time after driving, on the foregoing test variables, since these factors could not be investigated until after the test planks had been air-seasoned. Such a study was made possible because all nails for tests on withdrawal resistance and lateral load-carrying capacity were driven at that time of test performance when oak and beech were green and pine was partially air-dry.

Introduction

DIRECTLY or indirectly, nails are in everyday use by almost everyone. Without being in the limelight or conspicuous, they are essential to human comfort and living, since they are of fundamental importance in most wood products. Little is known about the behavior of nails once driven into wood. Experience governs their use. If one nail does not perform the job, a second one is used. If a large nail splits a piece of wood, one or two small ones are used instead. So many people want to know how to use nails properly, but few have the opportunity to collect enough experience to have the necessary know-how. To complicate matters, the number of types and sizes of nails in production and use is great. The round, triangular and square-shank nails are made as plain-shank, barbed, coated, twisted, spirally grooved, annularly grooved, nontempered or tempered nails with low or high-carbon steel, stainless steel, aluminum, copper, brass, bronze, silicon bronze, or other alloys; with short, medium, and long diamond, needle, chisel, duckbill, side or V-points; with standard, medium or large flat, countersunk, round, oval, brad or duplex heads. They are merchandised as common nails, finishing nails, fiberboard nails, plasterboard nails, wallboard nails, sheetrock nails, cork-insulation nails, lath nails, siding nails, sheeting nails, shingle nails, roofing nails, shade nails, concrete nails, flooring brads, pallet nails, box nails, case nails, basket nails, barrel nails, boat nails, wagon nails, car nails, foundry nails, fence nails, sign nails, hinge nails, clout nails, sinkers, corkers, coolers, etc.

In a recent U. S. Government publication (1),[2] sound and efficient nailing practices in home construction are suggested. These recommendations, although backed up by U. S. Forest Products Laboratory test data, are principally based on observed nailing practices, usually a matter of precedent, tradition, or individual judgment, however, as a rule, not fully taking into account the forces to be resisted. The use of plain-shank nails is recommended, presumably because of the unavailability of satisfactory design and test data on and field experience with relatively new nails with spirally or annularly grooved shanks, as shown in Fig. 1. Similarly, because test and design data on such improved

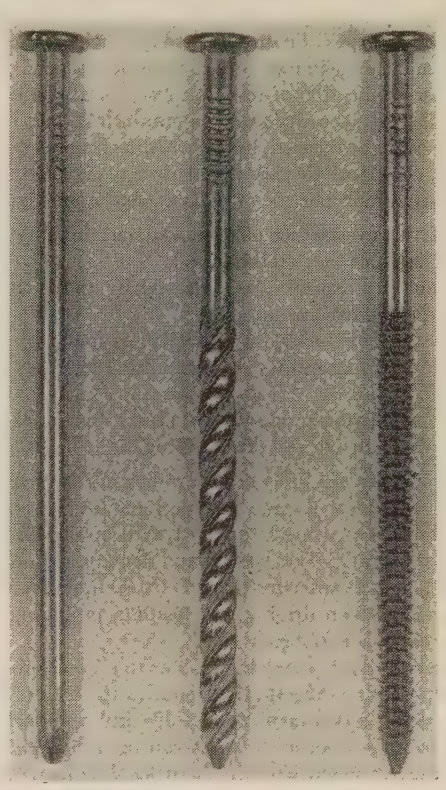

Fig. 1 Plain-Shank, Spirally Grooved, and Annularly Grooved 3 1/2-In-Long Nails

nails never have been available to the designing timber engineer, use of such improved nails for joints of timber structures has not been in the news, although such nails may have been occasionally used for such purposes. In contrast, the design of marine structures by naval architects with such spirally and annularly grooved nails has resulted in their widespread use in boat and ship construction. Automobile manufacturers have long taken advantage of these improved nails for fastening car linings to the body. Box and furniture manufacturers often have been in the position

[1] Research Professor, Department of Wood Construction, Virginia Polytechnic Institute. Mem. ASME.

Contributed by the Wood Industries Division and presented at the Annual Meeting, New York, N. Y., November 27–December 2, 1949, of The American Society of Mechanical Engineers.

Note: Statements and opinions advanced in papers are to be understood as individual expressions of their authors and not those of the Society. Paper No. 49—A-115.

[2] Number in parentheses refer to the Bibliography at the end of the paper.

to use these nails to great advantage, in many instances even in place of wood screws. Since 1939 these improved nails have found preferential acceptance for the construction of wooden pallets and were approved in recent recommendations by The National Wooden Pallet Manufacturers Association and Naval Specifications.

Annularly grooved brass, bronze, and stainless-steel nails have been used in carload quantities for butt-nailing asbestos side-wall shingles since early 1935. Lately the wood- and asphalt-shingle contractors have become convinced promoters of the use of grooved nails. Simultaneously, the building industry has become aware of the advantages of these nails for laying floors, fastening of insulation, nailing of siding and millwork. The extended use of these nails for application of metal roofing and building sheets has long been justified by their performance as convincingly exhibited in a recent treatise (2).

A considerable amount of technical information has been made available on plain-shank, barbed, and cement-coated nails. Before preliminary test and design data on spirally and annularly grooved nails had been published (3), first, cement-coated nails (4) and, later, chemically etched nails (5, 6) had been recommended for superior withdrawal resistance immediately after driving. These recommendations had been made despite the fact that these latter types of nails lose some of their holding capacity with time, and change in moisture content of the wood (5, 6).

For proper application of the improved spirally and annularly grooved nails, the necessity arose to obtain test data from which design data could be secured, in line with the generally established trend from empirical to theoretical design of wood structures. Effectiveness and proper use of nails depend upon the following:

1 The driving resistance offered, as determined by the energy required to hammer the nail into wood.

2 The holding capacity, as observed by the withdrawal resistance of the nail from wood.

3 The lateral load-carrying capacity, as found by the resistance of the nail to lateral forces transmitted through the nail to wood.

4 The nonsplitting properties, as shown by the resistance to splitting of wood during and after driving of the nail.

These properties are influenced significantly by (*a*) such nail-production variables as may be specified for material, design, manufacture, and treatment, and (*b*) such application variables as method of loading, wood species and density, member size and grain direction, moisture content and change in moisture content, time interval between driving and loading, preboring of undersized holes, clinching, and redriving.

This paper cannot present the answer to all nail problems. Its general purpose is to indicate the trends in the field of nailing, to show the special advantages of spirally and annularly grooved nails, and to give proof as to what can be accomplished by research and development work in the field of nailing. Its specific purpose is to determine proper design data for the tested spirally and annularly grooved nails,[3] so they may be used to best advantage in wood structures and important wood assemblies.

The test program included evaluation of type of nail (plain-shank, spirally grooved Screwtite with a 60-deg slope of thread, and annularly grooved Stronghold with 0.060-in. spacing from center to center of grooves), size of nail (length and diameter), type of steel (low-carbon and high-carbon), treatment of nail (nonhardened and hardened), surface coating (noncoated and cement-coated), type of nail point (diamond and V), and use of pilot.

Southern yellow pine, white oak, and beech were selected for test purposes as representative for the softwood, open-porous hardwood, and closed-porous hardwood species, respectively. The test planks consisted of select, partially air-dried (20 per cent moisture content), clear, straight-grain, dressed-four-sides, structrual 3 × 8-in. and 4 × 8-in. shortleaf pine from Virginia, similar green (46 per cent moisture content) white oak from Virginia, and similar green (45 per cent moisture content) beech from Indiana.

Replicate (duplicate quintuplicate) tests on each test variable were performed with different planks. The nails were spaced perpendicularly to the grain $1^1/_4$ in. apart, while nail spacing parallel with the grain was $1^1/_2$ in. In order to facilitate comparative testing with green and dry wood, the testing and matching schedules were prepared in such a way that adjacent locations in the fiber direction of the planks were used for testing with the green and, at a later date, with the dry wood. Nails for tests on withdrawal resistance and lateral load-carrying capacity were driven to $^2/_3$ shank penetration immediately before testing, in order to eliminate any time effect on the test data. Upon completion of these tests, the second series of nails was hammered into the respective adjacent locations for performance of tests upon air-drying of the planks to uniform equilibrium moisture content.

For tests on the driving resistance of nails, a 1000-in-lb-capacity nail driver was employed to drive nails with uniform centric impact force into wood, in order to obtain comparative data on the depth of nail-shank penetration as a result of application of a single impact stroke.

For all tests on withdrawal resistance and lateral load-carrying capacity, an Olsen universal testing machine with 1400 and 12,000-lb-capacity poises was provided with special jigs shown in Figs. 3 and 4.

A universal joint ascertained uniform and centric load application in the direction of the nail axis, provided the nail was driven perpendicular to the plane of the plank. Uniform rate of pulling was attained for all tests on the ultimate withdrawal resistance by the constant motion of the movable crosshead of the testing machine at 0.060 ipm. A test speed of 0.015 ipm was used for the performance of withdrawal tests for which load-deformation data were recorded.

Tests on the lateral load-carrying capacity of nails were performed by loading the projecting part of the nail shank with a free-turning, tight-fitting steel jig placed snugly between nail head and plank. The uniform rate of testing of 0.060 ipm for tests on the ultimate load-carrying capacity was reduced to 0.048 ipm for those tests for which load-deformation data were obtained.

Test Results

Nail Withdrawal Under Axial-Load Application. The relationship between withdrawal resistance in pounds and withdrawal in inches was determined experimentally in a separate test series for $2^1/_2$-in-long, 0.135-in-diam plain-shank, spirally grooved, and annularly grooved nails, as shown in Fig. 5. They penetrated for two thirds of their shank length into 3 × 8-in. southern yellow pine with a 13.9 per cent average moisture content, 0.57 specific gravity, 14 annual rings per inch, and 30 per cent summerwood.

The observed "slopes" for the three types of nails are similar, that is, 25,000, 26,800, and 22,400 lb/in., respectively. Thus the nails have a similar rigidity in withdrawal, hence cause a similar stiffness of nailed joints within the design range.

As soon as the shank friction of the plain-shank nail was exceeded, that is, upon a withdrawal of $^1/_{50}$ in. at a load of 420 lb,

[3] The nails selected for test purposes are general-purpose nails of standard design and conform to standard manufacturing procedure of the producer. Variations from these standards, to satisfy specific requirements, are numerous. Thus the test data obtained in this study may not be directly applied to other nails than those tested, although they are representative spirally and annularly grooved types of nails. Thus the presented data are only directly applicable to the spirally grooved "Screwtite" and annularly grooved "Stronghold" nails manufactured by the Independent Nail & Packing Company, Bridgewater, Mass.

the nail pulled for a small amount. This resulted in a decrease in applied load under the testing procedure employed. By continuing the test, the applied load could again be increased, however, only to a slightly smaller maximum, since the original friction and friction area between shank and wood were decreased by the initial failure. Further test continuation resulted in successive slipping whereby the holding capacity decreased step by step at a constant rate, until the test was discontinued at a withdrawal of approximately $^{3}/_{16}$ in.

The spirally grooved nail showed an "initial ultimate load" at a withdrawal of approximately $^{1}/_{25}$ in., if initial ultimate load is defined as the minimum load at which deformation begins to increase considerably with no appreciable increase in load at the constant rate of withdrawal. When the nail was allowed to turn during continuation of the test, the withdrawal resistance of the nail was increased, since a firmer grip between wood fibers and threaded nail shank was attained. At a withdrawal of $^{11}/_{32}$ in., a 25 per cent increase in load beyond the initial ultimate load of 475 lb was observed. When the nail head was prevented from turning, the low-carbon-steel shank of the nail countertwisted near the surface of the plank, as shown in Fig. 2 (*left*), since during withdrawal the further inserted part of the shank was forced by the wood fibers to thread itself out of the wood. The resistance offered by the wood fibers to withdrawal under this testing procedure resulted in a 33 per cent increase in withdrawal resistance beyond the initial ultimate load of 535 lb.

The annularly grooved nail attained its ultimate withdrawal

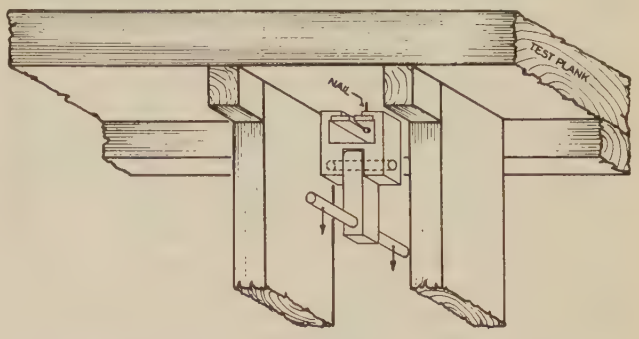

Fig. 3 Diagrammatic Test Setup for Performance of Withdrawal Tests

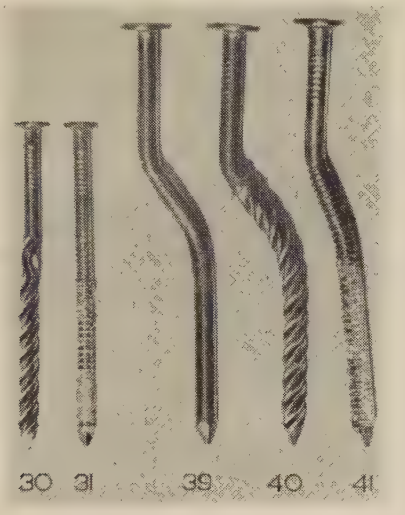

Fig. 2 Deformed Spirally Grooved and Wood-Filled Annularly Grooved Low-Carbon-Steel 3-In-Long Nails After Withdrawal-Test Performance Are Shown at Left—At Right, Plain-Shank, Spirally Grooved, and Annularly Grooved Low-Carbon-Steel 4-In-Long Nails After Performance of Lateral Nail-Shank Loading Tests

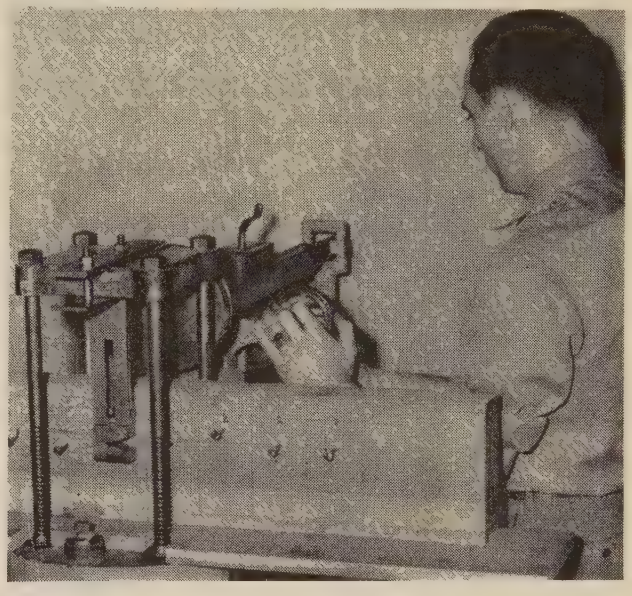

Fig. 4 Test Setup for Performance of Lateral Nail-Shank Loading Tests

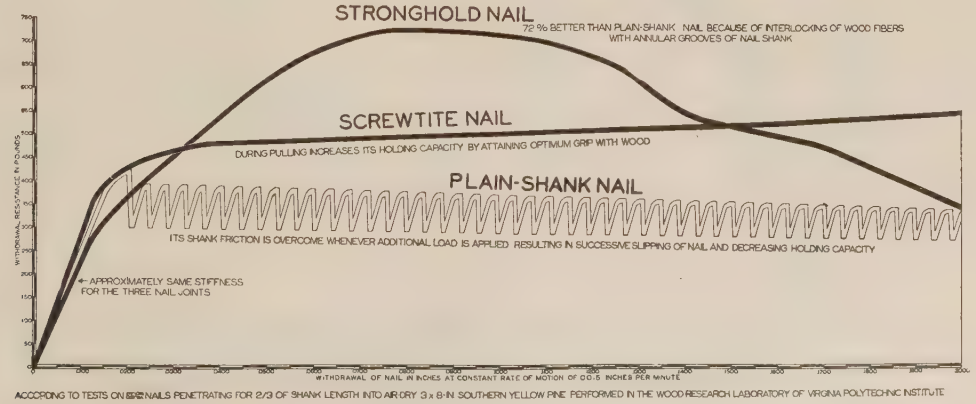

Fig. 5 Load-Withdrawal Diagram for Axially Loaded Low-Carbon-Steel $2^{1}/_{2}$-In-Long Plain-Shank, Spirally Grooved, and Annularly Grooved Nails in Partially Air-Dry Southern Yellow Pine

load of approximately 700 lb at a withdrawal of $^1/_{12}$ in. Beyond this peak load, its withdrawal resistance continuously decreased with increase in withdrawal. At a withdrawal of approximately $^1/_5$ in., the holding capacity of this nail approximated that of the plain-shank nail. Withdrawal of such a magnitude is seldom allowable from the design viewpoint. Therefore the greater withdrawal resistance of the annularly grooved nail, as compared with that of the plain-shank nail, cannot be considered lessened by this decrease in holding capacity (beyond its ultimate) if a loading procedure is used similar to that employed in these tests.

Nail Deformation Under Lateral-Load Application. Data on nail deformation during lateral loading of the nail shank are required for the design of nailed wood structures, if the structural design is limited or influenced by the actual deformation of the structure under load. For this test series, the same test material and $2^1/_2$-in-long, 0.135-in-diam nails were used as for the performance of tests on nail withdrawal. Additional data were obtained for hardened high-carbon-steel nails. The deformation of the nail shank is reported as the motion of a steel loading bar, fitting snugly around the protruding nail shank, relative to a horizontal line on the plank with the nail perpendicular to and intersecting this line. Diagrammatic test data are given in Fig. 6.

The slopes of the load-deformation curves indicate approximately the same stiffness for the three nail types within their design ranges.

The low-carbon-steel plain-shank nail deformed approximately $^1/_3$ in. before reaching an average maximum load of 620 lb. After having attained this peak load, the nail continued to deform. The shank finally sheared off at the loading edge nearest the plank at a total load of 325 lb and at a total deformation of $^7/_{16}$ in. The hardened plain-shank nail was too brittle to resist the shear-stress concentration along the edge of the loading bar. Thus the average ultimate load amounted to only 410 lb.

The low-carbon-steel spirally and annularly grooved nails sheared off at the start of the rolled-on shape at an average maximum test load of 840 lb, and a total deformation similar to that found for the plain-shank nail at its maximum test load. Those hardened spirally grooved nails, which did not shear off along the edge of the loading bar, failed $^1/_2$ in. inside from the plank surface at maximum lateral loads of 820 and 1010 lb, and at a total deformation of $^{13}/_{32}$ in. One of the hardened annularly grooved nails similarly failed at 980 lb and at a similar amount of deformation. Thus on the basis of the limited number of tests performed, spirally and annularly grooved nails appear to have similar rigidity within their complete lateral loading range.

Ultimate Test Data. In Table 1 the driving resistance of nails is given as the ultimate penetration of the nail shank into the plank, corrected for nonuniformity, within a species, in properties of the planks used for testing.

Test data on the ultimate withdrawal resistance for spirally grooved nails are not comparable to those for plain-shank and annularly grooved nails, since the ultimate for spirally grooved nails does not occur within the same range as do the ultimates for plain-shank and annularly grooved nails. On the other hand, the "initial ultimate loads" for spirally grooved and the ultimate loads for plain-shank and annularly grooved nails are attained within a relatively similar range of withdrawal and thus may be considered of a comparable nature. In consideration of this observation, the comparative data given in Table 1 on withdrawal resistance of spirally grooved nails refer to their initial ultimate loads.

The ultimate test data, as observed during lateral loading, were limited by rupture of the nail shanks in 45 per cent of all test cases, that is, in 63 per cent for hardened and in 27 per cent for nonhardened nails. The remaining test nails failed in withdrawal or excessive flexural deformation during lateral-load application.

Both ultimate-withdrawal and lateral-loading data were also

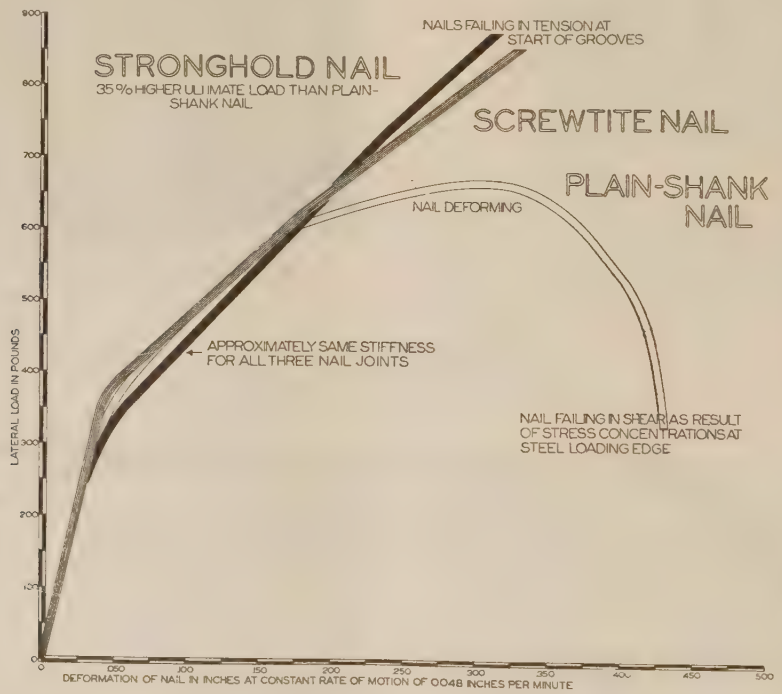

FIG. 6 LOAD-DEFORMATION DIAGRAM FOR LATERALLY LOADED LOW-CARBON-STEEL $2^1/_2$-IN-LONG PLAIN-SHANK, SPIRALLY GROOVED, AND ANNULARLY GROOVED NAILS IN PARTIALLY AIR-DRY SOUTHERN YELLOW PINE

TABLE 1 GRAND AVERAGES FOR MATCHED DECUPLE TESTS ON DRIVING RESISTANCE, WITHDRAWAL RESISTANCE, AND LATERAL LOAD-CARRYING CAPACITY FOR PLAIN-SHANK, SPIRALLY GROOVED, AND ANNULARLY GROOVED NAILS IN GREEN WHITE OAK, GREEN BEECH, AND PARTIALLY AIR-DRY SOUTHERN YELLOW PINE

Nail Size Length x Wire Dia. (In Inches)	Nail Type	Wood Species	Driving Resistance Shank Penetration (In Inches)			Withdrawal Resistance For 2/3 Shank Penetration (In Pounds)			Lat. Load-Carrying Cap. For 2/3 Shank Penetration (In Pounds)		
			Plain	Spirally Grooved	Annularly Grooved	Plain	Spirally Grooved	Annularly Grooved	Plain	Spirally Grooved	Annularly Grooved
2" x 0.120"	HC-NH-NC-D	Oak	1.04	——	——	313	——	——	604	——	——
		Beech	0.88	——	——	314	——	——	355	——	——
		SYP	1.08	——	——	205	——	——	406	——	——
	HC-H-NC-D	Oak	1.10	0.92	0.95	394	542	520	544	694	465
		Beech	0.87	0.70	0.75	419	494	416	370	342	347
		SYP	1.18	1.02	1.06	335	500	525	494	571	426
	HC-NH-NC-V	Oak	0.95	——	——	289	——	——	587	——	——
		SYP	1.06	——	——	140	——	——	383	——	——
	HC-H-NC-V	Oak	——	0.86	0.93	——	540	511	——	688	271
		SYP	——	0.91	1.05	——	455	478	——	612	280
2½" x 0.120"	HC-NH-NC-D	Oak	1.01	——	——	375	——	——	625	——	——
		Beech	0.84	——	——	468	——	——	511	——	——
		SYP	1.16	——	——	198	——	——	393	——	——
	HC-H-NC-D	Oak	1.06	0.88	0.96	471	658	662	398	497	518
		Beech	0.83	0.68	0.75	520	719	688	445	464	497
		SYP	1.18	1.01	1.09	380	600	619	356	563	415
	HC-NH-NC-V	Oak	0.91	——	——	374	——	——	612	——	——
		SYP	1.01	——	——	181	——	——	357	——	——
	HC-H-CC-D	Oak	——	0.91	0.90	——	652	662	——	708	391
		Beech	——	0.73	0.71	——	711	680	——	561	328
		SYP	——	1.13	1.09	——	630	576	——	756	403
	HC-H-NC-V	Oak	——	0.87	0.90	——	657	——	——	922	213
		SYP	——	0.92	1.01	——	533	——	——	551	207
	HC-H-NC-D-P	Oak	——	0.89	0.93	——	623	668	——	591	502
		Beech	——	0.69	0.72	——	674	644	——	567	294
		SYP	——	0.99	1.00	——	535	607	——	745	275
2½" x 0.135"	LC-NH-NC-D	Oak	0.93	0.73	0.72	401	645	732	700	799	597
		Beech	0.77	0.62	0.60	462	627	704	355	483	638
		SYP	1.08	0.86	0.82	264	331	644	500	751	620
	LC-NH-CC-D	Oak	0.93	——	——	515	——	——	732	——	——
		Beech	0.76	——	——	492	——	——	421	——	——
		SYP	1.12	——	——	438	——	——	638	——	——
3" x 0.135"	HC-NH-NC-D	Oak	0.85	——	——	408	——	——	773	——	——
		Beech	0.49	——	——	502	——	——	577	——	——
		SYP	1.06	——	——	243	——	——	467	——	——
	HC-H-NC-D	Oak	0.89	0.73	0.75	629	829	785	1178	1373	748
		Beech	0.53	0.35	0.40	702	841	851	685	681	742
		SYP	1.08	0.91	0.97	588	784	796	976	1252	782
3" x 0.148"	LC-NH-NC-D	Oak	0.75	0.63	0.60	541	688	866	906	1071	1080
		Beech	0.69	0.54	0.54	623	737	868	676	820	769
		SYP	0.90	0.75	0.75	366	362	825	567	830	1059
3½" x 0.162"	LC-NH-NC-D	Oak	0.68	0.56	0.56	663	929	1072	1081	1178	1235
		Beech	0.61	0.47	0.47	795	946	959	630	881	925
		SYP	0.80	0.67	0.64	429	609	1015	678	994	1198
4" x 0.177"	HC-NH-NC-D	Oak	0.62	——	——	834	——	——	1741	——	——
		Beech	0.50	——	——	1061	——	——	1224	——	——
		SYP	0.70	——	——	491	——	——	914	——	——
	HC-H-NC-D	Oak	0.64	0.50	0.55	1100	1444	1397	2106	2559	1345
		Beech	0.49	0.40	0.45	1232	1291	1273	1715	1522	1513
		SYP	0.74	0.53	0.61	792	1112	1100	1624	1939	1353
4" x 0.203"	LC-NH-NC-D	Oak	0.54	0.47	0.46	815	1093	1487	1743	1989	2031
		Beech	0.44	0.38	0.34	1093	1159	1256	1215	1595	1690
		SYP	0.64	0.54	0.53	403	664	1170	949	1545	1550

LC = low-carbon steel
HC = high-carbon steel
NH = nonhardened
H = hardened
NC = noncoated
CC = cement-coated
D = diamond point
V = V-point
P = pilot

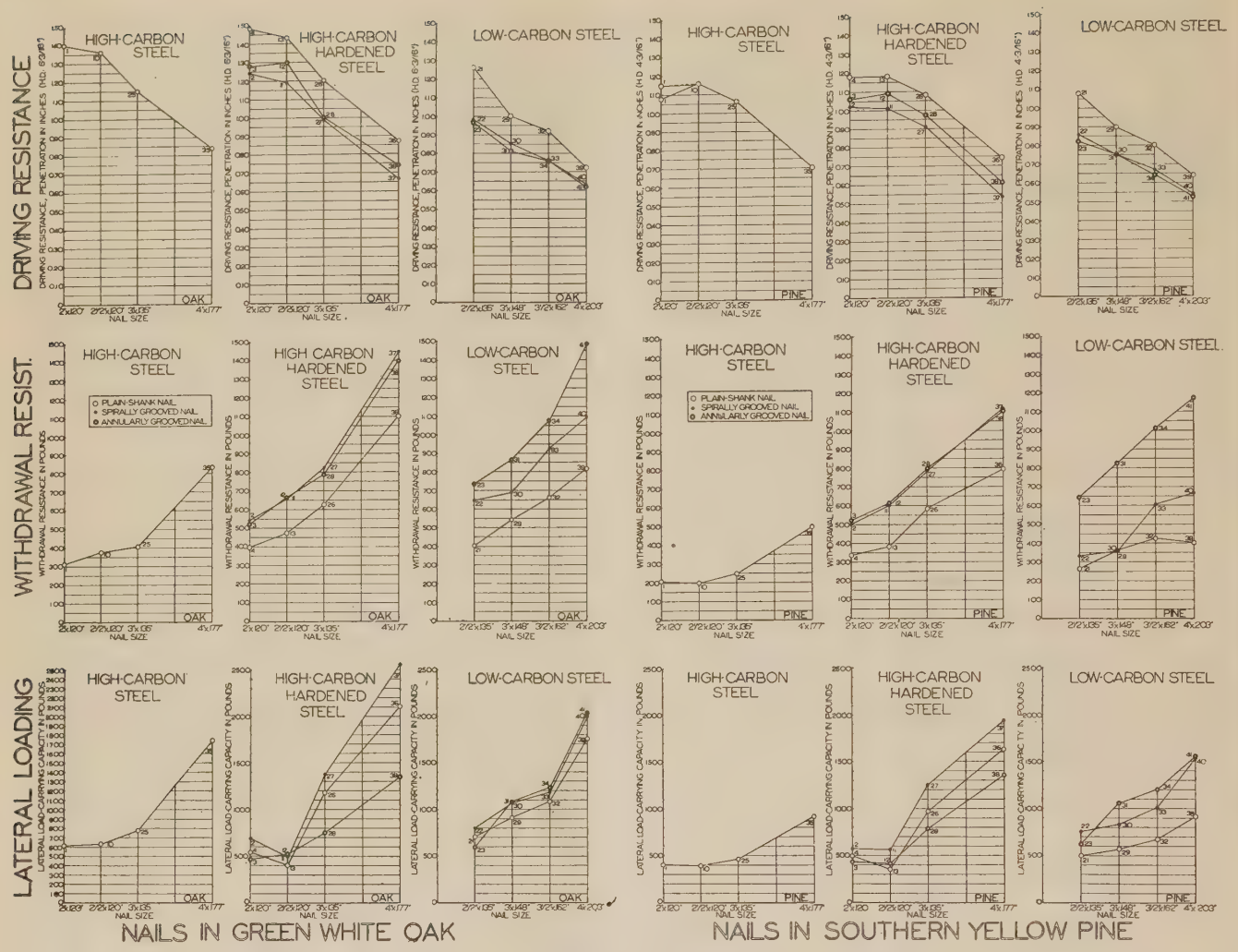

FIG. 7 INFLUENCE OF TYPE OF NAIL ON DRIVING RESISTANCE, WITHDRAWAL RESISTANCE, AND LATERAL LOAD-CARRYING CAPACITY OF 2, 2½, 3, 3½, AND 4-IN-LONG PLAIN-SHANK, SPIRALLY GROOVED, AND ANNULARLY GROOVED NAILS IN GREEN WHITE OAK, GREEN BEECH, AND PARTIALLY AIR-DRY SOUTHERN YELLOW PINE

corrected for nonuniformity in plank properties, if different planks within a species showed variations in their nail-withdrawal resistance and lateral load-carrying capacity.

INFLUENCE OF DESIGN VARIABLES

Nail Type. Comparative tests on driving resistance, withdrawal resistance, and lateral load-carrying capacity were performed with low-carbon-steel and hardened high-carbon-steel plain-shank, spirally grooved, and annularly grooved nails. The test results are given in Table 1 and graphically presented in Fig. 7. Because of their increased contact areas and frictional resistance between nail shank and surrounding wood, the grooved nails provided a larger withdrawal resistance and lateral load-carrying capacity than the plain-shank nails. These increases, however, were combined with an increase in driving resistance, although the latter increase proved to be somewhat smaller than those for withdrawal resistance and lateral load-carrying capacity.

The average driving resistance of the low-carbon-steel and hardened high-carbon-steel spirally grooved nails in green oak was 19 and 18 per cent, that in green beech was 20 and 21 per cent, and that in partially air-dry southern yellow pine was 19 and 16 per cent greater, respectively, than that of the plain-shank nails. The average driving resistance of the corresponding annularly grooved nails in oak was 20 and 13 per cent, that in beech was 22 and 13 per cent, and that in southern yellow pine was 21 and 11 per cent greater, respectively. Thus the average driving resistance of spirally and annularly grooved nails tested was between $^1/_5$ and $^1/_6$ greater than that of the plain-shank nails.

The average withdrawal resistance of the low-carbon steel and hardened high-carbon steel spirally grooved nails in oak was 39 and 34 per cent, that in beech was 17 and 16 per cent, and that in southern yellow pine was 34 and 43 per cent greater, respectively, than that of the plain-shank nails. The average withdrawal resistance of the respective annularly grooved nails in oak was 72 and 30 per cent, that in beech was 27 and 12 per cent, and that in southern yellow pine was 50 and 45 per cent greater.

The average lateral load-carrying capacity of low-carbon-steel spirally and annularly grooved nails in oak was 14 and 12 per cent, that in beech was 31 and 40 per cent, and that in southern yellow pine was 52 and 64 per cent greater, respectively, than that of the plain-shank nails; that of the hardened high-carbon-steel spirally grooved nails in oak was 21 per cent, in beech was 3 per cent, and in pine was 25 per cent greater. By use of more satisfactory heat-treating procedures, considerable improvement might have been attained in the lateral load-carrying capacity of

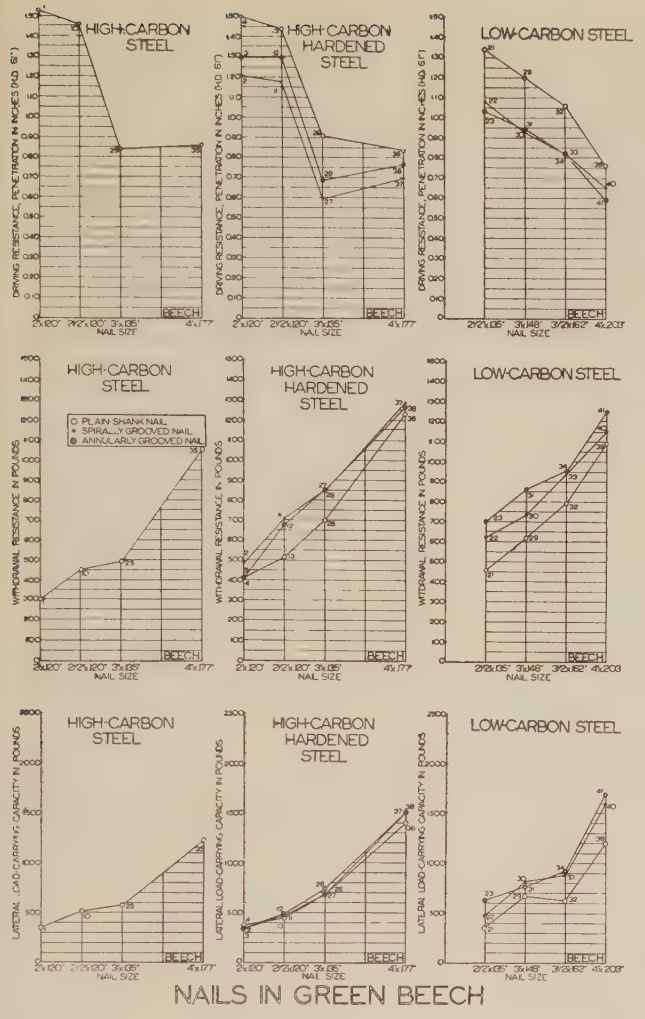

FIG. 7 (*Continued*)

these hardened high-carbon-steel nails. To this end, improved equipment has been installed by the nail manufacturer.

Nail Size. According to authoritative data (6), the withdrawal resistance per inch of penetration of plain-shank nails varies directly with the nail diameter. One of the exceptions is the withdrawal resistance, e.g., of 3½ and 4-in-long plain-shank nails in southern yellow pine, which is 5 and 10 per cent smaller, respectively, than if computed according to the foregoing correlation. Furthermore, according to this reference, the lateral load-carrying capacity of plain-shank nails varies with the 1.5th power of the nail diameter.

Comparative tests on driving resistance, withdrawal resistance, and lateral load-carrying capacity were performed with 2½, 3, 3½, and 4-in-long low-carbon-steel plain-shank, spirally grooved, and annularly grooved nails, and with 2, 2½, 3, and 4-in-long nonhardened high-carbon-steel plain-shank nails, and hardened high-carbon-steel plain-shank, spirally grooved, and annularly grooved nails. The test data are graphically presented in Figs. 8 and 9, in comparison with those advanced in reference (6) for low-carbon-steel common wire nails. This comparison is limited in value, since common wire nails are made of a wire with a slightly different diameter from the tested nails.

With increase in shank diameter, that is, the wire gage from which the nail was made, average driving resistance of both spirally and annularly grooved nails increased at a similar rate. This increase, however, was slightly larger than that of the plain-shank nail driven into southern yellow pine and, especially, into oak. On the basis of the relatively uniform test data, it may be justified to assume a curvilinear relationship between shank diameter and depth of penetration for plain-shank nails, and a similar curvilinear relationship for grooved nails.

The increase in withdrawal resistance per inch of penetration with increase in shank diameter of low-carbon-steel plain-shank and grooved nails was somewhat smaller than expected, according to reference (6) for low-carbon-steel plain-shank nails. Although some of the data are somewhat erratic, a general trend of curvilinear relationship may be expected, particularly if grand-average data for increase in withdrawal resistance of —2, 7, and 19 per cent for nails in oak, of 4, 8, and 22 per cent for nails in beech, and of 5, 18, and 13 per cent for nails in southern yellow pine are compared with increases in shank diameters of 10, 20, and 50 per cent.

The average withdrawal resistance per inch of penetration of the high-carbon-steel 3-in-long nails was only slightly larger, and that of the 4-in-long nails in oak 39 per cent, in beech 48 per cent, and in southern yellow pine 18 per cent larger than that of the 2 and 2½-in-long nails. The withdrawal resistance of some of the 3-in-long and, in particular, that of almost all 4-in-long nails should have been larger, according to the correlation suggested in reference (6), for low-carbon-steel plain-shank nails. The excessive brittleness of some of the test nails may have been of some influence on these data.

While the increase in lateral load-carrying capacity of low-carbon-steel plain-shank and spirally grooved nails in southern yellow pine, with increase in diameter, was similar to that expected, according to the general formula advanced in reference (6), the increase in capacity of these nails in oak and beech and of spirally grooved nails in oak, beech, and southern yellow pine was considerably larger. Thus with an increase in diameter of 10, 20, and 50 per cent for 3, 3½, and 4-in-long nails, on the basis of comparison with the 2½-in-long nail, the respective ratios of average increases in capacity for plain-shank and spirally grooved nails in southern yellow pine were 12 : 34 : 98, in beech were 80 : 80 : 236, and in oak were 32 : 50 : 149; those for annularly grooved nails in southern yellow pine were 71 : 87 : 150, in beech were 21 : 45 : 165, and in oak were 81 : 107 : 240.

The increase in lateral load-carrying capacity with increase in diameter of most of the high-carbon-steel nails tested was also considerably larger than that expected, according to the general formula presented in reference (6) for low-carbon-steel plain-shank nails. The erratic nature of some of the test data is explained by the considerable variation in brittleness of these nails.

The relatively small increase in efficiency with increase in shank diameter of some of the grooved nails, in comparison with that of the plain-shank nails, such as in withdrawal resistance in green beech, may be explained by the uniformity in spacing of spiral and annular grooves for all nail sizes. Smaller center-to-center spacing of the grooves of the large-size nails might have increased their efficiency, although to date, no data have been obtained to substantiate such an assumption.

Nail Point. Nails tapered to and terminating in a flat point do not split wood as much as nails with a sharp or diamond point. The withdrawal resistance of nails with a tapered and flat point is equal in dense wood, though, smaller in less dense wood than that of the corresponding nail with a sharp point. Splitting of wood by a nail may also be prevented by use of a shank point with a short wedge having a blunt end, such as the V-point. Although the angle of the wedge-point axis to the wood-fiber direction may be of influence on the efficiency of this nail, all V-point nails were driven without consideration being given to the direction of the wedge axis.

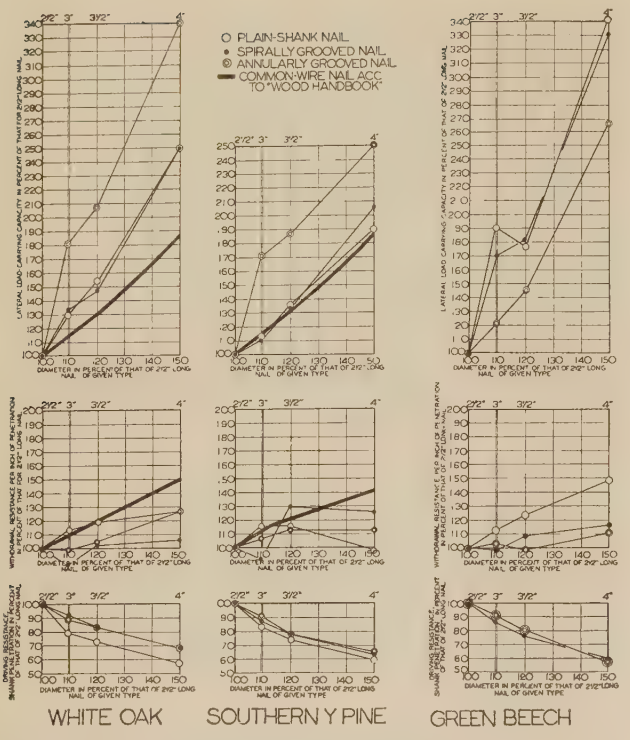

FIG. 8 EFFICIENCY DIAGRAM, WITH RESPECT TO WIRE DIAMETER OF NAIL SHANK, FOR PLAIN-SHANK, SPIRALLY GROOVED, AND ANNULARLY GROOVED LOW-CARBON-STEEL NAILS IN GREEN WHITE OAK, GREEN BEECH, AND PARTIALLY AIR-DRY SOUTHERN YELLOW PINE ACCORDING TO GRAND AVERAGES FOR DECUPLE TESTS

Comparative tests were performed with 2 and $2^1/_2$-in-long diamond-point and V-point, high-carbon-steel nonhardened plain-shank and hardened spirally and annularly grooved nails, manufactured from the same wire strand, and driven into green white oak and partially air-dry southern yellow pine. The V-point, in comparison with the diamond point, resulted in a 9, 8, and 4 per cent greater average driving resistance and a 10, 5, and 5 per cent smaller average withdrawal resistance for the nonhardened plain-shank, hardened spirally grooved, and hardened annularly grooved nails, respectively. The lateral load-carrying capacity of the nonhardened plain-shank nail with V-point was 4 per cent smaller than that of the diamond-point nail. The lateral load-carrying capacity of the hardened grooved nails with V and diamond points was influenced too much by variations in nail brittleness to yield satisfactory comparative data.

With few exceptions, the effect of the V-point was consistent for all tests on the driving resistance, withdrawal resistance, and lateral load-carrying capacity. However, the influence of the V-point, in comparison with that of the diamond point, on the foregoing properties was relatively small, thus insignificant from the practical viewpoint.

Shank Pilot. For ease in initial driving of nails with grooved shanks, a pilot may be used, that is, for a short length from the nail point, the nail shank is plain and grooving starts only beyond that length. The length of the pilot may vary. For tests on the $2^1/_2$-in-long hardened high-carbon-steel grooved nails with a pilot, a pilot length of $^3/_{16}$ in. was used.

According to the comparative data for spirally and annularly grooved nails, the pilot resulted in a 2.5 per cent greater average driving resistance and a 5 per cent smaller average withdrawal resistance. In view of the considerable variation in brittleness of the test nails, fully comparative data could not be obtained on the lateral load-carrying capacity of nails with and without pilots.

Thus it appears that as a short pilot was used for these comparative tests, it did not have any appreciable influence on both driving and withdrawal resistance of $2^1/_2$-in-long, hardened high-carbon-steel spirally and annularly grooved nails.

Steel Composition. Both "regular" low-carbon steel, SAE 1010, and high-carbon steel, SAE 1065, were used for the manufacture of the tested nails. Comparative data were obtained on the driving resistance, withdrawal resistance, and lateral load-carrying capacity of $2^1/_2$, 3, and 4-in-long plain-shank nails made from both steels, with the high-carbon-steel nails having 11.2, 8.8, and 12.8 per cent smaller diameters, respectively.

The average driving resistance of high-carbon-steel nails was 7 to 18 per cent, with a grand average of 12 per cent, smaller than that of the low-carbon-steel nails. An exception was the 3-in-long high-carbon-steel nail in beech with a 30 per cent larger driving resistance. The average withdrawal resistance of the high-carbon-steel nails was from 34 per cent smaller to 22 per cent larger, with a grand average of 10 per cent smaller, than that of the low-carbon-steel nails. Similarly, the lateral load-carrying capacity of the high-carbon-steel nails was from 25 per cent smaller to 44 per cent larger, with a grand average of 7 per cent, smaller than that of the low-carbon-steel nails.

Thus, because of the smaller diameters of the high-carbon-steel nails, as compared to the diameters of the low-carbon-steel nails of the same types and lengths, the high-carbon-steel nails were somewhat easier to drive and had a smaller withdrawal resistance and lateral load-carrying capacity than the respective low-carbon-steel nails.

Heat-Treatment. High-carbon-steel nails may be hardened to increase their buckling resistance during driving, their withdrawal resistance and lateral load-carrying capacity during use. Thus some of the high-carbon-steel nails were heat-treated at 1500 to 1600 F for 28 min, quenched in an oil bath, and tempered at 550 F for an additional 28 min. The nails thus treated varied considerably in brittleness although made from the same wire strand and issuing from the same nail batch, with some of the nails failing as a result of their brittleness and others failing only in exceeding their withdrawal resistance.

Comparative data were secured on the driving resistance, withdrawal resistance, and lateral load-carrying capacity of 2, $2^1/_2$, 3, and 4-in-long high-carbon-steel, nonhardened and hardened plain-shank nails.

The average driving resistance of the hardened nails was from 2 per cent larger to 9 per cent smaller, with a grand average of 3 per cent smaller than that of the nonhardened nails. The average withdrawal resistance of the hardened nails was 11 to 142 per cent, with a grand average of 50 per cent larger than that of the nonhardened nails. The lateral load-carrying capacity of the hardened nails was from 36 per cent smaller to 109 per cent larger, with a grand average of 21 per cent larger than that of the nonhardened nails. While the driving resistance of hardened nails was almost consistently, however, from the practical viewpoint, insignificantly smaller, the withdrawal resistance of the hardened nails was consistently larger than that of the nonhardened nails. The considerable variation in brittleness is the explanation for the relatively large variation in data on both the withdrawal resistance and lateral load-carrying capacity of hardened nails. However, since as a result of heat-treatment both withdrawal resistance and lateral load-carrying capacity of some of the nails were increased more than 100 per cent, it should be possible to increase consistently to a considerable degree both withdrawal resistance and lateral load-carrying capacity by use of fully satisfactory hardening methods with equipment only lately installed by the nail manufacturer.

Cement Coating. According to information given in reference

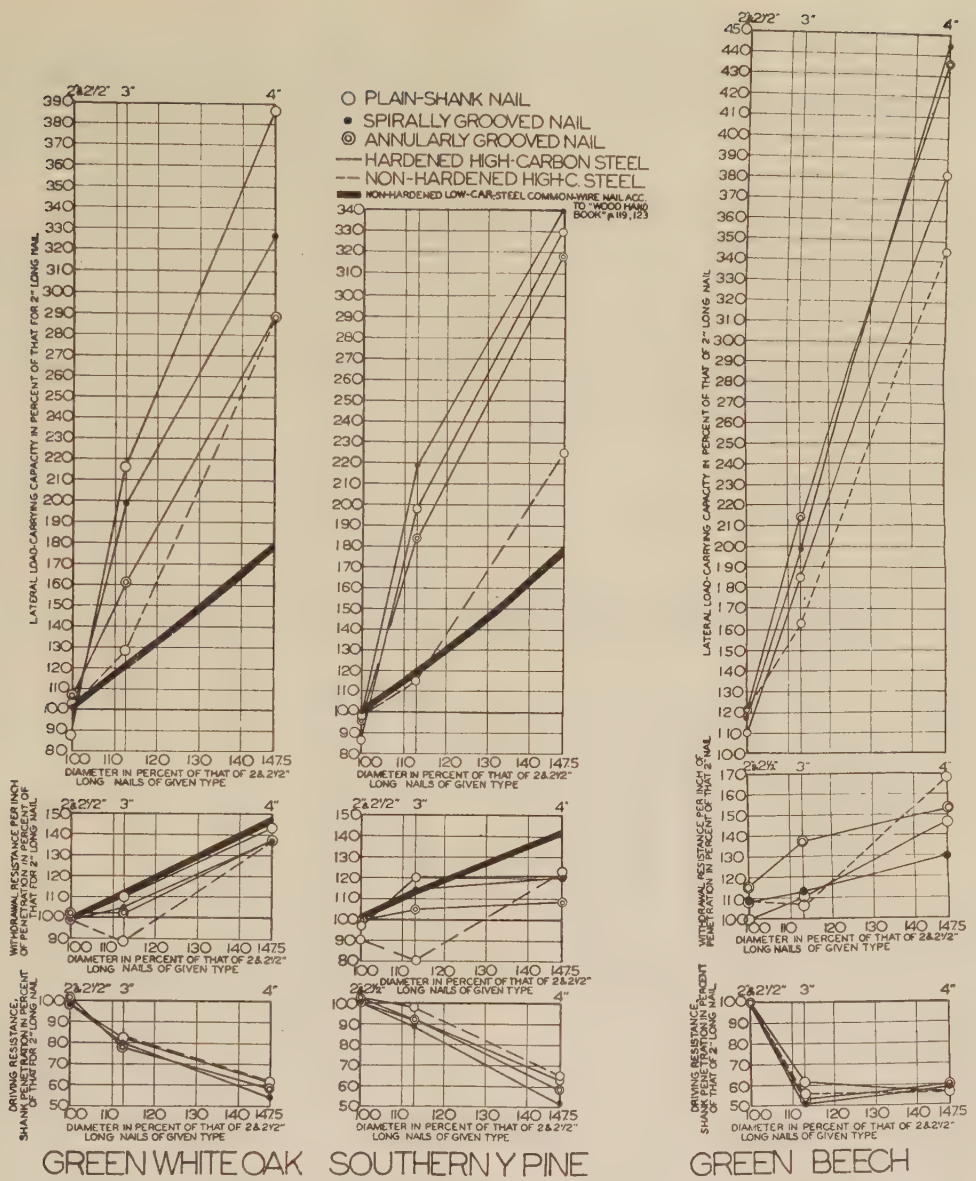

Fig. 9 Efficiency Diagram, With Respect to Wire Diameter of Nail Shank, for Plain-Shank, Spirally Grooved, and Annularly Grooved High-Carbon-Steel Nails in Green White Oak, Green Beech, and Partially Air-Dry Southern Yellow Pine According to Grand Averages for Decuple Tests

(6) the withdrawal resistance of plain-shank nails immediately after driving into light wood may be 85 to 100 per cent larger if the nails are properly cement-coated, while, with increase in wood density, the benefit of cement coating decreases to practically no advantage over noncoating.

Comparative tests were performed on the driving resistance, withdrawal resistance, and lateral load-carrying capacity of $2^1/_2$-in-long low-carbon-steel plain-shank nails and hardened high-carbon-steel spirally and annularly grooved nails. The cement-coating compound[4] used consisted of synthetic resin treated with linseed oil. It contained 65 per cent, by weight, petroleum naphtha as volatile carrier. It was applied in a tumbling process at normal temperature and uniformly covered the whole nail.

The average driving resistance of the noncoated and coated nails did not vary to any large extent. Cement coating increased the average withdrawal resistance of the plain-shank nail in oak 28 per cent, in beech 6 per cent, and in southern yellow pine 65 per cent. On the other hand, cement-coating of hardened high-carbon-steel spirally and annularly grooved nails was of no effect on their withdrawal resistance. The lateral load-carrying capacity of the coated plain-shank nail in oak was 5 per cent, in beech was 19 per cent, and in southern yellow pine was 28 per cent greater as a result of application of cement coating. The variation in brittleness of the hardened spirally and annularly grooved nails did not make it possible to obtain reliable data on the influence of cement coating on the lateral load-carrying capacity of these nails, although the coated spirally grooved nail showed consistently larger values than the noncoated nail. However, since the withdrawal resistance of these nails was not increased as a result of cement-coating, this increase in lateral load-carrying capacity may not be fully attributable to the coating.

[4] No. V-5071 Elastic Nail Coating by the M. B. Suydam Division of Pittsburgh Plate Glass Company.

The foregoing data on the withdrawal resistance of plain-shank nails are in general agreement with the information advanced in reference (6) for plain-shank nails. These data also indicate that cement-coating of spirally and annularly grooved nails may not be justified for purposes of improving their withdrawal resistance.

Summary

1 With relatively small increases in driving resistance of nails, large increases can be expected in both withdrawal resistance and lateral load-carrying capacity.

2 Spirally and annularly grooved nails offer larger withdrawal resistance and lateral load-carrying capacity than plain-shank nails. Annularly grooved low-carbon-steel nails offer a larger withdrawal resistance than spirally grooved low-carbon-steel nails, while the withdrawal resistance of spirally and annularly grooved hardened high-carbon-steel nails is approximately the same.

3 Typical data on the effectiveness of spirally and annularly grooved nail shanks in comparison with plain nail shanks are presented in Table 2.

TABLE 2 COMPARISON OF PER CENT EFFECTIVENESS OF LOW-CARBON-STEEL, DIAMOND-POINT, 2½-IN-LONG, 0.135-IN-DIAM PLAIN-SHANK, CEMENT-COATED PLAIN-SHANK, SPIRALLY GROOVED, AND ANNULARLY GROOVED NAILS ON BASIS OF COMPARISON WITH RESPECTIVE NON-COATED PLAIN-SHANK NAIL

Wood species	Property	Plain-shank nail		Spirally grooved nail	Annularly grooved nail
		Non-coated	Cement-coated		
In green white oak	Driving resistance	100	100	122	123
	Withdrawal resistance	100	128	161	183
	Lateral load-carrying capacity	100	105	114	85
In green beech	Driving resistance	100	101	119	123
	Withdrawal resistance	100	106	136	152
	Lateral load-carrying capacity	100	119	136	180
In partially air-dry southern pine	Driving resistance	100	96	120	124
	Withdrawal resistance	100	166	125	244
	Lateral load-carrying capacity	100	128	150	124

4 Both under withdrawal and lateral load, plain-shank and spirally or annularly grooved nails have similar rigidity within their design ranges; thus cause similar stiffness of nailed joints.

5 Under constant rate of withdrawal, plain-shank nails retain, within given limits, a slowly decreasing holding capacity somewhat below the ultimate holding capacity; spirally grooved nails continue to increase their holding capacity, although at a decreased rate of increase, after the "initial ultimate withdrawal resistance" has been reached; annularly grooved nails reach a considerably greater ultimate withdrawal resistance at a larger withdrawal than plain-shank and spirally grooved nails, while this withdrawal resistance decreases at a similar rate to that of increase up to the ultimate.

6 Under lateral load, the ultimate lateral load-carrying capacity of plain-shank and spirally or annularly grooved nails is reached at approximately the same amount of deformation.

7 Curvilinear relationships may be assumed between nail-shank diameter and both driving resistance and withdrawal resistance for plain-shank nails. Similar curvilinear relationships seem to exist for spirally and annularly grooved nails. The general correlation between nail-shank diameter and lateral load-carrying capacity, as presented in reference (6), seems to be somewhat conservative for plain-shank and spirally grooved nails in green white oak, green beech, and partially air-dry southern yellow pine.

8 The V-point, in comparison with the diamond point, has little effect on the driving resistance, withdrawal resistance, and lateral load-carrying capacity of plain-shank and spirally or annularly grooved nails.

9 A short pilot for grooved nails does not have any appreciable influence on either driving or withdrawal resistance.

10 High-carbon-steel nails, having smaller shank diameters than low-carbon-steel nails of the same lengths, are, type for type, somewhat easier to drive and have correspondingly smaller withdrawal resistance and lateral load-carrying capacity than low-carbon-steel nails with their larger diameters.

11 Although the driving resistance of hardened nails is similar to that of nonhardened nails, the withdrawal resistance and lateral load-carrying capacity of hardened nails can be considerably larger.

12 Cement coating results in considerably increased withdrawal resistance of plain-shank nails immediately after driving into the low-density southern yellow pine and an almost negligible increase in withdrawal resistance for high-density beech. However, cement coating does not increase withdrawal resistance or lateral load-carrying capacity of spirally or annularly grooved nails.

13 Because of the considerable difference in moisture content, the average driving resistance, withdrawal resistance, and lateral load-carrying capacity of nails in green white oak and beech on the one hand, and partially air-dry southern yellow pine on the other hand, did not differ greatly and as much as would be expected if the nails were tested in these species with like moisture content (7).

14 Driving resistance and withdrawal resistance increase with increase in wood density according to somewhat similar trends (7).

15 As a result of variation in physical structure of the plank, driving resistance, withdrawal resistance, and lateral load-carrying capacity may vary within the same plank cross section, even if the lumber is free of growth irregularities (7).

Acknowledgment

This study was performed in the VPI Wood Research Laboratory under the auspices of the VPI Research Foundation, Inc., and under the sponsorship of the Independent Nail & Packing Company of Bridgewater, Mass., manufacturer of the spirally grooved Screwtite and the annularly grooved Stronghold nails.

BIBLIOGRAPHY

1 "Technique of House Nailing," by U. S. Forest Products Laboratory in Cooperation with U. S. Housing & Home Finance Agency, U. S. Printing Office, November, 1947.

2 "The Effectiveness of Roofing Nails for Application of Metal Building Sheets," by H. Giese and S. M. Henderson, Iowa State College Agricultural Engineering Station Research Bulletin No. 355, November 1947.

3 "Influence of Depth of Penetration on Withdrawal Resistance of Nails," by E. G. Stern and A. E. Price, presented at the Annual Wood Industries Division Meeting of The American Society of Mechanical Engineers at High Point, N. C., October, 1948 (mimeographed); published in *The Journal of Southeastern Research*, vol. 1, April, 1949, pp. 14–16; also, *The Wooden Box & Crate*, vol. 11, May, 1949, pp. 21–25, and July, 1949, pp. 21–25.

4 "Fibre Box Memo 11," by Fibre Box Association, 1948.

5 "New Nail-Treating Process Increases Holding Power," by J. H. Gahagan and E. Beglinger, U. S. Forest Products Laboratory Report No. R970, July, 1932; also, *Barrel & Box & Packages*, vol. 37, no. 9, September, 1932.

6 "Wood Handbook," by U. S. Forest Products Laboratory, U. S. Government Printing Office, 1935.

7 "Driving Resistance, Withdrawal Resistance, and Lateral Load-Carrying Capacity of Nails," by E. George Stern and A. E. Price, VPI Wood Research Laboratory Release, February, 1949; Revised, June, 1949 (typewritten).

Discussion

T. D. Perry.[5] The nail is one of the most common items used in all kinds of woodworking, one of our largest industries. It is surprising that so little has been investigated, technically, with regard to the gripping power of nails having different shapes of shanks.

Excellent as this paper is, there are two points which need clarification in this as well as in the author's earlier paper on the subject.

Simplify the conclusions, by emphasizing major factors at the expense of less important ones, or break the results down into sections, so that the number of variables in each bracket is much reduced. Reading technical papers is no novelty to me, but I have to confess considerable confusion, even after a careful reading of this paper. Reading rapidly or scanning would not improve the casual reader's conclusions. The facts are there but they do not stand out clearly against the background of lengthy testing procedure.

Supplement the strength data by analyzing the economic factors. If 8 lb of grooved shank nails are needed to carry the same load as 10 lb of common plain shank nails, what is the relative cost of the two lots? In other words, and in the last analysis, the dominating reason for adopting such nails would be either more strength at the same cost, or equal strength at less cost.

H. J. Stone[6] states that with respect to the use of grooved nails in the field of building construction, the most important point is that ordinary nails are not nearly strong enough to equal the structural strength of the materials they fasten. To put this in another way, the frame used in the average home is, according to our tests, up to 5 times as strong as its fastenings. However, if properly grooved nails are used, their holding power can exceed the strength of the lumber they fasten, with the result that the frame of a house assembled with properly grooved nails will be fractured before the nails have yielded. It seems obvious that, since a house is ultimately not stronger than the fastenings which were used in its assembly, these fastenings should be as strong, if not stronger, than the lumber used in the construction of the house.

While it may be argued that most houses are never subjected to extraordinary stresses, there are in almost all sections of the country periods of high winds, extremes of temperatures, and other conditions which cause severe stresses on the house structure. These stresses often result in cracks, warpage, and distortions with resulting sticking of windows, door frames, and other comparatively minor distortions, which may result in repair bills, any one of which may exceed the additional cost of properly grooved nails.

The advantages of grooved nailing also apply to roofing, woodfinishing, door and window frames, and other elements which often deteriorate and cause trouble. An asphalt-shingle roof fastened with properly grooved roofing nails will never leak due to nail popping. Here again, a single roof leak may be more costly than the entire differential in cost between annularly grooved nails and ordinary roofing nails.

In the case of the grooved flooring nails, as compared with conventional nails, we have experiences with spirally grooved nails going back 15 or 16 years. We have no record of failure during that period of time. On the other hand, floors nailed with either conventional cut nails or common wire brads will in time squeak, buckle, and ultimately require renailing and refinishing.

Many of the cracks in walls and ceilings can be traced to failure of fastenings in the frame of a house and consequent settling of frames or distortion of walls. These conditions may be avoided with use of properly grooved nails which are proved in tests to exceed the strength of common nails as much as 1200 per cent.

If the contractor or home owner desires to offset the slight additional cost of properly grooved nails, this may be done by sheathing the house with one of several types of synthetic sheathing materials. While such materials are not as effective as boarding when common nails are used, they may safely be used if the house structure is assembled and the sheathing itself applied with the respective grooved nails. The use of these grooved nails also allows the use of lower grades of lumber without reducing the ultimate strength of the building itself.

Author's Closure

With respect to Mr. Perry's comments, it may be stated that this paper is to serve a twofold purpose. It is (*a*) to make available to the average engineer general information on the advantages of using improved nails; and (*b*) to present detailed data to the nail user concerned with a large number of variables of little interest to the average engineer. The information which may be too detailed for the former, may contain too little data for the latter. Thus a relatively large amount of information had to be crowded into a given space. For those wishing to obtain additional information, parts or complete copies of reference (7)[7] can be made available.

Since presentation of this paper, a considerable amount of additional information on improved nails and their effects has been obtained. To those interested in this information, a supplement to the Bibliography appears at the end of this closure.

Reference (10) contains a partial summary of fully comparative information on delayed nail-holding properties, as referred to in the paper and scheduled for later presentation. Thus it shows the effect of change in moisture content and elapsed time after nail driving on the test variables under discussion.

With respect to the economic aspects created by the mass-production of grooved nails, Mr. Perry overlooked the aspect of considerably increased service at somewhat increased cost. In this case, this aspect can be combined with better service at the same cost or equal service at less cost, since the better service rendered by the individual grooved nail makes it possible to reduce, under given conditions, the number of nails hitherto required.

One of the cases in which considerably better service can be obtained at even decreased cost for grooved nails, is that of the spirally grooved Screwtite flooring nails. In this particular case, 50 lb of grooved nails replace 100 lb of cut nails, with an increase in nail-holding power of 40 per cent, combined with a simultaneous saving of 28 per cent of the cost of the cut nail.

For a more complete analysis of the economic aspects of use of grooved nails, a cost analysis (Table 3) is presented which was advanced for a 50-ft × 24-ft $10,000 five-room house with attached garage.

Thus, at a cost of $10,000 for this house, the cost of all nails amounts to $65.70 or 0.657 per cent if of the plain-shank type, and to $106.25 or 1.0625 per cent if of the grooved type.[8] In other

[5] Engineer in Wood Work, Moorestown, N. J. Fellow ASME.

[6] General Manager, Independent Nail & Packing Company, Bridgewater, Mass.

[7] Reference is to Bibliography at the end of the paper.

[8] Reference (*a*) Table 3 of this closure.

TABLE 3 COST ANALYSIS OF NAILS FOR TYPICAL $10,000 HOUSE

Nail type	Nail size	Required amount lb	Quoted cost[a] Plain-shank nails	Quoted cost[a] Annularly grooved Stronghold nails
Framing	20d	110	$ 7.98	$13.85
	16d	75	5.44	9.44
	10d	60	4.44	7.58
	8d	130	9.75	16.51
	6d	5	0.40	0.66
Casing	10d	10	0.89	1.33
	6d	5	0.48	0.69
Finishing	10d	10	0.89	1.33
	8d	15	1.35	2.02
	6d	5	0.48	0.69
	4d	2	0.20	0.33
Flooring	8d	30	3.90[b]	2.81[c]
Siding	7d	35	4.81	5.86
Shingle	3d	65	10.40	16.71
Asphalt roofing	1 × 11	60	8.10	14.04
Lath	1⅛ × 13	45	6.19	12.40

[a] Based on retail quotations for products of the Independent Nail & Packing Company, Bridgewater, Mass.
[b] High-carbon-steel cut flooring nails.
[c] 15 lb of spirally grooved Screwtite flooring nails.

words, for an increase of $40.55 or less than ½ per cent of the total cost of the house, all the following advantages can be obtained, according to data presented in the paper and in references (8, 9, 10, 11). It is not a necessity, of course, to replace all plain-shank nails with grooved nails. To date, replacement for individual applications has been more or less the case. On the other hand, with the increased amount of knowledge as to the beneficial effect of use of grooved nails, total replacement of nails must be given consideration under certain conditions. The advantages follow:

1 For the increased expenditure of $20.03 or 0.2 per cent of the total cost of the house given as an example, the unsheathed framing can offer a 4 to 6 times greater lateral-thrust resistance, with the frame joints possibly even stronger than the framing lumber (9).

2 For a saving of $1.09, as a result of the use of 15 lb of spirally grooved Screwtite flooring nails instead of the twice as heavy cut flooring nails, the flooring and stair treads can be more easily and quickly laid; under normal conditions do not come loose, squeaky or springy, cup or buckle; split tongues can be averted; whereby 220 and 40 per cent, respectively, greater withdrawal resistances are obtained if comparison is made with the same-size plain-shank flooring brads and cut flooring nails (11).

3 For an increased expenditure of $1.05, all the siding may be fastened in such a way that the nails will not "creep" or "pop"; thus the siding remains firmly fastened to the structure.

4 For an increased expenditure of $6.31, assurance may be had that none of the wood or asbestos shingles will come loose since the use of grooved nails results in a 250 per cent greater holding power than attained by use of corresponding plain-shank nails.

5 For an increased expenditure of $5.94 for fastening asphalt-roofing shingles, assurance may be had that the nails will retain the shingles continuously tightly fastened as a result of the 50 per cent greater axial withdrawal resistance of the grooved nails in comparison with the plain-shank nails.

6 For an increased expenditure of $6.21, the plaster lath may be fastened permanently and firmly to the framework because of the 40 per cent increased holding power of the annularly grooved nails. Thus the possibility of formation of any cracks in plaster is considerably decreased.

7 For an increased expenditure of $2.10 for casing and finishing nails, the woodwork should never come loose. Thus a satisfactory fastening of all interior woodwork even after aging of the structure can be assured.

The cost increases cited result from the use of an equivalent number of properly grooved nails to replace plain-shank nails. In many cases, a smaller number of grooved nails may be used without detrimental effect. Thus the small increases in expenditure may even be decreased.

All the improvements in the structure immediately after erection and during its life, and the decreased cost of maintenance and repair, resulting exclusively from the use of grooved nails, can be attained for a cost amounting to less than ½ per cent of the total cost. This small difference in initial cost may be considered "an insurance premium of the entire value of the house for its lifetime, which will guarantee that the house will not deteriorate within its expected lifetime."

Although tables indicating the efficiency of grooved nails in comparison with plain-shank nails, as based on holding capacity per dollar value, could be presented according to the data made available in this and other papers (10, 11), it is believed that the foregoing cost analysis for nails in home construction answers the question raised by Mr. Perry as to the economic aspects of the use of grooved nails.

SUPPLEMENT TO BIBLIOGRAPHY

8 "Comparative Tests on Old and New Grooved Nails," by E. George Stern, *The Wooden Box and Crate*, vol. 11, December, 1949, pp. 21–25.

9 "Grooved Nails Strengthen House Frames," by E. George Stern, *Engineering News-Record*, vol. 144, April 6, 1950, pp. 32–34.

10 "Deterioration of Green Wood Along Steel Nail Shank and Its Influence on the Nail-Holding Properties," by E. George Stern, *Virginia Journal of Science*, vol. 1, July, 1950.

11 "Nails in End-Grain Lumber," VPI Wood Research Laboratory Release, October, 1949.

"Improved Nails for Building Construction," VPI Wood Research Laboratory Release, February, 1950. (Accepted for publication as Bulletin of the Virginia Polytechnic Institute, Engineering Experiment Station.)

Head and Flow Observations on a High-Efficiency Free Centrifugal-Pump Impeller

By W. C. OSBORNE[1] and D. A. MORELLI,[2] PASADENA, CALIF.

A series of studies of the flow through the various components of hydrodynamic machinery is in progress in the Hydraulic Machinery Laboratory of the California Institute of Technology. Observations have been made on an impeller patterned after the Grand Coulee design. The impeller was operated as an isolated unit hydraulically free of the casing. The flow pattern at the discharge has been determined quantitatively for one flow rate, and a head-capacity curve for the impeller has been obtained. This paper constitutes a report on the findings up to the present.

Introduction

In the past most of the experimental work carried on in the field of rotating machinery has dealt with the machine as a whole, and because of the technical difficulties involved, comparatively little has been done to determine the performance characteristics of the individual elements which make up the whole. As a rough classification, such a machine can be thought of as consisting of three parts, namely, (*a*) the stationary inlet member, (*b*) the rotating member, and (*c*) the stationary outlet member.

Some empirical work has been carried out in which various rotating members have been tested with the same stationary members and vice versa, but the test results obtained in these cases have been referred to the performance of the combination as a complete machine, and the effect of changes in the individual member has been inferred only through the effect of such changes on the over-all performance. Several laboratories, particularly those of Spannhake, Thoma, and Pfleiderer, in Germany (1–9),[3] have undertaken experimental investigations of the detailed characteristics of the flow in the rotating passages, and a few workers have explored the flow during its transition from the rotating member to the case. In practically all instances, however, the experimental machine has been greatly simplified, usually to the point of making the runner two-dimensional. The gain from such simplification has been twofold, namely, the experimental difficulties have been lessened appreciably, and the possibility of parallel analytical studies has been improved. Unfortunately, the losses accompanying the simplification have included large decreases in efficiency, lowered resistance to cavitation, and a general lack of similarity to the performance characteristics of modern hydraulic machines.

Much effort has been devoted to the development of a satisfactory analytical treatment of the flow in hydraulic machines. Considerable progress has been made in the analysis of the axial-flow machine based upon airfoil theories, especially in the zone of efficient operation. However, for abnormal operating conditions even in the axial-flow machines, and for all conditions in the machines having appreciable components of radial flow, the presently known analytical methods leave much to be desired. If the performance of the individual elements of machines having good characteristics and high efficiencies could be obtained experimentally, and especially if the details of the flow could be determined, as well as the over-all characteristics of the elements, it would greatly enlarge the possibilities of developing a satisfactory analytical treatment and at the same time improve design possibilities through the use of more detailed empirical information.

In an effort to meet this need, a project has been initiated at the Hydrodynamics Laboratory of the California Institute of Technology under the sponsorship of the Office of Naval Research for the primary purpose of making detailed studies, both experimental and analytical, of flow through various components of well-designed modern hydraulic machines. Since the existing facilities of the Hydraulic Machinery Laboratory (10) were not readily adaptable to the type of experimental work anticipated, a smaller more suitable laboratory was constructed.

Laboratory Facilities

The project is located on the mezzanine floor of the Hydraulic Machinery Laboratory. The equipment is arranged to provide a flow of water in a closed circuit which is shown schematically in Fig. 1 and which consists essentially of three principal sections. One section functions primarily as a supply reservoir and includes the necessary equipment to deliver and meter a steady flow of water at various pressures and flow rates. It includes the reservoir and service pump, the Venturi meters and the throttle valve. This part of the circuit is independent of whatever test arrangement is made.

The second section functions principally as a distribution circuit and includes an adaptable arrangement of distributing headers, valves, and piping which may be arranged in various combinations to carry the flow from the throttle valve to and from the test elements in the particular manner and direction required by the unit under observation. Fig. 1 shows two of the several flow circuits possible. The major portion of this section is expendable and may be modified as the research requires.

The test stand is the third part of the circuit. Here are provided facilities for mounting, operating, and testing hydraulic-machine elements. The principal parts are the approach piping, the test basin, and the vertical dynamometer. These components are all in duplicate and thus allow two different studies to be run alternately and effect a great saving of time. Fig. 2 shows the test equipment as arranged for the photographic studies herein reported. One of the vertical dynamometers has been removed and replaced by a centerless impeller-drive mechanism to allow a full view of the impeller. Windows have been installed in the test basin to facilitate lighting and provide additional observation points. Fig. 3 presents the parallel test setup on the opposite side of the test stand. With this arrangement over-all

---

[1] Research Engineer, Hydraulic Machinery Laboratory, California Institute of Technology. Jun. ASME.

[2] Senior Research Engineer, Hydraulic Machinery Laboratory, California Institute of Technology. Mem. ASME.

[3] Numbers in parentheses refer to the Bibliography at the end of the paper.

Contributed by the Hydraulic Division and presented at the Annual Meeting, New York, N. Y., November 27–December 2, 1949, of The American Society of Mechanical Engineers.

 Paper No. 49—A-108.

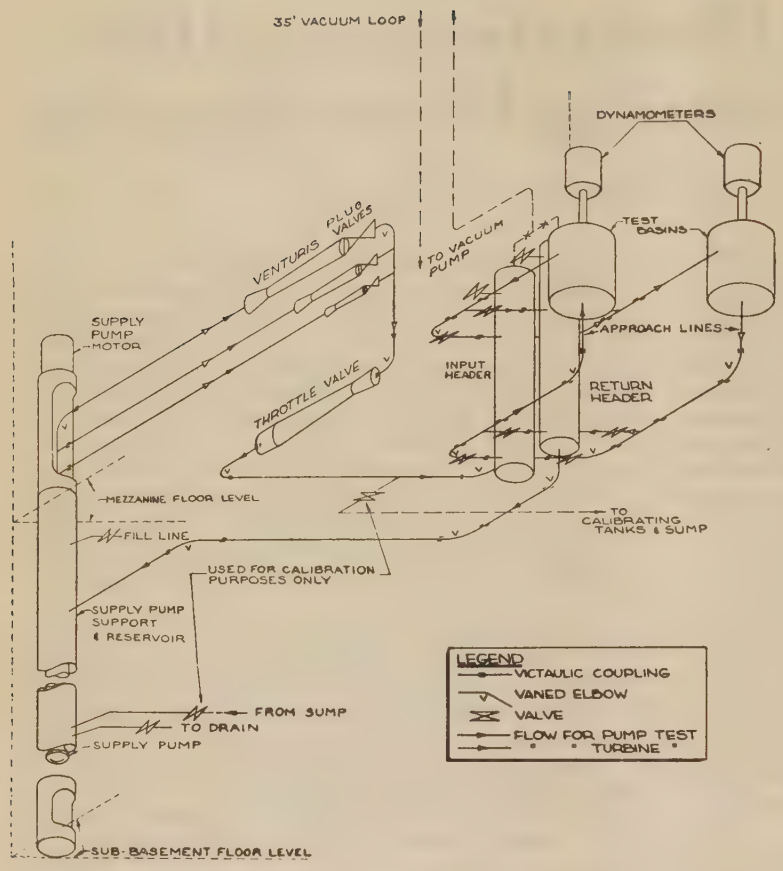

FIG. 1 DIAGRAM OF MAIN AND AUXILIARY FLOW CIRCUITS

head-capacity characteristics of the impeller were determined.

The project is a self-contained unit and can be operated independently of the other equipment in the building. However, to avoid duplication of equipment, the three Venturi meters may be connected to the main calibrating circuit of the Hydraulic Machinery Laboratory (10) and the existing facilities used for calibration. Fig. 2 shows the two points of interconnection.

The apparatus covers the following ranges:

1 Flow rates up to 4 cfs with a head differential of 66 ft at the test unit.

2 Power input or absorption up to 30 hp.

3 Dynamometers capable of rotative speeds of 100–2000 rpm in either direction.

The physical size of the test elements is not rigidly fixed. However, rotating channels up to 12 in. diam and diffuser or volute casings up to 30 in. diam may be accommodated.

Although the conventional opaque metal cast elements can be used in some test work, techniques have been developed at the laboratory for precision manufacture of these elements from transparent materials such as lucite. This not only makes possible the use of the various photographic techniques (12, 13) which have been developed and found to be extremely useful in observing and analyzing flow phenomena in the Hydrodynamics Laboratory (11), but it also offers advantages of controlled dimensions and guarantees symmetry and reproducibility to a degree essential for precise test work, which, ordinarily, are unattainable with standard cast elements.

OBJECT OF TESTS

The impeller of a centrifugal pump was chosen as the first machine element to be examined. The rotating member was selected since it may be considered as the primary element of the pump; the principal interchange of energy between the machine and the fluid takes place in its rotating passages. The initial studies were confined to observations of the flow pattern at the discharge section of the impeller and to determinations of the over-all head-capacity characteristics of the impeller running free of its case. The discharge section of a modern medium-specific-speed impeller lends itself more readily to observation than does the inlet section and hence was selected as a logical starting point for a series of investigations which eventually will cover the entire impeller passage. Likewise, the head-capacity is the beginning of a series of studies designed to cover the complete over-all operating characteristics of the impeller. It is the purpose of this paper to report the findings of these initial studies and to present the tentative conclusions that have been drawn.

THE TEST IMPELLER

The test impeller used was very similar in design to the Grand Coulee pump impeller. This pump is a high-efficiency unit of medium specific speed, $N_s = 100$ (Q in cfs), and its design is representative of modern practice. The entire series of Grand Coulee model pumps was tested in the Hydraulic Machinery Laboratory and thus there is much detailed information available on the over-all performance of the pumping unit (15). Fig. 4 is a scale drawing of the impeller and presents its principal dimensions. The shroud curvature, the discharge and inlet vane angles, and the vane length were modeled to scale directly from the Grand Coulee design. However, the slight curvature or spooning of the vane in the eye was omitted and the vane was terminated along a straight line in the meridional projection. Although this alteration speeded production of the test impeller, it is not a limitation of the manufacturing technique; exact curvature of the prototype can be duplicated in the model if tests indicate the necessity. The discharge-vane tips were left blunt for the present tests.

A FREE IMPELLER

It was required that the flow through the rotating impeller be independent of external effects. The flow was delivered to the impeller eye by a nozzle which matched the eye diameter exactly, and which was designed to give a uniform velocity profile at that section (14). The impeller was mounted directly above the nozzle and was rotated about a vertical axis. When using the centerless impeller mount, Fig. 2, the large journal bearing located between the impeller and the nozzle effects the necessary seal, whereas in the setup for the head-capacity measurements a ring of $\frac{1}{4}$-in-sq packing seated in a groove in the nozzle bears against the impeller and seals the suction side against leakage. It was intended originally that the impeller should be operated with a free atmospheric discharge, Fig. 5; however, as the capacity is reduced, thus lowering the static pressure in the eye, a point of instability is reached; the water breaks away from the top shroud and air flashes back into the impeller. This results in operating with passages partially filled, Fig. 6. Operating the impeller at extremely low speeds will avoid this difficulty, but the magnitude of the head generated and the flow rate are reduced correspondingly, and measurements become exceedingly difficult.

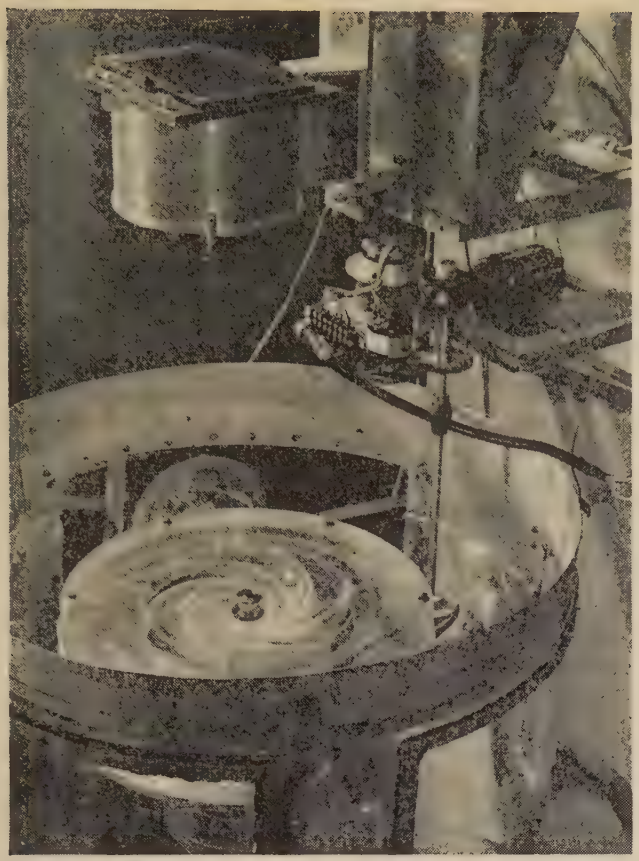

FIG. 2 EQUIPMENT FOR PHOTOGRAPHIC STUDIES OF FLOW

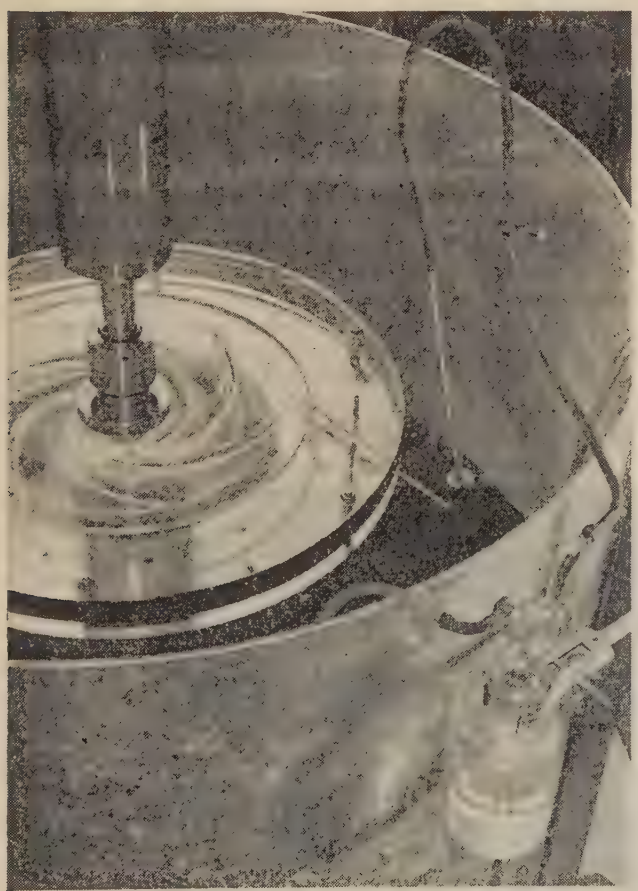

FIG. 3 EQUIPMENT FOR DETERMINING HEAD-CAPACITY CHARACTERISTICS

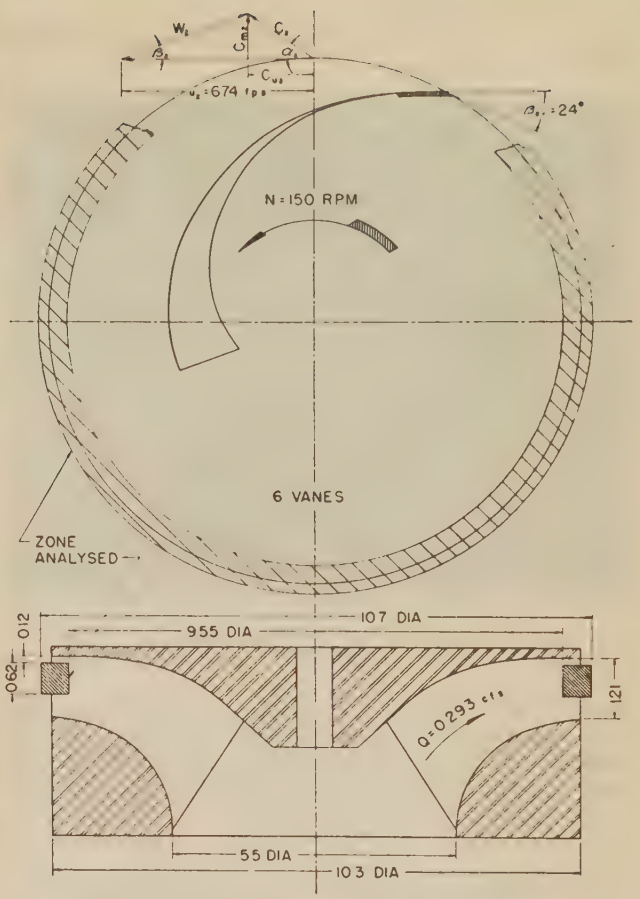

FIG. 4 PRINCIPAL DIMENSIONS OF TEST IMPELLER

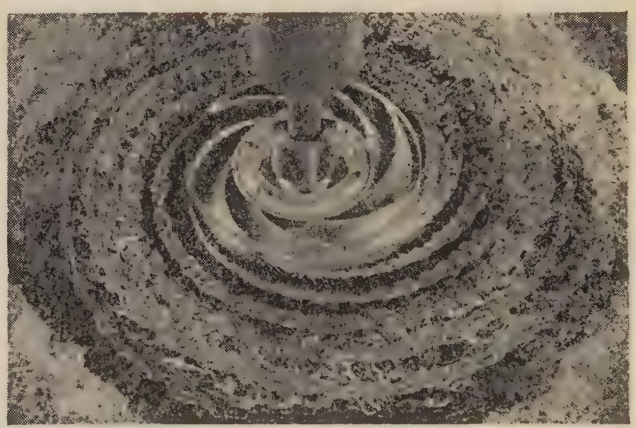

FIG. 5 AN IMPELLER DISCHARGING INTO A FREE BODY OF WATER AT HIGH CAPACITY; FULL PASSAGES

A symmetrical stationary collector about the discharge of the impeller furnished a satisfactory solution to the problem. The collector matches the impeller width at the periphery of the impeller and reduces to a smaller opening at its outer rim. A cylindrical weir is used to vary this opening and thus maintain a sufficiently high pressure in the collector and impeller to prevent flashback. The clearances between the impeller and the collector are close-running. Qualitative and quantitative studies of the flow pattern at the periphery of the impeller in the zone indicated in Fig. 4 were made with the impeller discharging freely, and also into the collector. These showed that the latter had no perceptible effect on the pattern of flow in that zone. With the exception of the flow in the boundary layer at the pe-

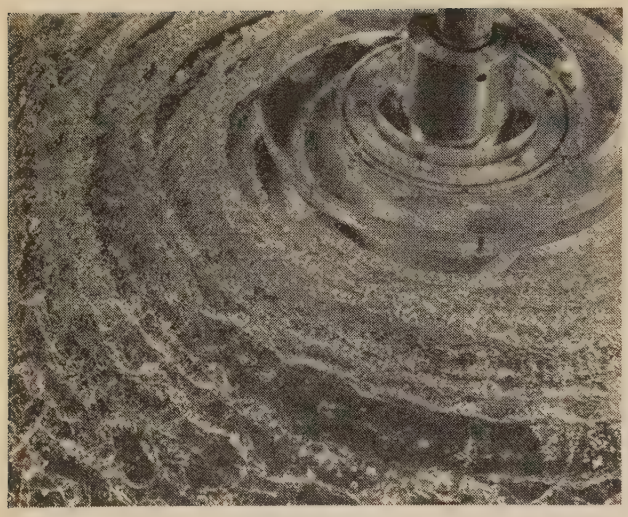

FIG. 6 AN IMPELLER DISCHARGING INTO A FREE BODY OF WATER AT LOW CAPACITY; PARTIALLY FILLED PASSAGES

riphery, it is believed that the flow pattern at the discharge and throughout the entire impeller is unaffected. The test unit so arranged is considered to be hydraulically independent of the test setup and hence is referred to as a "free impeller."

FLOW OBSERVATION

Instrumentation and Procedure. A three-dimensional photographic technique was used in making the quantitative flow studies. Thus the problems of instrument response and obstruction to the flow presented by mechanical methods were eliminated. However, photographic techniques required that the test passages be transparent and that suitable photographically identifiable particles be present in the stream. A mixture of dibutyl phthalate and kerosene proportioned to give a specific gravity equal to that of the water,[4] colored white and observed against a black background, was found to be satisfactory. This mixture is immiscible with water and, when injected into the flow, forms small globules which retain their identity and, when illuminated properly, are photographically discernible. Unlike the more common carbon tetrachloride-benzene solution, the mixture is not injurious to lucite. The tracers were released from a series of small capillary tubes arranged in the throat of the suction nozzle. Neglecting the minor surface-tension effect, the small tracers formed, $^1/_{32}$ to $^1/_{16}$ in. diam, may be considered to follow the same flow paths as the water itself.

The tracer paths were recorded with a stereoscopic camera. The stereoscopic technique was necessary to establish the axial position or third dimension of the tracers in the passages. In Fig. 2 is shown the camera located above the periphery of the test impeller. A series of exposures were made on each plate with a controlled burst of flashes of a high-speed multiflash lamp. When the flash rate was matched properly with the impeller speed, the familiar golf-ball-type pictures resulted, Fig. 7. In this manner a number of positions of a tracer were recorded. To determine the tracer velocity, the stereophotographic images were projected back into space through the same lens system, that is, the camera was used as the projector and the space positions of the tracers at each interval of time were located. In this manner the angular, radial, and axial position of the center of each tracer group, the inclination of the group to the tangent, and the displacement of the tracers within the group were obtained. Knowing the time interval, the average velocity of each group was calculated. The shaded peripheral zone in Fig. 4 indicates the region covered by the analysis. The centers of all tracer groups fell within this zone.

The test impeller was operated at 150 rpm and a capacity of 0.293 cfs. At this capacity it was possible to operate the impeller both with and without the collector and hence make the comparative studies mentioned previously. The unit capacity for this operating point is 0.165, Fig. 11. Referred to the Grand Coulee prototype performance, this represents approximately a capacity 40 per cent above the maximum efficiency point and approximately coincides with the upper operating limit of that installation.

Discussion of Results. Figs. 8 and 9 present the results of the tracer studies. The plotted points were all obtained from tracer groups selected at random, the only requirement being that they be within the zone under observation.

The wide scatter of the data is most interesting. At first it might be thought to be experimental error. However, a variation of ±50 per cent cannot be attributed to experimental errors which did not exceed ±2 per cent. The second explanation that might be proposed is that the scatter was caused in part by the inclusion of data at various impeller radii and depths within the zone. No correlation between these factors has been observed and hence this contention is not supported by experimental evidence. The scatter could be attributed to any asymmetry existing in the flow through the impeller. However, tracer data were recorded in one specific channel and also in channels at random,

[4] Equality was satisfactory when globules remained suspended in a sample of the water.

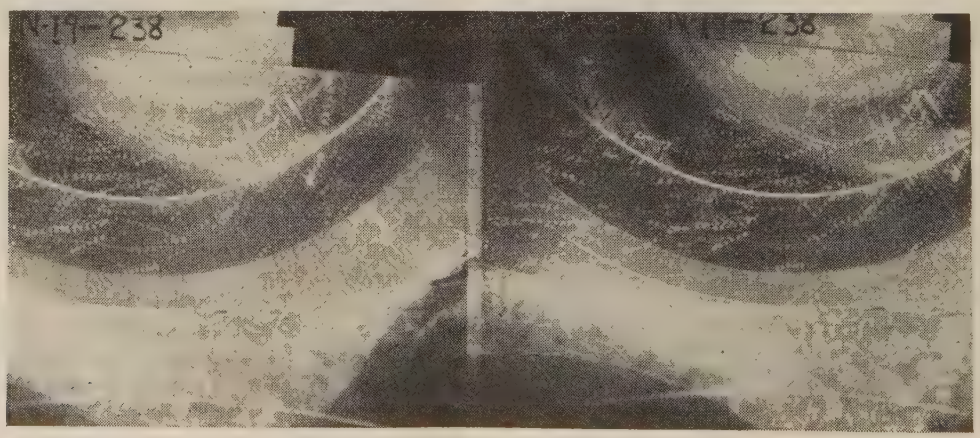

FIG. 7 STEREOSCOPIC PHOTOGRAPH OF TRACERS IN IMPELLER PASSAGES

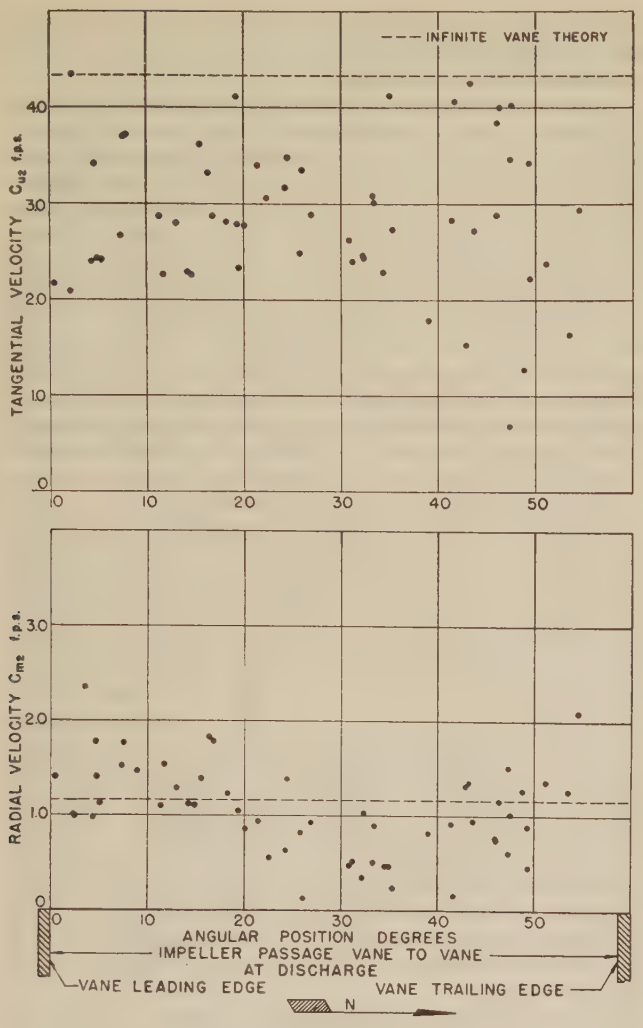

FIG. 8 RADIAL C_{m2} AND TANGENTIAL C_{u2} COMPONENTS OF ABSOLUTE VELOCITY AT DISCHARGE

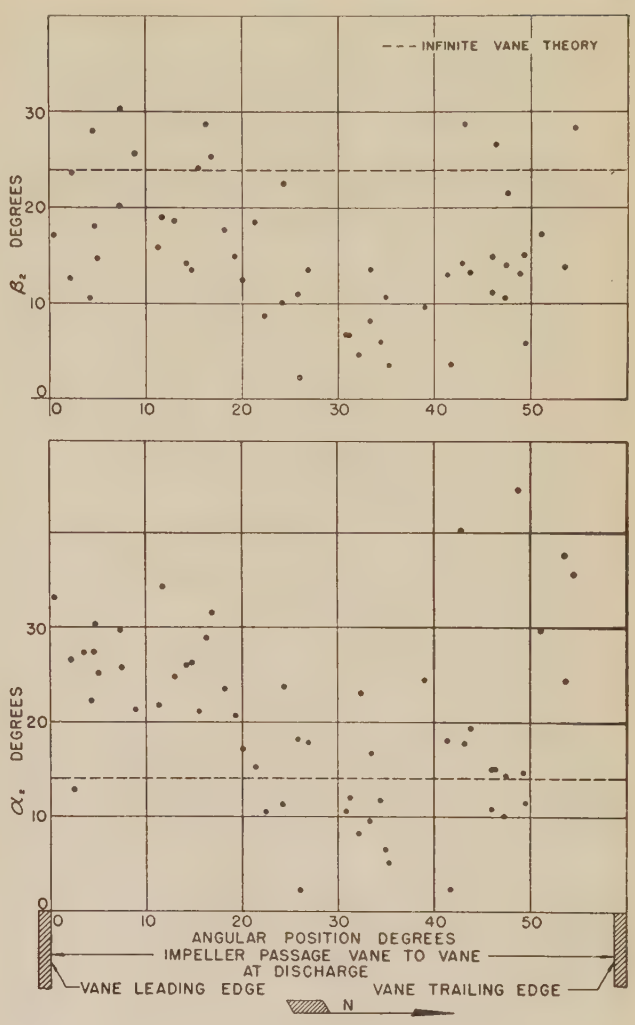

FIG. 9 RELATIVE AND ABSOLUTE ANGLES β_2 AND α_2 AT DISCHARGE

and no asymmetry could be detected. It is possible that large-scale turbulence, present in the incoming flow, might be the source of this dispersion of data. Dye-streak studies have been made in the impeller approach over a wide range of capacities. Large-scale turbulence was not observed until the dye streaks came into close proximity with the impeller passages. It is concluded that the point scatter is due to large-scale turbulence which develops within the impeller passages.

It is interesting to note the increase in the scatter in the region near the trailing edge of the vane which strongly suggests an unstable flow condition. However, although an instability has been noticed in other photographic studies recently completed, a large rolling eddy has not been observed. The scarcity of points close to the trailing edge of the vane is a limitation imposed by the photographic method employed. When a series of exposures are made on one plate, the vane images obscure that area. Stereoscopic high-speed motion pictures overcome this difficulty.

The pronounced dips at mid-passage of the radial velocity C_{m2}, the relative discharge angle β_2, and the absolute discharge angle α_2 are the most striking features of the data. The decrease in β_2 is to be expected from theory. Likewise, theoretical considerations show that C_{m2}, β_2, and α_2 must each be of equal magnitude at opposite sides of the vane passage, and this point is verified. However, the C_{m2} profile is not yet substantiated by theory. Although a three-dimensional analytical solution of the problem is not available, the analysis of a two-dimensional straight radial-vane impeller indicates that, for that special case C_{m2} varies almost sinusoidally about a uniform average through-flow, being least near the leading edge of the vane and greatest near the trailing edge. The present data do not show this trend to exist in a modern three-dimensional impeller. The α_2 variation must necessarily follow the trend indicated, once C_{m2} and β_2 are established.

The obvious dip present in the other plots is noticeably absent in the C_{u2} data. The points suggest that the time-average specific energy about the periphery of an impeller is constant.

The horizontal dotted lines represent values of C_{m2}, C_{u2}, β_2, and α_2 based upon the Euler infinite-vane theory, namely, the relative discharge flow angle β_2 equals the vane angle β_{2v} and is everywhere constant, and C_{m2} is constant about the periphery. It is interesting to note that the position of this line with respect to the averages of the test data is in agreement with theoretical deductions. The Euler line must represent the average radial velocity, whereas it should lie above the mean β_2 and C_{u2} and below the mean α_2.

The instantaneous absolute streamlines pictured in Fig. 10 were sketched from a large number of data prints. The streamlines are spaced at random and hence represent flow direction

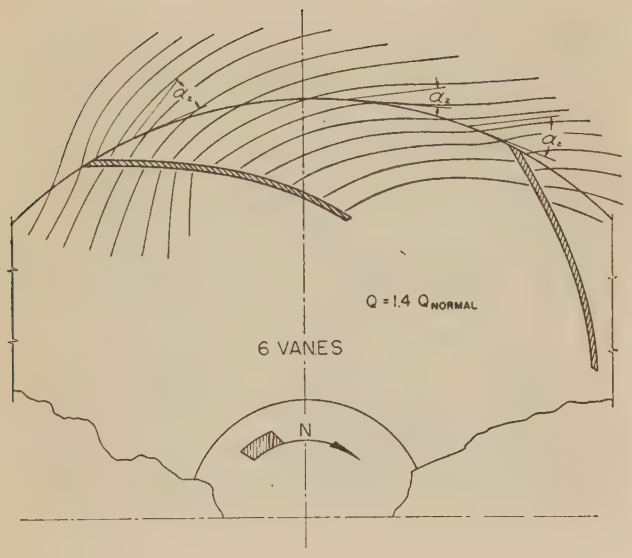

FIG. 10 INSTANTANEOUS ABSOLUTE STREAMLINES AT DISCHARGE; RANDOM SPACING

only. It is interesting to note that in the region following the vane there is no evidence of backflow.

DETERMINATION OF HEAD-CAPACITY CHARACTERISTICS

Instrumentation. The inevitable losses involved in the use of a measuring point at any distance from the impeller made it desirable to use total head tubes close to the inlet and outlet to determine the energy of the inflow and outflow from the test impeller. Although there is some doubt as to the correct reference pressure at the inlet, considerations of symmetry indicate that the total head at some point on the center line of the suction nozzle seemed to be a desirable location at which to measure the total head of the incoming flow. A total-head tube directed upstream was located at the inlet to the pump impeller at a point $^7/_8$ in. below the plane of the intersections of the vane leading edges with the suction shroud. The total-head tube at the outlet was mounted on a rotatable mount and was retractible through a sleeve set at right angles to the axis of rotation. By these means the inlet to the total-head tube could be set at any predetermined distance from the impeller, and its axis could be aligned with the approaching flow. The direction of the flow at the nose of the total-head tube was determined by a probe carrying a fine thread.

Since it has not been possible to obtain a pressure gage with an accuracy and frequency response sufficient to follow in detail the variations in total head, a damped water-column manometer connected directly to the metal total-head tube was used. The air side of the manometer was connected to the air space of a waterpot. The water side of the waterpot was supplied by the total-head tube at the inlet to the impeller; thus the differential head across the runner could be read directly. By adjusting the height of the water level in the pot a large range in head could be covered without great variations in the height of the water level in the manometer tube, Fig. 3.

The question always arises in applications where the measured total head fluctuates, as to the meaning of the reading obtained by the manometer. Experiments were made to determine the influence of the damping imposed on the measuring head, and it was found that a large degree of damping gave steadier readings which were fully consistent with the mean readings obtained with less damping. Since the total-head tube measures a fluctuating energy level directly, and since speed and flow control were of such quality that the fluctuations could be considered a steady-state condition, a viscously damped system should read the true average total head.

Variation of Total Head Across Outlet. Since the flow through a radial-flow pump involves essentially a change of direction from axial to radial, it was of interest to determine the variation in total head between the lowermost streamline that emerges at the suction or lower shroud and the uppermost streamline that emerges at the back or upper shroud. This is particularly interesting in view of the velocity field observed photographically and discussed previously. A location was chosen for the total-head tube $^1/_{16}$ in. distant from the periphery of the impeller. At this location the total-head tube was aligned with the mean streamline and traversed vertically across the width of the impeller. At the chosen flow rates it was found that the energy of the lowermost streamline was approximately 5 per cent greater than the energy of the uppermost streamline. On the basis of these observations a location was chosen halfway between the two shrouds at the outlet for the subsequent work reported here.

Influence of Prerotation on Accuracy of Observations. Experimental work on complete pumps has shown that the flow conditions in the inlet pipe are in many cases highly complex. This requires that justification be provided for measuring the inlet total head with the total-head tube close to the impeller at the center line of the suction nozzle. This was done in the following manner:

The outlet total-head tube was set at $^1/_{16}$ in. from the periphery of the impeller at mid-width, and the total head change between the inlet and the outlet was recorded for a large range of flow rates. A typical run is shown in Fig. 11 which is a dimensionless head-capacity characteristic for the test impeller. Since it is reasonable to suppose that the inlet effects, if any, must decrease in intensity as one recedes further from the disturbing influence, other runs were made using the piezometer taps located after the inlet straightening vanes which are some distance upstream from the impeller inlet and guarantee a smooth velocity profile in the approach pipe.

The results of these measurements are plotted in Fig. 11, including the necessary corrections for approach-velocity head, but omitting the small loss due to the friction of the finite length of

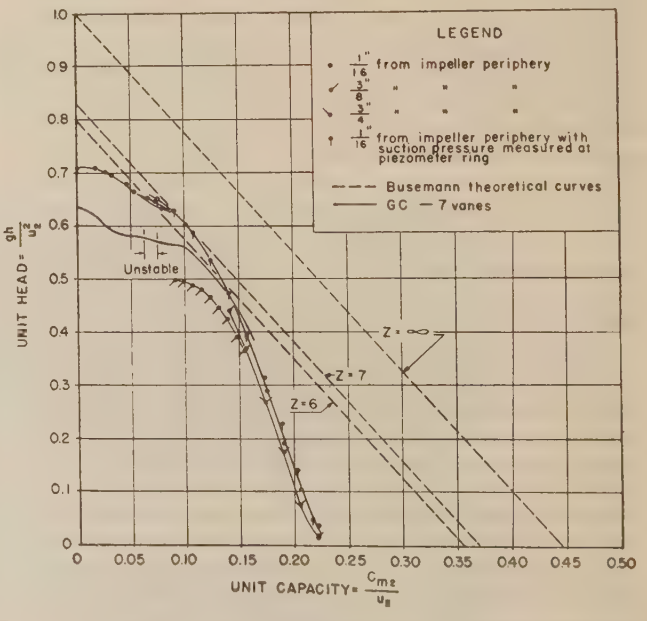

FIG. 11 DIMENSIONLESS HEAD-CAPACITY CHARACTERISTICS OF TEST IMPELLER

pipe between the piezometer taps and the impeller eye. This latter correction has not been applied to the typical run shown in Fig. 11 and would improve the agreement at the higher values of dimensionless capacity where its influence is appreciable.

It should be observed that the points plot along the same line as the points determined using the total-head tube in the inlet. This is believed to indicate that in this installation the backflows which may exist do not affect the accuracy of the total-head tube in the eye. Since total head is the measure of the energy of the fluid at the point of measurement, it seems that there has been no energy supplied by the pump to the incoming fluid at the measuring point. Visual observations with dye introduced at the eye indicate that the disturbances in the eye are localized close to the vane leading edges.

Impeller Characteristics. The type of observation discussed in the previous paragraphs may be used to study some of the detailed qualities of an impeller. Near the point of zero head, the head-capacity curve shown on the unit plot in Fig. 11 is closely linear. In the range of maximum efficiency of the prototype impeller, the linearity has disappeared and the characteristic turns smoothly without discontinuities. At a value of $C_{m2}/u_2 = 0.075$, the smooth trend of the characteristic is broken, and in this region a scatter of points was obtained which indicate that the operation of the impeller is unstable. The region of instability is indicated by the dip in the characteristic. After this region is passed, unique values are again obtained for the dimensionless head.

As a matter of interest, the unit characteristic of the prototype impeller is plotted in Fig. 11 and is marked "GC-7 Vanes." The zone of discontinuity for this impeller is marked by two vertical lines which fall in practical coincidence with the zone of discontinuity of the six-vane test impeller. Work has not yet been completed on the five-vane impeller based on the same prototype to enable definite conclusions to be drawn from this coincidence. It indicates, however, that the position of the unstable range may depend primarily on the vane shape for impellers having sufficient vane overlap.

Prerotation. It was observed very early in the experimental work that the impeller developed zero head at a flow which still showed a positive tangential component of absolute velocity at the outlet. This has been verified very carefully both by observations of the absolute flow and by measurements with the total-head tube at the outlet. Since this condition requires that the flow enter the eye with a positive prerotation, there seems to be no doubt that such a phenomenon occurs, although visual evidence indicates that this is a local effect. The absolute angle of emergence of the flow at the periphery is quite acute and cannot be attributed to experimental error in the measurement of the direction of the outflow.

Variation of Characteristic With Position of Outlet Total-Head Measurement. The type of total-head tube used in these investigations was not sensitive to yaw of the flow over the angles encountered at the outlet of the impeller except, perhaps, in the neighborhood of the vane tips. The vane tips were left wide and unsharpened. When runs are made with the Pitot head further from the outlet than has been used in the previous experiments, lower total heads are measured. Fig. 11 shows a few points taken at $^3/_8$ in. from the periphery and $^3/_4$ in. from the periphery, and they define a characteristic lower than the one obtained with the measuring point $^1/_{16}$ in. from the periphery. On the basis of present evidence it is not possible to explain this shift. Variations in instrumentation have not caused any noticeable difference in this phenomenon, and it cannot reasonably be ascribed to losses due to mixing or to the losses in the rudimentary collector ring.

The lowest curve in Fig. 11 was obtained with the measuring point distant from the periphery of the impeller before the behavior of the total head near the impeller was noticed. This curve represents a minimum and undoubtedly contains losses due to the collector ring.

The head-capacity line, based on an infinite number of vanes and the outlet vane angle, is also shown in Fig. 11, as well as two lines for six and seven vanes, based on Busemann's (16) solution of the two-dimensional radial-flow impeller with a finite number of logarithmic spiral vanes. The displacement between the GC-7 vane characteristic and the Busemann line for seven vanes indicates that the characteristic for the test impeller is too high in relation to its corresponding Busemann line for six vanes. This indicates that the experimental data based on a measuring point very close to the outlet contain a systematic error. However, this discrepancy does not affect the experimental procedure when general characteristics of the runner are being investigated and efficiency determinations are not involved.

Influence of Collector Ring. The collector ring used in the determination of the characteristic consists of two parallel plates set apart the width of the outlet which were necessary to prevent air from striking back from the free surface. In order to throttle the outflow, one cylindrical ring was attached to the circumference of each collector-ring plate, and these could be set apart a determined amount. A systematic series of runs showed that in the range of operation there was no influence of the throttle gap on the measurements.

Affinity Relation. The data presented in Fig. 11 were obtained at a rotative speed of 225 rpm; at this speed the maximum head reading was 2.06 ft. This permitted a high accuracy of measurement of the differential head except near zero head. Flow measurements were accurate to better than 1 per cent at all flows.

With this accuracy available, another series of runs were made at 150 rpm to detect, if possible, the influence of rotative speed on the characteristic which could be significant at the low speeds used in these tests. The correspondence between the dimensionless head-capacity plots for the 225-rpm series and the 150-rpm series was complete within the accuracy of the experimental data.

Acknowledgments

The authors acknowledge many suggestions of the laboratory staff, under the direction of Dr. R. T. Knapp, and particularly those of their collaborator, Mr. A. J. Acosta.

BIBLIOGRAPHY

1 "Untersuchung der Wasserströmung durch rotierendes Zellenkreiselrad," by H. Oertli, Rascher and Cie, Zurich, Switzerland, 1923.

2 "Verdrangungsströmungen bei Rotation zylindrischer Schaufeln in einer Flussigkeit mit freier Oberfläche," by W. Barth, Mitteilungen des Instituts für Strömungsmaschinen der Technischen Hochschule, Karlsruhe, Germany, No. 1, 1930, p. 39.

3 "Hilfsmittel zur Beobachtung und Messung an umlaufenden Kreiselradern," by A. Closterhalfen, *Forschung auf dem Gebiete des Ingenieurwesens*, vol. 2, No. 1, 1931, p. 2; no. 2, p. 52.

4 "Versuche an einer Schaukreiselpumpe," by A. Closterhalfen, *Forschung auf dem Gebiete des Ingenieurwesens*, vol. 2, July, 1931, p. 252.

5 "Investigation of the Flow Conditions in a Centrifugal Pump," by K. Fischer and D. Thoma, Trans. ASME, vol. 54, 1932, p. 141.

6 "Über die Relativ-Stromung in einem Pumpen-Laufrad von grossem Radien-Verhaltnis," by W. Stiess, Mitteilungen des Instituts für Strömungsmaschinen der Technischen Hochschule, Karlsruhe, Germany, No. 3, 1933, p. 77.

7 "Messungen des Druckverlaufes über Lauf und Leitschaufel einer Kreiselpumpe," by E. Hagmayer, PhD thesis, Technische Hochschule, Braunschweig, Germany, 1932.

8 "Wirebelbildung und Kraftewirkung an umlaufenden Kreisel-

schaufeln," by E. Frietsch, *Verein deutscher Ingenieure, Forschungsheft*, 384, 1937.

9 "Die Untersuchung der Strömung durch eine Flugelradturbine bei verschiedenen Schaufelzahlen," by K. Hahn, Mitteilungen des Instituts für Stromungsmaschinen der Technischen Hochschule, Karlsruhe, Germany, No. 4, 1939, p. 2.

10 "The Hydraulic Machinery Laboratory at the California Institute of Technology," by R. T. Knapp, Trans. ASME, vol. 58, 1936, pp. 649–661.

11 "The Hydrodynamics Laboratory of the California Institute of Technology," by R. T. Knapp, Joseph Levy, J. P. O'Neill, and F. B. Brown, Trans. ASME, vol. 70, 1948, pp. 437–457.

12 "Laboratory Investigations of the Mechanism of Cavitation," by R. T. Knapp and A. Hollander, Trans. ASME, vol. 70, 1948, pp. 419–435.

13 "Special Cameras and Flash Lamps for High-Speed Underwater Photography," by R. T. Knapp, *Journal, Society of Motion Picture Engineers*, vol. 49, July, 1947, pp. 64–82.

14 "On the Design of the Contraction Cone for a Wind Tunnel," by Hsue-Shen Tsien, *Journal of the Aeronautical Sciences*, vol. 10, February, 1943, pp. 68–70.

15 "Development of the Hydraulic Design for the Grand Coulee Pumps," by C. Blom, Trans. ASME, vol. 72, 1950, p. 53.

16 "Das Forderhohenverhaltnis Radialer Kreiselpumpen mit logarithmisch spiraligen Schaufeln," by A. Busemann, *Zeitschrift für angewandte Mathematik und Mechanik*, vol. 8, 1928, p. 372.

Discussion

A. J. Acosta.[5] The need for a series of investigations on the individual elements of a hydraulic machine has been recognized for some time. Due to the somewhat inconclusive experimental results to date, it has been impossible to evaluate the separate effects of the components of a hydraulic machine. For that reason, the interpretation of observed phenomena and correlation with any real or perfect-fluid theory has lagged. Accordingly, the study of an impeller or volute, wherein its effects are isolated, should enable the laboratory to perform for the first time definitive tests as to the nature of flow in hydraulic machinery.

In reference to the plots of C_{m2} and C_{u2} (Fig. 8 of the paper), the authors state that there is as yet no theoretical justification for their behavior. The writer has had occasion to make an analysis of the flow of an inviscid incompressible fluid in a two-dimensional rotating-vane system. Inasmuch as an "ideal" solution offers possibilities of interpreting test data, it seems pertinent to present it now. The geometry of the chosen idealized impeller consists of eight logarithmic spiral vanes with a characteristic angle of 45 deg and a radius ratio of 0.5. The analysis involves the numerical evaluation of the differential equation governing the flow subject to appropriate boundary conditions. In the case considered, an absolute co-ordinate system (stationary with respect to the inertial reference frame) was chosen so that the differential equation to be solved is Laplace's equation in two dimensions, i.e., $\partial^2 U/\partial x^2 + \partial^2 U/\partial y^2 = 0$ where U is either the stream function or velocity potential for the flow. The boundary conditions are: (a) there is no flow through the vanes; (b) there is no flow around the tip of the vanes at exit. This latter condition is merely a statement of the Kutta-Joukowsky principle for the flow around lifting surfaces. The vanes are taken to be infinitely thin, although this condition is not necessary for the solution of the problem. Finally, we require that the velocity diminish to zero at an infinitely great distance from the impeller. Then, to within an additive constant, the stream function and velocity potential for the flow are uniquely defined, and the velocities in the field may be computed from either. The flow rate through the impeller is accounted for by placing a line source at the origin. Rather than compute a number of solutions for separate flow rates only two need be found, since the resulting velocity field within the impeller can be resolved into two parts, namely, (a) the flow due to the rotation of the vanes without any net through-flow (corresponding to shutoff head); (b) the flow from a source through a set of radially disposed stationary guide vanes. Solutions of this latter sort are available.[6] Combined with the present work which is only for zero flow rate, the flow for any operating point on the head flow-rate diagram may be obtained by taking a linear combination of (a) and (b).

The solution itself was effected by the so-called "relaxation" method.[7] Briefly, the method for solving Laplace's equation is as follows: The value of the function in the region of interest is approximately determined at the intersecting points of a rectangular grid. Then, to the first order, the finite-difference equation representing Laplace's equation is $\psi_1 + \psi_2 + \psi_3 + \psi_4 - 4\Delta\psi_0 = 0$, where ψ_1 to ψ_4 are the values of the function at the nearest four intersecting points to the point 0. This equation is satisfied at each point in the region by a trial-and-error process. Ways in which this is readily accomplished are discussed by Southwell.[7]

The solution was carried out by the method described, and from it the variation of the radial velocity across the impeller-exit section was determined and is shown in the accompanying diagram, Fig. 12. The value of the unit head at zero flow rate is 0.79, which is the same as that given by Busemann's theory[8] for logarithmic vanes. Although it is unfortunate that the dimensions of the impeller chosen for analysis are somewhat different from those of the test impeller, the order of magnitude of the velocities and the general features of the flow will be the same.

Comparing Fig. 8 of the paper with Fig. 12 computed by the writer, one sees that the dip in the radial-velocity distribution is substantiated by theory. For logarithmic vanes of the angle and radius ratio used in the analysis and for the test impeller, the radial-velocity variation at the impeller exit is nearly unaffected by the flow rate; so we are justified in comparing the variation at zero flow rate with that of the experiment. The range of variation seen in Fig. 8 is about a radial velocity of 1 fps, or in a dimensionless form it is 0.15, arrived at by dividing

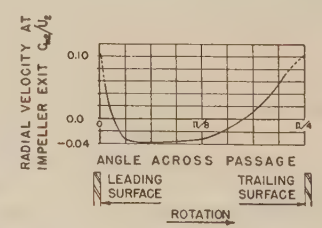

Fig. 12 Plot of Ratio of Radial Velocity to Peripheral Velocity at Exit Section Computed for a Two-Dimensional Impeller With Eight Logarithmic Spiral Blades Having a Vane Angle of 45 Deg and a Radius Ratio of 0.5 for Zero Flow Rate

by the peripheral velocity. The maximum variation computed from the two-dimensional ideal fluid case is about $\Delta C_{m2}/U_2 = 0.14$. The only noticeable departure in general trend between the two is found near the leading surface, where it is seen that the area of positive C_{m2} is much less for the computed case than for the test results. This is, however, the trend one would expect as the vane angle becomes steeper.

As the authors mentioned, the dip apparent in the C_{m2}, β_2, and

[5] Research Fellow in Hydrodynamics, California Institute of Technology, Pasadena, Calif. Jun. ASME.

[6] "Diagrams for Calculation of Airfoil Lattices," by A. Betz, NACA, T.M. 1022.

[7] "Relaxation Methods in Theoretical Physics," by R. V. Southwell, Oxford University Press, London, England, 1946.

[8] Refer to author's Bibliography (16).

α_2 is not evident in the C_{u2} (absolute tangential velocity at exit) plot. For the special case analyzed, the range of variation of C_{u2} compared with the mean value was found to be 18 per cent, 12.5 per cent being positive occurring at the boundary on the vane tip. It is, then, not surprising that a variation of this order of magnitude should not be observed on the authors' plot, in view of the large point scatter.

The general trend of the data presented is seen to follow that predicted by two-dimensional perfect-fluid theory, a surprising fact considering the high level of turbulence present in the flow. However, the limitations of perfect-fluid theory for flows of this sort are as yet unknown. The writer is interested in this problem and hopes to see it explored further.

This work was supported by the Office of Naval Research.

Authors' Closure

The authors thank Mr. Acosta for his discussion and consider it a valuable contribution. More complete and detailed studies made on a series of impellers since the completion of the paper indicate that in the region of the design point, the total head generated by the impeller matches rather well (within 8 per cent) the ideal Busemann value, and also that the head-capacity curve of the free impeller follows very closely the ideal straight-line relationship. In this region prerotation is nil; there is no separation within the passages and the discharge flow pattern is primarily two-dimensional. Hence, in this region, the two principal parameters present in the real fluid case but omitted in the ideal case are viscosity, μ, and the temporal velocity variations $\frac{\partial v}{\partial t}$. If through continued research the effects of these quantities on the ideal solution can be determined, an extremely powerful tool would be made available to the researcher and designer.

Unfortunately, the whole picture is not quite as simple as might be inferred. At off-design points, observations show that the flow separates from the channel walls and follows unknown and indeterminate boundaries. Cross flows develop and the discharge flow pattern does not remain two-dimensional. These elements impose serious limitations on the potential approach in the very regions where its use to predict off-design point performance would be most desirable. On top of all this, it must be remembered that the ideal situation applies only to a free impeller; an impeller operating in an infinite fluid medium with stationary boundaries only at infinity. Tests have shown that the characteristics of the complete pump, consisting of impeller and case, differ widely from those of the free impeller at all points except the design point. Hence the effect of the volute must be considered and incorporated in the final solution.

It is not meant to imply by these remarks that the potential solution is considered either impractical or impossible. The intent of the authors is to point out the long road ahead and the vast areas yet to be explored, and to underline the statement that at these early stages of the work it is most gratifying to find a good correlation between potential theory and experiment in some parts of the field.

The Flow Through Centrifugal Compressors and Pumps

By H. E. SHEETS,[1] AKRON, OHIO

The flow through centrifugal compressors and pumps is a three-dimensional flow problem and is of such a complex nature that an exact solution is not obtainable. The literature (1, 2)[2] shows the differential equations which the flow through an impeller must follow. An approximate solution to these equations is found by means of certain assumptions which are possible for impellers within a limited range of specific speeds. The solution gives the approximate velocity and pressure distribution in the impeller passages. The knowledge of the velocity distribution is used to analyze the phenomena of pulsation and blade stalling. The method has also been used in mixed-flow compressors and radial- and mixed-flow turbines. The application of this method for two impellers and test data are presented.

Nomenclature

The following nomenclature is used in the paper:

- a = distance between 2 blades normal to flow lines
- c = absolute velocity
- f = area
- l = blade length
- m = mass
- p = pressure
- r = impeller radius
- t = blade pitch
- u = tip speed of impeller
- w = relative velocity
- z = blade number
- n_s = specific speed
- Q = total flow
- R = blade radius of curvature
- β = blade angle
- $\gamma = 1/v$ = specific weight
- ω = angular velocity
- σ = blade solidity

Indexes:

- 2 = impeller exit
- 1 = impeller inlet
- * = arbitrary point in impeller passage

Other symbols will be defined in the text.

Derivation of Approximate Solution—Blade Center Section

The approximate solution of the flow problem considers the impeller-blade passage as a rotating channel for the center section. The first step is the determination of the approximate velocity distribution in this center section, and then the solutions for the exit and inlet of the blade passage are added. The result gives the nonuniform velocity distribution throughout the entire blade passage.

This method is therefore limited to blade passages which are long enough to permit a division in three sections, and it is necessary that the center section, treated as a rotating channel, extend at least over a limited length. Therefore the proposed method is limited to a range of blade solidity

$$\sigma = \frac{l}{t} = \frac{z}{2\pi \sin \beta} \log_e \frac{r_2}{r_1} \geqq 1.3 \quad \ldots\ldots\ldots [1]$$

or approximately

$$\sigma' = \frac{l}{t_2} = \frac{lz}{2\pi r_2} \geqq 1.2 \quad \ldots\ldots\ldots\ldots [1a]$$

This definition for blade solidity is given in reference (3).

Fig. 1 shows a schematic drawing of an impeller. For two-dimensional flow the blade width has a constant value, b = const. Considering the relative flow in the center section of the rotating channel in Fig. 1, we apply to the particle of mass dm the complementary forces $dm\, r\omega^2$ and $dm\, 2w\omega$. The normal acceleration toward the center of curvation is w^2/R, and we have the equation of motion

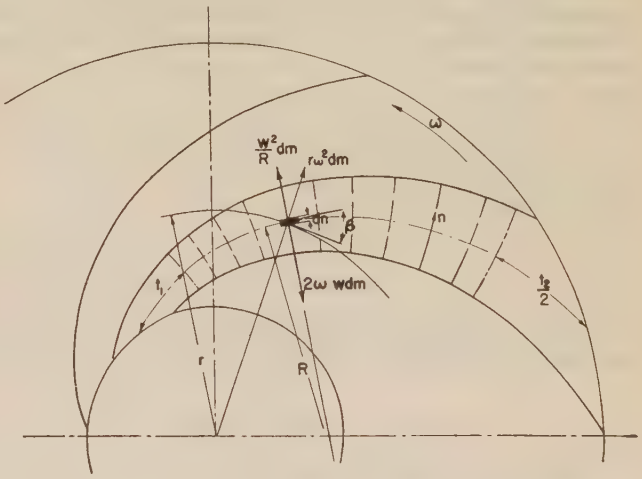

Fig. 1 Forces in a Rotating Channel With Backward Curved Vanes

$$dm \frac{w^2}{R} = df(p - p^*) + dm\, 2w\omega - dm\, r\omega^2 \cos\beta \ldots [2]$$

for backward-curved vanes.

Since

$$dm = dfdn \frac{\gamma}{g} = df\, dn \frac{1}{vg}$$

---

[1] Goodyear Aircraft Corporation. Mem. ASME.

[2] Numbers in parentheses refer to the Bibliography at the end of the paper.

Contributed by the Hydraulic Division and presented at the Annual Meeting, New York, N. Y., November 27–December 2, 1949, of The American Society of Mechanical Engineers.

Note: Statements and opinions advanced in papers are to be understood as individual expressions of their authors and not those of the Society. Revised manuscript received at ASME Headquarters, April 4, 1950. Paper No. 49—A-154.

and

$$dp = p - p^*$$

and according to Fig. 1, taking dn positive from the low-velocity side of the blade to the high velocity side

$$dr = dn \cos \beta$$

we get

$$\frac{w^2}{R} = vg \frac{dp}{dn} + 2w\omega - r\omega^2 \frac{dr}{dn} \quad [3]$$

The energy equation of a streamline is

$$\frac{w^2 - w^{*2}}{2g} = -\int_p^{p^*} vdp + \frac{u^2 - u^{*2}}{2g} \quad [4]$$

For infinitely close-lying points it is with $dw = w - w^*$

$$\frac{wdw}{g} = -vdp + r\omega^2 \frac{dr}{g} \quad [5]$$

Comparing Equations [3] and [5], we get

$$\frac{w}{R} + \frac{dw}{dn} - 2\omega = 0 \quad [6]$$

for backward-curved vanes. For forward-curved vanes we get

$$\frac{w}{R} + \frac{dw}{dn} + 2\omega = 0 \quad [6a]$$

For the purpose of our approximate solution we make the assumption that the radius of curvature of the streamlines is approximately constant for each line orthogonal to the flow lines. The radius of curvature may vary from vane inlet to exit. This assumption means

$$R = \text{const} \quad [7]$$

For the center section, Equation [7] is a good approximation, and for straight-bladed impellers it is correct.

Then Equation [6] becomes

$$\frac{dn}{R} = \frac{dw}{2\omega R - w} \quad [8]$$

For $n = 0$ the minimum velocity at the channel wall is designated as w' and the solution for Equation [8] becomes

$$w = (w' - 2\omega R)e^{-\frac{n}{R}} + 2\omega R \quad [9]$$

Developing the exponential function into a series and omitting third and higher powers of n/R we get

$$w = w' + \left(2n\omega - \frac{n}{R} w'\right)\left(1 - \frac{n}{2R}\right) \quad [10]$$

Defining the mean velocity as

$$w_m = \frac{Q}{ab} = \frac{\int^a wbdn}{ab} \quad [11]$$

a and b are the channel width and height, respectively.

Substitution of Equation [10] in [11] and some transformation give us the following for the extreme local velocities at the channel wall:

Minimum velocity for $n = 0$

$$w' = w_m \left[1 + \frac{a\left(1 - \frac{a}{3R}\right)}{2R - a\left(1 - \frac{a}{3R}\right)}\right] - a\omega \left[1 - \frac{a}{3R} + \frac{a\left(1 - \frac{a}{3R}\right)^2}{2R - a\left(1 - \frac{a}{3R}\right)}\right] \quad [12]$$

Maximum velocity for $n = a$

$$w'' = w_m \left[1 - \frac{a\left(1 - \frac{2a}{3R}\right)}{2R - a\left(1 - \frac{a}{3R}\right)}\right] + a\omega \left[1 - \frac{2a}{3R} + \frac{a\left(1 - \frac{a}{3R}\right)\left(1 - \frac{2a}{3R}\right)}{2R - a\left(1 - \frac{a}{3R}\right)}\right] \quad [13]$$

For straight blades $R = \infty$ these equations become

$$w_s' = w_m - a\omega \quad [12s]$$

$$w_s'' = w_m + a\omega \quad [13s]$$

For forward-curved blades we get similarly

$$w' = w_m \left[1 - \frac{a\left(1 - \frac{2a}{3R}\right)}{2R - a\left(1 - \frac{a}{3R}\right)}\right] - a\omega \left[1 - \frac{2a}{3R} + \frac{a\left(1 - \frac{a}{3R}\right)\left(1 - \frac{2a}{3R}\right)}{2R - a\left(1 - \frac{a}{3R}\right)}\right] \quad [12a]$$

$$w'' = w_m \left[1 + \frac{a\left(1 - \frac{a}{3R}\right)}{2R - a\left(1 - \frac{a}{3R}\right)}\right] + a\omega \left[1 - \frac{a}{3R} + \frac{a\left(1 - \frac{a}{3R}\right)^2}{2R - a\left(1 - \frac{a}{3R}\right)}\right] \quad [13a]$$

The flow through the impeller can be divided into two parts, the "through flow" associated with w_m and the "displacement flow" associated with ω. With $w_m = 0$ we get in Equations [12] and [13] the values for the displacement flow alone.

Blade Exit

It is known that the relative flow through a centrifugal impeller can be expressed by a relative flow function as a sum

$$\psi = \psi_1 + \psi_2 + \psi_3$$

where

ψ_1 = flow function for through flow

ψ_2 = flow function for displacement flow

ψ_3 = flow function for circulation flow

The flow functions ψ_2 and ψ_3 must be of such a nature that the infinite velocity at the inlet edge caused by the through flow is neutralized. Stodola (1) has shown that the solutions of the flow function ψ_2 and ψ_3 can be found by the membrane analogy or by torsional stress analogy. In the literature (4, 5) are published solutions for the stress analogy for a large number of simple shapes.

To determine the shape of the blade-exit channel, we assume that the end effects extend a distance $t_2/2 = (D_2/2z)\pi$ from the end of the blade inward. This distance is taken along the mean flow line. A line orthogonal to the flow lines is the separation line between the center section and the blade exit. The velocity distribution up to the separation line is known according to Equations [12] and [13]. We have now to determine the variation of the velocities from the separation line to the blade exit, where the velocity on both sides of the blade must be uniform and equal to the through-flow velocity.

The shape of the blade exit thus determined is usually very simple so that the variation of velocity can be taken directly from the stress analogy for such shapes as sector of a circle, triangle, and many others. For more complex shapes, an approximate solution can be found according to the energy method of the torsional problem as proposed by Ritz and Trefftz (4). With this method the velocity distribution can be found for any polygon-shaped channel exit.

For an exit channel of nearly rectangular shape, the results of the stress analogy (5) show a velocity variation approximately according to a parabola from a known value at the separation line of the center section to zero at the blade exit.

Blade Inlet

The blade inlet can be treated like the blade exit. Therefore it becomes necessary to determine the shape of the blade-inlet channel. In this case we assume that inlet effects extend to a distance $t_1 = D_1\pi/z$ from the blade inlet inward. This distance is taken along the mean flow line. A potential line orthogonal to the flow lines is the separation line between the center section and the blade inlet. The velocity distribution at the separation line is known according to Equations [12] and [13]. In this case we have to determine the velocity distribution from the stagnation point of the blade at the inlet to the known values at the separation line with the center section.

The blade-inlet velocity distribution can be determined according to the method of Betz (6, 7), and Ackeret (8) for the axial inducer-type impeller.

It is thus possible by starting with the calculation of the velocity distribution in the center section, according to Equations [12] and [13], to find the velocity distribution in the entire blade channel.

Three-Dimensional Flow

For three-dimensional flow the blade height is not constant and usually decreases from impeller inlet to impeller outlet. Frequently the flow turns in the vicinity of the impeller inlet from axial to radial direction. This means that the mean velocity w_m changes as a function of the blade height and must be determined.

At first we determine the absolute velocity c_m for the hypothetical case of the fluid flowing through a stationary impeller of identical shape. We designate the radius of curvature with ρ, and taking n again from the low-velocity side of the flow, i.e., the convex side in this case, we get from considerations similar to Equations [2] to [6]

$$\frac{dn}{\rho} - \frac{dw}{w} = 0 \qquad [14]$$

A graphical solution for the velocity distribution according to Equation [14] can be found according to the method of Flugel (1).

Another method which permits direct calculation of the velocity distribution is possible if the impeller contours can be approximated by two hyperbolas following the equation

$$r^2 x = C \qquad [15]$$

Then the velocity calculated according to the basic equation from Durand (9) is

$$c_m = \frac{C}{2\pi}\sqrt{(2x)^2 + r^2} \qquad [16]$$

According to either method, the absolute velocity c_m is determined for the mean streamline as well as for the inner and outer contours of the impeller, c_{mi} and c_{mo}, respectively.

The relative velocity is

$$w_m = \frac{c_m}{\sin\beta} \qquad [17]$$

where β is the local blade angle at the location of c_m. Equation [17] assumes that the mean relative velocity follows the blade contour, and this assumption is justified for the center section or rotating channel of the impeller. For impellers within the specified solidity range, Equation [17] gives also a good approximation for inlet and exit of the blade channel.

For impellers with large inducers, Equation [17] must be replaced for the blade-inlet condition by more accurate equations following the theory of axial machines (3).

Thus w_{mi} and w_{mo} can be determined for the inner and outer contour of the impeller and these velocities exist at the mean streamline between two blades.

Equation [17] cannot be used when large secondary flows occur, such as those caused by blade stalling or the impeller operating under considerably larger or smaller flow than design point.

Compressibility and Friction

The effect of compressibility is taken into consideration by calculating the area of the impeller-flow channel for an arbitrary number of stations along the mean flow line. The velocity w_m^* is calculated from the total flow on the basis of the known area and an estimated compressibility. Later w_m^* is recalculated according to correct compressibility. The enthalpy increase from the conditions at the inlet to the compressor to an arbitrary station inside the impeller is

$$H^* - H_0 = \frac{u^{*2} - u_1^2}{2g} + \frac{w_{m1}^2 - w_m^{*2}}{2g} - \frac{c_1^2 - c_0^2}{2g} \qquad [18]$$

The first two terms in Equation [18] define the enthalpy increase in the impeller, and the last term defines the inlet depression caused by the acceleration of flow from the known conditions to the impeller inlet.

Part of this total enthalpy increase is transformed into pressure and the other part into heat. The amount of enthalpy transformed into pressure is defined as

$$\Delta H_{AD} = \eta_c (H^* - H_0) = \frac{k}{k-1} RT_0 \left[\left(\frac{p^*}{p_0} \right)_{AD}^{\frac{k-1}{k}} - 1 \right] \qquad [19]$$

where η_c is the impeller channel efficiency, which is a function of the channel Reynolds number, turbulence, friction coefficient, and boundary-layer condition; η_c must be assumed on the basis of experience.

Equation [19] permits the calculation of the pressure rise $(p^*/p_0)_{AD}$. The temperature increase is

$$\frac{T^*}{T_0} = 1 + \frac{H^* - H_0}{c_p T_0 J} \quad [20]$$

and the volume change becomes

$$\frac{V^*}{V_0} = \frac{T^*}{T_0}\left(\frac{p_0}{p^*}\right)_{AD} \quad [21]$$

The correct volumes and velocities can be calculated according to Equations [18] to [21], and the original estimate of the compressibility is replaced by the accurate value of Equation [21]. Thus the correct values of the velocity w_m in Equations [12] and [13] are calculated. Then the following velocities are calculated, at first on the basis of incompressible flow, w_{mi}; w_{mo} along the inner and outer contour of the impeller and the local velocities w', w''; w_i', w_i'', w_o', and w_o'', according to Equations [12] and [13]. If any of the foregoing velocities vary greatly from its corresponding value of w_m, the compressibility correction is calculated in the same manner.

This analysis permits calculation of the impeller-velocity distribution and gives a complete map of the velocity values for the three-dimensional compressible flow through the impeller.

The velocity distribution shall be represented as a function of the blade length and, for dimensionless representation, the values shall be divided by tip speed and impeller-tip radius, respectively.

Accuracy of Approximate Solution

For the theoretical case of two-dimensional flow through radial-flow impellers, we can compare the results of the approximate solution with a flow analysis which has been calculated according to the relaxation method by Professor Emmons (10) for two types of impellers. In this report the velocity distribution is determined separately for the through flow and the displacement flow. The two types of impellers, which have been analyzed, are a straight radial-vane, $\beta_2 = 90$ deg, 22-blade unit, and a backward-curved $\beta_2 = 30$ deg logarithmic spiral-blade unit. Both impellers have a radius ratio $r_1/r_2 = 0.333$, constant blade width b, and a solidity of $\sigma = 3.84$.

Fig. 2 compares the velocity distributions of the displacement flow for the straight radial-vane unit. The solid line shows the velocity distribution according to the relaxation method of Professor Emmons, and the dash line according to the approximate solution of Equations [12] and [13] with $w_m = 0$. A comparison on the basis of the displacement flow will show any discrepancies more clearly because total flow consists of the sum of displacement flow and through flow. Fig. 3 shows the velocity distribution for the displacement flow for the backward-curved unit, again with the solid line and dash line indicating the values of the relaxation method and the approximate solution, respectively. The two results indicate very good agreement for almost the entire blade passage and justify the use of the approximate solution.

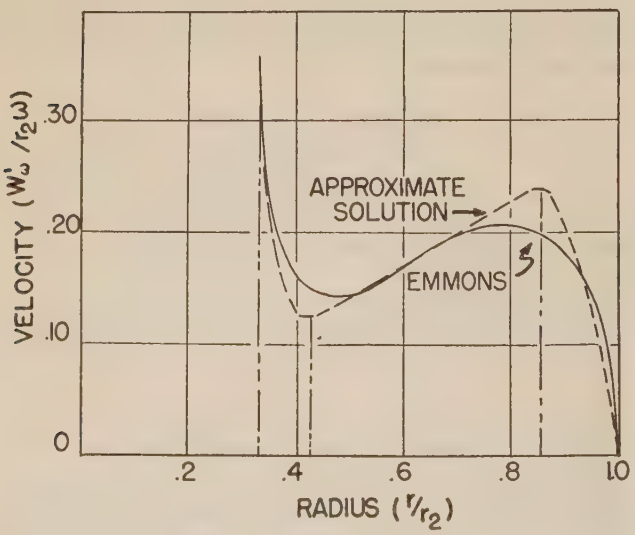

Fig. 2 Velocity Distribution of Displacement Flow for Radial-Vaned Impeller, $z = 22$

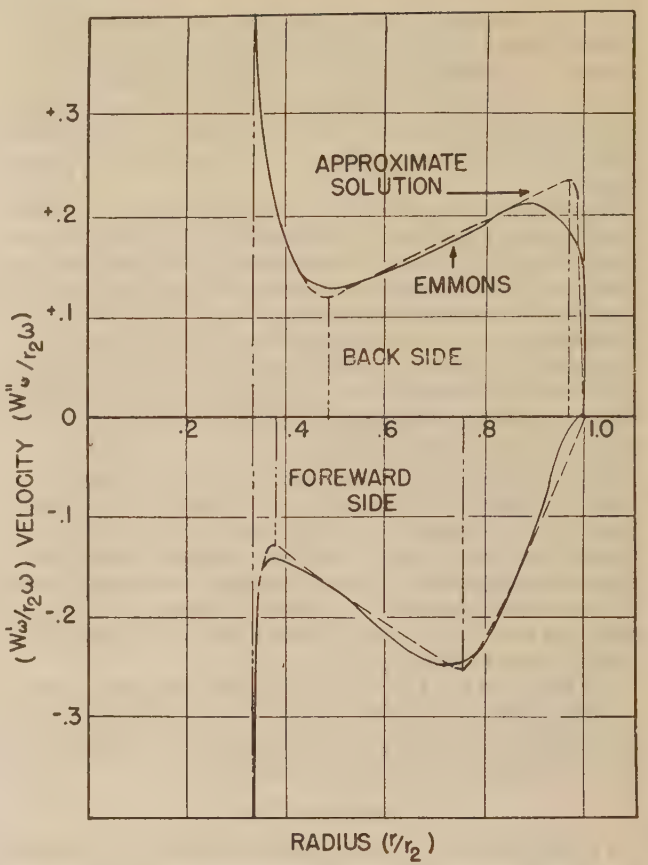

Fig. 3 Velocity Distribution of Displacement Flow for Impeller With Backward-Curved Vanes, $z = 11$; $\beta_2 = 30$ Deg

We can also calculate the effect of finite blade number on the relative exit velocity. For the range of solidity under consideration this effect may be ascribed to the displacement flow only, and the influence of the circulation flow may be neglected (3). The calculation is identical with the stress or membrane-analogy methods discussed before, except that we calculate this time the velocity distribution along the impeller-exit diameter. This velocity distribution is again taken from the stress analogy. From the velocity distribution we calculate the mean value of this circumferential velocity Δw_u. This is the desired velocity correction for the finite number of blades. For nearly rectangular exit shapes, the velocity distribution is, as before, approximately a parabola, and the maximum velocities are proportionate to the width and height of the shape. The maximum velocity on the sides of the exit shape exists at the separation line between the center section and exit section and is known from the values of Equations [12] and [13] with $w_m = 0$.

The velocity Δw_u has been calculated for the two cases mentioned previously. The values are compared with the values for Δw_u

TABLE 1 RELATIVE VELOCITY CORRECTION

Relative velocity correction	Stodola[a] Δw_u	Busemann[b] Δw_u	Emmons Δw_u	This method Δw_u
Radial vanes 90 deg, $z = 22$	$0.143 \times u_2$	$0.105 \times u_2$	$0.086 \times u_2$	$0.108 \times u_2$
Backward-curved vanes 30 deg, $z = 11$	$0.143 \times u_2$	$0.137 \times u_2$	$0.136 \times u_2$	$0.137 \times u_2$

[a] $\Delta w_u = \frac{\pi \sin \beta_2}{z} \times u_2$ Reference (1).

[b] Reference (3).

calculated according to the theories of Stodola, Busemann, and Emmons. Table 1 shows the results.

For the backward-curved impeller the theories of Busemann and Emmons agree with the results of this calculation, and, for the radial-vaned impeller, the results of this calculation agree with the theory of Busemann, but the value is somewhat above that of Emmons.

Practical Applications

The application of the analysis will be shown for two cases. The first case relates to a compressor A which had a very narrow range of operation and pulsation outside this range of operation. An analysis of this impeller was suggested in order to find whether the range of operation could be improved. Fig. 4 shows the velocity distribution for this impeller. The vertical lines indicate the separation between the inlet, the center and exit section of the flow channel. The mean velocity w_m shows a decrease from inlet to exit of the impeller but does not permit any conclusion regarding the stability range of the unit. Backflow or pulsation of an impeller will start if the local velocity on the forward side of the blade becomes zero, and, in this impeller, the local velocity distribution indicates narrow range of operation. In this case the velocity difference $w_m - w'$ is a function of the angular velocity ω and channel width a only, according to Equation [12], with $R = \infty$, and does not change with w_m in the critical region of lowest values of w' on the forward side of the blade. Therefore a reduction in total flow of 13 per cent reduces the mean velocity in the same proportion and results in a value of mean velocity equal to $w_m - w'$ in the critical region; thus making the value of local velocity w' on the forward side zero. Backflow will occur if the flow is reduced 13 per cent.

Another item of importance is the amount of deceleration on either side of the blade per unit length. Too large an amount of deceleration causes high pressure gradients and stalling of the blades. While the velocity-distribution diagram permits predicting pulsation caused by backflow, the stalling of the blades cannot be analyzed quantitatively from the diagram, because stalling is affected by boundary-layer thickness, turbulence, and blade finish. However, on the basis of comparison of similar velocity distributions, experience can be gained indicating which velocity distributions tend to avoid stalling. The large decelerations on both pressure and velocity side of the blade of impeller A indicate a danger of stalling and thick boundary layers even under normal operation.

The second case relates to a compressor which was designed by use of the foregoing velocity-distribution method. The specifications called for a pressure ratio of 3 at 40,000 ft altitude, a wide range of stability, and a certain maximum flow capacity. Since this unit was tested under sea-level conditions, the specifications were recalculated for sea-level conditions as follows:

Flow, $Q = 4850$ cfm $\qquad Q$ max $= 5280$ cfm

Pressure ratio, $\rho = 2.54$

Speed, $n = 19{,}600$ rpm $\qquad n_s = \bar{n} \frac{\sqrt{\bar{Q}}}{g^{3/4} H^{3/4}} = 0.096$

In order to get the desired range of stability, the design point

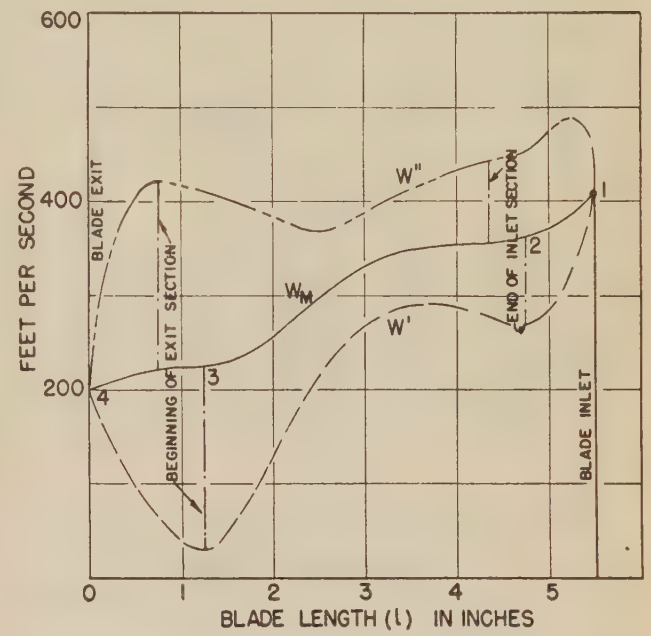

FIG. 4 UNDESIRABLE VELOCITY DISTRIBUTION IMPELLER A ($D_2 = 13.25$ in., $u_2 = 700$ fps, $n_s = 0.110$.)

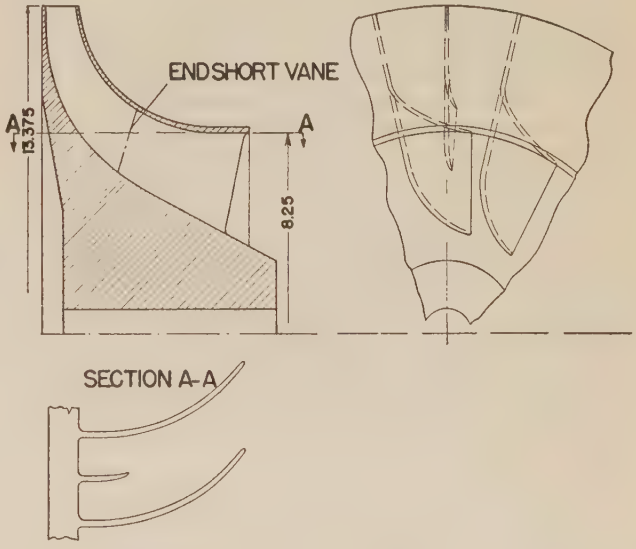

FIG. 5 IMPELLER B, 14 SHORT VANES, 14 FULL VANES

was chosen 8 per cent below the point of maximum capacity. Fig. 5 shows this compressor. This impeller has 14 full vanes and 14 short vanes. Fig. 6 shows the velocity diagram with regard to the mean relative velocity for this impeller. The various regions of the flow channel are separated by vertical lines.

The mean relative velocity shows decreasing values from inlet to exit, as well as a continuous change in decrease to the smaller

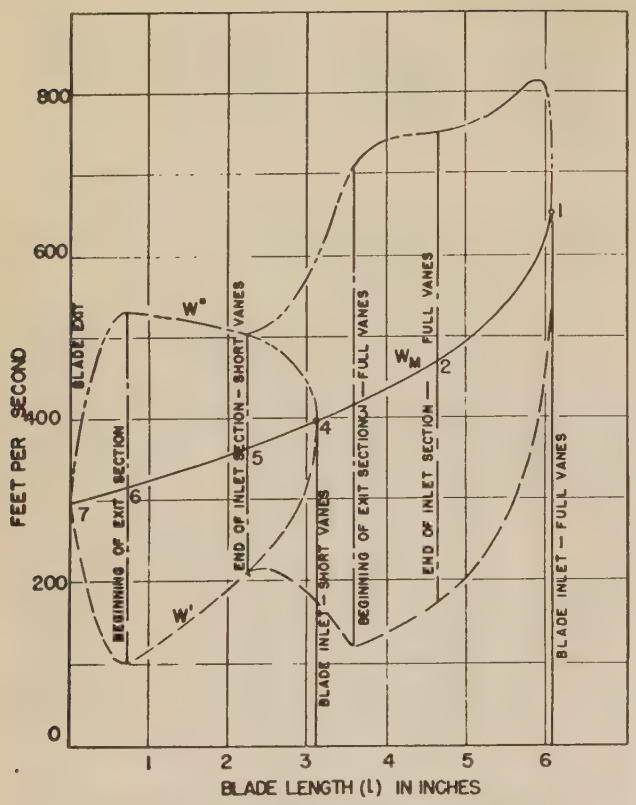

FIG. 6 VELOCITY DISTRIBUTION FOR MEAN FLOW PATH OF IMPELLER B

decelerations at the discharge end. The local velocites indicate the same characteristics on the high-pressure side of the blade, giving the largest decelerations at the blade entrance of the full and half-vanes, respectively. The low-pressure side of the blade shows little change in velocity, except at the discharge end of the blade and at the entrance into the half-vanes. The lowest value of local velocity occurs in a region where $R = \infty$; therefore, according to Equation [12], the velocity difference $(w_m - w')$ is a function of the angular velocity ω and channel width a only. Thus, reducing the through flow 33 per cent results in a value of mean velocity equal to $w_m - w'$ in the critical region, $l = 0.70$, and the value of the local velocity w' becomes zero. This means that backflow has progressed to the center of the blade channel and pulsation will occur. The beginning of pulsation can be analyzed by calculating the velocity distribution for the inner and outer contours of the impeller. From the curve, Fig. 6, it can be seen that this impeller would pulsate without the half-vane at its design flow and that half-vanes permit the extension of the operating range by reducing the value of local velocities.

Fig. 7 shows the velocity distribution of the impeller for the inner contour with the mean value w_{mi} and for the outer contour, mean value w_{mo}. All velocities have been calculated by taking into consideration an approximate value of the boundary-layer thickness. From the local velocity distribution a revised estimate of the stability range can be made. The lowest local velocity occurs on the forward side of the blade near the impeller disk. The critical value is again near the blade exit, $l = 0.70$, because in this region the value of w_{mi} is near its minimum value and $R = \infty$. Thus $(w_{mi} - w_i')$ is independent of w_{mi}, according to Equation [12]. Therefore a reduction of 27 per cent of the design capacity will result in the first local velocity value of $w_i' = 0$ initiating backflow. At a slightly larger reduction, 28 per cent of design capacity, the local velocity w' also becomes zero in the second critical region at $l = 4.45$ near the inducer exit of the full vanes at the impeller disk. At this flow the local velocity value w' in the critical region near the impeller exit is negative at the impeller disk and backflow progresses toward the center of the flow channel.

The local velocity w_o'' on the back side of the blade close to the impeller shroud has the maximum value near the inducer inlet. This is the maximum value of velocity in the entire blade channel. An increase of 9 per cent above design capacity will result in the first occurrence of local sound velocity at this location. This analysis, therefore, indicates a total operating range of about 36 per cent.

Fig. 8 shows test data of the performance curve for this compressor at 1100 and 1140 fps tip speed. These performance curves indicate an operating range of 28 per cent from the design point to the beginning of pulsation, and a range of 10 per cent from the design point to maximum capacity, giving a total range of about 38 per cent at which the compressor efficiency is above 70 per cent.

Therefore the performance curve verifies the predicted result of the velocity-distribution curves. The maximum efficiency is above 79 per cent, and it should be remembered that this unit operates at an unusually low specific speed. Due to the instrumentation, flow losses in the 90-deg inlet turn are charged to the compressor efficiency. The entire performance of this compressor with regard to efficiency, pressure ratio, and stability is significant in that it was possible to calculate the performance of this unit and achieve the results shown in the curve, Fig. 8, without any modifications after tests.

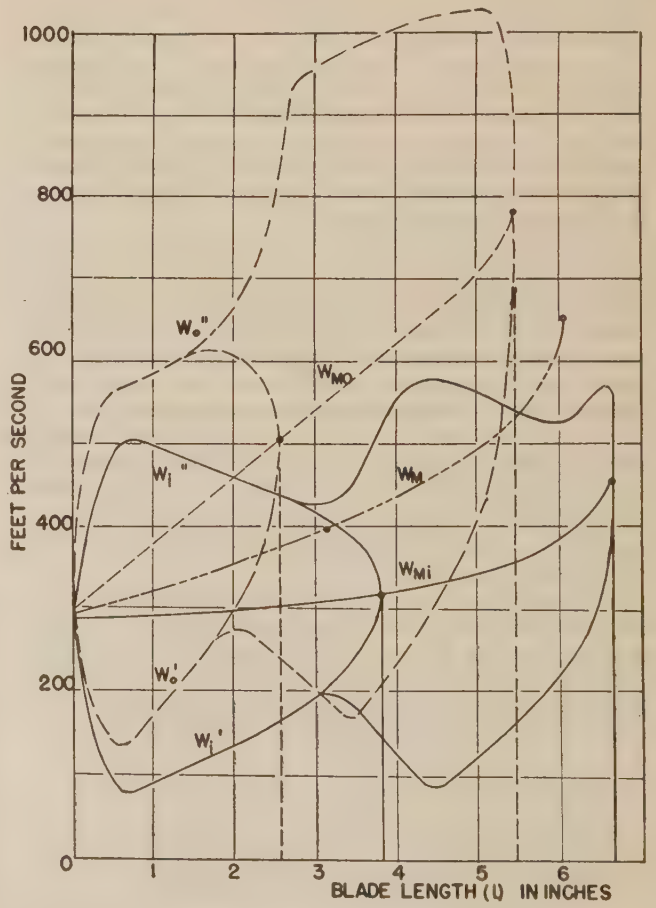

FIG. 7 VELOCITY DISTRIBUTION FOR INNER AND OUTER CONTOURS OF IMPELLER B

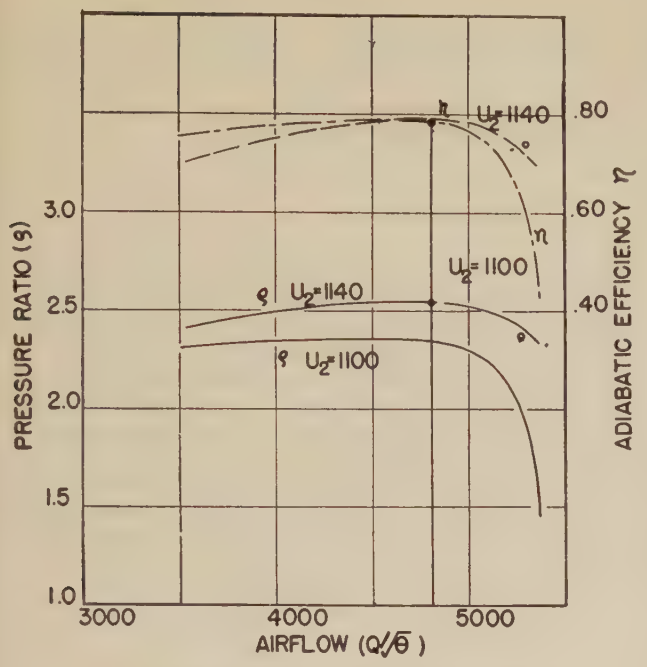

FIG. 8 COMPRESSOR PERFORMANCE CURVE IMPELLER B

CONCLUSIONS

The analysis permits calculation of the impeller velocity distribution and gives a complete map of the velocity values for the three-dimensional compressible flow through the impeller of a compressor.

The use of the velocity-distribution curves permits the prediction of pulsation of the compressor. Pulsation occurs when the local velocity reaches values of zero or below.

A qualitative analysis can be made with regard to blade stalling by comparing velocity-distribution curves for similar types of impellers. The criterion for stalling may be defined as the deceleration per unit length $(\Delta w)/(\Delta l)$, or the pressure gradient per unit length $(\Delta p)/(\Delta l)$.

In making the qualitative analysis it must be pointed out that stalling is a function of boundary-layer thickness, and the boundary layer is affected by centrifugal force which acts to remove the boundary layer from certain locations of the blade. Hence it may be stated that radially ending vanes, or vanes which easily permit complete removal of the boundary layer due to centrifugal force, can have considerably larger values of the local pressure gradients before stalling occurs. On the other hand, impellers with backward leading blades, or vane shapes which do not permit removal of the boundary layer by centrifugal force but only a relocation of the boundary layer, are much more subject to stalling, and frequently, in units with small blade exit angle, stalling occurs before pulsation (11). The analysis of the velocity distribution also leads to the conclusion that impellers of maximum efficiency should, within certain limits, have fewer blades, thus increasing the Reynolds number but decreasing stability.

Finally, the flow in any machine is not frictionless but does follow the laws of an imperfect fluid. However, with the knowledge of the local velocity and pressure gradients, it should be possible to make better predictions about the behavior of the boundary layer and secondary flows. The knowledge of pressure gradients permits the application of the analysis of flow, including friction, as shown by J. R. Weske (12) and Goldstein (13), to these impellers.

The proposed method is applicable to mixed-flow compressors and to radial and mixed-flow turbines as well.

ACKNOWLEDGMENT

The author is deeply indebted to Prof. H. W. Emmons of Harvard University and the Elliott Company, Jeannette, Pa., for their permission to show the results of the relaxation method in Figs. 2 and 3, and to the Continental Aviation and Engineering Corporation, Detroit, Mich., for their permission to publish Figs. 5 to 8. The author is also indebted to Prof. J. R. Weske of Brown University, for the derivation of, and permission to publish, Equation [16].

BIBLIOGRAPHY

1 "Steam and Gas Turbines," by A. Stodola, translation by L. C. Loewenstein, P. Smith, New York, N. Y., 1945.

2 "Die Kreiselpumpen," by C. Pfleiderer, Verlag von Julius Springer, Berlin, Germany, 1932.

3 "Fluid Mechanics of Turbo-Machinery," by G. F. Wislicenus, McGraw-Hill Book Company, Inc., New York, N. Y., 1947.

4 "Theory of Elasticity," by S. Timoshenko, McGraw-Hill Book Company, Inc., New York, N. Y., 1934.

5 "Resistance of Materials," by F. B. Seely, second edition, John Wiley & Sons, Inc., New York, N. Y., 1935.

6 "Diagrams for Calculation of Airfoil Lattices," by A. Betz, NACA Technical Memorandum No. 1022, 1942.

7 "Calculation of Rotor Blades," by A. Betz and I. Flugge-Lotz, *Ingenieur Archiv.*, vol. 9, 1938, p. 486.

8 "Zum Entwurf dichtstehender Schaufelgitter," by J. Ackeret, *Schweizerische Bauzeitung*, vol. 120, August, 1942, p. 103.

9 "Aerodynamic Theory," by W. F. Durand, editor in chief, Durand Reprinting Committee, California Institute of Technology, vol. 1, 1943, p. 209.

10 "Flow Through a Two-Dimensional Centrifugal Impeller With Backward Leading Vanes," by H. W. Emmons, unpublished report to the Elliott Company, Jeannette, Pa., February, 1945.

11 "Investigation of Flow in a Centrifugal Pump," by K. Fischer, NACA Technical Memorandum No. 1089, 1946.

12 "Investigation of the Flow in Curved Ducts at Large Reynolds Numbers," by J. R. Weske, *Journal of Applied Mechanics*, Trans. ASME, vol. 70, 1948, p. A-344.

13 "Modern Developments in Fluid Dynamics," by S. Goldstein, Oxford University Press, New York, N. Y., 1938.

Possibilities of the Regenerative Steam Cycle at Temperatures Up to 1600 F

By P. H. KNOWLTON[1] and R. W. HARTWELL[2]

The regenerative-steam-cycle heat-rate gains that may be realized at temperatures up to 1600 F are presented in this paper. These gains are calculated for a theoretical cycle and also for a practical cycle wherein such losses as extraction-piping pressure drop, heater-terminal temperature differences, and the like, are considered. An economic evaluation of the anticipated turbine heat-rate differences for various throttle conditions is presented. This evaluation includes such factors as fuel costs, load characteristics, auxiliary-power requirements, boiler efficiencies, and annual fixed charges. A method of comparing the heat-rate gains due to higher steam temperatures with those made possible by resuperheating is provided.

THE purpose of this paper is to present the results of a study of the theoretical and practical possibilities of the regenerative steam cycle at throttle temperatures up to 1600 F. It also presents an economic evaluation of these gains which indicates the amount of capital investment which could be justified for the installation of high-temperature power-generating equipment.[3]

As the cost of fuel increases, it becomes more important to evaluate the savings which might be effected by increasing the steam temperatures in the power plant of the future. Because of the wide general interest in this problem, the ASME Special Research Committee on High Temperature Steam Generation requested the authors to prepare a paper covering (1) the probable thermal gains by the use of high-temperature steam in the regenerative cycle, and (2) the possible fuel savings that might result.

The use of steam for electric power generation has been characterized by a fairly steady increase in the steam temperature. This has made possible steady gains in the thermal efficiency of steam power plants. The increase in maximum steam temperatures used in power plants constructed during the past 45 years is shown in Fig. 1. This curve shows that the temperature has increased an average of 12 F per year. Perhaps more important is that the temperatures increased in steps as new high-temperature materials became available. During the past 20 years, temperatures have increased faster than the average rate of 12 F per year.

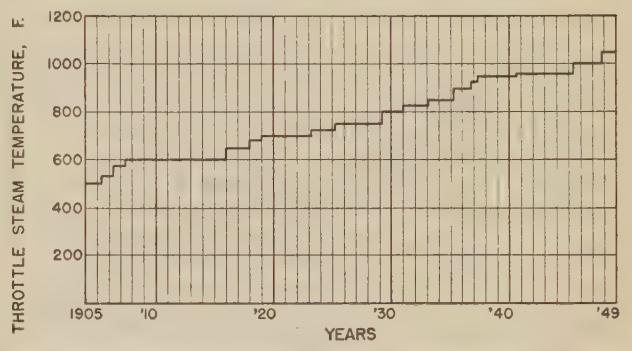

Fig. 1 Maximum Throttle Steam Temperatures for Past 45-Year Period

Theoretical Possibilities at Higher Temperatures

Selvey and Knowlton[4] published theoretical regenerative-steam-cycle heat rates for temperatures up to 1200 F and pressures up to 3200 psia. To facilitate a comparison over a wide range of pressure-temperature conditions, these data have been extended herein to 1600 F over the higher range of pressures, using the same theoretical cycle. As stated in the Selvey and Knowlton paper, the heat rates are for a regenerative steam cycle of the following component parts:

1 A turbine, having no mechanical losses, through which steam is expanded at constant entropy (engine efficiency is 100 per cent).

2 A regenerative feedwater system having an infinite number of bled-steam heaters heating to the saturation temperature, corresponding to the throttle steam pressure, and with zero terminal difference between the saturation temperature of the bled steam and the temperature of the feedwater leaving the heater, even when superheat is present in bled steam, and an attendant feed pump of 100 per cent efficiency with each heater to step up the feedwater pressure to the level of the next higher heater.

3 An electric generator of 100 per cent efficiency, which supplies, without line loss, the boiler feed pumps.

4 A steam generator of 100 per cent efficiency, in which blowdown, soot-blowing losses, etc., are zero.

Since energy required to drive fans, fuel equipment, general services, and so forth, is considered zero in a theoretical cycle, auxiliary-power usage other than that required for the boiler feed pumps, as described in item (2), is not included.

The theoretical heat rates are given in Table 1 and are presented in curve form in Fig. 2. This information shows that there is a steady improvement in the theoretical cycle economy with higher steam temperatures, but that the rate of improvement is diminishing as the temperatures are increased. Fig. 3 presents the theoretical heat-rate gains on a percentage basis with the 1250 psia-950 F throttle condition as a base. These curves provide a means of comparing theoretical and practical heat rates. The latter are discussed in the following section.

[1] Thermodynamic Engineer, Turbine Divisions, General Electric Company, Schenectady, N. Y. Mem. ASME.

[2] Engineer, Mechanical Engineering Division, Engineering Department, The Detroit Edison Company, Detroit, Mich. Jun. ASME.

[3] The data on steam in all calculations are from "Thermodynamic Properties of Steam," by J. H. Keenan and F. G. Keyes, John Wiley & Sons, Inc., New York, N. Y., 1936.

Contributed by the Research Committee on High Temperature Steam Generation, Joint ASTM-ASME Committee on Effect of Temperature on the Properties of Metals, and Power and Heat Transfer Divisions and presented at the Annual Meeting, New York, N. Y., November 27–December 2, 1949, of The American Society of Mechanical Engineers.

Note: Statements and opinions advanced in papers are to be understood as individual expressions of their authors and not those of the Society. Paper No. 49—A-33.

[4] "Theoretical Regenerative-Steam-Cycle Heat Rates," by A. M. Selvey and P. H. Knowlton, Trans. ASME, vol. 66, 1944, pp. 489–500; discussion, pp. 501–512.

TABLE 1 THEORETICAL REGENERATIVE STEAM-CYCLE HEAT RATES IN BTU PER KWHR
(1 In. Hg abs Exhaust Pressure)

Throttle pressure, psia	Throttle temperature – 900 F	950 F	1000 F	1100 F	1200 F	1400 F	1600 F
1000	7095		7993	6896	6802	6599	6412
1250	6912	6867[a]	6821	6729	6637	6457	6285
1450	6792		6707	6620	6529	6358	6197
2000	6542		6464	6384	6307	6156	6016
2500	6378		6306	6232	6161	6020	5892
3000	6246		6176	6109	6042	5912	5788

[a] Base condition assumed in Fig. 3.

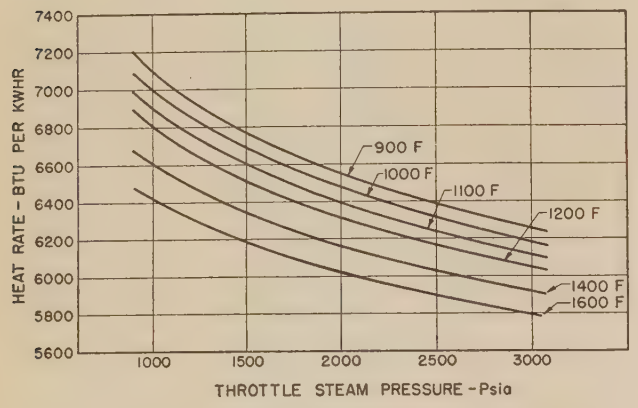

FIG. 2 THEORETICAL REGENERATIVE STEAM-CYCLE HEAT RATES

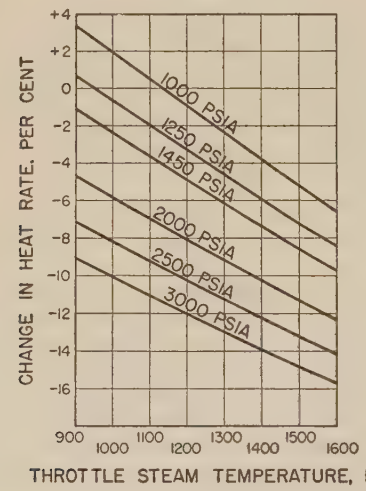

FIG. 3 PER CENT CHANGE IN THEORETICAL CYCLE HEAT RATE VERSUS INITIAL TEMPERATURE
(Base condition, 1250 psia, 950 F, 1 in. Hg abs exhaust pressure.)

PRACTICAL POSSIBILITIES AT HIGHER TEMPERATURES

Fig. 4 shows comparative per cent change in regenerative-cycle heat rates which are considered practical from the design and operating standpoint. These heat-rate changes, computed for the same high-temperature and pressure range as was selected for the theoretical heat-rate calculations, include the effects of such losses as extraction-piping pressure drop, heater-terminal temperature differences, etc. From a specified heat rate for a particular turbine generator, the heat rate for any other condition may be calculated with the data included in Fig. 4.

As in Fig. 3, the base steam conditions chosen are 1250 psia, 950 F. The per cent change in heat rate from this base condition to any other condition may therefore be read directly. If it is desired to obtain correctly the difference in heat rate between any other two sets of steam conditions in terms of the heat rate at one of these conditions, the difference, as read from Fig. 4, must be corrected for the change in base. For example, if we wish to get the difference between heat rates at 1450 psia, 1250 F and at 1450 psia, 1000 F, in terms of the heat rate at 1450 psia, 1000 F, this difference is

$$\frac{7.9 - 2.4}{1 - \frac{(2.4)}{(100)}} = \frac{5.5}{0.976} = 5.6 \text{ per cent}$$

Practical Cycle Assumptions. In making the calculations to

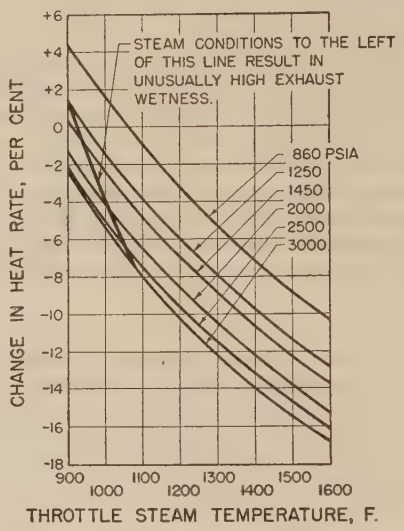

FIG. 4 PER CENT CHANGE IN PRACTICAL CYCLE HEAT RATE VERSUS INITIAL TEMPERATURE
(Base condition, 1250 psia, 950 F, 1 in. Hg abs exhaust pressure.)

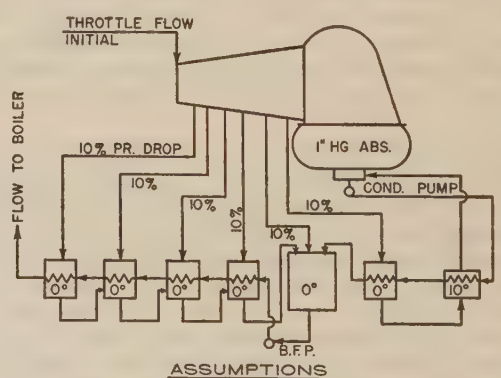

ASSUMPTIONS

1 - TERMINAL DIFFERENCES AS INDICATED
2 - 10% PRESSURE DROPS FROM STAGE TO HEATER

3 - STEAM PRESS.	860	1250	1450	2000	2500	3000
4 - B.F.P. DISCH. PRESS.	1000	1450	1700	2300	2900	3450
5 - ENTHALPY RISE IN B.F.P., BTU/LB.	4.1	6.3	7.6	10.3	12.9	15.4
6 - NO. OF HEATERS (CHANGING NUMBER OF H.P. HEATERS)	4	5	6	7	9	10
7 - BOILER FEED TEMP., F.	380	434	458	516	556	590

8 - ENTHALPY RISE IN CONDENSATE PUMP 0.6 B.T.U./LB.

FIG. 5 PRACTICAL CYCLE HEATER ARRANGEMENT FOR HEAT-RATE CALCULATIONS

arrive at the values plotted in Fig. 4, the following assumptions have been made:

1 The cycle arrangement and associated apparatus have been assumed to be as shown in Fig. 5 which presents the same arrange-

ment as was used by Harris and White.[5] The present calculations have been extended to higher temperatures and pressures than those assumed by Harris and White and are based upon somewhat lower boiler feedwater temperatures. Power required to drive the boiler feed pump has been deducted from the generator terminal output.

2 As was done in the Harris and White paper, turbine and generator efficiencies have been assumed to correspond to those obtained in present-day turbine generators. The turbine-generator efficiency assumptions correspond to those made by Warren and Knowlton.[6] This implies that at temperatures above present-day levels, new features of turbine design, or new materials, or both, must be developed if the general level of efficiency obtained in the past is to be maintained.

3 The exhaust loss from the turbine has been assumed to be a constant fraction of the turbine power output for all steam conditions.

4 It is assumed that the turbine-generator output is about 100,000 kw. This must be borne in mind particularly when comparing the heat rates at various initial pressures, since turbines of smaller capacities than 100,000 kw probably would show poorer relative performance at the higher pressures.

Steam Flows. Throttle and condenser steam rates, based on the practical cycle assumptions, have been computed to indicate the relative size of the generating equipment. The throttle and

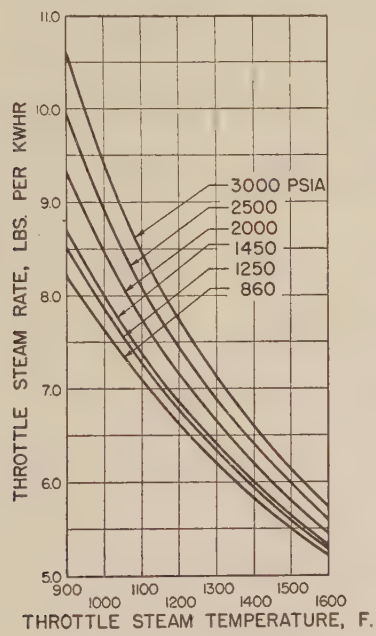

Fig. 6 Throttle Steam Rate Versus Initial Temperature (1 in. Hg abs exhaust pressure.)

condenser steam rates are presented in Figs. 6 and 7, respectively. These are shown on the basis of the generator-terminal output, whereas the heat-rate change curves, Fig. 4, show the net change after deduction of boiler-feed-pump power from the generator-terminal output.

Heat-Rate-Difference Evaluation

In considering the merits of one steam condition over another, it is desirable to evaluate the anticipated difference in heat rates. Because the practical heat rates represent results which at present appear possible at the higher steam conditions, these anticipated heat rates were used in this evaluation rather than the theoretical heat rates.

Basic Factors. The basic factors included in this evaluation are the cost of fuel, load characteristics, auxiliary-power requirements, boiler efficiency, turbine heat rates, and annual fixed charges on plant investment. Table 2 presents the results of an evaluation of heat-rate differences wherein a base condition of 1250 psia, 950 F has been used for comparing all of the other conditions. The figures shown in Table 2 represent the additional investment in dollars over the cost of 100,000 kw of 1250 psia 950 F capacity that is justified by the differences in heat rates. In computing the data it was assumed that plant availability and operating and maintenance personnel would be the same in all cases. No attempt was made to allow for possible differences in the extent of maintenance required.

Cost of Fuel. A 10-cent to 35-cent per million Btu fuel-cost range has been covered in the evaluation.

Load Characteristics. An annual plant-factor variation from 50 to 80 per cent has been included in the tabulation. The annual plant factor is the ratio of the kilowatthours generated on the machine in a year to the product of the kilowatt nameplate rating times 8760.

Auxiliary-Power Requirements. The following types of pulverized-coal-fired boilers were assumed in computing fan and mill power requirements.

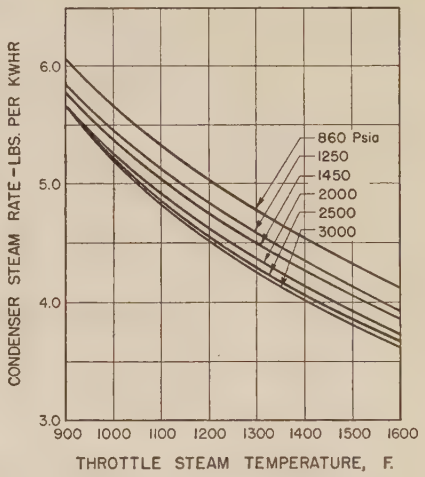

Fig. 7 Condenser Steam Rate Versus Initial Temperature

(*a*) For throttle pressures up to and including 2000 psia; natural-circulation boilers.

(*b*) For 2500 psia throttle pressure; steamotive-cycle boilers with recirculating pumps which handle 130 per cent of steam flow.

(*c*) For 3000 psia throttle pressure; once-through forced-circulation-cycle boilers.

Allowances for miscellaneous auxiliary-power demands were included in all cases.

Boiler Efficiency. A boiler manufacturer indicated that even with feedwater temperatures approaching 600 F on these high-pressure high-temperature boilers, the exit-gas temperature could be held to about 300 F. Assuming pulverized-coal boilers operating with an average grade of coal, it was estimated that boiler efficiencies would vary from 87.7 to 88.8 per cent, depending upon the feedwater temperature.

[5] "Developments in Resuperheating in Steam Power Plants," by E. E. Harris and A. O. White, Trans. ASME, vol. 71, 1949, pp. 685.

[6] "Relative Engine Efficiency Realizable From Large Modern Steam-Turbine Generator Units," by G. B. Warren and P. H. Knowlton, Trans. ASME, vol. 63, 1941, pp. 125–135.

TABLE 2 EVALUATION OF HEAT-RATE DIFFERENCES: ADDITIONAL JUSTIFIED INVESTMENT PER 100,000 KW OF CAPACITY OVER COST OF 1250 PSIA, 950 F PLANT

(Cost figures in thousands of dollars)

	Coal Cost Cents per Million Btu	1250 Psia				1450 Psia				2000 Psia				2500 Psia				3000 Psia			
		Annual Plant Factor--Per Cent				Annual Plant Factor--Per Cent				Annual Plant Factor--Per Cent				Annual Plant Factor--Per Cent				Annual Plant Factor--Per Cent			
		50	60	70	80	50	60	70	80	50	60	70	80	50	60	70	80	50	60	70	80
900 F	10	- 61	- 74	- 86	- 98	- 16	- 19	- 22	- 25	62	74	86	99	97	116	136	155	106	127	148	169
	15	- 92	- 110	- 129	- 147	- 24	- 28	- 33	- 38	93	111	130	148	145	174	203	232	158	190	222	253
	20	- 123	- 147	- 172	- 196	- 32	- 38	- 44	- 50	123	148	173	198	194	232	271	310	211	253	296	338
	25	- 153	- 184	- 215	- 245	- 39	- 47	- 55	- 63	154	185	216	247	242	290	339	387	264	317	369	422
	30	- 184	- 221	- 258	- 295	- 47	- 57	- 66	- 76	185	222	259	296	290	348	407	465	317	380	443	507
	35	- 215	- 258	- 301	- 344	- 55	- 66	- 77	- 88	216	259	303	346	339	407	474	542	369	443	517	591
1000 F	10	59	71	83	95	108	129	151	172	183	220	256	293	227	272	318	363	242	291	339	388
	15	89	106	124	142	162	194	226	259	275	330	384	439	340	408	476	544	363	436	509	581
	20	118	142	166	189	215	259	302	345	366	439	513	586	454	544	635	726	484	581	678	775
	25	148	177	207	237	269	323	377	431	458	549	641	732	567	681	794	907	606	727	848	969
	30	177	213	248	284	323	388	453	517	549	659	769	879	681	817	953	1,089	727	872	1,017	1,163
	35	207	248	290	331	377	453	528	603	641	769	897	1,025	794	953	1,112	1,270	848	1,017	1,187	1,356
1100 F	10	169	203	237	270	213	255	298	341	289	347	405	463	342	410	478	546	357	428	499	570
	15	254	304	355	406	319	383	447	511	434	520	607	694	512	615	717	820	535	642	749	856
	20	338	406	473	541	426	511	596	681	578	694	809	925	683	820	957	1,093	713	856	998	1,141
	25	423	507	592	676	532	639	745	851	723	867	1,012	1,156	854	1,025	1,196	1,367	891	1,070	1,248	1,426
	30	507	609	710	811	639	766	894	1,022	867	1,041	1,214	1,388	1,025	1,230	1,435	1,640	1,070	1,284	1,497	1,711
	35	592	710	828	947	745	894	1,043	1,192	1,012	1,214	1,416	1,619	1,196	1,435	1,674	1,913	1,248	1,497	1,747	1,997
1200 F	10	259	311	362	414	306	367	428	489	381	458	534	610	430	516	602	688	459	551	643	735
	15	388	466	544	621	459	550	642	734	572	687	801	916	645	774	903	1,032	689	827	965	1,103
	20	518	621	725	828	611	734	856	978	763	916	1,068	1,221	860	1,032	1,204	1,376	919	1,103	1,287	1,470
	25	647	777	906	1,035	764	917	1,070	1,223	954	1,144	1,335	1,526	1,075	1,290	1,505	1,720	1,149	1,378	1,608	1,838
	30	777	932	1,087	1,243	917	1,101	1,284	1,467	1,144	1,373	1,602	1,831	1,290	1,548	1,807	2,065	1,378	1,654	1,930	2,205
	35	906	1,087	1,268	1,449	1,070	1,284	1,498	1,712	1,335	1,602	1,869	2,136	1,505	1,807	2,108	2,409	1,608	1,930	2,251	2,573
1400 F	10	427	513	598	684	470	564	659	753	541	649	757	865	593	712	830	949	626	752	877	1,002
	15	642	769	898	1,026	706	847	988	1,129	811	974	1,136	1,298	890	1,067	1,245	1,423	940	1,127	1,315	1,503
	20	855	1,026	1,197	1,368	941	1,129	1,317	1,505	1,082	1,298	1,515	1,731	1,186	1,423	1,661	1,898	1,253	1,503	1,754	2,004
	25	1,069	1,282	1,496	1,710	1,176	1,411	1,646	1,881	1,352	1,623	1,893	2,164	1,483	1,779	2,076	2,372	1,566	1,879	2,192	2,505
	30	1,282	1,539	1,795	2,052	1,411	1,693	1,976	2,258	1,623	1,947	2,272	2,596	1,779	2,135	2,491	2,847	1,879	2,255	2,631	3,006
	35	1,496	1,795	2,095	2,394	1,646	1,976	2,305	2,634	1,893	2,272	2,651	3,029	2,076	2,491	2,906	3,321	2,192	2,631	3,069	3,507
1600 F	10	564	676	789	902	605	726	847	968	675	810	946	1,081	724	869	1,014	1,158	754	905	1,055	1,206
	15	846	1,015	1,184	1,353	908	1,090	1,271	1,453	1,013	1,216	1,418	1,621	1,086	1,303	1,520	1,738	1,131	1,357	1,583	1,809
	20	1,127	1,353	1,578	1,804	1,211	1,453	1,695	1,937	1,351	1,621	1,891	2,161	1,448	1,738	2,027	2,317	1,508	1,809	2,111	2,412
	25	1,409	1,691	1,973	2,255	1,513	1,816	2,118	2,421	1,688	2,026	2,364	2,702	1,810	2,172	2,534	2,896	1,884	2,261	2,638	3,015
	30	1,691	2,029	2,367	2,706	1,816	2,179	2,542	2,905	2,026	2,431	2,837	3,242	2,172	2,607	3,041	3,475	2,261	2,714	3,166	3,618
	35	1,973	2,367	2,762	3,157	2,119	2,542	2,966	3,390	2,364	2,837	3,309	3,782	2,534	3,041	3,548	4,055	2,638	3,166	3,694	4,221

Turbine Heat Rates. Turbine heat-rate differences represented in Fig. 4, which are based on the practical values, were used in the evaluation.

Annual Fixed Charges. An annual fixed-charge rate of 10 per cent was assumed in computing the justified additional investments. The investment figures shown in Table 2 may be adjusted for other fixed-charge rates as follows:

$$\text{Investment from Table 2} \times \frac{0.10}{\text{New fixed charge rate}} = \text{adjusted investment}$$

Example. An example will illustrate the use of Table 2.

Throttle conditions to be compared: 1450 psia, 1000 F
3000 psia, 1400 F

Assumptions:

Coal cost	20 cents per million Btu
Annual plant factor	60 per cent
Fixed-charge rate	10 per cent

Additional investment figures from Table 2:

1450 psia, 1000 F	$ 259,000
3000 psia, 1400 F	1,503,000

The amount that could be spent for 100 mw of 3000 psia, 1400 F capacity over the cost of a 1450 psia, 1000 F installation is

$$\$1,503,000 - 259,000 = \$1,244,000$$

High Steam Temperatures Versus Resuperheating

It is of interest to compare the heat-rate gains resulting from higher steam temperatures with those made possible by resuperheating. An approximate comparison may be made directly by comparing gains shown in Fig. 4 with various charts by Harris and White, and by Reynolds.[7] These two references do not exactly agree on the gain due to reheat, presumably because of differences in the assumptions made by the authors in setting up their calculations.

The assumptions made by Harris and White differ from those made in this paper on the following points:

1 The boiler feed temperatures are lower in the present case than were assumed by Harris and White. This difference makes a minor change in the gain due to reheat. For the order of magnitude of the effect of this on the reheat gain, refer to Reynolds' paper.[8]

2 The heat-rate gains in Fig. 4 of the present paper are on the basis of a fixed percentage exhaust loss, whereas Harris and White assumed, in calculating their reheat gain, that their nonreheat machines had a 4.5 per cent exhaust loss and their reheat machine a lesser exhaust loss obtainable from keeping the same exhaust-end size and the same rating for their reheat turbine. The assumptions made by Reynolds regarding the exhaust loss as between reheat and nonreheat are not stated in his paper.

However, we are able in the present case to show the effect of considering either two cases:

(*a*) The use of a "constant percentage exhaust loss," regardless of throttle-steam conditions. In this case, as we proceed to higher throttle temperatures, the exhaust size per unit rating decreases, and the gains expected are as shown in Fig. 4.

(*b*) The use of a "constant size of exhaust per unit rating," regardless of throttle-steam conditions. In this case, the percentage exhaust loss decreases when throttle temperature increases, and a further gain results from this, over and above the gains indicated in Fig. 4. The magnitude of this change in exhaust loss can be calculated by the use of Fig. 8, if the exhaust loss at a base condition is known. For any two sets of steam conditions shown on Fig. 8, the ratio of exhaust-loss percentage is the ratio of the ordinates therein.

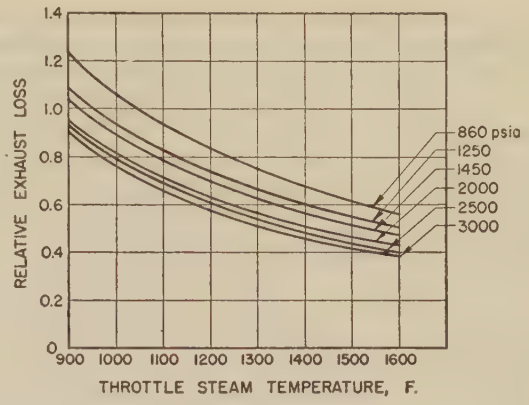

Fig. 8 Relative Exhaust Loss Versus Initial Temperature

An example will illustrate this point:

Assume a base condition of 1450 psia, 1000 F, and compare heat-rate gains due to the following:

1 Reheat to 1000 F at 450-psia reheat pressure.
2 Raising throttle temperature to 1250 F, nonreheat.

The answer to (1) can be read from Harris and White[9] as 5.2 per cent gain due to reheat, on the basis of constant exhaust size per unit rating.

The answer to (2) is given here in two parts, corresponding to the foregoing items (*a*) and (*b*), as follows:

(*a*) For constant percentage exhaust loss from Fig. 4, the gain at 1450 psia, 1000 F is 2.4 per cent, and at 1450 psia, 1250 F is 7.9 per cent. This gives a net gain of $\frac{7.9 - 2.4}{1 - 0.024} = 5.6$ per cent.

(*b*) For constant size of exhaust per unit rating, the relative exhaust-loss factors from Fig. 8 are as follows:

1450 psia, 1000 F	0.89
1450 psia, 1250 F	0.66

Revised exhaust-loss percentage from the assumed 4.5 per cent

$$4.5 \times \frac{0.66}{0.89} = 3.4 \text{ per cent}$$

Additional heat-rate gain due to exhaust-loss correction

$$4.5 - 3.4 = 1.1 \text{ per cent}$$

Total gain due to temperature increase

$$5.6 + 1.1 = 6.7 \text{ per cent}$$

It will be noted that the additional gain due to a change in the exhaust loss with fixed exhaust size depends directly upon the magnitude of the exhaust loss itself.

In comparing heat-rate gains due to higher steam temperatures with those made possible by resuperheating as presented by Harris and White, an exact evaluation should include the exhaust-loss correction described in item (*b*).

Conclusion

The curves for practical performance in Fig. 4 exhibit trends similar to those for the theoretical performance in Fig. 3. However it will be seen that the practical cycle shows less improve-

[7] "Reheating in Steam Turbines," by R. L. Reynolds, Trans. ASME, vol. 71, 1949, pp. 701–706.

[8] Ibid., Fig. 5.

[9] Footnote 5, Fig. 11.

ment with increasing pressure, and more improvement with increasing temperature, than the theoretical cycle. This relationship results from the fact that the practical turbine loses in efficiency with increasing pressure, and gains in efficiency with increasing temperature, while the theoretical turbine is assumed to be always 100 per cent efficient. These trends are not at all new; the only novel feature is the extrapolation of the trends to show what economies may be expected at temperatures up to 1600 F and pressures up to 3000 psia. It is believed that this has been done in a reasonable manner consistent with past practice.

Use of steam temperatures in power plants above the present maximum of 1050 F will depend on the development of suitable materials for the higher temperatures and on the design of acceptable equipment, particularly boilers and turbines, at a cost commensurate with the thermal gains to be realized. Since the costs of such materials and equipment are not presently available, this paper has presented only the total investment which could be justified on the basis of the thermal gains expected at the higher steam conditions.

Acknowledgment

The authors wish to express their appreciation for the advice and assistance of Mrs. Jean Harrison Higley and Mr. E. E. Harris of the General Electric Company, Mr. A. E. Raynor of the Babcock & Wilcox Company, and Messrs. H. A. Wagner and H. S. Walker of The Detroit Edison Company.

Discussion

W. E. Caldwell.[10] This paper indicates the thermal performance and evaluated savings obtainable by increasing initial steam temperature for the regenerative steam cycle. This cycle offers advantages over the reheat cycle, from the standpoint of simplicity, although it would result in more water in the exhaust stages for the same heat rate. It is indicated that an initial temperature of about 1170 F with the regenerative cycle would yield about the same heat rate as a 1000–1000 reheat cycle with the same initial pressure and heater arrangement. In the arrangement of heating stages and distribution of extraction heaters, the regenerative cycle offers more attractive thermal possibilities than the reheat cycle. The question of economic justification for the regenerative cycle above present temperature limits must await practical developments in high-temperature metallurgy.

In both the reheat and high-temperature regenerative cycles the improved performance results from utilization of a larger proportion of high-level heat than is presently employed, which aggravates surface-cleaning problems in the boiler plant, aside from metallurgical considerations.

In a 1000–1000 reheat cycle, the heat required to superheat the steam and reheat it is equivalent to a drop of about 1350 deg F in boiler gas temperature. To this must be added 600 deg F saturation temperature, 200 deg F for temperature difference or heat head between gas and steam, and 150 deg F for gas stratification, resulting in temperature zones above 2200 F in the superheater bank. With the equivalent regenerative cycle a lower gas temperature suffices, but in both cases the required gas temperature is substantially above 2000 F, which is the approximate rejection limit for some abundant low-cost coals with low-fusion ash. Improvements in design and disposition of the superheater surface should, in time, lessen the cleaning requirements and extend the range of acceptable fuels for high-temperature installations. Geographical location of plants and characteristics of available fuels will continue to be a major consideration in the choice of steam conditions.

[10] Staff Engineer, Consolidated Edison Company of New York, Inc., New York, N. Y. Mem. ASME.

This paper exemplifies our dependence upon the steam tables, and some comments on their use for the higher temperatures would be of interest. The upper temperature line on Mollier charts with the 1936 tables ends at 1200 F. Was a condition curve plotted for the expansions from the various initial temperature, or was some other procedure employed?

E. E. Harris.[11] This paper will be a very useful tool for the industry. The user will be able to compare the gains to be expected as well as the amount of additional money that may be justified for obtaining a gain in station economy.

This paper, together with the paper by E. E. Harris and A. O. White,[5] will give the user considerable information that may be used for determining the future trend in the power-plant field.

Fig. 4 of the paper was obtained from calculations that were made for the Harris and White paper with additional calculations made for the higher pressures and temperatures. The added calculations followed the same method as was used in the original paper, correcting for volume flow, pressure, and superheat, the superheat correction taking into account the change in moisture. It was assumed, in making the calculations and arriving at the gains to be obtained with higher pressures and temperatures, that materials will be available as well as design and ability to build such turbine units without sacrificing efficiency or gain.

At 1450 psia, 1000 F initial conditions, reheating to 1000 F will show a gain of approximately 5 per cent in station heat rate. If the same gain is to be obtained by operating at a higher initial temperature without reheat, the initial temperature will be about 1175 F. The 5 per cent gain in heat rate will justify an expenditure of $632,000 over 1450 psia, 1000 F nonreheat with a coal cost of 30 cents per million Btu and 60 per cent annual plant factor. It is felt that a reheat station will have a lower increment cost than the nonreheat plant with 1175 deg to obtain the same gain.

Sometime in the future, materials will be available as well as design and know-how for building units for the higher temperatures for nonreheat. When such information is available, reheating to the same initial temperature may be used with approximately the 5 per cent gain over the nonreheat plant.

A. E. Raynor.[12] The authors have made an interesting and useful survey which should be helpful to those who are looking forward to the time when they may find it desirable to go to higher pressures and higher temperatures. Dollar values have been established and given in Table 2, which indicate approximately how much may be spent economically for the higher pressures and higher temperatures.

The data are presented with the bases used in establishing the dollar values, so that corrections may be made readily by anyone wishing to modify these data and correct for conditions which may differ somewhat from those arbitrarily used by the authors. Any correction which the user may wish to make, such as a different value for fixed charges, annual plant factor, etc., can be made readily, the additional justified investment quickly determined, and proper design conditions established.

The authors have been wise in extending the pressures to 3000 psia and the temperatures to 1600 F, even though manufacturers are not now equipped with materials to satisfy, particularly, the higher temperatures. It may be that we are now in a similar situation to the designers of, say, 20 years ago, when a temperature of 1050 F appeared to be very far in the future. However, in about 20 years, temperatures have gone from something less than 800 F to 1050 F, and higher temperatures will be used when satisfactory materials are available. Inasmuch as the wall

[11] General Electric Company, Schenectady, N. Y.

[12] Executive Assistant, New York Proposition Division, The Babcock & Wilcox Company, New York, N. Y. Mem. ASME.

thickness of some of the present 2½-in. 18 Cr, 8 Ni-Cb tubes used in the hot end of superheaters designed for 2300 psia and 1050 F are 0.56 in. thick, leaving but little internal area for the flow of steam, it is quite obvious that temperatures much higher than 1050 F will call for metals with higher available stresses than those currently being used. Many engineers in the steel and allied industries are working on this problem, and time alone will tell when the better high-temperature materials will be available for use. When one considers the economies gained by the use of higher temperatures, it may be that some will find it desirable to use higher temperatures even at the risk of shorter life of the material in the hot portions of the superheater, piping, and turbines. Therefore earlier replacement of parts of the equipment than now contemplated may be economically justified.

The authors indicate that, based upon certain assumptions, $1,244,000 more may be spent for a 100,000-kw plant designed for 3000 psia, 1400 F than for a 1450 psia-1000 F installation. Using the same assumptions, $773,000 more may be spent for a 2500 psia-1200 F installation than a 1450 psia-1000 F unit. In either case a considerable amount of money is involved. This alternative example is used because metals are already available and being used in reheat designs for 2080 psi 1050 F and 1000 F reheat, also 1500 psia 1000 F-1000 F reheat. The latter is about equivalent in cycle efficiency to the nonreheat 2500 psia-1200 F unit.

This presumably accounts for several companies purchasing reheat units during the past few years, the steam conditions being about as follows:

1300 psia, 950 F and 950 F reheat
1500 psia, 1000 F and 1000 F reheat
2080 psia, 1050 F and 1000 F reheat

Design engineers have had and will continue to have problems where a considerable amount of judgment is required in determining the best pressure and temperature to satisfy the conditions of a given project. The data submitted in this paper should be helpful in future studies and encourage engineers and metallurgists to solve the material problem as rapidly as possible in order that higher temperature metals may be available for early use.

R. L. Reynolds.[13] In this paper the authors present the thermal advantages of high pressures and temperatures and point out the additional investment which can be justified by these reductions in fuel costs. Such a comparison with what are now considered established steam conditions (1250 psia, 950 F) will serve as a valuable guide for analyzing the benefits to be derived from these increased steam pressures and temperatures. It also offers a challenge to designers of steam generators and turbines to develop equipment to meet these advanced conditions.

Of particular interest are the curves in Fig. 4, which show the change in heat rates for pressures from 860 to 3000 psia and temperatures from 900 to 1600 F. We feel that the values given on these curves are consistent with past practice and are reasonable estimates of what can be expected in the future, provided developments in design and materials keep pace with increases in steam pressures and temperatures.

At the present time the maximum operating steam temperature on central-station turbines is 1050 F. Although operation at this temperature, in general, has been satisfactory, further successful operation should be experienced before extending this limit materially. In the meantime a thermal gain equivalent to about 175 deg F increase in throttle temperature can be realized by the use of the reheat cycle.

[13] Land Turbine Engineering, Central Station Turbine Section, Westinghouse Electric Corporation, South Philadelphia, Pa. Mem. ASME.

The authors refer to the writer's paper,[6] and point out that values for thermal improvement derived from the reheat cycle do not agree with those given by Harris and White,[5] due to differences in the assumptions made.

These differences in assumptions are as follows:

(*a*) The writer's comparisons were made upon the turbine alone. It was pointed out that additional advantages were obtained due to a reduction of from 15 to 18 per cent in boiler-feed-pump power, but this factor was not included. Power requirements for condenser and boiler auxiliaries are also reduced by the use of the reheat cycle.

(*b*) The writer's data were based upon 1.5 in. Hg abs exhaust pressure, as compared with 1.0 in. Hg used by Harris and White. The increased exhaust pressure results in a smaller differential in the thermal advantages of the reheat cycle.

(*c*) The writer's values also were based upon a constant exhaust loss expressed in Btu per pound. It was pointed out that, if constant exhaust area for a given set of initial steam conditions were used, the 7 or 8 per cent decrease in exhaust volume would result in a decrease in exhaust loss and thus increase the thermal benefits from the reheat cycle.

When reduced to the same basis, the values given by Harris and White agree quite closely with the writer's.

The evaluation figures tabulated in the authors' paper have been based upon the assumption that equal reliability can be obtained for all sets of conditions. This may at first appear unjustified and certainly would be if the increased temperatures were attempted at this time, but, when operating experiences over a long period of time are studied, it is evident that the reliability of steam turbines is now higher than ever, despite a large increase in steam pressures and temperatures. Although each new step may result temporarily in some reduction in reliability until the problems associated with this advance are solved, we feel that, if these changes are made gradually and in a fundamentally sound manner, no decrease in reliability will be suffered.

L. B. Schueler.[14] The authors have performed an excellent service in projecting the useful data on steam-electric unit heat rates into the field of higher steam temperatures, even into the extremes where most of us will probably never see their practical realization. However they give us an important sense of direction and show that there are real possibilities if we do not accept half-way measures in many respects.

The problem of whether to adopt higher steam temperatures rapidly resolves itself into some simple but definite economic limitations. The extremely high cost of alloy materials suitable for higher temperatures is the heart of the problem. The turbine builders already have taken the big step in going to austenitic materials for the high-temperature portion of the 1050 F units. It should be possible to extend the application of these materials up to about 1200 F for turbine construction.

The superheater design, wherein maximum metal temperatures are usually about 100 deg F higher than the steam temperature, indicates a limit of about 1000 F for the lower-cost ferritic-alloy materials. Higher temperatures involve correspondingly greater quantities of costly austenitic-alloy tubing—all based upon present allowable stresses as established by the ASME Boiler Construction Code. These present allowable stresses, while presumably based on reasonably long life along with a substantial safety factor, often represent conditions of indefinite life, say, more than 40 years. In these cases, and there are many of them, an extremely high initial investment is made in materials which might be difficult to justify in the light of experience.

[14] Engineer, Mechanical Engineering Division, American Gas & Electric Service Corporation, New York, N. Y. Mem. ASME.

It is proposed that designers and users give consideration to the relative merits of designing superheater and reheater materials, particularly in the extreme high-temperature zones, with the deliberate intent that they shall have a limiting life, probably somewhere between 5 and 20 years. Careful studies of this proposal appear warranted, particularly in the light of substantial experience along these very lines in oil-cracking-still units. If studies indicate possible economic merit, then it becomes necessary to establish another set of higher allowable stresses, to be used in such applications, by the appropriate regulatory bodies.

On the basis of a double-stress standard, a preselected portion of a superheater or reheater could be built to long or short-life standards, as desired, with the manufacturer and purchaser working out the best over-all arrangement, and with the user being reconciled to periodic replacement of a small portion of the superheater or reheater. If it were limited to superheater and reheater tubing materials only, and up to a limiting tube diameter, the safety element would be kept adequately under control.

The ASME Special Research Committee on High Temperature Steam Generation is embarking on a broad program of research to investigate materials which are suitable for steam temperatures up to 1500 F.

It seems advisable that an analytical study of the proposed double-stress standard be made at once so that the research work can be planned more effectively. This study can and should be made jointly by manufacturers and users to arrive at the proper relationship of physical and economic limitations.

Authors' Closure

The authors agree with Mr. Caldwell and Mr. Harris in their finding that the data presented show that an increase by about 175 F in initial temperature gives a gain in heat rate equivalent to that obtainable from reheat, and that at present this gain is more economically obtained from reheat than from such a considerable increase in temperature.

The authors are grateful to Mr. Caldwell for inquiring as to how the turbine calculations were made. This point probably should have been more fully covered in the paper. The Keenan and Keyes Steam Table extends to 1600 F (the chart is plotted only to 1200 F) although very much skeletonized above 1200 F. It was necessary to extend the chart to 1600 F and fill in intermediate values between those given in the table by calculation. This was done by graphical means, using a large-scale plot of the constant-pressure specific heat to smoothly interpolate between table values. No extrapolation was necessary. The chart thus extended was used for plotting the turbine expansion lines, in accordance with the assumptions as stated in the paper.

Mr. Raynor's remarks concerning tube thicknesses presently required illustrate very well the necessity for stronger materials for very elevated temperatures. His suggestion that perhaps some parts should be considered as requiring more frequent replacement is interesting, but it is not clear that such considerations would result in any economic improvement.

The authors are also grateful for Mr. Reynolds' statements, both as to general corroboration of the findings of the present paper, and as to clarification of his own previous paper, reference 7. Further, the authors are in agreement with Mr. Reynolds' remarks concerning relative reliability.

Mr. Schueler's statements are quite to the point. The high cost of satisfactory materials, according to present knowledge, is the main reason why higher temperatures are not presently used. It seems to be too early to judge effectively whether stresses currently allowed are overconservative. However, the company with which Mr. Schueler is associated has for many years been building power plants using high temperatures and pressures, so their experience is very valuable.

Oil Holes and Grooves in Plain Journal Bearings

By S. A. McKEE[1] and H. S. WHITE,[1] WASHINGTON, D. C.

Data are presented showing the performance of plain journal bearings having various arrangements of oil holes and grooves operating in a four-bearing friction machine with forced-feed lubrication. Tests cover operation where the oil is fed through the bearing shell by means of five arrangements, including one, two, or four oil holes; one axial or one circumferential groove. Tests were also run with three arrangements for feeding oil from the center of a hollow shaft. These were one or two oil holes in the shaft, or one oil hole terminating in a flat on the surface of the shaft. Two clearance-diameter ratios were used with each arrangement. Test runs were made at constant speed and at a number of loads, which were unidirectional relative to the bearings. The data cover operation with one oil at one oil-inlet temperature and two speeds. In some of the tests the loads were increased until unstable lubrication was reached. The test results include the frictional characteristics, values of *ZN/P* at transition between stable and unstable lubrication, and data on thermal behavior and on oil flow. A summary of the general behavior of the various arrangements is given.

Nomenclature

The following nomenclature is used in the paper:

- D = journal diameter, in.
- L = bearing length, in.
- C = running clearance (difference between bearing diameter and journal diameter), in.
- W = total load acting on bearing, lb.
- P = W/LD = pressure on projected area of bearing, psi
- N = speed of journal, rpm
- F = tangential frictional force, lb
- f = F/W = coefficient of friction
- Z = absolute viscosity of lubricant at atmospheric pressure and bearing temperature, centipoises (cp)
- H_t = rate of heat supplied to one bearing from both entering oil and bearing friction, in-lb per min
- ΔT_b = temperature rise above ambient of loaded side of bearing shell (average of four bearings), deg F
- ΔT_0 = temperature rise above ambient of oil leaving ends of bearings (average of four bearings), deg F
- Q = rate of oil flow per bearing, cu in. per min
- ZN/P = generalized operating variable
- p = oil-feed pressure (corrected for drop between gage and bearings and for centrifugal force when oil is fed through shaft), psi

[1] National Bureau of Standards.

Contributed by the Special Research Committee on Lubrication and presented at the Spring Meeting, Washington, D. C., April 12–14, 1950, of The American Society of Mechanical Engineers.

Note: Statements and opinions advanced in papers are to be understood as individual expressions of their authors and not those of the Society. Manuscript received at ASME Headquarters, January 6, 1950. Paper No. 50—S-9.

Introduction

One of the problems in the lubrication of plain journal bearings is the method of admitting the oil to the bearing. The concept of the load-carrying film indicates the desirability of avoiding the use of oil holes or grooves which interfere with the normal development of hydrostatic pressure to support the load. In some bearing installations, however, it is not always possible to satisfy this requirement. With bearings where loads are fluctuating in both intensity and direction, it is sometimes impracticable to apply the oil to the unloaded side throughout the complete load cycle. Also in some cases, provision must be made for a continuous flow of oil to some other moving part.

The tests reported in this paper were made to determine the comparative performance of journal bearings having various arrangements of holes or grooves when using forced-feed lubrication under conditions where in each case the load was unidirectional on the bearing. The work comprised two separate series of tests. The first covers operation with three arrangements of oil holes and two types of oil grooves in the surface of the bearing. The second covers operation with three arrangements for feeding the oil from the center of a hollow shaft. Each of these arrangements is located at the axial center of the bearing.

This investigation was part of a research program on the lubrication of plain journal bearings which was conducted at the National Bureau of Standards with the financial support of the National Advisory Committee for Aeronautics.

Apparatus

Four-Bearing Friction Machine. The four-bearing friction machine used in this investigation has been described in a previous publication (1).[2] The complete apparatus is shown in Fig. 1, and the major elements of the machine disassembled in Fig. 2. The machine consists essentially of four similar test bearings enclosed in a housing and mounted on a common shaft. Loads are applied by hydraulic jacks which form the base of the housing. The complete unit of bearings and housing acts as a cradle dynamometer. The frictional torque is measured by a dynamometer scale acting through a torque arm fitted to the housing. An automatic device is provided in the hydraulic system to release the load under the high-torque conditions occurring near bearing seizure.

In the first series of tests, oil was fed to each bearing through conventional pipe and tubing, using flexible connections to the bearing housing. In the second series, the oil was fed to the end of the hollow shaft through a rotating joint. The lubricating system was provided with a vane pump having a variable-speed drive and a relief valve. Runs could be made at constant oil-feed pressure or at a constant rate of oil flow. The oil-feed line also was fitted with a filter consisting of two layers of sheet cellulose, electric heaters for controlling the oil-inlet temperature, and a flowmeter used chiefly for control purposes. Determinations of oil flow also were made by weighing the amount of oil that flowed for a given time interval from the housing outlet into a measuring vessel.

[2] Numbers in parentheses refer to the Bibliography at the end of the paper.

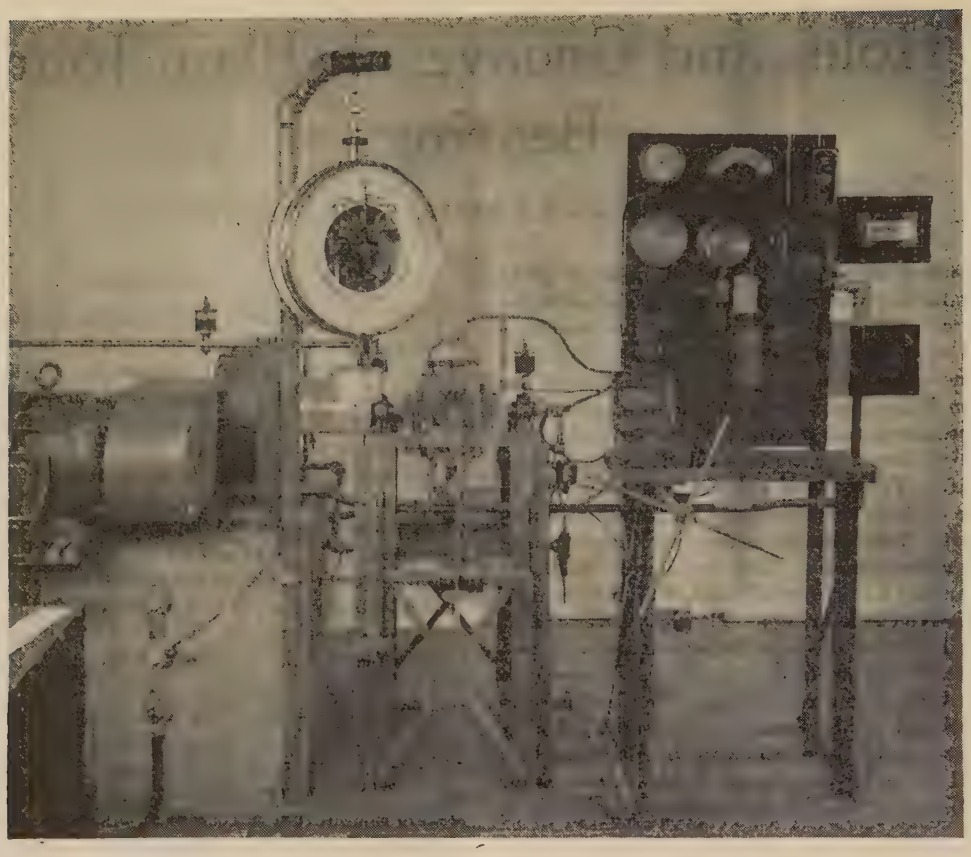

FIG. 1 FRICTION-MACHINE INSTALLATION

Operating temperatures were measured with copper-constantan thermocouples. One was fastened to the loaded side of each of the four bearings, and four thermocouples of equal resistance connected in parallel, were spaced around the shaft, in the oil streams at the end of each bearing.

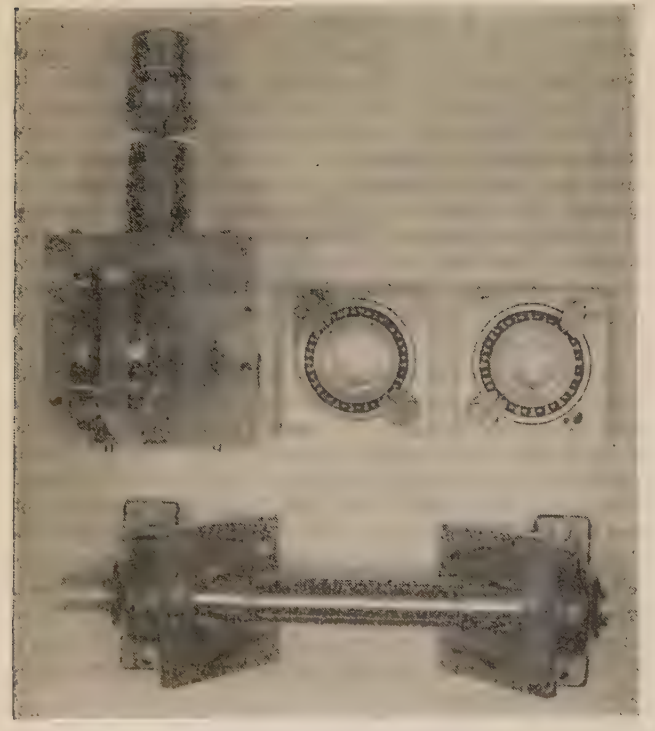

FIG. 2 FRICTION-MACHINE PARTS

Shafts and Bearings. One solid test shaft was used in all of the first series of tests. It was made of SAE 3115 steel, carburized, and heat-treated to a hardness of 55 Rockwell C. The three hollow test shafts, $^{27}/_{64}$ in. inside bore, used in the second series of tests, were made of SAE 4615 steel, carburized, and heat-treated to hardnesses ranging from 58 to 61 Rockwell C. The surface roughness of each shaft was measured at 90-deg intervals at each of the four journal positions.

The averages of the observations for each shaft ranged from 4 to 5 microinches (rms profilometer). The journal diameters were measured 90 deg apart at each of the four journals on each shaft. The observations of diameters were accurate to 0.00005 in. at 68 F.

The shaft used in the first series of tests had no holes or grooves. In the second series, the shaft used with bearing sets S31, and S51 (see Fig. 3), had one radial oil hole at the mid-point of each bearing. The holes were 0.125 in. in diam and were chamfered to a diameter of approximately 0.180 in. at the shaft surface. The one used with bearing sets S32 and S52 was similar, except that two holes 180 deg apart were used for each bearing. The shaft for bearing sets S33 and S53 was similar to the shaft with one hole per bearing, except that instead of a chamfer, a flat, $^{5}/_{8}$ in. long (axially) and $^{3}/_{16}$ in. wide (depth about 0.004 in.), was located symmetrically at the end of each hole. The edges of the chamfers and flats were stoned and polished to remove sharp edges.

The test bearings were solid steel sleeves with copper-lead linings conforming to Pratt and Whitney Aircraft specification 121. They were pressed in the bearing retainers, rough-bored in a lathe, pushed in the self-aligning ball-bearing swivels, and then

TABLE 1 ESSENTIAL DIMENSIONS OF SHAFTS AND BEARINGS

Design of oil feed	Bearing set	Length of bearing, L, inches	Avg diam of bearing, inches	Avg diam of shaft, D, inches	Avg clearance, C, inches	Diameter-clearance ratio, D/C	Length-diameter ratio, L/D
1 hole in bearing	31	1.275	2.0579	2.0548	0.0031	663	0.620
	51	1.275	2.0599	2.0548	0.0051	403	0.620
2 holes in bearing	32	1.275	2.0579	2.0548	0.0031	663	0.620
	52	1.275	2.0599	2.0548	0.0051	403	0.620
Axial groove in bearing	33	1.275	2.0579	2.0548	0.0031	663	0.620
	53	1.275	2.0599	2.0548	0.0051	403	0.620
4 holes in bearing	34	1.275	2.0579	2.0548	0.0031	663	0.620
	54	1.275	2.0599	2.0548	0.0051	403	0.620
Circum groove in bearing	35	1.125*	2.0579	2.0548	0.0031	663	0.547*
	55	1.125*	2.0599	2.0548	0.0051	403	0.547*
1 hole in shaft	S31	1.275	2.0580	2.0549	0.0031	663	0.620
	S51	1.275	2.0600	2.0549	0.0051	403	0.620
2 holes in shaft	S32	1.275	2.0579	2.0548	0.0031	663	0.620
	S52	1.275	2.0599	2.0548	0.0051	403	0.620
1 hole with flat in shaft	S33	1.275	2.0577	2.0546	0.0031	663	0.620
	S53	1.275	2.0597	2.0546	0.0051	403	0.620

*Allowance is made for circumferential groove.

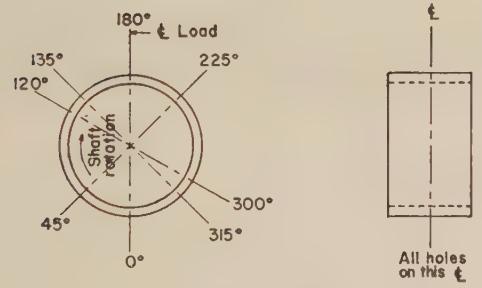

Sets 31 & 51, oil hole at 0°
Sets 32 & 52, oil holes at 120° & 300°
Sets 34 & 54, oil holes at 45°, 135°, 225°, & 315°
All holes 0.125" diameter, chamfered to 0.18" diameter at edge

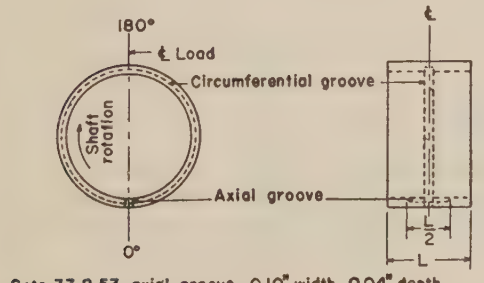

Sets 33 & 53, axial groove, 0.10" width, 0.04" depth
Sets 35 & 55, circumferential groove, 0.150" width, 0.075" depth

FIG. 3 ARRANGEMENTS OF OIL HOLES AND GROOVES IN BEARINGS

finished to size with a special type of bearing reamer having a single cutting edge. With each bearing, determinations of four diameters 45 deg apart were made at each of three axial positions, one at the center, and one near each end. Bearings having circumferential grooves were measured on each side of the groove as well as at the ends. These measurements were accurate to 0.0001 in. at 68 F.

Bearings with one, two, or four oil holes, or with one circumferential or one axial groove were used in the first series of tests. Sketches showing the details of these arrangements are given in Fig. 3. With any of these arrangements each hole or groove was connected with the source of oil supply. In the second series of tests, the bearings had plain cylindrical surfaces. Two sets of bearings of different clearance were run for each type of oil feed.

The essential dimensions of the shafts and bearings are given in Table 1.

LUBRICANT

The oil used in these tests was an SAE 20 motor oil having an absolute viscosity of 70.8 centipoises at 100 F and 8.12 centipoises at 210 F.

FRICTION DATA

Tests at High ZN/P. With each set of bearings, tests first were made in the region of stable lubrication at the higher values of ZN/P (see nomenclature) in order to obtain characteristic data with a minimum of change in bearing surface. Each test run was made at a constant speed with a number of constant loads which were successively increased at intervals during each run. The apparatus was "warmed up" before the start of each test run and the data were obtained with the bearings in a steady state of temperature distribution.

Friction data obtained in these tests are given in Figs. 4, 5, 6, 7, 8, 9, 10 and 11 for the eight oil-feed systems. These results cover operation at an oil-inlet temperature of 200 F, two speeds, 2030 and 3040 rpm, and a range of loads from approximately 300 to 3000 psi on the projected area. In these figures f, the coefficient of friction, is plotted against the operating variable ZN/P. The values of Z used are based on temperature observations obtained with the thermocouples on the loaded side of each bearing shell.

With the bearings having a circumferential groove, the effective area of the loaded side of the bearing is reduced, and in plotting the data shown in Fig. 8, the values of P used were based on the effective area (total area minus area of groove). The slopes of the curves would be somewhat less if P were based on the total projected area of the bearing as was the case with the curves for the other designs of bearings.

Lines representing the Petroff equation for concentric running (2) for the respective D/C ratios used are also shown in the figures. The experimental data for a given bearing can be represented by a straight line roughly of the same general slope but displaced toward greater values of f than is given by the Petroff line for a given D/C ratio. This general trend of the data is similar to that obtained in an earlier investigation (3) where it was shown that the friction of a journal bearing could be represented approximately by the equation $f = k(ZN/P)(D/C) + \Delta f$, where Δf was an L/D correction and represents the difference (approximately) between the experimental data and the Petroff equation.

For purposes of comparison, values of Δf at $ZN/P = 10$ and $ZN/P = 70$ for each set of bearings tested are given in Table 2. The table also lists the average value of Δf (over the range of ZN/P from 10 to 70) for each set, and the average value for each type of bearing (two D/C ratios). The latter values are used as

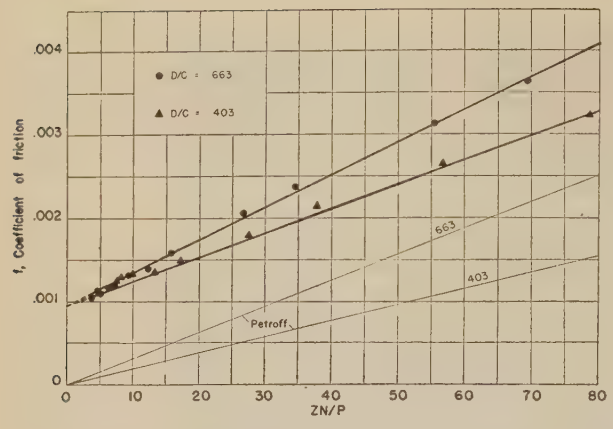

FIG. 4 FRICTION IN STABLE REGION FOR 2-IN. × 1¼-IN. COPPER-LEAD BEARINGS HAVING ONE OIL HOLE IN BEARING

(Operating at 2030 rpm with 15 cu in. per min oil flow, and 3040 rpm with 22.5 cu in. per min oil flow; SAE 20 oil at 200 F oil-inlet temperature.)

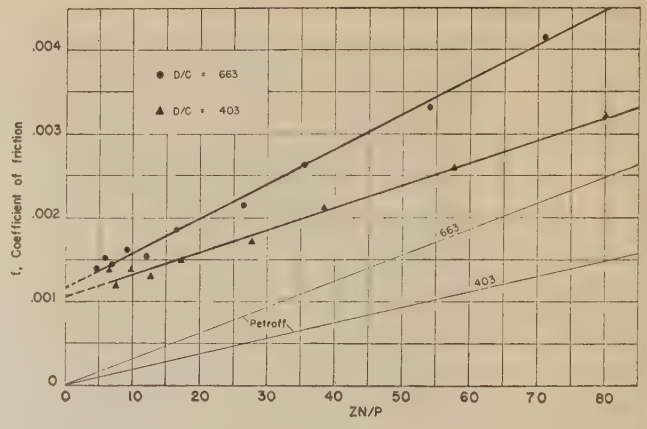

FIG. 5 FRICTION IN STABLE REGION FOR 2-IN. × 1¼-IN. COPPER-LEAD BEARINGS HAVING TWO OIL HOLES IN BEARING

(Operating at 2030 rpm with 15 cu in. per min oil flow, and 3040 rpm with 22.5 cu in. per min oil flow; SAE 20 oil at 200 F oil-inlet temperature.)

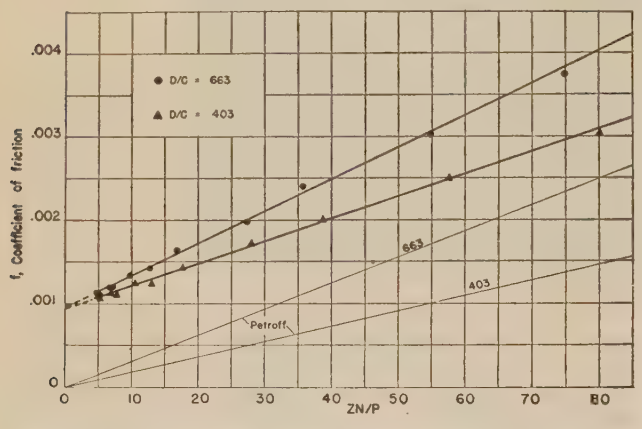

FIG. 6 FRICTION IN STABLE REGION FOR 2-IN. × 1¼-IN. COPPER-LEAD BEARINGS HAVING AN AXIAL GROOVE IN BEARING

(Operating at 2030 rpm with 15 cu. in. per min oil flow, and 3040 rpm with 22.5 cu in. per min oil flow; SAE 20 oil at 200 F oil-inlet temperature.)

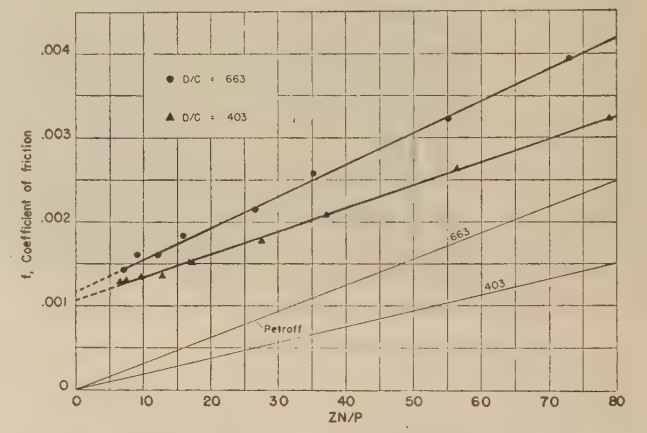

FIG. 7 FRICTION IN STABLE REGION FOR 2-IN. × 1¼-IN. COPPER-LEAD BEARINGS HAVING FOUR OIL HOLES IN BEARING

(Operating at 2030 rpm with 15 cu in. per min oil flow, and 3040 rpm with 22.5 cu in. per min oil flow; SAE 20 oil at 200 F oil-inlet temperature.)

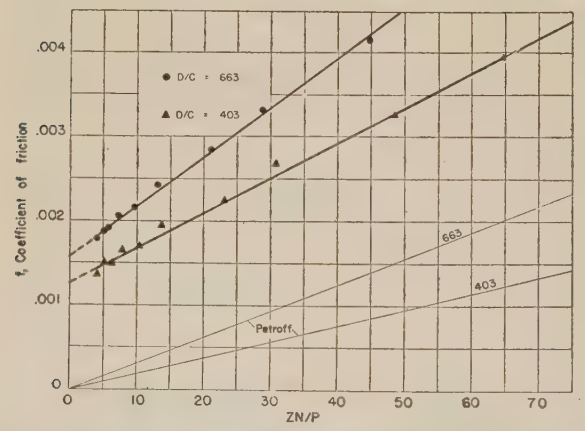

FIG. 8 FRICTION IN STABLE REGION FOR 2-IN. × 1¼-IN. COPPER-LEAD BEARINGS HAVING A CIRCUMFERENTIAL GROOVE IN BEARING

(Operating at 2030 rpm with 15 cu in. per min oil flow, and 3040 rpm with 22.5 cu in. per min oil flow; SAE 20 oil at 200 F oil-inlet temperature.)

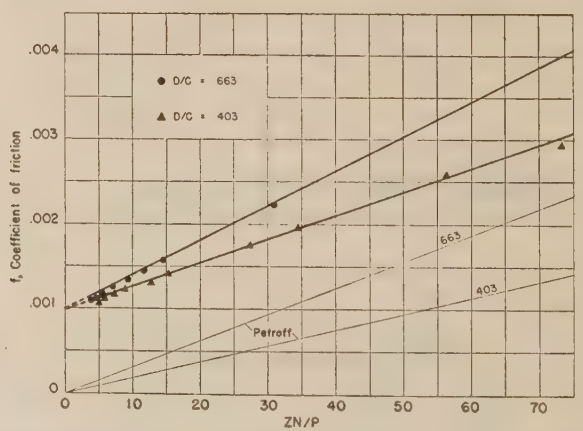

FIG. 9 FRICTION IN STABLE REGION FOR 2-IN. × 1¼-IN. COPPER-LEAD BEARINGS WITH ONE OIL HOLE IN SHAFT

(Operating at 2030 and 3040 rpm, 15 cu in. per min oil flow, SAE 20 oil at 200 F oil-inlet temperature.)

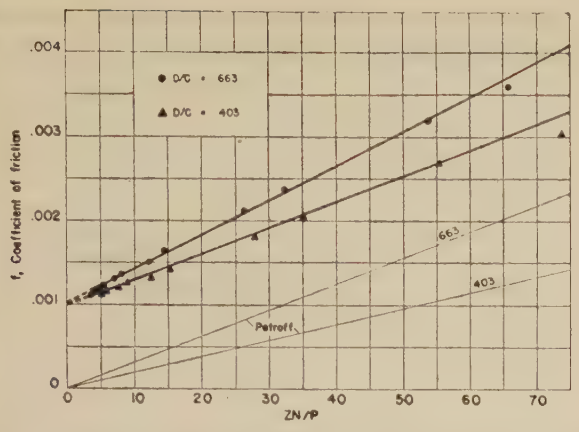

FIG. 10 FRICTION IN STABLE REGION FOR 2-IN. × 1¼-IN. COPPER-LEAD BEARINGS WITH TWO OIL HOLES IN SHAFT
(Operating at 2030 and 3040 rpm, 15 cu in. per min oil flow, SAE 20 oil at 200 F oil-inlet temperature.)

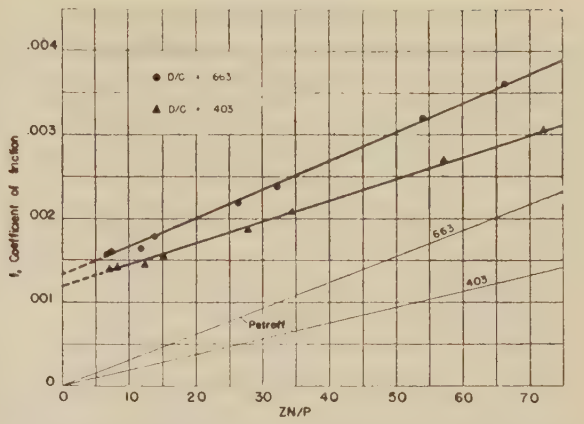

FIG. 11 FRICTION IN STABLE REGION FOR 2-IN. × 1¼-IN. COPPER-LEAD BEARINGS WITH ONE HOLE WITH FLAT IN SHAFT
(Operating at 2030 and 3040 rpm, 15 cu in. per min oil flow, SAE 20 oil at 200 F oil-inlet temperature.)

a basis for rating the different types of bearings from the standpoint of friction. Since the differences between some types are within the probable experimental error, the ratings are given in three general groups: Group A, bearings of relatively low friction; B, intermediate; and C, high.

One of the most marked effects shown by the data given in this table is the relatively high friction obtained with the bearings having a circumferential groove, where the bearing is divided into two narrow bearing surfaces. This confirms the results obtained by Clayton (4). It also is in agreement with previously published data obtained at the National Bureau of Standards (3), which indicate that for L/D ratios less than unity, a decrease in L/D increases the friction. The data for this type of bearing were based on the effective area rather than the total area. If the latter is considered, the average value of Δf for this type of bearing would become 0.00217 instead of 0.00240 as given in Table 2.

The data for the bearings having two oil holes and four oil holes, of which one and two holes, respectively, were on the loaded side of the bearing, showed a slightly higher friction than for the sets having one hole or one axial groove, where the loaded side was undisturbed.

It is of interest that with the sets where the oil was fed through the shaft, there was only a relatively small increase in friction, although, during part of a revolution of the shaft, an oil hole was passing through the loaded portion of the bearing. This small increase is especially interesting with sets S33 and S53 where there was a relatively large flat on the shaft.

Tests at Low ZN/P. After the tests at high ZN/P, the range of operation with each set of bearings was extended to cover the lower values of ZN/P at and below the point of minimum f. In each test the speed and rate of oil flow were held constant and the load was increased in steps until unstable lubrication was reached.

TABLE 2 FRICTION RATINGS OF BEARINGS

Design of oil feed	Bearing set	ZN/P=10 Δf	ZN/P=70 Δf	Average Δf for each set	Average Δf for each design	Friction rating
1 hole in bearing	31	0.00101	0.00149	0.00125	0.00130	A
	51	0.00106	0.00164	0.00135		
2 holes in bearing	32	0.00128	0.00187	0.00158	0.00147	B
	52	0.00113	0.00159	0.00136		
Axial groove in bearing	33	0.00101	0.00143	0.00122	0.00124	A
	53	0.00101	0.00149	0.00125		
4 holes in bearing	34	0.00125	0.00165	0.00145	0.00143	B
	54	0.00116	0.00166	0.00141		
Circum groove in bearing	35	0.00186	0.00340	0.00263	0.00240	C
	55	0.00149	0.00284	0.00217		
1 hole in shaft	S31	0.00109	0.00166	0.00138	0.00136	A or B
	S51	0.00107	0.00162	0.00134		
2 holes in shaft	S32	0.00112	0.00169	0.00140	0.00143	B
	S52	0.00111	0.00181	0.00146		
1 hole with flat in shaft	S33	0.00137	0.00153	0.00145	0.00146	B
	S53	0.00126	0.00166	0.00146		

One of the chief difficulties in obtaining representative data in the unstable region of lubrication is that the frictional characteristics of the bearings are affected by the roughness, geometry, and metallurgical features of the bearing surfaces, and, under operation, these frequently do not remain constant very long. Usually a bearing first tends to improve from the so-called running-in action (5), but when operation is continued under relatively high loads, speeds, and temperatures, the performance frequently is impaired and sometimes to a considerable degree. Accordingly, in running these tests, precautions were taken to minimize such effects by holding the bearings at a given load and speed for a relatively short time (2 min).

Friction data obtained in the first and fourth test runs when operating at 2030 rpm and with 15 cu in. per min oil flow with each of the eight designs of bearings are given in Figs. 12, 13, 14, 15, 16, 17, 18, and 19, where f is plotted against ZN/P. In Fig. 16 (as was the case in Fig. 8), the values of ZN/P used in plotting the data are based upon the effective area of the bearings.

In Figs. 12 to 19, inclusive, the differences between the curves for the first and fourth runs provide an indication of the change in bearing performance with running-in for a given set of bearings.

In these tests the bearings were operated at a given load for a period of 2 min (as was previously mentioned), and observations of the frictional torque were made at 1-min intervals. The values of f given in the figures are based upon the second observation where conditions were more nearly in a steady state. One ex-

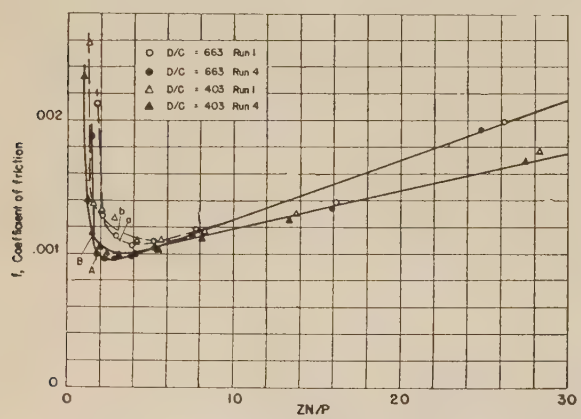

FIG. 12 FRICTION IN UNSTABLE REGION FOR 2-IN. × 1¼-IN. COPPER-LEAD BEARINGS HAVING ONE OIL HOLE IN BEARING
(Operating at 2030 rpm, 15 cu in. per min oil flow, SAE 20 oil at 200 F oil-inlet temperature.)

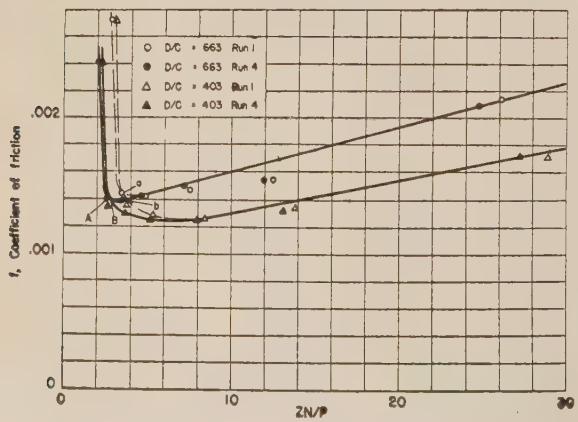

FIG. 13 FRICTION IN UNSTABLE REGION FOR 2-IN. × 1¼-IN. COPPER-LEAD BEARINGS HAVING TWO OIL HOLES IN BEARING
(Operating at 2030 rpm, 15 cu in. per min oil flow, SAE 20 oil at 200 F oil-inlet temperature.)

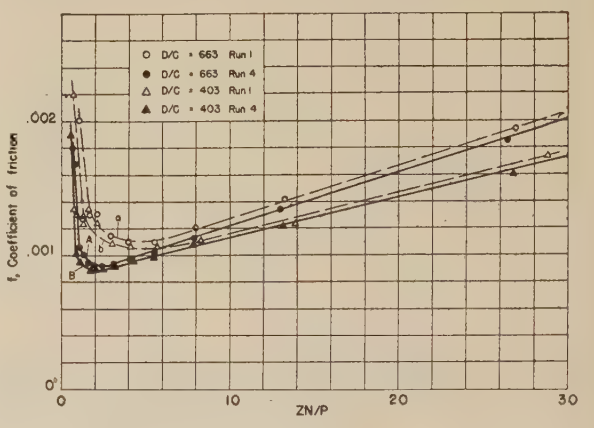

FIG. 14 FRICTION IN UNSTABLE REGION FOR 2-IN. × 1¼-IN. COPPER-LEAD BEARINGS HAVING AN AXIAL GROOVE IN BEARING
(Operating at 2030 rpm, 15 cu in. per min oil flow, SAE 20 oil at 200 F oil-inlet temperature.)

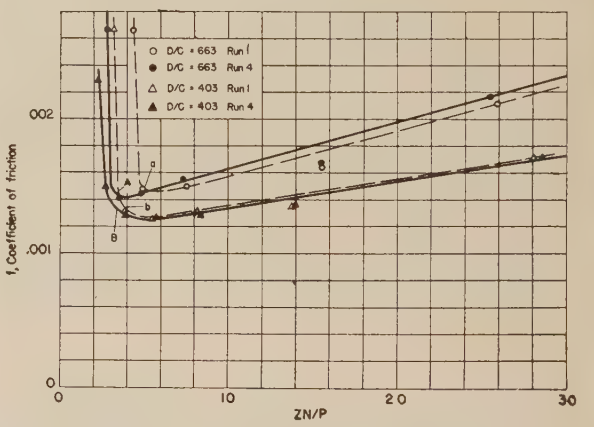

FIG. 15 FRICTION IN UNSTABLE REGION FOR 2-IN. × 1¼-IN. COPPER-LEAD BEARINGS HAVING FOUR OIL HOLES IN BEARING
(Operating at 2030 rpm, 15 cu in. per min oil flow, SAE 20 oil at 200 F oil-inlet temperature.)

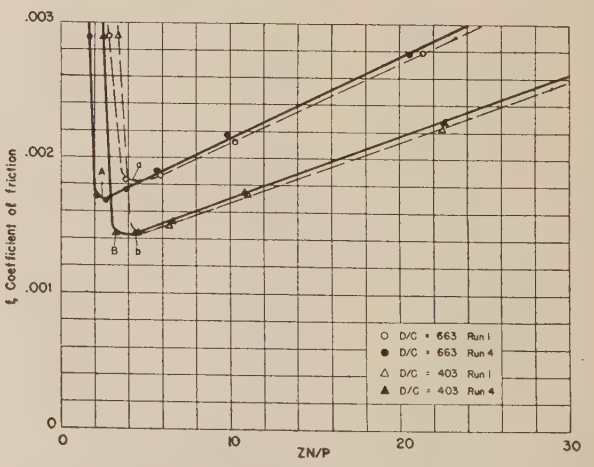

FIG. 16 FRICTION IN UNSTABLE REGION FOR 2-IN. × 1¼-IN. COPPER-LEAD BEARINGS HAVING A CIRCUMFERENTIAL GROOVE IN BEARING
(Operating at 2030 rpm, 15 cu in. per min oil flow, SAE 20 oil at 200 F oil-inlet temperature.)

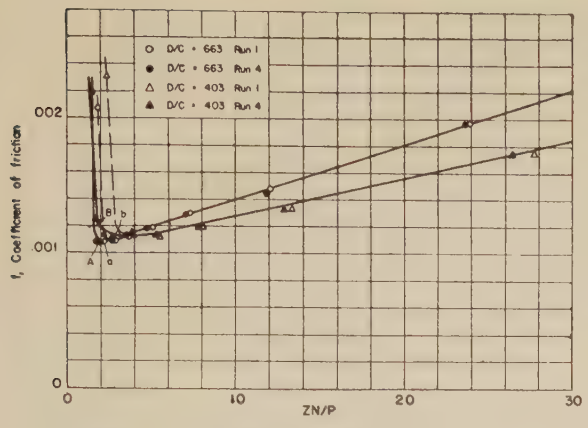

FIG. 17 FRICTION IN UNSTABLE REGION FOR 2-IN. × 1¼-IN. COPPER-LEAD BEARINGS WITH ONE OIL HOLE IN SHAFT
(Operating at 2030 rpm, 15 cu in. per min oil flow, SAE 20 oil at 200 F oil-inlet temperature.)

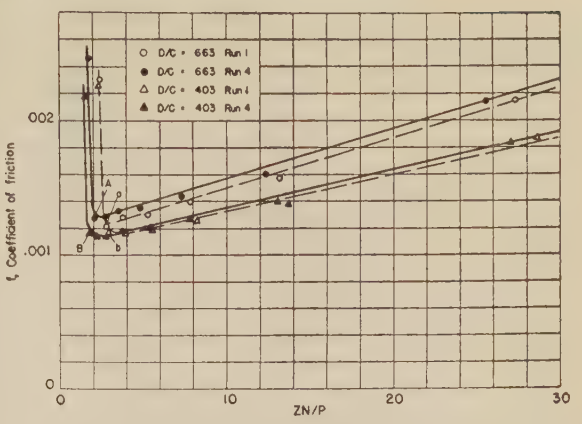

FIG. 18 FRICTION IN UNSTABLE REGION FOR 2-IN. × 1¼-IN. COPPER-LEAD BEARINGS WITH TWO OIL HOLES IN SHAFT
(Operating at 2030 rpm, 15 cu in. per min oil flow, SAE 20 oil at 200 F oil-inlet temperature.)

ception to this is at the highest load in a given run where the friction rose rapidly and the automatic load release usually acted within 30 sec. When operation was in the region of stable lubrication, the second torque reading was either equal to or lower than the first, depending upon the particular rates of heating and cooling and the time required to reach a steady state.

As the loads were increased, the bearings eventually reached the unstable operating condition where the friction increased with an increase in temperature. In some of these tests this transition from stable to unstable conditions is fairly well defined by the friction curves, because the frictional torque rose rapidly and usually in a very short time reached a value high enough to trip the load release. In others, however, the change in the friction curve was more gradual, and the transition is more definitely indicated by the condition where the second torque reading is higher than the first. In Figs. 12 through 19, the approximate locations of these points of transition between stable and unstable lubrication obtained during the first test run with the bearings having a D/C ratio of 663 are indicated by the letter a and for the fourth run by A. Corresponding points obtained with the bearings having a D/C ratio of 403 are indicated by the letters b and B.

The critical values of ZN/P at which these transition points occur for the first and fourth runs with each set of bearings are given in Table 3. Also listed are the average values obtained with each type. Since the first run with each set of bearings may be significantly affected by the condition of the original surface finish, the values for the fourth run are used as a basis for rating the different types. These ratings provide an indication of the relative load-carrying capacity of the bearings when operating under the given conditions. They are indicated by letters rather than the numerical values, since (as was the case with the friction data at high ZN/P) the differences between some types are within the probable experimental error.

From the data given in Table 3 it will be noted that the values of ZN/P when unstable lubrication was reached were, in general, lower with the bearings having no holes or grooves on the loaded side (sets 31, 51, 33, and 53). In this connection, however, it is of interest that while the values obtained with the sets having one or two holes in the shaft were somewhat higher, they were sufficiently low to receive an A rating. Under the conditions of operation in these tests, the passage of an oil hole through the loaded portion of the bearing had relatively small effect on the points of transition between stable and unstable lubrication.

With the sets having a flat on the shaft, the reduction in area

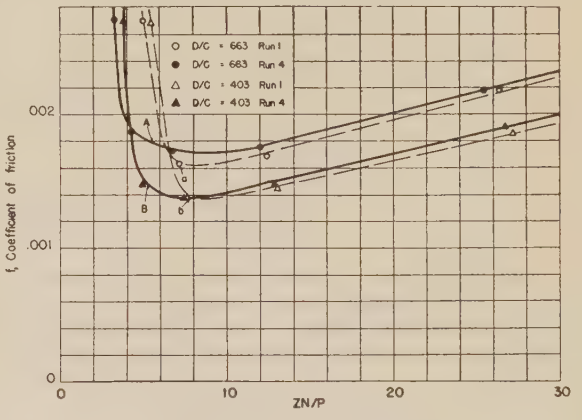

FIG. 19 FRICTION IN UNSTABLE REGION FOR 2-IN. × 1¼-IN. COPPER-LEAD BEARINGS WITH ONE HOLE WITH FLAT IN SHAFT
(Operating at 2030 rpm, 15 cu in. per min oil flow, SAE 20 oil at 200 F oil-inlet temperature.)

was sufficient to cause a marked increase in the value of the critical ZN/P, and these sets have the lowest load-carrying capacity rating.

Because of the interference to the formation of a load-carrying film with the bearings having two holes, four holes, or a circumferential groove, the operation was impaired sufficiently to result in intermediate ratings. If the total area is considered for the bearings with a circumferential groove, the average critical value of ZN/P would increase from 2.8 to 3.1 and would change the rating from B to C.

The small difference between the bearings with the axial groove and with one oil hole indicates that the groove may be somewhat more effective in the distribution of the oil for maintaining the load-carrying film.

THERMAL BEHAVIOR

Data pertaining to the thermal behavior of these bearings were obtained in the tests at high ZN/P values under a steady state of temperature distribution. In the analysis of these data, consideration is given to the total heat supplied to the bearing. Since the oil-inlet temperature was higher than the ambient temperature, the temperature rise of the bearings was not only dependent upon the heat generated by shearing the oil in the bearings but also upon the heat delivered by the oil entering the bearings.

TABLE 3 LOAD-CARRYING CAPACITY RATINGS OF BEARINGS

Design of oil feed	Bearing set	First Run		Fourth Run		Load-carrying capacity rating
		Critical ZN/P for each set	Average critical ZN/P for each design	Critical ZN/P for each set	Average critical ZN/P for each design	
1 hole in bearing	31	3.2	3.2	1.7	1.6	A
	51	3.1		1.5		
2 holes in bearing	32	3.5	3.6	2.6	2.7	B
	52	3.8		2.8		
Axial groove in bearing	33	3.3	2.9	1.5	1.4	A
	53	2.5		1.2		
4 holes in bearing	34	5.0	4.1	3.4	3.4	C
	54	3.9		3.3		
Circum groove in bearing	35	4.2	4.2	2.4	2.8	B
	55	4.2		3.2		
1 hole in shaft	S31	2.2	2.6	1.8	1.8	A
	S51	3.0		1.8		
2 holes in shaft	S32	2.7	2.8	2.0	1.9	A
	S52	3.0		1.8		
1 hole with flat in shaft	S33	7.2	7.4	5.5	5.4	D
	S53	7.7		5.2		

The thermal data obtained with the two sets of bearings of different C/D ratios having a circumferential groove (sets 35 and 55) are given in Fig. 20. In this figure, H_t, the total rate of heat supply to one bearing from both the entering oil and bearing friction (expressed in in-lb per min) is plotted against the temperature rise above the ambient. The solid points indicate the rise in temperature above the ambient of the oil leaving the bearings (ΔT_0), as determined by thermocouples located in the oil streams at the ends of each bearing, while the open points represent the temperature rise of the bearings (ΔT_b) as determined by thermocouples placed in the loaded sides of the bearing shells. Since these tests were made at a steady state of temperature distribution, the data are also indicative of the rate of heat dissipation.

Analysis of the data in this figure indicates that the relation between the rate of total heat supplied to the bearings and the temperature rise above the ambient is dependent chiefly upon factors affecting the rate of heat dissipation by the oil, namely, rate of oil flow, specific heat of the oil, and temperature rise of the oil. This method of analysis has been outlined in detail in a previous publication (6), which also describes a method for determining from the data the rate of heat dissipation through the apparatus itself by radiation, conduction, and convection.

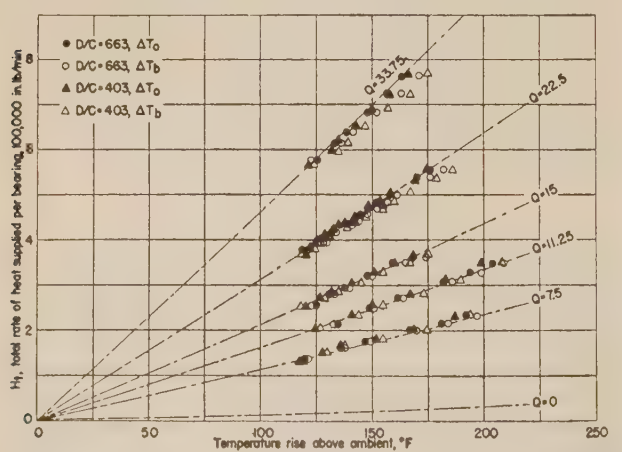

FIG. 20 THERMAL BEHAVIOR OF 2-IN. × 1¼-IN. COPPER-LEAD BEARINGS HAVING A CIRCUMFERENTIAL GROOVE IN BEARING Operating at 2030 and 3040 rpm. SAE 20 oil at 200 F oil-inlet temperature.)

The lines drawn in Fig. 20 represent the H_t versus ΔT_0 relationship for the indicated constant rates of oil flow (Q expressed as cu in. per min). The line $Q = 0$ represents the heat losses through the apparatus itself, and is used as a base for computing the lines representing the H_t versus ΔT_0 for the different values of Q. These are obtained by computations involving the product of the rate of oil flow indicated, the temperature rise, and the average specific heat of the oil over the given temperature range. From the figure it will be noted that these computed lines are in reasonable agreement with all the experimental data based upon values of the average temperature above the ambient of the oil leaving the bearings.

In Figs. 21 and 22, H_t versus ΔT_0 data are given for all sixteen sets of bearings when operating at 2030 rpm and a rate of oil flow of 15 cu in. per min. From these figures it will be noted that the data for all the bearings, having various arrangements of holes, or grooves, show the same general trend and fall reasonably well on the computed lines. This indicates that under the conditions covered, the heat-dissipation characteristics of the bearings were dependent chiefly upon the rate of oil flow through the bearings and were practically independent of clearance or the type of hole or groove used.

OIL FLOW

Measurements of the rate of oil flow at various oil-feed pressures were made also with each set of bearings when operating at a given load and speed. The flow-pressure data obtained with the bearings having a D/C ratio of 663, when operating at a load of 3008 lb per bearing ($P = 1148$ psi) and a speed of 2030 rpm, are given in Fig. 23, where Q, the rate of flow per bearing in cubic inches per minute is plotted against p the corrected oil-feed pres-

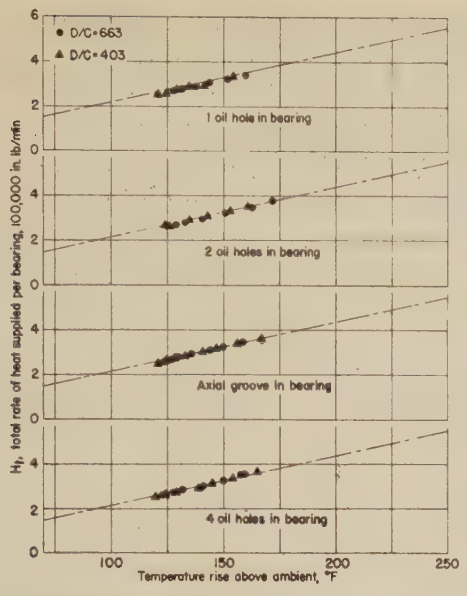

FIG. 21 THERMAL BEHAVIOR OF 2-IN. × 1¼-IN. COPPER-LEAD BEARINGS

(Operating at 2030 rpm, 15 cu in. per min oil flow, SAE 20 oil at 200 F oil-inlet temperature.)

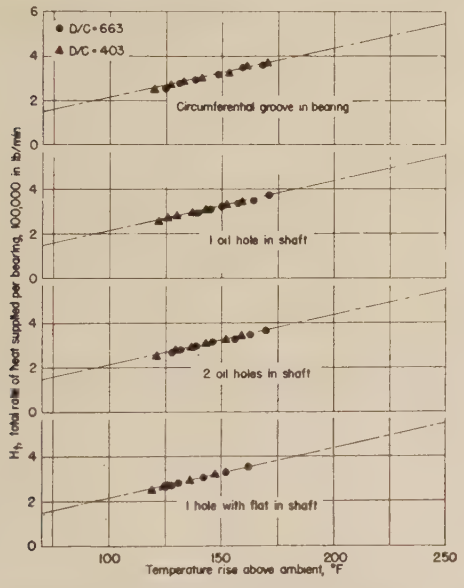

FIG. 22 THERMAL BEHAVIOR OF 2-IN. × 1¼-IN. COPPER-LEAD BEARINGS

(Operating at 2030 rpm, 15 cu in. per min oil flow, SAE oil at 200 F oil-inlet temperature.)

sure in pounds per square inch. Similar data for the bearings, having a D/C ratio of 403, are given in Fig. 24.

It should be pointed out that the data in these figures were obtained at constant load and speed but because of temperature changes caused by differences in friction and oil flow they were not obtained at constant viscosity.

The flow characteristics shown by these curves are dependent upon the particular operating conditions, hence the relative values are not necessarily applicable to other conditions. They are also dependent upon the particular dimensions of the holes and grooves used and changes in these dimensions may affect the relative values materially.

The most marked characteristics shown by these oil-flow data are the relatively high rates of flow obtained with the bearings

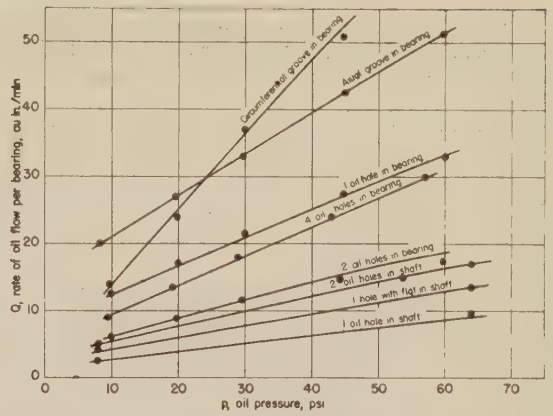

FIG. 23 OIL-FLOW VERSUS OIL-PRESSURE CURVES FOR THE DIFFERENT OIL-FEED ARRANGEMENTS WITH 2-IN. × 1¼-IN. COPPER-LEAD BEARINGS

(D/C = 663, operating at 2030 rpm and 3008 lb load, SAE 20 oil at 200 F oil-inlet temperature.)

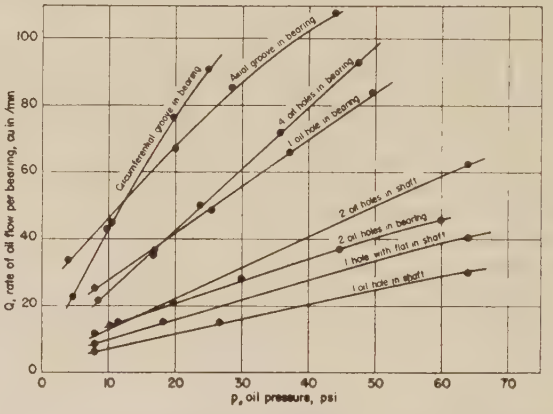

FIG. 24 OIL-FLOW VERSUS OIL-PRESSURE CURVES FOR THE DIFFERENT OIL-FEED ARRANGEMENTS WITH 2-IN. × 1¼-IN. COPPER-LEAD BEARINGS

(D/C = 403, operating at 2030 rpm and 3008 lb load, SAE 20 oil at 200 F oil-inlet temperature.)

having the axial or circumferential oil grooves and the generally low rates obtained with the sets where the oil was fed through the shaft.

Since the rate of heat dissipation of the bearings depended chiefly upon the rate of oil flowing through the bearings, these flow data provide an indication of the relative heat-dissipation characteristics of the bearings tested under the operating conditions covered.

CONCLUSION

The influence of the various arrangements of oil holes and grooves on the behavior of bearings is as follows:

One Oil Hole in Bearing. With this arrangement, the absence of holes or grooves on the loaded side of the bearing provides for normal development of pressure in the oil film. Consequently, the bearing has relatively low friction and low ZN/P at transition between stable and unstable lubrication. While the single hole does not provide the highest oil flow, it would seem to be sufficient to provide adequate heat dissipation for most conditions.

Two-Oil-Hole Arrangement in Bearing. The single hole on the loaded side with this arrangement apparently disturbs the normal development of pressure in the film to make a measurable increase in friction and in ZN/P at the transition point. The par-

ticular location of the oil hole on the unloaded side is adverse from the standpoint of oil flow, hence the rate of heat dissipation is somewhat lower than the arrangement with one hole in the bearing.

Axial Groove in Bearing. This arrangement apparently provides a slightly better distribution of oil for the development of the load-carrying film than the arrangement with one hole in the bearing. Consequently, the bearing has low friction and lowest critical ZN/P, and the high oil flow provided is advantageous where forced cooling is necessary.

Four-Hole Arrangement in Bearing. This arrangement has two holes on the loaded side which disturbs the development of pressure in the film to a greater extent than the arrangement with two holes in the bearing, and its critical ZN/P is higher, but the friction is comparable. The two holes on the unloaded side are not in advantageous positions, and its oil flow and rate of heat dissipation is comparable to the arrangement with one hole in the bearing.

Circumferential Groove in Bearing. The groove dividing the bearing into two narrower parts increases the friction and causes a relatively high critical ZN/P. The high friction is counteracted by high oil flow and rate of heat dissipation.

One Oil Hole in Shaft. The passage of one oil hole across the loaded portion of the oil film has relatively small effect on both friction and critical ZN/P, which are only slightly higher than for the arrangement with one hole in the bearing. When the hole is exposed to some portions of the loaded area, the oil feed is practically shut off and consequently this arrangement results in the lowest oil flow and rate of heat dissipation.

Two Oil Holes in Shaft. With two oil holes for each journal, the disturbance to film-pressure development occurs twice in a revolution, resulting in slightly higher friction and critical ZN/P than with the arrangement with one hole in the shaft. The two holes also provide a greater oil flow and rate of heat dissipation. In this respect it is comparable to the arrangement with two holes in the bearing.

One Oil Hole With Flat in Shaft. The flat at the end of the oil-hole causes considerable disturbance to the development of pressure in the oil film, increases the friction, and markedly increases the critical value of ZN/P. Its oil flow and rate of heat dissipation are higher than the arrangement with one hole in the shaft without the flat but not sufficient to counteract the effect of its high ZN/P at transition from stable to unstable lubrication.

The results of these tests apply directly to unidirectionally loaded bearings for the particular range of conditions covered. The indicated differences between the various arrangements are not necessarily strictly indicative of more complex conditions where the load varies in both intensity and direction with respect to the bearings. It is believed, however, that the relative values obtained may be useful qualitatively in estimating the over-all effects of various arrangements of holes or grooves under more complex loading conditions, especially if proper consideration is given to conditions present throughout the complete load cycle.

BIBLIOGRAPHY

1 "Performance Characteristics of Journal Bearings With Forced-Feed Lubrication," by S. A. McKee, H. S. White, A. D. Bell, and J. F. Swindells, NACA Wartime Report ARR No. 4H15, August, 1944.

2 "Friction in Machines and the Effect of the Lubricant," by N. Petroff (*a*) in Russian, *Engineering Journal*, St. Petersburg, Russia, 1883; No. 1, p. 71; No. 2, p. 228; No. 3, p. 377; No. 4, p. 535. (*b*) German translation by L. Wurzel, Hamburg, Germany, L. Voss, 1887, 187 pp.

3 "Friction of Journal Bearings as Influenced by Clearance and Length," by S. A. McKee and T. R. McKee, Trans. ASME, vol. 51, 1929, p. 161.

4 "Oil Grooves in Plain Bearings," by D. Clayton, *Engineering*, vol. 159, 1945, pp. 158–178.

5 "Effect of Running In on Journal-Bearing Performance," by S. A. McKee, *Mechanical Engineering*, vol. 49, 1927, p. 1335; vol. 50, 1928, p. 528.

6 "Measurements of the Combined Frictional and Thermal Behavior in Journal-Bearing Lubrication," by S. A. McKee, H. S. White, and J. F. Swindells, Trans. ASME, vol. 70, 1948, p. 409.

Discussion

M. D. Hersey.[3] Can the authors compare their results at any point with the work of Clayton and others, and amplify their application to engine bearings?

Authors' Closure

With reference to Mr. Hersey's question, the case of the bearings with 360-degree circumferential groove provides the closest approach to a direct comparison between our results and those of Clayton (4). Clayton's bearing h and our bearing set 35 are similar in diameter and length but differ in D/C ratio, that value for bearing h being 800 and for set 35 being 663. In Table 1 in his paper Clayton reports a value of the coefficient of friction of 0.0026 for bearing h when operating at a speed of 3000 rpm, a load of 1500 psi, and with the viscosity of the oil at 10.0 centipoises. Under these conditions the value of ZN/P is 20. The value of f for $ZN/P = 20$ for set 35 is about 0.00275. This is shown in Fig. 8 of our paper. An approximate correction to this value (based on the Petroff equation) to correspond to a D/C ratio of 800 would raise the value to about 0.00288. This would indicate that the value we obtained was about 10 per cent higher than that obtained by Clayton. In this connection, however, it should be pointed out that the NPL friction machine used by Clayton measures the bearing friction, whereas the NBS four-bearing friction machine measures the journal friction (see Norton's "Lubrication," 1942, p. 23). This difference in f in the two cases would seem to indicate that along a line perpendicular to the load the center of the journal was displaced from the center of the bearing about 0.00028 in., and, if it is assumed that the film thickness at the point of closest approach is somewhat smaller than the 0.0002 in. estimated by Clayton for bearing a (bottom hole), the angle between the line of the load and the point of closest approach would be of the order of 14 degrees. Since both of these values appear to be reasonable, it is believed that the friction data for the two bearings check rather closely.

Somewhat greater differences in f are shown when comparing Clayton's bearing a (one oil hole in unloaded side) with our set 31. However, this can be accounted for by the difference in L/D, which was 0.875 for bearing a and 0.620 for set 31.

Comparison of the data on oil flow is more difficult because of the complex relations between the factors involved. Rough corrections for differences in clearance, length, viscosity, and oil-feed pressure indicate that values from the two laboratories for similar types of bearings are of the same order of magnitude, but no attempt was made to evaluate the effects of differences in such factors as oil-inlet temperature, load, speed, or eccentricity.

[3] U. S. Naval Engineering Experiment Station, Annapolis, Md.

Film Thickness Between Gear Teeth

A Graphical Solution of Karlson's Problem

By M. D. HERSEY[1] and D. B. LOWDENSLAGER[2]

This investigation completes a solution, undertaken by K. G. Karlson in his little-known Swedish paper of 1926, for the oil-film thickness between gear teeth. Karlson's problem is characterized by the use of a parabolic curve for the viscosity-pressure relation. The numerical results here obtained are comparable with those previously published by Gatcombe, who used a more conventional viscosity-pressure formula. It is hoped that the present analysis will help to clarify the assumptions and calculations required in the hydrodynamic theory of gear-tooth lubrication. As an aid to its practical application, the relative film thicknesses found for geometrically similar pairs of gears are here shown by a chart constructed in terms of the appropriate dimensionless variables, and extending from zero to 10 microinches per in. of pitch diameter of the pinion. The limiting case of a lubricant whose viscosity is unaffected by pressure, for which an analytical solution had been given by Karlson, is represented by a straight line on this chart.

Introduction

IT would be useful in studies of gear-tooth lubrication, particularly when efforts are being made to increase the load capacity of gear teeth, to be able to estimate, even roughly, the probable or possible thickness of the oil film between two contacting teeth under hydrodynamic conditions.

Three principal investigations toward this end have already been published, those of *Engineering* in 1916 (1),[3] of Karlson in 1926 (2), and of Gatcombe in 1945 (3). The article in *Engineering*, though unsigned, is generally recognized as the pioneer investigation in our field. It does not, however, take into account the effect of high pressure on viscosity. The study by Karlson is based upon a parabolic equation for the viscosity, Z, of the lubricant as a function of the gage pressure p, namely

$$Z = Z_1 \left(\frac{p + k}{k}\right)^2 \quad \ldots\ldots [1]$$

where Z_1 is the viscosity at atmospheric pressure and k is a constant of the lubricating oil. Gatcombe's study is based upon a widely used exponential formula

$$Z = Z_1 (10)^{p\delta} \quad \ldots\ldots [2]$$

where δ is an empirical constant analogous to k.

Karlson's investigation was left unfinished, his integral for the load capacity of the film not being evaluated. Gatcombe's study was carried through and applied to a series of numerical examples. These numerical results were generalized by Hersey and Hopkins (4), in the form of a chart for the relative film thickness in geometrically similar gears. However, Blok (5) has questioned the accuracy of Gatcombe's mathematical approximations leading to the results utilized by Hersey and Hopkins. Accordingly, the present authors found it necessary to make a fresh approach to the subject, and therefore undertook a graphical solution of Karlson's problem.

Basic Assumptions

The physical assumptions which are customary in the theory of lubrication, and others pertinent to the gear-tooth problem, notably the following, have been made:

1 The lubricant is incompressible and without inertia; it has the same physical properties at every point and in every direction; it adheres to the solid surfaces and follows Newton's law of viscous flow.

2 The gear teeth are rigid and geometrically perfect, and therefore free from any appreciable effects of deformation, misalignment, manufacturing errors, surface roughness, or wear.

3 The gears are running at constant speeds without dynamic loading or appreciable vibration.

4 The temperature is uniform throughout the film at any moment, though it may vary greatly with operating conditions.

5 The mechanical action of the film has reached a practically steady state at every phase of contact, or angular position of the tooth; the approach process being so nearly completed that the minimum film thickness in every such position may be treated as a constant with respect to time.

These various assumptions define the scope of our investigation and limit it severely compared to what might ideally be desired (6, 7). It is hoped, however, that the present analysis may be useful in the absence of more exact knowledge, and that it may be followed by discussions which will greatly clarify the background of gear-tooth lubrication theory, thus facilitating the work that lies ahead.

Integration for Load Capacity

The normal tooth load F_n, which is the resultant force per unit of face width exerted by one tooth upon another at right angles to the tooth surface through the medium of the oil film, is given by

$$F_n = \int p \, dx \quad \ldots\ldots [3]$$

where p denotes the fluid pressure at any distance x measured in the direction of motion from the point of nearest approach.

Karlson's expression for the pressure distribution, derived from the usual hydrodynamic assumptions together with Equation [1] may be written

$$p = \frac{4\,HT\,k}{(1 + T^2)^2 - 4\,HT} \quad \ldots\ldots [4]$$

---

[1] Mechanical Engineer, U. S. Naval Engineering Experiment Station, Annapolis, Md. Fellow ASME.

[2] School of Mathematics, University of Virginia, Charlottesville, Va.; Mathematics Aide, U. S. Naval Engineering Experiment Station, summer of 1949.

[3] Numbers in parentheses refer to Bibliography at end of paper.

Contributed by the Research Committee on Lubrication and presented at the Spring Meeting, Washington, D. C., April 12–14, 1950, of The American Society of Mechanical Engineers.

Manuscript received at ASME Headquarters, January 11, 1950. Paper No. 50—S-10.

Here T is the tangent of Gatcombe's angle S, and may be defined by

$$T \equiv \frac{-x}{\sqrt{2\,r\,h_0}} \quad [5]$$

where h_0 denotes the film thickness at the point of nearest approach; and r denotes the effective contact radius, defined by

$$\frac{1}{r} \equiv \frac{1}{r_1} + \frac{1}{r_2} \quad [6]$$

in which r_1 and r_2 are the radii of curvature of the pinion tooth and gear tooth, respectively. The dimensionless number H in Equation [4] is defined by

$$H \equiv \frac{Z_1 U \sqrt{2\,r\,h_0}}{k\,h_0^2} \quad [7]$$

where U denotes the mean tangential velocity $(U_1 + U_2)/2$ of the contacting surfaces, U_1 referring to the pinion and U_2 to the gear. It happens that H is equal to $^1/_{12}$ the ratio of Gatcombe's constant G to Karlson's constant k, both of which have the dimensions of pressure.

From Equation [4] it will be noted that $p = 0$ when $T = 0$, and, therefore, when $x = 0$. Thus the film pressure is assumed to vanish at the point of nearest approach. This assumption is known as Sommerfeld's condition, in contrast with Reynolds' condition under which both the film pressure and the pressure gradient vanish together at some point in the divergent portion of the film, appreciably removed from the point of nearest approach in the direction of motion. While the present authors subscribe to Reynolds' condition, they have tolerated the other for simplicity in completing Karlson's integration. A trial calculation indicates the difference in load capacity under the two assumptions to be of the order of 15 per cent, more or less, Reynolds' condition leading to the greater load capacity; hence our solution will be on the safe side. Both schools of thought concur for practical purposes in disregarding the region of negative pressure; hence the integration of Equation [3] need be carried out only on one side of the point of nearest approach.

Substituting from Equations [4] and [5] into [3] gives for the normal load per unit width

$$F_n = \frac{2\,Z_1\,Ur}{h_0}\left(\frac{J}{H}\right) \quad [8]$$

where by definition

$$J \equiv \int_0^\infty \frac{4\,HT\,dT}{(1+T^2)^2 - 4\,HT} \quad [9]$$

Equation [8] in conjunction with Equation [9] expresses the essential relation sought for, connecting load capacity with the minimum film thickness h_0. Although these equations should be credited to Karlson, they have been confirmed by an independent derivation.

To evaluate the factor J/H occurring in Equation [8], we have found it sufficient to plot the integrand of Equation [9] as a function of T for five suitably spaced values of H and to measure the area under each curve. It may be shown analytically that $J/H = 2$ when $H = 0$, and that for perfectly rigid teeth, the maximum pressure p_m is infinite when $H = 0.770$. Thus by differentiating Equation [4], the maximum pressure is found to occur when T equals $1/\sqrt{3}$. It is then given by

$$p_m = k\left(\frac{1}{1 - \frac{3}{4}\sqrt{3}\,H} - 1\right) \quad [10]$$

which becomes infinite when $H = 4\sqrt{3}/9$, or approximately 0.77. The values of J/H so obtained are recorded in Table 1, and plotted against H in Fig. 1.

TABLE 1 RESULTS OF GRAPHICAL INTEGRATION

H	J/H
0.00	2.00
0.25	2.52
0.50	3.62
0.625	5.22
0.70	7.86
0.75	16.5
0.77	∞

NOTE: H and J are dimensionless; see Equations [7] and [9].

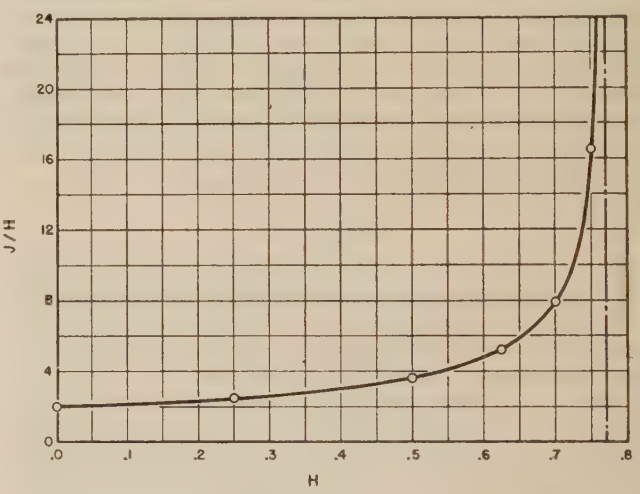

FIG. 1 PLOT OF VALUES FOUND BY GRAPHICAL INTEGRATION

To convert F_n values into the component F of tooth load per unit width acting tangentially to the pitch circle, which will be needed for computing the torque on the drive shaft, a factor C_0, depending on the gear geometry, must be introduced, such that

$$F = C_0 F_n \quad [11]$$

where

$$C_0 \equiv k_0\,L_c \cos\alpha \quad [12]$$

Here k_0 is the ratio of the average supporting action of the film at all tooth positions to its value F_n for the pitch-point phase; L_c is the average number of pairs of teeth meshing simultaneously, which governs the effective length of contact; and α the pressure angle. Gatcombe in the reference cited gave values for these constants applicable to a gear and pinion having a 5:1 reduction ratio with 24 teeth in the pinion, and to a rack and pinion described in the *Engineering* article (1) with 54 teeth in the pinion. The values of C_0 ranged from about 1.26 to 1.50.

CALCULATION OF FILM THICKNESS

Eliminating F_n between Equations [8] and [11], we obtain

for the relative film thickness, D being the pinion diameter at the pitch circle

$$\frac{h_0}{D} = C_1 \left(\frac{J}{H}\right) \quad [13]$$

where

$$C_1 \equiv \frac{2\,C_0\,Z_1\,Ur}{F\,D} \quad [14]$$

To find the correct value of J/H for use in Equation [13], we may solve Equation [7] for h_0 and substitute the expression so obtained into Equation [13], after which the resulting equation may be solved for J/H, giving

$$\frac{J}{H} = \frac{C_2}{H^{2/3}} \quad [15]$$

where

$$C_2 \equiv \frac{\sqrt[3]{2r}}{C_1\,D} \left(\frac{Z_1 U}{k}\right)^{2/3} \quad [16]$$

Thus for any value of C_2, representing the data of a given problem, we may plot the graph of Equation [15] in Fig. 1, or such portion as may be required to locate the intersection point. The ordinate of this point is the desired value of J/H.

It is more convenient in practice to express F in terms of P, the load per unit of projected area, this area being arbitrarily chosen as the product of the face width into the pitch diameter of the pinion. Thus

$$F \equiv PD \quad [17]$$

Similarly, it is more convenient to express U in terms of the pinion speed, or number of revolutions per unit time N. At the pitch point $U = U_1 = U_2$, where U_1 and U_2 are the tangential velocities of the tooth surfaces of pinion and gear, respectively. The effects of variations from pitch-point contact are included in the factor C_0 as shown briefly by Gatcombe (3), although a more complete exposition would be reassuring. If now ω_1 and r_1 denote, respectively, the angular velocity of the pinion tooth and its radius of curvature at the pitch point, it follows from the reference cited that U is equal to $\omega_1 r_1$. But ω_1 equals $2\pi N$, therefore

$$U = 2\pi N r_1 \quad [18]$$

Making these substitutions, the working constants become

$$C_1 = \frac{4\pi\,C_0\,r_1\,r}{D^2} \left(\frac{Z_1 N}{P}\right) \quad [19]$$

and

$$C_2 = \frac{\pi^{-1/3}}{2\,C_0} \cdot \frac{D}{r_1^{1/3}\,r^{2/3}} \left(\frac{P}{k}\right)^{2/3} \left(\frac{Z_1 N}{P}\right)^{-1/3} \quad [20]$$

Constants of the Lubricating Oil

Evaluating Z_1, the viscosity at atmospheric pressure, offers no difficulty aside from determining the mean effective equivalent film temperature, which has been assumed uniform—an important problem outside the scope of this paper. Evaluating Karlson's constant k requires an experimental knowledge of the viscosity-pressure curve for the lubricating oil at the temperature in question.

When the logarithm of the relative viscosity Z/Z_1 is plotted against the gage pressure p at constant temperature, the graphs for most lubricating oils are by no means straight lines. They are commonly convex upward and can only be fitted by straight lines for a short interval near the origin, after which they bend over conspicuously. Karlson's equation takes account of this fact. From Equation [1] it will be seen that the logarithm of Z/Z_1 equals twice the logarithm of $(p + k)/k$ and approaches direct proportionality to the logarithm of p/k as the pressure approaches infinity. However, the graph of Karlson's equation falls somewhat below the true curve for the usual lubricating oil, just as the graph of Equation [2] falls too high, assuming that all three graphs have the same slope at the origin. This difficulty can be corrected to a first approximation by assigning a suitable value to the constant k, such that the graph will start out too steep, intersect the true curve near the middle of its pressure range, and drop below it at the high-pressure end, averaging about right.

Let b denote the pressure coefficient of viscosity at atmospheric pressure, elsewhere frequently denoted by b_1. The pressure coefficient is the relative or fractional increase in viscosity per unit increase of pressure. Its value at atmospheric pressure is equal to the initial slope of the curve obtained when the natural logarithm of the viscosity is plotted against the pressure; and it may be taken equal to 2.30 times this slope when the common logarithm is plotted. Upon differentiating Equation [1], it will be seen that b is equal to $2/k$, from which

$$k = \frac{2}{b} \quad [21]$$

Now let b_0 denote the observed value of the initial pressure coefficient while b is the adjusted, or raised value, corresponding to the desired effective value of k. The adjustment ratio b/b_0 will evidently be greater, the greater the range of pressure over which a fit is required. A perfect fit at the origin would be obtained when b/b_0 equals unity. The corresponding value of k for use in Equation [1] is given by

$$k = \frac{2/b}{b/b_0} \quad [22]$$

Values of the adjustment ratio b/b_0 for two representative lubricating oils are plotted in Fig. 2 as a function of p_m, the maximum film pressure expected. These values were found by a trial fitting of Karlson's formula to the curves for petroleum oil 42 at 77 and 212 F, and castor oil at 167 F, given by Hersey and Hopkins in their paper of 1945 (4), Fig. 4. This fitting should be extended to a wider variety of oils and to higher temperatures. Equation [22] has been plotted in Fig. 3.

Numerical Examples

In Tables 2 and 3 are given the results obtained by Equations [13], [15], [19], and [20], and associated procedure, for the five problems which had been solved in Gatcombe's paper (3). It is surprising what close agreement is found, considering (*a*) that the accuracy of his integration has been questioned, (*b*) that the viscosity-pressure relations used in his paper are based on a straight-line logarithmic equation, and (*c*) that our own adjustments for evaluating the viscosity constants are far from precise.

The symbols appearing in the tables have all been defined previously except for the abbreviations of units, most of which are familiar. The abbreviation m following the viscosity Z_1 refers to the millionth part of the pound-second per square inch, a convenient unit coming into more frequent use, equal to approximately 6.9 centipoises. This abbreviation is again employed in tabulating the values of Z_1N/P, which are 60×10^6

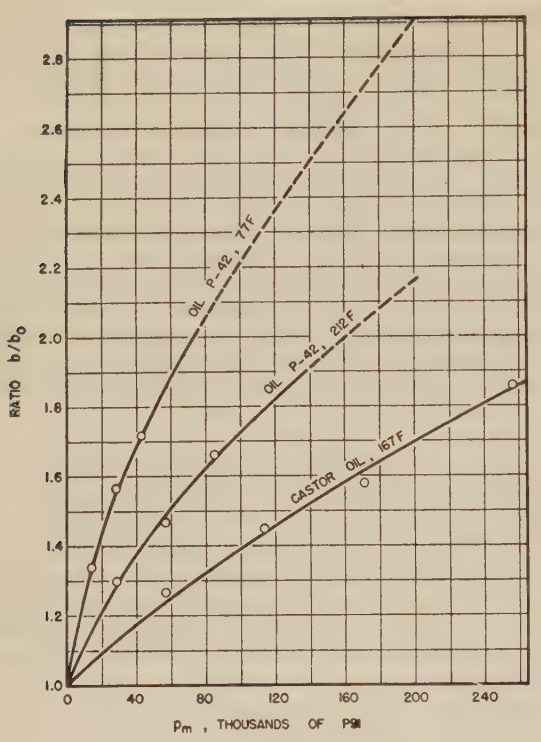

FIG. 2 ADJUSTMENT RATIO FOR PRESSURE COEFFICIENT

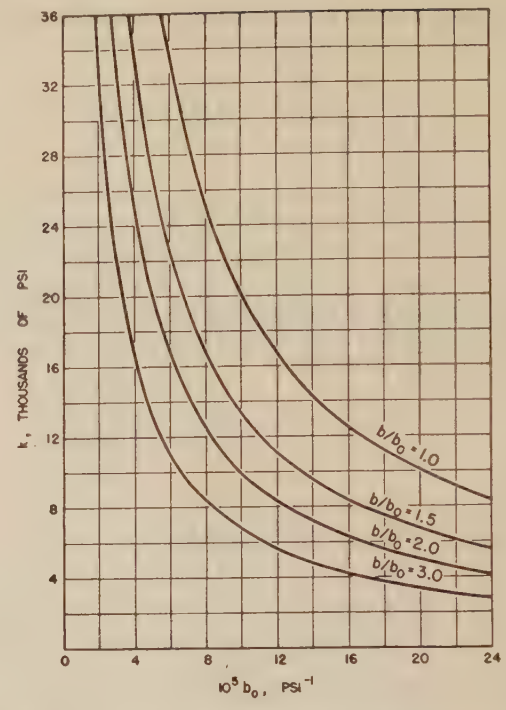

FIG. 3 KARLSON'S CONSTANT AND OBSERVED PRESSURE COEFFICIENT

times as great as the values required for use in theoretical equations like [19] and [20].

In Table 3 the first two columns of h_0/D values are, respectively, those computed by Professor Gatcombe in the paper cited, and by the present authors, as explained in footnotes *a* and *b* of the table. The third column contains the limiting values for the imaginary case of zero-pressure coefficient, computed from Equation [13] with J/H set equal to 2.0, which is the value corresponding to $H = 0$ or $k =$ infinity in Equation [7]. The value 9.1 microinches per in. in problem No. 5 is recorded for comparison with the value 8.9 reported by *Engineering*. Finally, in the last column of Table 3 the influence of pressure on viscosity is plainly shown by tabulating the ratio of the film thickness, calculated for a given pressure coefficient, to that calculated for a zero coefficient this ratio varying from approximately 1 to 10.

Film-Thickness Charts

Under the basic assumptions stated, dimensional analysis shows that the relative thickness h_0/D for geometrically similar pairs of gears can be plotted against the operating variable Z_1N/P and represented completely by a single family of curves, each identified by a constant value of one dimensionless parameter, provided the viscosity-pressure curve can be represented by an empirical equation containing only one constant besides Z_1. Both Equations [1] and [2] satisfy this condition. When Equation [2] is chosen, and δ replaced by its equivalent $b_0/2.3$, the required parameter turns out to be b_0P. Such a chart was given by Hersey and Hopkins in Fig. 2 of their paper (4), the notation b_1P then being used, and its value recorded as a percentage.

A chart of the same general type is now given in Fig. 4 using the parameter k/P based on Equation [2]. The value of k required in the application of this chart is that providing the best

TABLE 2 DATA FOR PROBLEMS

(Abbreviation m denotes millionths of a lb-sec/sq in.

Problem no.	N rpm	F lb/in.	P psi	$10^{-3}p_m$ psi	Temp deg F	Z_1 m	$10^5\delta$ psi^{-1}	10^5b_0 psi^{-1}
1	1750	197	98.5	56	95	5.5	8.74	20.1
2	1160	300	150	100	95	5.5	8.74	20.1
3	1750	197	98.5	206	199	0.26	4.14	9.54
4	1750	197	98.5	82	198	3.5	3.97	9.14
5	846	267	19.1	7.3	100	10.2	7.14	16.5

TABLE 3 SOLUTION OF PROBLEMS

(Mi/in. denotes microinches per inch of pinion pitch diameter; m denotes millionths of a lb-sec/sq in.)

Problem no.	b/b_0	k psi	k/P	Z_1N/P m rpm/psi	h_0/D mi/in.[a]	h_0/D mi/in.[b]	h_0/D mi/in.[c]	Pressure effect[d]
1	1.80	5530	56	97.8	8.4	8.1	1.52	5.3
2	2.13	4660	32	42.6	6.4	6.8	0.66	10.3
3	2.12	9890	100	4.6	0.7	0.7	0.7	1.1
4	1.28	17100	174	62.2	3.7	3.0	0.97	3.1
5	1.17	10500	550	456	10.4	11.4	9.1	1.3

[a] From E. K. Gatcombe's paper (3).
[b] By calculations of present paper.
[c] For viscosity unaffected by pressure.
[d] Ratio of h_0/D for the given pressure coefficient to that for zero coefficient.

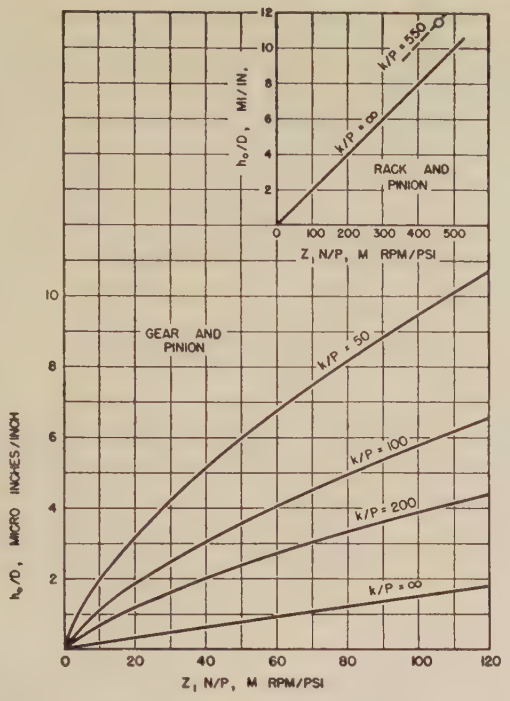

FIG. 4 FILM THICKNESS IN GEOMETRICALLY SIMILAR GEARS

fit of Karlson's formula to the experimental viscosity-pressure curve. Figs. 2 and 3 have been offered as a tentative guide in evaluating k until more systematic information can be made available.

The three curves labeled $k/P = 50$, 100, and 200, were computed from Equations [13], [15], [19], and [20], and Fig. 1, without the aid of Figs. 2 and 3. These latter diagrams are called for only in the application, not in the construction of Fig. 4. The straight graph, identified by $k/P =$ infinity, was constructed from Equation [13] in the special form corresponding to $H = 0$, namely

$$\frac{h_0}{D} = \frac{8\pi C_0 r_1 r}{D^2}\left(\frac{Z_1 N}{P}\right) \quad \text{[23]}$$

Equation [23] is equivalent to an equation published by Karlson (2), connecting the film thickness h_0 with the normal tooth load F_n. The small diagram in the upper corner of Fig. 4 shows on a compressed scale the corresponding graph for the rack and pinion described in *Engineering* (1), together with an isolated point representing our solution of problem No. 5. The h_0/D values computed for Table 3 fall exactly into place on Fig. 4 and might have been determined directly from the chart by interpolation.

The main family of curves in Fig. 4 should be found applicable not only to the gear and pinion described, but to any pair geometrically similar to these, regardless of absolute size; and to any lubricant following Karlson's equation, regardless of absolute viscosity. Moreover, it should be possible from the calculations developed in this paper to construct the appropriate charts for any pair of spur gears operating in accordance with the basic assumptions outlined. From an intercomparison of such charts the influence of the purely geometrical factors might be more clearly brought out.

ACKNOWLEDGMENTS

This brief study was undertaken as part of a survey of gear lubrication requested by the Bureau of Ships, Navy Department. The authors are indebted to Mr. H. Blok of Delft, Holland, and to Prof. E. K. Gatcombe of the U. S. Naval Post Graduate School, and to the ASME Research Committee on Lubrication, for information and comments that have been helpful in formulating the problem to be solved.

BIBLIOGRAPHY

1 "The Lubrication of Gear Teeth," *Engineering*, vol. 102, 1916, pp. 119–121.

2 "Kontaktproblem" (Contact Problem), by K. G. Karlson, *Teknisk Tidskrift, Mekanik*, vol. 56, Jan. 16, 1926, pp. 1–6.

3 "Lubrication Characteristics of Involute Spur Gears," by E. K. Gatcombe, Trans. ASME, vol. 67, 1945, pp. 177–188.

4 "Viscosity of Lubricants Under High Pressure. Co-Ordinating the Data From Ten Investigations," by M. D. Hersey and R. F. Hopkins, *Mechanical Engineering*, vol. 67, 1945, pp. 820–824; vol. 68, 1946, pp. 676–683.

5 "Gear Wear as Related to the Viscosity of the Gear Oil," by H. Blok, Proceedings of the Summer Conference on Mechanical Wear, Massachusetts Institute of Technology, June, 1948 (in press); see also *De Ingenieur*, vol. 61, July 24, 1949, pp. 39–46.

6 "Physical Concepts of the Establishment of the Lubricating Oil Wedge and Its Associated Load Carrying Capacity for the Mating Tooth Surfaces of High Speed Gears," by E. K. Gatcombe, Symposium on Lubrication of High-Speed Turbine Gear Equipment, Technical Publication No. 92, American Society for Testing Materials, Philadelphia, Pa., 1949, pp. 14–19.

7 "Tooth Contact Conditions in Spur and Helical Gears," by R. M. Macarthur, *Engineering*, vol. 168, 1949, pp. 654–657.

NOTATION

The following notation is used in the paper:

- C_0 = dimensionless constant depending only on the gear geometry; defined by Equation [12]
- C_1 = dimensionless constant defined by Equation [14]
- C_2 = dimensionless constant defined by Equation [16]
- D = pinion pitch diameter
- F = component of F_n tangential to pitch circle
- F_n = normal force on tooth per unit of face width due to film pressure
- H = dimensionless quantity proportional to Z_1U/k and depending also on film thickness; defined by Equation [7]
- J = dimensionless quantity proportional to tooth load; defined as a function of H in Equation [19].
- L_c = average number of teeth meshing simultaneously
- N = pinion speed in revolutions per unit time
- P = tooth load per unit of projected area formed by face width multiplied by pitch diameter; or ratio F/D, Equation [17]
- T = ratio of distance along tooth profile to square root of $2rh_0$, defined by Equation [5]
- U = mean of U_1 and U_2
- U_1 = tangential velocity of pinion-tooth surface
- U_2 = tangential velocity of gear-tooth surface
- Z = viscosity of lubricant at any point in film, as affected by pressure and temperature
- Z_1 = viscosity at atmospheric pressure but at temperature of film
- b = pressure coefficient of viscosity at atmospheric pressure, evaluated for optimum fit between theoretical and observed viscosity-pressure curves
- b_0 = observed pressure coefficient at atmospheric pressure
- h_0 = film thickness at point of nearest approach, also called minimum film thickness
- k = empirical constant in Karlson's parabola, Equation [1], expressing the viscosity-pressure relation
- k_0 = ratio of average F_n for all contact phases to value of F_n for contact at pitch point
- p = fluid pressure at any point in film as a function of x or T
- p_m = maximum value of p

r = effective contact radius defined by Equation [6]
r_1 = radius of curvature of pinion tooth at contact point
r_2 = corresponding radius of curvature of gear tooth
x = distance along tooth profile from point of nearest approach, considered positive in the direction of motion
α = pressure angle fixed by gear geometry
δ = empirical constant in Equation [2] proportional to pressure coefficient of viscosity
π = as usual, 3.1416
ω_1 = angular velocity of pinion

Discussion

H. Blok.[4] The paper touches upon the following important question, which forms the background to the present discussion: What are the limits inherent in the hydrodynamic lubrication of straight spur gears? Under the authors' five basic assumptions the answer doubtless is: There are no such limits, if viscosity increases quadratically with pressure according to Karlson's parabolic Equation [1]. This can easily be verified by referring to the critical cases, that is, the limiting cases where maximum oil pressure p_m becomes infinitely high (H assumes its critical value $4/3\sqrt{3} = 0.770$, as indicated by Expression [10], where H is defined by Equation [7]). In fact, it was shown by the authors that in the critical cases hydrodynamic load capacity F_n, as expressed by Equations [8] and [9], will become infinite. In this connection it is noteworthy that, in any given spur gear (given effective contact radius r; see [7]) for any given atmospheric viscosity Z_1, velocity U, and tolerable minimum film thickness h_0, the critical value of H can in principle always be reached by proper choice of the empirical oil constant k, that is, of the oil. This indeed leads to the conclusion that, as long as all of the authors' basic assumptions as well as Karlson's viscosity-pressure relationship can be upheld, hydrodynamic load capacity in principle is unlimited.

It remains to be seen whether or not the basic assumptions and Karlson's relationship can be upheld, when the critical cases are approached.

In so far as Karlson's relationship is concerned, this was acknowledged by the authors to break down for the high oil pressures involved in the cases contemplated. Then, the following generalized viscosity-pressure relationship would have to be substituted for Karlson's

$$Z = Z_1(1 + p/k)^n \quad [24]$$

where n would be greater than 2; particularly, the higher the maximum oil pressure to be accounted for, the higher would n have to be.

With the foregoing generalized relationship, it is found that the critical cases, where maximum oil pressure becomes infinitely high, occur when the quantity H (see Expression [7]) becomes equal to its critical value H_c

$$H_c = 4/3\sqrt{3}\,(n - 1) \quad [25]$$

For instance, for $n = 8$, which the authors found to hold good for castor oil, H_c would amount to $4/21\sqrt{3} = 0.110$.

Further, it proves that, in contrast with $n = 2$ as in the paper (or more generally, $n \leqslant 3$), as soon as n is greater than 3, hydrodynamic load capacity in the critical cases no longer becomes infinitely high, but remains finite, notwithstanding that maximum oil pressure continues to be infinitely high.[5] This can be shown in the following way:

With Equation [24] instead of Karlson's relationship, Equation [1] of the paper, it can easily be deduced that the distribution of oil pressure p in the film, as a function of the variable T, is given by

$$p = k\left[\left\{1 - (n-1)\cdot H\cdot 4T/(1+T^2)^2\right\}^{-\frac{1}{n-1}} - 1\right] \quad [26]$$

so that maximum pressure p_{max}, which occurs in the film section defined by $T = 1/\sqrt{3}$, is

$$p_{max} = k\left[\left\{1 - (n-1)\cdot\frac{3\sqrt{3}}{4}\cdot H\right\}^{-\frac{1}{n-1}} - 1\right] \quad [27]$$

In fact, for $n = 2$, Equation [26] reduces to the authors' Equation [10] and, for $H = H_c$ (compare Equation [25]), p_{max} becomes infinitely high.

With Equation [26], instead of the authors' Equation [8], we now arrive at the more general expression for hydrodynamic load capacity F_n (compare Equation [3] of the paper):

$$F_n = \frac{2Z_1Ur}{h_0}\cdot\left(\frac{J_n}{H}\right) \quad [28]$$

where J_n represents the integral

$$J_n = \int_0^\infty\left[\left\{1 - \frac{16}{3\sqrt{3}}\cdot\frac{H}{H_c}\cdot\frac{T}{(1+T^2)^2}\right\}^{-\frac{1}{n-1}} - 1\right]dT \quad [29]$$

For the critical cases $H = H_c$, it now follows from analytical inspection of the singularity then occurring in the integrand of Equation [29] at $T = 1/\sqrt{3}$, that, in fact, as soon as $n > 3$, hydrodynamic load capacity remains finite, as then the Integral [29] converges.

By numerical evaluation it was found that for $n = 4$ and 6, in the critical cases $H = H_c$, the factor J_n/H amounts, respectively, to 11.9 and 7.25; this means that in these critical cases, the relative gains in hydrodynamic load capacity, as compared with the classical case where viscosity is assumed to be independent of oil pressure, are 5.95 and 3.63.[6] It can be shown that at increasing values of n the critical J_n/H from Integral [29] monotonously decreases toward an asymptotic limit; this could be checked if the authors would communicate the critical value of the integral, Equation [29], that they computed for their value of $n = 8$.

Thus it would appear that with $n > 3$ the generalized viscosity-pressure relationship, Equation [24], in fact, results in a gain in hydrodynamic load capacity; this in contradistinction to the authors' case $n = 2$, where the gain is infinitely great. In this respect it should be noted that values of n greater than 3 (such as 8) are more representative of actual lubricating oils than the originally proposed value $n = 2$. Let us consider this point further in the light of the theory by Gatcombe,[7] who used the same basic assumptions as the authors, but based his calculations on a viscosity-pressure relationship different from Equations [1] and [24],

[4] Senior Research Engineer, Koninklijke/Shell-Laboratorium, Delft, Holland.

[5] By utilizing the method worked out by W. Weibull in his paper: "Glidlagerteori med variabel Viskositet" (Theory of Slider Bearings With Variable Viscosity) in the Swedish journal *Teknisk Tidskrift, Mekanik*, vol. 55 (1925), pp. 164–167, it can also be shown that, if in Equation [24] the exponent n is smaller than unity, there are no critical cases at all; in other words, maximum oil pressure then could never become infinitely high.

[6] It should be noted that for pressure-independent viscosity the factor J_n/H from Equation [28] assumes the value 2.

[7] Reference is to author's Bibliography (3).

that is, on the exponential relationship Equation [2] of the paper.

Now, the authors themselves have already compared Gatcombe's results with theirs (Table 3), but, as Gatcombe had not been able to evaluate his theory in an exact analytical way, for their purpose the authors had to confine themselves to Gatcombe's "approximate" evaluation. However, it can be shown by the following arguments that the approximation involved is no longer tolerable when a critical case is approached.

Gatcombe's exact result can be written in the form of Equation [28], if the numerical factor (J_n/H) is replaced by B

$$B = -\frac{1}{A}\int_0^{\frac{\pi}{2}} \ln[1 - A(\sin 2S + \tfrac{1}{2}\sin 4S)] \cdot \sec^2 S \cdot dS \quad \ldots\ldots [30]$$

where the nondimensional quantity A is defined by

$$A = \frac{1}{12} G\delta \ln 10 \ldots\ldots [31]$$

if Gatcombe's notation is upheld, or, if rewritten in the authors' notation by

$$A = Z_1 U(2r)^{1/2} \cdot h_0^{-3/2}\delta \ln 10 \ldots\ldots [32]$$

Gatcombe's approximation amounts to the same thing, as replacing the exact value of B Integral [30] by the approximate one

$$B \approx \frac{\pi}{120} \cdot \left[4\pi \ln 10 - \frac{27}{A} \cdot \ln\left(1 - \frac{3\sqrt{3}}{4} A\right)\right] \ldots [33]$$

As was shown by Gatcombe, with the exponential viscosity-pressure relationship, Equation [2] of the paper, critical cases arise, that is, maximum pressure theoretically becomes infinitely high, when A becomes equal to its critical value[8] of $4/3\sqrt{3}$.

Whereas, for the critical value of A, the integrand of Integral [30] shows a singularity at $S = \pi/6$, it can be shown by analytical inspection that yet this integral converges, so that the corresponding value of B or, say, hydrodynamic load capacity remains finite in the critical cases. On the other hand, Gatcombe's approximate value for B (see Expression [33]) becomes infinite for the critical value of A. This proves that, in fact, Gatcombe's approximation is no longer tolerable when a critical case is reached or approached.

In view of the background to the present discussion, we are left with the problem of computing, from Integral [30], a workable expression for B that is applicable at least to the critical and the near critical cases. Fortunately, it proves that an exact evaluation of the integral of Equation [30] is possible, so that this evaluation is even applicable to the whole physically significant range $0 \leqslant A \leqslant 4/3\sqrt{3}$. The method of exact evaluation found will now be elucidated, the more so as it is also applicable to the authors' Integral [9].

Changing to the authors' variable T, and partially integrating Integral [30], it is easily found that

$$B = 12\int_0^{\infty} \frac{T\,dT}{(1+T^2)^2 - 4AT} - 16\int_0^{\infty} \frac{T\,dT}{(1+T^2)[(1+T^2)^2 - 4AT]} \ldots [34]$$

The foregoing two integrals can, in fact, be evaluated in terms of elementary functions by observing that the integrands can be resolved into partial fractions of no higher than the second degree, namely, as follows:

According to Descartes' well-known method of solving biquadratic equations, the form $[(1+T^2)^2 - 4AT]$ can be resolved into the product of two quadratic forms

$$(1+T^2)^2 - 4AT = (T^2 - uT + v)(T^2 + uT + w). [35]$$

where u, v, and w are determined, for any given A, by the positive root of Descartes' "cubic resolvent"[9]

$$y^3 + 4y^2 - 16A^2 = 0 \ldots\ldots [36]$$

That is, u, v, and w follow consecutively from the formulas

$$u = \sqrt{y} \ldots\ldots [37a]$$

$$v = \tfrac{1}{2}\left(2 + y - 4A/\sqrt{y}\right) = \tfrac{1}{2}(2 + u^2 - 4A/u) \ldots [37b]$$

$$w = \tfrac{1}{2}\left(2 + y + 4A/\sqrt{y}\right) = \tfrac{1}{2}(2 + u^2 + 4A/u) \ldots [37c]$$

In this way, the integrals in Equation [34] were actually evaluated in an exact analytical way. As, however, for an arbitrary value of A, within the range $0 \leqslant A \leqslant 4/3\sqrt{3}$ to be considered, the expression for B is rather unwieldy, the expression for the critical case only of $A = 4/3\sqrt{3}$ will be given here, namely

$$B = \frac{3}{2} \cdot \left[(\sqrt{3} - \sqrt{2}) \cdot \pi + \ln 3 + 2\sqrt{2} \cdot \tan^{-1}\left(2\sqrt{2}\right)^{-1}\right] = 4.588 \ldots\ldots [38]$$

Thus we arrive at the conclusion that, with the exponential viscosity-pressure relationship Equation [2] of the paper, in the critical cases hydrodynamic load capacity is only $4.588/2 = 2.294$ times as high as it would be when viscosity is constant, that is, not affected by pressure. This entails, of course, that Gatcombe's approximation can no longer be upheld in those cases where it predicts a relative gain (called "pressure effect," in the last column of the authors' Table 3) in hydrodynamic load capacity that is greater than 2.294. Such cases are represented by Gatcombe's problems Nos. 1, 2, and 4; thus only to problems Nos. 3 and 5 can some significance be attached for the authors' purpose of comparing their results with Gatcombe's.

So far, the authors' and Gatcombe's basic assumptions have been upheld; it remains to be seen, however, whether these assumptions are permissible, and if not sufficiently so, when they will break down. Here we shall solely consider the question of the validity of the assumption about the perfect rigidity of the mating tooth faces. The reason that it can be made acceptable is that only the elastic distortion of the tooth faces, such as actually occurs when oil pressures in the film are sufficiently high,[10] can, in conjunction with the increase in viscosity with pressure, contribute substantially to hydrodynamic load capacity; thus we might arrive at an explanation of the remarkable fact that in practice there are many cases of gears where hydrodynamic load capacity obviously is very much greater than would be predicted by Martin's anonymous paper (1)[11] on the elementary theory of hydrodynamic lubrication of gear teeth.

It will be evident that tooth faces may no longer be considered

[8] By sheer coincidence the critical value for A happens to be the same as the one for the authors' H in their case of $n = 2$.

[9] It is easily demonstrated that, for $0 \leqslant A \leqslant 4/3\sqrt{3}$, which is the physically significant range of A, the cubic Equation [36] has one positive root only.

[10] The type of elastic distortion meant here was called "hydrodynamic depression" in the present writer's paper: "Fundamental Mechanical Aspects of Thin-Film Lubrication," (read on March 4, 1950, before the New York Academy of Sciences); in this paper further particulars about the relevant gain in hydrodynamic load capacity can be found.

[11] Reference is to authors' Bibliography (1).

to be perfectly rigid in those cases where the maximum film pressure, as calculated by the theory to be checked, attains or exceeds the order of magnitude of the Hertzian contact pressure that would obtain for the load considered if there were no oil film at all. In fact, in such cases the elastic distortions of the tooth faces under the high oil pressures must be comparable with those according to the Hertzian theory of elastic contact. This means, however, that, with the small minimum film thicknesses involved, the geometry of the film, and thereby the distribution of film pressures and hence the corresponding hydrodynamic load capacity, must be altered appreciably. Examples of the foregoing cases are provided by all of Gatcombe's problems, except No. 5 (compare the authors' Table 3).

It would also appear that the somewhat disturbing critical cases with their infinitely high maximum oil pressures would disappear automatically when the elastic distortions of the tooth faces are taken into account. Anyway, in cases representative of the beneficial effects on hydrodynamic load capacity of the increase of viscosity with pressure, the additional beneficial effects of the elastic distortions mentioned have to be accounted for simultaneously. Of course this renders the computer's task much more difficult; however, some headway has already been made and it is hoped that the results can be published in the not too distant future.

Authors' Closure

It is reassuring to have Mr. Blok's opinion that the effect of elastic deformation is to increase the film thickness. This confirms the authors' belief that the assumption of rigid teeth gives film thickness values on the safe side, the true values being greater than calculated. It was not the authors' desire to defend that assumption but only to treat it as a limiting case. Let us hope that new investigations will soon be available in which elastic deformation is combined with hydrodynamic action. Meldahl[12] took a long step in this direction but did not include the viscosity-pressure effect.

Mr. Blok offers constructive comment in two principal directions: first, by explaining the question he had raised (5) regarding the accuracy of Gatcombe's theory, and providing an exact analytical solution; second, by outlining a solution for rigid teeth based on a more general form of the viscosity-pressure relation, namely Equation [24].

This equation is a fairly obvious generalization of Karlson's parabola, the only change being the substitution of an empirical exponent n in place of the parabolic exponent 2. The same generalization had also been investigated by the authors, and the main results stated during the oral presentation of the paper. These are summarized below in response to Mr. Blok's inquiry regarding the critical value of the load integral in Equation [29] when $n = 8$.

Proceeding as in Karlson's paper except for the use of n in place of 2, the authors had arrived at relations identical with Equations [26] to [29] by completely analytical steps. Equation [29] was then integrated graphically for chosen values of H, leading to the round number $J_n/H = 6$ when $n = 8$ and H has the critical value $H_c = 0.110$. An analytical proof that the load integral remains finite in the critical case if n is greater than 3 had been given by Mr. Lowdenslager.

A more precise solution was then made in which the area under the pressure curve was evaluated by a semianalytical method. The tail of the diagram from T_1 to infinity, where T_1 is large compared to the value T_0 at which the formula gives infinite pressure, was computed by treating T_0/T as a negligible quantity. The peak area was evaluated by neglecting T-T_0 in comparison with T_0, using a factored expression kindly suggested by Prof. J. T. Burwell, Jr., of M.I.T. The mean of both methods gave $J_n/H_c = 6.2$. This is in good agreement with a more exact value, 6.23, communicated by Mr. Blok. In fact, Mr. Blok and the authors, working independently, arrived at similar conclusions on every essential aspect of the problem.

All the values found for J_n/H_c are plotted in Fig. 5 as a function of n. Fig. 6 has been constructed with the aid of Fig. 5 and can be offered as a tentative generalization of Fig. 1. In Fig. 6 the dashed curves for $n = 3$, 4, 6, and 12 have been drawn in freehand from $H = 0$ to their known end-points corresponding to $H_c = 0.384$, 0.257, 0.154, and 0.070 respectively, and faired by cross-plotting of H against n at constant values of the ordinate.

From Fig. 6 and its future refinements, in conjunction with Equations [13], [15], [19], and [20] of the paper it should be possible to generalize the film-thickness chart, Fig. 4, for all values of n. In the meantime, the practical use of Fig. 4, with Karlson's exponent 2, requires only that suitable values be selected for the empirical constant k with the aid of Fig. 3, as described in the paper.

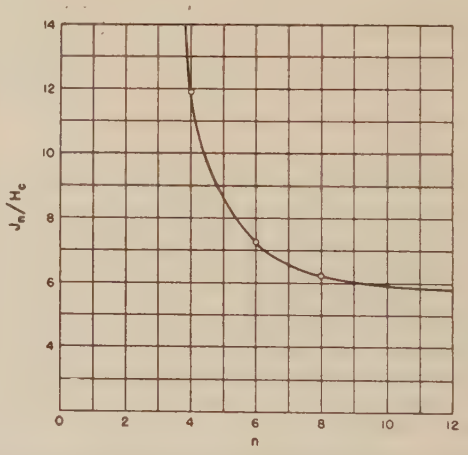

Fig. 5 Critical Load Factor for Different Exponents n

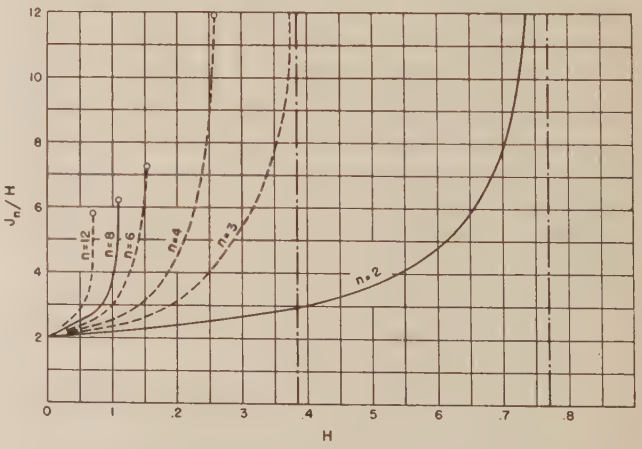

Fig. 6 Load Factor Plotted Against H for Stated Values of n

[12] "Contribution to the Theory of the Lubrication of Gears and of the Stressing of the Lubricated Flanks of Gear Teeth," by A. Meldahl, *Brown Boveri Review*, vol. 28, 1941, pp. 374–382.

Thermal-Shock and Other Comparison Tests of Austenitic and Ferritic Steels for Main Steam Piping

By W. C. STEWART[1] and W. G. SCHREITZ,[1] ANNAPOLIS, MD.

Thermal-shock tests of 6-in. pipe-and-valve assemblies, representing both austenitic and ferritic steels in 80 and 160 schedules, are described. The shock-testing procedure was devised to simulate conditions resulting from carry-over of boiler feedwater into main steam lines operating at 900 or 2000 psi pressure, 1050 F temperature. Other test procedures described include cyclic deflection tests of full-size mock-ups consisting of 160 schedule pipe and valves for simulating expansion bends. Results are reported for mock-ups of both austenitic and ferritic materials which were tested at 2000 psi pressure, 1050 F temperature. Each assembly was subjected to 4000 or more deflections corresponding to expansion cycles that would obtain on heating up a piping system from room temperature to 1050 F once every 2 days for approximately 20 years.

Introduction

DECISION to investigate the feasibility of utilizing 18–8 chromium-nickel-type steel for main steam piping for 1050 F temperature service was prompted by the superior strength properties of the material at temperatures above 1000 F. Moreover, the superior high-temperature properties of the austenitic steels over the ferritic steels for temperatures above 1000 F are reflected in the higher working stresses allowed by the ASME Boiler Code. The higher working stresses for austenitic steel should permit the use of thinner and lighter pipe which, at the higher pressures, is particularly advantageous from the standpoint of increased flexibility and weight saving. On the other hand, thermal expansion is greater for austenitic steel than for ferritic steel, and this fact must not be overlooked in considering flexibility factors.

No experience with austenitic steel for main steam piping has been reported, although the material has been used for boiler feed lines. H. Weisberg[2] has reported on cyclic heating tests of main steam-piping joints between ferritic and austenitic steels. Reports from the oil industry of failures of components in pipe lines used to convey charges of hot oil from cracking stills created doubt as to the suitability of austenitic steel for main steam piping.

It is reported that components in austenitic-steel pipe lines have shown much greater susceptibility to cracking as a result of thermal shock produced by the periodic flow of hot oil than have similar components of ferritic-steel pipe lines. In view of this information it did not seem unreasonable to assume that austenitic steel might exhibit similar susceptibility in steam service under conditions of thermal shock occasioned by boiler-water carry-over. Moreover, experience has been cited which indicates strength deficiencies for austenitic-steel castings as well as for welded joints between austenitic pipe and castings.

There are numerous points of difference between pipes carrying hot oil as previously mentioned and main steam lines. In the case of oil pipe lines, the pressures are fairly low and the temperature of the oil high. For steam lines under consideration the pressure is high and the temperature intermediate by comparison. In the oil pipe lines conditions producing high thermal gradients recur regularly, while conditions producing similar gradients in steam lines occur only infrequently as a result of boiler-water carry-over. Then, there is the difference in heat-transfer characteristics for the two processes which appears to be an important factor in favor of steam applications. Hot oil on passing through a relatively cold pipe causes the inside layer to expand. This expansion is resisted by the colder outer layers with the result that the inside is stressed in compression. Cracking occurs on cooling when the inside of the pipe is in tension.

The introduction of a quantity of boiler water along with the steam flow cools the inside surface, producing a thermal gradient in the pipe wall. Contraction of the quenched layer is resisted by the outer layers of the pipe which are at higher temperature, with the result that the inside of the pipe is subjected to a tensile stress. Therefore any tendency to cracking in steam pipes under thermal shock associated with feedwater carry-over would be expected to occur on quenching.

In setting up the test program, it was decided to subject full-scale pipe-and-valve assemblies to thermal-shock conditions simulating boiler-water carry-over. It was reasoned that this procedure would produce the maximum temperature gradient in the pipe wall that could be expected in service. A second series of tests included in the program consisted of subjecting full-scale mock-ups to deflection cycles designed to simulate stress conditions produced in expansion loops on heating and cooling. At the outset, it was the intention to test only the austenitic material under thermal shock. Later, it was decided to conduct parallel tests of $2^1/_4$ Cr-1 Mo steel throughout.

In order that information on the strength properties of the particular test materials might be available, a laboratory test program was included as a phase of the investigation. Specimens for this purpose were fabricated from sections of 6-in., 80, and 160-schedule pipes and cast cylinders designed to simulate cast valve bodies. The same welding procedures were employed in fabricating these test sections as were used in welding the thermal-shock assemblies and mock-ups.

Welding of the original test assemblies, including the specimens for the laboratory test program, was performed by a large commercial fabricator utilizing production welding practices with regard to qualification of welders, number of welders employed on the job, shift work, and extent of supervision exercised over the welders.

---

[1] United States Naval Engineering Experiment Station.

[2] "Cyclic Heating Tests of Main Steam-Piping Joints Between Ferritic and Austenitic Steels—Sewaren Generating Station," by H. Weisberg, Trans. ASME, vol. 71, 1949, pp. 643–649.

Contributed by the Power Committee and presented at the Spring Meeting, Washington, D. C., April 12–14, 1950, of The American Society of Mechanical Engineers.

Note: Statements and opinions advanced in papers are to be understood as individual expressions of their authors and not those of the Society. Manuscript received at ASME Headquarters, February 27, 1950. Paper No. 50—S-23.

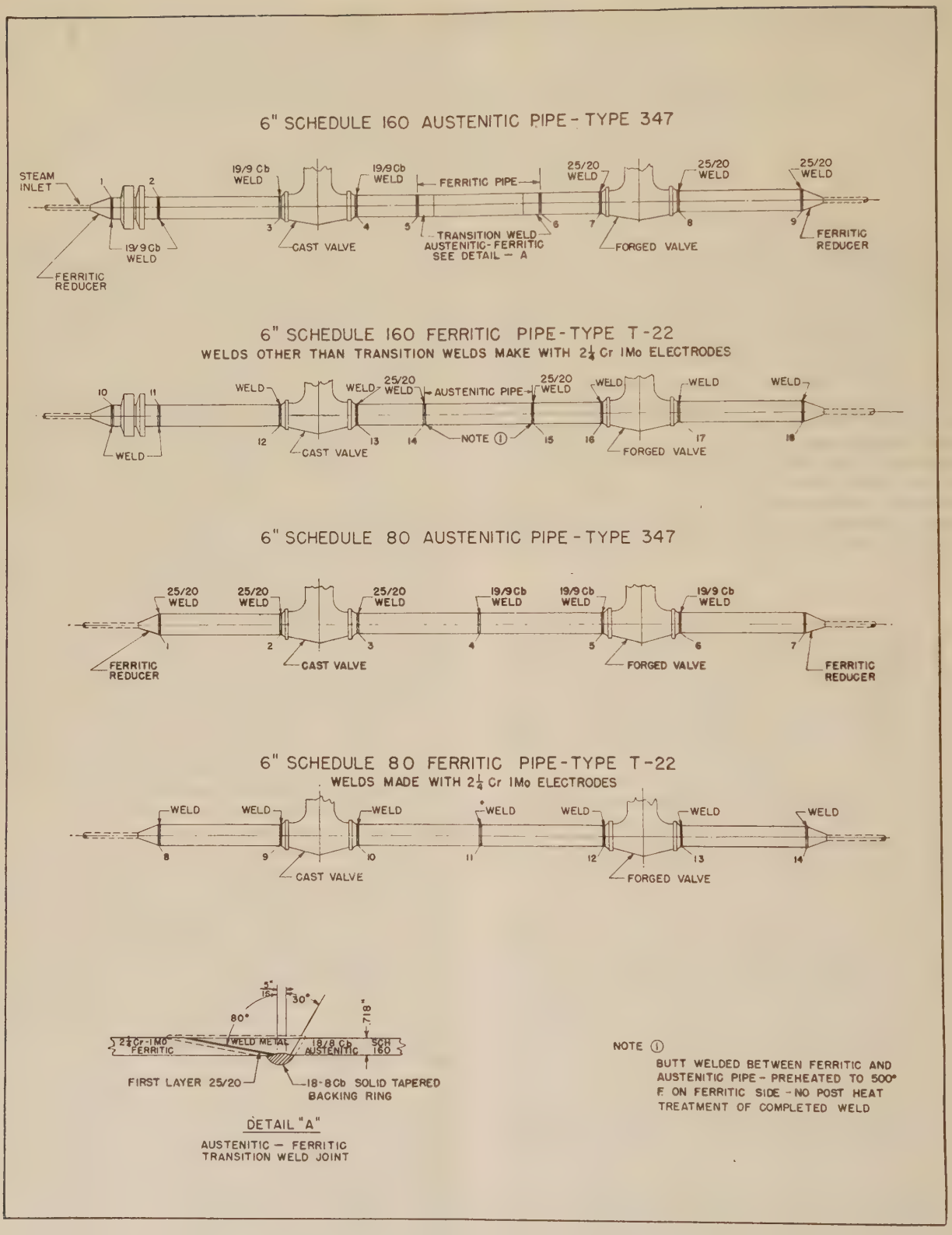

FIG. 1 DETAILS OF THERMAL-SHOCK TEST SPECIMEN

Description of Thermal-Shock Test Assemblies

Details of the thermal-shock test assemblies are shown in Fig. 1. Four 6-in. assemblies are shown. Two are of austenitic steel, type 347, in 80 and 160 schedules, and the other two ferritic steel, Type T-22 in the same schedules. The lighter assemblies were prepared for testing at 900 psi pressure, 1050 F temperature, and the heavier specimens for testing at the same temperature, but at 2000 psi pressure. Each assembly contains two pressure-seal bonnet gate valves, one of cast material and the other of forged material, both of similar composition to the pipe. The 160 schedule austenitic assembly contains a 36-in. length of 2¼ Cr-1 Mo steel pipe at mid-length, while the ferritic assembly contains a similar length of austenitic-steel pipe. This arrangement permitted the simultaneous testing of joints between the dissimilar steels. In the austenitic assembly a transition type of welded joint was employed, while the dissimilar materials in the ferritic assembly were joined by means of V-type welds. Details of the transition-type joint are given in Fig. 1. No dissimilar metal sections were incorporated in the 80-schedule thermal-shock assemblies.

Fig. 2 shows the design of the V-type weld employed in welding the thermal-shock assemblies. The welds of the ferritic-steel assemblies, except for the welds joining the dissimilar pipe section, were made with 2¼ Cr-1 Mo electrodes. The dissimilar pipes were welded with 25–20 chromium-nickel electrodes. The V-welds of the austenitic assemblies are of two types, those made with 19–9 Cb electrodes and those made with 25–20 electrodes as indicated in Fig. 1.

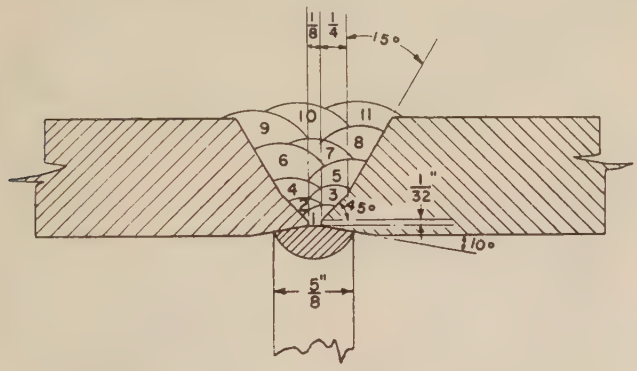

Fig. 2 Details of V-Type Welded Joint

The 2¼ Cr-1 Mo steel pipe is in accordance with ASTM A158–46T, except that chemical requirements are as per ASTM Specification A213–46T for Grade T-22.

The prescribed welding procedure included the following:

All joints of 2¼ Cr-1 Mo steel were preheated to a minimum temperature of 400 F for welding, and this temperature was maintained until final heat-treatment was accomplished. After welding and while the interpass temperature was held, a circumferential band on each side of the weld, having a width of not less than 6 times the section thickness of the pipe, was heated uniformly to a temperature within the range 1325–1350 F. The zone was maintained at this temperature for a period of time equivalent to 2 hr per in. of thickness. Retarded rates of cooling were employed.

The 18–8 Cb pipe is in accordance with ASTM A158–46T for Grade P8d. The pipe was stabilized at 1550 F temperature as a final operation, pickled, plus all supplementary requirements of specification. No preheat or postheat was employed in welding the austenitic-steel pipe.

The material for the cast austenitic-steel valve bodies is in accordance with ASTM Specification A157, Grade C9, except 0.10 per cent maximum carbon and columbium stabilized. Material for the forged austenitic valve bodies is as per AISI Type 347. All bodies were given the following treatment:

Heated to 1850 F minimum, held for 4 hr, and cooled in air blast until black. Stabilizing treatment consisted of heating to 1575–1625 F, holding for 8 hr, and cooling in air.

The material of the cast ferritic-steel valve bodies is as per ASTM Specification A217, Grade WC3. The chemical composition of the forged valves is as per ASTM Specification A213–46T, Grade T-22. The valve bodies were heat-treated as follows:

Cast Bodies:

Normalizing treatment
Heated to 1775–1825 F, held for 4 hr, cooled in air
Air-quench treatment
Heated to 1675–1725 F, held for 4 hr, cooled in air
Tempering treatment
Heated to 1275–1325 F, held for 4 hr, cooled in air

Forged Bodies:

Air-quench treatment
Heated to 1550–1600 F, held for 4 hr, cooled in air
Tempering treatment
Heated to 1275–1325 F, held for 4 hr, cooled in air

Prior to welding, the thermal-shock specimens were drilled for thermocouples as shown in Fig. 3. The thermocouple holes are 0.136-in. diam and are located on the underside of the pipe about 6-in. upstream from the cast valves, where the quenching action would be most severe. The thermocouples are held against the metal at the bottom of the wells by coil springs. Drilling these

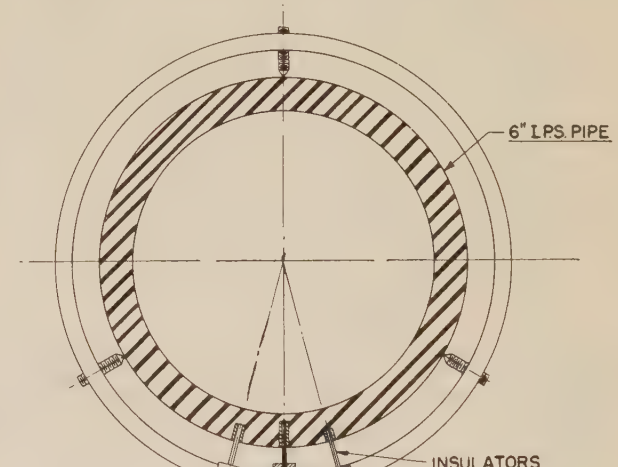

THERMOCOUPLE DESIGNATION	WALL THICKNESS AT BOTTOM OF THERMOCOUPLE HOLE— INCHES			
	18:8 160 SCH.	2¼ Cr-1 Mo 160 SCH.	18:8 80 SCH.	2¼ Cr-1 Mo 80 SCH.
T_1	.032	.021	.017	.024
T_2	.147	.146	.094	.090
T_3	.348	.338	.179	.195
* T_4 & T_5	.679	.670	.412	.419

* THERMOCOUPLES PEENED IN OUTSIDE PIPE WALL

Fig. 3 Thermocouple Location in Pipe Wall

holes prior to welding permitted more accurate depth measurements to be made. Leads from the thermocouples were connected to jacks mounted in a panel board, and the circuits to the instruments were completed by plugging in on the panel.

Characteristics of the temperature recorders used in the investigation are as follows:

Four-point recorder, chart speed 8 ipm, 0 to 1200 F, minimum time between printed points 1 sec.

Continuous pen recorder, 0 to 1200 F, chart speed 8 ipm, maximum pen speed 4.5 sec for full scale travel.

Continuous pen recorder, double range 0 to 12 mv and 0 to 1200 F. Chart speed 8 ipm, maximum pen speed 2.2 sec for full scale travel.

Thermal-Shock Tests

The thermal-shock specimens were set up for test as shown in Fig. 4. Steam was supplied from a Bessler boiler and separately fired superheater, and thence through a booster superheater before entering the test assemblies. The temperature of the steam on leaving the Bessler superheater was approximately 930 F. The steam at the outlet of the booster superheater was maintained at 2000 psi pressure, 1065 F temperature, which insured steam at 1050 F at the test assemblies. The flow of steam was maintained constant by means of orifice plates in the discharge lines; about 7500 lb of steam per hr was passed through each assembly. Steam on leaving the assemblies was passed through a desuperheater, thence to a condenser.

As shown in Fig. 4, two thermal-shock specimens of the same

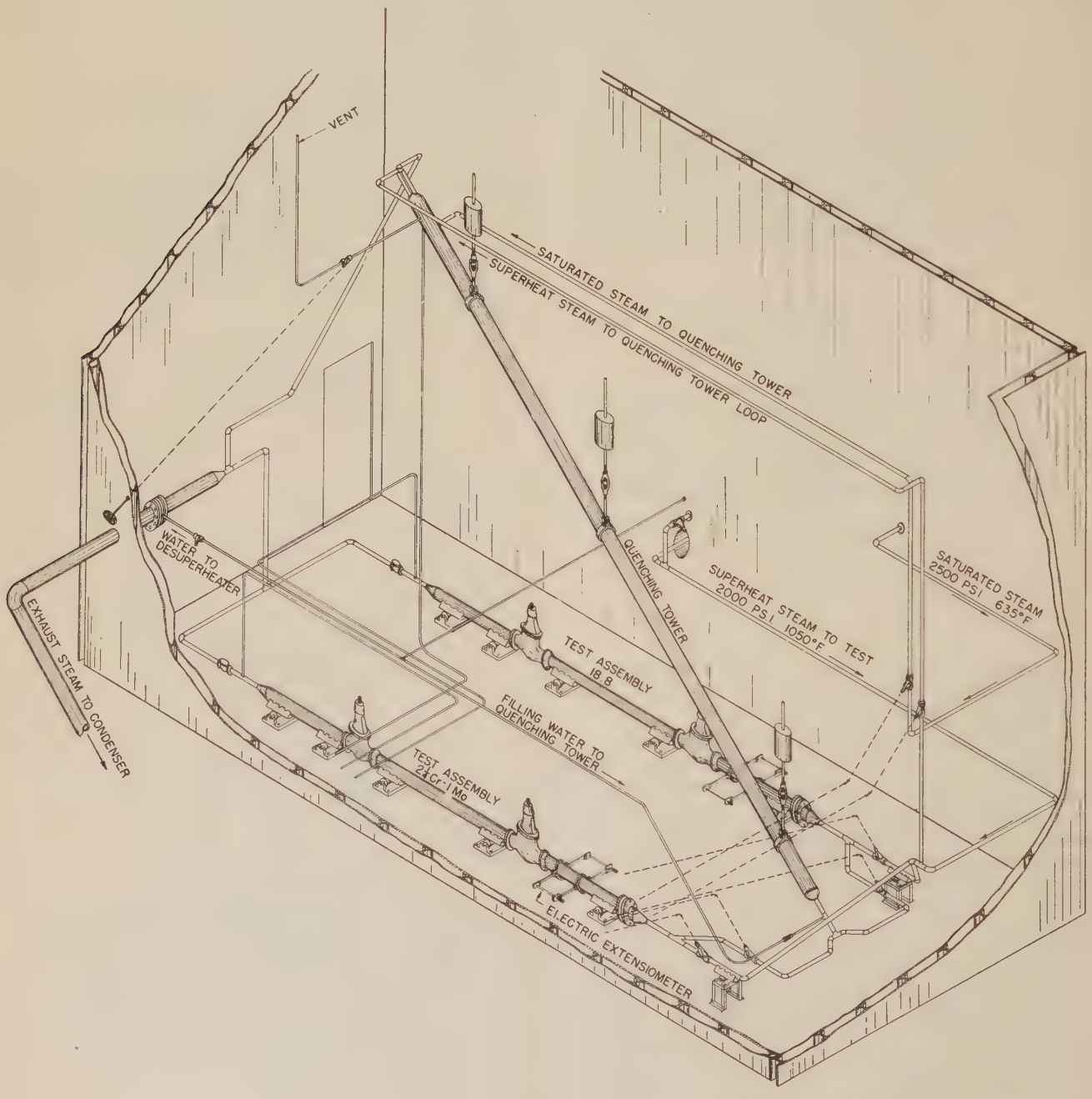

Fig. 4 Layout of Thermal-Shock Test Specimens

schedule are arranged in parallel with the quenching tower suspended between them. The tower is provided with four thermocouple wells distributed over its length. Thermocouples placed in these wells indicate the water level in the tower. The test assemblies are mounted on rollers to prevent longitudinal restraint. Thermal shock is produced by introducing water at the saturated temperature into the assemblies after the latter have attained temperature equilibrium. The water is introduced along with the flow of superheated steam in order more nearly to simulate actual service conditions.

The original plan of test called for shocking the austenitic and ferritic assemblies alternately. A few preliminary runs showed that this was impracticable as the procedure caused too much fluctuation on the boiler, and besides, the main valves were difficult to operate with long rods extending outside the protective enclosure. Accordingly, one assembly was tested at a time. The assemblies were shocked with either 60 or 88 lb of water, corresponding to levels 2 and 3 of the quenching tower. The volume of quenching water, whether 60 lb or 88 lb, had no significant effect on the temperature gradients produced in the pipe walls.

A temperature record was taken for each thermal shock, the order of taking thermocouple records being varied so that all combinations of temperature differences would be obtained. For several runs, records were obtained on a multipoint recorder which gave a complete record. However, the printing speed of the multipoint recorder was not sufficient to obtain maximum temperature differentials. Temperature gradients given in the paper represent a composite of several average runs. Readings obtained with a differential recorder were not in good agreement with the corresponding temperature differentials obtained for iron-constantan thermocouples, but the records do serve to confirm a peculiar behavior observed for one of the regular thermocouples. This circumstance will be referred to later in the paper.

Test data obtained for the thermal-shock specimens are given in Table 1.

TABLE 1 TEST DATA FOR THERMAL-SHOCK TEST SPECIMENS

	Ferritic assemblies quenched with 60 or 88 pounds of water		Austenitic assemblies quenched with 60 or 88 pounds of water	
	⟵Schedule⟶		⟵Schedule⟶	
Condition	80	160	80	160
Number of thermal shocks	100	125	100	102
Approximate time for 1 shock cycle, hr	0.5	1	0.5	1
Maximum temperature difference between inside and outside of pipe wall during quench, deg F	225	210	115	170
Average time required to produce maximum temperature differential in pipe wall, sec	2	4–5	3	17
Steam pressure during heating part of cycle, psi	900	2000	900	2000
Boiler steam pressure, psi	1020	2300	1020	2300
Temperature of pipe prior to quench, deg F	1050	1050	1050	1050
Temperature of quench water, deg F	533	635	533	635

NOTE: All four thermal-shock assemblies withstood the 100 or more quenching cycles without failure by rupture.

Time-temperature curves for four locations in the pipe walls of the 160-schedule austenitic and ferritic assemblies are shown in Figs. 5 and 6. These assemblies were quenched with water at the saturation temperature (635 F). In Fig. 5 the curve for thermocouple T–1 is shown as crossing the curve for thermocouple T–2 at 16 sec and recrossing at 26 sec. This anomaly was observed only in the case of the austenitic assembly, as will be seen by a comparison of the time-temperature curves in Figs. 5 and 6.

Differential thermocouple readings obtained for the austenitic assembly also indicated a higher temperature for T–1 than for T–2 over a short period of time, thus confirming results obtained with regular thermocouples. Similar differential thermocouple records for the ferritic assembly showed no corresponding anomalous behavior. Temperature differentials obtained from curves T–1 and T–4 in Figs. 5 and 6 are plotted in Fig. 7. The slow response of thermocouple T–1 of the austenitic assembly on quenching is indicated by the lower portion of the curve. No satisfactory explanation for this behavior is available.

Similar time-temperature curves for the 80-schedule austenitic and ferritic assemblies are shown in Figs. 8 and 9. During these tests, trouble developed in thermocouples T–2 and T–3 of the austenitic assembly, and in T–3 of the ferritic assembly. In view of this, results obtained for these thermocouples are not included in the paper. Temperature differentials for thermocouples T–1 and T–4 of the 80-schedule assemblies as taken from the time-temperature curves in Figs. 8 and 9 are presented in Fig. 10.

Stress Calculations

Thermal stresses produced in the 160 schedule assemblies as a result of the quenching action were calculated from Timoshenko's[3] thermoelastic formula. As the temperature was measured at four positions, three positions within the pipe wall and on the outside of the pipe, it was necessary to interpolate to find the temperature at points between the locations where it was actually measured. This interpolation was done under the assumption that the temperature varied linearly between successive readings, from thermocouple to thermocouple. It was possible to find the temperature of the inside wall by extrapolating the values from the first two thermocouples as these were quite near the wall.

The stresses at radii corresponding to the four thermocouples were calculated from four integrals which were added to get the corresponding integral for outside radius to inside radius. As a check the integral from outside radius to inside radius was calculated in a similar manner, assuming that the temperature varied linearly throughout the pipe wall. These yielded values are very near the values as calculated by thermocouple-to-thermocouple integration. The maximal tensile stress developed in each of the assemblies as calculated by this method was about the same, namely, 32,000 psi. The maximal tangential stress was computed using the formula,[4] developed under the assumption that the temperature varied linearly from wall to wall. Results checked closely with the largest of the stresses computed by the method previously described.

Description of Mock-Ups

On completion of the thermal-shock tests of the 160-schedule assemblies, the valves with connecting section of pipe were removed for rewelding in mock-ups for cyclic deflection tests. In sectioning the thermal-shock specimens, one cut was made about 5 in. upstream from the cast valve, and the other 12 in. downstream from the forged valve. A 7-in-long section of pipe was welded to the pipe adjacent to the cast valve to make the assembly symmetrical. Then, S-bends were welded to the ends of the pipe and valve assemblies, producing a mock-up as shown in Fig. 11. The design of these welds differed somewhat from the original welds in that a flat split backing ring with four pins to maintain $^3/_8$ in. root spacing for the austenitic pipe and $^1/_4$ in. root spacing for the ferritic pipe was employed.

As shown in Fig. 11, one end of the loop is anchored and the other end pinned to the piston of a hydraulic cylinder having an 8-in. bore. The free end of the loop is restrained from moving in any but the horizontal direction by a 30-in-long sleeve bearing. The hydraulic cylinder is supplied with oil at the rate of 50 cu in. per min by a motor-driven pump. The direction of the piston is reversed by means of an electrically operated four-way valve, the length of the stroke being controlled by microswitches. Three

[3] "Strength of Materials," by S. Timoshenko, second edition, The Macmillan Company, New York, N. Y., vol. 2, 1931, p. 261.

[4] Ibid., p. 174.

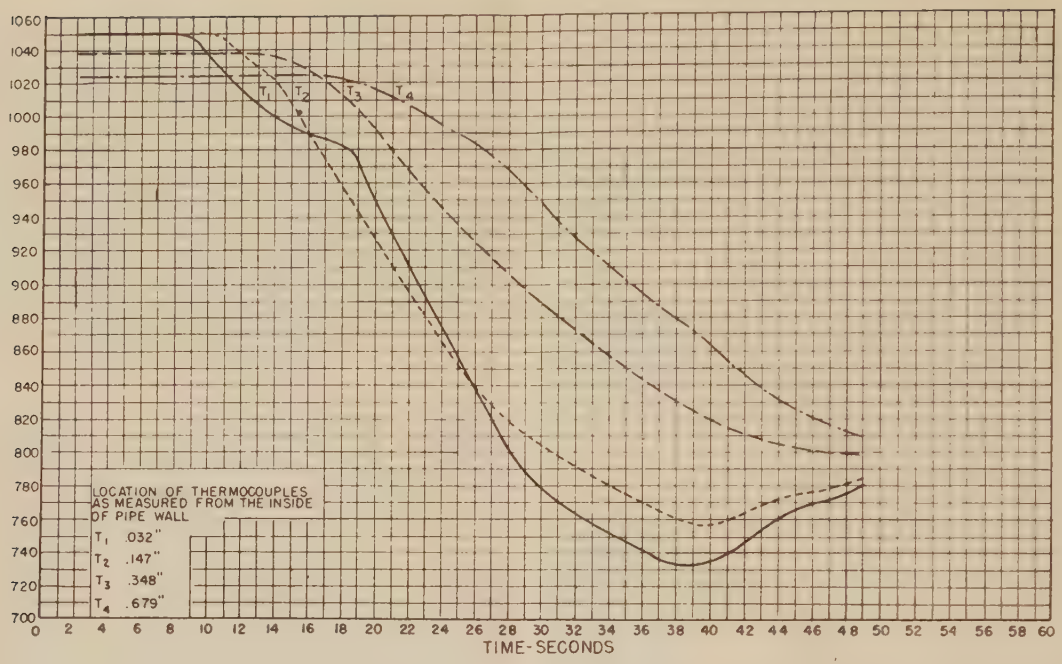

FIG. 5 THERMAL GRADIENTS FOR 18 CR-12 NI-0.8 CB 6-IN. PIPE, 160 SCHEDULE, WHEN QUENCHED WITH 635 F WATER

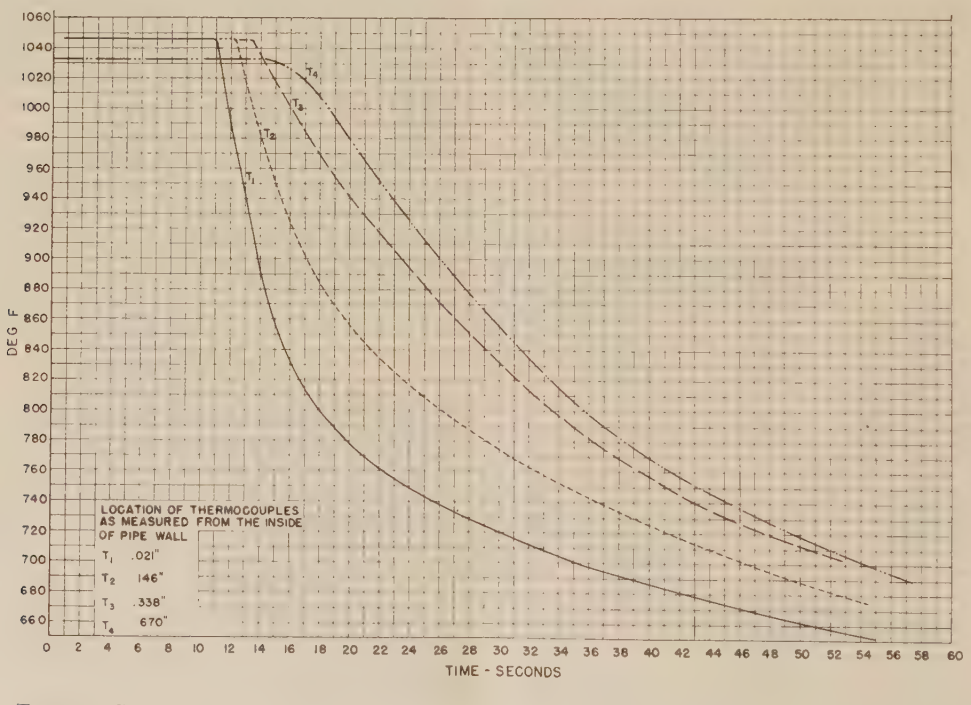

FIG. 6 THERMAL GRADIENTS FOR 2¼ CR-1 - MO 6-IN. PIPE, 160 SCHEDULE, WHEN QUENCHED WITH 635 F WATER

safety devices are contained in the hydraulic system, i.e., (1) a pressure-relief valve set at 300 psi, (2) a pressure switch adjusted to shut down the pump when the pressure exceeds 275 psi, and (3) a by-pass valve in a line connecting the ends of the cylinder.

RESULTS OF MOCK-UP TESTS

Deflection tests were made of the 160-schedule mock-ups at room temperature after mounting resistance-type strain gages at a number of locations as indicated in Fig. 11. Readings were taken on all gages after removing the pin from the shackle of the piston so as to insure a free-end condition. The connecting pin was then replaced without producing appreciable change in the initial readings. Next, 2000-psi hydrostatic pressure was applied to the assembly, and another set of readings taken. Strain-gage readings were obtained for different positions of the piston while compressing the loop. Readings were taken about every 0.3-in. movement of the piston for a total movement of 2 in.

The relationship between deflection and strain or equivalent stress having been established at normal temperature, it was only necessary to multiply the normal temperature deflection by the

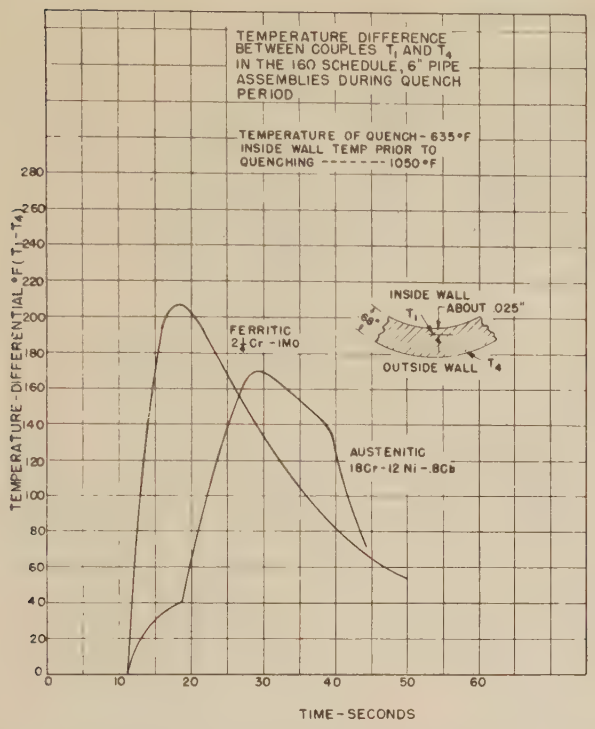

FIG. 7 TEMPERATURE DIFFERENCE BETWEEN COUPLES T–1 AND T–4 IN THE 160-SCHEDULE, 6-IN. PIPE ASSEMBLIES DURING QUENCH PERIOD

ratio of moduli of elasticity of the material at normal and 1050 F temperatures to obtain the deflection necessary to produce the corresponding stress at the elevated temperature. For the austenitic steel this ratio is 28.8/23.0 = 1.25; and for the ferritic steel 30.4/21.0 = 1.45.

Steam was passed through the mock-up at the rate of 5000 lb per hr, temperature equilibrium at 1050 F temperature being established after 6 hr. The unrestrained position of the free end of the assembly was determined within 0.02 in. In the case of the 160-schedule austenitic mock-up, the stroke was adjusted to produce an equivalent stress of approximately 21,500 psi for the extreme end of the stroke, and a corresponding stress of 11,500 psi for the opposite end of the stroke, the variable equivalent stress being 10,000 psi. For the 160-schedule ferritic mock-up the corresponding stress range was 15,750 to 9750 psi, and the variable equivalent stress 6000 psi. The stroke and equivalent-stress relationships were based upon strain values obtained for gages e and f as shown in Fig. 11. In taking the strain readings on the ferritic mock-up, a rosette strain gage containing a 45-deg element was placed at location ef. This permitted evaluation of shear stress which was found to be negligible.

The principal stresses computed from the strain-gage readings for the cold condition, including the equivalent stresses, are given in Table 2. The stresses were computed from the following relationships:

$$S_x = \frac{E(\epsilon_x + \mu\epsilon_y)}{1 - \mu^2}$$

$$S_y = \frac{E(\epsilon_y + \mu\epsilon_x)}{1 - \mu^2}$$

$$S = \sqrt{S_x^2 + S_y^2 - S_x S_y}$$

where

S_x = longitudinal stress, psi
S_y = circumferential stress, psi
S = equivalent stress, psi
ϵ_x = unit strain in x-direction
ϵ_y = unit strain in y-direction
μ = Poisson's ratio = 0.3

In setting up the test procedure for the mock-ups, it was decided to subject the members to 4000 deflection cycles. This number of cycles was selected as representing the contraction and expansion that a piping system would undergo if brought up to 1050 F from normal temperature once every 2 days for approximately 20 years.

The 160-schedule austenitic mock-up was subjected to 4100 deflection cycles, and the corresponding ferritic mock-up to 4300 cycles. Neither mock-up showed any effect of the test which could be discerned by the operating personnel. The average inlet and outlet steam temperatures for the austenitic assembly were 1055 F and 1045 F. The corresponding temperatures for the

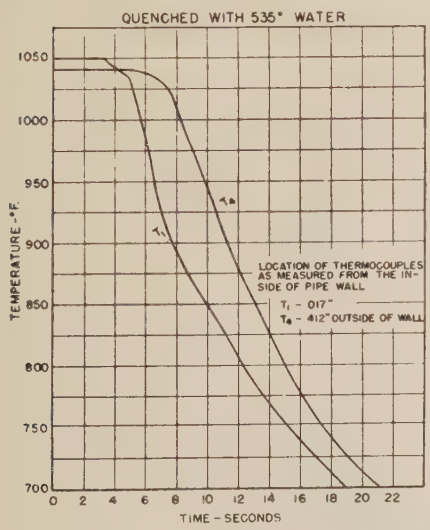

FIG. 8 THERMAL GRADIENTS FOR AUSTENITIC-STEEL 18 CR-12 NI- 0.8 CB, 6-IN. PIPE, 80 SCHEDULE, WHEN QUENCHED WITH 535 F WATER

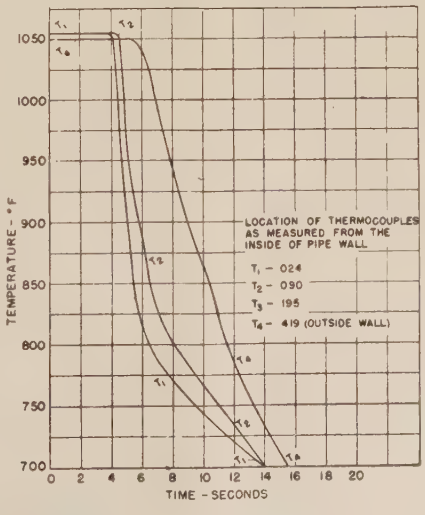

FIG. 9 THERMAL GRADIENTS FOR FERRITIC-STEEL 2¼ CR-1 MO, 6-IN. PIPE, 80 SCHEDULE, WHEN QUENCHED WITH 533 F WATER

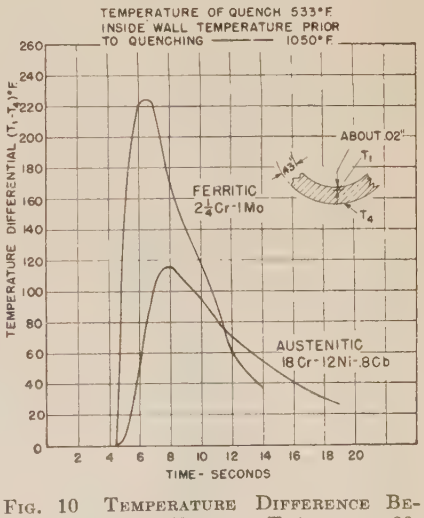

FIG. 10 TEMPERATURE DIFFERENCE BETWEEN COUPLES T–1 AND T–4 IN THE 80-SCHEDULE 6-IN. PIPE ASSEMBLIES DURING QUENCH PERIOD

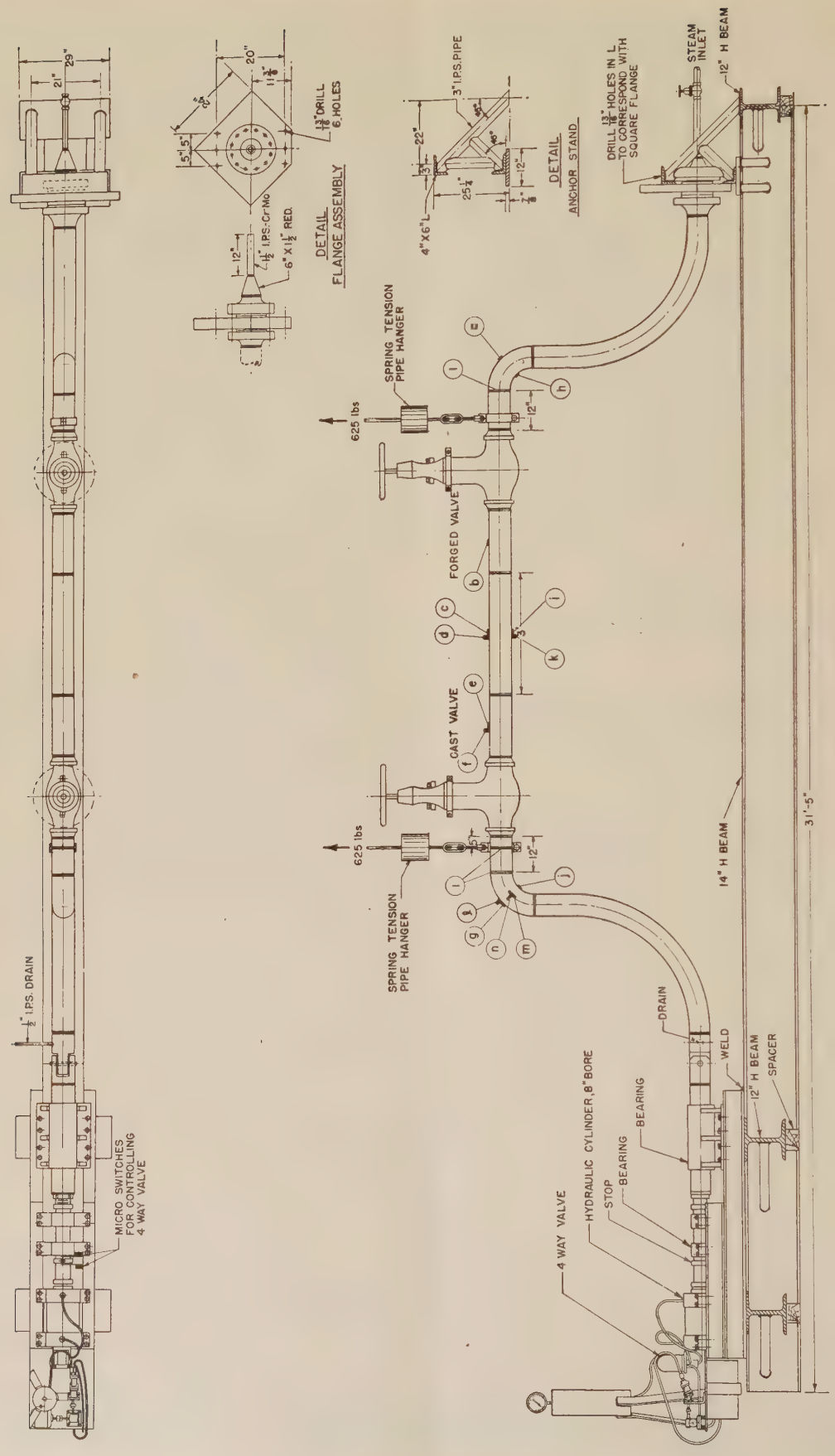

FIG. 11 DETAILS OF MOCK-UP

TABLE 2 DATA OBTAINED FROM COLD DEFLECTION TESTS OF 160-SCHEDULE MOCK-UPS

Strain-gage location shown in Fig. 11	Direction on pipe	Principal stresses computed from strain readings, psi: Austenitic mock-up 160 schedule (a)	(b)	Ferritic mock-up 160 schedule (a)	(b)	Equivalent stress, psi: Austenitic Mock-up 160 schedule (a)	(b)	Ferritic Mock-up 160 schedule (a)	(b)
e	Long	24500	13100	18200	11300				
f	Trans	6800	6100	6100	6100	21900	11200	16000	9800
g	Long	12500	7200	8000	5400				
l	Trans	−15000	−4800	−13500	−5200	23800	10500	18800	9100
m	Long	17800	9400	21900	13400				
n	Trans	25800	14700	26800	17600	22800	12900	24800	15900
c	Long	21800	11800	17000	10700				
d	Trans	6500	6200	7600	7100	19400	10200	14800	9500
i	Long	−16300	−6400	−11000	−3900				
k	Trans	3800	3800	5700	5700	18500	8900	14700	8300

(*a*), Values for maximum inward deflection of loop.
(*b*) Values for minimum inward deflection of loop.

ferritic mock-up were 1057 F and 1048 F. The austenitic mock-up was under test approximately 135 hr at 30.4 cycles per hr. The ferritic mock-up was under test 116 hr at 37 cycles per hr.

The next phase of the investigation will consist of similar tests of the 80-schedule mock-ups.

Following the cyclic deflection tests, zero points for the free-end condition were determined. The zero point of the free end of the austenitic assembly after 4100 deflection cycles indicated that the assembly was 0.44 in. shorter than at the start of the test. The ferritic assembly after 4300 cycles showed a corresponding shortening of 0.86 in.

It appears that shifting of the zero point was caused by yielding which tended to alter the form of the loop somewhat. At the conclusion of the test the maximum stress in the austenitic mock-up was 18,000 psi and the minimum stress 8000 psi, as compared to an initial range of 21,900 to 11,200 psi. For the ferritic mock-up, the maximum stress was 10,600 psi and the minimum stress 5500, as compared to the range 15,750 to 9750 psi at the start of the test. Inasmuch as the tests were conducted at constant deflection, the value of the variable stress would not be expected to change materially.

Examination of Thermal-Shock Assemblies and Mock-Up Following Tests

The necessity for removing the valves and connecting pipe intact from the thermal-shock specimens for rewelding in the mock-ups has precluded destructive examination of any of the welds excepting those at the ends of the assemblies. In Fig. 1 the various welds of the assemblies are numbered for convenience of reference.

Thermal-Shock Assemblies—160 Schedule. All welds contained in the 160-schedule thermal-shock assemblies were examined by an oil-powder method of flaw detection prior to the thermal-shock test. Also, transition weld No. 6 was macroetched and examined at low power for cracks. Following the thermal-shock test the welds again were examined by the oil-powder method. Those welds showing indications of defects were macroetched and examined. In addition, welds, 5, 6, and 9 were x-rayed, and welds 2 and 9 subjected to a peel test which consisted of removing the weld metal from the groove in increments ranging from 0.0075 to 0.030 in. until no indications of cracks were revealed by oil-powder inspection.

Prior to the thermal-shock test, no cracks were observed in the weldments of the 160-schedule assemblies as a result of oil-powder and macroexamination methods of inspection. Following the thermal-shock test, the oil-powder technique revealed cracks which were not evident prior to the shock treatment. The distribution of these cracks was toward the bottom of the assemblies.

The welds joining austenitic-ferritic pipe, namely, 25–20 in V-type joints and 19–9 Cb in transition-type joints, showed the greatest tendency to develop cracks. The etched surfaces of the transition joints indicated variations as regards the deposition technique employed, in that, in some portions of the joints the weld metal was deposited stringerwise while in others in oscillations or weaves up to 1 in. in width.

The 19–9 Cb weld metal in the austenitic piping revealed the least tendency toward fissuring. Others[5] have observed that chromium-nickel compositions of this type, which promote the formation of ferrite, are more resistant to fissuring than are the fully austenitic weld metals. Results of the peel test performed for welds Nos. 2 and 9 showed that cracks indicated on the surface were removed completely after machining to a depth of 0.023 in. for weld No. 2 (19–9 Cb), but persisted to a depth of 0.375 in. for weld No. 9 (25–20).

The welds of the 160-schedule ferritic assembly also revealed cracks following the thermal-shock test, but the number of cracks was less than in the austenitic assembly. The majority of cracks occurred in welds Nos. 10 and 15.

Thermal-Shock Assemblies—80 Schedule. The welds of the 80-schedule assemblies were examined after the manner described for the 160-schedule assemblies. No cracks were observed prior to thermal-shock treatment. Following the thermal-shock tests, cracks were revealed by the oil-powder method but were less numerous and more uniformly distributed than in the 160-schedule specimens. Of the two 80-schedule specimens, the austenitic assembly showed the greater tendency toward fissuring, the number of fissures being much greater in the 25–20 weld No. 2 which happened to be located near the inlet end of the assembly.

The welding technique employed in producing the 25–20 welds in the 80-schedule assembly was at variance with that for similar welds in the 160-schedule assembly in that deposition was stringerwise.

Austenitic Mock-Up—160 Schedule. Further examination of the welds following 4100 deflection cycles of the 160-schedule austenitic mock-up showed an increase in the number and magnitude of cracks in the 25–20 V-joint welds 7 and 8, and in the transition welds 5 and 6. In the case of joint 5, the concentration of defects was apparently on the ferritic side of the joint along the line of fusion between the layer of 25–20 weld metal and the main body of the 19–9 Cb weld metal.

Testing of the 160-schedule ferritic mock-up was not completed in time to include results of oil-powder inspection in the paper.

The fact that cracks or fissures were not revealed in the welds by the oil-powder method until after the thermal-shock treatment might indicate that the defects were potentially present as planes

[5] "The Effect of Alloying Elements on the Tensile Properties of 25–20 Weld Metal," by H. C. Campbell and R. D. Thomas, Jr., *Welding Journal*, vol. 25, 1946, pp. 760s–768s.

TABLE 3 CHEMICAL COMPOSITION AND TENSILE PROPERTIES

Material	Type	C	S	P	Mn	Si	Cr	Ni	Mo	Cb	Temp of Test-°F	Tensile Properties: Tensile Strength	Yield Strength (.2% set)	Elongation in 2 inches	Reduction of Area
		Percent										Lb per Sq Inch		Percent	
Pipe, 6", 160 schedule 2-1/4 Cr- 1 Mo	T-22 ASTM (A213-46)	.12	.019	.015	.36	.35	2.23	.15	1.08	-	75	71900	37800	25.2	72.9
											1100	42100	23000	51.5	85.8
Cast cylinder simulating valve casting 2-1/4 Cr- 1 Mo	Grade WC9 ASTM (A217-47T)	.13	.015	.013	.57	.48	2.25	—	.89	-	75	77800	42300	27.0	51.5
											1100	41400	28200	45.0	77.2
All -weld metal from longitudinal weld laid down between two quarter sections of 6" schedule 160 pipe.(2-1/4Cr-1Mo)Note(c)		.08	.036	.013	.51	.43	2.35	—	.95	-	75	83000	64000	20.0	43.5
											1100	42100	29600	23.0	45.4
Pipe, 6", 160 schedule 18-8 Cb Type 347	Grade P8d ASTM (A158-46T)	.08	.010	.020	1.69	.39	18.13	12.34	-	.80	75	90600	58900	40.5	65.5
											1100	56600	43400	26.7	57.7
Cast cylinder simulating valve casting 18-8 Cb	Grade C9 ASTM (157-44)	.06	.015	.017	.65	.83	18.82	9.03	-	.24	75	71000	28500	29.5	60.1
											1100	42600	18200	30.0	56.9
All-weld metal from longitudinal weld laid down between two quarter sections of 6", schedule 160 pipe 19-9 Cb. Note (b)		.06	.013	.01	1.75	.38	20.23	10.15	-	.62	75	94600	70600	36.0	50.1
											1100	59400	47200	21.7	46.9
All-weld metal from longitudinal weld laid down between two quarter sections of 6" schedule 160 pipe 25-20. Note (a)		.14	.013	.013	1.78	.43	25.88	21.80	.02	-	75	91000	57500	36.7	43.7
											1100	61200	36000	33.5	38.2

Welding electrodes - (a) The 25-20 electrodes were of the lime DC type, the titania content of the coating not exceeding 2% by weight, as per N.D. Spec. 46E4 (INT) Grade IV, Class 1 mod. except that Si, P and S of the deposited weld metal not to exceed the following:

Si 0.50%
P 0.02%
S 0.02%

(b) The 19-9 Cb electrodes were in accordance with N.D. Spec. 46E4 (INT) Grade II except for Si, P and S contents which are the same as for the 25-20 electrodes. Columbium not less than 10 times carbon content but not more than 1%.

(c) Electrodes 2-1/4 Cr - 1 Mo, coating lime-titania type.

TABLE 4 TENSILE TEST RESULTS FOR 0.505-IN. SPECIMENS TAKEN ACROSS V-TYPE WELDS

Description of Specimen	Temp. of Test °F	Tensile Strength	Yield Strength (.2% Set)	Elongation in 2"	Red. of Area	
		Lb per Sq Inch		Percent		
Specimens taken across V-type welded joints in 18–8 Cb 160 schedule 6-inch pipe – welded with 19–9 Cb electrodes.	Room	90400	59300	22.0	25.5	Failed in weld.
		85600	56900	16.5	29.5	
	900	59900	43900	18.0	41.3	Failed in weld.
	1000	59400	42200	25.0	57.3	Broke in base metal.
		59900	- - -	19.5	54.4	Broke in weld.
	1050	55000	40700	11.0	25.8	Broke in weld.
	1100	57700	41400	23.5	56.5	Broke in base metal.
		56800	42200	17.0	27.5	Broke in weld.
Specimens taken across V-type welded joints in 18–8 Cb 160 schedule 6-inch pipes – welded with 25–20 electrodes.	Room	88400	55400	18.0	28.5	Broke in weld.
		76100	53900	11.0	26.8	Broke in weld.
	1000	59400	37700*	22.0	57.3	Broke in base metal.
	1100	52400	34400	8.0	21.3	Broke in weld metal.
Specimens taken across V-type welded joints joining cast 18–8 cylinders – welded with 19–9 Cb electrodes.	Room	78700	35400	45.0	59.5	Broke in cast metal.
	550	53400	28000	23.0	59.9	Broke in cast metal.
	1000	53700	27800	23.0	49.7	Broke in cast metal.
	1050	45900	23400	22.0	52.7	Broke in cast metal.
	1100	44100	24800	22.0	64.8	Broke in cast metal.

* .1% set

of weakness from the beginning, and that the stress conditions imposed by the test caused development into fine cracks. If this is correct, it would be expected that continued stressing would further aggravate the defects as has been mentioned for the 25–20 V-joints, welds 7 and 8, and transition welds 5 and 6 of the 160-schedule austenitic assembly. These welds were subjected to both thermal shock and deflection cycles. On the other hand, fissures would not be expected to develop in sound austenitic weldments as a result of the thermal stresses imposed.

Careful and painstaking control of the entire welding process is necessary to avoid fissuring in welds of heavy sections. Opinion differs as to the relative importance of the various factors. The effect of certain residual elements for increasing the susceptibility to cracking in a number of the chromium-nickel weld metals was pointed out by R. D. Thomas, Jr.[6] The same author observes that cracks may arise from changes in composition of the weld metal by dilution from a dissimilar base metal. O. R. Carpenter and N. C. Jessen[7] present data to the specifying of core-wire analysis which will produce a minimum of microdefects in deposited 25–20 welds. Anton L. Schaeffler[8] has presented a graphical method for predicting weld-metal composition and structure in dissimilar welds. Slight deviations from the applicable technique such as a slower rate of progression, a wider weave, higher preheat, or a higher current have been mentioned by others as contributing factors to the development of fissures in austentic welds.

Laboratory Test Program

The chemical composition and tensile properties at normal temperature and 1100 F for the test materials are given in Table 3. The tensile properties were determined with standard 0.505-in-diam specimens, most of the results being the average of two or more determinations.

Tensile test results obtained for 0.505-in-diam specimens taken across V-type welds in 6-in. 160-schedule austenitic assemblies are given in Table 4.

Stress-rupture test results at 1000 and 1100 F temperatures for specimens prepared from the austenitic and ferritic pipe meterials and cast cylinders are presented in Fig. 12. Similar results for all-weld-metal specimens and specimens taken across V-type welds are shown in Fig. 13. The cast cylinders for simulating valve bodies were $12^1/_2$-in. long with the bore tapering from mid-point, the maximum wall thickness of $1^5/_{16}$-in. being at mid-point.

Fatigue tests were made at 1100 F temperature of conically tapered rotating cantilever specimens prepared from the 160-schedule pipes, the austenitic all-weld metals, and of specimens

[6] "Crack Sensitivity in Chromium-Nickel Stainless Weld Metal," by R. David Thomas, Jr., *Metal Progress*, vol. 50, 1946, pp. 474–479.

[7] "Some Factors Controlling the Ductility of 25% Cr, 20% Ni Weld Deposits," by O. R. Carpenter and N. C. Jessen, *Welding Journal*, vol. 26, 1947, pp. 727s-740s.

[8] "Selection of Austenitic Electrodes for Welding Dissimilar Metals," by A. L. Schaeffler, *Welding Journal*, vol. 26, 1947, pp. 601s-620s.

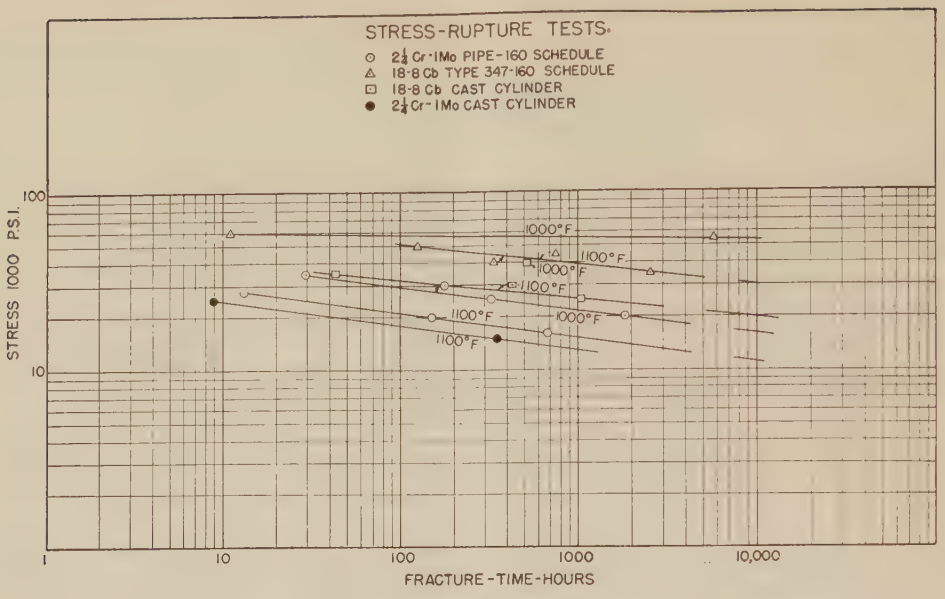

FIG. 12 STRESS-RUPTURE TESTS

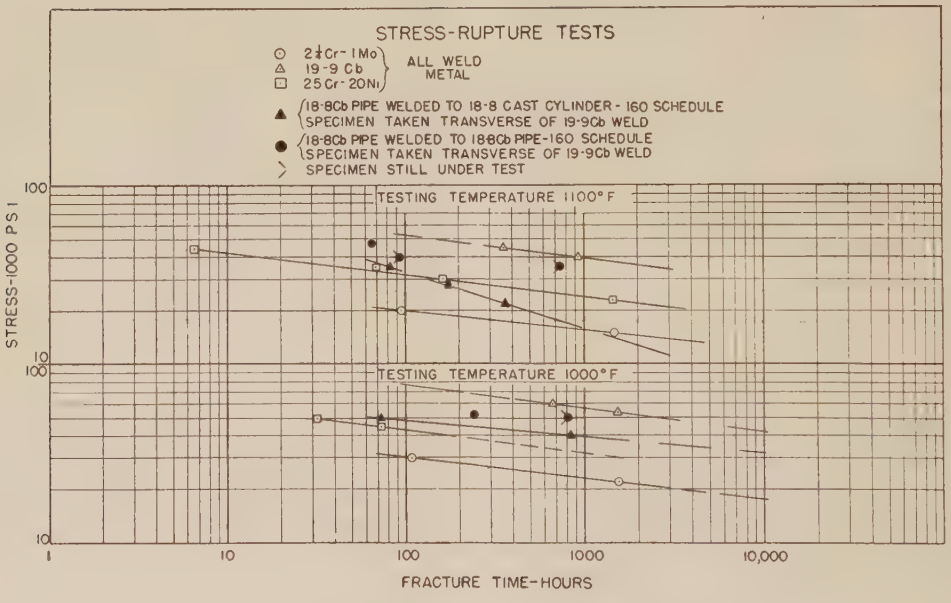

FIG. 13 STRESS-RUPTURE TESTS

taken across V-type welds. The weld zone of the latter was located in the middle of the test length of the specimen, the critical diameter of the tapered test section being 0.357 in. Results of test plotted on a semilogarithmic scale are presented in Fig. 14.

SUMMARY

Thermal-shock tests have been conducted of 6-in. pipe-and-valve assemblies representing both type 347 and 2¼ Cr-1 Mo steels in 80 and 160 schedules. The nominal pipe-wall thickness for 80-schedule pipe is 0.432 in. and for 160-schedule pipe, 0.718 in. Each assembly contained two valves, one cast and the other forged, of similar composition to the pipe material. The 160-schedule thermal-shock specimens contained a 36-in. length of dissimilar pipe at mid-length, the type 347 austenitic assembly being provided with a length of 2¼ Cr-1 Mo steel pipe, and the ferritic assembly with a length of type 347 pipe. The joints of the austenitic assemblies were of two kinds, namely, 19–9 Cb and 25–20 chromium-nickel. Transition-type welds were employed between the dissimilar materials in the austenitic assembly. A V-type joint made with 25–20 electrodes was employed between the dissimilar materials in the ferritic assembly. Dissimilar pipe sections were not contained in the 80-schedule assemblies.

The thermal-shock tests were designed to simulate the effect of carry-over of boiler feedwater into main steam lines operating at 900 or 2000 psi pressure, 1050 F temperature. The assemblies were shocked by introducing either 60 or 88 lb of boiler water at the saturation temperature along with the flow of superheated steam. Each assembly was subjected to 100 or more shocks. Temperature differentials in the pipe walls showed that the maximum temperature difference between the inside and outside of the wall was obtained for the ferritic-steel assemblies. Moreover, the maximum temperature difference occurred in a much

shorter time in the case of the ferritic steel. All four thermal-shock specimens withstood 100 or more shocks without failure by rupture.

Measurements of the assemblies following the tests showed that the ends of the 160-schedule assemblies had been distorted upwardly about 0.10 in. at the inlet end and 0.20 in. to 0.25 in. at the outlet end. The rate of decrease in fracture stress with time at 1100 F temperature, as shown in Fig. 13, for specimens taken across welds joining a section of austenitic-steel pipe and an austenitic-steel casting was disconcerting. However, similar tests of specimens taken across welds joining two sections of austenitic-steel pipe have indicated normal behavior in this respect.

Fatigue tests at 1100 F temperature have shown considerable superiority for the 18–8 Cb pipe material. The fatigue strength for the 19–9 Cb all-weld metal is considerably lower than for the pipe material and apparently controls the fatigue strength of specimens taken across 19–9 Cb welds joining sections of pipe. Similar specimens taken across welds joining 18–8 Cb pipe to austenitic castings showed lower fatigue strength. Comparable fatigue values between 10^7 and 10^8 cycles are indicated for 25–20 weld metal and $2^1/_4$ Cr-1 Mo pipe material at 1100 F temperature.

Acknowledgments

The guidance and assistance received from the Special Subcommittee under the chairmanship of Mr. N. L. Mochel throughout the course of this investigation is gratefully acknowledged. The authors also wish to express their appreciation to Capt. W. D. Leggett, Jr., U.S.N., Director of the Naval Engineering Experiment Station, and Capt. C. G. Grimes, U.S.N., Assistant Director of Laboratories, for their encouragement and support.

Discussion

M. L. Ireland, Jr.[9] The marine and stationary power-plant industries are both fortunate to have available the important results presented in this paper.

It is reassuring that the piping materials withstood tests of such severity with only the small amount of damage indicated. Presumably these tests correspond to the expected number of thermal shocks and normal heating and cooling cycles which will be received by similar pipe in a service life of 20 years.

Such tests are of too-short duration to give much indication of the effect of long-time exposure under sustained pressure stresses. It has been suggested that the reported cracks in the welding zone are due to enlargement of microfissures which may have been present before the test.

If this explanation is accepted then does it not appear likely that further enlargement will occur during long-time exposure at the service temperature, even if the only stresses present are those due to internal pressure?

In view of this fact, it would appear desirable to perform stress-rupture or creep tests on specimens cut from the affected areas but at moderate stress levels, corresponding to the operating conditions.

Since this program was initiated, a rational method for calculating temperature gradients in a pipe subjected to thermal shock has become available.[10] However, this method requires use of a constant value for the internal surface heat-transfer coefficient. A value of 1000 Btu/hr ft^2 F was used in these calculations since it was expected that surface evaporation would occur.

[9] Engineering Department, Technical Division, Newport News Shipbuilding and Dry Dock Company, Newport News, Va. Mem. ASME.

[10] "Heat Transfer," by Max Jakob, John Wiley & Sons, vol. 1, 1949, p. 270.

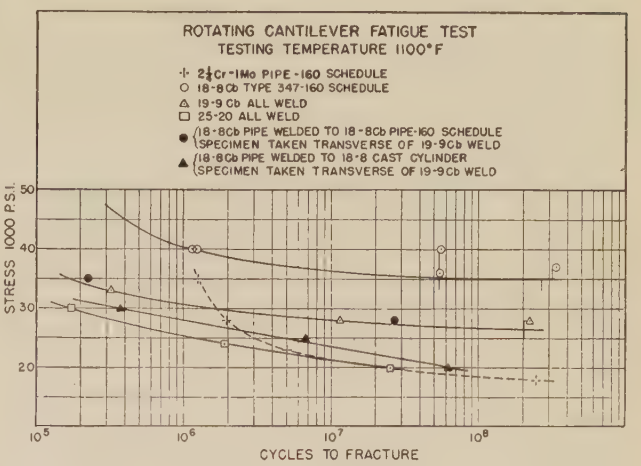

Fig. 14 Rotating Cantilever Fatigue-Test; Testing Temperature 1100 F

The following illustrations show how the calculated temperatures compare with the test values reported in the paper. Fig. 15 is for the ferritic schedule-160 piping and shows quite good agreement except for thermocouples T–3 and T–4.

The initial difference shown for thermocouple T–4 before start of the quench indicates that this element was subject to some error. It is possible that this was caused by heat losses due to partial exposure.

Another possibility is that wet superex insulation may have been applied over this element and the insulation insufficiently dried out before testing. The writer has recently employed thermocouples peened on the outside of a pipe to measure steam temperatures and found an error of the same order (25 F) which persisted throughout an entire one-day sea trial. Laboratory tests showed that about 24 hr at temperature were required to dry out the insulation sufficiently to give accurate readings.

Fig. 16 is a similar comparison of test and calculated values for the ferritic schedule-80 piping and shows about the same numerical difference but in the opposite direction.

The test temperatures near the outer wall are higher than the calculated values for schedule-160 pipe, but lower than calculated values for schedule-80 pipe.

Comparisons for the two thicknesses of austenitic piping are shown in Figs. 17 and 18. In both these cases the observed temperature differences across the pipe are very much less than calculated, and the discrepancy is too great to be ascribed to errors in temperature measurement.

In order to explain this discrepancy the indicated surface heat-transmission rates were computed from the test data by summing up the pipe-wall temperature changes for any interval of time. The surface temperature gradient was assumed to be the difference between thermocouple T–1 and the saturation temperature. The log-mean temperature difference was used for the initial phase when the inner pipe-wall temperature was changing rapidly. The results of these calculations are shown in Fig. 19.

These results are considerably different from the assumed surface heat-transfer coefficient of 1000, and, in general, account for the differences between observed and calculated temperatures in the pipe wall.

However, the differences in test heat-transfer coefficients still remain to be accounted for. It appears reasonable to expect some delay in establishing the full value of this coefficient, but it is difficult to understand why the 18–8 piping should have a much slower response and reach lower final values. The rapid drop in value for the schedule-80 ferritic piping is also curious.

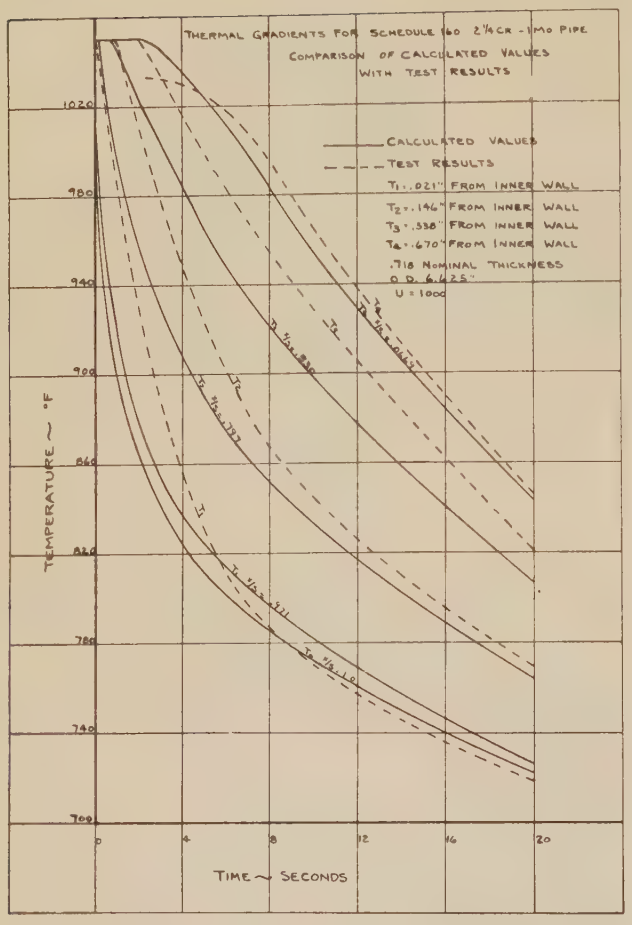

FIG. 15 THERMAL GRADIENTS FOR SCHEDULE-160 2¼ CR - 1 MO PIPE. COMPARISON OF CALCULATED VALUES WITH TEST RESULTS

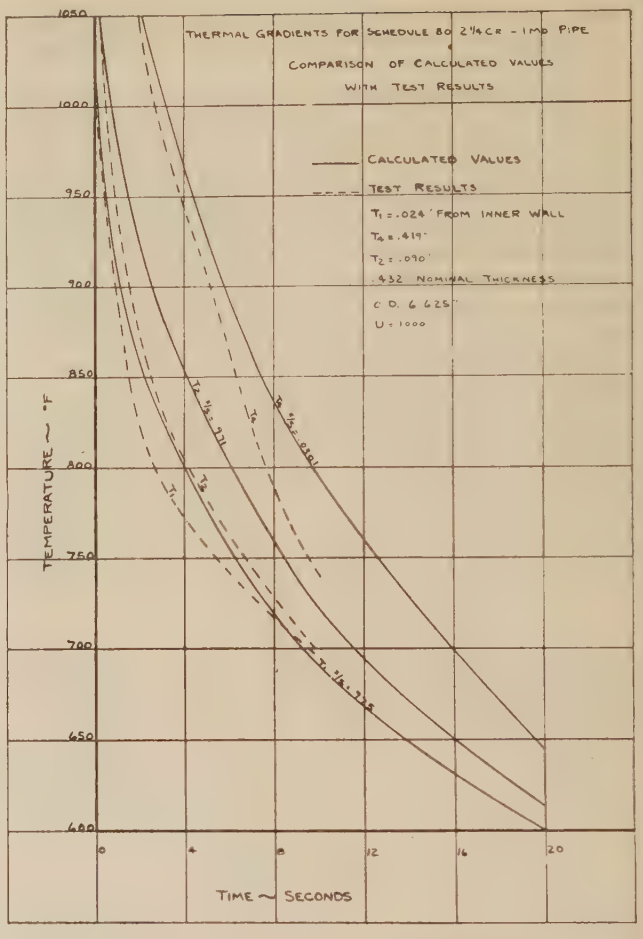

FIG. 16 THERMAL GRADIENTS FOR SCHEDULE-80 2¼ CR - 1 MO PIPE. COMPARISON OF CALCULATED VALUES WITH TEST RESULTS

It would be helpful to know just how consistent the thermocouple readings were between successive quenches of the same piping assembly, as this would indicate what variation is to be expected in the heat-transfer curves in Fig. 19.

One further item which should be established is the actual pipe-wall thickness at the points of temperature measurement. It is assumed that the piping was ordered to minimum wall specifications, in which case there is a permissible overthickness tolerance of 22 per cent.

It is hoped that this discussion has suggested some further lines of inquiry which ultimately will add to the value of the test results.

V. T. MALCOLM[11] AND SIDNEY LOW.[12] For many years it has been the hope of both the power-plant and refinery design engineers that they would have a sufficient amount of information with regard to this elusive condition. Due to the lack of knowledge of the conditions existing in high-temperature steam lines, flange joints were gradually abolished and replaced with welded joints.

The selection of materials for service at elevated temperatures above 900 F is a complex problem and usually results in a compromise of a number of important design and fabricating features, such as the following:

1 Strength and ductility at operating temperatures.
2 Resistance to oxidation and scaling.
3 Resistance to corrosive attack.
4 Retention of satisfactory mechanical and other properties after extended exposure under operating conditions.
5 Resistance to thermal stresses in applications involving intermittent heating and cooling which eventually may cause deformation or cracking.
6 Weldability of the materials.
7 Structural stability.
8 Ease of fabrication.
9 Cost.

Adequacy of a given design, from a structural standpoint, requires that it be strong enough under the anticipated service conditions and that the stress imposed at the operating load and temperature be less than the strength of the material for long periods. At the same time, the imposed stress should not be much less than the strength of the material at temperature, if the design is to be practicable. Therefore all factors must be considered individually, especially such factors as consequence of failure, economic production, and degree of performance and life desired.

In the introduction we find that the authors were prompted to use the 18–8 chromium-nickel steel for 1050 F service due to the fact that it had superior high-temperature properties over the ferritic types of steel and would permit the use of thinner and lighter pipe at higher pressures. This is common practice among many design engineers who have based their designs on weight saving due to better stress values, but this thinking is

[11] Director of Research, The Chapman Valve Manufacturing Company, Indian Orchard, Mass.

[12] Research Engineer, The Chapman Valve Manufacturing Company. Jun. ASME.

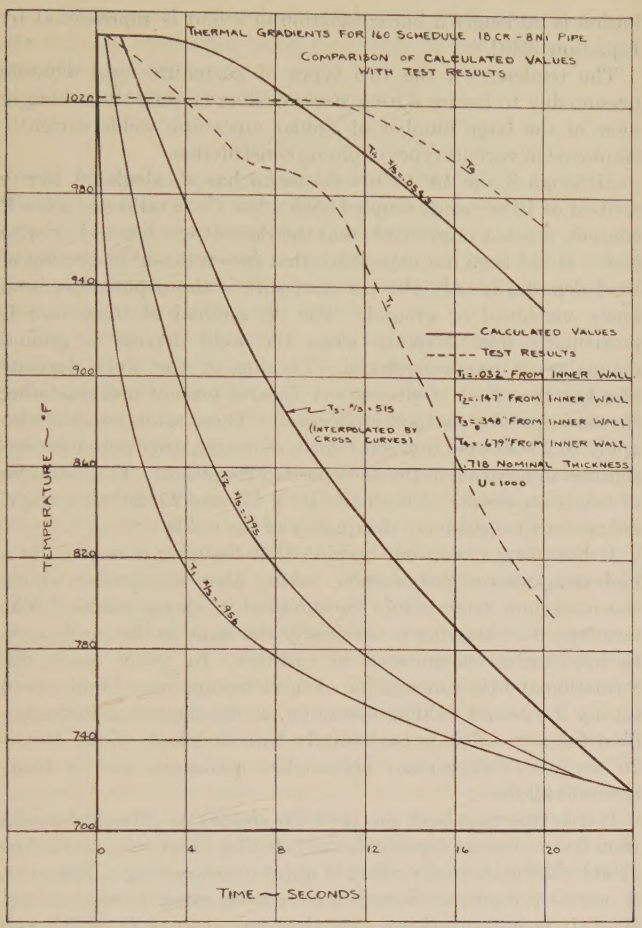

FIG. 17 THERMAL GRADIENTS FOR 160-SCHEDULE 18 CR - 8 NI PIPE. COMPARISON OF CALCULATED VALUES WITH TEST RESULTS

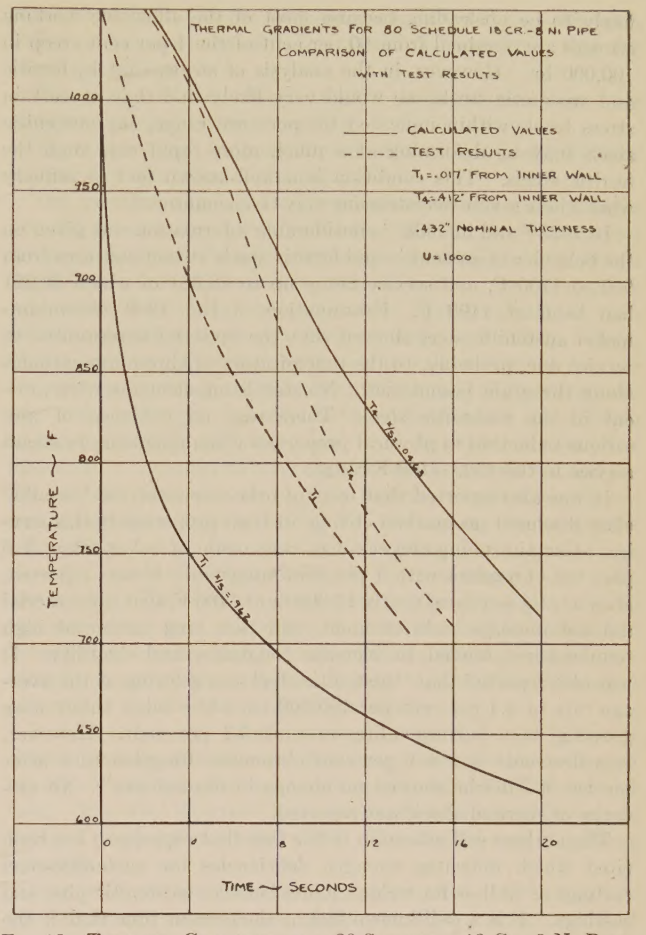

FIG. 18 THERMAL GRADIENTS FOR 80 SCHEDULE 18 CR - 8 NI PIPE. COMPARISON OF CALCULATED VALUES WITH TEST RESULTS

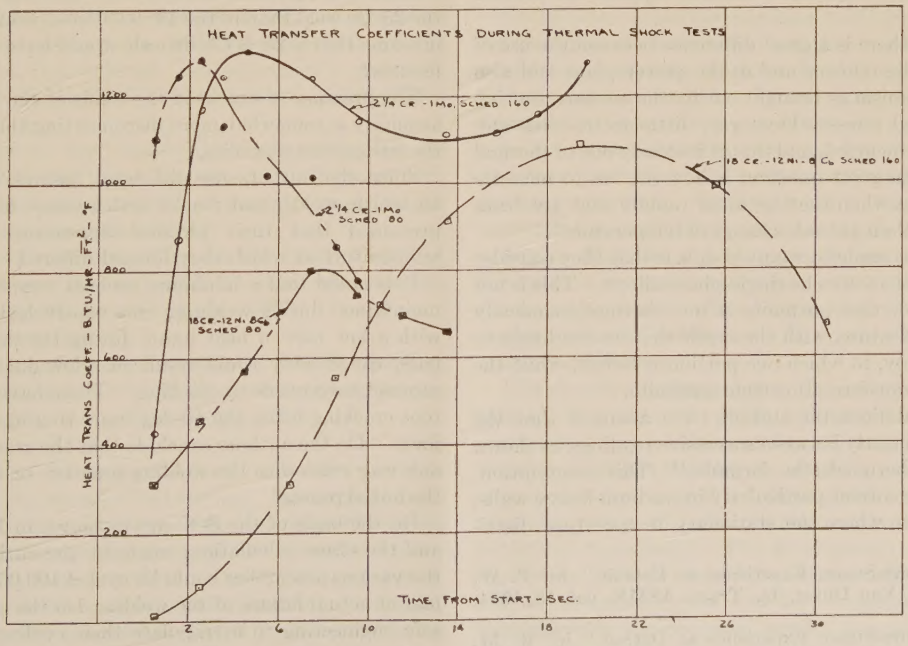

FIG. 19 HEAT-TRANSFER COEFFICIENTS DURING THERMAL-SHOCK TESTS

likely to be misleading because most of the allowable working stresses are obtained from 80 per cent of the 1 per cent creep in 100,000 hr. However, in the analysis of steels, that is, ferritic and austenitic steels, we would very likely find that at certain stress levels within indicated temperature range, the austenitic steels may be deforming at a much more rapid rate than the ferritic steels. This condition is a well-known fact in refinery work where severe overstressing may be encountered.

In 1933[13] and in 1938,[14] considerable information was given on the behavior of austenitic and ferritic steels at temperatures from 900 to 1100 F, and service hours up to 48,361 of which 38,921 had been at 1100 F. Examination of the 18–8 chromium-nickel austenitic steel showed that the material deteriorated in service due, probably, to the precipitation of chromium carbides along the grain boundaries. No stabilizing elements were present in the austenitic steel. There was no evidence of any serious reduction in physical properties when operating in steam service in the 1000–1100 F range.

It was also reported that tests of other steels of the low-alloy class disclosed no marked change in their properties in this service. Certain tubing and castings were made of a low-alloy, 4–6 per cent chromium with 1 per cent tungsten. It was reported, after a total service of nearly 11,000 hr at 1100 F, that the material did not undergo embrittlement, and that long service at high temperatures tended to increase toughness and ductility. It was also reported that "austenitic steel was growing at the average rate of 4.4 per cent per 100,000 hr, while alloy tubes were growing at a corresponding rate of 5.3 per cent. However, measurements of a 4–6 per cent chromium–tungsten tube after service of 7465 hr showed no change in dimensions." No evidence of thermal shock was reported.

The authors call attention to the fact that experience has been cited which indicates strength deficiencies for austenitic-steel castings as well as for welded joints between austenitic pipe and castings. It is a well-known fact at the present time that if the composition of austenitic steel is carefully controlled, with respect to the chromium and nickel equivalents, strength will not be lacking. This same composition balance applies to welded joints.

The writers agree there is a great difference between the use of austenitic steels in the refinery and in the power plant and also agree with the mechanism as brought out by the authors, but believe that mechanical stresses have very little to do with any damage that may be incurred, and that it is clearly one of thermal stress. However, the great question is how are we to measure these thermal stresses when they occur so rapidly and are transient in effect rather than a steady change of temperature?

One of the mistakes made by many people is that they consider the austenitic steels of 18–8 to be single-phase alloys. This is not true because we know that austenite is not thermodynamically stable at room temperature, with the result that we are likely to have a two-phase alloy, in which one portion is ferrite, while the other is undergoing transformation from austenite.

In the stress calculations the authors have assumed that the temperature varied linearly between successive readings, as shown by Timoshenko's thermoelastic formula.[15] This assumption, however, may not be correct particularly in medium-heavy walls, as denoted by a valve where the stationary temperature distribution is no longer a linear function of r and is represented by Equation [239].[16]

The tendency of the two types of austenitic weld deposits presumably to fissure during stress cycling is quite disturbing in view of the large number of similar austenitic welds currently employed in various types of piping construction.

Although if the 19–9 Cb weld metal has a calculated ferrite content of 10 per cent, coupled with a low C: Si ratio and a low P content, it is not improbable that the deposit was fissured prior to test. It has been our experience that penetrant-oil inspection of weld deposits is only 100 per cent sure if the deposit has been finely machined or ground. The oil method of inspection is particularly unsatisfactory when the weld deposit is ground manually or rough-machined. Peening of the weld deposits also has the effect of closing any fissures present and rendering the oil-inspection method ineffectual. These same remarks also apply to 25–20 weld deposits which, of course, are even more susceptible to fissuring in the as-deposited condition. The inclusion of bend-test results of both the 19–9 Cb and 25–20 welds might define more conclusively the quality of the welds.

It has always been our opinion that fissuring is essentially a high-temperature phenomenon, taking place appreciably above the maximum temperature encountered in steam service. The mechanism of fissuring is essentially the same as the mechanism of hot-tearing encountered in castings. In many cases, the formation and the propagation of these fissures may be observed during the actual welding operation, as the deposit solidifies behind the arc. This is particularly true of alloys of the 10 Cr-20 Ni type and certain high-nickel corrosion- and/or heat-resistant alloys.

If it is true that both the 19–9 Cb and the 25–20 weld deposits were fissure-free as deposited, the fact that fissures formed below 1100 F during thermal cycling is quite disconcerting. However, if macro- (or micro-) fissures were present prior to thermal cycling, it is not surprising that they would grow in width and length sufficiently to permit their detection by oil inspection (in view of the relatively high notch sensitivity of these materials).

Since the authors observed that fissuring was more severe in the 25–20 weld than in the 19–9 Cb weld, would it not be logical to presume that a 20–8 Cb deposit would have less (or perhaps no) fissures?

The presence of cracks in the welds of the 160-schedule ferritic assembly is somewhat more disconcerting than those observed in the austenitic assemblies.

Since the authors use the term fissures with respect to the austenitic welds, and cracks with respect to ferritic welds, it is presumed that their physical appearance differed, and the temperature at which they formed differed.

It is noted that a minimum preheat temperature of 400 F was maintained during welding; this relatively low preheat, coupled with a low rate of heat input during the deposition of the first pass, conceivably could result in a low ductility-transformation product susceptible to cracking. There have also been reports of root cracking using the 10-deg taper ring in a poorly "fitted-up" joint. Do the authors conclude that the cracks observed were in any way related to the welding practice, or to the "ingotism" of the initial passes?

On the basis of the S-N curves shown in Fig 14 of the paper, and the stress calculations made by the authors, it appears that the various assemblies could be cycled 100,000 times without any fear of actual failure of the welds. Do the authors feel that it is safe engineering to extrapolate their cycling test results on the basis of the S-N curves?

[13] "High-Temperature-Steam Experience at Detroit," by P. W. Thompson and R. M. Van Duzer, Jr., Trans. ASME, vol. 56, 1934, pp. 497–506.

[14] "High-Temperature-Steam Experience at Detroit," by R. M. Van Duzer, Jr., and Arthur McCutchan, Trans. ASME, vol. 61, 1939, pp. 383–398.

[15] Authors' reference (3), p. 261.

[16] Author's reference (3), p. 262.

C. T. Evans.[17] Were the welds cracked before the tests were started, the cracks not being detectable by conventional methods of inspection?

Were the tests abnormally severe?

Authors' Closure

Mr. Ireland's thorough analysis of our results is greatly appreciated. It is certainly true that it would be desirable to perform stress rupture and creep tests on samples cut from the test members and particularly from areas which show small cracks. It is planned to do this when it is decided that no further tests on the complete assemblies will be carried out.

The method for predicting unsteady-state temperatures in a cylindrical shell as referred to in the discussion is based on the assumption that the pipe wall is a flat plate. Other approximate methods are of course, available, such as the graphical or numerical method employing finite increments, and the electrical analog, and these can employ a variable coefficient of heat transfer. In so far as is known here the mathematical method based on a constant heat-transfer coefficient has not yet been applied to this case. In view of the uncertainty of necessary assumption, it would seem that the agreement between the test and calculated results indicated in Figs. 15 and 16 of the paper, is quite satisfactory. It must be remembered that these are in the nature of operating tests, rather than research experiments conducted under rigidly uniform conditions. While the test assemblies were uniform in arrangement it is possible that the flow of quench water, fairly reproducible in any one setup, was not exactly the same in all four. This might possibly account for the surface transfer coefficients being lower at the thermocouple positions in the case of the austenitic samples. It is also possible that the austenitic alloy surface has by nature a lower heat-transfer coefficient for the boiling of water.[18] Figs. 17, 18, and 19 of the paper, can be interpreted, in general, by either of these explanations. In fact, if the latter be correct, the ferritic alloy in these tests is actually being shocked more severely than the austenitic alloy.

The initial temperature drop from T–1 to T–4 can be shown to be approximately what would be expected under the conditions of insulation at the location of the thermocouples, namely, radiation from the hot pipe to the room, with one intermediate baffle of larger size. Thus, it is believed that any errors in the thermocouples are considerably smaller than the temperature differences from T–1 to T–4.

The general shape of the time-temperature curves for the several thermocouples were in good agreement. The maximum temperature differentials for a number of quenches made on the 160 schedule austenitic assembly follow:

Average maximum temperature difference between T–1 and T–4 thermocouples for 27 quenches with 60 lb of water when couples T–1 and T–4 were recorded simultaneously—180 F.

Standard deviation—12.6 F.

Average maximum temperature difference between T–1 and T–4 thermocouples for 6 quenches with 88 lb of water when couples T–1 and T–4 were recorded simultaneously—179 F.

Standard deviation—10.8 F.

As shown in Fig. 3 of the paper, the thermocouples are held in wells in the pipe wall by means of coil springs. An opening about 3 in. square was left in the insulation to accommodate the spring assembly. Although this opening was a relatively dead air space, it would account for some heat loss. The writer's precaution against the use of wet insulating material is well taken. Actually, the insulation was in dry block form; first 2 in. of diatomaceous earth, then 2 in. of 85 per cent magnesia, followed by a seal coat. Only the seal coat was put on wet, and, subsequently, this was thoroughly dried.

The pipe wall and depth of the thermocouple wells were measured carefully prior to welding.

The authors wish to thank Messrs. Malcolm and Low for their informative discussion of the paper.

The question was raised as to whether austenitic steels might not deform at a more rapid rate than ferritic steels at certain stress levels within the indicated temperature range. At certain stress levels and temperatures, transition from second-stage to very active third-stage creep may occur in austenitic steels even after thousands of hours at a fairly constant creep rate. Hence, the importance of knowing the time of transition between second- and third-stage creep. Yield-strength values at 0.2 per cent offset for the austenitic cast steel at room temperature and 1100 F, as shown in Table 3 of the paper, are lower than for the other materials. Consequently, highly stressed components of austenitic cast steel would be more likely to deform, and this observation is supported by experience. For this reason, and because of inferior high-temperature strength of welds adjacent to castings, the use of austenitic steel castings is not contemplated for main steam lines. The thermal-shock tests produced less distortion in the austentitic test assemblies than in the ferritic assemblies. However, the assemblies were of welded construction and contained no austenitic cast-steel flanges. Maximum distortion occurred in the 80 schedule ferritic assembly.

Stabilized types of austenitic chromium-nickel steel in lieu of similar types containing no stabilizing elements are indicated for the service temperatures mentioned by Messrs. Malcolm and Low. The steel they refer to as showing deterioration after a long time at temperature below 1000 F contained no stabilizing elements.

It is realized that the austenitic steels of the 18-8 type are not necessarily single-phase alloys. In fact a reference cited in the paper observed that chromium-nickel compositions which promote the formation of ferrite are more resistant to fissuring than are fully austenitic weld deposits.

At the outset of the investigation it was considered that thermal stresses might be more important than mechanical stresses when considering austenitic steel for steam piping for high-pressure, high-temperature service. It was with this in mind that the thermal-shock assemblies were fabricated and tested.

In the stress calculations presented in the paper the assumption was made that the temperature varied linearly between successive readings. While this method is not strictly valid, it was considered sufficiently accurate for the purpose.

Messrs. Malcolm and Low remark that the tendency for the two types of austenitic weld deposits to presumably fissure during stress cycling is quite disturbing in view of the large number of similar austenitic welds currently employed in various types of piping construction.

This situation is disturbing to the authors as well. The presence of fissures in the welds indicates a serious need for improved welding procedures and guidance for the welding of high-pressure, high-temperature steam piping. This need would not appear so conspicuous if the defects had been found only in the austenitic welds, for after all, the austenitic material was the subject of experiment. The development of similar defects in the ferritic welds is cause for serious consideration. This material was included in the test for comparison purposes and its suitability for the proposed service was not questioned. It is believed that sufficient technical information is available to insure sound conventional type welds in these materials provided painstaking control of the entire process is exercised.

Although oil powder and zyglo methods of inspection failed to

[17] Chief Metallurgist, Elliott, Company, Jeannette, Pa.

[18] "Heat Transmission," by W. H. McAdams, second edition, McGraw-Hill Book Company, Inc., New York, N. Y., 1933, pp. 300–304.

reveal fissures before the tests, the defects were probably present in an incipient stage. The 19–9 weld deposits showed much less tendency toward fissuring than did the 25–20 weld deposits. It does not seem unlikely that fissures might be disclosed in austenitic welds in service if the surfaces are smoothly finished and carefully examined.

The authors did not intentionally use the term fissure with respect to the austenitic welds and crack with respect to the ferritic welds. The two terms indicate the same type of defect, that is, parting of the metal or a tear.

Root cracks observed in the welds are associated with lack of fusion at the root which points to undesirable features in the joint design. Subsequent experiments have indicated the desirability of increasing the root opening from $^1/_8$ in. to $^3/_8$ in. and employing a flat, split backing ring in lieu of the backing ring shown in Fig. 2 of the paper. It is also indicated that deposition should be stringerwise, the thickness of each stringer not to exceed $^1/_8$ in.

The authors would not advise extrapolating the cycling test results for the full-scale assemblies on the basis of S-N curves obtained for laboratory test specimens. However, they do consider it advisable to continue the testing of the mock-ups at higher stress levels until failures are produced.

In answer to Mr. Evan's questions:

The oil powder and zyglo methods of inspection failed to reveal the surface defects before the tests were started.

The thermal-shock test of 100 cycles might be considered rather severe but not necessarily more severe than might occur during the service life of a piping system. The 4000 deflection cycles imposed on the mock-ups represent stress conditions produced on heating up a piping system every other day for approximately 20 years, the maximum allowable stress being 25 per cent greater than that permitted by the ASME Boiler Code.